City University London
School of Engineering and Mathematical Sciences

Advanced Robust Non-Invasive Foetal Heart Detection Techniques during Active Labour Using One Pair of Transabdominal Electrodes

by

Walid A. Zgallai

A thesis submitted in partial fulfilment of the requirements
for the degree of Doctor of Philosophy in Electrical Engineering

Electrical, Electronic and Information Engineering Division,
Northampton Square, London EC1V 0HB, UK

April 2007

Table of contents

List of Tables

4,873. The average fetal heart detection rate is 93.52% for coincident mother and fetal QRS-complexes. The average fetal heart detection rate is 99.5% for non-coincident mother and fetal QRS-complexes. Model order is fixed at 11 + 4. 330

List of Figures

List of abbreviations

ACF	Auto-Correlation Function
ADC	Analogue to Digital Converter
AEMG	Abdominal electromyographic signal
AIC	Akaike Information Criteria
ANN	Artificial Neural Network
AR	Auto-Regressive
ARMA	Auto-Regressive Moving Average
BIC	Bispectral contour template matching technique
BPM	Beats Per Minute
BSS	Blind Source Separation
BSSS	Blind Source Subspace Separation
CPU	Central Processing Unit
CRLB	Cramer-Rao Lower Bound
CTG	Cardiotocogram
DSP	Digital Signal Processing
ECG	Electrocardiogram
EV	Eigen-vector Decomposition
EMG	Electromyogram
FECG	Fetal electrocardiogram
FFT	Fast Fourier Transform
FHB	Fetal Heartbeat
FHDR	Fetal Heart Detection Rate
FHR	Fetal Heart Rate
FIR	Finite Impulse Response
FMCG	Fetal magnetocardiogram
FO	Fourth Order
FP	False Positive
FPPP	Fetal Principal Pseudo-spectral Peak
FS TOC	Fetal scalp cardiac cycle TOC

FS TOC D	Fetal scalp cardiac cycle TOC diagonal slice
FS TOC W	Fetal scalp cardiac cycle TOC wall slice
FT	Fourier Transform
FT ECG TOC D	Fetal transabdominal ECG TOC diagonal slice
FT ECG TOC W	Fetal transabdominal ECG TOC wall slice
HOS	Higher-Order Statistics
ICA	Independent Component Analysis
LMS	Least-Mean Squares
LMSCV	Least-Mean Squares-based Cubic Volterra
LMSQV	Least-Mean Squares-based Quadratic Volterra
LMF	Least-Mean Fourth
LMFCV	Least-Mean Fourth-based Cubic Volterra
LMFQV	Least-Mean Fourth-based Quadratic Volterra
MA	Moving Average
MBP-MLP	Modified Back Propagation Multi-Layer Perceptron
MC TOC	Maternal-chest cardiac cycle TOC
MC TOC D	Maternal-chest cardiac cycle TOC diagonal slice
MC TOC W	Maternal-chest cardiac cycle TOC wall slice
MC QRS TOC	Maternal-chest QRS complex TOC
MC QRS TOC D	Maternal-chest QRS complex TOC diagonal slice
MC QRS TOC W	Maternal-chest QRS complex TOC wall slice
MECG	Maternal electrocardiogram
MEM	Maximum Entropy Method
MHR	Maternal Heart Rate
MIT/BIH	Massachusetts Institute of Technology / Beth Israel Hospital
ML	Maximum Likelihood
MLP	Multi-Layer Perceptron
MPPP	Maternal Principal Pseudo-spectral Peak
MSE	Mean Square Error
MT TOC	Maternal-transabdominal cardiac cycle TOC
MT TOC D	Maternal-transabdominal cardiac cycle TOC diagonal slice
MT TOC W	Maternal-transabdominal cardiac cycle TOC wall slice
MT QRS TOC	Maternal-transabdominal QRS complex TOC
MT QRS TOC D	Maternal-transabdominal QRS complex TOC diagonal slice

MT QRS TOC W	Maternal-transabdominal QRS complex TOC wall slice
MUCS MUSIC	Modified uterine contraction interference signal incorporated pseudo-spectral multiple signal classification
MUSIC	Multiple Signal Classification
MVDR	Minimum Variance Distortionless Response
PC	Personal Computer
PCA	Principal Component Analysis
PDF	Probability Density Function
PFA	Probability of False Alarm
PHD	Pisarenko Harmonic Decomposition
PPP	Principal Pseudo-spectral Peak
PSD	Power Spectral Density
QRS-free TOC D	QRS-free third-order cumulant diagonal slice
QRS-free TOC W	QRS-free third-order cumulant wall slice
RLS	Recursive Least Square
SNR	Signal to Noise Ratio
SO	Second Order
SOS	Second-Order Statistics
SQUID	Super conducting Quantum Interference Device
SVD	Singular Value Decomposition
TN	True Negative
TOC	Third-Order Cumulants
TP	True Positive

Acknowledgements

I would like to express my sincere appreciation and thanks to my supervisor, Dr. M. Sabry-Rizk for her encouragement and guidance at every stage of this work. Particularly, I would like to thank her for her patience and painstaking effort during the process of writing up this thesis.

The author would like to thank Dr. D. Romare for useful discussions on adaptive filtering, Dr. S. H. Elkhafif for useful discussions on the representation of straight lines in three-dimensional space, Dr. J. O'Riordan (North Middlesex Hospital), Dr. P. Hardiman (North Middlesex Hospital), and Prof. A. B. MacLean (Royal Free and University College Medical School), for their help and support. Throughout this work I much appreciated the help of the departmental secretaries Mrs. J. Rivellini and Mrs. L. Carr.

I am grateful to my family for their patience and support. Last, but by no means least, I would like to pay a special tribute to my parents who have supported me in many ways throughout my studies and to whom this thesis is dedicated.

Declaration

I hereby grant powers of discretion to the University Librarian to allow this thesis to be copied in whole or in part without further reference to me. This permission covers only single copies made for study purposes, subject to normal conditions of acknowledgement.

Abstract

The thesis proposes and evaluates **three** state-of-the-art signal processing techniques to detect fetal heartbeats within each maternal cardiac cycle, during labour contractions, using only a pair of transabdominal electrodes. The first and second techniques are, namely, the structured third-order cumulant-slice-template matching and the bispectral-contours-template matching for fetal QRS identification, respectively. The third technique is based on the modified and appropriately weighted spectral multiple signal classification (MUSIC) with incorporated covariance matrix for uterine contraction noise-like interfering signals also contaminated with noise. Essentially, two modifications to the standard MUSIC have been developed in order to enhance the performance of the spectral estimator in our applied work. The first modification involves the introduction of an optimised weighting function to the segmented ECG covariance matrix, and is chiefly aimed at enhancing the fetal QRS major spectral peak which occurs at around 30 Hz against the mother QRS major spectral peak usually occurring around 17 Hz and all other noise contributions. Additional optional pseudo-bispectral enhancement to sharpen the maternal and fetal spectral peaks, in particular when the mother and fetal R-waves are temporally coincident, have been achieved. The second modification to the spectral MUSIC is the removal of the unjustified assumption that only white Gaussian noise is present and the incorporation of the actual measured labour uterine contraction covariance matrix in reconfigured subspace analysis. This inevitably leads to the generalised eigenvectors – eigenvalues decomposition modern signal processing. This is now coined the modified, interference incorporated pseudo-spectral MUSIC. The above mentioned first and second techniques are higher-order statistics-based (HOS) and **hybrid** involving both signal processing and NN classifiers. The third technique is second-order statistics-based (SOS). In all techniques, the removal of signal non-linearity with the aid of non-linear Volterra synthesisers plays a crucial part in the fetal detection integrity.

Accurately assessed fetal heart classification rates as high as 95% have been achieved during labour, thus helping to provide non-invasive transparency to fetal intrapartum welfare. Performance analysis and evaluation processes involved more than 30 critical cases classified as "fetal under stress in labour" recorded in a London hospital database and used both transbadominal ECG electrodes and fetal scalp electrodes. The latter facilitates detection of the instantaneous fetal heart rate which is then used as the Reference Fetal Heart Rate in the assessment of the classification rate of each of the above mentioned techniques. It will be shown that the fetal heartbeats are completely masked by uterine activity and noise artefacts in all the recorded transabdominal maternal ECG signals. The fetal scalp electrode was, therefore, deemed necessary to provide the highest accurate measure of fetal heart functionality (from the hospital viewpoint), and in the assessment of the three non-invasive techniques presented in this thesis. The techniques may also be used during gestation and as early as 10 weeks.

CHAPTER ONE

INTRODUCTION

Worldwide, the standard method of monitoring the foetus during labour is the display of continuous fetal heart rate (FHR) and the uterine activity which together constitutes the cardiotocogram (CTG) (Figure 1.1). By analysis and appropriate interpretation of changes in the CTG obstetricians hope to prevent the delivery of dead or impaired babies who had suffered as a result of a lack of oxygen during labour and delivery.

1.1 The fetal electrocardiogram

The fetal heart rate is routinely obtained during labour from the electrocardiogram (ECG), the electrical activity of the heart or ultrasound. The ECG is obtained invasively by measuring differentially between an electrode clipped on the fetal scalp and a standard electrode (see Figures 1.2 and 1.3). In practice, to measure the fetal heart rate a suitable DSP algorithm is employed to detect, in hardware or software, successive QRS-complexes and from these to calculate the R-to-R intervals and the corresponding FHR. Most QRS-complex detection methods assume that the shape of the fetal QRS-complex is known *a priori*, but that its time of occurrence is unknown. This assumption is reasonable in the case of fetal scalp electrode ECG monitoring as the QRS-complex is visible and the SNR is high. However, it is not always valid as the shape of the QRS-complex may change from one subject to another and indeed within the same subject. Thus by comparing the ECG signal against a known, representative QRS-complex template the location of the QRS-complexes in the ECG can be determined based on some measure of similarity, for example a high value of cross-correlation. Like the adult ECG, normal fetal ECG is characterised by five peaks and valleys labelled with successive letters of the alphabet P, Q, R, S, and T. Thus, the ECG is said to consist of the P-wave, QRS-complex, and T-wave, as typified in Figure 1.2.

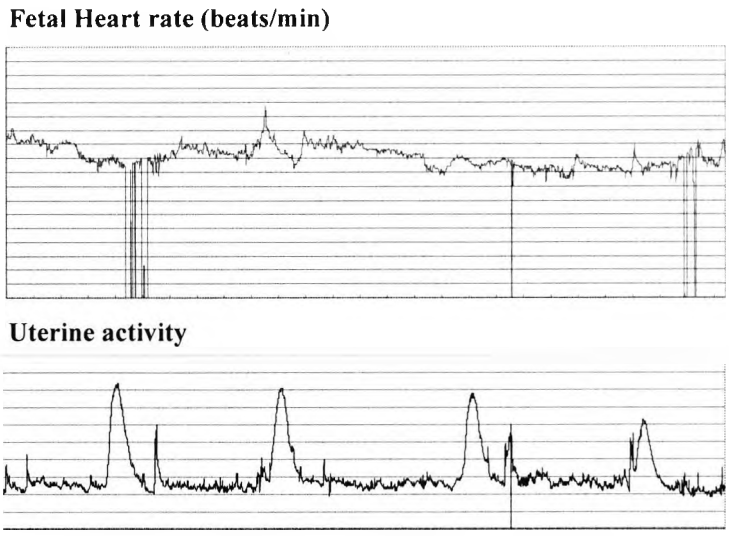

Figure 1.1: *An example of a cardiotocogram (CTG). The CTG consists of the fetal heart rate pattern (top panel) and the uterine activity (bottom panel).*

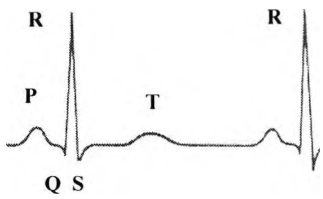

Figure 1.2: *The electrocardiogram (ECG).*

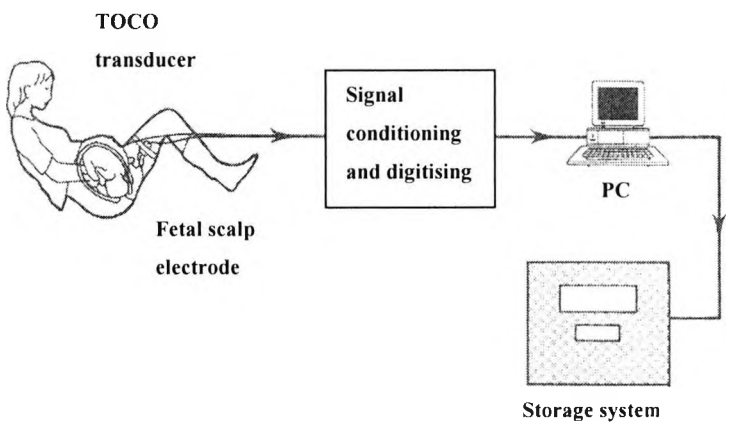

Figure 1.3: *Measurement of fetal electrocardiogram.*

As shown in Figure 1.2, the reciprocal of the heart period, that is the time interval between the R-to-R peaks (in milliseconds), multiplied by 60,000 gives the instantaneous heart rate. The FHR pattern in the upper half of Figure 1.1 is a plot of successive instantaneous heart rates.

Figure 1.4 shows the fetal heart rate before, during, and after labour uterine contractions; observe the boundaries of tachycardia and bradychardia. Also, observe the fetal heart rate deceleration duration after the peak pressure region of uterine contraction. These observation regions are extremely important in assessing fetal wellbeing.

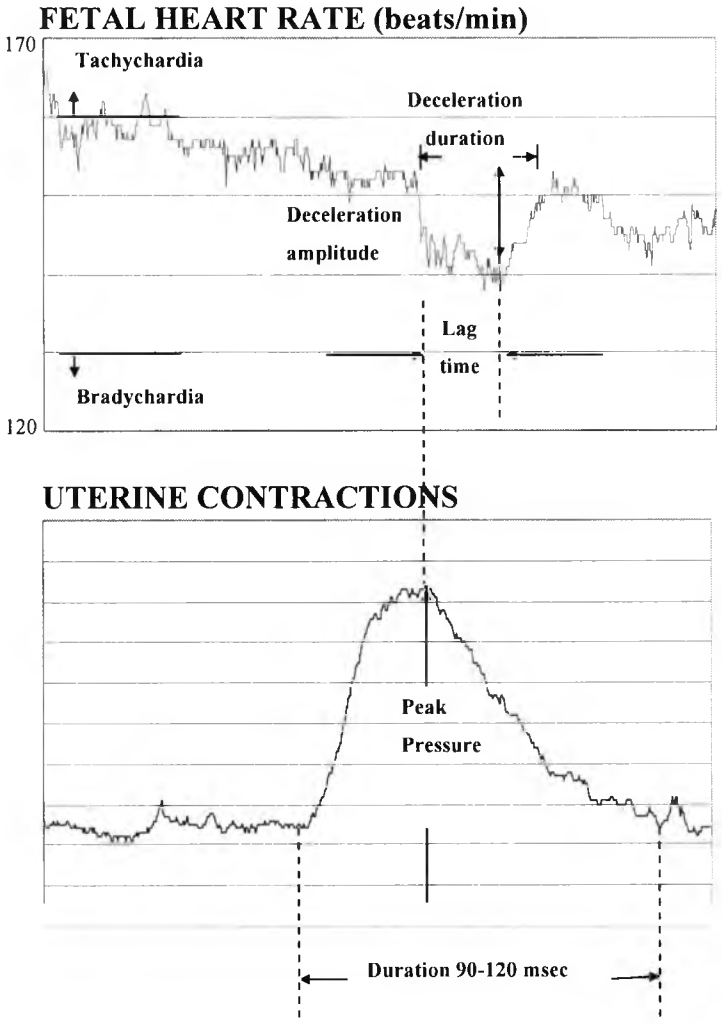

Figure 1.4: *Fetal heart rate (top panel) and uterine contraction activity (bottom panel).*

An important aspect of achieving the highest possible fetal heart detection rate, which is the aim of this thesis, is the ability not only to predict the outcome of labour all in good time, but also to assess FHR accelerations and decelerations (measured relative to the baseline of more than or less than 15 bpm), in sympathy with every dominant uterine contraction peak. For example, variable decelerations vary in time and / or shape, and are considered ominous only when:

- The decrease is 60 bpm or more.
- The decrease lasts 60 seconds or more.
- The decrease is associated with reduced variability.
- There is a slow return to baseline, or
- The baseline rate is abnormal.

Variable decelerations are seen with umbilical cord compression, but asphyxial features may be superimposed.

Late decelerations are when there is either:

- A lag time between the onset of uterine contraction and the deceleration, or
- A lag time between the end of the uterine contraction and the return of the baseline FHR to normal.

They are considered ominous, and may indicate uteroplacental insufficiency and fetal hypoxia, especially when they occur with 50% of contractions, or with loss of baseline variability.

In order to assess FHR accelerations and decelerations, the FHR is calculated from the R-R interval (the R-wave resides at the peak of the QRS-complex as shown in Figure 1.2). A fundamental problem is the reliable detection of the QRS-complexes. Missing 20 fetal heartbeats in a row around the uterine contraction peak can happen very often with all non-invasive FHR detection schemes* particularly when applied during labour. Other less severe signal degradation due, for example, to baseline wander, mains interference, ADC saturation and movement of the baby or mother will also lead to false detection or missed complexes and these are all common problems encountered in fetal heart monitoring even in the invasive fetal scalp electrode cases. Obviously all

*** To our knowledge, ultrasound and all other modern non-invasive ECG techniques reported in the literature fail to provide uninterrupted FHR recordings around the uterine contraction peak.**

problems are grossly exacerbated in transabdominal fetal heart monitoring as opposed to fetal scalp electrode FHR monitoring.

1.2 Brief discussion highlighting problems in detecting fetal ECG, non-invasively, from maternal transabdominal ECG signals

1. In a low-noise interval, SNR = 0 dB or worse, the basic problem is to extract the fetal QRS-complex from the composite transabdominal maternal ECG signal obtained from the abdominal lead, where the overlapping maternal QRS-complex is ten times stronger. Sometimes, even the maternal P-wave may swamp the weak fetal QRS-complex.
2. There are frequently occurring episodes of coincident mother's and fetal QRS-complexes. This is the most challenging problem, which is imminent in about 10% of the recorded ECG data.
3. Common types of noise in ECG measurements such as baseline wander, electromyographic (EMG), and motion artefacts are still, to this date, problematic in fetal heartbeat detection, as their spectra overlap both the mother's and fetal power spectra and this precludes the use of the power spectrum in detection. Current DSP techniques only offer partial solutions to suppress noise measurements.
4. During labour, uterine contractions result in very strong signal and noise artefacts that can easily drown the faint fetal QRS-complex signal. Essentially, it has been found that the uterine activity has a frequency peak overlapping that of the fetal QRS at 30 Hz [119]. This, undoubtedly, presents a formidable problem in extracting fetal heartbeats in the time or the frequency domain during labour.
5. It is noted, in this thesis, that the nature of the signals representing the maternal and fetal QRS-complexes is non-linear, and the physical channel through the uterus layers and the abdominal layers is also non-linear. Therefore, it is of paramount importance, in the first instance, to use non-linear techniques to synthesise, model, and remove as much as possible the non-linearity.
6. Close proximity of the mother's and fetal non-linear QRS-complex signals results in non-stationarity and presents a formidable detection problem.
7. There are limitations to some of the SOS-based detection methods based on spectral estimation such as the FFT, the AR, the Yule-Walker, the MEM…etc. Apart from the assumption of stationarity, the conventional

SOS-based methods lack sharpness of the peaks and thus have restricted ability to resolve spectral peaks.

8. The parametric spectral estimation methods assume white Gaussian noise and moderate to high signal-to-noise ratios (SNRs). If the data is contaminated with non-Gaussian or coloured noise then this would influence the estimation.
9. There is the issue of resolvability if the spacing between the mother's and fetal QRS-complexes is less than the shorter autocorrelation length. This is demonstrated in Figure 1.5 which depicts the autocorrelation function (ACF) for a fetal QRS-complex of 60 msec duration and a maternal chest QRS-complex of normal maximum 110 msec duration. The spacing between the mother's and fetal R-waves is 35 msec. The length of the autocorrelation function is 39 msec and 51 msec, for the fetal scalp electrode QRS-complex and the maternal chest QRS-complex, respectively. Since the length of the ACF is larger than the spacing between the mother's R-wave and the fetal R-wave, their respective QRS-complexes will not be resolvable. And since the power spectrum forms a Fourier Transform pair with the autocorrelation function, it has the same information presented in the ACF and it will not be able to resolve the spectral peaks of the mother's and fetal QRS-complexes when their respective R-wave spacing is comparatively small. This precludes the use of the power spectrum as a tool to identify and detect the fetal QRS-complexes.

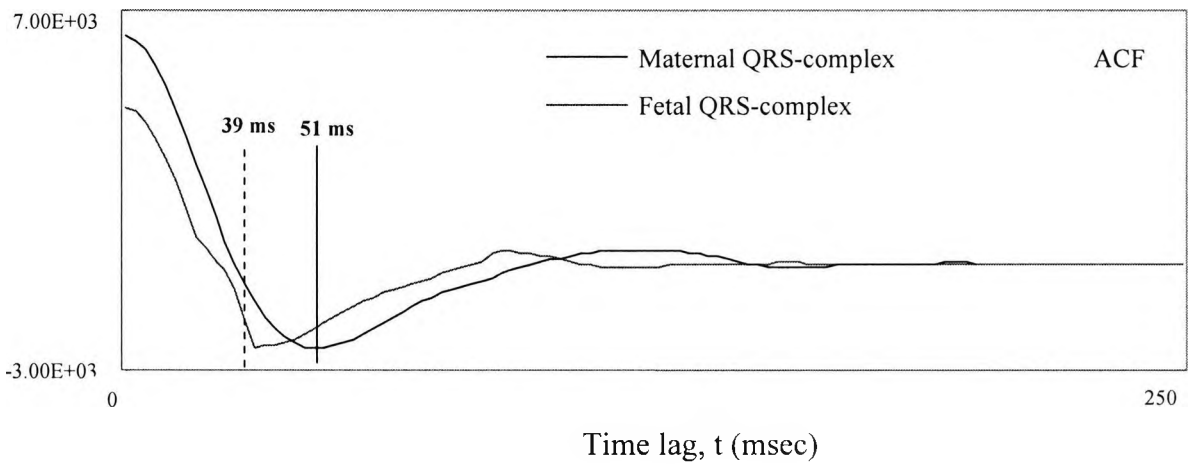

***Figure 1.5**: The autocorrelation function (ACF) for a maternal QRS-complex of 110 msec duration and a fetal QRS-complex of 60 msec duration. The correlation lengths are 39 msec and 51 msec, respectively. The spacing between the maternal and fetal R-waves is 35 msec. (Code: 16-31).*

10. For methods that rely on multiple surface electrodes, such as Blind Source Separation (BSS), and when spatial orthogonalisation is a key element in mother's and fetal signal subspace orthogonalisation, such ECG signals are picked up using a large number of electrodes, up to 32 in some reported work [98, 114-115]. The latter comes within the broad spectrum category of Singular Value Decomposition (SVD)* [110-111, 126-128] of mother, fetal, and noise methodologies. In such cases, the fetal heartbeat (FHB) detection is hampered by the rather unpredictable configuration of the volume conductor and the bioelectric sources when projected on 16 or even 32 surface electrodes. The utility of such methods in a real clinical environment is rather limited and very often renders FHB detection susceptible to electrode locations, human interaction, stage of pregnancy, and position of the foetus. So far, all the reported studies referred to herein, however, have not been assessed properly using the scalp electrode FHB as the FHB reference. Only high to moderate signal-to-noise ratios (SNRs) have been involved in these methods. In fact, all the FHBs were visible in their recordings which defies the purpose of using such sophisticated signal processing methods. Such methods will be appraised in this Chapter (Section 1.5) and in Chapter Four (Section 4.2).

1.3 Selection of some early work on fetal heartbeat detection

In the second half of the last century, some of the non-invasive fetal heartbeat detection techniques with variable success rates, as claimed by the authors but have not been properly assessed against fetal scalp electrode FHB reference, were reported in the literature. Here are some worth mentioning;

(i) Matched filtering applied to the fetal QRS-complex

Generally, matched filters can maximise the signal-to-noise ratio for the detection of a known signal in noise. However, the design of optimal matched filters requires knowledge of both the signal (mother's and fetal QRS-complexes) and the correlation statistics of the noise. The non-stationary nature of the signal and noise in an ECG

*** Fetal heart detection methods involving the generalised singular value decomposition (GSVD) methodology will be appropriately addressed in Chapter Six alongside with the new modified sequentially optimised and weighted MUSIC with the incorporation of the uterine contraction interference signal modified covariance matrix (MUCS MUSIC).**

represents an obstacle in the application of matched filtering to QRS-complex detection even for adults [55]. Later on, Xue et al. [54] developed a linear adaptive matched filter for the detection of adult QRS-complexes in extreme noise [54]. This filter attempts to adjust itself to compensate for changing signal shapes and noise conditions. This linear adaptive filter may have performed better than the non-adaptive types. However, the ECG is a non-linear signal generated from a non-linear system- the human body. It is difficult to adapt to a non-linear signal using a linear model. Towards the end of the last century, Xue et al. [18] replaced their linear filter by an ANN-based adaptive matched filter for adult QRS-complex detection. But no attempt has been made to apply this to fetal QRS-complex detection.

(ii) Maternal QRS-complex cancellation applied to transabdominal signals

Widrow et al. [15] proposed an adaptive filtering and adaptive noise cancellation method to extract the FECG from the composite maternal ECG signal; multiple MECG signals obtained from chest leads were used to cancel the MECG component identified as noise in the composite maternal ECG signal. A variant of the same approach was used by Longini et al. [108], where the FECG was obtained through a direct scaled subtraction of the thoracic ECG from the transabdominal ECG. Among the other methods, autocorrelation and cross correlation techniques were used by Van Bemmel [109]; methods termed as "spatial filtering" were used by Bergveld and Meijer [52] and Van Oosterom [110], where the FECG signal was produced through a weighted combination of signals from multiple electrodes.

All these methods have a common requirement of multiple maternal thoracic ECG signals together producing an estimate of the MECG component, which is eliminated from the composite maternal ECG signal to obtain the FECG component. Some of the problems of the multiple electrode methods are as follows; In the multiple electrode methods, there is the need to generate (either through adaptive weighting of the thoracic signals [15, 52, 108-110] or otherwise [23, 56, 111]) an estimate of the MECG component, which is close to that appearing in the composite maternal ECG signal. To achieve this, the number of thoracic as well as transabdominal ECG signals is sometimes heuristically chosen. Although some works reportedly use specific numbers of thoracic signals (for example 4 in [15] and 3 in [111]), the extraction is sensitive to the accuracy in the absolute as well as collective placement of the thoracic electrodes

[23, 56, 111]. Further, parametric methods [15, 52] may have estimation problems if the underlying dynamics keep changing. Another aspect often ignored is the problem of eliminating the effects of differential interferences due to extraneous reasons (e.g., due to respiratory activity [112]) on the thoracic signals and on the composite abdominal signals. All multiple electrode methods suffer from this problem.

1.4 Current non-invasive techniques

The short- and long-term recording of the fetal heart rate (FHR) is the most frequently used diagnostic measurement to determine the fetal health status [17], [84]. Recently, it has been discovered that by using sophisticated algorithms it is possible to have high acquisition rates for FHR as early as the 12^{th} gestational week. Routine medical analysis of the recorded FHR diagram is of great clinical importance, and since its introduction it has led to the drastic reduction of prenatal and post-natal child mortality [86]. Currently, there are several different non-invasive methods used in medical practice for the measurement of the FHR:

- The ultrasound cardiotocography (CTG) is the most commonly applied diagnostic tool which provides an accurate determination of the long-term fetal cardiac performance. In recent years, combined ultrasound transducers have appeared, which are capable of detecting the fetal heart activity and the uterine contractions as well. Frequent measurements of FHR are recommendable, however, the cost of high quality CTG devices is unfortunately so high that this technology is not viable for low-cost devices used in the home care sector. The CTG has typically 2 MHz radiated at 10 mW / cm^2 intensity on the fetus. However, this is regarded as unrisky. There are two disadvantages with CTG, namely, the loss of acquisition (i) during a time window in gestation, and (ii) due to the baby's movement.
- Fetal Magnetocardiography (FMCG) is also applied for the detection of fetal heart activity, but primarily for short-term recordings. This technique uses a super-conducting quantum interference device (SQUID) to detect changes in the magnetic field created by changes in the intracellular current density within the fetal heart. It has the advantage of not having any interference from the maternal ECG complexes and abdominal muscle action. It requires high-value superconductor sensors and a special recording environment (magnetically shielded room). Another advantage of this method is that it allows a proper segmentation of the P-wave,

QRS-complex, and ST-segment of the fetal cardiac cycle. A study of 106 pregnant women between 20 and 42 weeks gestation using the SQUID technique has resulted in a 67% success rate in detecting the fetal QRS-complex in unaveraged recordings, 75% detection rate of the fetal P-wave, and 72% detection rate of the fetal T-wave [30]. FMCG and FECG recordings of similar quality have been consecutively obtained from the same patients [27]. The main disadvantages of the system are the high cost of the SQUID, the especially purpose-built, non-metal chair and the shielded environment required to reduce interference.

- Auscultation is one of the oldest medical tools in history, which has also been applied in fetal diagnostics, using specially-formed stethoscopes. The modern form of auscultation called phonocardiography, provides for absolutely non-invasive electronic recording and computerised analysis of the acoustic cardiac signals. Further use has been reported which concerns the analysis of the recorded acoustic vibrations, such as electronic stethoscope and heart noise analysis [88-90]. Unfortunately, the fetal heart activity produces much less acoustic energy, and in addition it is surrounded by a highly noisy environment. This makes the detection of fetal heart sounds a very complicated problem. Several methods have already been proposed for fetal phonocardiographic measurements [91-93]. However, currently there are no fetal phonocardiographic devices available.
- Fetal Electrocardiography (FECG) using non-invasive surface electrodes placed on the maternal abdomen (transabdominal) is another tool for FHR recording. There are numerous methods proposed for the rejection of the disturbing maternal ECG signal. These can be found in [17, and references therein]; the automated long-term evaluation of FECG is regarded as less robust than CTG. In [17] a failure rate of approximately 30% is quoted as an almost unanimous norm [5, 26, 29, 94-96]. The advantage of FECG is that it can be implemented in small and relatively low-cost devices [97].

Some of the most advanced techniques will now be briefly appraised in the following section.

1.5 Modern antepartum techniques for non-invasive fetal electrocardiogram monitoring

1.5.1 Blind Source Separation (BSS) based on the method of Independent Component Analysis (ICA)

(a) Background

Blind source separation describes the process of extracting a number of individual signals emitted by statistically independent sources from combinations received by an array of sensors. The term "blind" is used to indicate that no prior information or training data is available concerning the individual sources or the manner in which they have been combined.

It is assumed here that the combination mechanism is linear, instantaneous, and time invariant. It is well documented that under these circumstances the signals cannot be separated using only second-order statistics. Performing a conventional Principal Component Analysis (PCA) based on second-order statistics serves to identify the number of signals present and to identify noise components but does not separate the signals completely. The principal component signal waveforms are uncorrelated (in the noiseless real-mixture two-source sensor scenario, the observations are whitened, de-correlated and normalised) but not necessarily statistically independent. They are related to the original independent signals by means of an unknown rotation matrix. Determining this rotation matrix necessitates the use of Higher-Order Statistics (HOS) usually represented by cumulants of order higher than two. Since the third-order cumulants of a symmetric distribution are zero, the fourth-order cumulants are most commonly used. Note that signals with Gaussian statistics cannot be separated in this way since a Gaussian distribution is specified completely by its mean and variance and the expected values of the higher order cumulants are zero.

The use of higher-order statistics to separate unknown, independent signals (following an initial principal component analysis) is often referred to as Independent Component Analysis (ICA). The definitive work on ICA was published by Comon [116]. He used the term contrast function to denote a higher-order statistical measure which attains its minimum (maximum) value for multiple signals only when the signals are independent.

As a convenient form of contrast functions, Comon chose to use the sum of the squares of the fourth-order auto-cumulants. For normalised, zero-mean signals (as generated by the initial PCA), this should attain a maximum value when the signals are statistically independent.

An alternative algorithm for ICA has been developed by Clarke [117-118] and applied with great success to a wide range of communication signals received by various sensors. This algorithm, known as BLISS, exploits the same sequence as that proposed by Comon but differs in the choice of contrast function used to estimate the rotation angles.

(b) Appraisal of techniques involving independent component analysis

Some research workers [98, 114-115] have recently been using Independent Component Analysis (ICA), also known as Blind Source Separation (BSS), in pursuit of separating mother's and fetal ECG signals from cutaneous measurements. Perhaps it is more prudent to appraise the technique here as a concept for non-invasive fetal heartbeat detection and resort to an appendix to provide an informative background. The ICA-method itself is discussed at a conceptual level in Appendix A2 part 1 and the extraction of FECG by means of BSS in Appendix A2 part 2.

In the publications [98, 114-115] the ICA has been carried out under the following assumptions, the validity of each has been challenged in the author's joint paper [99] (a copy of our publication is given in Appendix A3); (1) Sensors (electrodes) are assumed to form an instantaneous linear mixture of mother and fetal source signals. (2) Noise is assumed to have an additive Gaussian perturbation. (3) Mother's and fetal ECG signals are assumed to be stationary and linear, mutually statistically independent and statistically independent from noise. (4) Most of the second-order and fourth-order Blind Source Separation (BSS) methods developed to date assume that all ECG third-order cumulants vanish, which shows their lack of understanding of ECG statistics, hence the need to use the fourth-order cumulants. Furthermore, a crucial factor in using Independent Component Analysis (ICA) is the accurate positioning of the individual cutaneous electrodes connected to channels numbering from six up to 32 in aid of signals' orthogonalisation.

References [98, 114-115] have succeeded in separating fetal heartbeats (FHBs) using just eight electrodes (channels). But, the collection of data used has been rather limited to clean segments taken during gestation periods, and very conveniently chosen to have very high signal-to-noise ratio (SNR), and cleverly avoiding data with intrapartum cyclic uterine contractions or serious motion artefacts. Furthermore, the aforementioned publications **have failed to include in their assessment the imminently and most frequently occurring episodes of coincident mother's and fetal heartbeats. This is the most challenging problem which is imminent in around 10% of the measured data.** As mentioned before, due to the non-linear nature of the maternal and fetal QRS-complexes and the non-linear physical channel through the uterus layers and the abdomen layers, quadratic and higher-order coupling is generated between the mother's and fetal ECGs as their separate signals propagate through the inner tissues. This also results in non-stationarity and presents a formidable detection problem even when higher-order statistics are used as DSP tools.

Independent Component Analysis (ICA) essentially requires high signal-to-noise ratios (SNRs) and has, so far, been used antepartum without appropriate assessment (i.e., no provision of fetal scalp electrode ECG reference to confirm the detection of fetal QRS-complexes) [98, 114-115].

These methods have been criticised in our paper "Virtues and Vices of Source Separation Using Linear Independent Component Analysis for Blind Source Separation of Non-linearly Coupled and Synchronised Fetal and Mother ECGs" [99] where the following issues have been raised: In our paper [99], there is evidence of non-linear quadratic and cubic coupling and non-stationarity in the transabdominally measured signals when the fetal and maternal heartbeats are coincident or even close enough. This, therefore, requires a high degree of sophistication in the non-linear modelling of both the maternal and fetal ECG signals to be able to establish the extent of quadratic coupling (cubic coupling is very weak) and incorporate it in the analysis. At this juncture, any justification of **the key assumption of linearity and mutual statistical independence** of both maternal and fetal ECG signals which is the basis for the ICA techniques, is now questionable [99]. We report in Chapter Three the use of non-linear Volterra structures which caters for quantifying the linear, quadratic, and cubic parts of both the maternal and fetal ECG signals. The subsequent analysis is much more

simplified by including only the linear non-Gaussian component of the ECG signals and noise. The analysis referred to includes; (1) the third-order cumulant template matching technique (**TOC template matching**), (2) the bispectral contour template matching technique (**BIC template matching**), and (3) the modified spectral multiple signal classification (MUSIC) with incorporated covariance matrix for uterine contraction combined with noise. It is worth reporting at the end of this short appraisal that present techniques for non-linear ICA only cater for non-linear mixtures and are definitely not adequate to separate non-linear sources such as the mother's / fetal ECGs in non-linear noise artefacts which is the case during labour.

1.5.2 Appraisal of techniques involving wavelet transform

This is based on the detection of singularities obtained from the composite abdominal signal, using the modulus maxima in the wavelet domain [100]. Modulus maxima locations of the abdominal signals are used to discriminate between maternal and fetal signals. Two different approaches have been considered. In the first approach, at least one thoracic signal is used prior to performing the classification whereas in the second approach no thoracic signal is needed. A reconstruction method is utilised to obtain the fetal ECG signal from the detected fetal modulus maxima. It is worth noting that:

1. The proposed technique [100] is different from the classical time-domain methods, in that it exploits the most distinct features of the signal, leading to more robustness with respect to signal perturbations.
2. The algorithm is validated using data with high SNR and this is evidenced by the visual tracking of all fetal heartbeats which can be detected using a simple threshold procedure yielding far less computational overhead.

1.5.3 Appraisal of techniques involving dynamic modelling

The authors [7] described and applied a technique which is an outcome of the theory of non-linear dynamical systems. In deterministic dynamical systems, the post-transient trajectory of the system is frequently confined to a set of points in state space called an "attractor". Filters based on the concept of an attractor in state space are often found to be dramatically superior to linear filtering methods when applied to chaotic systems. The improvement in performance comes from exploiting the geometrical information the attractor provides. Whenever a multi-dimensional reconstruction of a signal can be approximated by a low-dimensional surface (or attractor), projections onto this (hyper)

surface can improve the signal-to-noise ratio. In this application, the fetal component in the first sweep is treated as a contamination of the maternal ECG, when noise reduction techniques are suitable for signal separation. It proved to be a much more stable procedure to first extract all contaminations from the maternal trace, and then subject the output- containing the fetal and noise- to a second sweep of the projective filter. Basically there are two key issues related to the questionable assumption of signal-to- noise-ratio quantification.

1. Like the methods mentioned in sections 1.5.1 and 1.5.2, the data has comparatively high SNR and the fetal heartbeats can be detected by an adaptive matched filter like the one previously developed for adult QRS-complex detection (see footnote for specific references*) and requires much shorter data samples than the dynamic modelling. Thus, the dynamic modelling apparent success at high SNR is offset by the required lengthy data (at least 10,000 samples).
2. Due to the beat-to-beat fluctuations of the shape and duration of the ECG waveform, the normal ECG cannot be considered to be deterministic [83, 113]. In our previous publications, we have proved that determinism is found in all adult and fetal ECGs for data lengths of 10,000 samples.

1.6 Conventional noise cancellation and adaptive adults' ECG filtering

Adaptive filtering algorithms are self-adjusted techniques that can be applied to the analysis of signals with unknown or time varying statistics [6]. Adaptive filtering techniques have shown to be useful in many biomedical applications [7]. The basic idea behind adaptive filtering has been summarised by Widrow et al. [9] and

* [1] T. Schreiber, and D Kaplan, "Signal separation by nonlinear projections: The fetal electrocardiogram," Phys. Rev. E, Vol. 53, p. R4326, 1996.

[2] E. Cicinelli, A. Bartone, I. Carbonara, G. Incampo, M. Bachicchio, G. Ventura, S. Montanaro, and G. Aloisio, "Improved equipment for abdominal fetal electrocardiogram recording: description and clinical evaluation", Int. J. Biol. Med. Comput., Vol. 35, pp. 193-205, 1994; De Callerts et al., "Description of a real time system to extract the fetal electrocardiogram", Clin. Phys. Physiol. Meas., Vol. 10, Suppl. B, pp. 7-10, 1989. D. Callerts, B. DeMoor, J. Vanderville, W. Sansen, "Comparison of SVD methods to extract the fetal electrocardiograms", Med. Biol. Eng. Comput., Vol. 28, pp. 217- 224, 1990.

[3] T. Schreiber and D. Kaplan, "Nonlinear noise reduction for electrocardiograms", CHAOS, Vol. 6, pp. 87-92, 1996.

used in a variety of ECG signal processing applications [8-9]. Adaptive filtering is necessary in ECG applications because the filter coefficients need to adapt to changing signal conditions and noise characteristics. This is due to changes in the signal morphology and the noisy environment. Also, there is a spectral overlap between the ECG signal and some noise components, and the noise band might be unknown or time-varying. This is very serious especially when the noise is non-linearly coupled to the signal or has a recursive and / or non-stationary nature.

One simple but important application is in 50 Hz power-line interference cancellation. Yelderman et al. [8] used the idea that the maternal chest ECG recording from one of the leads can be used as a correlated noise source for adaptive cancellation. To improve the signal-to-noise ratio (SNR) multiple channels are employed for adaptive filtering. The ECG signal was employed [11] as the reference input to the adaptive filter to cancel the cardiogenic artefact from the thoracic signal.

Before discussions regarding different noise cancellation schemes it is prudent to describe in sufficient detail the spectral characteristics of adult and fetal scalp electrode ECGs.

1.6.1 The Power spectrum of adults' ECG components in noise and fetal scalp electrode ECG

The power spectrum of the ECG signal can provide somewhat limited but useful information about the QRS-complex frequency bands and its localised power. This section gives an interpretation of the power spectrum of the adults QRS-complex. In order to obtain this information, the QRS-complex of the ECG signal must be selected as a template over an 250 msec interval*, and zero-padded prior to the power spectrum analysis. The peak of the frequency spectrum obtained corresponds to the peak energy of the QRS-complex at 17 Hz. However, the peak of the overall ECG occurs at 14 Hz which demonstrates the previously mentioned limitations of FFT-based spectral estimators.

*** The special length of this temporal window will be addressed in Chapters Four, Five, and Six.**

The ECG waveform contains, in addition to the QRS-complex, the P- and T-waves. The templates for the P- and T-waves were taken from our research ECG databank, each over an 250 msec interval [123]. Figure 1.6 (a) summarises the relative power spectra of adult ECG, QRS-complexes, P- and T-waves, motion artefacts, and muscle noise. The latter two noise artefacts were isolated from the MIT/BIH Normal Sinus Rhythm (NSR) database [50-51]. The peak of the frequency spectrum obtained corresponds to the peak energy of the QRS-complex at 17 Hz. However, the peak of the overall ECG occurs at 14 Hz which demonstrates the previously mentioned limitations of the FFT-based spectral estimators. Observe the high spectral content at very low frequencies attributed to motion artefact and muscle noise. Figure 1.6 (b) shows a prominent fetal ECG spectral peak at 30 Hz. Again, templates extracted from our fetal scalp electrode databases have been used in this study. Figure 1.6 (c) is based on a previous paper entitled "Novel decision strategy for P-wave detection utilising nonlinearly synthesised ECG components and their enhanced pseudospectral resonances", Dr. M. S. Rizk, et al. IEE Proceedings Science, Measurement and Technology, Special section on Medical Signal Processing, vol. 147, No. 6, pp. 389-397, November 2000 [123], and gives a picture of two multi-window structures which have been used to detect the MUSIC pseudo-spectral peaks for the maternal and fetal QRS-complexes based on innovative techniques reported in the above joint paper [123]. Figure 1.6 (c) will be referred to in Section 1.7.

The 50 Hz noise from power-line interference, and possibly other interference from electro-surgery equipment in the operating room were extracted using the conventional Butterworth filter. Another method is briefly mentioned in the next subsections.

1.6.2 Baseline Wander Reduction

The drift of the baseline with respiration can be represented as a sinusoidal component at the frequency of respiration added to the ECG signal. The amplitude and frequency of the sinusoidal component should be variables. The amplitude of the ECG signal also varies by about 15% with respiration. The variation could be reproduced by amplitude modulation of the ECG by the sinusoidal component which is added to the baseline.

Van Alste and Schilder described an efficient finite impulse response (FIR) notch filter that is rather effective at removing baseline wander and power line interference [102].

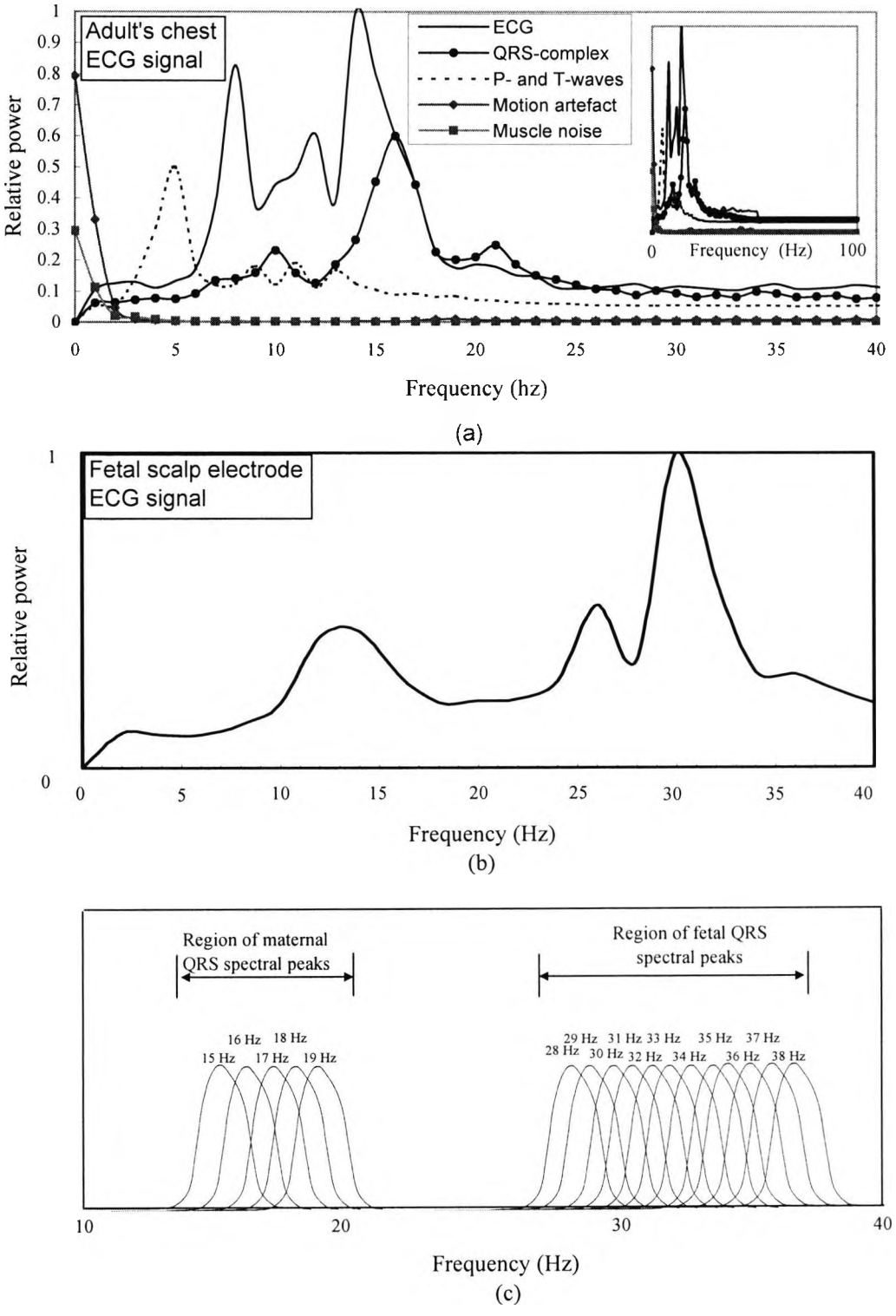

Figure 1.6: *Relative power spectra based on averaging of ten cardiac cycles of (a) adult's ECG signals, QRS-complexes, P- and T-waves, motion artefact and muscle noise (the inset shows an extended spectrum), and (b) fetal scalp electrode ECG. The Welch averaged periodogram method is used to calculate the power spectrum.(c) Optimised Kaiser windows. Each window is designed to enhance one of the MUSIC pseudo-spectral peaks for the maternal or the fetal QRS-complex. Part (c) is based on [123]. courtesy of the IEE Proceedings Science, Measurement and Technology.*

The adaptive filter to remove baseline wander is a special case of notch filtering, with the notch at zero frequency (dc). Only one weight is needed, and the reference input is a constant with a value of 1. This filter has a zero at dc. Frequencies in the range of 0 to 0.5 Hz should be removed to reduce baseline drift. If the sampling rate is 500 Hz, the convergence parameter μ should be smaller than 0.003. The parameter μ may be dynamically adjusted to obtain the desired low-frequency response. This filter converges slowly and therefore cannot track abrupt transients produced by motion artefacts.

1.6.3 Adaptive 50 Hz and 60 Hz Canceller

Power-line interference consists of 50 Hz (or 60 Hz) pickup and harmonics which can be modelled as sinusoids and combination of sinusoids. Furno and Tompkins [103] and Sahakian and Furno [104] described filter designs that subtract 60 Hz sinusoids from ECG signals. Widrow et al. [15] described a filter employing two weights so that in-phase and out-of phase components of the 60 Hz can be cancelled. In general, however, the power-line noise is not a pure 50 Hz (or 60 Hz) sinusoid, but is distorted. Therefore it was suggested to use the true interference signal as a reference [59]. The common-mode signal, usually recorded at the right leg reference electrode, is truly correlated with the noise in the ECG signal to be filtered, and the reference signal is the common-mode signal.

1.6.4 Multi-lead Canceller for EMG Noise

Muscle contractions cause artefactual millivolt-level potentials to be generated. The baseline electromyogram (EMG) is usually in the microvolt range and is, therefore, usually insignificant. The signals resulting from muscle contraction can be assumed to be transient bursts of zero-mean band-limited Gaussian noise. The variance of the distribution may be estimated from the variance and duration of bursts. EMG noise has a broad bandwidth which sometimes overlaps that of the ECG [105]. Simple low-pass filtering, therefore, is not adequate. It is suggested to employ more than one ECG lead [59]. Since electrodes are placed at different locations, the EMG noise from various leads may be uncorrelated. Uncorrelated inputs to the filter are ensured by selecting two orthonormal ECG leads. Noise in orthonormal leads is expected to be uncorrelated.

1.6.5 Motion Artefact Canceller

Motion artefacts are transient baseline changes caused by changes in the electrode-skin

impedance with electrode motion. As this impedance changes, the ECG amplifier sees a different source impedance, which forms a voltage divider with the amplifier input impedance. Therefore, the amplifier input voltage depends on the source impedance, which changes as the electrode position changes. The usual cause of motion artefacts is assumed to be vibrations or movement of the subject. Motion artefact is usually the most difficult form of noise to be eliminated from ECG signals. This is because its spectrum completely overlaps with that of the ECG, and its morphology often resembles that of the P- and T-waves and QRS-complexes [106], [107]. Most linear filtering approaches fail to solve this problem. The adaptive recurrent filter [63] is useful in cancelling noise from signals that have a repetitive morphology. The primary input to the filter is the ECG signal with motion artefact, and the reference signal is an impulse that is coincident with the beginning of each P-QRS-T complex. The adaptation takes place only for the samples spanning the signal complex, and subtraction of this complex from the ECG leaves the motion artefact as residue. Note that since the filter does not adapt between QRS-complexes, the baseline between complexes is simply interpolated. This clearly results in some signal distortion.

1.6.6 Electrode Contact Noise

Electrode contact noise is a type of transient interference caused by loss of contact between the electrode and the skin of the subject. The loss of contact can be permanent, or can be intermittent as would be the case when a loose electrode is brought in and out of contact with the skin as a result of movements or vibration. This switching action at the measurement system input can result in large artefacts since the ECG signal is usually capacitively coupled to the system. With the amplifier input disconnected, the 50 Hz (or 60 Hz) interference may be significant. Electrode contact noise can be modelled as a randomly occurring rapid baseline transient which decays exponentially to the baseline value and has a superimposed 50 Hz component. This transition may occur only once or may rapidly occur several times in succession. Characteristics of this noise signal include the amplitude of the initial transition, the amplitude of the 50 Hz component, and the time constant of the decay.

1.6.7 Electro-surgical noise

Electro-surgical noise completely destroys the ECG signal and can be represented by large amplitude sinusoids with frequencies approximately between 100 KHz and

1 MHz. Since the sampling rate of an ECG signal is between 250 Hz and 1000 Hz, an aliased version of this signal would be added to the ECG signal. The amplitude, duration and possibly the aliaised frequency should be variable.

1.6.8 Noise generated by electronic devices

Artefacts generated by electronic devices in the instrumentation system cannot be corrected by a QRS-complex detection algorithm. The input amplifier may saturate and no information about the ECG can reach the detector. In this case an alarm must be raised to take corrective action.

1.7 Non-invasive fetal heartbeat detection: New innovative techniques to overcome and tame Gaussian and non-Gaussian noise, non-linear noise, and unwanted strong non-linear deterministic signals

In this study, which has led to three innovative techniques to boost the accuracy of fetal heartbeat detection non-invasively, before and after the onset of labour, HOS including SOS and super-resolution techniques, all incorporating the adaptive non-linear Volterra synthesisers have been tested and appraised using ECG data recorded from more than 30 women in labour and a few women in gestation. Having discussed the problems encountered, the main issues here and potential solutions are as follows;

(1) To provide signal HOS domains that are not only free from Gaussian noise, but also devoted in their unique 2-d representations of the ECG signals to capturing and enhancing discriminant patterns to be used as standard templates of; (i) the mother's QRS-complex deduced from the chest ECG, (ii) the fetal QRS-complex, P-, and T-waves deduced from the fetal scalp electrode ECG. The reason for using the whole fetal cardiac cycle in the development of templates as opposed to the fetal QRS-complex is to avoid using the short data of 60 msec occupied by the fetal QRS-complex. The latter would yield high HOS variances and also violate one of the conditions given in the literature to separate and orthogonalise the signal and noise subspaces in the third MUSIC-based technique presented in Chapter Six. The HOS templates will be stored in the template databank and will be used for cross matching cumulants and bispectral contours created from the transabdominally measured ECG signals that contain the mother's, fetal and uterine contraction signals as well as noise. The latter is referred to as the transabdominal HOS domain. Apart from non-Gaussian

noise, it also contains the signal HOS representative associated with the uterine activities. It has been reported in previous studies [120-122] that the uterine contraction is a deterministic chaotic type of signal, but this applies to lengths of data comprising tens of maternal cardiac cycles. Within the maternal cardiac cycle, the uterine contraction signal supports the third- and higher-order statistics and is definitely non-linear. It will be shown in Chapter Six that removing the non-linearity from the transabdominally measured ECG signals is not adequate to guarantee the effectiveness of the MUSIC-based super-resolution detection technique and that the modelling and incorporation of the covariance matrix representing the linearised uterine contraction signals (in the absence of any mother's or fetal QRS-complex events) is of absolute necessity prior to performing the generalised singular value decomposition (GSVD) involved in the orthogonalisation of the signal and interference plus noise subspaces.

(2) To exploit the pseudo-spectral uniqueness of the mother's and that of the fetal ECG so that when there is coincident mother's and fetal QRS-complexes, one can resort to such individual uniqueness in order to discriminate between the mother and the fetal. Each of the mother's and fetal QRS-complexes has its own unique eigenvector discriminant pattern. Such mother and fetal patterns are combined together in the matrix obtained from the transabdominally measured ECG signal. Therefore, individual weightings are principally used to enhance a particular spectral feature (spectral peak) and suppress other features. This is done sequentially for the mother's QRS-complex and then for the fetal QRS-complex every time the mother's QRS-complex is scanned (read). If the two QRS-complexes are coincident temporally, they can only be separated due to their different "colours" in the frequency or pseudo-frequency domain. For instance, the subspace containing the combined mother and fetal ECG signals can be weighted to yield a spectrum with enhanced peak at 17 Hz for the mother's QRS-complex whilst suppressing the 30 Hz-peak of the fetal QRS-complex, and sequentially vice versa. Because each subject may have a different frequency peak, the 17 Hz is one frequency in a cluster of frequencies [123-125]. Similarly, the 30 Hz of the fetal QRS-complex pseudo-spectral peak is one frequency in a cluster of frequencies. One fetal ECG may produce pseudo-spectral QRS peaks that span the whole cluster. Therefore, there is a requirement of a sufficient number (5 - 10) of optimised windows centred at the frequencies of 15 Hz, 16 Hz, 17 Hz, 18 Hz, and 19 Hz for the mother's spectrum, and at the frequencies of 28 Hz, 29 Hz, 30 Hz, 31 Hz, 32 Hz, 33 Hz, 34 Hz, 35 Hz, 36 Hz, 37 Hz, and 38 Hz for the fetal spectrum (see Figures 1.6 (a), (b), and (c)).

Unlike other methods that fall in the broad spectrum category of generalised singular value decomposition (GSVD) [98, 114-115], this method does not require orthogonalising the mother subspace and the fetal subspace in order to separate them. In other words, there is no need for an elaborate electrode configuration on the mother's abdomen to result in two orthogonal predominant mother and fetal signal subspaces. In summary, this new subspace-based method relies, in the first instance, on orthogonalising the desired signal subspace which contains both the mother and fetal QRS-complexes against the interference subspace which contains the electrical signal emanating from the uterus electro-mechanical activity plus noise artefact. This is followed by enhancing the mother's pseudo-spectral principal peak at 17 Hz against the fetal and sequentially enhancing the fetal principal pseudo-spectral peak at 30 Hz against the mother's. Each is performed using specially adapted weights on pre-selected segmentations during the maternal cardiac cycle, see (4).

(3) To eliminate the signal or noise quadratic and cubic non-linearity, thereby primarily leaving only the linear portions of the mother's QRS- and fetal QRS-complexes to be used as their unique representative signatures or discriminant patterns in their respective HOS domains or subspaces during the detection or classification procedures. The removal of the above non-linearity from all non-linear background noise or other interfering signals is also carried out as a by-product of the operation of the non-linear adaptive Volterra processor.

(4) To provide a good estimate for the modified covariance matrix of the noise-contaminated interference signal associated with uterine activity to be incorporated in the above solutions. An accurate model for the long-term uterine activities has already been published elsewhere [119-122].

1.8 Data collection

During the last decade, several ECG recordings were borrowed on loan from the North Middlesex Hospital and the Royal Free and University College Medical School. Measurements took place between 1995 and 1997 at the North Middlesex Hospital, London, and between 1997 and 1999 at the Royal Free and University College Medical School, London. Essentially, each of the ECG recordings has one-minute duration and consists of synchronised maternal chest, maternal transabdominal, and fetal scalp electrode ECG signals. The subjects included 30 pregnant women during gestation and at full-term, 40 weeks gestation. The transabdominal signals were obtained with the

consent of women using a pair of electrodes, Sonicaid 8000, a Pentium II PC and an interface card. Ag-AgCl Beckman electrodes of 8 cm in diameter, and 25-cm spaced centres are positioned on the abdominal wall after careful preparation of the skin, which lowers the inter-electrode impedance of about 10 kΩ. The electrode pair is set over the umbilicus, and lined up with the median vertical axis of the uterus. The ground electrode is located on the woman's hip. An ECG monitor device (Sonicaid, Oxford Instruments) was used to record fetal scalp electrode, maternal chest and maternal transabdominal ECG signals. Data sets are sampled at 500 Hz. The ECG monitoring device has built-in filters to eliminate the baseline wander, high frequency components and 50 Hz noise in the signal.

1.9 Data Pre-processing

Data were analysed in this thesis without the need for any pre-processing. However, in some cases, as will be seen in Chapters Four, Five, and Six, a second- or third-order Volterra synthesiser was used to extract the linear part of the signal before applying higher-order statistics to that part only and ignore the quadratic and cubic parts of the signal.

1.10 Assessment and validation strategy

The following definitions are used throughout the thesis.

Definitions

1- The Sensitivity (Se) is defined as the ratio of the True Positives (TP) to the sum of the True Positives and the False Negatives (FN). The sensitivity reports the percentage of the true beats that are correctly classified by the algorithm.

2- The Specificity (Sp) is defined as the ratio of the True Positives (TP) to the sum of the True Positives (TP) and the False Positives (FP). It reports the percentage of classified heartbeats which are in reality true beats.

3- The classification rate: The mean value of the sensitivity and the specificity is used as the criterion for the effectiveness of the technique.

1.11 Outline of the thesis

The first few sections of Chapter Two are devoted to definitions and properties of

cumulants and cumulant spectra. This is followed by familiarisation with the unique structural properties of the third-order cumulants and typified examples of an adult male chest ECG, maternal chest ECG, transabdominally-measured ECG, as well as fetal ECG signal using scalp-electrode are presented. Section 2.9 shows results of calculating the third-order cumulants (TOC) and their diagonal and wall slices for fetal scalp electrode, maternal chest, and maternal transabdominal ECG signals, and segments of the latter. Section 2.9 also shows results of calculating the bispectra and their slices for the above mentioned signals. Section 2.10 shows examples of calculating the bicoherence squared for the aforementioned signals. Section 2.11 shows the effect of the proximity of the mother's QRS- and the fetal QRS-complexes on the non-stationarity of the signal. Section 2.12 depicts the bispectra and bicoherence squared of three types of noise in ECG signals. These types are, namely, the baseline wander, electromyographic (EMG), and motion artefact noise. A summary is given in Section 2.13.

Chapter three introduces the LMS- and the LMF-based quadratic and cubic Volterra synthesisers. Brief summaries of the standard LMS and LMF algorithms are given in Section 3.2. This is followed by description of the LMS- and LMF-based second- and third-order Volterra structures in section 3.3. Section 3.4.1 describes the model order selection criterion. Section 3.4.2 shows results of directly applying the LMS- and LMF-based adaptive algorithms to predict ECG signals, and assess the resultant mean-squared errors. Adaptive LMS-based second- and third-order Volterra structures are then applied to synthesise ECG signals in Section 3.4.3. The LMS- and LMF-based second- and third-order Volterra synthesisers are then applied to fetal scalp electrode, maternal chest, and maternal transabdominal ECG signals in Section 3.4.4. A summary is given in Section 3.5.

Chapter Four starts by discussing the following issues; (1) ECG cumulant database, (2) classification, (3) ECG segmentation and window minimum length, (4) window overlapping, (5) calculation of an averaged fetal heart rate within one maternal cardiac cycle, (6) the effect of using more than one slice and linearisation on the classification rate, and (7) shortcomings of the cumulant matching technique. Section 4.2 presents previous work on independent component analysis with its virtues and vices. Section 4.3 provides a brief description of the detection key operations of the TOC template matching technique. Section 4.4 briefly describes the equations for the TOC 1-d

diagonal and wall slices, examines the effect of reducing the length of segmentation on the variance of the third-order cumulants, the effect of reducing the length of segmentation on the variance, skewness, and kurtosis for white Gaussian noise, and the effect of linearisation on third-order cumulants. Typical examples of the TOCs and their diagonal and wall slices with and without linearisation are then shown, and the TOC variance is calculated. Section 4.5 describes the back-propagation with momentum algorithm. It then describes the optimisation of the parameters of the single-hidden-layer classifier. Results are shown for the maternal QRS-complex and fetal heartbeat classification rates for different TOC slices with and without linearisation employing second- and third-order Volterra synthesisers with LMF update. A summary and conclusions are given in Section 4.6.

Chapter Five is divided as follows. Section 5.2 references previous joint work on non-invasive fetal heartbeat detection using the bispectrum. Section 5.3 refers to the detection key operations. Section 5.4 caters for displaying the effect of linearisation in conjunction with a number of second-order statistics (SOS) spectral estimators, namely, (i) the FFT, (ii) the auto-regressive (AR), (iii) the Yule-Walker, and (iv) the maximum entropy (MEM). Section 5.5 presents preliminary investigations of ECG bispectrum, including typical examples of bispectra and their contours, followed by the estimation of the variance. Section 5.6 gives a detailed description of the second hybrid system which uses several bispectral contours as the discriminants in detecting the occurrences of fetal heartbeats within each maternal cardiac cycle. Section 5.6.1 shows the results of optimising the single-hidden-layer classifier. Section 5.6.3 shows the results of maternal QRS-complex and fetal heartbeat classification with and without linearisation, and employing both second- and third-order Volterra synthesisers with LMF update. Summary and conclusions are given in Section 5.7.

Chapter Six describes a third method for non-invasive fetal heartbeat detection using the sequentially optimised, weighted spectral MUSIC with the incorporation of the modified covariance matrix of the uterine activity during labour. Section 6.2 provides discussions of some relevant issues. These issues include the role of ECG linearisation and the issue of coincident mother and fetal QRS-complexes. Section 6.3 addresses some problems associated with mother and fetal spectral resolution in a labour environment, and the proposed solutions. Section 6.4 reviews some relevant previous studies that paved the

way for the development of the new technique. Section 6.5 presents a detailed statement of research. It describes a particular class of modified MUSIC, namely, *the sequentially optimised, weighted spectral MUSIC* algorithm, also involving a *reconfigured interference plus noise subspace* to incorporate *the modified covariance matrix of the uterine activity* in such a spectral estimator. For convenience, the mathematical formulation of the conventional MUSIC is presented in Section 6.6. Section 6.7 is devoted to the mathematical formulation of the new class of MUSIC, and deals with the incorporation of the modified covariance matrix of the linearised non-Gaussian uterine contraction interference signal (UCS) in the sequentially optimised, weighted MUSIC. Also, the concepts of oriented energy and signal-to-signal ratio, and the alternative projection method of Gram-Schmidt orthogonalisation are then briefly described. Results are detailed in Section 6.8. Summary and conclusions are given in Section 6.9. Chapter seven draws conclusions for the thesis.

1.12 References

[1] A. Cohen, *Biomedical Signal Processing*, Boca Raton Fla CRC, 1986.

[2] Friesen, G. M., Jannett, T. C., Jadallah, M. A., Yates, S. L., and Quint, S. R., "A comparison of the noise sensitivity of nine QRS detection algorithms," IEEE Transactions Biomedical Engineering, vol. BME-37, pp. 85-105, 1990.

[3] M. Sabry-Rizk, D. Romare, W. Zgallai, K. T. V. Grattan, P. Hardiman, and J. O'Riordan, "Higher order statistics (HOS) in signal processing: Are they of any use," IEE Colloquium, Digest #111, pp. 1/1-1/6, London, May 1995.

[4] A. G. Favret, "Computer matched filter location of fetal R-waves," Medical and Biological Engineering, vol. 6, pp. 467-475, 1968.

[5] J. M. Herbert, W. Peasgood, X. B. Huang, J. A. Crowe, M. S. Woolfson, N. Reed, and E. M. Symonds, "Antepartum Fetal Electrocardiogram Extraction and Analysis," Proceedings of Computers in Cardiology, pp. 875-877, 1993.

[6] P. P. Kanjilal, S. Palit, and G. Saha, "Fetal ECG Extraction from Single Channel Maternal ECG Using Singular Value Decomposition," IEEE Transactions on Biomedical Engineering, vol. 44, No. 1, pp. 51-59, January 1997.

[7] M Richter, T Schreiber, and D Kaplan, "Fetal ECG Extraction with Non-Linear State-Space Projections," IEEE Transactions on Biomedical Engineering, vol. 45, No. 1, pp. 133-137, January 1998.

[8] K. Greene and J. Westgate, "The ST waveform ," *in A Critical Appraisal of Fetal Surveillance* (H. P. Van Geijn and F. J. A. Copray, eds.), pp. 388-398, Amsterdam: Elseveir, 1994.

[9] H. M. L. Jenkins, E. M. Symonds, D. L. Kirk and P. R. Smith, "Can the fetal electrocardiogram improve the prediction of antepartum acidosis?," British Journal of Obstetrics and Gynaecology, vol. 93, pp. 6-12, 1986.

[10] S. Arulkumaran, M. Yang, I. Ingermarsson et. Al., "Augmentation of labour: does oxytocin titration to achieve pre-set active contraction area values produce better obstetric outcome?," Asia-Oceania Journal of Obstetrics and Gynaecology, vol. 15, pp. 333-337, 1989.

[11] J. W. Westgate, R. D. Keith, J. S. Curnow, et. Al., " Suitability of fetal scalp electrodes for monitoring the fetal electrocardiogram during labour," Clinical Physics and Physiological Measurements, vol. 11 (4), pp. 297-306, 1993.

[12] D. Rowlands, *Understanding The Electrocardiogram: Section 3: Rhythm Abnormalities*, Imperial Chemical Industries, 1987.

[13] W. J. Tompkins, *Biomedical Digital Signal Processing*, Prentice Hall, 1993.

[14] J. Hampton, *The ECG made easy*, Churchill Livingstone, Edinburgh, 1986.

[15] B. Widrow et al., " Adaptive Noise Cancellation: Principles and Applications," Proceedings of IEEE, Vol. 63, No. 12, pp. 1692-1716, December 1975.

[16] E. R. Ferrera, and B. Widrow, " Fetal Electrocardiogram Enhancement by Time-Sequenced Adaptive Filtering." IEEE Transactions on Biomedical Engineering, vol. BME-29, pp. 458-460, 1982.

[17] J. Gardosi, Bailliere's Clinical Obstetrics and Gynaecology, International Practice and Health, Intrapartum Surveillance, Vol. 10, No. 2, 1996.

[18] Q. Xue, Y. H. Hu, and W. J. Tompkins, " Neural network-based adaptive matched filtering for QRS detection," IEEE Transactions on Biomedical Engineering, Vol. BME-39, No. 4, pp. 317-328, April 1992.

[19] H. P. Van Geijn, "Developments in CTG analysis," in *Baillier's clinical obstetrics and gynaecology, international practice and research, intrapartum surveillance*, (J. Gardosi, ed.), vol. 10, No. 2, pp. 185-208, 1996.

[20] K. Rosen and R Luzietti, "The fetal electrocardiogram," Journal of Perinatal Medicine, vol. 22, pp. 501-512, 1994.

[21] C. Sureau, "Historical perspectives: forgotten past, unpredictable future," in *Baillier's clinical obstetrics and gynaecology, international practice and research,*

intrapartum surveillance, (J Gardosi, ed.), vol. 10, No. 2, pp. 167-184, 1996.

[22] S. Arulkumaran, U. Nicotini and N. M. Fisk, "Direct antenatal fetal electrocardiographic waveform analysis," British Journal of Obstetrics And Gynaecology, Vol. 98, pp. 829-831, 1991.

[23] J. Vanderschoot, D. Callaerts, W. Sansen, J. Vandewalle, G. Vantrappeen and J. Janssens, "Two methods for optimal MECG elimination and FECG detection from skin electrode signals," IEEE Transactions on Biomedical Engineering, Vol. 34, No. 3, pp. 233-240, March 1987.

[24] Y. Li, J. Razavilar and K. J. Ray Liu, "A high-resolution techniques for multi-dimensional NMR spectroscopy," IEEE Transactions on Biomedical Engineering, vol. 45, No. 1, pp. 78-86, January 1998.

[25] Y. H. Hu, S. Palreddy and W. J. Tompkins, "A patient-adaptable ECG beat classifier using a mixture of experts approach," IEEE Transactions on Biomedical Engineering, vol. 44, No. 9, pp. 891-899, September 1997.

[26] M. C. Carter, P. Gunn and R. W. Beard, "Fetal heart rate monitoring using the abdominal fetal electrocardiogram," British Journal of Obstetrics and Gynaecology, vol. 87, pp. 396-401, 1980.

[27] J. A. Crowe, J. M. Herbert, X. B. Huang et al., "Sequential recording of the abdominal fetal electrocardiogram and magnetogram, Physiological Measurements, vol. 16, pp. 43-47, 1995.

[28] T. F. Oostendorp, A. Van Oosteorm and H. W. Jongsma, "The effect of changes in the conducting medium on the fetal ECG throughout gestation," Clinical Physics and Physiological Measurements, vol. 10 (Supplement B), pp. 11-20, 1989.

[29] T. F. Oostendorp, A. Van Oosteorm and H. W. Jongsma, "The fetal ECG throughout the second half of gestation," Clinical Physics and Physiological Measurements, vol. 10 (2), pp. 147-160, 1989.

[30] Quinn, A. Weir, U. Shahani et al., "Antenatal magnetography: A new method for fetal surveillance?," British Journal of Obstetrics and Gynaecology, Vol. 101, pp. 866-870, 1994.

[31] J. Gondry, C. Marque, J. Duchene, D. Cabrol, "Uterine EMG processing during pregnancy: preliminary report," Biomedical Instrum Technology, vol. 27, pp. 318-24, 1993.

[32] C. M. Steer, G. J. Hertsch, "Electrical activity of the human uterus in labour- the electrohysterograph," American Journal of Obstetrics and Gynecology, Vol. 59, pp.

25-40, 1950.

[33] S. Skrablin, T. Canic, I. Kuvaic, R. Gobac, D. Hodzic, "Uterine electromyography in pregnancies with symptoms of preterm labour," Jugosl Ginekol Perinatol, Vol. 31 pp. 6-11, 1980.

[34] L. V. Dill, R. M. Maiden, "The electrical potentials of the human uterus in labour," American Journal of Obstetrics and Gynecology, vol. 52, pp. 735-745, 1946.

[35] E. J. G. Hon, C. D. Davis, "Cutaneous and uterine electrical potentials in labour-an experiment," Obstetrics and Gynaecology, Vol. 12, pp. 47-53, 1958.

[36] G. M. J. A. Wolfs, H. Rottinghuis, "Electrical and mechanical activity in the human uterus during labour," Arch Gynakol, Vol. 208, pp. 373-85, 1970.

[37] C. Marque, J. Duchene, S. Leclercq, G. Panczer, J. chaumaont, "Uterine EHG processing for obstetrical monitoring," IEEE Transactions on Biomedical Engineering,, Vol. 33, pp. 1182-1187, 1986.

[38] C. Marque, J. Duchene, "Human abdominal EHG processing for uterine contraction monitoring," in: Applied Biosensors (D. L. Wise, ed.). Stoneham. Butterworth pp. 187-226, 1989.

[39] E. Levy-Solal, P. Morin, F. Zacouto, "Analyse obstetricale des potentiels d'action de 1' uterus en travail," (electro-uterographie) Presse Med, Vol. 60, pp. 1335-1338, 1952.

[40] C. M. Steer, "The electrical activity of the human uterus in normal and abnormal labour," American Journal of Obstetrics and Gynecology, Vol. 68, pp. 867-890, 1954.

[41] J. G. Planes, R. Favretto, H. Grangjean, J-P. Morucci, "External recording and processing of fast electrical activity of the uterus in human parturition," Medicine and Biology in Engineering Computation, vol. 22, pp. 585-591, 1984.

[42] N. Val, B. Dubuisson, F. Goubel, "Aide du diagnostic de l'accouchement par l'electromyogramme abdominal: selection de caracteres," Reconaisseance des Formes et Intelligence Artificielle, Vol. 3, pp. 42-48, 1979.

[43] R. Caldeyro-Barcia, J. J. Poseiro, "Physiology of the uterine contraction," Clinical Obstetrics and Gynaecology, vol. 3, pp. 386-408, 1960.

[44] J. Mizrahi, Z. Karni, W. Z. Polishuk, "Strain uterography in labour," British Journal of Obstetrics and Gynaecology, vol. 84, pp. 930-936, 1977.

[45] H. Kantz, T. Schreiber, "Human ECG: nonlinear determinism versus stochastic aspects," IEE Proceedings- Science, Measurement and Technology, vol. 145, pp.

279-284, November 1998.

[46] E. Ciccinelli, A. Bortone, I. Carbonara et al, "Improved equipment for abdominal fetal electrocardiogram recording: description and clinical evaluation," International Journal of Biomedical Computing, vol. 35, No. 3, pp. 193-205, 1994.

[47] S. W. Nam and E. J. Powers, "Application of Higher Order Spectral Analysis to Cubically Non-Linear System Identification," IEEE Transaction on Signal Processing, vol. 42, No. 7, pp. 1746-1765, July 1994.

[48] W. Zgallai, M. Sabry-Rizk, P. Hardiman, and J. O'Riordan, "MUSIC-based bispectrum detector: A novel non-invasive detection method for overlapping fetal and mother ECG," Proceedings of the 19th IEEE International Conference on Engineering in Medicine and Biology, EMB, pp. 72-75, USA, October 1997.

[49] M. Sabry-Rizk, W. Zgallai, P. Hardiman, and J. O'Riordan," Third-order cumulant signature matching technique for non-invasive fetal heart beat identification," IEEE International Conference on Acoustics, Speech, and Signal Processing (ICASSP), vol. 5, pp 3781-3784, Germany, 1997.

[50] MIT/BIH Database: ECG Database Applications Guide, 10th Edition, 1997. Harvard-MIT Division of Health Sciences and Technology, MIT Room 20A-113, Cambridge, MA 02139, USA.

[51] MIT/BIH Database: ECG Database Programmer's Guide, 9th Edition, 1997. Harvard-MIT Division of Health Sciences and Technology, MIT Room 20A-113, Cambridge, MA 02139, USA.

[52] P. Bergveld, and W J H Meijier, "A New Technique for the Suppression of MECG," IEEE Transactions on Biomedical Engineering, vol. 28, pp. 348-354, 1981.

[53] W. J. Tompkins and J. G. Webster (eds.), *Design of Microcomputer-based Medical Instrumentation*. Prentice Hall, Englewood Cliffs, NJ, 1981.

[54] P. S. Hamilton and W. J. Tompkins, "Adaptive Matched Filtering for QRS Detection," in Proceedings of the 10th IEEE International Conference of Engineering in Medicine and Biology Society (EMB), pp. 145-146, 1988.

[55] S. E. Dobbs, N. M. Schmit, and H. S. Ozemek, "QRS Detection by Template Matching Using Real Time Correlation on a Microcomputer," Journal of Clinical Engineering, vol. 9, pp. 197-212, 1984.

[56] D. Callaerts, J. Vanderschat, J. Vandewalle, and W. Sanson, "An Adaptive On-Line method For the Extraction of the Complex Fetal Electrocardiogram From

Cutaneous Multilead Recordings," Journal of Perinatal Medicine, vol. 14, pp. 421-433, 1986.

[57] B. C. Lipman And T. Cascio, *ECG Assessment and Interpretation*, F. A. Davis company, Philadelphia, 1994.

[58] S. Haykin, *Adaptive Filter Theory*, Prentice Hall, 1991.

[59] N. V. Thakor and Y. S. Zhu, "Applications of adaptive filtering to ECG analysis: Noise cancellation and arrhythmia detection," IEEE transactions on Biomedical Engineering, vol. BME-38, No. 8, pp. 785-793, August 1991.

[60] M. Yelderman and B. Widrow et al., " ECG Enhancement by Adaptive Cancellation of Electrosurgical Interference," IEEE Transactions on Biomedical Engineering, vol. 30, pp. 392-398, 1983.

[61] R. A. DuFault and A. C. Wilcox, " Dual Channel P-wave Detection in the Surface ECG via the LMS Algorithm," in Proceedings of the 8th IEEE Annual Conference of Engineering in Medicine and Biology Society, pp. 325-328, 1986.

[62] A. Sahakian and K. H. Kuo, " Cancelling Cardiogenic Artifact in Impedance Pneumographic," in Proceedings of the 7th IEEE Annual Conference of Engineering in Medicine and Biology Society, pp. 855-859, 1985.

[63] Y. Zhu and N. V. Thakor, " P-Wave Detection by Adaptive Cancellation of QRS-T Complex," in Proceedings of the 8th IEEE Annual Conference of Engineering in Medicine and Biology Society, pp. 329-331, 1986.

[64] P. O. Borjesson et al, "Adaptive QRS Detection Based on Maximum a Posteriori Estimation," IEEE Trans. on Biomedical Engineering, vol. 29, pp. 341-351, 1982.

[65] J. Pan and W. J. Tompkins, "A Real-Time QRS Detection Algorithm," IEEE Transactions on Biomedical Engineering, vol. BME-32, pp. 230-236, 1985.

[66] P. S. Hamilton and W. J. Tompkins, "Quantitative Investigation on QRS Detection Rules Using MIT/BIH Arrhythmia Databases," IEEE Transactions on Biomedical Engineering, vol. BME-33, pp. 1157-1165, 1986.

[67] M.L. Ahlstrom and W.J. Tompkins, "Automated high-speed analysis of holter tapes with microcomputers," IEEE Trans. Biomed. Eng., vol. 30, pp. 651-657, Oct. 1983.

[68] R.A. Balda, Trends in Computer-Processed Electrocardiograms. Amsterdam: North Holland, 1977, pp. 197-205.

[69] J. Fraden and M.R. Neumann, "QRS wave detection," Med. Bioi. Eng. Comput., vol. 18, pp. 125-132,1980.

[70] D. Gustafson, "Automated VCG interpretation studies using signal analysis techniques," R-I044 Charles Stark Draper Lab., Cambridge, MA,1977.

[71] A. Ligtenberg and M. Kunt, " A robust-digital QRS-detection algorithm for arrhythmia monitoring," Comput, Biomed.Res., vol. 16, pp. 273-286, 1983.

[72] B., Cellar, Y.C.C. Grace, and C. Phillips, "ECG analysis and processing using wavelets and other methods," Biomed. Eng. Appl. Basis Commun., vol. 9, no. 2, pp. 81-90,1997.

[73] Y.H. Hu, W.J. Tompkins, J.L. Urrusti, and V.X. Afonso, "Applications of artificial neural networks for ECG signal detection and classification," J. Electrocardiology, vol. 26 (Suppl.), pp. 66-73,1993.

[74] M.G. Strintzis, G. Stalidis, X. Magnisalis, and N. Maglaveras, "Use of neural networks for electrocardiogram (ECG) feature extraction, recognition and classification," Neural Netw. World, vol. 3, no. 4, pp. 313-327,1992.

[75] A. Kyrkos, E. Giakoumakis, and G. Carayannis, "Time recursive prediction techniques on QRS detection problem," in Proc. 9th, Annu. Conf. IEEE Engineering in Medicine and Biology Society, 13-16 Nov., Boston, MA, pp. 1885-1886, 1987.

[76] D.A. Coast, R.M. Stem, G.G. Cano, and S.A. Briller, "An approach to cardiac arrhythmia analysis using hidden Markov models," IEEE Trans. Biomed. Eng., vol. 37, pp. 826-836, 1990.

[77] P.E. Trahanias," An approach to QRS complex detection using mathematical morphology," IEEE Trans. Biomed. Eng., vol. 40, no. 2, pp. 201-205,1993.

[78] A. Ruha, S. Sallinen, and S. Nissila, "A real-time microprocessor QRS detector system with a 1-ms timing accuracy for the measurement. Of ambulatory HRV," IEEE Trans. Biomed. Eng., vol. 44, pp. 159-167, 1997.

[79] R. Poli, S. Cagnoni, and G. Valli, "Genetic design of optimum linear and nonlinear QRS detectors," IEEE Trans. Biomed. Eng., vol. 42, pp. 1137-1141, 1995.

[80] S.-K. Zhou, J.-T. Wang, and J.-R. Xu, "The real-time detection of QRS-complex using the envelop of ECG," in Proc. 10th Annu. Int. Conf., IEEE Engineering in Medicine and Biology Society, New Orleans, LA, 1988, p. 38.

[81] F. Gritzali, "Towards a generalized scheme for QRS detection in ECG waveforms," Signal Processing, vol. 15, pp. 183-192, 1988.

[82] G. Belforte, R. De Mori, and F. Ferraris, "A contribution to the automatic

processing of electrocardiograms using syntactic methods," IEEE Trans. Biomed. Eng., vol. 26, pp. 125-136, Mar. 1979.

[83] M. Sabry-Rizk, W. Zgallai, E. R. Carson A. MacLean, K. T. V. Grattan, "Multi-fractility in Fetal Heart Beat Dynamics," 2nd European Medical & Biological Engineering Conference Vienna (Austria), December 04-08, 2002.

[84] G. S. Dawes, C. R. Houghton, C. W. Redman, G. H. Visser, "Pattern of the normal human fetal heart rate," British Journal of Obstetrics and Gynaecology, Vol. 89, pp. 276-284, 1982.

[85] M. Sabry-Rizk, W. Zgallai, "Novel robust modified pseudo-spectral MUSIC algorithm for on-line QRS detection in electrocardiogram signals", to be published.

[86] G. S. Dowes, M. Moulden, C. W. Redman, "Improvements in computerized fetal heart rate analysis," Antepartum Journal Perinatal Medicine, Vol. 24, pp. 25-36, 1996.

[87] T. Menendez, S. Achenbach, W. Moshage, M. Flug, E. Beinder, A. Kollert, A. Bittel, K. Bachmann, "Prenatale registrierung fetaler herzaktionen mit magnetokardiographie," Zeitschrift Kardiologie, Vol. 86, pp. 111-118, 1998.

[88] J. M. Bentley, P. M. Grant, J. T. E. McDonnel, "Time-frequency and time-scale techniques for the classification of native and bioprosthetic heart valve sounds," IEEE Transactions on Biomedical Engineering, Vol. 45, pp. 125-128, 1998.

[89] I. Cathers, "Neural network assisted auscultation," Artificial Intelligence in Medicine, Vol. 7, pp. 53-66, 1995.

[90] J. Ritola, S. Lukkarinen, "Comparison of time-frequency distributions in the heart sounds analysis," Medical and Biological Engineering and Computing, Vol. 34, pp. 89-90, 1996.

[91] A. J. Zuckerwar, R. A. Pertlow, J. W. Stoughton, D. A. Baker, "Development of a piezopolimer pressure sensor of the phonocardiogram board of the matching pursuit method," IEEE Transactions on Biomedical Engineering, Vol. 40, pp. 963-969, 1993.

[92] D. G. Talbert, W. L. Davies, F. Johnson, N. Abraham, N. Colley, D. P. Southall, "Wide bandwidth fetal phonocardiography using a sensor matched to the compliance of the mother's abdominal wall," IEEE Transactions on Biomedical Engineering, Vol. 33, pp. 124-130, 2000.

[93] E. Kovaes, M. Torok, I. Habermajer, "A rule-based phonocardiogrphic method for long-term fetal heart rate monitoring," IEEE Transactions on Biomedical

Engineering, Vol. 47, pp. 124-130, 2000.

[94] H. G. Murray, "The fetal electrocardiogram: current clinical developments in Nottingham," Journal of Prenatal Medicine, Vol. 14, pp. 399-404, 1986.

[95] H. G. Murray, "The intrapartum fetal electrocardiogram- a study of time intervals," in G. Genser, K. Marshall, N. Svenningsen and Lindstron (eds.) Fetal and neonatal physiological measurement III, Proceedings of the 3rd International Conference on Fetal and Neonatal Measurement, Sweden, pp. 133-148, 1989.

[96] H. G. Murray, "Evaluation of the fetal electrocardiogram (ECG), MD Thesis, University of Nottingham, 1992.

[97] C. Lin, H. Wu, T. Liu, N. Lee, T. Kou, S. Young, "A portable monitor for fetal heart rate and uterine contraction," IEEE EMBS Magazine, pp. 80-84, Nov./Dec., 1997.

[98] L. De Lathauwer, B. De Moor, and J. Vandewalle, "Fetal electrocardiogram extraction by blind source separation," IEEE Transactions on Biomedical Engineering, Vol. 47, No. 5, pp. 567- 572, May 2000.

[99] M Sabry-Rizk, W. Zgallai, A. McLean, E. R. Carson, and K. T. V. Grattan, "Virtues and Vices of Source Separation Using Linear Independent Component Analysis for Blind Source Separation of Non-linearly Coupled and Synchronised Fetal and Mother ECGs," IEEE Engineering in Medicine and Biology Conference, USA, 2001.

[100] A. Khamene, S. Negahadariapour, "A new method for the extraction of fetal ECG from the composite abdominal signal," IEEE Transactions on Biomedical Engineering, Vol. 47, No. , pp. 507 – 51, April 2002.

[101] Sabry-Rizk, M. Transabdominal foetal mother ECG signals deinterleaver using a neural network. NNESMED '96, 2nd International conference on Neural Networks and Expert Systems in Medicine and Healthcare, Plymouth, UK,1996.

[102] J. A. Van Alste and T. S. Schilder, "Removal of baseline wander and power-line interference from the ECG by an efficient FIR filter with a reduced number of taps," IEEE Transactions on Biomedical Engineering, vol. 32, pp. 1052-1062, 1985.

[103] G. S. Furno and W. J. Tompkins, "A learning filter for removing noise interference," IEEE Transactions on Biomedical Engineering, vol. 30, pp. 234-235, 1983.

[104] A. V. Sahakian and G. S. Furno, "An adaptive filter for distorted line-interference

noise," Biomedical Science Instrumentation, vol. 19, pp. 47-52, 1983.

[105] J. Slocum, A. Sahakian, and S. Swiryn, "Computer detection of atroventricular dissociation from surface electrocardiograms during wide QRS complex tachycardias," Circulation, vol. 72, pp. 1028-1036, 1985.

[106] J. C. huhta and J. G. Webster, "60 Hz interference in electrocardiography," IEEE Transactions on Biomedical Engineering, vol. 20, pp. 91-101, 1973.

[107] N. V. Thakor, J. G. Webster, and W. J. Tompkins, "Estimation of QRS complex power spectra for design of QRS filters," IEEE Transactions on Biomedical Engineering, vol. 31, pp. 702-706, 1984.

[108] R. L. Longini, T. A. Reichert, J. M. Yu, and J. S. Crowley, Near orthogonal basis functions: A real time fetal ECG technique," IEEE Transactions on Biomedical Engineering, Vol. 24, pp. 39-43, 1977.

[109] J. H. Van Bemmel, "Detection of weak electrocardiograms by autocorrelation and cross correlation envelopes," IEEE Transactions on Biomedical Engineering, Vol. 15, pp. 17-23, 1968.

[110] A. Van Oosterom, "Spatial filtering of the fetal electrocardiogram," Journal of Perinatal Medicine, vol. 14, pp. 411-419, 1986.

[111] D. Callaerts, B. De Moor, J. Vandewalle, and W. Sansen, "Comparison of SVD methods to extract the foetal electrocardiogram from cutaneous electrode signals," Med. Biological Eng. And Computing, Vol. 28, pp. 217-224, 1990.

[112] R. Pallas-areny, J. Colominus-balague, and F. J. Rosell, "The effect of respiration-induced heart movements on the ECG," IEEE Transactions on Biomedical Engineering, Vol. 6, pp. 585-590, 1989.

[113] M. Sabry-Rizk, W. Zgallai, A. MacLean, and E. R. Carson, "Multi-fractility in labour contraction dynamics," The 2nd Joint Conference of the IEEE Engineering in Medicine and Biology Society and the Biomedical Engineering Society,23-26 October 2002, Houston, Texas, USA.

[114] V. Zarazoso, A. K. Nandi, and E. Bacharkis, "Maternal and foetal separation using blind source separation methods," IMA Journal of Mathematics Applied in Medicine and Biology, vol. 14, pp. 207-225, Oxford University Press, 1997.

[115] V. Zarazoso and A. K. Nandi, "Comparison between blind separation and adaptive noise cancellation techniques for fetal electrocardiogram extraction," IEE Colloquium, pp. 1/ -1/6., 1999.

[116] P. Comon, "Independent component analysis, A new concept?", Signal

Processing, Vol. 21, pp. 287-314, 1994.

[117] I. J. Clarke, "Direct exploitation of non-Gaussianity as a discriminent", Proc. EUSIPCO IX, pp. 2057-60, 1998.

[118] J G McWhirter, and I. J. Clarke, "Higher order statistics, blind signal separation and multilinear algebra," IEE Collocium, IEE, London, pp. 4/1-4/3, 1999.

[119] M. Sabry-Rizk, W. Zgallai E. R. Carson, K. T. V. Grattan, P. Hardiman, P. Thompson and A. Maclean, "Modified MUSIC Pseudospectral Analysis Reveals Common Uterus and Fetal Heart Resonances During Labour Contractions", the 22nd Annual International Conference of the IEEE Engineering in Medicine and Biology Society, EMB2000, USA, 23-28/7/2000.

[120] M. Sabry-Rizk, W. Zgallai, A. MacLean, K. T. V. Grattan, E. R. Carson, "The Application of a Novel Class of Embedded Dynamic Cubic Volterra to Long-Term Prediction of Chaotic and Multi-Fractal Electromyographic Signals During Labour," the 4th International Conference on Neural Networks and Expert Systems in Medicine and Healthcare, Greece, June 2001.

[121] M. Sabry-Rizk, W. Zgallai, E. R. Carson, K. T. V.Grattan, A. MacLean, and P. Hardiman, "Non-linear dynamic tools for characterising abdominal electromyographic signals before and during labour," Transactions of the Institute of Measurement and Control, Vol. 22, pp. 243-270, 2000.

[122] M. Sabry-Rizk, W. Zgallai, "Novel Volterra Predictor Based on State-Space Equilibrium of Nonlinear Single- or Multi-Fractal Signals", Proceedings of the SPIE's 45th Annual Meeting, the International symposium on Optical Science and Technology, SPIE2000, Advanced Signal Processing Algorithms, Architectures, and Implementations X, USA, Vol. 4116, pp. 322-333, 30/7-4/8/2000.

[123] M. Sabry-Rizk, W. Zgallai, C. Morgan, S. El-Khafif E. R. Carson, and K. T. V. Grattan, "Novel decision strategy for P-wave detection utilising nonlinearly synthesised ECG components and their enhanced pseudospectral resonances," IEE Proceedings Science, Measurement and Technology, Special section on Medical Signal Processing, vol. 147, No. 6, pp. 389-397, November 2000.

[124] M. Sabry-Rizk, W. Zgallai, E. R. Carson, S. El-Khafif, C. Morgan, and K. T. V. Grattan, "Novel decision strategy for P wave detection utilising non-linearly synthesised ECG components and their enhanced pseudospectral resonances", IASTED-SIP 2001, Honolulu, Hawaii, USA, August 2001.

[125] M. Sabry-Rizk, W. Zgallai, E. R. Carson, S. El-Khafif, C. Morgan, and K. T. V. Grattan, "Novel decision strategy for P wave detection utilising non-linearly synthesised ECG components and their enhanced pseudospectral resonances", IEE International conference, MEDSIP2000, Bristol, UK, September 2000.

[126] A. Van Oosterom and J Alsters, "Removing the maternal component in the fetal ECG using singular value decomposition," In Electrocardiography '83. I. Ruttkay-Nedecky and P. MacFarlane, Eds., Exceptra Medicine, Amesterdam, The Netherlands, pp. 171-176, 1984.

[127] D. Callaerts, J. Vanderschoot, J. Vandewalle, W. Vantrappen, and J. Janssens, "An adaptive on-line method for the extraction of the complete fetal electrocardiogram from cutaneous multilead recordings," J. Perinat. Med., Vol. 14, No. 6, pp. 421-433, 1986.

[128] D. Callaerts, J. Vanderschoot, J. Vandewalle, and W. Sansen, "An on-line adaptive algorithm for signal processing using SVD," In Signal Processing III, Elsevier Science/ North Holland/, Amesterdam, The Netherlands, EURASIP 86, The Hague, pp. 953-956, 1986.

CHAPTER TWO

HIGHER-ORDER STATISTICS: APPLICATION TO ECG SIGNALS

2.1 Introduction

2.1.1 Motivations behind using higher-order statistics in processing ECG signals

Essentially, adequate knowledge of the higher-order statistics (HOS) of both the mother's and fetal ECG signals must first be acquired in order to pave the way for fetal QRS-complex identification and detection. There are several motivations behind using higher-order statistics in processing ECG signals. These motivations will be discussed further in the context of the material presented in the next few chapters:

(i) ECG signals are predominantly non-Gaussian [46], [50], and exhibit quadratic and higher-order non-linearities supported by third- and fourth-order statistics, respectively. It is worth mentioning that, in general, the third-order cumulants can support any of the following; (a) linear non-Gaussian signal, (b) non-linear signal, and (c) both (a) and (b).

(ii) The mother's and fetal QRS-complex bispectral contours do not overlap with that of the baseline wander and that of the EMG above –20 dB normalised to the peak of the maternal QRS-complex bispectrum (as will be seen in Section 2.12). So it is comparatively easy to detect and classify either using the bispectral contour template matching technique (BIC template matching).

(iii) In the higher-order statistics domain (higher than the second-order domain), Gaussian noise diminishes in the HOS domains if the data length is adequate [3-4]. This implies that it is possible, under certain conditions, to process the ECG signal in Gaussian noise-free domains. We have found ([46, 50], also see sections 4.4.3 and 4.4.4) that for ECG signals a minimum length of 1 sec is adequately long to suppress Gaussian noise in the higher-order statistical domains, whilst not long

enough to violate Hinich's criterion of "local" stationarity [59]. Hinich tests for Gaussianity and linearity are performed on ECG signals in Appendix A4. In general, ECG signals are non-stationary in the statistical sense, but relatively short data can be successfully treated with conventional signal processing tools primarily designed for stationary signals. For example, when dealing with individual cardiac cycles, non-stationarity is not an issue but when one takes on board the heart rate time series which is chaotic and multi-dimensional then it is not wise to assume stationarity for analysis purposes [56-57].

(iv) In the third-order domain all sources of noise with symmetric probability density functions (pdfs), e.g., Gaussian and uniform, will vanish. The ECG signals are retained because they have non-symmetric distributions [58].

(v) Our previously published results show that all ECG signals do contain measurable quantities of quadratic and, to a lesser extent, cubic non-linearities [47, 57, 60]. Such measurable quantities of non-linearity if not synthesised and removed before any further processing for the purpose of signal identification and classification could lead to poor performance with regard to fetal QRS-complex detection rates.

In this thesis, the adaptive third-order Volterra structure shown in Figure 2.1 (a) has been used to synthesise the linear, quadratic, and cubic components of ECG signals. The conventional frequency domain Volterra model of a cubically non-linear system modelling with a non-Gaussian input shown in Figure 2.1 (b) and used by Nam and Powers [4] has not been used in this thesis.

It will be shown in Chapters Four and Five that the removal of non-linearities in the transabdominal ECG signal yields an increase in the fetal heartbeat detection rates by up to 7% in the third-order cumulant matching technique (Chapter Four), and 3% in the bispectral contour template matching technique (Chapter Five).

2.1.2 Layout of the rest of the Chapter

The first few sections of this chapter are devoted to definitions and properties of cumulants and cumulant spectra. This is followed by familiarisation with the unique structural properties of the third-order cumulants of an adult male's chest ECG, maternal chest ECG, transabdominally-measured ECG, as well as fetal ECG signal

using scalp-electrode. The non-linearity and non-stationarity of ECG signals are investigated in Sections 2.10 and 2.11 using the bispectrum and bicoherence squared, respectively.

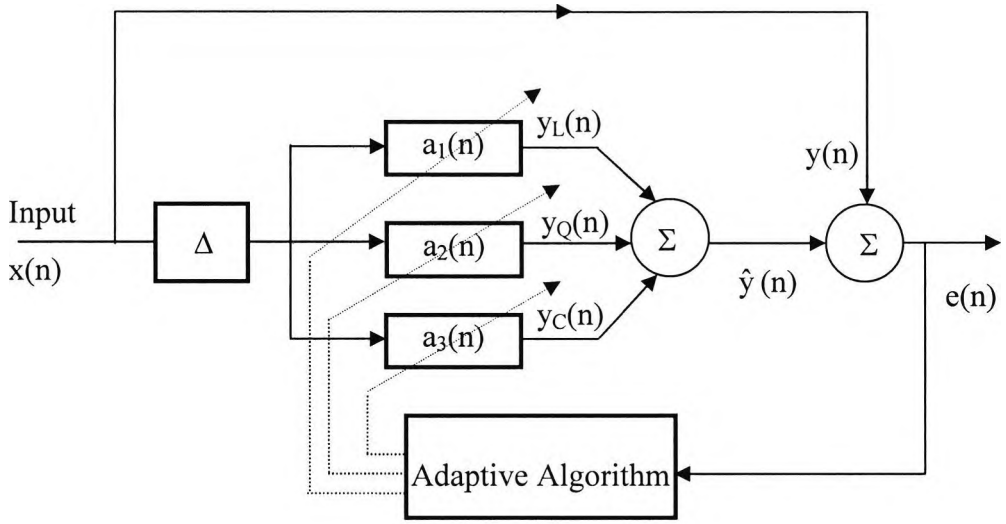

(a)

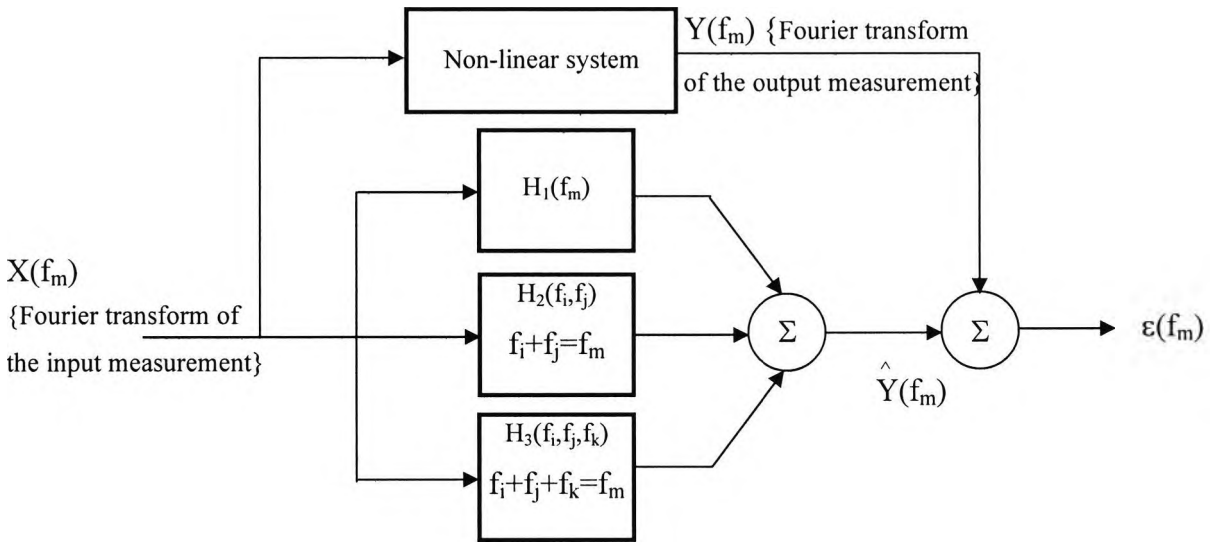

(b)

Figure 2.1: *(a) An adaptive third-order Volterra structure. (b) Frequency domain Volterra model of a cubically non-linear system.* $Y(\lambda)$ *is defined by the equation;*

$$Y(\lambda) = H_1(\lambda)X(\lambda) + \sum_{\omega 1}\sum_{\omega 2} H_2(\omega_1,\omega_2)X(\omega_1)X(\omega_2)$$

$$+ \sum_{\omega 1}\sum_{\omega 2}\sum_{\omega 3} H_3(\omega_1,\omega_2,\omega_3)X(\omega_1)X(\omega_2)X(\omega_3)$$

For noise identification and characterisation in the third-order statistical domain, good use is made of all the recorded normal ECG signals contained in the MIT/BIH NSR and

AR databases; user guide and manual are found in references [51] and [52], and a brief description of a number of individual records is given in Appendix A5. The third-order cumulants, bispectra, and bicoherence squared of some noise components, namely, the baseline wander, electromyographic (EMG), and motion artefact noise isolated from the MIT/BIH NSR and AR database are analysed in Section 2.12. By knowing the statistics of these noise components, this serves to facilitate the detection of ECG signals against a cocktail of background noise in either the cumulant or the bispectrum domain. As will be seen in Chapter Five, higher detection rates of fetal QRS-complex can be easily achieved in the enhanced fetal QRS-complex bispectrum domain against both maternal and motion artefact bispectral contribution. It is important to mention that bispectral enhancement has been carried out after removing the baseline wander, and in difficult cases, after linearisation (removing the non-linearity from the noise contaminated maternal transabdominal signal). Conclusions are given in Section 2.13.

2.2 Cumulants

Given a set of n real variables $\{x_1, x_2, \ldots, x_n\}$, their joint moments of order $r = k_1 + k_2 + \ldots + k_n$ are given by [1]:

$$\text{Mom}\,[x_1^{k1}, x_2^{k2}, \ldots, x_n^{kn}] \stackrel{\nabla}{=} E\{x_1^{k1}, x_2^{k2}, \ldots, x_n^{kn}\} = (-j)^r \left. \frac{\partial^r \phi(\omega_1, \omega_2, \ldots, \omega_n)}{\partial\omega_1^{k1}\,\partial\omega_2^{k2} \ldots \partial\omega_n^{kn}} \right|_{\omega_1=\omega_2=\ldots=\omega_n=0}, \quad (2.1)$$

where $\phi(\omega_1, \omega_2, \ldots, \omega_n) \stackrel{\nabla}{=} E\{e^{j(\omega_1 x_1, \omega_2 x_2, \ldots, \omega_n x_n)}\}$ is their joint characteristic function. $E\{.\}$ denotes the expectation operator. Another form of the joint characteristic function is defined as the natural logarithm of $\phi(\omega_1, \omega_2, \ldots, \omega_n)$, i.e.,

$$\tilde{\Psi}(\omega_1, \omega_2, \ldots, \omega) \stackrel{\nabla}{=} \ln[\phi(\omega_1, \omega_2, \ldots, \omega)]. \quad (2.2)$$

For Gaussian processes, the logarithm of the characteristic function is a polynomial of degree two. Hence, all cumulants of order three and higher will be identically zero. The joint cumulants of order r of the same set of random variables, are defined as the

coefficients in the Taylor expansion of the second characteristic function about zero, i.e.,

$$\text{Cum}[x_1^{k1}, x_2^{k2}, .., x_n^{kn}] \overset{\nabla}{=} E\{x_1^{k1}, x_2^{k2}, .., x_n^{kn}\} = (-j)^r \left. \frac{\partial^r \tilde{\Psi}(\omega_1, \omega_2, .., \omega_n)}{\partial \omega_1^{k1} \partial \omega_2^{k2} .. \partial \omega_n^{kn}} \right|_{\omega_1 = \omega_2 = .. = \omega_n = 0} . \quad (2.3)$$

Thus, the joint cumulant can be expressed in terms of the joint moments of a set of random variables. For example, the moments of the random variable $\{x_1\}$ are defined as:

$$m_1 = \text{Mom}[x_1] = E\{x_1\}. \quad (2.4)$$

$$m_2 = \text{Mom}[x_1, x_1] = E\{x_1^2\}. \quad (2.5)$$

$$m_3 = \text{Mom}[x_1, x_1, x_1] = E[x_1^3]. \quad (2.6)$$

They are related to its cumulants by

$$c_1 = \text{Cum}[x_1] = m_1. \quad (2.7)$$

$$c_2 = \text{Cum}[x_1, x_1] = m_2 - m_1^2. \quad (2.8)$$

$$c_3 = \text{Cum}[x_1, x_1, x_1] = m_3 - 3\, m_2\, m_1 + 2\, m_1^3. \quad (2.9)$$

For three random variables x_1, x_2, and x_3 the third-order cumulants are defined as [1]:

$$\text{Cum}[x_1, x_2, x_3] = E\{x_1 x_2 x_3\} - E\{x_1\}.\, E\{x_2 x_3\} - E\{x_2\}.\, E\{x_1 x_3\} - E\{x_3\}.\, E\{x_1 x_2\} + 2\, E\{x_1\}.\, E\{x_2\}.\, E\{x_3\}, \quad (2.10)$$

Or defined in terms of three lags of a variable x,

$$\overset{x}{c}_3(\tau_1, \tau_2) = \overset{x}{m}_3(\tau_1, \tau_2) - \overset{x}{m}_1 [\overset{x}{m}_2(\tau_1) + \overset{x}{m}_2(\tau_2) + \overset{x}{m}_2(\tau_2 - \tau_1)] + 2 \cdot (\overset{x}{m}_1)^3 \quad (2.11)$$

If the set of random variables is jointly Gaussian, then all the information about their distribution is contained in the moments of order $n \leq 2$. Therefore, all the moments of order greater than two ($n > 2$) have no new information to provide. This leads to the fact that all joint cumulants of order $n > 2$ are identically zero for Gaussian random variables. Hence, the cumulants of order greater than two, in some sense, measure the non-Gaussian nature of a time series. The third-order cumulant has six symmetry regions,

$$c_3^x(\tau_1,\tau_2) = c_3^x(\tau_2,\tau_1) = c_3^x(-\tau_2,\tau_1-\tau_2) = c_3^x(\tau_2-\tau_1,-\tau_1) = c_3^x(\tau_1-\tau_2,-\tau_2) = c_3^x(-\tau_1,\tau_2-\tau_1) \quad (2.12)$$

2.3 Properties of cumulants

1. Cum $[a_1x_1, a_2x_2, \ldots, a_nx_n] = a_1a_2 \ldots a_n$ Cum $[x_1, x_2, \ldots, x_n]$.
2. Cumulants are symmetric functions in their arguments, e.g., $\text{Cum}[x_1,x_2,x_3] = \text{Cum}[x_2,x_1,x_3] = \text{Cum}[x_3,x_2,x_1]$, and so on.
3. If the random variables $\{x_1, x_2, \ldots, x_n\}$ can be divided into any two or more groups which are statistically independent, their nth-order cumulant is identical to zero; i.e., $\text{Cum}[x_1, x_2, \ldots, x_n] = 0$, whereas in general $\text{Mom}[x_1, x_2, \ldots, x_n] \neq 0$.
4. If the sets of random variables $\{x_1, x_2, \ldots, x_n\}$ and $\{y_1, y_2, \ldots, y_n\}$ are independent, then

$$\text{Cum}[x_1+y_1, x_2+y_2, \ldots, x_n+y_n] = \text{Cum}[x_1, x_2, \ldots, x_n] + \text{Cum}[y_1, y_2, \ldots, y_n], \quad (2.13)$$

whereas in general

$$\text{Mom}[x_1+y_1, x_2+y_2, \ldots, x_n+y_n] \neq \text{Mom}[x_1, x_2, \ldots, x_n] + \text{Mom}[y_1, y_2, \ldots, y_n]. \quad (2.14)$$

5. If the set of random variables $\{x_1, x_2, \ldots, x_n\}$ is jointly Gaussian, then all the information about their distribution is contained in the cumulants of order $n \leq 2$. Therefore, all cumulants of order greater than two ($n > 2$) have no new information to provide. This leads to the fact that all joint cumulants of order $n > 2$ are identical to zero for Gaussian random vectors. Hence, the cumulants of order greater than two, in some sense, measure the non-Gaussian nature of a time series.

2.4 One-dimensional third-order cumulant slices

Since higher-order cumulants and spectra are multi-dimensional functions, their computation may be impractical in some applications due to excessive crunching. This is caused by the large CPU time taken to calculate HOS functions, compared to SOS functions. It was suggested to use 1-d slices of multi-dimensional cumulants, and their 1-d Fourier transforms, as ways of extracting useful information from higher-order statistics of non-Gaussian stationary processes [9].

The third-order cumulants of a non-Gaussian process, {x(k)}, is given by [3]:

$$c_3^x(\tau_1,\tau_2) = \mathrm{Cum}\{x(k), x(k+\tau_1), x(k+\tau_2)\}. \tag{2.15}$$

One-dimensional slices of $c_3^x(\tau_1,\tau_2)$ can be defined as:

$$r_{2,1}^x(\tau) \triangleq \mathrm{Cum}\{x(k), x(k), x(k+\tau)\} = c_3^x(0,\tau), \text{ and} \tag{2.16}$$

$$r_{1,2}^x(\tau) \triangleq \mathrm{Cum}\{x(k), x(k+\tau), x(k+\tau)\} = c_3^x(\tau,\tau), \tag{2.17}$$

Define the following even and odd functions:

$$s_{2,1}^x(\tau) \triangleq \frac{1}{2}[r_{2,1}^x(\tau) + r_{1,2}^x(\tau)], \text{ and} \tag{2.18}$$

$$q_{2,1}^x(\tau) \triangleq \frac{1}{2}[r_{2,1}^x(\tau) - r_{1,2}^x(\tau)]. \tag{2.19}$$

A 1-d spectrum could be defined as:

$$R_{2,1}^x(\omega) = \sum_{\tau=-\infty}^{\infty} r_{2,1}^x(\tau) e^{-j\omega\tau} = \sum_{\tau=-\infty}^{\infty} \{s_{2,1}^x(\tau)\cdot\cos(\omega\tau) - jq_{2,1}^x(\tau)\cdot\sin(\omega\tau)\}. \tag{2.20}$$

2.5 Cumulant spectra

Higher order spectra[1] are defined as the multi-dimensional Fourier transforms of the higher order statistics[2] of the superimposed signals in the presence of noise [10-12]. The nth-order cumulant spectrum of a process {x(k)} is defined as the (n-1)-dimensional Fourier transform of the nth-order cumulant sequence. The nth-order cumulant spectrum is thus defined as [3]:

$$C_n^x(\omega_1,\omega_2,\ldots,\omega_{n-1}) = \sum_{\tau_1=-\infty}^{+\infty} \cdots \sum_{\tau_{n-1}=-\infty}^{+\infty} c_n^x(\tau_1,\tau_2,\cdots,\tau_{n-1})\ e^{-j(\omega_1\tau_1+\omega_2\tau_2+\ldots,\omega_n\tau_{n-1})}, \quad (2.21)$$

where $|\omega_i| \le \pi$ for $i = 1,2,\ldots n-1$, and $|\omega_1 + \omega_2 + \ldots + \omega_{n-1}| \le \pi$.

Special cases

(1) Power spectrum (n = 2):

$$C_2^x(\omega) = \sum_{\tau=-\infty}^{+\infty} c_2^x(\tau)\ e^{-j\omega\tau}, \quad (2.22)$$

where $c_2^x(\tau)$ is the covariance.

(2) Bispectrum (n = 3):

$$C_3^x(\omega_1,\omega_2) = \sum_{\tau 1=-\infty}^{+\infty} \sum_{\tau 2=-\infty}^{+\infty} c_3^x(\tau_1,\tau_2)\ e^{-j(\omega_1\tau 1+\omega_2\tau 2)}, \quad (2.23)$$

where $c_3^x(\tau_1,\tau_2)$ is the third-order cumulant. Key steps of calculating the bispectrum using the indirect and the direct methods are summarised in Figure 2.2.

(3) Trispectrum (n = 4):

$$C_4^x(\omega_1,\omega_2,\omega_3) = \sum_{\tau_1=-\infty}^{+\infty} \sum_{\tau_2=-\infty}^{+\infty} \sum_{\tau_3=-\infty}^{+\infty} c_4^x(\tau_1,\tau_2,\tau_3)\ e^{-j(\omega_1\tau_1+\omega_2\tau_2+\omega_3\tau_3)}, \quad (2.24)$$

where $c_4^x(\tau_1,\tau_2,\tau_3)$ is the fourth-order cumulant.

---

[1] Polyspectra, including bispectrum and trispectrum.

[2] Cumulants or moments.

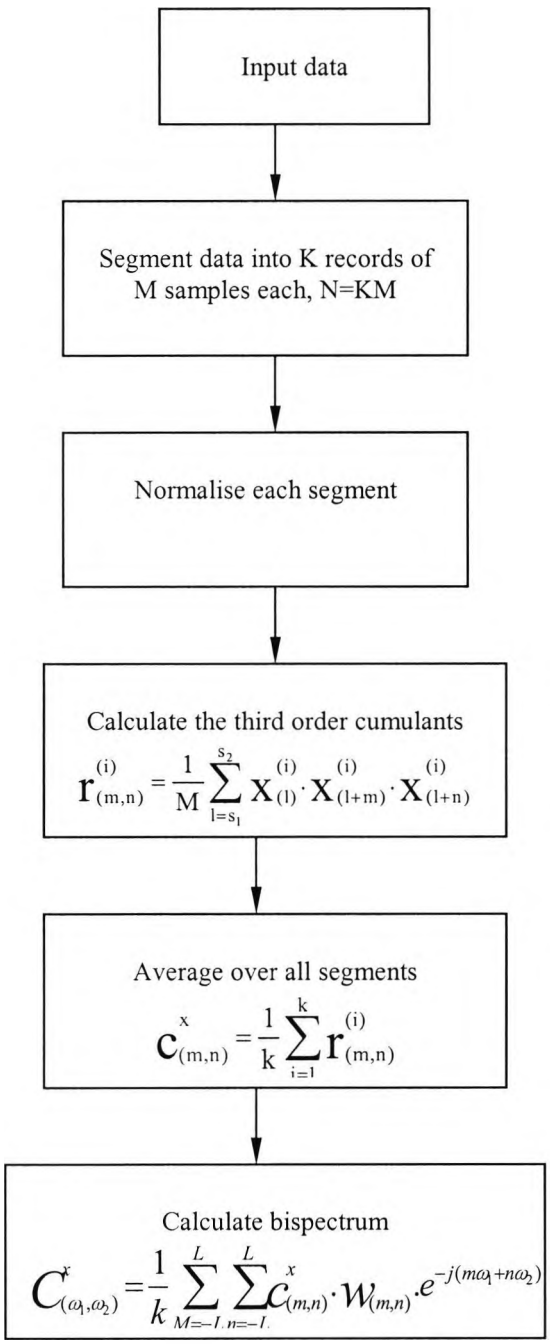

where i=1, 2, …, k. s_1=max(0,-m,-n). s_2=min(M-1,M-1-m,M-1-n). L<M-1,

w(m,n) is a 2-d window function.

(a)

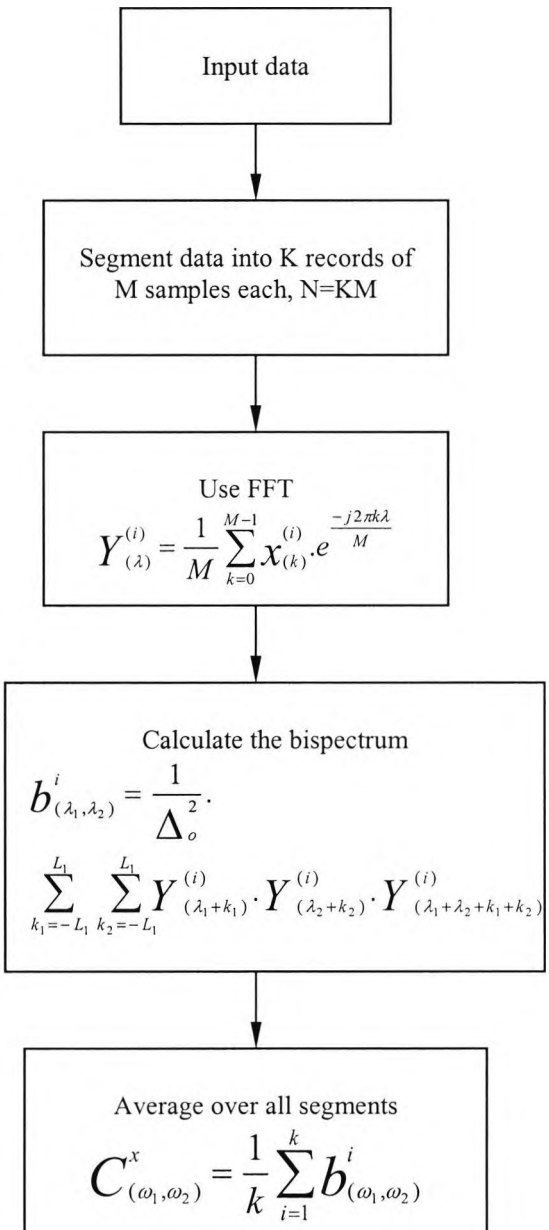

$\Delta_o = f_s / N_o$ is the required spacing between frequency samples. λ=0, 1, …, M/2. i=1,2,…,k. $0 \le \lambda_2 \le \lambda_1$. $\lambda_2+\lambda_1=f_s/2$. $\omega_1 = \frac{2\pi f_s}{N_o}\lambda_1$,

$\omega_2 = \frac{2\pi f_s}{N_o}\lambda_2$.

(b)

Figure 2.2: *Flowchart of the key calculations of the bispectrum using (a) the indirect method, and (b) the direct method.*

Conventional higher-order statistics (HOS) estimates are asymptotically unbiased and consistent [9], and easy to implement using FFT-based methods. The ability to resolve harmonic components is limited by the uncertainty principle of the Fourier transform. There are numerous methods for higher-order spectrum (polyspectrum) estimation based on parametric methods. MA models have been treated in [14-16]. Spectral estimation methods based on non-causal AR models were developed in [17-19]. Methods based on ARMA models have been published [20-21]. The description of MA, AR and ARMA methods based on higher-order statistics is the subject of tutorial papers [22-24]. A review of cumulant spectra and the asymptotic properties of their estimators were given in [31]. Practical considerations for bispectral estimation were given [32] and the relationship between the bispectrum and conventional methods for their estimation was discussed [33-35].

2.6 Nth-order coherency function

A normalised cumulant spectrum or the nth-order coherency index is a function that combines the cumulant spectrum of order n and the power spectrum. It is defined as [3]

$$P_n^x(\omega_1,\omega_2,\ldots,\omega_{n-1}) \nabla \frac{C_n^x(\omega_1,\omega_2,\ldots,\omega_{n-1})}{[C_2^x(\omega_1).C_2^x(\omega_2)\cdots C_2^x(\omega_{n-1}).C_2^x(\omega_1+\omega_2+\ldots+\omega_{n-1})]^2}. \qquad (2.25)$$

The third-order (n = 3) coherence index is also called bicoherence. The nth order coherence index is useful for the detection and characterisation of non-linearities in time series via phase relations of their harmonic components. The coherency index is used to differentiate between linear non-Gaussian processes and non-linear processes when both have non-zero cumulants. If the coherency index is zero, then the process is linear and Gaussian. If the n^{th} order coherency index is not frequency dependent, then the process is linear non-Gaussian. If the coherency index is frequency dependent, then the process is non-linear [3].

2.7 Non-stationarity and the OT region of the bispectrum

The bispectrum of a stationary sampled process must be zero in the triangle region OT (Figure 2.3), i.e., in the region defined by the triangle OT = $\{\omega_1, \omega_2 : \omega_2 \leq \omega_1, \pi \leq \omega_1 + \omega_2 \leq 2\pi - \omega_1\}$ (chapter 8, pp. 373 in [3]). The bispectrum in the OT region

(Figure 2.3) will be non-zero if the process is non-stationary. The bispectrum has 12 symmetric regions. The knowledge of the bispectrum in one triangular region is enough for a complete description of the bispectrum of a real process.

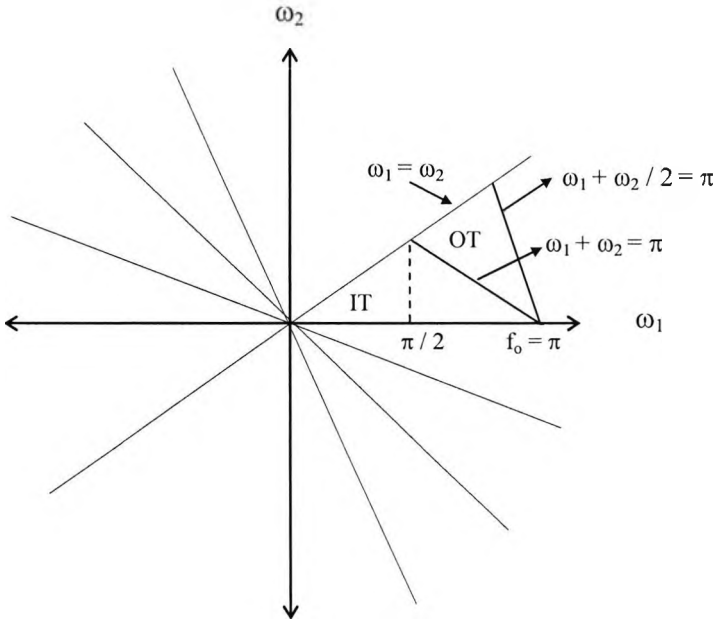

Figure 2.3: *Symmetry regions of the bispectrum showing discrete-time principal domain.*

2.8 Statistical measures

A second-order statistical measure is the variance which is defined as:

$$\gamma_2^x \underline{\underline{\nabla}} c_2^x(0) = \frac{1}{2\pi} \int_{-\pi}^{\pi} C_2^x(\omega).d\omega \,. \tag{2.26}$$

Two higher-order statistics measures are called the skewness and the kurtosis. Skewness and kurtosis have their own physical meanings. The skewness measures the asymmetry of a distribution around its mean. A positive skewness indicates that the distribution is skewed to the right, whereas a negative skewness indicates that the distribution is skewed to the left. The kurtosis measures how peaky or flat a distribution is with respect to a Gaussian distribution. A positive kurtosis indicates that a density is more peaked around its mean value than the density of a Gaussian distribution, whereas a negative kurtosis indicates that a density is more flat around its mean value than the density of a Gaussian distribution.

The skewness is defined as $\gamma_3^x \underline{\underline{\nabla}} c_3^x(0,0) = \frac{1}{(2\pi)^2} \int_{-\pi}^{\pi} \int_{-\pi}^{\pi} C_3^x(\omega_1, \omega_2).d\omega_1.d\omega_2$, (2.27)

and the kurtosis is defined as

$$\gamma_4^x \underline{\underline{\nabla}} c_4^x(0,0,0) = \frac{1}{(2\pi)^3} \int_{-\pi}^{\pi} \int_{-\pi}^{\pi} \int_{-\pi}^{\pi} C_4^x(\omega_1, \omega_2, \omega_3).d\omega_1.d\omega_2.d\omega_3 . \quad (2.28)$$

A statistical measure could be described as an unbiased estimate when the expected value of the estimated statistic is, asymptotically, equal to the true value. For example an estimate of the cumulant spectra is said to be unbiased if

$$E\left|\hat{C}_3^x(\omega_1, \omega_2)\right| = C_3^x(\omega_1, \omega_2). \quad (2.29)$$

The bias is defined as the difference between the true value and the expected value.

2.9 Statistics of ECG signals

A. Second-order statistics

2.9.1 The Probability Density Functions (pdfs) of ECG signals

Here, we concern ourselves with the three essential ECG signals used in the fetal QRS-complex detection; 1) the maternal chest ECG signal. This is measured using one surface electrode positioned on the chest and one reference electrode on the thigh. 2) The transabdominally-measured ECG signal which contains both maternal and fetal contributions amongst other deterministic and chaotic signals plus noise artefacts [60]. This is acquired using twin surface electrodes positioned near the mother's umbilicus and synchronised with the maternal chest signal. And 3) the fetal scalp electrode ECG signal which will always be used as a reference signal in the assessment of any particular QRS detection technique based on non-invasive transabdominally-measured

ECG signals[*, **]. The non-symmetry of the probability density functions (pdfs) of the above mentioned signals is shown in the histograms of Figure 2.4 and supports their third-order cumulants.

2.9.2 The second-order cumulants (autocorrelation functions) of ECG signals

Figure 2.5 (a) shows a full maternal transabdominal cardiac cycle (1000 msec) which has been divided into four segments, I, II, III, and IV. These segments represent (I) the predominantly maternal QRS-complex, (II) the first fetal heartbeat with maternal contribution, (III) QRS-free ECG, and (IV) the second fetal heartbeat with maternal contribution, respectively. Figure 2.5 (b) shows a typical example of the second-order cumulants (autocorrelation functions) for the segments shown in Figure 2.5 (a). The auto-correlation function (ACF) of the maternal QRS-complex (I) could be distinguished from the three other ACFs in (II, III, and IV) as it crosses the x-axis in a much smaller lag time. The ACF of the fetal heartbeat with maternal contribution segments (II and IV) could be distinguished from that of the QRS-free ECG (III) in that they decay smoothly with less peaks.

2.9.3 The power spectrum of ECG signals

Figure 2.6 depicts the power spectrum using the FFT method for (a) fetal scalp electrode ECG signal (data length 500 msec), (b) maternal transabdominal ECG (data length 1000 msec), and (c) segment II of the transabdominal signal (inset) containing fetal heartbeat with maternal contribution (data length 250 msec). The maternal cardiac cycle begins 50 msec before the R-wave and ends 50 msec before the next R-wave. The subject is at the first stage of labour (40 weeks gestation). The FFT method reveals a fetal scalp electrode ECG principal spectral peak at 30 Hz. The FFT method for the transabdominal cardiac cycle reveals the maternal principal spectral peak of 15 Hz. However, the FFT does not clearly show a fetal spectral peak from the segmented transabdominal signal. There is a shallow peak at 28 Hz and a shifted peak at 42 Hz.

* Sensitivity: $S_e = \frac{TP}{TP + FN}$

** Specificity: $S_p = \frac{TP}{TP + FP}$

where TP is the number of true positives, FN is the number of false negatives, and FP is the number of false positives. The sensitivity S_e reports the percentage of true beats that were correctly detected by the algorithm. The specificity reports the percentage of detected heartbeats which were in reality true beats.

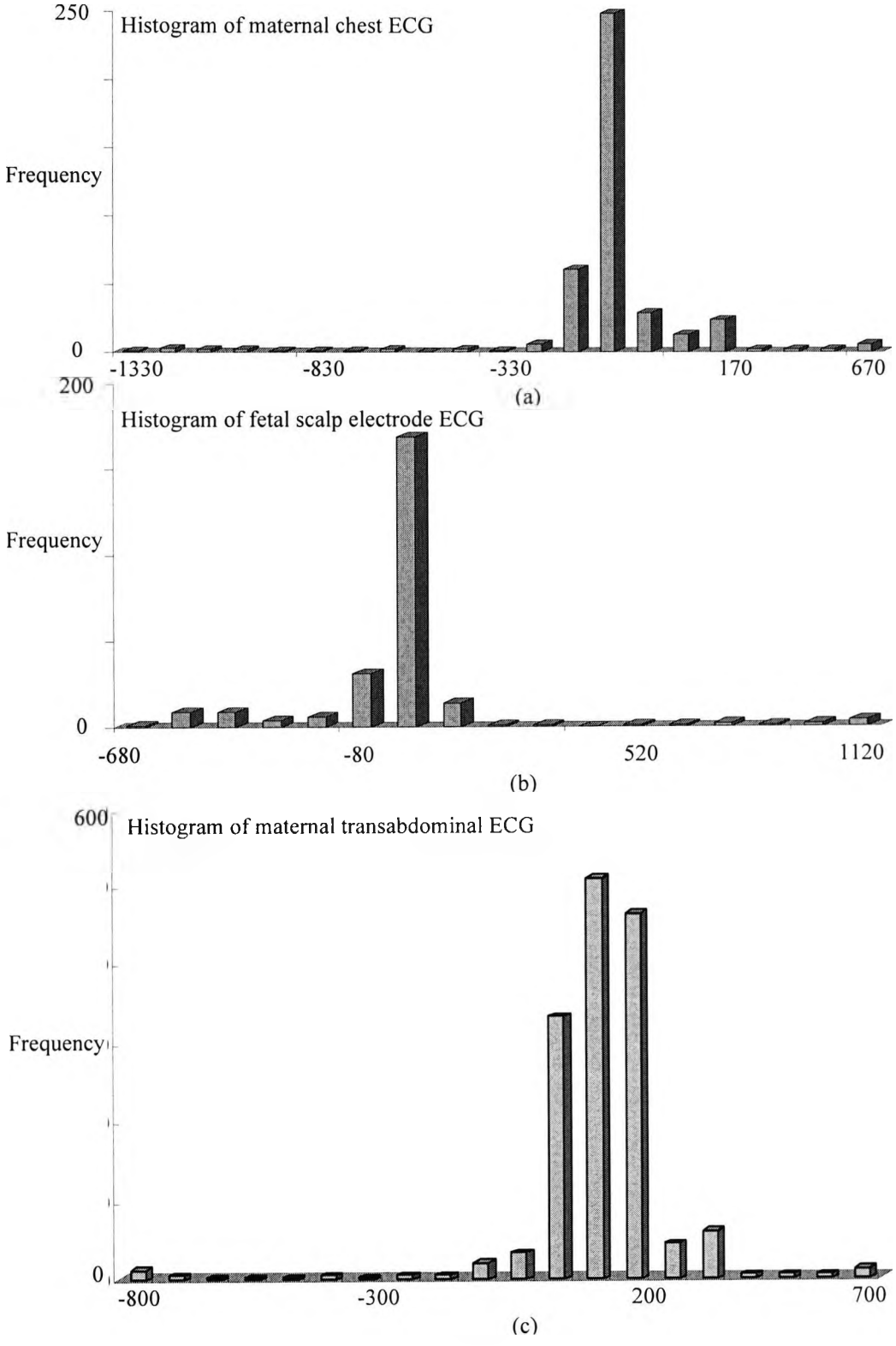

Figure 2.4: *Histograms of typical templates of (a) a maternal chest ECG, (b) a fetal scalp electrode FECG, and (c) a maternal transabdominal ECG. They all show non-Gaussian distribution.*

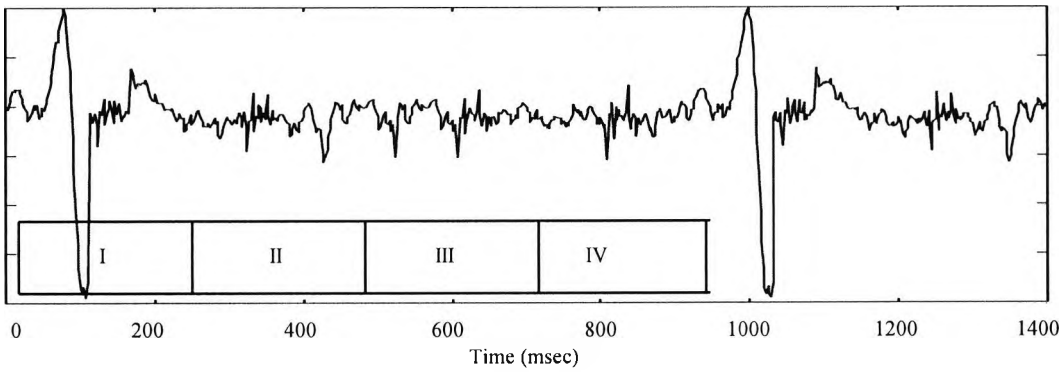

Figure 2.5 (a): *Maternal transabdominal cardiac cycle (1000 msec) which has been divided into four segments; (I) maternal QRS-complex, (II) the first fetal heartbeat with maternal contribution, (III) QRS-free ECG, and (IV) the second fetal heartbeat with maternal contribution. The maternal cardiac cycle begins 50 msec before the R-wave and ends 50 msec before the next R-wave. The subject is at the first stage of labour (40 weeks gestation).*

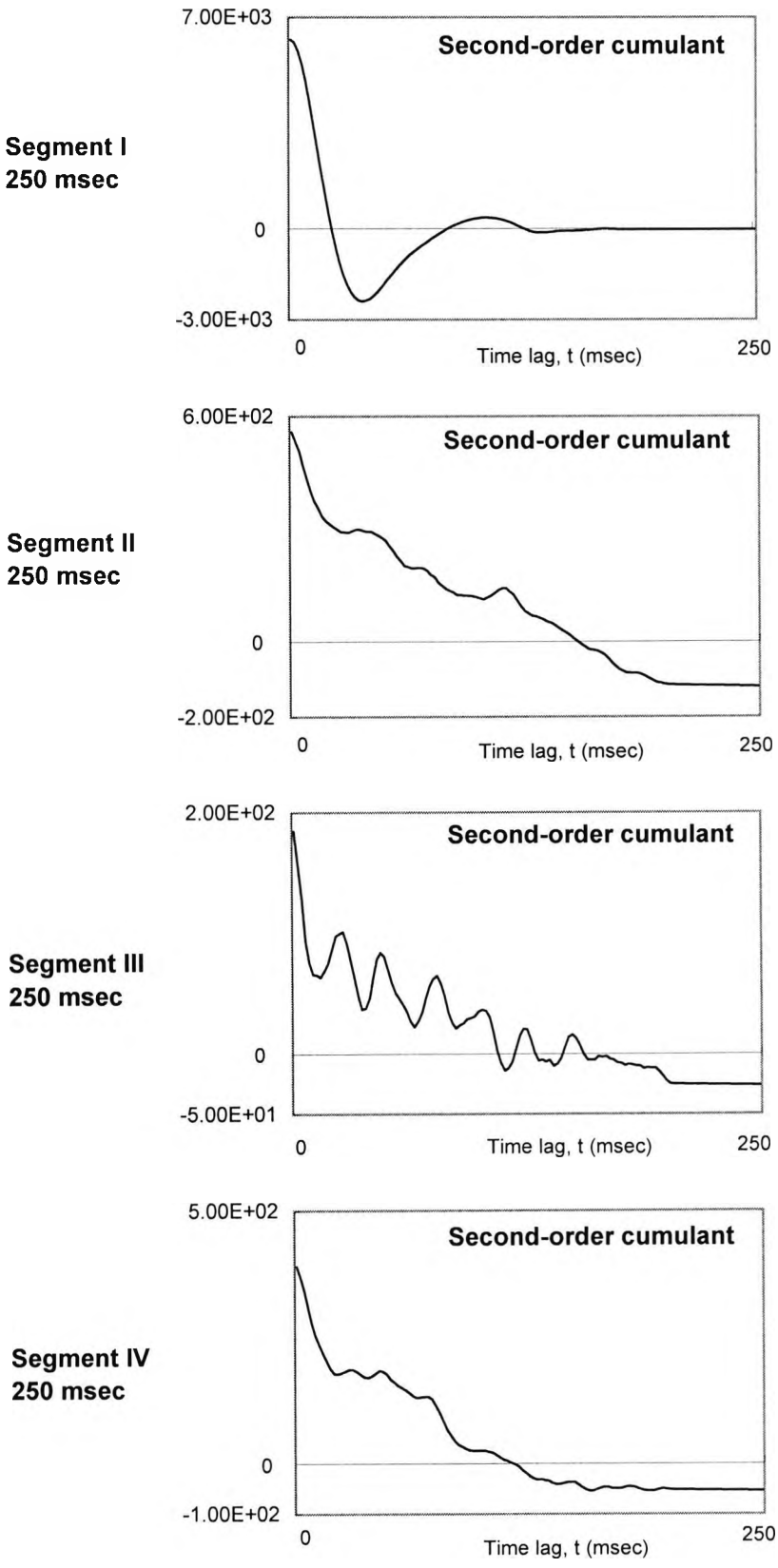

Figure 2.5 (b): *Typical examples of the second-order cumulants computed using the segments I, II, III, and IV shown in Figure 2.5 (a) of maternal transabdominal ECG.*

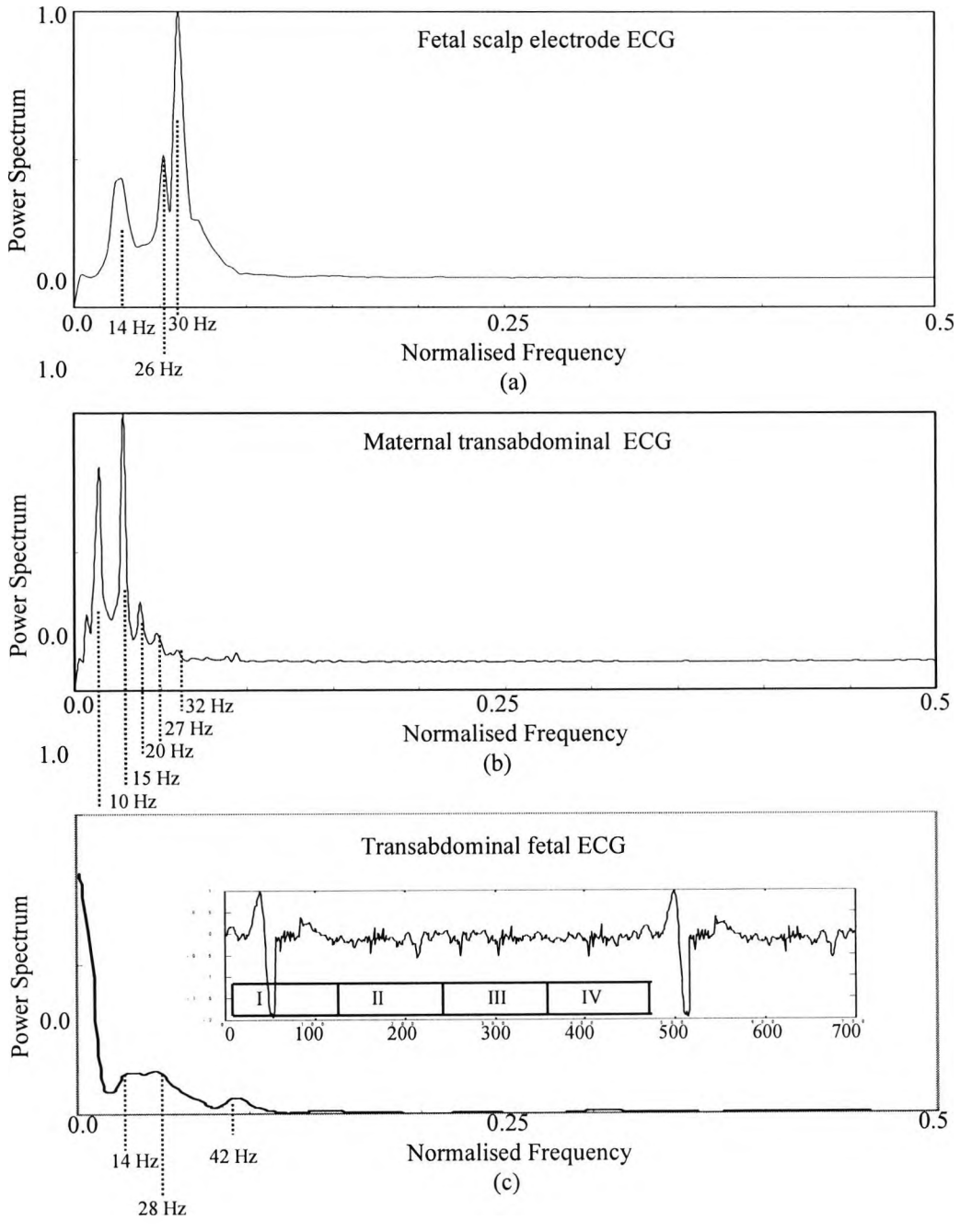

Figure 2.6: *The power spectrum using the FFT method for (a) fetal scalp electrode ECG (data length 500 msec), (b) maternal transabdominal ECG signal (data length 1000 msec), and (c) segment II of the transabdominal signal (inset) containing a fetal heartbeat with maternal contribution (data length 250 msec). The maternal cardiac cycle begins 50 msec before the R-wave and ends 50 msec before the next R-wave. The subject is at the first stage of labour (40 weeks gestation).*

B Third-order statistics

2.9.4 Typified examples of cumulants and their slices for individual cardiac cycles

The maternal chest ECG is measured using the standard three-lead electrode system. The maternal transabdominally-measured signals are obtained using two surface electrodes. The electrode pair is set over the umbilicus, and lined up with the median vertical axis of the uterus. The ground electrode is located on the woman's hip. The fetal scalp electrode is used when deemed necessary. Multi-dimensional TOCs were computed for the above ECG signals (full cardiac cycles) as well as for the four segments of the maternal transabdominal cardiac cycles. The four segments were coded as I, II, III, and IV, each of length 250 msec which has been considered short enough as not to satisfy the assumption of non-stationarity, and long enough to meet the threshold of the higher-order statistical variances. The four coded segments ascribe to the following often occurring scenario; (I) Segment I, 0 – 250 msec; Predominantly maternal QRS-complex (no fetal QRS-complex present), (II) Segment II, 251 msec – 500 msec; The first fetal heartbeat with maternal contribution, (III) Segment III, 501 msec – 750 msec; QRS-free ECG, and (IV) Segment IV, 751 msec – 1000 msec; The second fetal heartbeat with maternal contribution.

Figure 2.7 (a), (b), (c), and (d) each depicts ECG signals (upper panel) and their third-order cumulants (lower panel) for fetal scalp ECG (550 msec), maternal chest ECG (900 msec), and two different and randomly picked transabdominally-measured maternal ECGs (1000 msec each). The subject is at 40 weeks gestation after the water has been broken hence facilitating fetal scalp measurements. The maternal cardiac cycle begins 50 msec before the R-wave and ends 50 msec before the next R-wave.

A quick glance at the similarities of the four cumulant patterns in Figure 2.7 (a), (b), (c) and (d), gives some hope of successful detection of the fetal presence in the maternal cardiac cycle. To complicate matters further, the two transabdominal cumulants in Figure 2.7 (c) and (d) look dissimilar even though both contain two fetal QRS-complexes. However, the best way to distinguish between those patterns is to slice them and look for discriminant features as will be shown next.

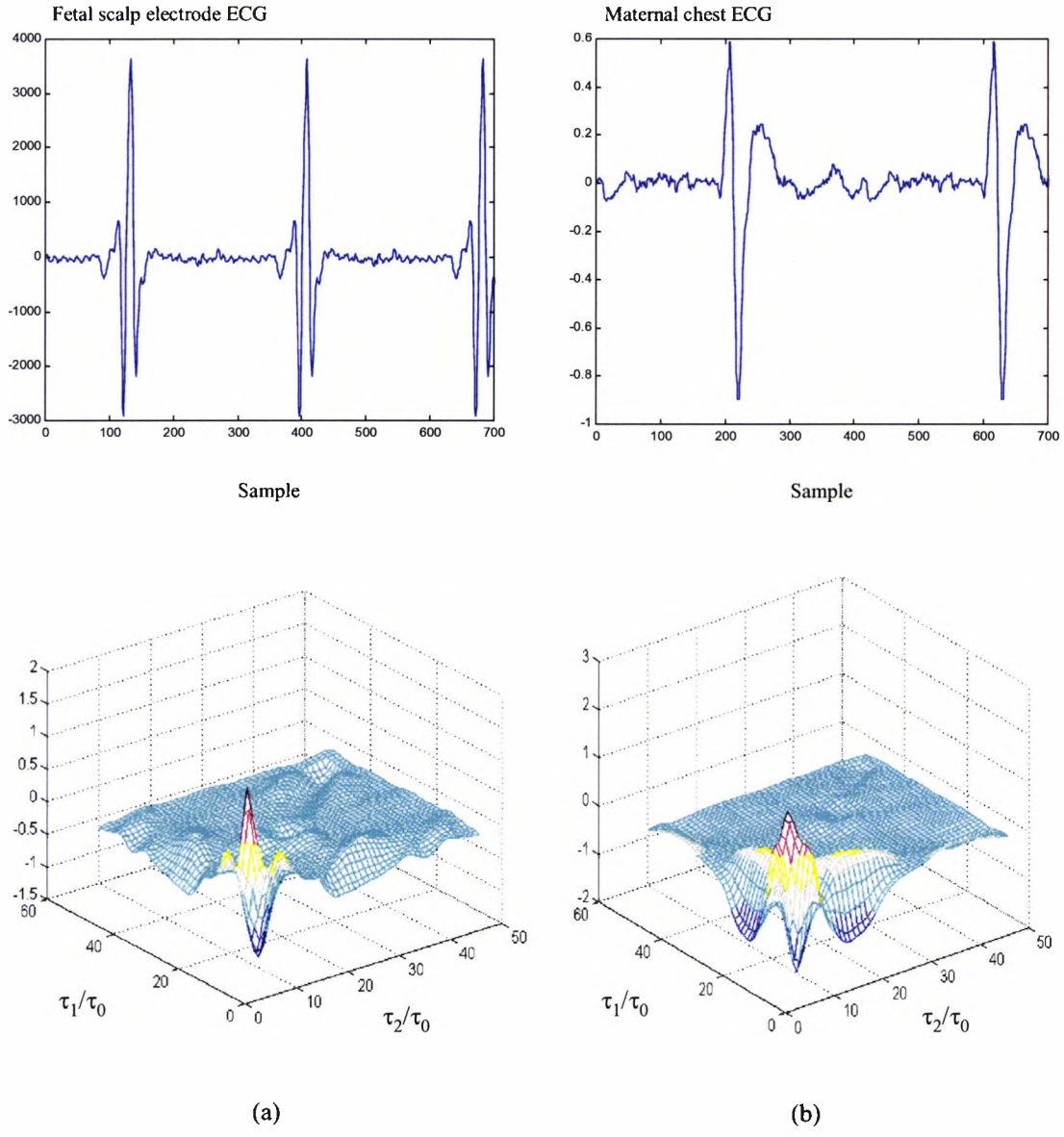

Figure 2.7: *ECG signals (upper panel) and their third-order cumulants (lower panel) for (a) fetal cardiac cycle using fetal scalp electrode (data length 550 msec), (b) maternal chest cardiac cycle using one surface electrode and a reference electrode (data length 900 msec), (c) and (d) are two maternal transabdominal cardiac cycles measured using twin surface electrodes (data length 1000 msec each). The maternal cardiac cycle begins 50 msec before the R-wave and ends 50 msec before the next R-wave. The subject is at the first stage of labour, 40 weeks, (Code: cycle 5-31 and 5-1679).*

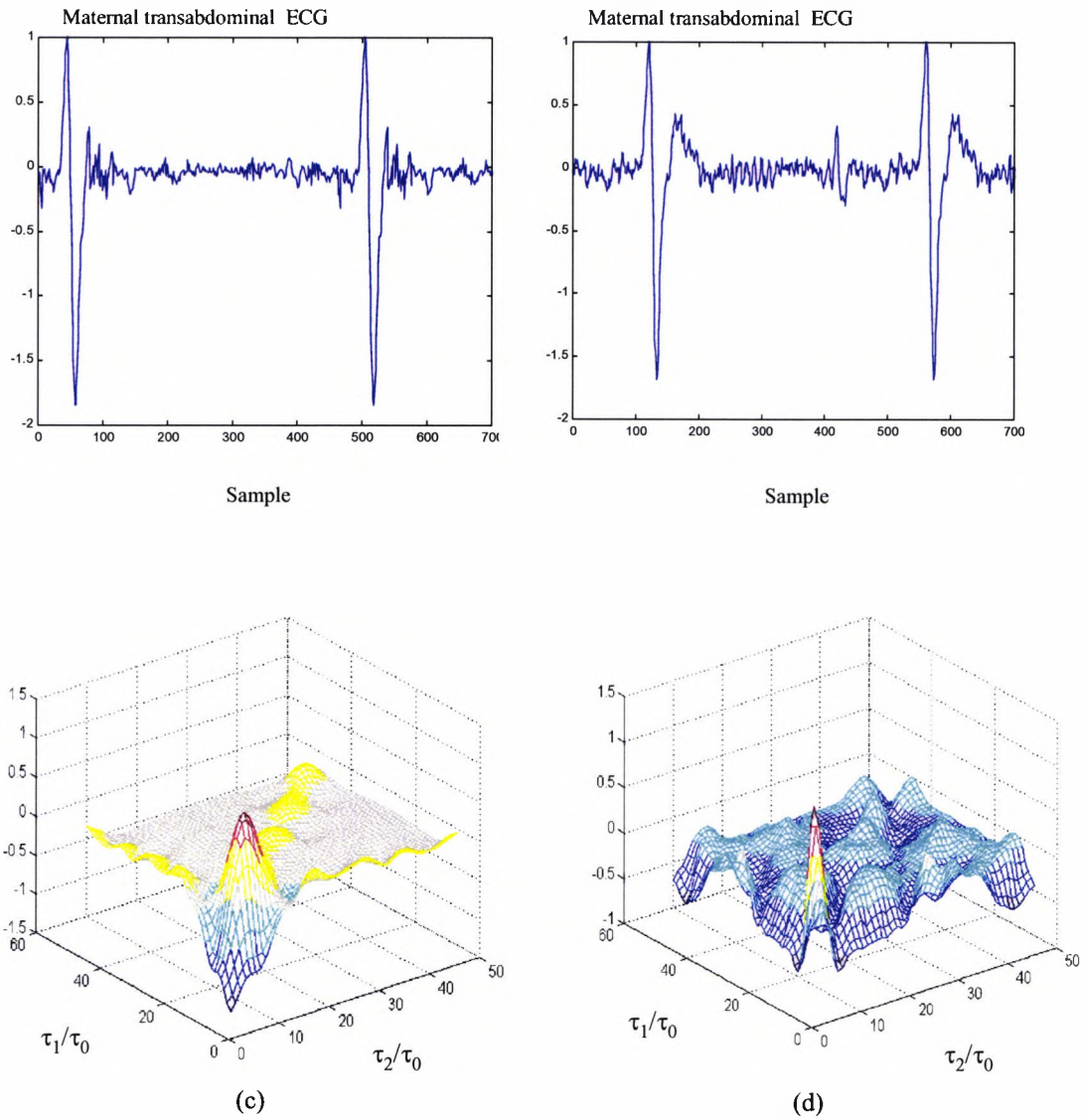

Figure 2.7 *(continued): ECG signals (upper panel) and their third-order cumulants (lower panel) for (a) fetal cardiac cycle using fetal scalp electrode (data length 550 msec), (b) maternal chest cardiac cycle using one surface electrode and a reference electrode (data length 900 msec), (c) and (d) are two maternal transabdominal cardiac cycles measured using twin surface electrodes (data length 1000 msec each). The maternal cardiac cycle begins 50 msec before the R-wave and ends 50 msec before the next R-wave. The subject is at the first stage of labour, 40 weeks gestation, (Code: cycle 5-31 and 5-1679).*

Figure 2.8 shows the third-order cumulants and their diagonal (l.h.s.) and wall (r.h.s.) slices of one transabdominal cardiac cycle which is segmented into four segments of 250 msec each for (I) predominantly maternal QRS, (II) the first fetal heartbeat with maternal contribution, (III) QRS-free ECG, and (IV) the second fetal heartbeat with maternal contribution. The diagonal and wall TOC slices of the maternal segment (I) are easily distinguished from the diagonal and wall TOC slices of segments (II), (III), and (IV). Furthermore, the diagonal and wall TOC slices of the fetal QRS segments (II) and (IV) are distinguishable from the diagonal and wall TOC slices of the QRS-free ECG segment (III) in that there is a distinguishable and well-formed peak at the origin in both diagonal and wall TOC slices. The peak of the QRS-free ECG segment is much narrower and more related to motion artefact than a signal.

Note that having computed the two-dimensional TOC, either the diagonal or the wall slice could be used in the detection / classification process. Therefore, computing the full multi-dimensional TOC and then extracting individual slices is an unnecessary waste of the CPU time. So, why not compute any arbitrary 1-d slice directly without firstly having to compute the three-dimensional TOC and secondly extract the 1-d slice? In fact, the TOC-diagonal and the TOC-wall slices are straightforward to compute directly, by freezing one of the two cumulant lags and changing the other one. However, to compute any other arbitrary slice requires the development of an *auxiliary algorithm* which is described in Chapter Four, and to my knowledge it has not been previously reported in the relevant literature. It has been found that performing direct computations of the 1-d TOC slices instead of computing the 2-d TOC firstly and secondly extracting individual 1-d slices results in saving of more than 99% of the CPU time.

Figure 2.9 shows four selected slices of the third-order cumulants computed using one cardiac cycle for each of the following; (a) and (b) an adult male and female chest, respectively, (c) maternal transabdominal, and (d) fetal scalp electrode ECG signal.

2.9.5 Typified examples of the bispectrum, contour maps and slices for individual cardiac cycles

Now, in a similar fashion to the third-order cumulants and cumulant slices analyses presented in section 2.9.4, we proceed with the bispectral analysis. Figure 2.10 shows the 2-d bispectrum magnitudes (upper panel) and the corresponding contours (lower

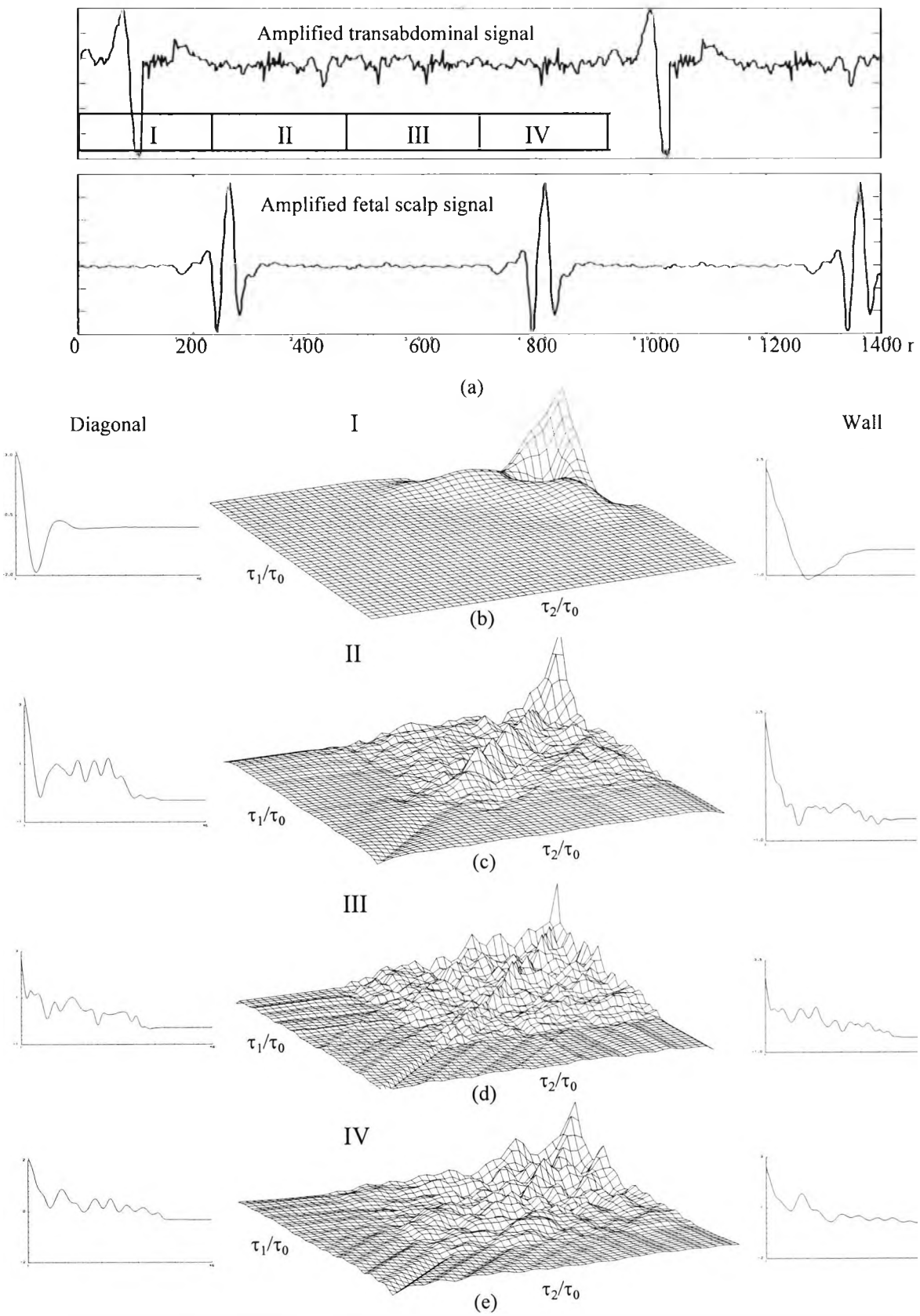

Figure 2.8: *(a) Maternal transabdominal ECG signal (upper panel) and the synchronised fetal ECG signal measured using fetal scalp electrode (lower panel). (b), (c), (d) and (e) are the third-order cumulants and their diagonal (l.h.s.) and wall (r.h.s.) slices for segments I, II, III, and IV, respectively, each segment is 250 msec. Segment I: pre-dominantly maternal QRS-complex, segment II, the first fetal heartbeat with maternal contribution, segment III: QRS-free ECG, and segment IV: the second fetal heartbeat with maternal contribution. The maternal cardiac cycle begins 50 msec before the R-wave and ends 50 msec before the next R-wave. (Code: cycle 5-14).*

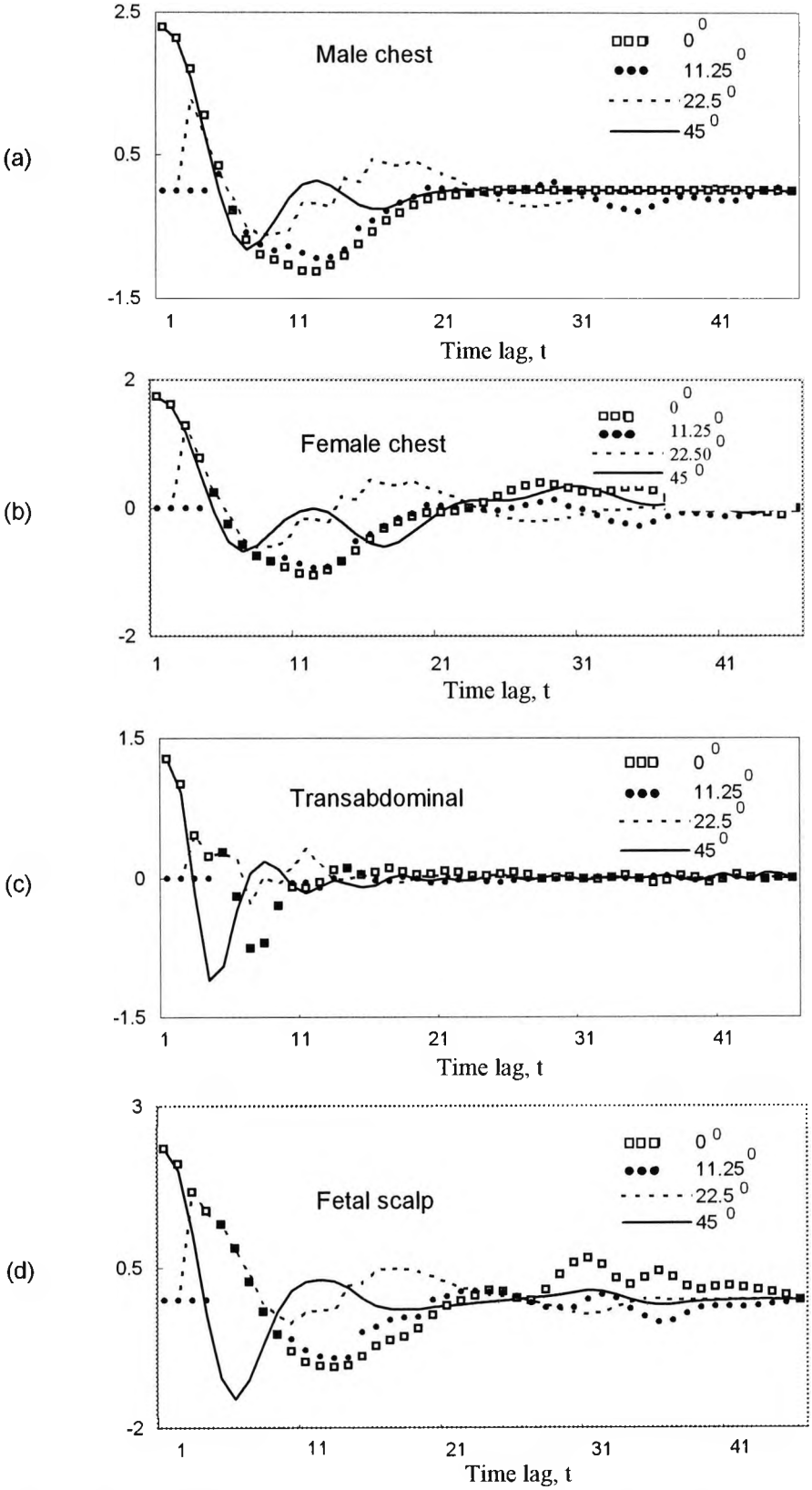

Figure 2.9: *Third order cumulant slices at 0° (wall), 11.25° , 22.50°, and 45° (diagonal) for (a) male chest cardiac cycle using one surface electrode (data length 1180 msec), (b) maternal chest cardiac cycle using one surface electrode (data length 900 msec), (c) maternal transabdominal cardiac cycle using twin surface electrodes (data length 1000 msec), and (d) fetal cardiac cycle using fetal scalp electrode (data length 550 msec). The maternal cardiac cycle begins 50 msec before the R-wave and ends 50 msec before the next R-wave. The female subject is at the first stage of labour, 40 weeks gestation. (code: (a) 7-1, (b) 5-15, (c) 5-7, and (d) 5-1).*

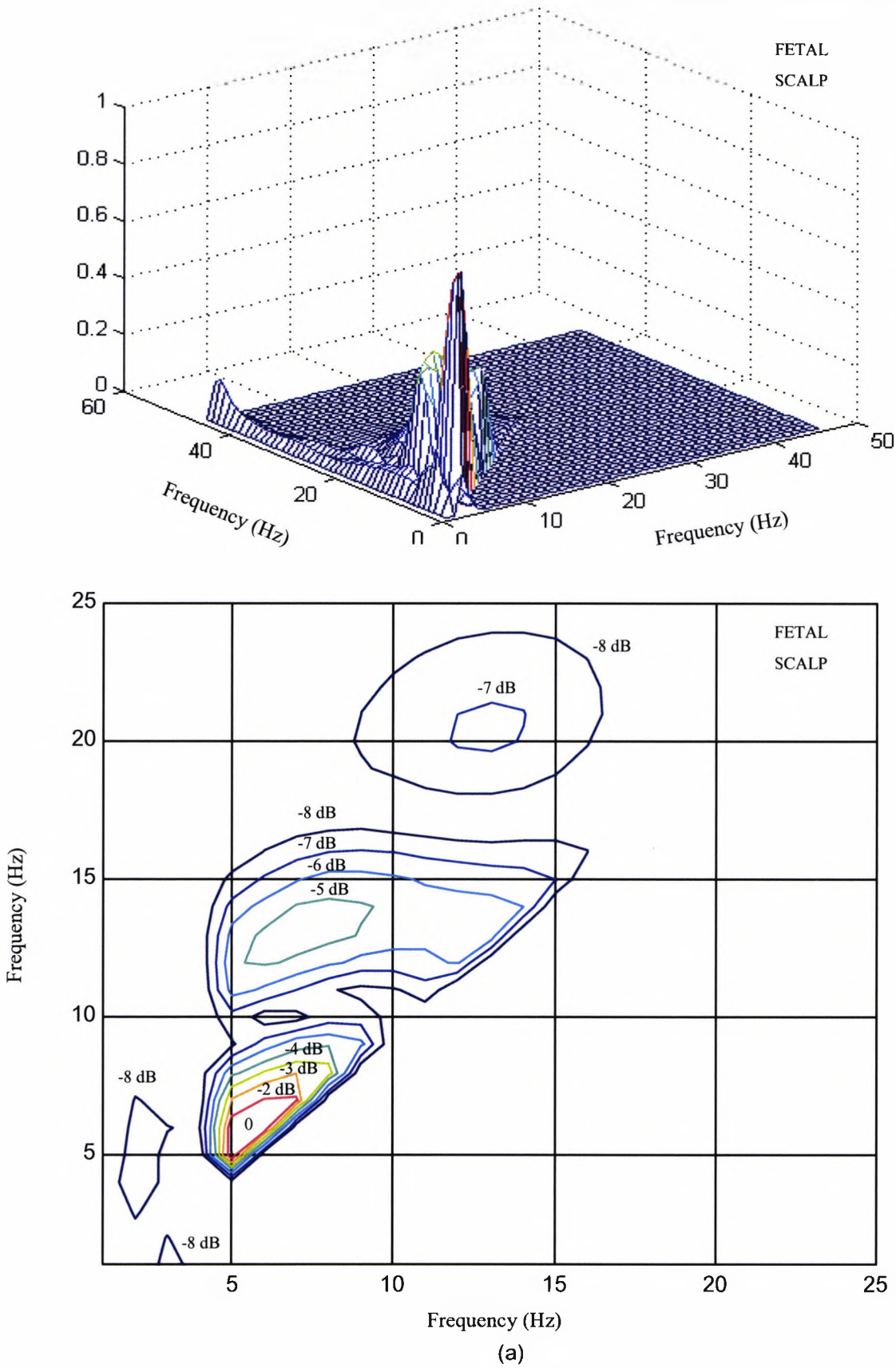

Figure 2.10: *The bispectrum magnitude (upper panel) and contour map (lower panel) for (a) a fetal cardiac cycle using fetal scalp electrode (data length 550 msec), (b) a maternal chest cardiac cycle (data length 1000 msec), and (c) a maternal transabdominal cardiac cycle (data length 1000 msec). The maternal cardiac cycle begins 50 msec before the R-wave and ends 50 msec before the next R-wave. The subject is at the first stage of labour, 40 weeks gestation. The direct method is used to calculate the bispectrum. (Code: 5-1).*

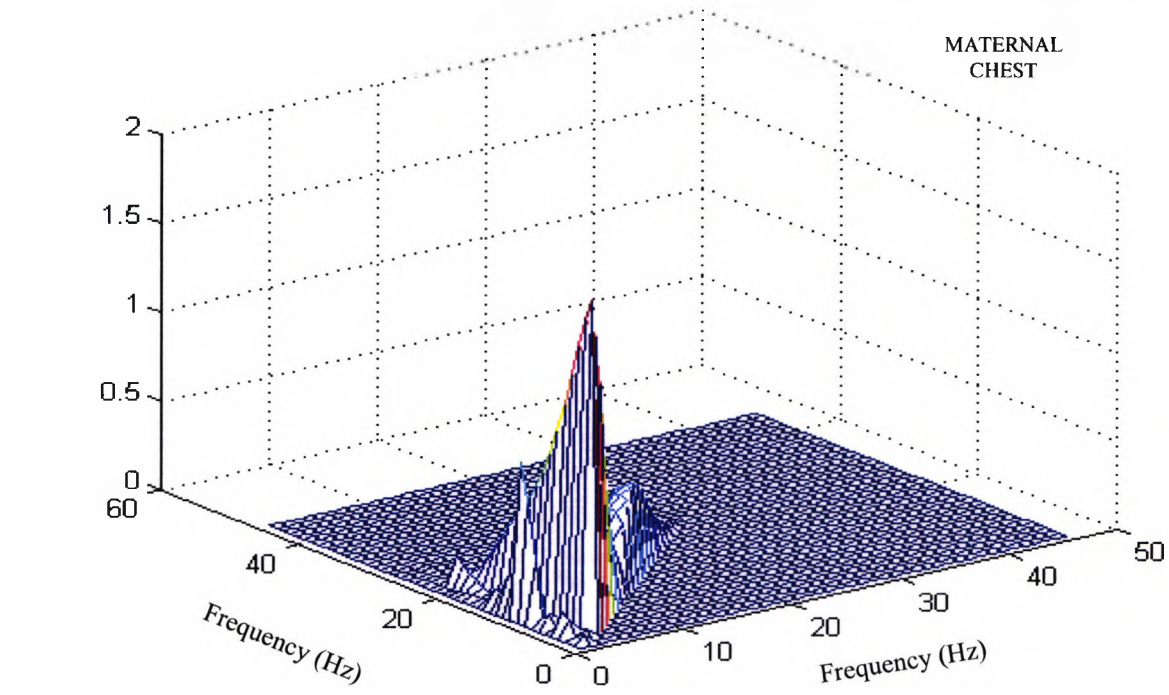

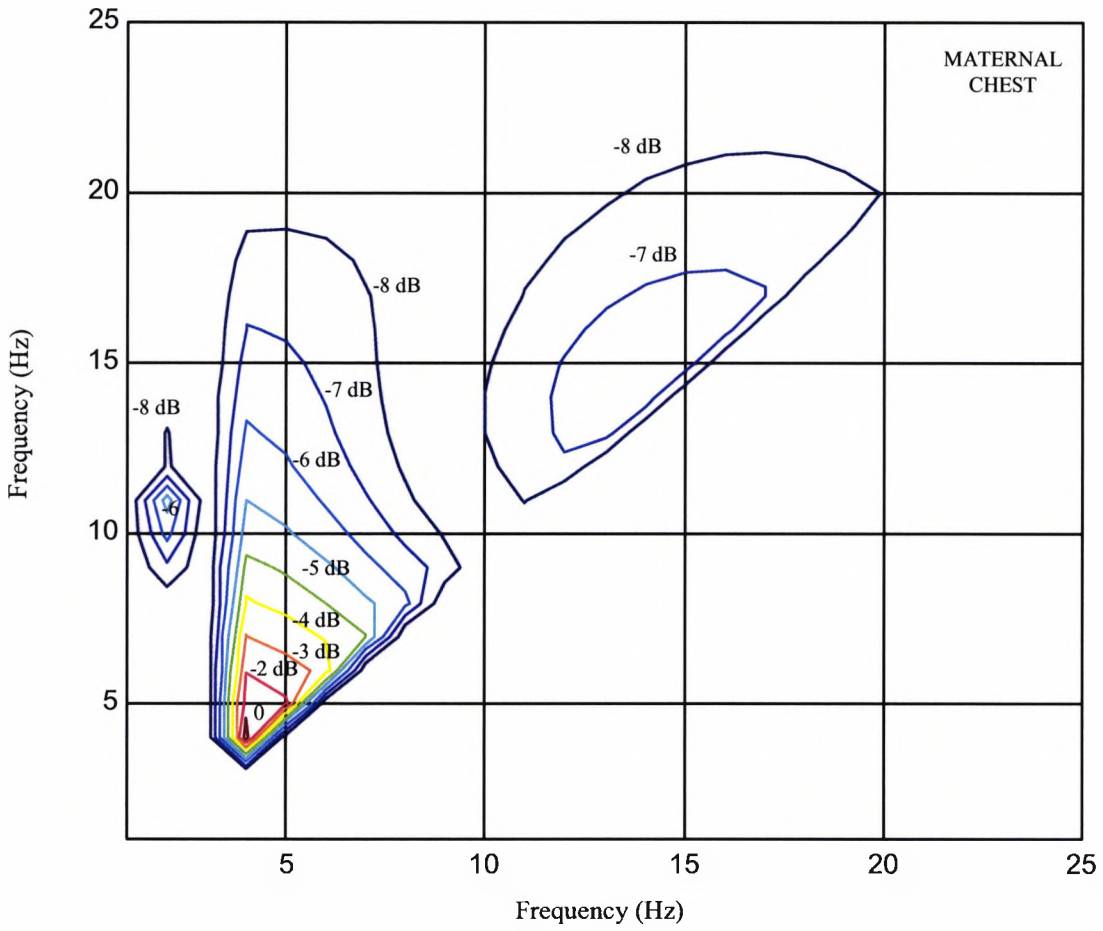

(b)

Figure 2.10 *(continued): The bispectrum magnitude (upper panel) and contour map (lower panel) for (a) a fetal cardiac cycle using fetal scalp electrode (data length 550 msec), (b) a maternal chest cardiac cycle (data length 1000 msec), and (c) a maternal transabdominal cardiac cycle (data length 1000 msec). The maternal cardiac cycle begins 50 msec before the R-wave and ends 50 msec before the next R-wave. The subject is at the first stage of labour, 40 weeks gestation. The direct method is used to calculate the bispectrum. (Code: 5-1).*

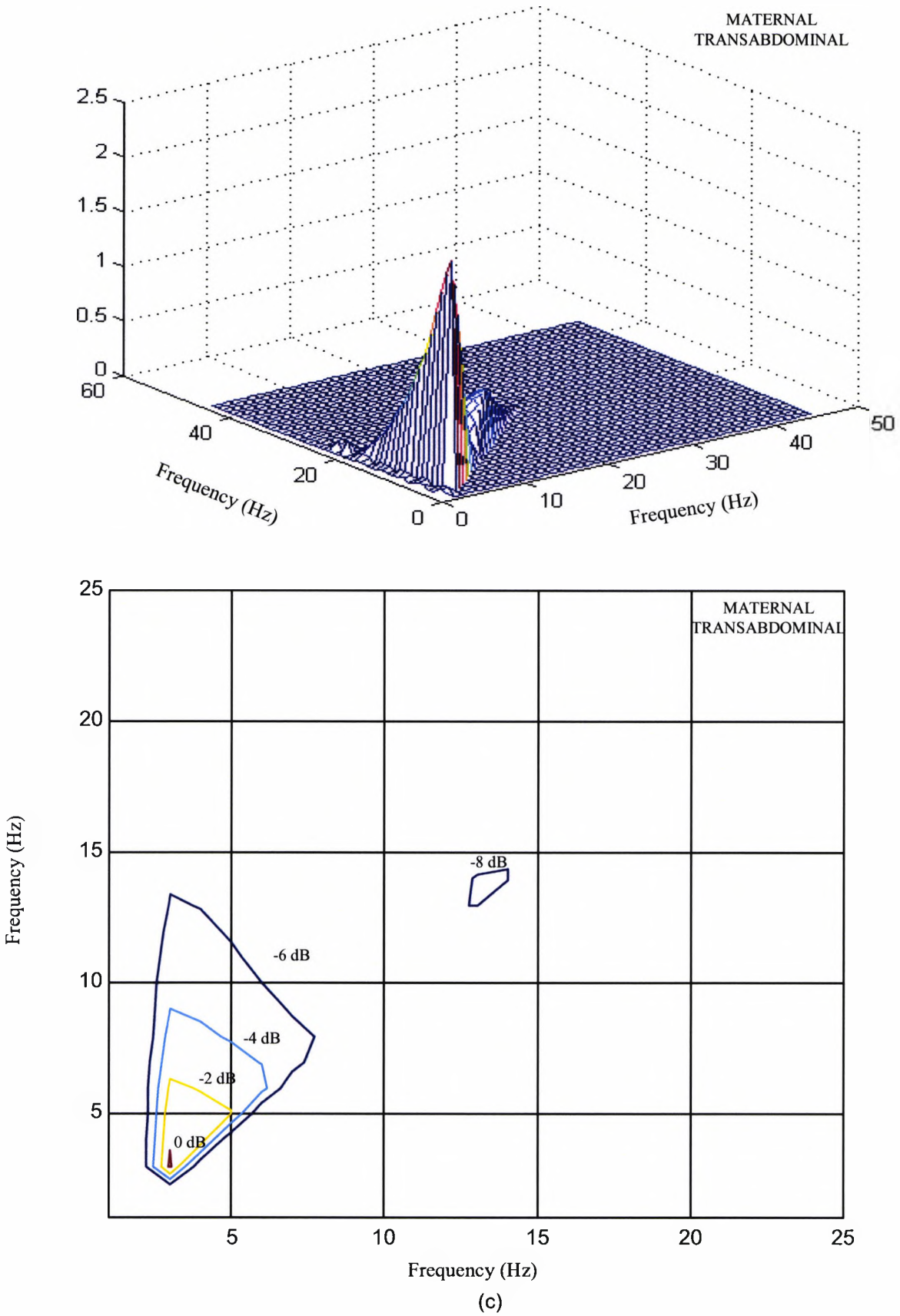

Figure 2.10 *(continued): The bispectrum magnitude (upper panel) and contour map (lower panel) for (a) a fetal cardiac cycle using fetal scalp electrode (data length 550 msec), (b) a maternal chest cardiac cycle (data length 1000 msec), and (c) a maternal transabdominal cardiac cycle (data length 1000 msec). The maternal cardiac cycle begins 50 msec before the R-wave and ends 50 msec before the next R-wave. The subject is at the first stage of labour, 40 weeks gestation. The direct method is used to calculate the bispectrum. (Code: 5-1).*

panel) using one cardiac cycle for; (a) fetal scalp electrode ECG, (b) maternal chest ECG, and (c) maternal transabdominal ECG signal.

Before attempting to assess any advantages of the ECG bispectrum over and above the power spectrum one should regress, for a moment, to view the power spectrum and locate the frequency ranges for adult's and fetal QRS-complexes. The power spectrum of appropriately sampled ECG showed the QRS-complex principal peak in the frequency range from 15 Hz to 20 Hz, and 25 Hz to 40 Hz, for the mother's chest ECG and fetal scalp electrode ECG, respectively. Unfortunately, the power spectrum has limitations as an estimator in terms of resolution, variance, and clarity of the spectrum to be able to produce clear and distinguishable peaks for the P-waves. Therefore, an alternative spectrum estimator was used instead, namely, the multiple signal classification (MUSIC) pseudo-spectrum. In separate publications [62-65], the MUSIC-based pseudo-spectrum also showed that the principal peaks for the p-waves occupy a range from 5 Hz to 8 Hz for adults. The principal peaks for the P-waves of the fetal scalp electrode ECG occupy a range from 8 Hz to 10 Hz. The same MUSIC-based spectral estimators have revealed high local energy peaks around 5 Hz due to motion artefact.

Now returning to the cardiac cycle bispectra shown in Figure 2.10, it is clearly seen that all significant twin-frequency peaks occur at frequencies lower than the p-wave and QRS-complex frequencies. In fact it is very difficult to observe any p-wave or QRS-complex frequencies. The only thing that could be construed from these results is that the combined effect of the low temporal resolution resulting from using the whole cardiac cycle and the low spectral resolution inherent in the bispectrum formation, the QRS-complex twin peaks which should occur at frequency ranges from (15 Hz,15 Hz) to (20 Hz,20 Hz) for adults and from (25 Hz,25 Hz) to (40 Hz,40 Hz) for fetal scalp electrode ECG are completely masked and cannot be found even at –30 dB normalised to any significant low frequency peak. Instead, only low frequencies predominate.

Figure 2.11 shows the bispectra of fetal scalp electrode and maternal chest ECG signals (upper panel) and the corresponding contour maps (lower panel). The maternal cardiac cycle begins 50 msec before the R-wave and ends 50 msec before the next R-wave. The subject is at the first stage of labour, 40 weeks gestation. The bispectrum is calculated

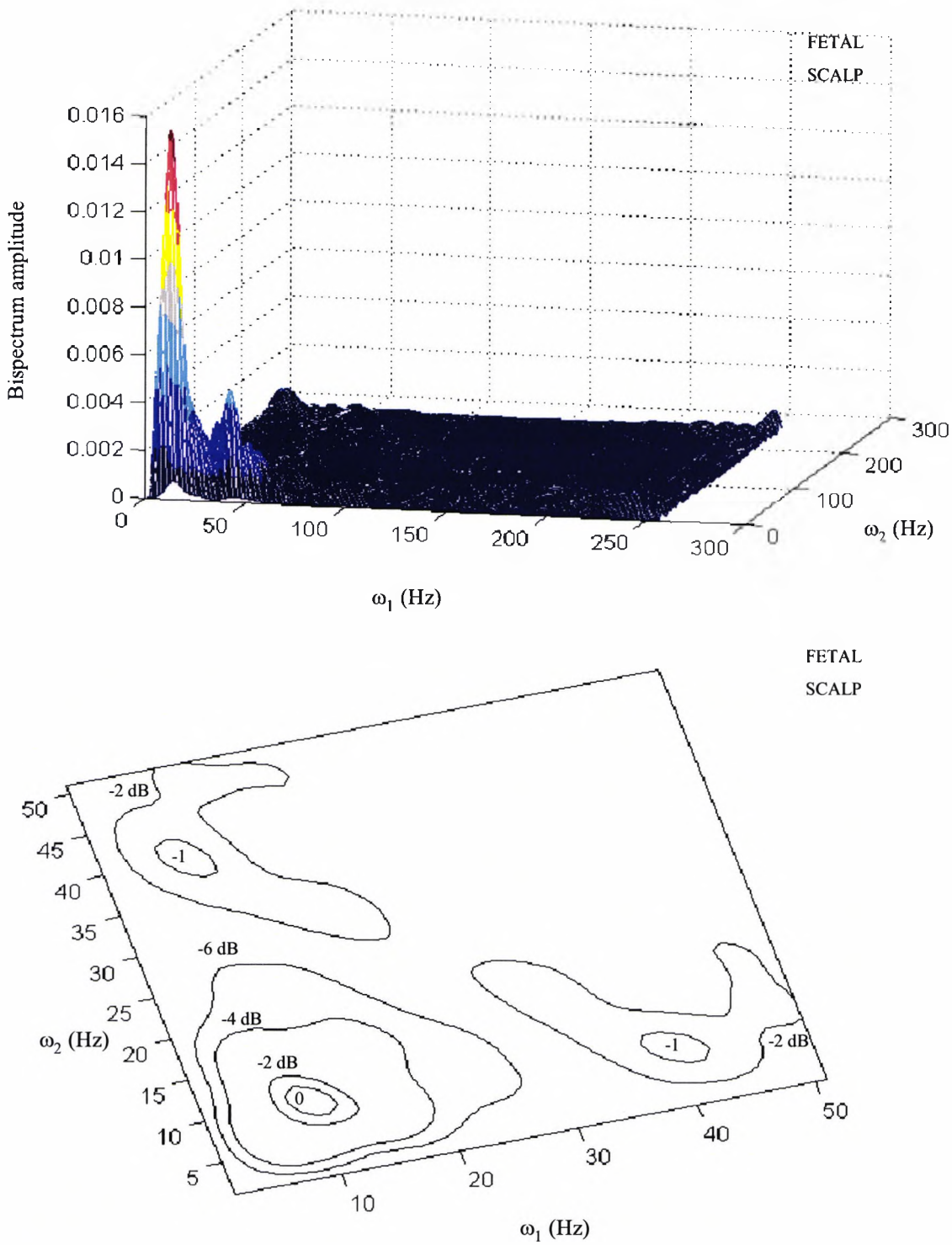

(a)

Figure 2.11: *The bispectra of (a) a fetal scalp and (b) a maternal chest ECG signal (upper panel) and the corresponding contour maps (lower panel). The maternal cardiac cycle begins 50 msec before the R-wave and ends 50 msec before the next R-wave. The subject is at the first stage of labour, 40 weeks gestation. The bispectrum is calculated using the direct method. A Hanning window is used to calculate the bispectrum which is averaged for smoothing. (Code: cycle 5-21).*

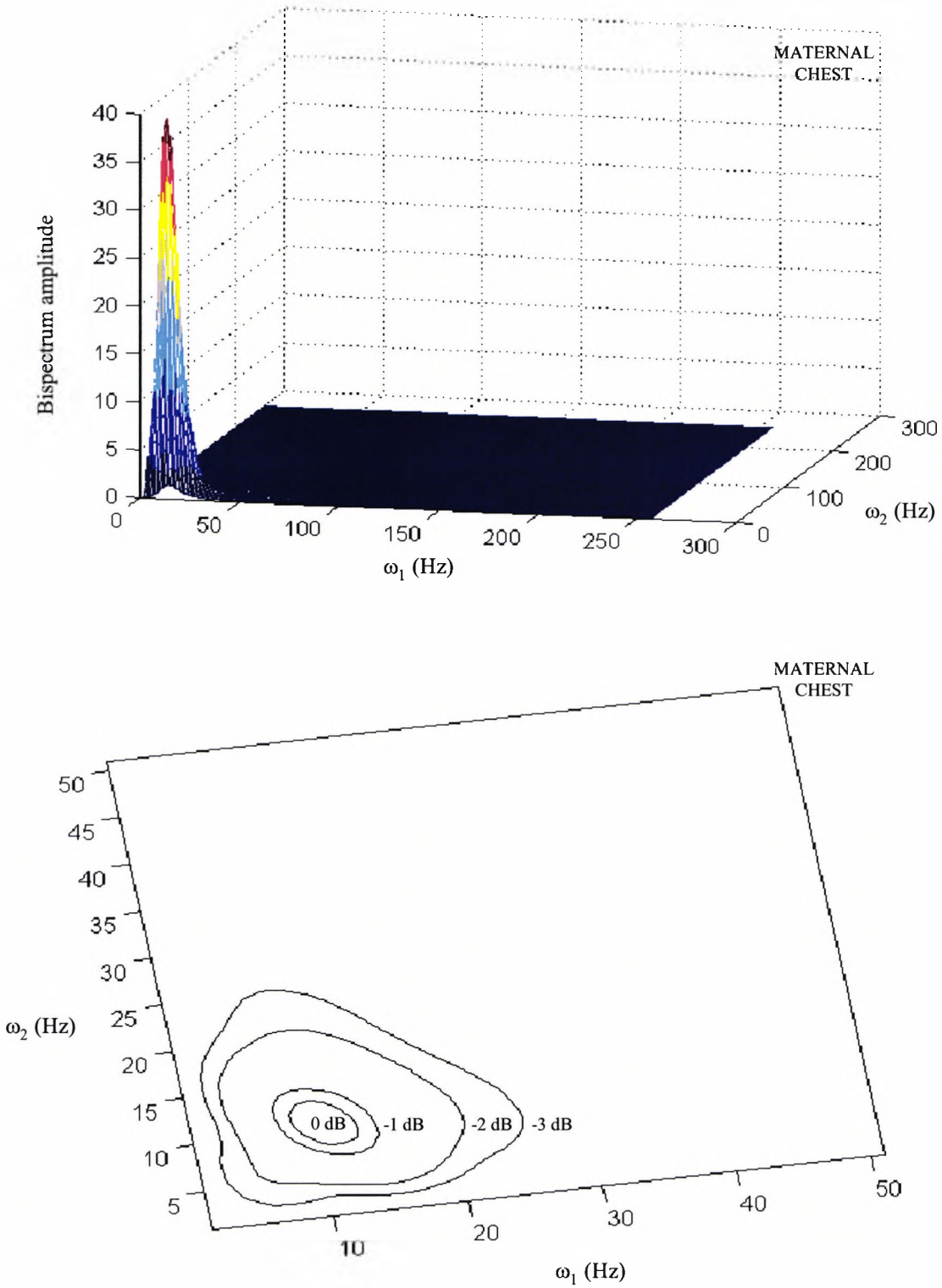

(b)

Figure 2.11: *The bispectra of (a) a fetal scalp and (b) a maternal chest ECG signal (upper panel) and the corresponding contour maps (lower panel). The maternal cardiac cycle begins 50 msec before the R-wave and ends 50 msec before the next R-wave. The subject is at the first stage of labour, 40 weeks gestation. The bispectrum is calculated using the direct method. A Hanning window is used to calculate the bispectrum which is averaged for smoothing. (Code: cycle 5-21).*

using the direct method which involves calculating a two-dimensional Fourier transform. The Hanning window is used in calculating the bispectrum which is averaged for smoothing. The bispectral peaks of the fetal scalp electrode and maternal chest QRS-complexes exist at (40 Hz,40 Hz) and (13 Hz,13 Hz), respectively. However, they are shifted, shallow and inconclusive even though they are centred near the right frequency pairs, (30 Hz,30 Hz) for the fetal scalp electrode and (17 Hz,17 Hz) for the maternal chest ECG.

The next step is to try to improve the temporal resolution by applying appropriate segmentations to the QRS-complexes. Instead of taking one cardiac cycle for an adult, which is on average 1000 msec, now we concern ourselves with the 250 msec QRS-complex segment which is centred on the R-wave and runs 125 msec in opposite direction. This also applies to the fetal scalp electrode ECG signal but with a reduced QRS-complex length of typically 60 msec. Figure 2.12 (top) depicts bispectral slices of the fetal QRS-complex which shows the correct position of a spectral peak at 30 Hz but only on the diagonal slice. Figure 2.12 (middle and bottom) show maternal chest and transabdominal QRS-complex bispectrum slices. The maternal chest and abdomen both exhibit spectral frequencies of 17 Hz and 15 Hz, respectively, but only on the diagonal slice. As we can see, considerable improvement has resulted due to improving the temporal resolution prior to the bispectral calculations for both fetal and maternal chest segmented QRS-complexes. However, looking at the maternal chest and transabdominal bispectral diagonal slices, we observe lowering of the QRS peak frequency from 17 Hz to 15 Hz.

A possible cause of this shifting in the QRS-complex frequency peak is the susceptibility and lack of predictability of the bispectral representation of highly-complex multi-frequency signals. As reported in [5], during labour contractions the presence of very strong deterministic and chaotic signals emanating from the uterus, and the accompanying motion artefacts result in highly dimensional transabdominal signals [5]. Consequently it is very difficult to isolate with integrity the maternal and fetal QRS-complex spectral peaks without first resorting to super-resolution algorithms using eigenvector-based projections as will be revealed in Chapter Six.

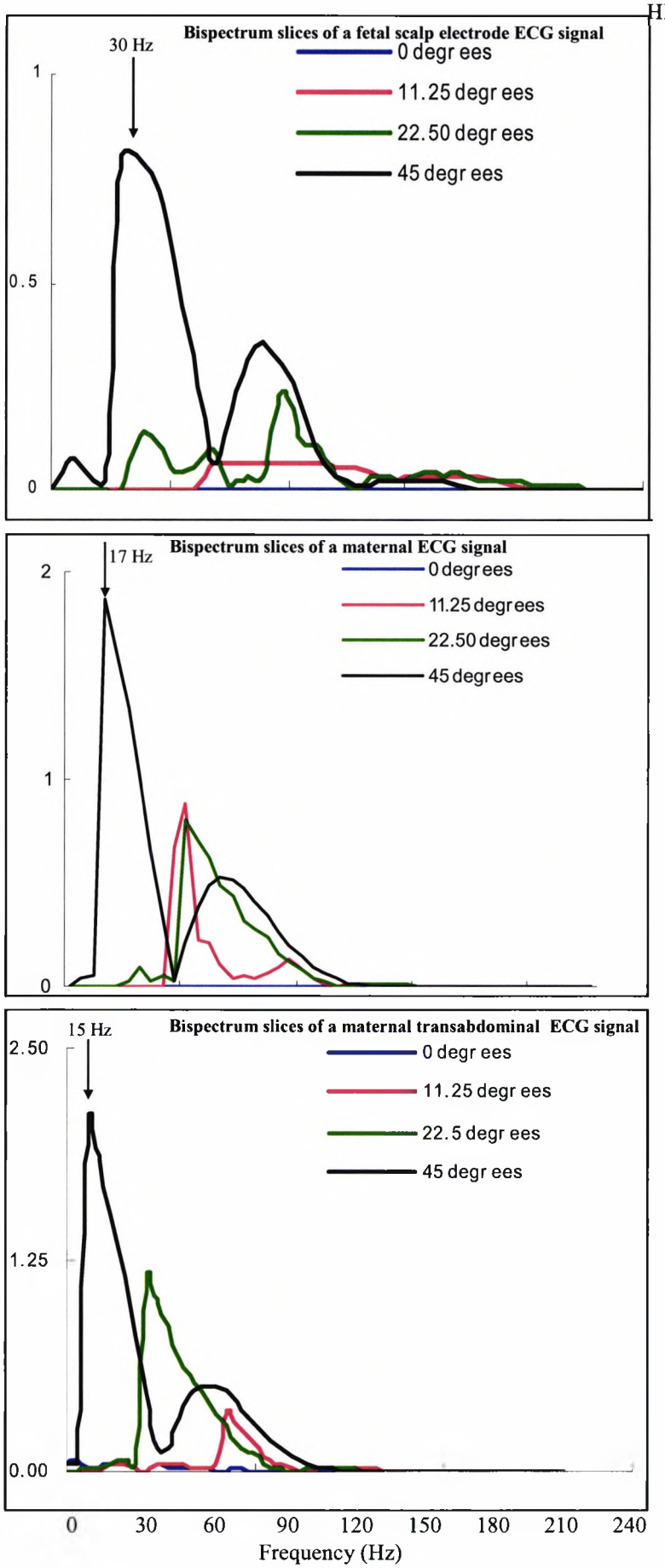

Figure 2.12: *Bispectrum slices at 0º (wall), 11.25º , 22.50º, and 45º (diagonal) for 250 msec segments of; fetal cardiac cycle using fetal scalp electrode (upper panel), maternal chest cardiac cycle (middle panel), and maternal transabdominal cardiac cycle (lower panel). The maternal cardiac cycle begins 50 msec before the R-wave and ends 50 msec before the next R-wave. The subject is at the first stage of labour, 40 weeks gestation. (code: 5-1).*

2.10 Non-linearity of ECG Signals

The non-linearity in the ECG signal can be detected using the bicoherence squared. Figure 2.13 depicts the bicoherence squared and their corresponding contour maps using one cardiac cycle for a fetal scalp electrode, maternal chest, and maternal transabdominal ECG. The bicoherence squared has peaks at the frequency pairs of (6 Hz,15 Hz) and (14 Hz,14 Hz) for the fetal scalp cardiac cycle, (15 Hz,15 Hz) for the maternal chest cardiac cycle, and (7.5 Hz,7.5 Hz) for the maternal transabdominal cardiac cycle. These bicoherence peaks support non-linearity.

2.11 The effect of proximity of the mother's and fetal non-linear QRS- complexes

There is a general consensus that individual cardiac cycles are locally stationary. This will be substantiated in Appendix A4 by the Hinich test [8]. However, when applying a highly dimensional signal such as the transabdominal ECG that has several individual non-linear and deterministic signals overlapping both in the time and frequency domains, all coexisting in a cocktail of noise and motion artefact, it is prudent to re-examine the validity of the stationarity assumption in relation to such signals. It is only natural to expect that the proximity of two non-linear signals such as the mother's and fetal QRS-complexes would result in non-linear (quadratic and higher-order) coupling and this in turn would invoke non-stationarity. This has already been the subject of several investigations [60] and it is beyond the scope of this thesis.

This section, however, demonstrates the above to be true by inspecting the bispectral OT region shown in Figure 2.14. Shown in the Figure are two typical transabdominally-measured maternal ECG cycles, ((a1), (a2)), and two synchronised fetal scalp ECG cycles ((b1), (b2)). The lower parts of the Figure, (c1) and (c2), consist of the corresponding maternal bispectral contour maps at a level of -30 dB. The two R-waves of the maternal and fetal QRS-complexes in (a1) and (b1), respectively, are separated by 200 msec. The resultant bispectrum in (c1) does not support the OT region. However, the situation is totally different when the two R-waves are as close as 35 msec as shown in Figure 2.14 (a2) and (b2). Now the OT region of the bispectrum in (c2) is fully occupied and non-stationary. This means we cannot use conventional signal processing techniques to separate the mother's and fetal QRS-complexes. This problem has been adequately solved by linearising (at least removing the quadratic coupling) the

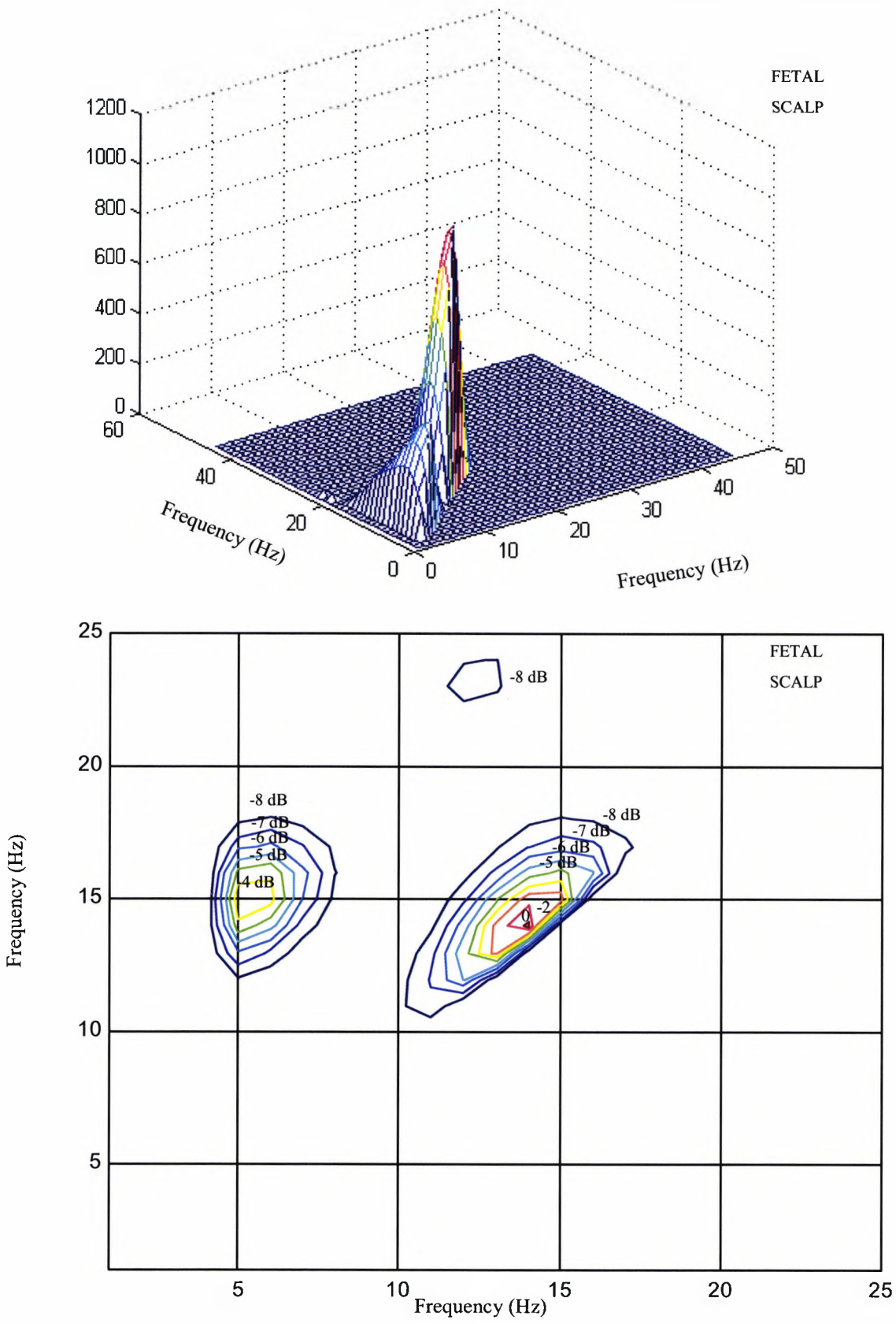

(a)

Figure 2.13: *The bicoherence squared (upper panel) and contour map (lower panel) for (a) a fetal cardiac cycle using fetal scalp electrode (data length 550 msec), (b) a maternal chest cardiac cycle (data length 1000 msec), and (c) a maternal transabdominal cardiac cycle (data length 1000 msec). The maternal cardiac cycle begins 50 msec before the R-wave and ends 50 msec before the next R-wave. The subject is at the first stage of labour, 40 weeks gestation. The bispectrum is calculated using the direct method. A Hanning window is used to calculate the bispectrum which is averaged for smoothing. (Code: 5-51).*

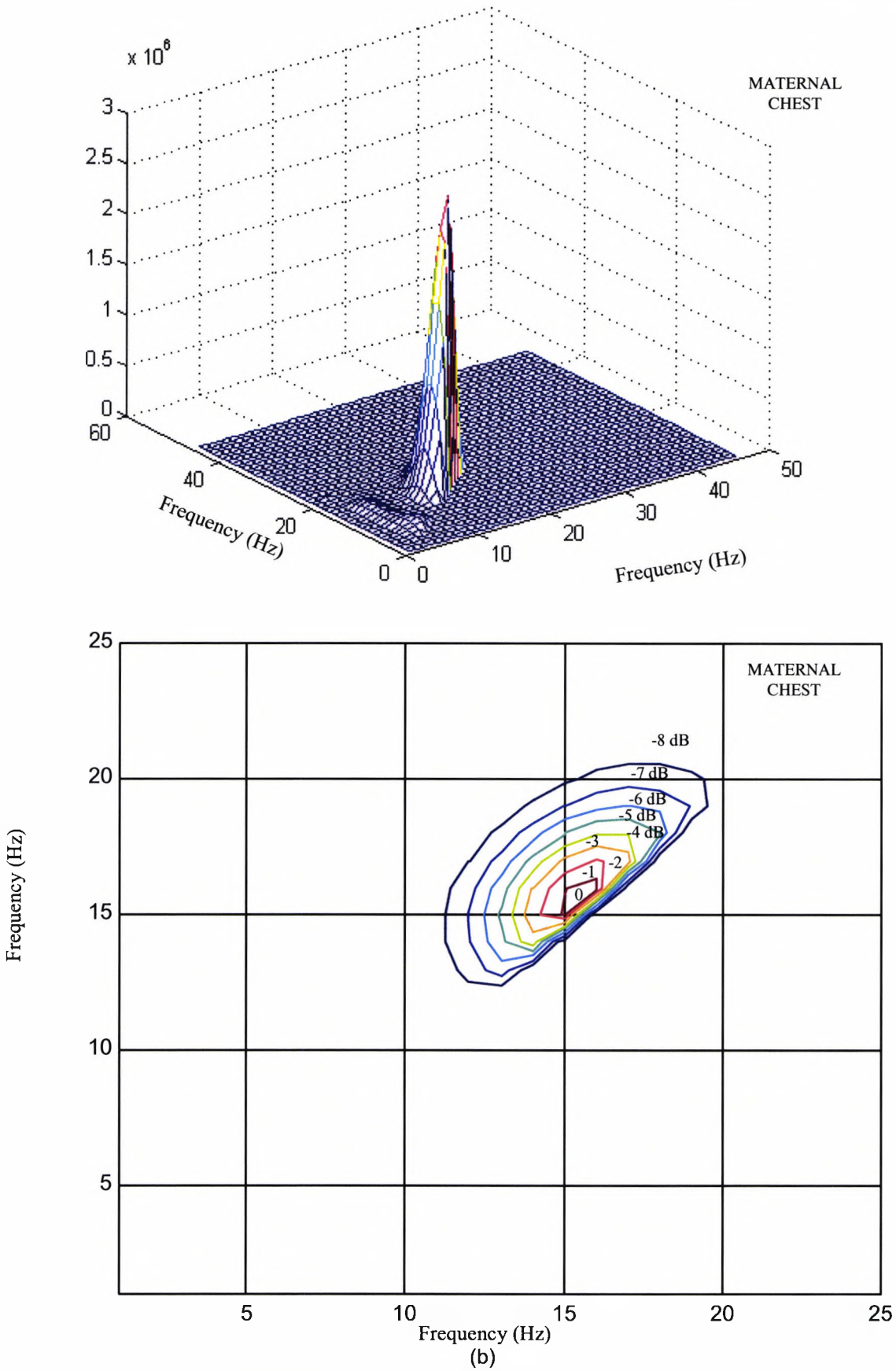

Figure 2.13 *(continued): The bicoherence squared (upper panel) and contour map (lower panel) for (a) a fetal cardiac cycle using fetal scalp electrode (data length 550 msec), (b) a maternal chest cardiac cycle (data length 1000 msec), and (c) a maternal transabdominal cardiac cycle (data length 1000 msec). The maternal cardiac cycle begins 50 msec before the R-wave and ends 50 msec before the next R-wave. The subject is at the first stage of labour, 40 weeks gestation. The bispectrum is calculated using the direct method. A Hanning window is used to calculate the bispectrum which is averaged for smoothing. (Code: 5-51).*

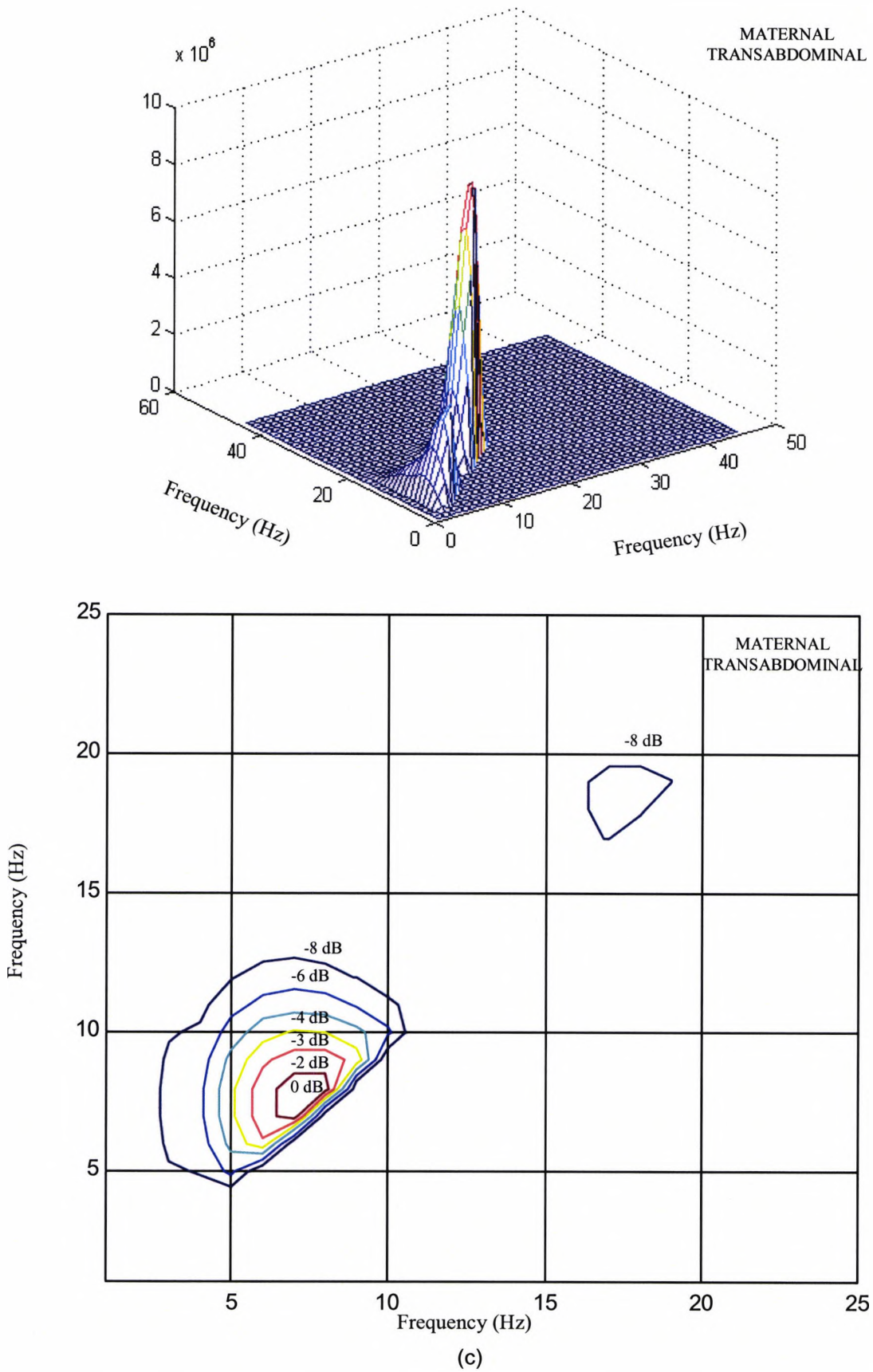

Figure 2.13 *(continued): The bicoherence squared (upper panel) and contour map (lower panel) for (a) a fetal cardiac cycle using fetal scalp electrode (data length 550 msec), (b) a maternal chest cardiac cycle (data length 1000 msec), and (c) a maternal transabdominal cardiac cycle (data length 1000 msec). The maternal cardiac cycle begins 50 msec before the R-wave and ends 50 msec before the next R-wave. The subject is at the first stage of labour, 40 weeks gestation. The bispectrum is calculated using the direct method. A Hanning window is used to calculate the bispectrum which is averaged for smoothing. (Code: 5-51).*

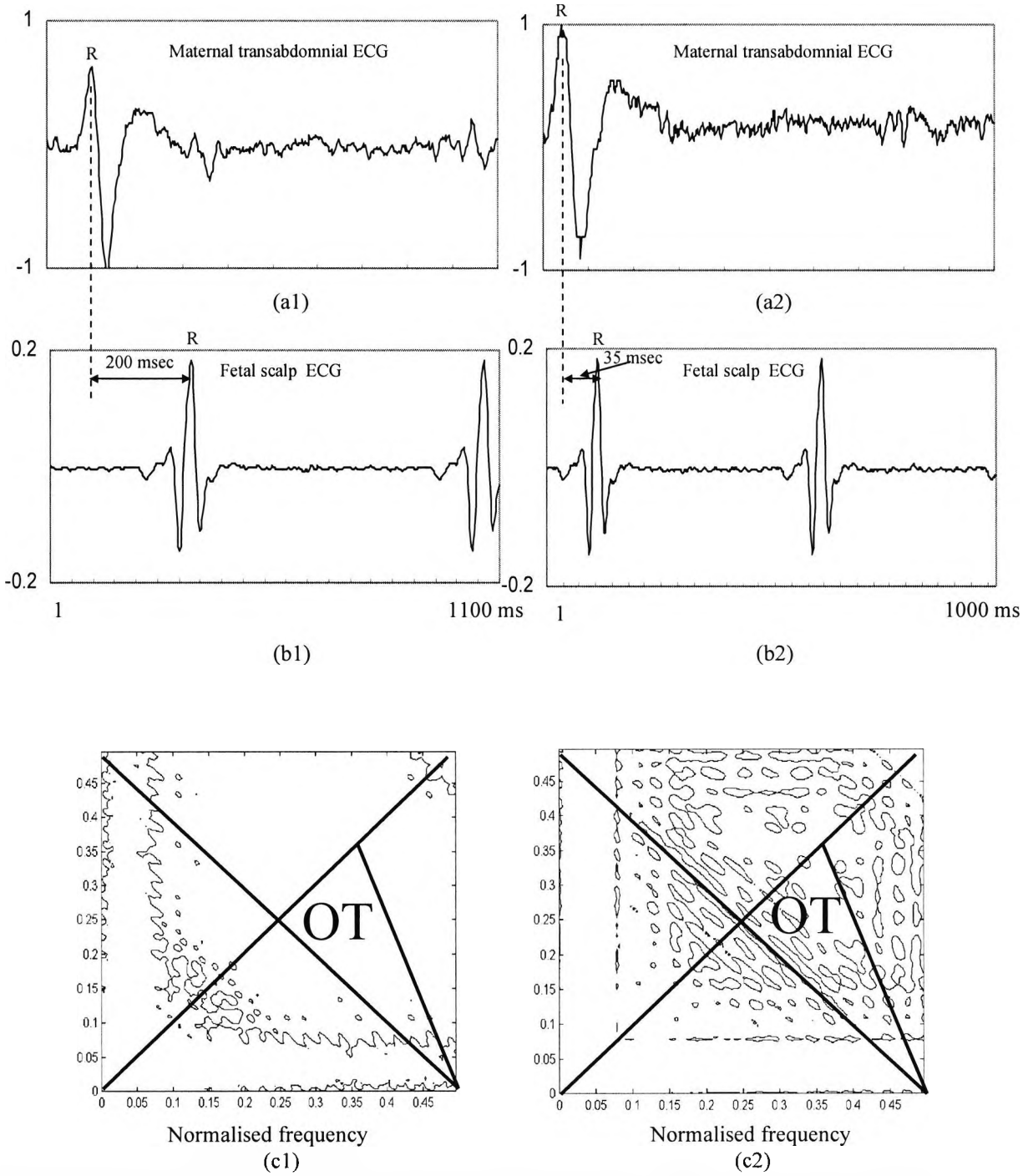

Figure 2.14: *(a1), (a2) Two typical examples of maternal transabdominal cardiac cycles, (b1) and (b2) are the corresponding fetal ECG signal using fetal scalp electrode. The first fetal QRS-complex in (b1) is separated from the maternal QRS-complex in (a1) by 200 msec. The first fetal QRS-complex in (b2) is separated from the maternal QRS-complex in (a2) by 35 msec. The corresponding bispectrum contour maps at a level of -30 dB for the two cycles in (a1) and (a2) are shown in (c1) and (c2), respectively. The R-wave of the first fetal QRS-complex in (b1) is separated from the R-wave of the maternal QRS-complex in (a1) by 200 msec. The corresponding bispectrum in (c1) does not show extra activity in the OT region. The R-wave of the first fetal QRS-complex in (b2) is separated from the R-wave of the maternal QRS-complex in (a2) by 35 msec. The corresponding bispectrum in (c2) shows extra activities in the OT region due to non-linear coupling between the mother and the baby. The maternal cardiac cycle begins 50 msec before the R-wave and ends 50 msec before the next R-wave. The subject is at the first stage of labour, 40 weeks gestation. Fetal cardiac cycle data length is 550 msec, and transabdominal ECG cardiac cycle data length is 1000 msec. (Code: (a) 5-1, (b) 5-31).*

transabdominal signal before attempting to separate individual QRS-complexes (Chapters Four, Five and Six).

2.12 Cumulants and Bispectra of noise components

The MIT/BIH NSR and AR databases [51-52] have recordings of the three main types of noise in ECG signals, namely, (a) baseline wander, (b) electromyographic (EMG) noise, and (c) motion artefact. The following statistics help in the processing stages of the fetal heartbeat detection. It will be shown in later chapters that, when using super-resolution techniques the requirement for Gaussian and non-Gaussian extraction and suppression is eliminated except for the conventional removal of baseline wander which is embedded in all data acquisition systems (baby monitors).

(a) Baseline Wander noise

Figure 2.15 depicts second- and third-order statistics of a baseline wander noise segment of 10,000 samples (approximately 30 sec) extracted from the MIT/BIH NSR and AR databases. Both the bispectrum and the bicoherence squared show high peaks at low frequencies (< 5 Hz). This means that the effect of the baseline wander noise on both maternal and fetal QRS-complexes at 15 Hz and 30 Hz, respectively, is not significant. However, it is prudent to eliminate such noise in the pre-processing stage. One conventional method of eliminating baseline wander employs a high-pass filter such as Butterworth high-pass filter of order 5, cut-off frequency of 1 Hz, a transition period of 1 Hz, a minimum ripple of –50 dB outside the main frequency lobe. As mentioned in Section 1.6.2, the frequency range of the baseline wander is 0 - 0.5 Hz.

(b) Electromyographic noise

Figure 2.16 shows some statistics of an electromyographic (EMG) noise segment of 10,000 samples extracted from the MIT/BIH NSR and AR databases. The noticeable feature is that the bispectrum is confined to low frequencies less than (10 Hz,10 Hz). This means that it will not interfere with the isolation of the adult QRS-complex bispectrum peak which occupies frequencies between (15 Hz,15 Hz) and (20 Hz,20 Hz), provided that an appropriate super-resolution technique is employed. But the bicoherence squared of the EMG noise is spread over a wide band of frequencies, up to (120 Hz ,120 Hz). The carpet effect of the non-linearity attributed to the EMG noise will be eliminated by linearising the transabdominal signal prior to fetal QRS-complex

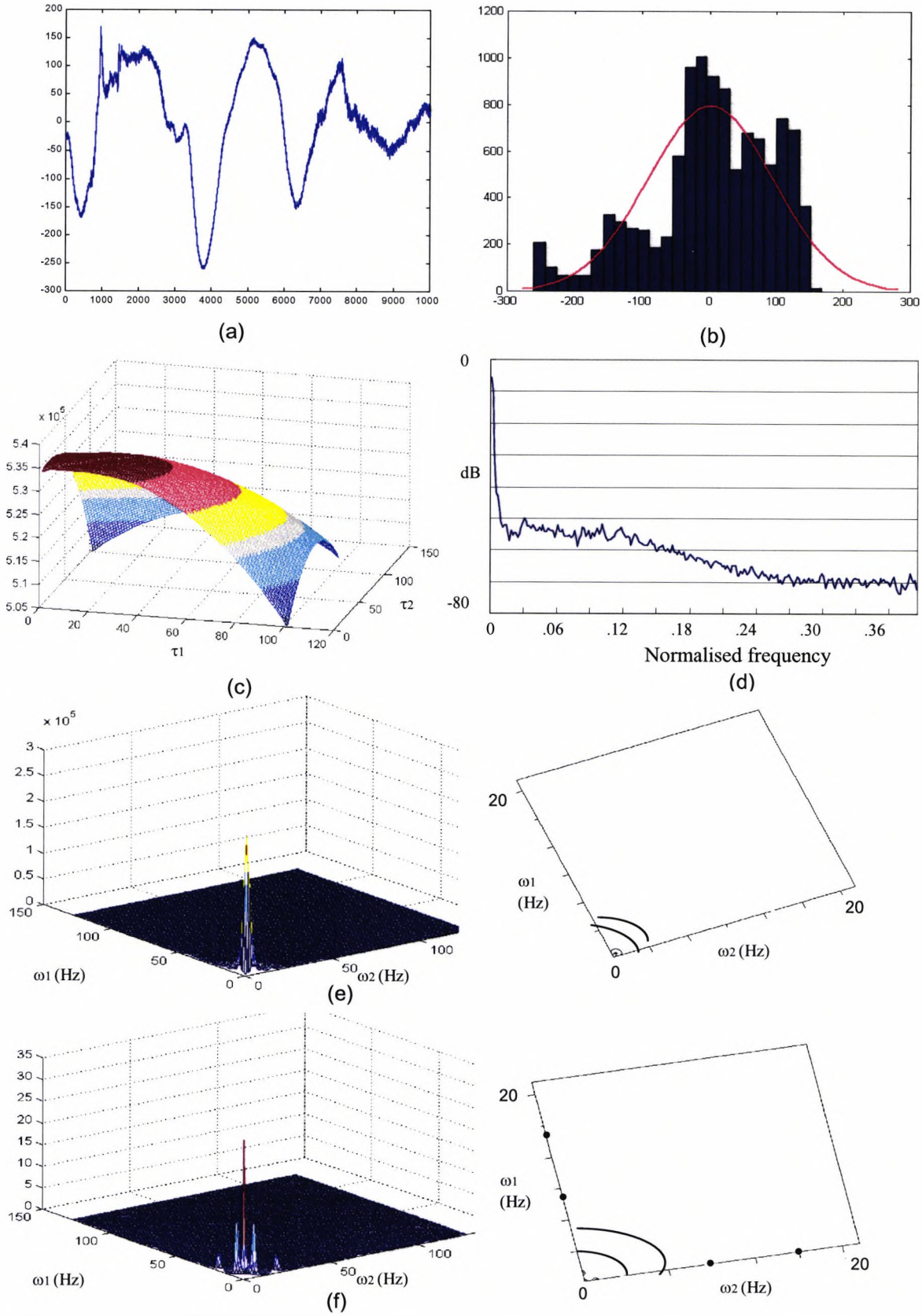

Figure 2.15: *Characterisation of 10,000 samples of baseline wander noise extracted from the MIT/BIH database and sampled at 360 samples per second. (a) time series, (b) its histogram showing non-Gaussian pdf, (c) third-order cumulants, (d) power spectrum using the averaged periodogram method, (e) the bispectrum (l.h.s.) calculated using the direct method with contour maps (r.h.s.) and (f) the bicoherence squared (l.h.s.) with contour maps (r.h.s.).*

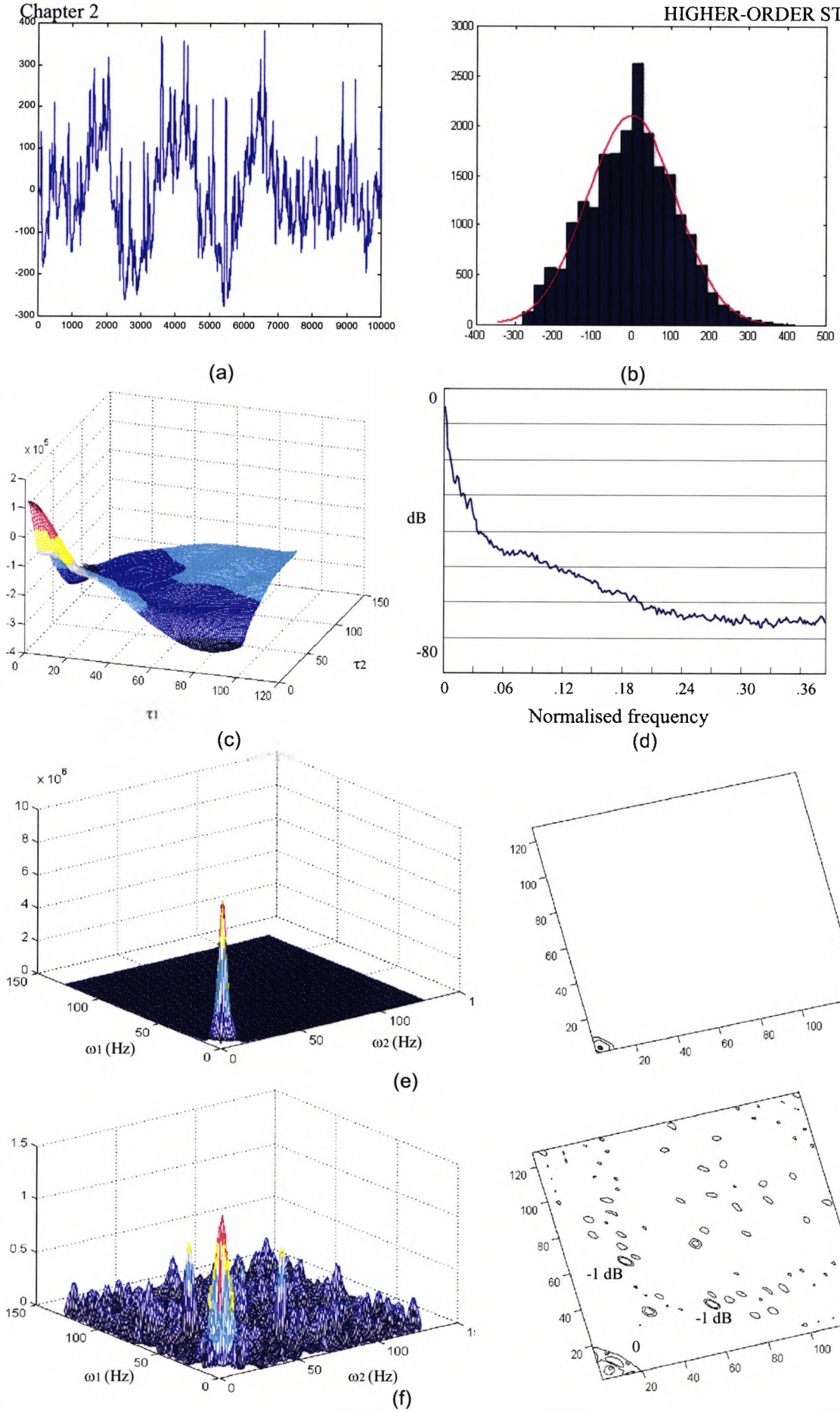

Figure 2.16: *Characterisation of 10,000 samples of electromyographic noise extracted from the MIT/BIH database and sampled at 360 samples per second. (a) time series, (b) its histogram, showing non-Gaussian pdf,(c) third-order cumulants, (d) power spectrum using the averaged periodogram method, (e) the bispectrum (l.h.s.) calculated using the direct method with contour maps (r.h.s.) and (f) the bicoherence squared (l.h.s.) with contour maps (r.h.s.).*

detection in the third-order statistical domain. Under broad signal and noise conditions, linearisation of the transabdominal ECG signal not only removes to a great extent the signal non-linearity, but also partially eliminates other types of non-linearity due to noise.

(c) Motion artefact noise

Figure 2.17 depicts second- and third-order statistics of a motion artefact noise segment of 10,000 samples extracted from the MIT/BIH NSR and AR databases. The bispectrum has many frequencies in the triangle region of (0 Hz,0 Hz), (0 Hz,35 Hz) and (35 Hz,0 Hz). These bispectral frequencies of motion artefact would be overlapping with those of the maternal and fetal QRS-complexes, albeit at around –20 dB level. However, the level of noise at the QRS-complex spectra is comparatively small and it will be shown in Chapter Six that the effect of motion artefact on the detection of QRS-complexes is not noticeable. Figure 2.17 (f) reveals that the bicoherence squared is rather confined to very low frequencies. As mentioned above, linearisation plays a definitive role.

2.13 Discussions

The objective of this chapter is to introduce the subject of higher-order statistics (HOS) and its applications to the non-linear / non-Gaussian ECG signals encountered in this thesis. This is to pave the way for employing HOS-based techniques as the solution to the formidable problem of transabdominal fetal heartbeat detection during labour. Indeed, high detection rates can be accomplished by invoking the HOS-based techniques, namely, the third-order cumulant or the **TOC template matching** and the bispectral contours template matching which is abbreviated as the **BIC template matching**, and which utilises a set of different levels of bispectral contours.

The key question we attempt to answer at this juncture is why do HOS-based techniques yield the highest possible FHRs? The reasons behind achieving high FHRs when using the HOS-based well-refined techniques are; (1) Under broad signal and noise conditions, higher-order cumulants and their spectra become high signal-to-noise ratio domains where detection, parametric estimation and signal classification can be performed. (2) The Gaussian noise diminishes in the HOS domains if the data length is adequate. We have found that for ECG signals a minimum length of 1 sec is sufficiently

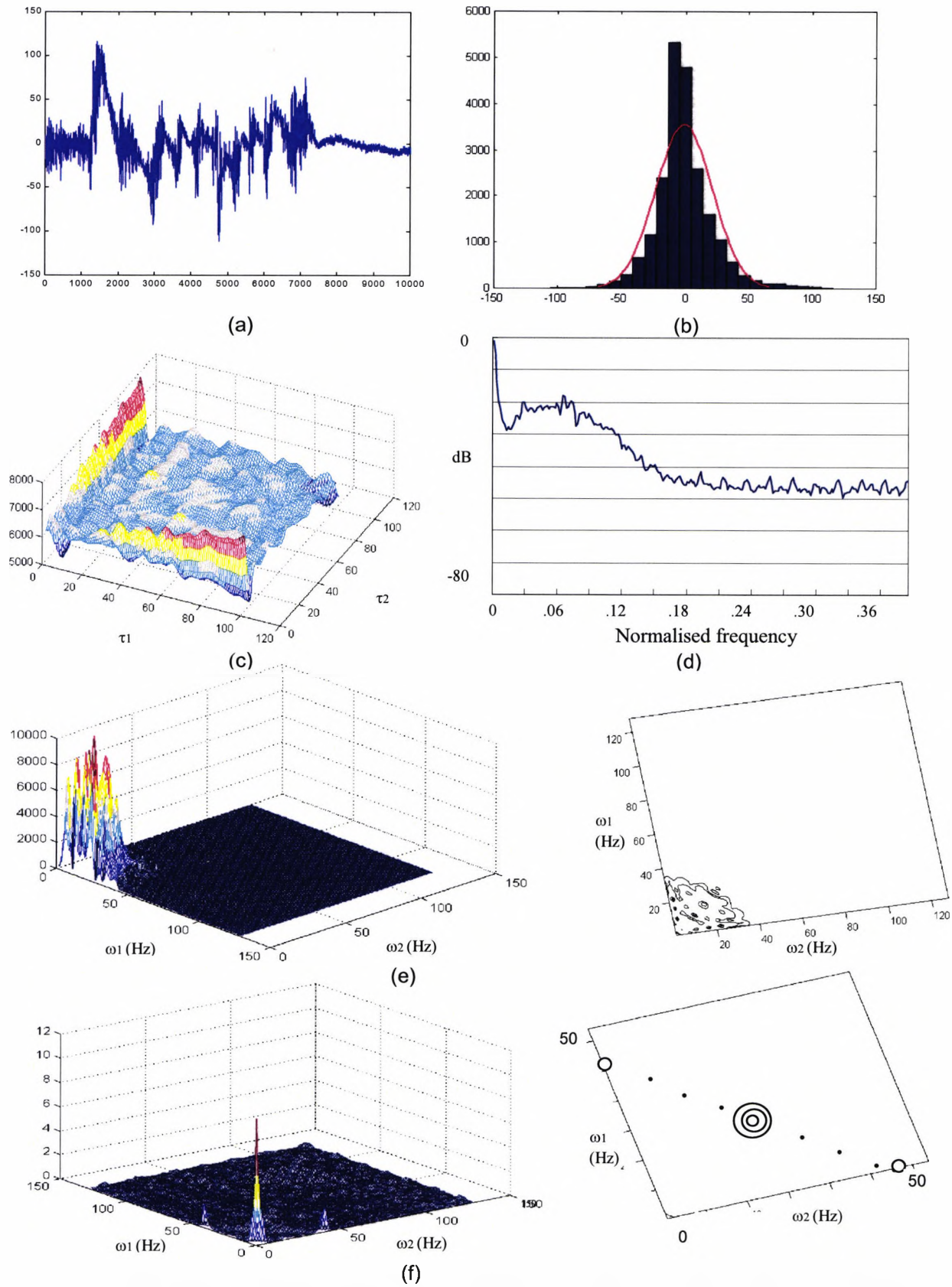

Figure 2.17: *Characterisation of 10,000 samples of motion artefact noise extracted from the MIT/BIH database and sampled at 360 samples per second. (a) time series, (b) its histogram, showing non-Gaussian pdf,(c) third-order cumulants, (d) power spectrum using the averaged periodogram method, (e) the bispectrum (l.h.s.) calculated using the direct method with contour maps (r.h.s.) and (f) the bicoherence squared (l.h.s.) with contour maps (r.h.s.).*

long to suppress Gaussian noise and maintain a low level of HOS variances in the HOS domains, whilst not sufficiently long to violate Hinich's criterion for "local" stationarity. (3) In the third-order domain all sources of noise with symmetric probability density functions (pdfs), e.g., Gaussian and uniform, will vanish. The ECG signals are retained because they have non-symmetric distributions. This implies that it is more than adequate to utilise only the TOCs and their bispectrta. There is no need to seek higher-than-third-order statistics as implicated in all the Independent Component Analysis applications to FHR detection. (4) The mother's QRS- and the fetal QRS-bispectral contours, which are used as the discriminant patterns in the identification and classification, only overlap with the bispectra of the baseline wander and that of the EMG at very low levels (around –20 dB normalised to the peak of the maternal QRS-complex bispectrum). Therefore, it is comparatively easy to detect and classify QRS-complexes in ECG signals utilising either the **TOC** or the **BIC** template matching techniques.

Detection key operations

Apart from the initial ECG pre-processing and critical segmentation the following key operations are performed;

(1) Signal linearisation as a key step in the identification and classification process

The ECG signals are inherently non-linear. They exhibit quadratic, cubic and higher-order non-linearities supported by the third-, fourth-, and higher-order cumulants. However, using TOC- and BIC-templates could compromise the identification and classification of the mother's QRS- or the fetal QRS-complexes. Because the inherent ECG non-linearities can at certain levels interact with the non-linearity of the physical channel, particularly, when there are strong uterine activities and this results in serious distortions to the individual TOC or BIC discriminant patterns. This could result in a significant mismatch when using the TOC or BIC templates to identify the maternal and the fetal QRS-complexes in transabdominally-measured ECG signals. It is, therefore, very important to remove, as much as possible, all types of non-linearities in the transabdominally-measured ECG signals and leave only the "refined" linear non-Gaussian components. This will be appreciated in later chapters.

The types of non-linearity of individual ECG signals, namely, the maternal chest full cardiac cycle, the fetal scalp electrode full cardiac cycle, and the maternal

transabdominally-measured full cardiac cycle, have been first identified and quantified using the bicoherence squared and subsequently removed using the adaptive non-linear Volterra filtering structures. Essentially, now all attention is given to the detection of QRS-complexes that are almost linear non-Gaussian in the presence of linear non-Gaussian noise.

(2) Data scenarios

Multi-dimensional TOCs were computed for the above ECG signals (full cardiac cycles) as well as for the four segments of the maternal transabdominal cardiac cycles. The four segments were coded as I, II, III, and IV, each of length 250 msec which, as mentioned earlier, must satisfy the two criteria of HOS low variance and pseudo-stationarity. It is interesting to report that the four coded segments have often ascribed to one of the following scenarios;

Scenario 1:

(I) Segment I, 0 – 250 msec; Predominantly maternal QRS-interval (no fetal heartbeat present),

(II) Segment II, 251 msec – 500 msec; The first fetal heartbeat with maternal contribution,

(III) Segment III, 501 msec – 750 msec; QRS-free ECG, and

(IV) Segment IV, 751 msec – 1000 msec; The second fetal heartbeat with maternal contribution.

Scenario 2:

(I) Segment I, 0 – 250 msec; Both maternal and fetal QRS-complexes,

(II) Segment II, 251 msec – 500 msec; QRS-free ECG,

(III) Segment III, 501 msec – 750 msec; The second fetal heartbeat with maternal contribution, and

IV) Segment IV, 751 msec – 1000 msec; Either QRS-free ECG or possibly the third fetal heartbeat with maternal contribution.

Obviously noise and uterine contractions are present in all transabdominally-measured ECG signals. The above critical segment length assumes, on average, a mother heart rate (MHR) of 60 bpm. For faster or slower MHR, the segment length is adaptively decreased or increased accordingly in order to accommodate any such variations in MHR. Obviously, any reduction below the critical window length of 250 msec would

result in an increase of the HOS variance. In the worst reported case by 0.5 dB for MHR = 100 bpm.

(3) Direct computations of individual 1-d TOC slices

It is also shown that, having computed the two-dimensional TOC, either the diagonal or the wall slice or a combination of the diagonal and wall slices is used in the detection / classification process. Therefore, computing the full multi-dimensional TOC and then extracting individual slices is an unnecessary waste of the CPU time. So, why not compute any arbitrary 1-d slice directly without firstly having to compute the two-dimensional TOC and secondly extract the 1-d slice? In fact, the TOC-diagonal and the TOC-wall slices are straightforward to compute directly, by freezing one of the two cumulant lags and changing the other one. However, to compute any other arbitrary slice requires the development of an *auxiliary algorithm* which is described in Chapter Four, and to my knowledge it has not been previously reported in the relevant literature. It has been found that performing direct computations of the 1-d TOC slices instead of computing the 2-d TOC firstly, and secondly extracting individual 1-d slices results in saving of more than 99% of the CPU time. The same applies to the 2–d bispectrum. However, it has to be borne in mind that it is the matching of the horizontal bispectral contours that will be used in the BIC template matching technique instead of the 1-d polar bispectral slices. Because in order to use the 1-d polar bispectrum slices effectively one needs to use a minimum of 24 polar slices so as not to miss the capturing of rapid changes or null features in the bispectrum that could be used as discriminant patterns. Whereas for BIC contours the number of discriminant horizontal slices required for detection / classification does not exceed 10.

Bispectral features of QRS-complexes

The power spectrum of appropriately sampled ECG showed the QRS-complex principal peak in the frequency range from 15 Hz to 20 Hz, and 25 Hz to 40 Hz, for the mother's chest ECG and fetal scalp electrode ECG, respectively. Unfortunately, the power spectrum has limitations as an estimator in terms of resolution, variance, and clarity of the spectrum to be able to produce clear and distinguishable peaks for the P-waves. Therefore, an alternative spectrum estimator was used instead, namely, the multiple signal classification (MUSIC) pseudo-spectrum. In separate publications [62-65], the MUSIC-based pseudo-spectrum also showed that the principal peaks for the p-waves

occupy a range from 5 Hz to 8 Hz for adults. The principal peaks for the P-waves of the fetal scalp electrode ECG occupy a range from 8 Hz to 10 Hz. The same MUSIC-based spectral estimators have revealed high local energy peaks around 5 Hz due to motion artefact.

As with cumulants, their bispectra were computed for the above mentioned ECG data samples and segmentations using the direct method which involves calculating a two-dimensional Fourier transform. The following bispectral peaks have been observed only on the bispectral diagonal slice;

(1) At (17 Hz,17 Hz) and (15 Hz,15 Hz) for the maternal chest and the transabdominal ECGs, respectively. So, there is a shift in the bispectral peak from 17 Hz to 15 Hz in the transabdominal ECG.

(2) At (30 Hz,30 Hz) and less prominently at (20 Hz,20 Hz) for the fetal scalp electrode ECG.

Quadratic coupling in transabdominally measured ECG signals

It has been found in maternal transabdominal ECG signals that close proximity of the mother's and fetal QRS-complexes initiates additional quadratic and higher-order non-linearities that could be due to higher-order "coupling" or mixing of the mother's and fetal own harmonics and the concomitant mixing of the ECG signals and the non-linear uterine contraction interference signal. This so called "coupling" between mother's and fetal ECGs was mentioned in [60] and manifested in a newly formed bicoherence squared peak(s) which did not exist in either of the isolated mother's bicoherence squared or the isolated fetal bicoherence squared computed form their respective ECG signals. The non-linear second-order or third-order Volterra structure has been used [60] to quantify the effect of this coupling, in part. The rest of the quantification process is carried out using the bicoherence squared.

Although it is beyond the scope of this thesis, it is worth mentioning that, depending on the bispectrum estimation method employed, the techniques for the detection and quantification of quadratic phase coupling are divided into two categories: the conventional and the parametric. Conventional techniques are based on the bicoherence spectrum and they are better qualifiers of the phase coupling [29, 66]. However, their resolution is limited by the "uncertainty principle" of the Fourier transform. On the other

hand, parametric techniques are based on the auto-regressive (AR) modelling of the third-order cumulants. Although the parametric AR methods are not good quantifiers, they possess a high-resolution capability, much higher than the frequency resolution of the conventional methods [10, 38]. The so-called "coupling" results in non-stationarity in the transabdominal ECG signal. This is evidenced by the filling of the bispectrum OT region which is used as a measure of non-stationarity in non-Gaussian signals (see Figure 2.3).

Noise identification in male and non-pregnant female adults

For noise identification and characterisation in the third-order domain, good use is made of the MIT/BIH NSR and AR databases [51-52]. Apart from Gaussian noise, there exist three types of non-Gaussian noise in ECG signals, namely, baseline wander, electromyographic (EMG), and motion artefact noise. 10,000 samples of each of these three types of noise are analysed. A brief summary of their second- and third-order statistics is shown in Table 2.1.

The effect of the baseline wander noise on both the maternal and the fetal QRS-complexes at 17 Hz and 30 Hz, respectively, is not significant. We can see from Table 2.1 that only the bispectrum of the motion artefact and the bicoherence squared of the EMG noise have frequencies that would potentially overlap with those of the QRS-complexes of the mother and the fetal, albeit at –20 dB level. Again referring to the MIT/BIH NSR and AR databases, the bicoherence squared of the EMG noise is spread over a wide band of frequencies, up to (120 Hz ,120 Hz). The carpet effect of the non-linearity attributed to the EMG noise will be significantly reduced by linearising the transabdominal signal prior to fetal QRS detection in the third-order statistical domain. Under broad signal and noise conditions, linearisation of the transabdominal ECG signals not only removes to a great extent the signal non-linearity, but also partially eliminates other types of non-linearity due to noise or non-linearity due to strong uterine contractions.

Also, we can deduce from Table 2.1 that there would be overlapping between the bispectral frequencies of motion artefact and those of the maternal and the fetal QRS-complexes, albeit at around –20 dB level. However, the level of noise at the QRS-complex spectra is comparatively small and it will be shown in Chapter Six that by

Noise type / 2nd & 3rd order statistics	Baseline wander	Electromyographic	Motion artefact
pdf	Non-symmetric	Non-symmetric	Non-symmetric
3rd order cumulants	Support	Support	Support
Bispectrum	Frequencies < 5 Hz	Frequencies < 10 Hz	Frequencies < 35 Hz
Bicoherence Sq.	Frequencies < 5 Hz	Frequencies < 120 Hz	Frequencies < 5 Hz

Table 2.1: *Summary of second- and third-order statistics of three types of noise in ECG signals, namely, baseline wander, electromyographic noise, and motion artefact.*

using QRS-complex tailor-made spectral windows, the effect of motion artefact on the detection of the QRS-complexes is not noticeable.

2.14 References

[1] V. Kravtchenko-Berejnoi et al., "On the use of tricoherent analysis to detect nonlinear wave-wave interactions," Signal Processing, vol. 42, pp. 291-309, 1995.

[2] P. A. Delaney and D. O. Walsh, "A Bibliography of Higher-Order Spectra and Cumulants," IEEE Signal Processing Magazine, pp. 61-70, July 1994.

[3] C. L. Nikias and A. P. Petropulu, *Higher Order Spectra Analysis: A Nonlinear Signal Processing Framework*, Prentice Hall, 1993.

[4] S. W. Nam and E. J. Powers, "Application of Higher Order Spectral Analysis to Cubically Non-Linear System Identification," IEEE Transaction on Signal Processing, vol. 42, No. 7, pp. 1746-1765, July 1994.

[5] M Sabry-Rizk, W Zgallai, E. R. Carson, K. T. V. Grattan, A. MacLean, and P.

Hardiman Non-linear dynamic tools for characterising abdominal electromyographic signals before and during labour. Trans Inst Measurement and Control, vol. 22, pp. 243-270, 2000.

[6] R. O. Schmidt, *A Signal Subspace Approach To Multiple Emitter Location And Spectral Estimation*, PhD Dissertation, Department of Electrical Engineering, Stanford University, USA, 1981.

[7] M. J. Hinich, "Testing for Gaussianity and Linearity of a Stationary Time Series," Journal of Time Series Analysis, vol. 3, No. 3, pp. 169-176, 1982.

[8] M. J. Hinich, "Test for Gaussianity and linearity of a stationary time series," Journal of Time Series Analysis, vol. 3, No. 3, pp. 169-176, 1982.

[9] Y. Nagata, "Lag joint probability, higher-order covariance function and higher-order spectrum," Bulletin de la socie'te' Franco-Japonaise d'oceanographic, vol. 8, Part 2, pp. 78-94, May 1970.

[10] C. L. Nikias and M. R. Raghuveer, "Bispectrum estimation: A digital signal processing framework," IEEE Proceedings, vol. 75, No. 7, pp. 869-891, July 1987.

[11] M. Rosenblatt, *Statistical Sequences and Random Fields*, Birkhauser, USA, 1985.

[12] D. R. Brillinger, "An Introduction to Polyspectra," Annals of Mathematical Statistics, vol. 36, pp. 1351-1374, 1965.

[13] L. Pflug, G. E. Ioup, J. W. Ioup, and R. L. Field, "Properties of Higher-Order Correlations and Spectra for Bandlimited, Deterministic Transients," Journal of the Acoustical Society of America, vol. 91, No. 2, pp. 975-988, February 1992.

[14] C. L. Nikias, "ARMA bispectrum approach to nonminimum phase system identification," IEEE Transaction on Acoustics, Speech, and Signal Processing, vol. ASSP-36, pp. 513-524, April 1988.

[15] G. B. Giannakis and J. M. Mendel, "Identification of nonminimum phase systems using higher-order statistics," IEEE Transaction on Acoustics, Speech, and Signal Processing, vol. ASSP-37, pp. 360-377, March 1989.

[16] B. Friedlander and B. Porat, "Performance analysis of MA parameter estimation algorithms based on higher-order moments," Proceedings of IEEE International Conference on Acoustics, Speech and Signal Processing (ICASSP), pp. 2412-2415, NY, April 1988.

[17] M. Huzzi, "Estimation of coefficients of an autoregressive process by using higher order moments," Journal of time series analysis, vol. 2, pp. 87-93, 1981.

[18] J. K. Tugnait, "Fitting non-causal autoregressive signal plus noise models to noisy non-Gaussian linear processes," IEEE Transactions on Automatic Control, vol. AC-32, pp. 547-552, June 1987.

[19] J. K. Tugnait, "On selection of maximum cumulant lags for non-causal autoregressive model fitting," Proceedings of IEEE International Conference on Acoustics Speech, and Signal Processing (ICASSP), pp. 2372-2375, NY, April 1988.

[20] K. S. Lii, "Non-Gaussian ARMA model identification and estimation," Proceedings of Business and Economics Statistics, ASA, pp. 135-141, 1982.

[21] G. B. Giannakis and A. Swami, "New results on state-space and input-output identification of non-Gaussian processing using cumulants," Proceedings conference of the International Society of Optical Engineers, vol. 826, CA, 1987.

[22] J. M. Mendel, "Use of Higher Order Statistics in Signal Processing and System Theory: An Update," Proceedings of SPIE, vol. 975, Advanced Algorithms and Architectures for Signal Processing III, pp. 126-144, 1988.

[23] J. M. Mendel, "A Compendium of New Theoretical Results Associated with Using Higher-Order Statistics in Signal Processing and System Theory," *in Spectral Analysis in One and two dimensions*, pp. 163-182, August 1990.

[24] J. M. Mendel, "Tutorial on Higher Order Statistics (Spectra) in Signal Processing and System Theory: Theoretical Results and Some Applications," Proceedings of the IEEE, vol. 79, No. 3, pp. 278-305, March 1991.

[25] P. Huber, B. Kleiner, and T. Gassar, "Statistical methods for investigating phase relations," IEEE Transactions on Audio and Electroacoustics, vol. 19, pp. 78-86, 1971.

[26] K. Lii, M. Rosenblatt, and C. Van Atta, "Bispectral Measurements in Turbulence," Journal of Fluid Mechanics, vol. 77, pp. 45-62, 1976.

[27] C. Van Atta, "Inertial Range Bispectra in Turbulence," The Physics of Fluids, vol. 22, pp. 1440-1442, 1979.

[28] K. Helland, K. Lii, and M. Rosenblatt, "Bispectra and Energy Transfer in Grid-Generated Turbulence," in *Developments in Statistics*, vol. 2, (P. Krishnaiah, ed.), Academic Press, NY, pp. 125-155, 1979.

[29] Y. Kim and E. Powers, "Digital Bispectral Analysis of Self-Excited Fluctuation Spectra," The Physics of Fluids, vol. 21, pp. 1452-1453, 1978.

[30] M. J. Hinich and C. S. Clay, "The Application of the Discrete Fourier Transform

in the Estimation of Power Spectra, Coherence, and Bispectra of Geophysical Data," Review of Geophysics, vol. 6, pp. 347-363, 1968.

[31] M. Rosenblatt, "Cumulants and Cumulant Spectra," in *Handbook of Statistics*, vol. 3, (D. Brillinger, and P. Krishnaiah, eds.), Amesterdam, Holland, pp. 369-387, 1983.

[32] T. Subba Rao, "The Bispectral Analysis of Nonlinear Stationary Time Series with Reference to Bilinear Time Series Models," in *Handbook of Statistics*, vol. 3, (D. Brillinger, and P. Krishnaiah, eds.), Amesterdam, Holland, pp. 293-319, 1983.

[33] D. R. Brillinger and M. Rosenblatt, "Asymptotic Theory of Kth Order Spectra," in *Spectral Analysis of Time Series* (B. Harris, ed.), pp. 189-232, Wiley, NY, 1967.

[34] M. Rosenblatt, *Stationary sequences and random fields*, Burkhauser, 1985.

[35] I. G. Zurbenko, *The spectral analysis of time series*, Ch. 6, North-Holland Series in Statistics and Probability, vol. 3, pp. 169-176, 1982.

[36] P. L. Brockett, M. J. Hinich, and D. Patterson, "Bispectral-Based Tests for the Detection of Gaussianity and Linearity in Time Series," Journal of the American Statistical Association, vol. 83, No. 403, pp. 657-664, 1988.

[37] M. J. Hinich and G. R. Wilson, "Detection of Non-Gaussian Signals in Non-Gaussian Noise Using the Bispectrum," IEEE Transactions on Acoustics, Speech, and Signal Processing, vol. 38, No. 7, pp. 1126-1130, July 1990.

[38] M. R. Raghuveer and C. L. Nikias, "Bispectrum estimation via parametric modeling," Signal Processing, Special issue on modern trends of spectral analysis, vol. 10, pp. 35-48, Jan. 1986.

[39] R. Pan and C. L. Nikias, "The Complex Cepstrum of Higher-Order Cumulants and Nonminimum Phase System Identification," IEEE Transactions on Acoustics, Speech, and Signal Processing, vol. ASSP-36, pp. 186-205, February 1988.

[40] A. Petropulu and C. L. Nikias, "The Complex Cepstrum and Bicepstrum: Analytic Performance Evaluation in Additive Gaussian Noise," IEEE Transactions on Acoustics, Speech, and Signal Processing, vol. 38, No. 7, pp. 1246-1256, July 1990.

[41] C. L. Nikias and F. Liu, "Bicepstrum computation based on second- and third-order statistics with applications," Proceedings of IEEE International Conference on Acoustics Speech, and Signal Processing, ICASSP, pp. 2381-2385, April 1990.

[42] A. W. Lohmann and B. Wirnitzer, "Tripple correlations," Proceedings of IEEE, vol. 72, pp. 889-901, July 1984.

[43] H. O. Bartlett, A. W. Lohmann, and B. Wirnitzer, "Phase and amplitude recovery

from bispectrum," Applied Optics, vol. 23, pp. 3121-3129, September 1984.

[44] N. Pan and C. L. Nikias, "Phase reconstruction in the trispectrum domain," IEEE Transactions on Acoustics, Speech, and Signal Processing, vol. ASSP-35, pp. 895-897, June 1987.

[45] A. Petropulu and C. L. Nikias, "Signal reconstruction from phase of the bispectrum," IEEE Transactions on Signal Processing, vol. SP-40, No. 3, pp. 601-610, March 1992.

[46] M. Sabry-Rizk, D. Romare, W. Zgallai, K. T. V. Grattan, P. Hardiman, and J. O'Riordan, "Higher order statistics (HOS) in signal processing: Are they of any use?," IEE Colloquium, Digest #111, pp. 1/1-1/6, London, May 1995.

[47] M. Sabry-Rizk, W. Zgallai, S. El-Khafif, E. Carson, and K. Grattan, "Higher-Order Ambulatory Electrocardiogram Identification and Motion Artifact Suppression With Adaptive Second- and Third-Order Volterra Filters," SPIE98 Advanced Signal Processing Algorithms, Architectures, and Implementations VIII, vol. 3461, pp. 417-431, San Diego, USA, 19-24 July 1998.

[48] M. Sabry-Rizk, W. Zgallai, S. El-Khafif, E. Carson, K. Grattan, P. Thompson, "Highly Accurate Higher Order Statistics Based Neural Network Classifier of Specific Abnormality in Electrocardiogram Signals," IEEE International Conference on Acoustic Speech and Signal Processing, ICASSP99, vol. II, Speech processing II Audio and Electrtoacoustics Neural Networks for Signal Processing, pp. 1033-1036, USA, 15-19/3/1999.

[49] H. Pozidis and A. Petropulu, "Use of selected HOS information for low variance estimate of bandlimited systems with short data records," ICASSP, IEEE International conference on Acoustics, Speech and Signal Processing, paper #DSP11.5, Seattle, Washington, USA, May 1998.

[50] M. Sabry-Rizk, W. Zgallai, "Higher Order Statistics Are Indispensable Tools in The Analysis of Electrocardiogram Signals," IEE Colloquium on Statistical Signal Processing, January 1999.

[51] MIT/BIH Database: ECG Database Applications Guide, 10th Edition, 1997. Harvard-MIT Division of Health Sciences and Technology, MIT Room 20A-113, Cambridge, MA 02139, USA.

[52] MIT/BIH Database: ECG Database Programmer's Guide, 9th Edition, 1997. Harvard-MIT Division of Health Sciences and Technology, MIT Room 20A-113, Cambridge, MA 02139, USA.

[53] A. Swami and J. M. Mendel, "Time and lag recursive computation of cumulants from a state space model," USC-SIPI Report 121, Los Angeles, CA, 1988; also in IEEE Transactions on Automatic Control, January 1990.

[54] J. W. Brewer, "Kronecker products and matrix calculus in system theory," IEEE Transactions on Circuits and systems, Vol. 25, pp. 772-781, 1978.

[55] P. Carre, H. Leman, C. Fernandez, and C. Marque, "Denoising of the uterus EHG by an undecimated Wavelet transform," IEEE Transactions on Biomedical Engineering, Vol. 45, No. 9, pp. 1104-1113, September 1998.

[56] M. Sabry-Rizk, W. Zgallai, E. R. Carson A. MacLean, K. T. V. Grattan, "Multi-fractility in Fetal Heart Beat Dynamics," 2nd European Medical & Biological Engineering Conference Vienna (Austria), December 04-08, 2002.

[57] M. Sabry-Rizk, W. Zgallai "Novel Volterra Predictor Based on State-Space Equilibrium of Nonlinear Single- or Multi-Fractal Signals" SPIE's 45th Annual Meeting, the International symposium on Optical Science and Technology, SPIE2000, Advanced Signal Processing Algorithms, Architectures, and Implementations X, USA, vol. 4116, pp. 322-333, 30/7-4/8/2000.

[58] W. Zgallai, M. Sabry-Rizk, P. Hardiman, and J. O'Riordan, "Third-order cumulant signature matching technique for non-invasive fetal heart beat identification," ICASSP, IEEE International Conference on Acoustics, Speech, and Signal Processing, vol. 5, pp 3781-3784, Germany, 1997.

[59] P. L. Brockett, M. J. Hinich, and D. Patterson, "Bispectral-Based Tests for the Detection of Gaussianity and Linearity in Time Series," Journal of the American Statistical Association, vol. 83, No. 403, pp. 657-664, 1988.

[60] M Sabry-Rizk, W. Zgallai, A. McLean, E. R. Carson, and K. T. V. Grattan, "Virtues and Vices of Source Separation Using Linear Independent Component Analysis for Blind Source Separation of Non-linearly Coupled and Synchronised Fetal and Mother ECGs," IEEE Engineering in Medicine and Biology Conference, USA, 2001.

[61] W. J. Tompkins, *Biomedical digital signal processing*, Prentice Hall, 1993.

[62] W. Zgallai, M. Sabry-Rizk, P. Hardiman, and J. O'Riordan, "MUSIC-based bispectrum detector: A novel non-invasive detection method for overlapping fetal and mother ECG," Proceedings of the 19th IEEE International Conference on Engineering in Medicine and Biology, EMB, pp. 72-75, USA, October 1997.

[63] M. Sabry-Rizk, W. Zgallai, C. Morgan, S. El-Khafif E. R. Carson, and K. T. V.

Grattan, "Novel decision strategy for P-wave detection utilising nonlinearly synthesised ECG components and their enhanced pseudospectral resonances," IEE Proceedings Science, Measurement and Technology, Special section on Medical Signal Processing, vol. 147, No. 6, pp. 389-397, November 2000.

[64] M. Sabry-Rizk, W. Zgallai, E. R. Carson, S. El-Khafif, C. Morgan, and K. T. V. Grattan "Novel decision strategy for P wave detection utilising non-linearly synthesised ECG components and their enhanced pseudospectral resonances", IASTED-SIP 2001, Honolulu, Hawaii, USA, August 2001.

[65] M. Sabry-Rizk, W. Zgallai, E. R. Carson, S. El-Khafif, C. Morgan, and K. T. V. Grattan "Novel decision strategy for P wave detection utilising non-linearly synthesised ECG components and their enhanced pseudospectral resonances", IEE International conference, MEDSIP2000, Bristol, UK, September 2000.

[66] S. B. Kim and E. J. Powers, "Estimation of Volterra kernels via higher-order statistical signal processing," in *Higher order statistical signal processing*, (Boashash, Powers, and Zoubier, eds.), Ch. 7, pp. 213-267, 1995.

CHAPTER THREE

THE APLICATION OF ADAPTIVE LMS- AND LMF-BASED SECOND- AND THIRD-ORDER VOLTERRA SYNTHESISERS TO ECG SIGNALS

3.1 Introduction

3.1.1 Aim

As mentioned in the previous chapters the maternal transabdominal ECG signal is non-Gaussian and possesses quadratic and cubic non-linearities. The contaminating noise contains Gaussian, non-Gaussian, and non-linear components. The maternal transabdominal ECG signal is a combined maternal and fetal ECG and there is also another formidable signal combined with it, namely, the uterine contraction interference signal (UCS) during labour. Each one of these three combined signals is non-linear by its own right. The objective of this chapter is to decompose the maternal transabdominal ECG signal into its linear, quadratic and cubic parts and retain only the linear part for further signal processing. A non-linear predictor / synthesiser is sought to carry out this task because employing a linear structure to cater for such non-linear signals would lead to a suboptimal solution. The predictor / synthesiser will try to model as faithfully as possible the linear, quadratic and cubic parts of the transabdominal ECG signal. This is done by predicting each sample of the maternal transabdominal full cardiac cycles before segmentation. The linear (and non-Gaussian) synthesised part of each segment of the maternal transabdominal cardiac cycle will be used for fetal heartbeat classification and detection in the following three chapters. In order to synthesise and linearise (retain only the linear part and remove the quadratic or the quadratic and cubic parts as applicable) the ECG signals, non-linear structures should be utilised. The main concern of this chapter, therefore, is to synthesise and linearise the fetal scalp electrode, the maternal chest, and more importantly the maternal transabdominal ECG signals using adaptive Least-Mean-Square- (LMS) and Least-Mean-Fourth-based (LMF), second- and

third-order Volterra structures. The reason for synthesising the fetal scalp electrode and maternal chest ECG signals is that they are used to create higher-order statistics templates to be used in conjunction with the first and second hybrid systems as it will be shown in Chapters Four and Five. In this thesis, the following abbreviations are followed;

LMSQV	LMS-based Quadratic (second-order) Volterra
LMFQV	LMF-based Quadratic (second-order) Volterra,
LMSCV	LMS-based Cubic (third-order) Volterra, and
LMFCV	LMF-based Cubic (third-order) Volterra,

The reason for applying an LMF-based filter to the above mentioned ECG signals is because it has the ability to track higher-order statistical variations while the LMS algorithm is limited to tracking variations in the second-order statistics domain only. The LMF algorithm is based on updating the error to the power four, which makes it converge faster than the LMS algorithm, which is based on updating the squared error. It will be shown that this is an advantage when dealing with ECG signals.

3.1.2 Layout of the Chapter

The structure of the chapter is as follows. First brief summaries of the standard LMS and LMF algorithms are given in Section 3.2. This is followed by descriptions of the LMS- and LMF-based second- and third-order Volterra structures in Section 3.3. Section 3.4.1 describes the model order selection criterion. Section 3.4.2 shows results of directly applying the LMS- and LMF-based adaptive algorithms to predict ECG signals (Figure 3.1), and assess the resultant mean-squared errors. Adaptive LMS-based second- and third-order Volterra structures are then applied to synthesise ECG signals in Section 3.4.3. The LMS- and LMF-based second- and third-order Volterra synthesisers are then applied to fetal scalp electrode, maternal chest, and maternal transabdominal ECG signals in Section 3.4.4. Conclusions are given in Section 3.5.

3.2 Adaptive LMS and LMF Algorithms

3.2.1 Background

Filtering implies extracting information from a signal at time t by using data before and including time t. Prediction, however, is aimed at deriving information about the signal

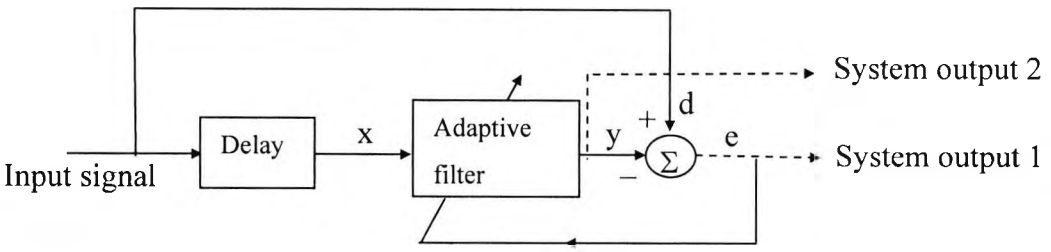

Figure 3.1: *Prediction as a basic class of adaptive filtering applications.*

at time $t + \Delta$ in the future by using data available before and including time t. The design of Wiener filters, which is a class of optimum linear discrete-time filters, requires prior information about the statistics of the data to be processed. However, adaptive filters do not require such information. For adaptive filters, the parameters of the filter are updated from one iteration to the next. The parameters become data dependent which makes it possible for the filter to perform satisfactorily in an environment where complete knowledge of the relevant signal statistics is not available. In a stationary environment, after successive iterations of the adaptive filtering algorithm it converges to the optimum Wiener solution in some statistical sense. In a non-stationary environment, the algorithm offers a tracking capability, whereby it can track time variations in the statistics of the input data, provided that the variations are sufficiently slow. Adaptive algorithms have fast speed of operation in terms of the CPU time and they are computationally efficient. There are four basic classes of adaptive filtering applications: (a) class I: identification; (b) class II: inverse modelling; (c) class III: prediction (see Figure 3.1); and (d) class IV: interference cancellation [31]. In this chapter the prediction operation will be considered.

The issue of prediction is one of the most basic and pervasive learning tasks. It is a temporal signal processing problem in that we are given a set of N past samples x(n-1), x(n-2), …, x(n-N) that are usually uniformly spaced in time, and the requirement is to predict the present sample x(n). Prediction may be solved using error-correction learning in a supervised manner in the sense that the training examples are drawn directly from the time series itself. Specifically, the sample x(n) serves the purpose of the desired response; hence given the corresponding prediction x(n) produced by the structure on

the basis of the previous samples x(n-1), x(n-2), ..., x(n-N), we may compute the prediction error as:

$$e(n) = x(n) - \hat{x}(n|n-1, \ldots, n-N), \tag{3.1}$$

and thus use the error-correction learning to modify the step-size parameter of the structure. Prediction may be viewed as a form of model building in the sense that the smaller we make the prediction error in a statistical sense, the better will the structure serve as a statistical model of the underlying process responsible for the generation of the time series. The problem of designing an optimum linear filter that provides the theoretical framework for linear adaptive filters was first conceived by Kolmogorov [71] and solved shortly afterwards independently by Wiener [72].

3.2.2 The Least-Mean-Square (LMS) Algorithm

The steepest descent adaptive filter, which is a gradient search technique, is an iterative procedure for obtaining the parameters that minimises a function. At each iteration of the steepest descent procedure, the values of the weights are modified in the direction in which the error function decreases most rapidly. According to the steepest descent algorithm, the weights of the filter assume time-varying form, and their values are adjusted in an iterative fashion along the error surface with the aim of moving them progressively towards the optimum solution. The LMS algorithm is a stochastic implementation of the method of the steepest descent. When the filter operates in an unknown environment, the exact measurements of the gradient vector are not possible since this requires a prior knowledge of both the autocorrelation and cross-correlation functions.

A standard linear LMS filter with transversal, tapped-delay, structure is shown in Figure 3.2. The output of the filter is related to its input by the relation:

$$y_{(n)} = \sum_{i=0}^{N-1} a_i x_{(n-i)} , \tag{3.2}$$

and the weights of the filter are updated using a standard LMS adaptation rule, which is

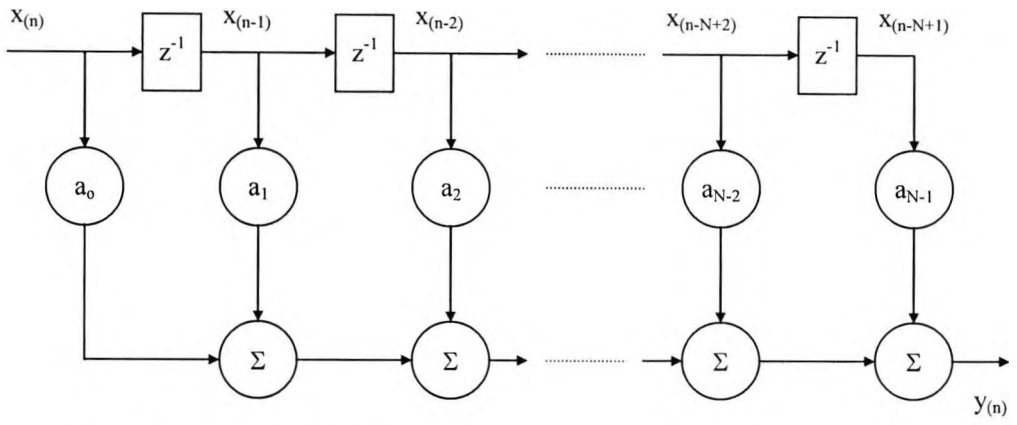

Figure 3.2: *A Transversal LMS Linear filter.*

derived from the Widrow-Hoff algorithm that uses an instantaneous estimation of the gradient.

$$\mathbf{a}(n+1) = \mathbf{a}(n) + 2\mu \quad e(n)x(n), \tag{3.3}$$

where $\mathbf{x}(n)$ is the input vector, $\mathbf{y}(n)$ is the output vector, $\mathbf{a}(n)$ is the N x 1 tap weight coefficients vector and μ is the step-size parameter. Figure 3.3 (a) shows a flowchart of the standard LMS algorithm. The LMS algorithm was introduced for adaptive noise cancellation [3]. Since then many variations and improvements were suggested and implemented. They show faster convergence or better tracking abilities. A thorough examination of the LMS performance analysis was provided in [6]. The LMS algorithm is not demanding in computational complexity. It is relatively simple to implement. The LMS does not require measurements of the pertinent correlation functions, nor does it require matrix inversion.

3.2.3 The least-mean-fourth (LMF) Algorithm

The least-mean-square (LMS) algorithm minimises the expected value of the squared difference between the estimated output and the desired response, i.e., $\{E\,|\,e(n)|^2\}$. A more general case is to minimise $E\{e(n)^{2N}\}$ [7]. This represents a general class of steepest descent algorithms for adaptive filtering which allow error minimisation in the mean fourth, sixth, .. etc. N = 1 is the Least-Mean-Square (LMS) and N = 2 is the Least-Mean-Fourth (LMF), which is summarised in Figure 3.3 (b). The LMF algorithm

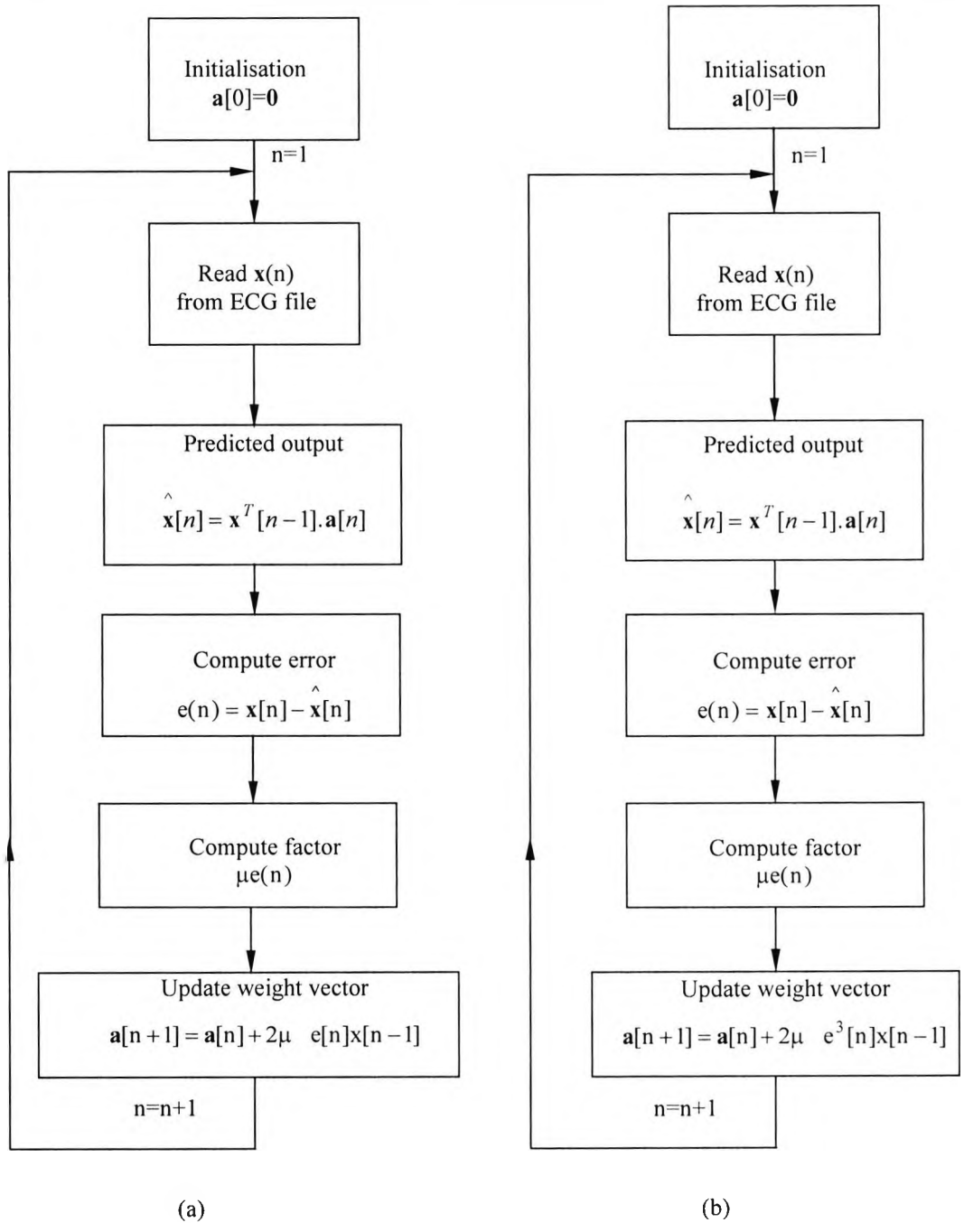

Figure 3.3: *Flowcharts of two adaptive prediction algorithms: (a) the LMS, and (b) the LMF.*

updates the weights as follows:

$$\mathbf{a}_i(n+1) = \mathbf{a}_i(n) + 2\mu_i \, .e^3(n).x(n). \tag{3.4}$$

The LMF has, in general, a faster convergence than the LMS algorithm. It has generally a lower weight noise than the LMS algorithm, with the same speed of convergence. It was shown to have 3 dB to 10 dB lower mean-squared error (MSE) than the LMS algorithm [7].

There are three parameters to optimise in order to achieve the best performance for ECG signals. These parameters are: the number of tap weight coefficients of the filter, N, the step size parameter, μ and the number of delay elements, Δ. The choice of the optimum values of these parameters is based, by and large, on trial and error. The optimum values are found in three steps. Each time two of the parameters are given fixed initial guesses and the third parameter is changed.

3.3 Volterra Structures

3.3.1 Background

Linear adaptive filters are based on the minimum mean-squared error criterion. The Wiener filter, that results from the application of such a criterion, can only relate to second-order statistics of the input data and no higher. This constraint limits the ability of a linear adaptive filter to extract information from the input data that are non-Gaussian. The use of a Wiener (linear) adaptive filter to extract signals of interest in the presence of non-Gaussian processes will yield sub-optimal solutions. We may overcome this limitation by incorporating some form of non-linearity in the structure of the adaptive filter. One type of adaptive non-linear filters is a Volterra filter. In Volterra filters, the non-linearity is localised at the front end of the filter. A non-linear adaptive filter may be decomposed into a non-linear Volterra expander followed by a linear FIR adaptive filter. The Volterra filter is attractive since it can deal with a general class of non-linear systems while its output is still linear with respect to its various higher-order system kernels or impulse responses. A formal solution to the optimum non-linear filtering problem is mathematically intractable. Nevertheless, in the 1950s a great deal of brilliant work was done by Zadeh [73], Wiener et al. [74] and others that did much to

clarify the nature of the problem. Gabor was the first to conceive the idea of a non-linear adaptive filter [75] and built such a filter [76]. Gabor proposed a shortcut through the mathematical difficulties of non-linear adaptive filtering by constructing a filter that optimises its response through learning. The output of the filter is expressed in the form

$$y(n) = \sum_{i_1=1}^{N} a^1_{i_1} x_{k-i_1+1} + \sum_{i_1=1}^{N}\sum_{i_2=1}^{N} a^2_{i_1,i_2} x_{k-i_1+1} x_{k-i_2+1} + \ldots. \qquad (3.5)$$

where x(0), x(1), …, x(N) are samples of the filter input. Nowadays, this polynomial is referred to as the Gabor-Kolomogrov polynomial or a discrete form of the Volterra series. The first term of the polynomial represents a linear filter characterised by a set of coefficients $\{a^1_{i1}\}$. The second term characterised by a set of dyadic coefficients $\{a^2_{i1i2}\}$ is non-linear; this term contains the products of two samples of the filter input, and so on for the higher-order terms. The coefficients of the filter are adjusted via gradient descent to minimise the mean squared value of the difference between a desired response d(n) and the actual filter output, y(n).

The Volterra series is a well-known method of describing non-linear dynamic systems. It is a generalisation of the Taylor series expansion of a function. However, the Volterra series has a drawback, which is the large number of parameters to be estimated leading to a large CPU time. The recent popularity of the Volterra filtering is due to the advancement in computer technology, which in turn allows one to estimate the relevant higher-order statistics required to calculate the higher-order Volterra kernels for non-linear systems [19-20]. The truncated Volterra series (the Volterra filter) is an attractive non-linear system representation because the parameters of this model are linearly related to the output.

Consider a single input single output discrete time-invariant system with non-linearities, a polynomial of order N and filter length M. The output Y_k is expressed in terms of the inputs x_k as follows:

$$Y_k = a^0 + \sum_{i_1=1}^{N} a_{i_1}^1 x_{k-i_1+1} + \sum_{i_1=1}^{N}\sum_{i_2=1}^{N} a_{i_1,i_2}^2 x_{k-i_1+1}x_{k-i_2+1} + \ldots.$$
$$+ \sum_{i_1=1}^{N}\ldots\sum_{i_N=1}^{N} a_{i_1,\ldots,i_N}^N x_{k-i_1+1}\ldots.x_{k-i_N+1} \qquad (3.6)$$

where $a^n_{i_1,\ldots,i_n}$, $i_1,\ldots,i_n \in \{1,\ldots M\}$ are referred to as the Volterra Kernels.

The Volterra non-linear system identification involves the estimation of the Volterra kernels in the time domain or the Volterra transfer functions in the frequency domain. The following section describes more realistic truncated second- and third-order Volterra structures.

3.3.2 Second- and third-order Volterra Structures

The basic Volterra structure as given below is a series of polynomial terms. These terms are formed from known values of a given time series $\{\mathbf{x}(n)\}$. Such series have been used widely in the field of system identification [21]. An estimate of x(n+1) can be derived via:

$$\hat{x}(n+1) = a_0 + \sum_{i_1=0}^{N-1} a_{i_1}^1 x_{n-i_1} + \sum_{i_1=1}^{N}\sum_{i_2=1}^{N} a_{i_1,i_2} x(n-i_1)x(n-i_2) + \ldots.$$
$$+ \sum_{i_1=1}^{N}\ldots\sum_{i_N=1}^{N} a_{i_1,\ldots,i_N} x(n-i_1)\ldots.x(n-i_N) \qquad (3.7)$$

where N is the number of samples. From Eq. (3.6) we can see that a second-order Volterra structure consists of a parallel combination of linear and quadratic filters and has the form of:

$$Y_k = a^0 + \sum_{i_1=1}^{N} a_{i_1}^1 x_{k-i_1+1} + \sum_{i_1=1}^{N}\sum_{i_2=1}^{N} a_{i_1,i_2}^2 x_{k-i_1+1}x_{k-i_2+1}\ . \qquad (3.8)$$

Based on Eq. (3.6), a third-order-order Volterra structure has the form of:

$$Y_k = a^0 + \sum_{i_1=1}^{N} a_{i_1}^1 x_{k-i_1+1} + \sum_{i_1=1}^{N}\sum_{i_2=1}^{N} a_{i_1,i_2}^2 x_{k-i_1+1}x_{k-i_2+1} + \sum_{i_1=1}^{N}\sum_{i_2=1}^{N}\sum_{i_3=1}^{N} a_{i_1 i_2, i_3}^3 x_{k-i_1+1}x_{k-i_2+1}x_{k-i_3+1} \quad (3.9)$$

From the structure of the series, it is evident that the number of terms involved will quickly become computationally unmanageable as p and N are increased. For p = 3, the number of terms $M_{\text{third-order Volterra}}$ grows as a cubic polynomial i.e.,

$$M_{\text{third-order Volterra}} = (6 + 11\,N + 6\,N^2 + N^3) / 6. \quad (3.10)$$

Rank deficiency is exploited in Appendix A4 to reduce redundancy in the number of Volterra coefficients and to reduce the CPU processing time without compromising the mean-squared error (MSE) threshold. A third-order Volterra structure is shown in Figure 3.4. Throughout this chapter, second- and third-order Volterra structures are used.

3.3.3 LMF-based second- and third-order Volterra synthesisers

Conventional methods of estimating the parameters of Volterra structures use the LMS algorithm to update the estimates. In this section, adaptive LMF-based second- and third-order Volterra structures are developed and then applied in Section 3.5 to fetal scalp electrode, maternal chest, and maternal transabdominal ECG signals. In the sequel, these filters will be referred to as second-order LMF-Volterra and third-order LMF-Volterra. The conventional adaptive LMS algorithm in the Volterra structure is replaced by an adaptive LMF algorithm. The linear, quadratic, and cubic weights of the LMF-based Volterra structure are updated as:

$$\mathbf{a}_{i_1}(n+1) = \mathbf{a}_{i_1}(n) + 2\mu_{i_1}.e^3(n).x(n) \quad (3.11)$$

$$\mathbf{a}_{i_1 i_2}(n+1) = \mathbf{a}_{i_1 i_2}(n) + 2\mu_{i_1 i_2}.e^3(n).x(n).x(n) \quad (3.12)$$

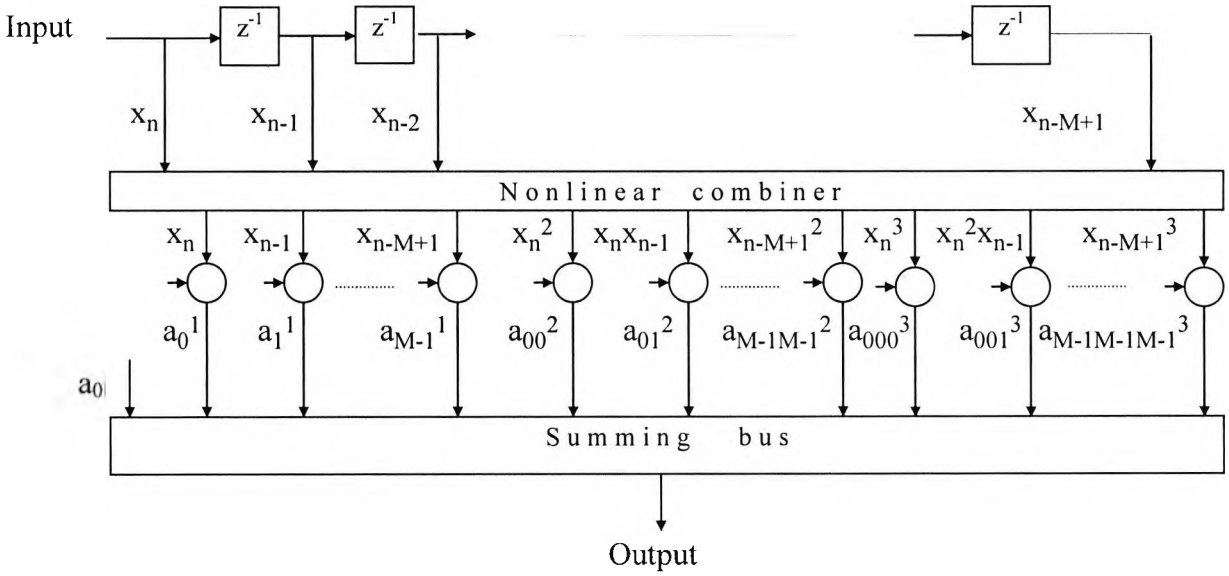

Figure 3.4: *A third-order Volterra structure.*

$$\mathbf{a}_{i_1i_2i_3}(n+1) = \mathbf{a}_{i_1i_2i_3}(n) + 2\mu_{i_1i_2i_3}.e^3(n).x(n).x(n).x(n) \tag{3.13}$$

The extension of the conventional LMS-based Volterra to the LMF-based Volterra is done to make use of the advantages of higher-order statistics, especially its robustness to Gaussian noise and its tracking capability in the higher-order statistics domain. The parameters of the LMF algorithm were optimised by trial and error to achieve the best performance in terms of the speed of convergence, minimum mean-squared error and tracking.

3.4 Results

3.4.1 Model order selection

The best choice of the filter order, N, is not generally known *a priori* and it is usually necessary to postulate several model orders then compute error criteria that indicate which model order to choose. One well-known criterion is the Akaike Information Criteria (AIC). The AIC determines the model order by minimising an information theoretic function

$$AIC(N) = N_d \ln(\hat{\rho}_N) + 2N \tag{3.14}$$

Where N_d is the number of data samples and ρ_N is the estimated white noise variance, the linear prediction error variance will be used for this estimate, $\hat{\rho}_m = \sum_t |e_m(t)|^2$.

Figure 3.5 shows the model order selection using Akaike Information Criteria (AIC) with values of AIC(N) plotted versus model orders for three transabdominally-measured cardiac cycles (data length 3000 msec). The step-size parameter is 0.03 for the linear adaptive LMS algorithm. The best order, or filter length, is to be chosen between 6 and 10. Three cardiac cycles were used so that the model order can be chosen within 3 sec to be able to start synthesising the ECG signal prior to any classification or detection.

3.4.2 Mean-squared error comparison of LMS- and LMF-based FIR predictors when applied to maternal transabdominal ECG signals

The LMS and LMF adaptive algorithms have been used in conjunction with an optimised FIR filter to predict the formidable maternal transabdominal ECG signal during the first stage of labour. Figure 3.6 (a-b) shows that the LMS algorithm takes about seven cardiac cycles to converge to a minimum mean-squared error (MSE) of 0.05. Figure 3.6 (c-d) shows that the LMF algorithm takes the same time to converge with a slightly smaller MSE of 0.04. The parameters of the LMS and LMF are, respectively, filter length = 10 and 23, delay = 4 and 6, and step-size parameter = 0.03, 0.008. The level of the errors at the output is –13 dB and -14 dB for the LMS and the LMF filters, respectively. Therefore, the LMF-based filter has a slightly better performance in terms of its mean-squared error for the same convergence time than that of the LMS-based filter.

3.4.3 LMS-based Volterra synthesiser when applied to fetal scalp, maternal chest, and maternal transabdominal ECG signals

In this section an LMS-based Volterra structure is used to decompose fetal scalp, maternal chest, and maternal transabdominal ECG signals into their linear, quadratic and cubic parts and the linear part only is retained for further analysis of the signal.

Figure 3.7 shows a third-order Volterra structure that represents the signal as linear, quadratic and cubic parts. The output is taken from the linear part to represent the linear

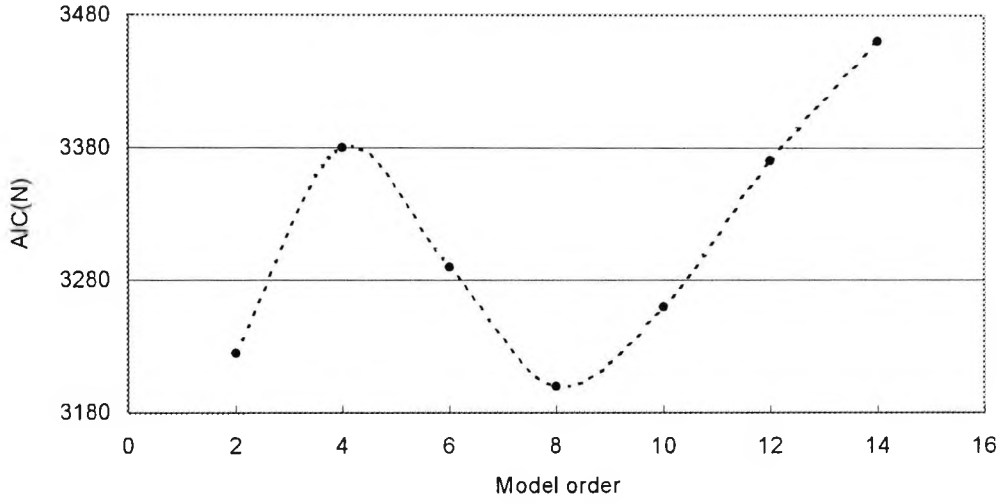

Figure 3.5: *Model order selection using Akaike Information Criteria (AIC). The values of AIC(N) are plotted against several model orders for three maternal transabdominal cardiac cycles (data length 3000 msec). The step-size parameter is 0.03 for the linear adaptive LMS-algorithm. Code: 5.*

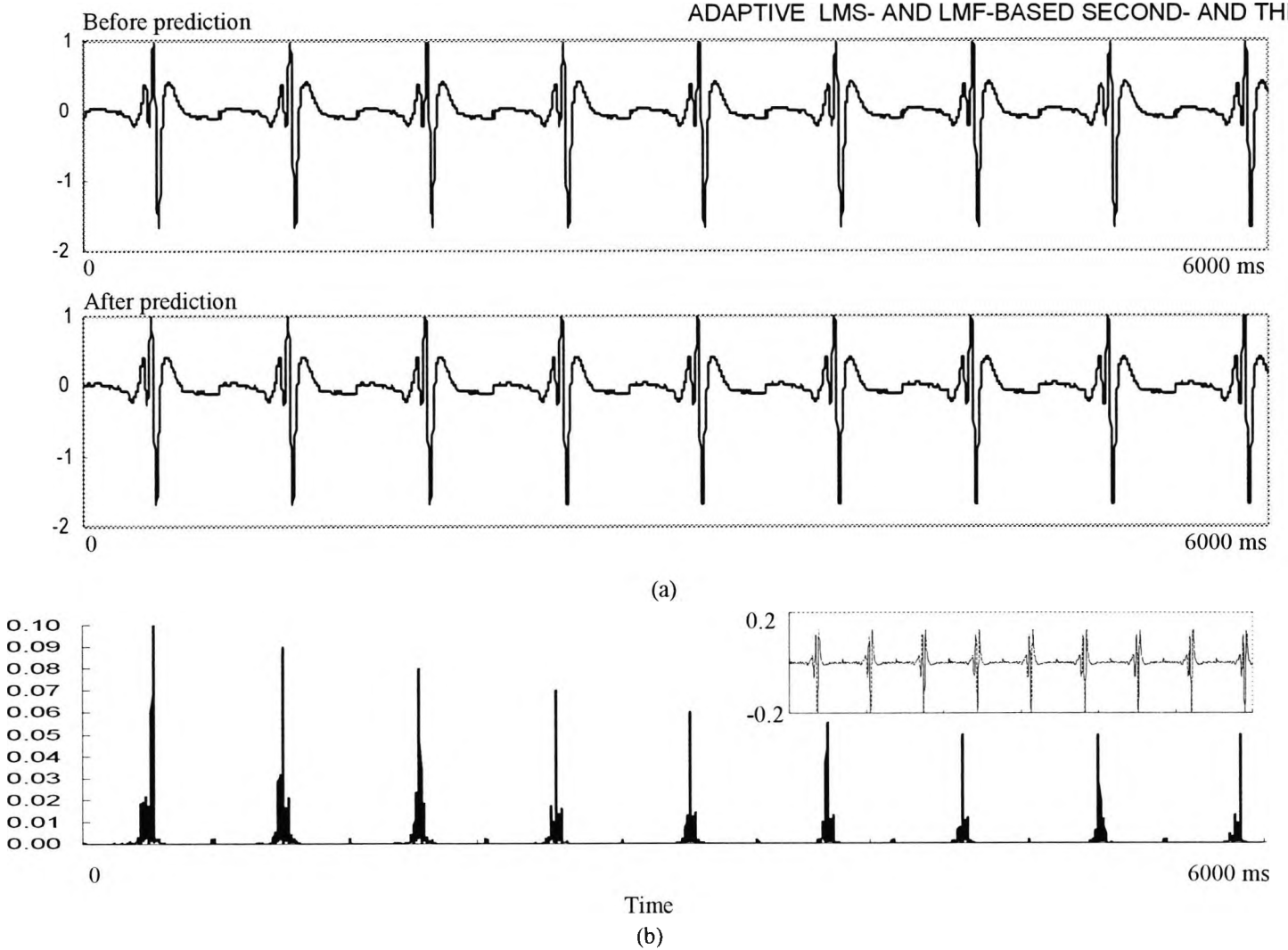

Figure 3.6: The application of the LMS and the LMF algorithms to eight maternal transabdominally measured cardiac cycles (twin surface electrodes). (a, c) Eight cardiac cycles before and after the application of the LMS and the LMF algorithms, respectively. (b, d) The mean-squared error of the eight cardiac cycles for the LMS and the LMF algorithms, respectively. The error signals are shown as insets. The optimised parameters are; The LMS filter: N = 6, μ = 0.03, Δ =2. The LMF filter: N = 8, μ = 0.04, Δ =3. The maternal cardiac cycle begins 50 msec before the R-wave and ends 50 msec before the next R-wave. The subject is at the first stage of labour, 40 weeks gestation. Code: 5-1-9.

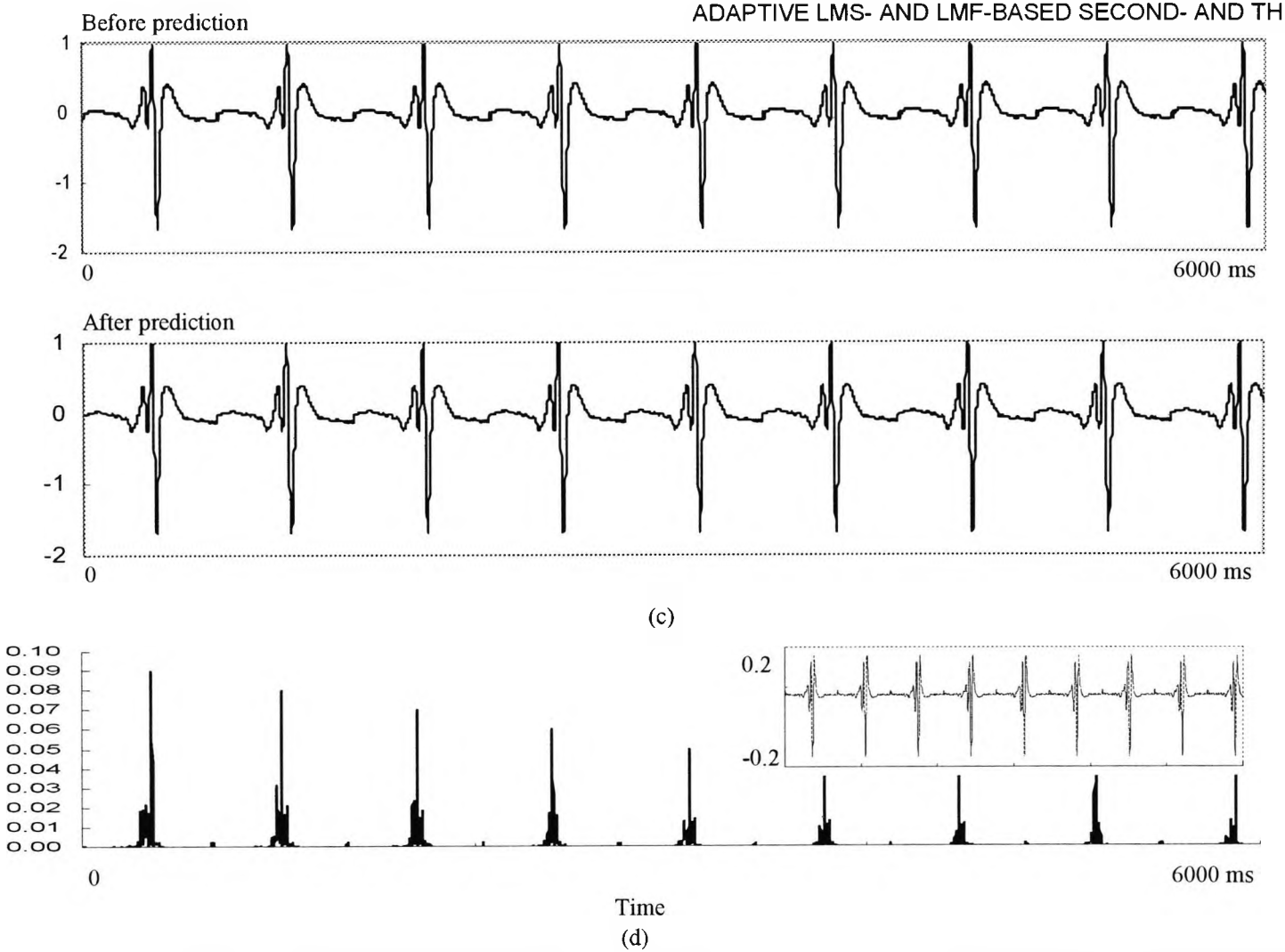

Figure 3.6 (continued): The application of the LMS and the LMF algorithms to eight maternal transabdominally measured cardiac cycles (twin surface electrodes). (a, c) Eight cardiac cycles before and after the application of the LMS and the LMF algorithms, respectively. (b, d) The mean-squared error of the eight cardiac cycles for the LMS and the LMF algorithms, respectively. The error signals are shown as insets. The optimised parameters are; The LMS filter: N = 6, μ = 0.03, Δ=2. The LMF filter: N = 8, μ = 0.04, Δ=3. The maternal cardiac cycle begins 50 msec before the R-wave and ends 50 msec before the next R-wave. The subject is at the first stage of labour, 40 weeks gestation. Code: 5-1-9.

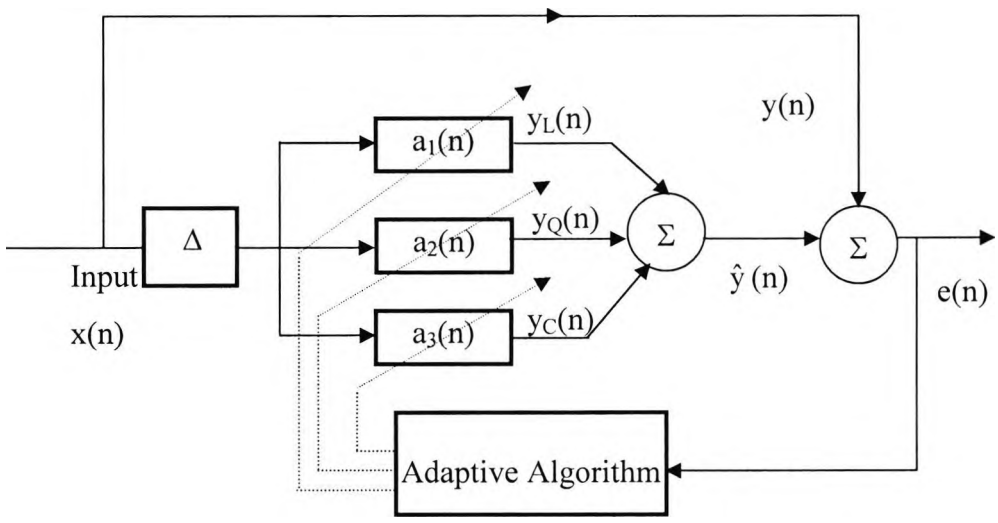

Figure 3.7: *An adaptive third-order Volterra structure with the output taken as the linear part of the structure,* $y_L(n)$.

part of the signal alone. A flowchart of the third-order Volterra structure is shown in Figure 3.8, where $\mathbf{a}_{i_1}$, $\mathbf{a}_{i_1 i_2}$ and $\mathbf{a}_{i_1 i_2 i_3}$ are the weighting vectors for the linear, quadratic and cubic parts of the third-order Volterra structure, respectively. The corresponding step-size parameters are μ_{i_1}, $\mu_{i_1 i_2}$ and $\mu_{i_1 i_2 i_3}$.

Figure 3.9 depicts the linear, quadratic and cubic parts of the fetal scalp electrode, maternal chest and maternal transabdominal ECG signals. These signals are tested for Gaussianity and linearity in Appendix A4, Section A4.2. Figure 3.10 shows the corresponding Volterra linear, quadratic and cubic kernels. Figure 3.11 shows the linear, quadratic and cubic Volterra parts of four 250 msec maternal transabdominal segments; these segments are; the predominantly maternal QRS-complex, the first fetal heartbeat with maternal contribution, QRS-free ECG, and the second fetal heartbeat with maternal contribution. This representation will be used later on in Chapters Four, Five and Six.

3.4.4 Mean-squared error comparison of the LMS- and LMF-based second- and third-order Volterra synthesisers when applied to fetal scalp electrode, maternal chest, and maternal transabdominal ECG signals

Using as input the fetal scalp electrode, maternal chest, and maternal transabdominal ECG signals, the MSE performance of the LMSQV synthesiser is compared with that of the LMFQV synthesiser. This is followed by comparing the MSE performance of the

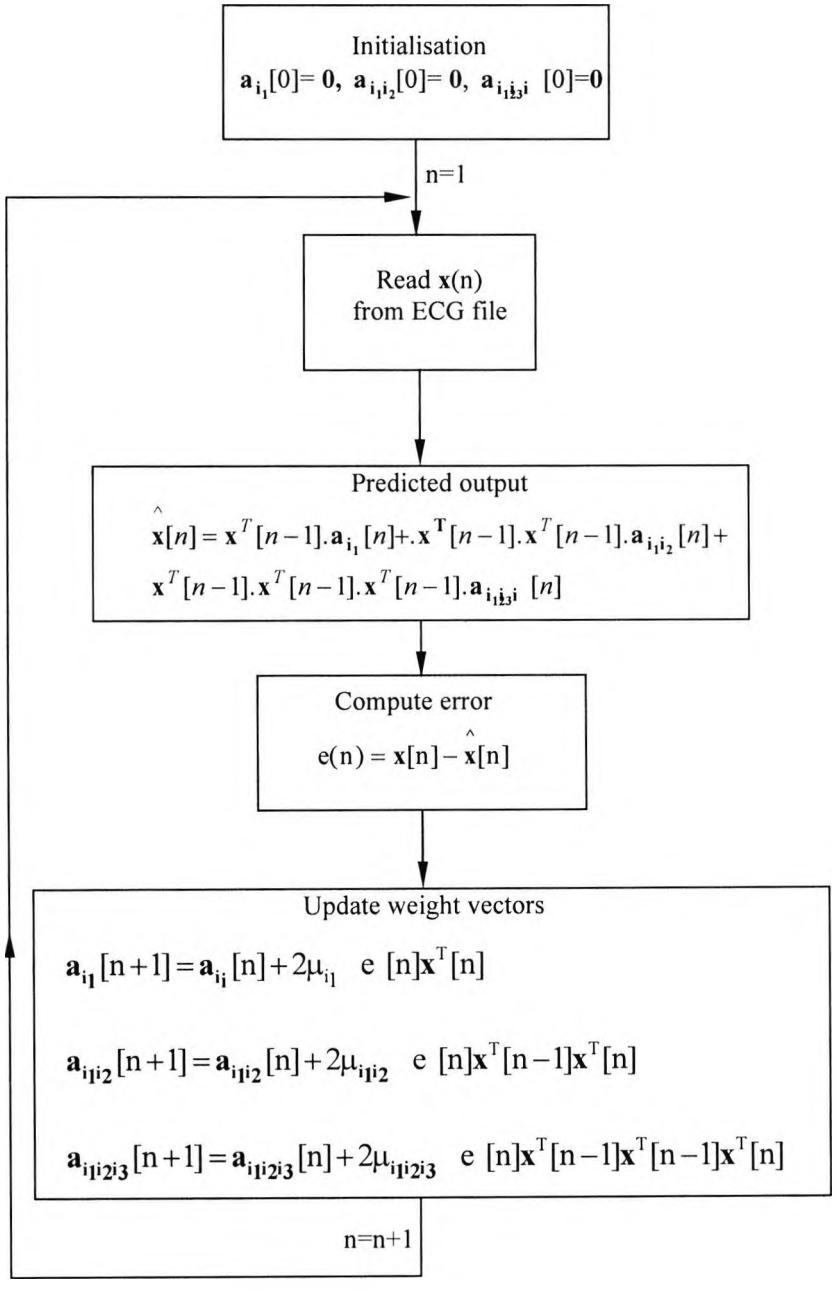

Figure 3.8: *A Flowchart of the adaptive LMS-based third-order Volterra algorithm.*

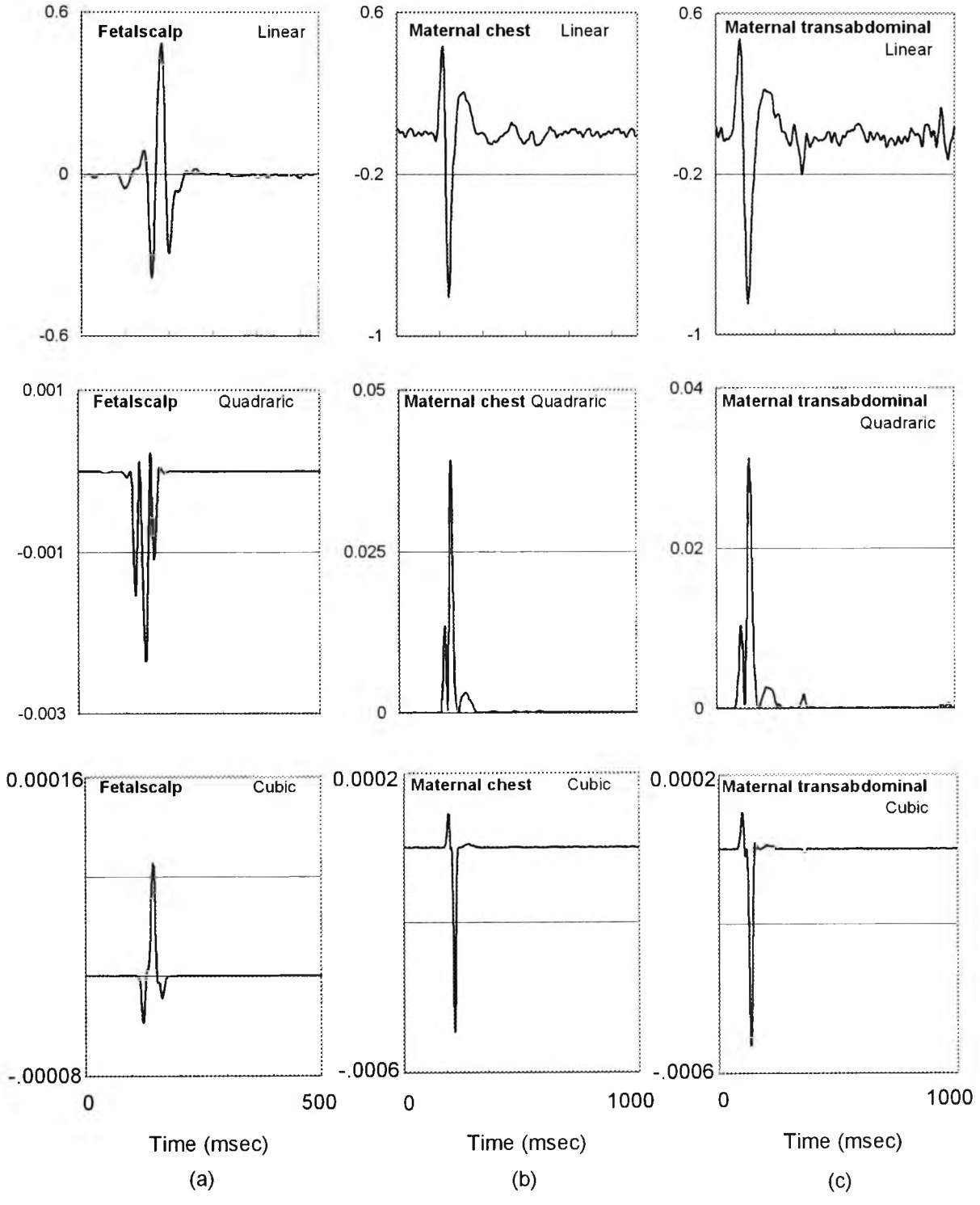

Figure 3.9: *Third-order Volterra synthesised signals. Linear (top panel), quadratic (middle panel) and cubic (bottom panel) parts of the third-order Volterra representation of (a) a fetal ECG signal using fetal scalp electrode, (b) a maternal chest ECG signal, and (c) a maternal transabdominal ECG signal. The maternal cardiac cycle begins 50 msec before the R-wave and ends 50 msec before the next R-wave. The subject is at the first stage of labour, 40 weeks gestation. The Volterra parameters are as follows; fetal ECG signal: filter length = 8, delay = 2, step-size parameters = 0.002, 0.0002, 0.0002, maternal chest ECG signal: filter length = 6, delay = 4, step-size parameters = 0.002, 0.0002, 0.0002, transabdominal ECG signal: filter length = 6, delay = 4, step-size parameters = 0.004, 0.0004, 0.0004. The length of the cardiac cycle is 550 msec for (a) and 1000 msec for (b) and (c).*

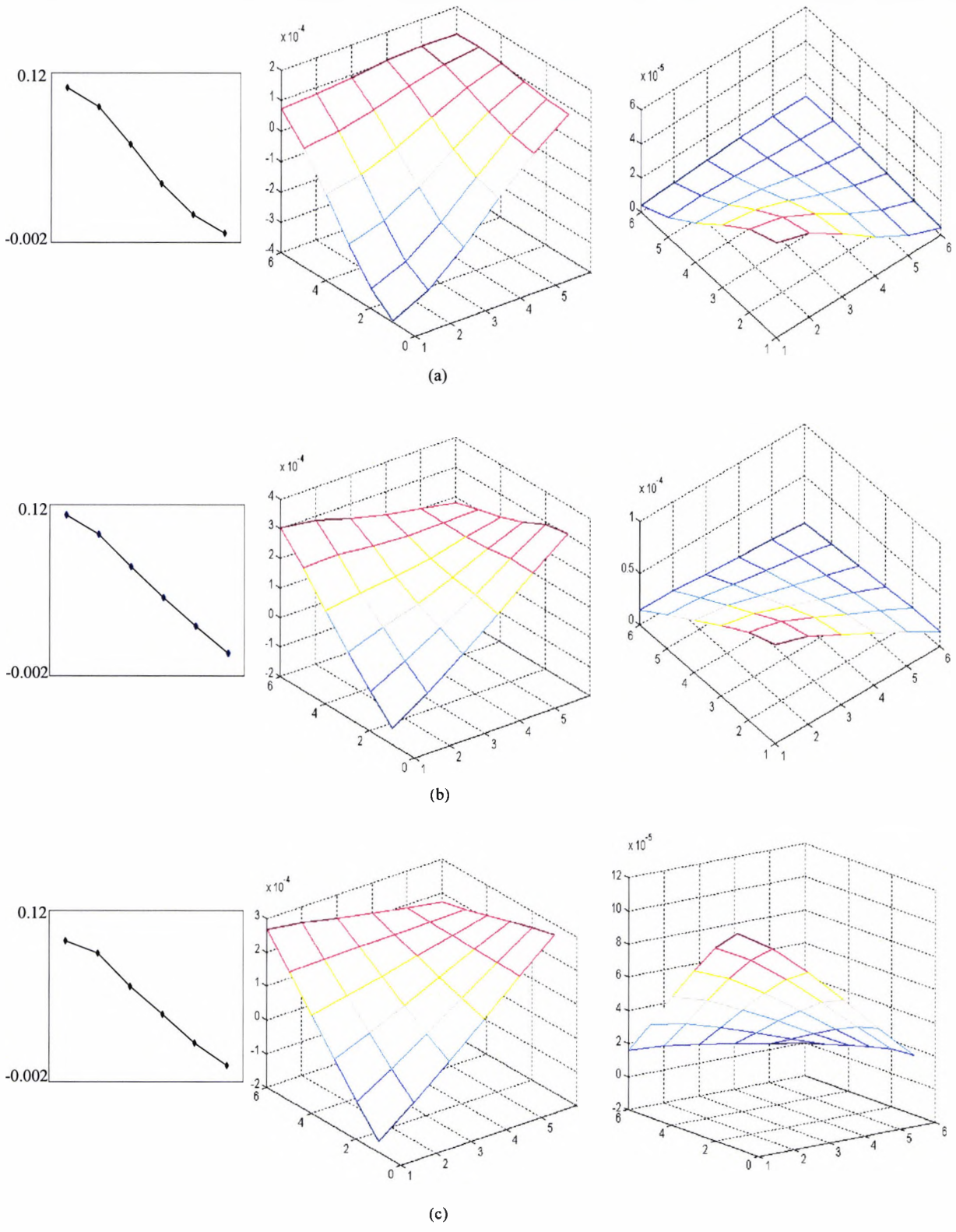

Figure 3.10: *Third-order Volterra coefficients (linear coefficients (l.h.s.), quadratic coefficients (middle), and diagonal tensor of cubic coefficients (r.h.s.) of (a) a fetal cardiac cycle using fetal scalp electrode (data length 550 msec), (b) a maternal chest cardiac cycle (data length 1000 msec), and (c) a transabdominally measured maternal cardiac cycle (twin surface electrodes, data length = 1000 msec). The third-order Volterra filter parameters are as follows; fetal scalp ECG signal: filter length =6, delay = 1, step-size parameter = 0.001, 0.0001, 0.0001. Maternal chest ECG signal: filter length =6, delay = 6, step-size parameter = 0.001, 0.0001, 0.0001. Trabsabdominal ECG signal: filter length =6, delay = 4, step-size parameter = 0.004, 0.0004, 0.0004.*

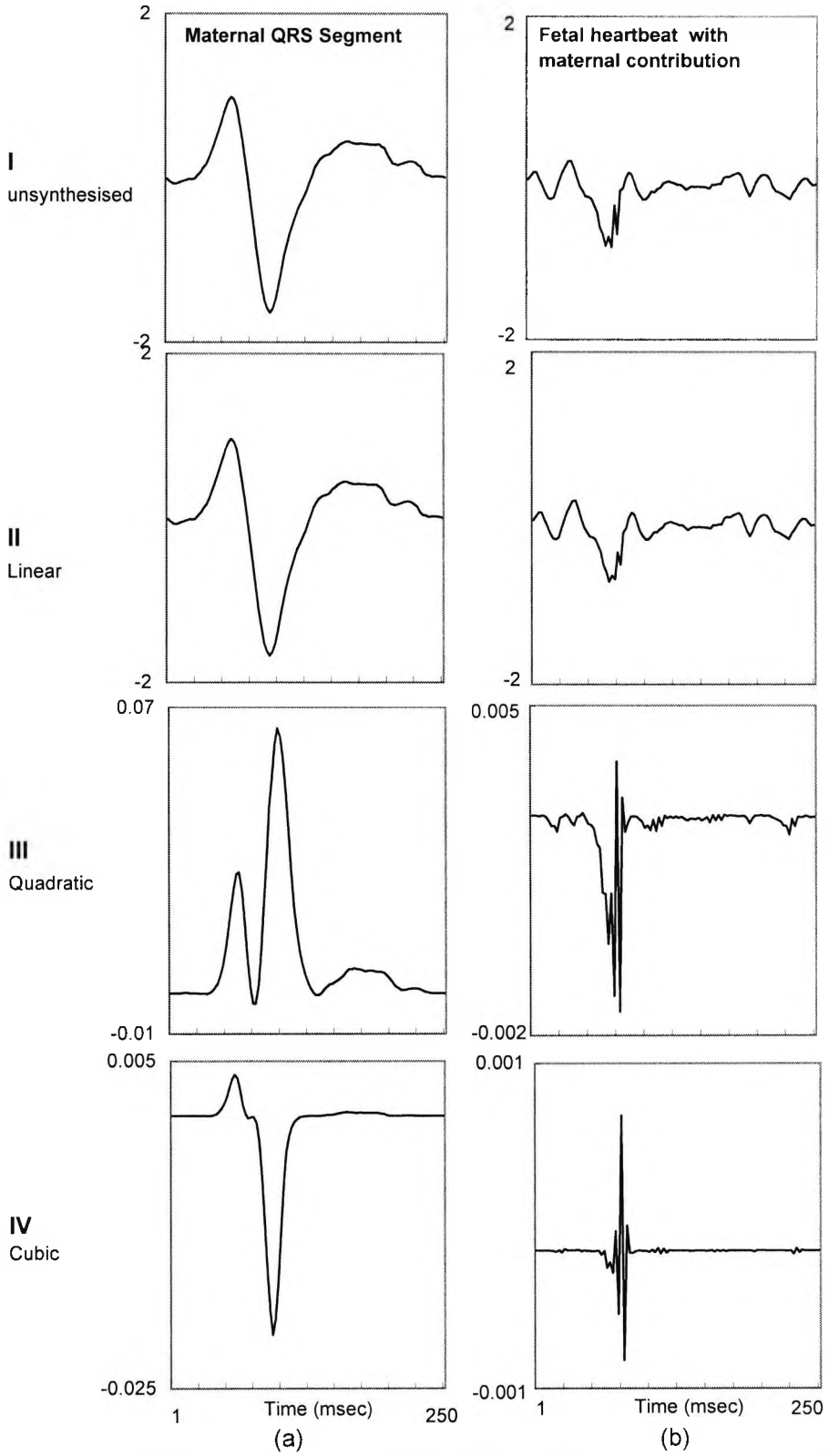

Figure 3.11: *Third-order Volterra Synthesis of four 250 msec segments of the maternal transabdominal cardiac cycle of Figure 3.9; (a) the predominantly maternal QRS-complex segment and (b) the first fetal heartbeat with maternal contribution. (I) the unsynthesised segment, and its (II) linear, (III) quadratic, and (IV) cubic parts. The Volterra synthesiser parameters for the maternal QRS-complex segment are: filter length = 6, delay = 2, step-size parameters =0.001, 0.0001, 0.00001, for the linear, quadratic and cubic parts, respectively. The Volterra synthesiser parameters for the first fetal heartbeat segment are: filter length = 8, delay = 4, step-size parameters =0.01,0.001, 0.0001, for the linear, quadratic and cubic parts, respectively. Code: cycle 5-1.*

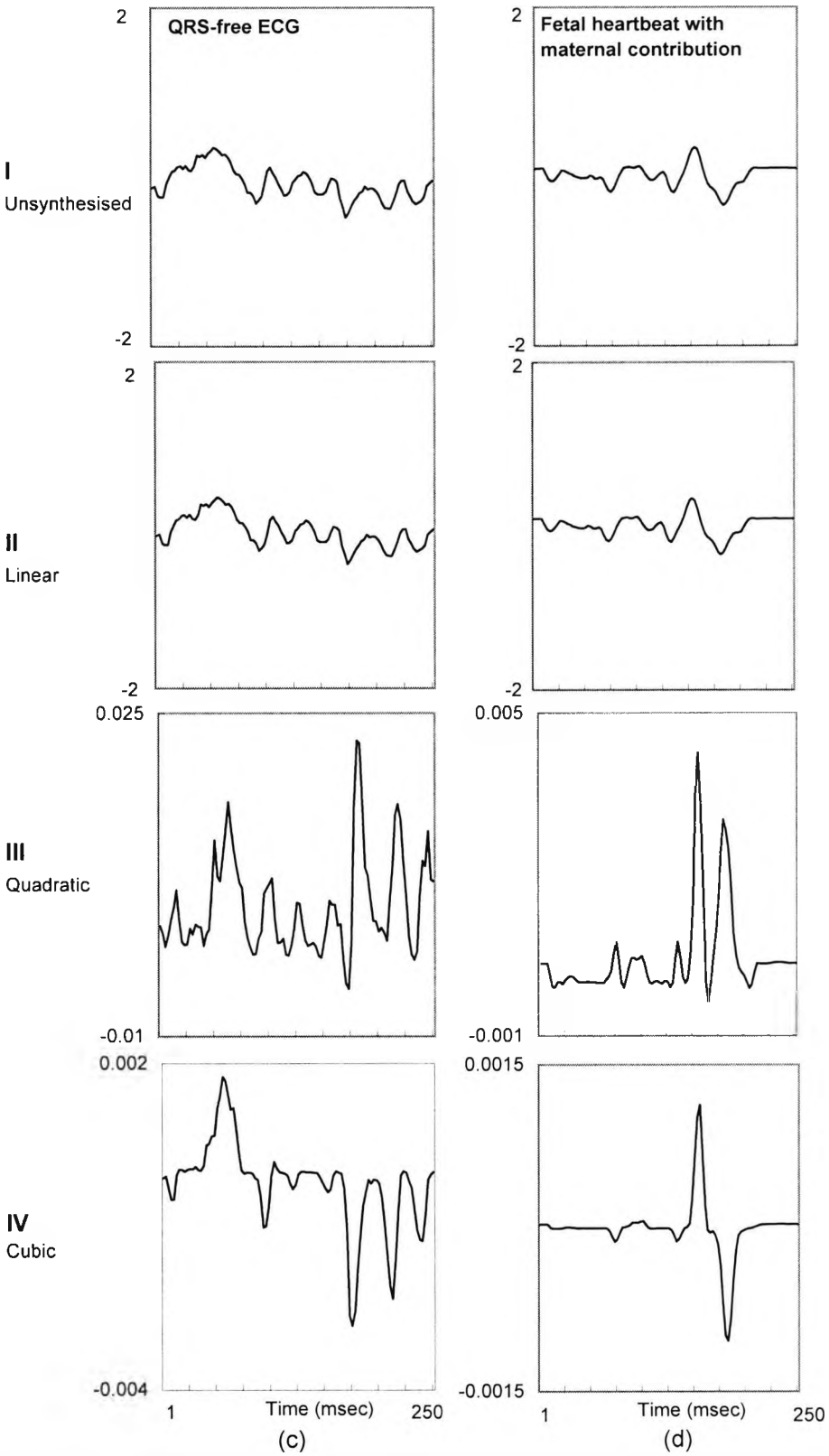

Figure 3.11 *(continued): Third-order Volterra Synthesis of four 250 msec segments of the maternal transabdominal cardiac cycle of Figure 3.9; (c) the QRS-free ECG segment and (d) the second fetal heartbeat with maternal contribution. (I) the unsynthesised segment, and its (II) linear, (III) quadratic, and (IV) cubic parts. The Volterra synthesiser parameters for the QRS-free ECG and the second fetal heartbeat segments are: filter length = 8, delay = 4, step-size parameters =0.01, 0.001, 0.0001, for the linear, quadratic and cubic parts, respectively. Code: cycle 5-1.*

LMSCV synthesiser with that of the LMFCV synthesiser. In each case the parameters have been optimised to yield the best performance for individual signals.

(i) LMSQV versus LMFQV synthesisers

Figure 3.12 shows the MSE of both the LMSQV and the LMFQV synthesisers when applied to a fetal scalp electrode ECG signal. At the start of the iterations, the MSE of the LMFQV is about 3 dB below that of the LMSQV. Then, both synthesisers equalise towards convergence. It is interesting to note that the fetal scalp electrode ECG signal is predominantly linear and is decomposed as follows; input = 0 dB, output = - 0.03 dB linear and –20 dB quadratic.

Figure 3.13 shows the MSE of both the LMSQV and LMFQV synthesisers when applied to a maternal chest ECG signal. At the start of the iterations, the MSE of the LMFQV is about 3 dB below that of the LMSQV. Then, both synthesisers equalise towards convergence. Note that the maternal chest ECG signal is predominantly linear and is decomposed as follows; input = 0 dB, output = - 0.02 dB linear and –19 dB quadratic.

Figure 3.14 shows the MSE of both the LMSQV (l.h.s.) and LMFQV (r.h.s.) synthesisers when applied to a maternal transabdominal ECG signal. The LMFQV starts with an initial error which is about 39% of that of the LMSQV. The LMFQV takes only two cardiac cycles to converge whilst the LMSQV converges in nine cardiac cycles. Also, the LMFQV approaches convergence with an MSE of 2.5×10^{-4} which is less than that of the LMSQV (7.4×10^{-3}); a definite improvement of 14 dB. Note that the maternal transabdominal ECG signal is predominantly linear and is decomposed as follows; input = 0 dB, output = - 0.015 dB linear and –17 dB quadratic.

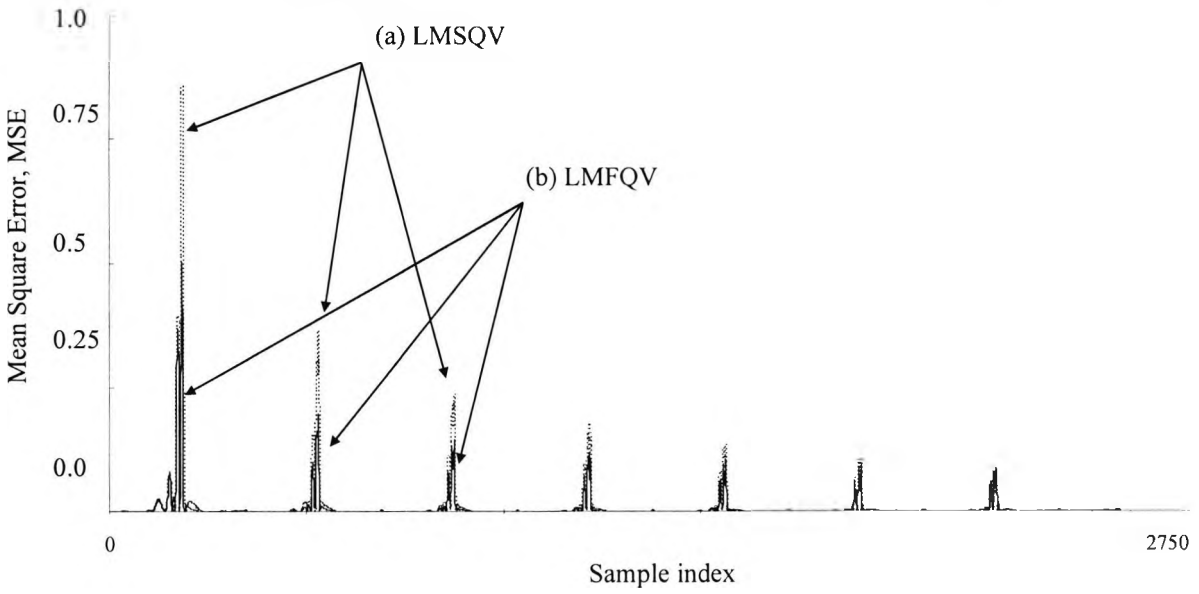

Figure 3.12: *The mean-squared error of (a) the LMSQV and (b) the LMFQV Synthesisers when applied to the fetal scalp electrode ECG signal of Figure 3.9. (Code: 5-78-80).*

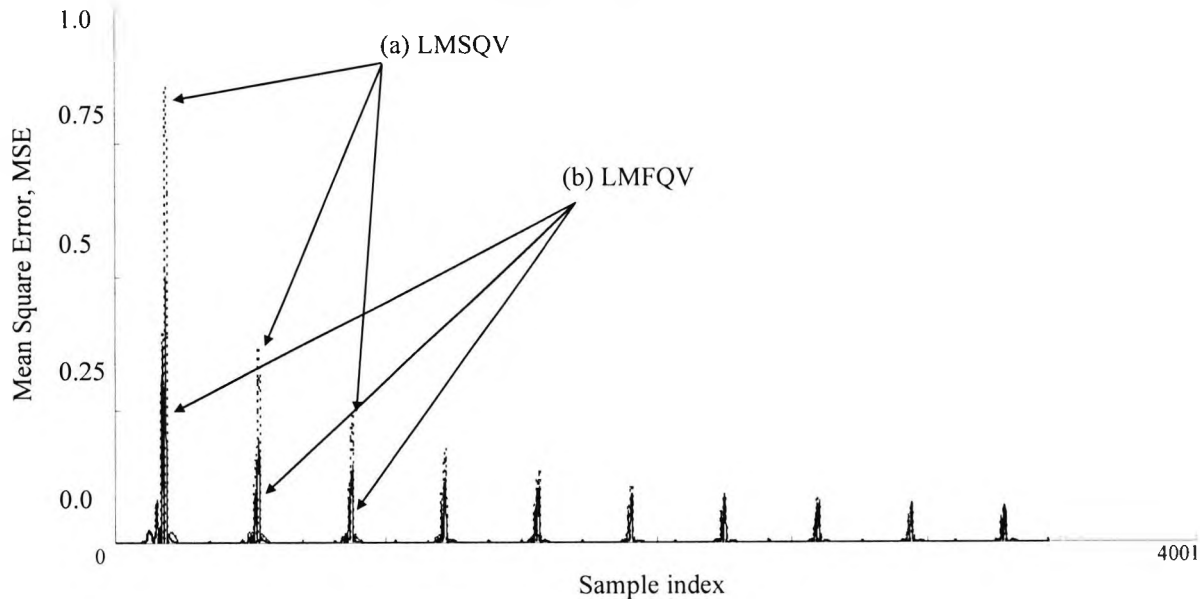

Figure 3.13: *The mean-squared error of (a) the LMSQV and (b) the LMFQV synthesisers when applied to the maternal chest ECG signal of Figure 3.9. (Code: 5-78-87).*

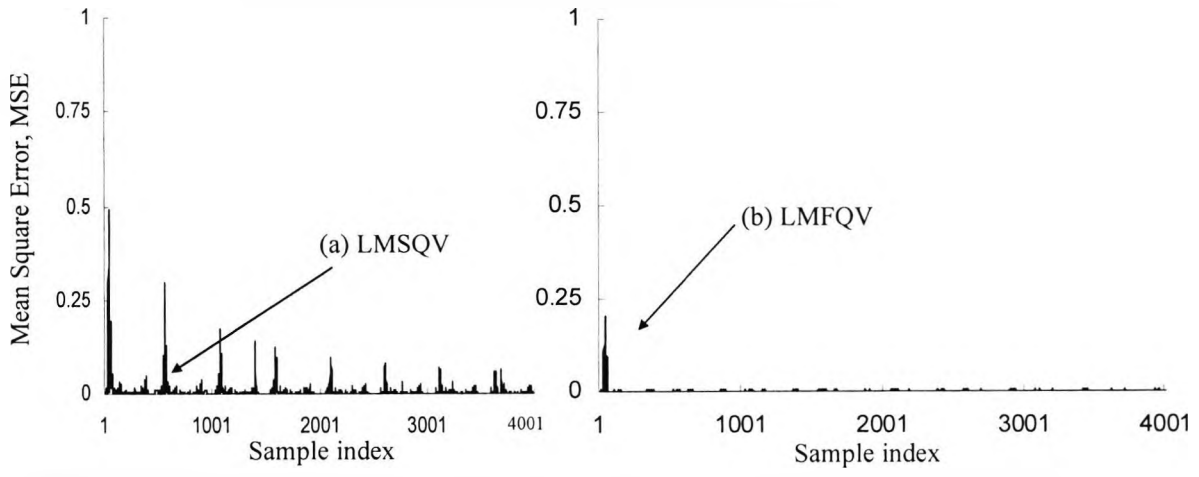

Figure 3.14: *The mean-squared error of (a) the LMSQV and (b) the LMFQV synthesisers when applied to the maternal transabdominal ECG signal of Figure 3.9 (Code: 5-78-87).*

(ii) LMSCV versus LMFCV synthesisers

Figure 3.15 shows the MSE of both the LMSCV and LMFCV synthesisers when applied to a fetal scalp electrode ECG signal. At the start of the iterations, the MSE of the LMFCV is about 3 dB below that of the LMSCV. Then, both synthesisers equalise towards convergence. Note that the fetal scalp electrode ECG signal is predominantly linear and is decomposed as follows; input = 0 dB, output = - 0.03 dB linear, –20 dB quadratic, and -39 dB cubic.

Figure 3.16 shows the MSE of both the LMSCV and LMFCV synthesisers when applied to a maternal chest ECG signal. At the start of the iterations, the MSE of the LMFCV is about 3 dB below that of the LMSCV. Then, both synthesisers equalise towards convergence. Note that the maternal chest ECG signal is predominantly linear and is decomposed as follows; input = 0 dB, output = - 0.02 dB linear, –19 dB quadratic, and -36 dB cubic.

Figure 3.17 shows the MSE of both the LMSCV (l.h.s.) and LMFCV (r.h.s.) synthesisers when applied to a maternal transabdominal ECG signal. At the start of iterations, the LMFCV is 6 dB below that of the LMSCV. The LMFCV takes only two cardiac cycles to converge whilst the LMSCV converges in nine cardiac cycles. Also, the LMFCV has a steady-state (after convergence) mean-squared error of 1.5×10^{-6} whilst that of the LMSCV is 3×10^{-5} which is an improvement of approximately 13 dB. Note that the maternal transabdominal ECG signal is predominantly linear and is decomposed as follows; input = 0 dB, output = - 0.015 dB linear, –17 dB quadratic, and -33 dB cubic.

The parameters for the adaptive LMS- and LMF-based quadratic and cubic Volterra synthesisers are summarised in Table 3.1.

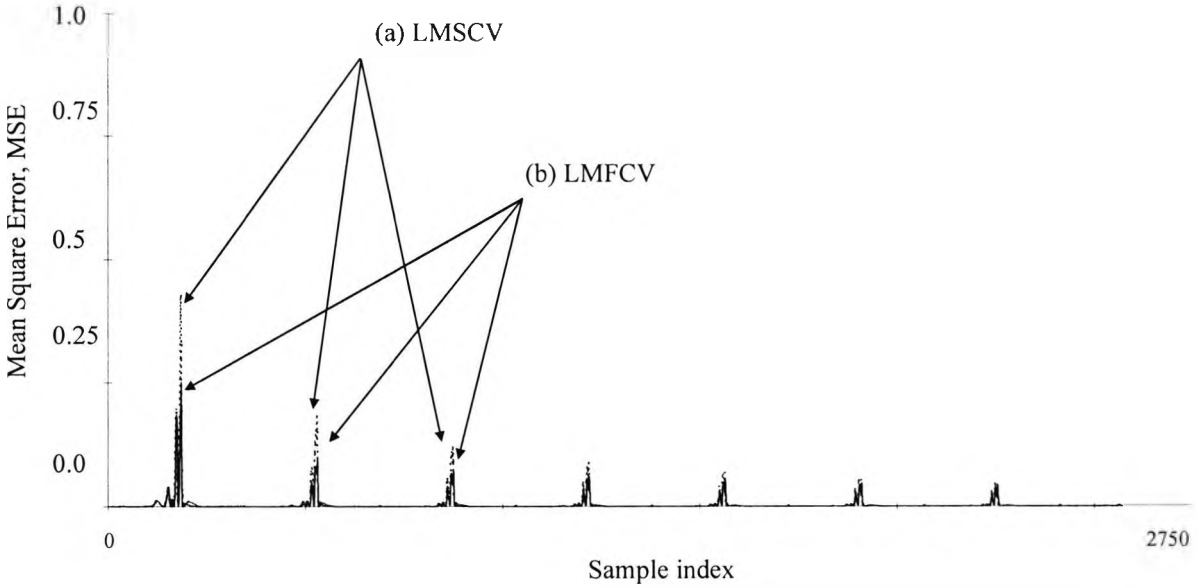

Figure 3.15: *The mean-squared error of (a) the LMSCV and (b) the LMFCV synthesisers when applied to the fetal scalp electrode ECG signal of Figure 3.9. (Code: 5-78-80).*

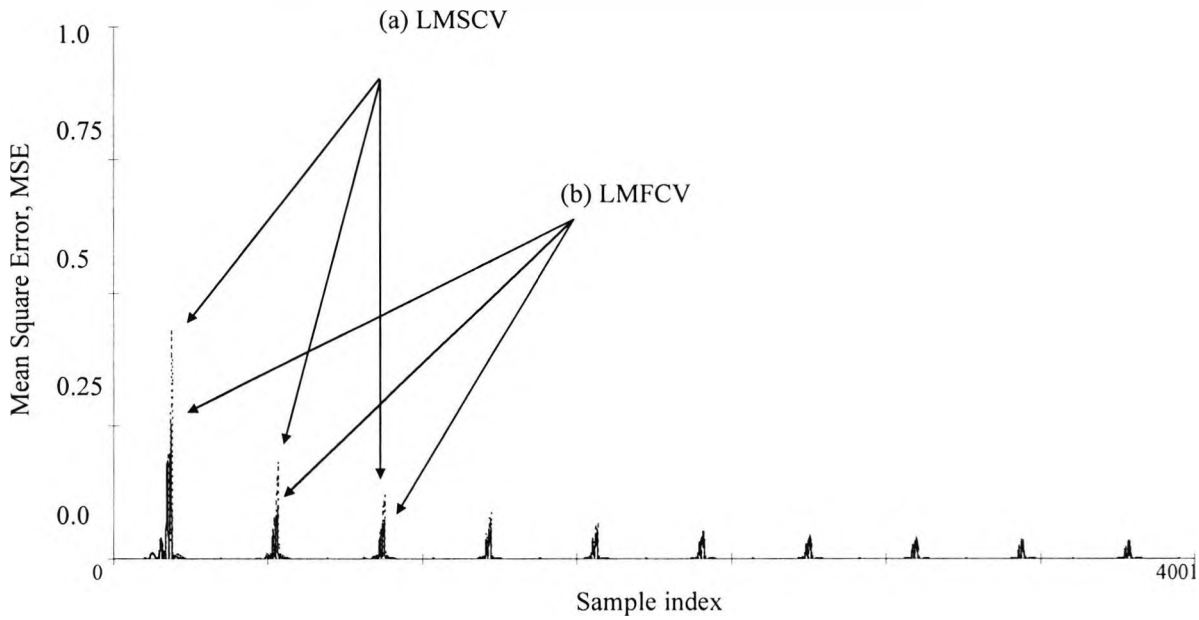

Figure 3.16: *The mean-squared error of (a) the LMSCV and (b) the LMFCV synthesisers when applied to the maternal chest ECG signal of Figure 3.9. (Code: 5-78-87).*

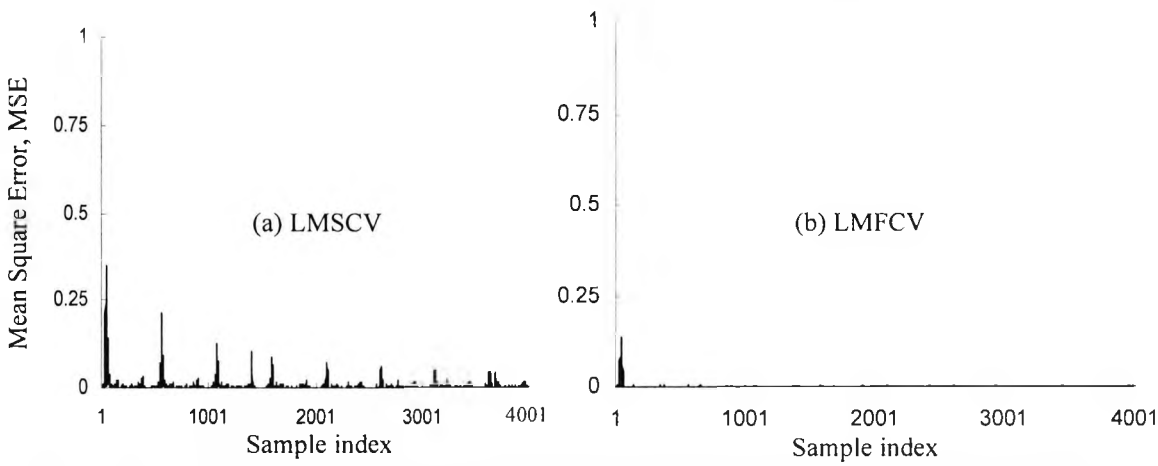

Figure 3.17: *The mean-squared error of (a) the LMSCV and (b) the LMFCV synthesisers when applied to the maternal transabdominal ECG signal of Figure 3.9. (Code: 5-78-87).*

Algorithm	Number of elements, N	Delay, Δ	Step-size parameter, μ	CPU (msec)
LMS Quadratic Volterra	8	6	0.002, 0.0004	25
LMS Cubic Volterra	6	6	0.001,0.0001, 0.0001	350
LMF Quadratic Volterra	8	5	0.001, 0.0002	40
LMF Cubic Volterra	6	5	0.001,0.0002, 0.0004	450

(a)

Algorithm	Number of elements, N	Delay, Δ	Step-size parameter, μ	CPU (msec)
LMS Quadratic Volterra	6	2	0.002, 0.0004	35
LMS Cubic Volterra	6	2	0.001,0.0001, 0.0001	700
LMF Quadratic Volterra	6	2	0.001, 0.0002	50
LMF Cubic Volterra	6	2	0.001,0.0002, 0.0004	850

(b)

Algorithm	Number of elements, N	Delay, Δ	Step-size parameter, μ	CPU (msec)
LMS Quadratic Volterra	6	2	0.002, 0.0004	35
LMS Cubic Volterra	6	2	0.001,0.0001, 0.0001	700
LMF Quadratic Volterra	6	2	0.001, 0.0002	50
LMF Cubic Volterra	6	2	0.001,0.0002, 0.0004	850

(c)

Table 3.1: *The optimised parameters of the LMSQV, LMSCV, LMFQV, and LMFCV adaptive algorithms compared in Figures 3.12 to 3.17 for (a) fetal scalp electrode, (b) maternal chest, and (c) maternal transabdominal ECG signals.*

3.5 Summary and conclusions

General discussions

The objective of this chapter is to decompose the maternal transabdominal ECG signal into its linear, quadratic, and cubic parts and retain only the linear part. The maternal transabdominal ECG signal is a combined maternal and fetal ECG and there is also another formidable signal combined with it, namely, the uterine contraction interference signal (UCS) during labour. Each one of these three combined signals is non-linear by its own right. To synthesise the maternal transabdominal ECG signal, a non-linear predictor / synthesiser is sought to carry out this task because employing a linear structure to cater for such non-linear signals would lead to a suboptimal solution. The predictor / synthesiser will try to model as faithfully as possible the linear, quadratic and cubic parts of the ECG signal. This is done by predicting each sample of the maternal transabdominal full cardiac cycles before employing segmentation. The linear (and non-Gaussian) part of each segment of the maternal transabdominal cardiac cycle will be used for fetal heartbeat classification and detection in the following three chapters.

Prediction may be viewed as a form of model building in the sense that the smaller we make the prediction error in a statistical sense, the better will the structure serve as a statistical model of the process responsible for the generation of the time series. When this process is of a non-linear nature, the use of a Volterra structure provides a powerful method for solving the prediction problem by virtue of the non-linear processing units built into its construction. The only exception to the use of non-linear units, however, is the output of the structure, which is linearly related to its inputs. The coefficients of the Volterra filter are adjusted via gradient descent to minimise the mean squared value of the difference between the desired response and the actual filter output.

Detailed results

1. Summary of the LMS and LMF algorithms

The adaptivity of the Volterra structure is carried out using two candidate algorithms, namely, the LMS and the LMF algorithms. The LMS algorithm is simple to implement, able to operate satisfactorily in an unknown environment and able to track time variations of the input statistics. The LMF algorithm however, is able to track variations in the higher-order statistics of the input signal. The LMS and LMF algorithms are

summarised in Tables 3.2 and 3.3, respectively. Figures 3.18 and 3.19 show signal-flow graph representations of the LMS and the LMF algorithms, respectively.

1. Initialisation: Set $a_i(1) = 0$
for k = 1, 2, …, p
2. Filtering: For time n = 1, 2, .. compute
$y_{(n)} = \sum_{i=0}^{N-1} a_i x_{(n-i)}$,
$e(n) = d(n) - y(n)$,
$\mathbf{a}(n+1) = \mathbf{a}(n) + 2\mu \quad e(n)x(n)$,
for k = 1, 2, …, p.

Table 3.2: *Summary of the LMS algorithm.*

1. Initialisation: Set $a_i(1) = 0$
for k = 1, 2, …, p
2. Filtering: For time n = 1, 2, .. compute
$y_{(n)} = \sum_{i=0}^{N-1} a_i x_{(n-i)}$,
$e(n) = d(n) - y(n)$,
$\mathbf{a}_i(n+1) = \mathbf{a}_i(n) + 2\mu_i \; .e^3(n).x(n)$.
for k = 1, 2, …, p.

Table 3.3: *Summary of the LMF algorithm.*

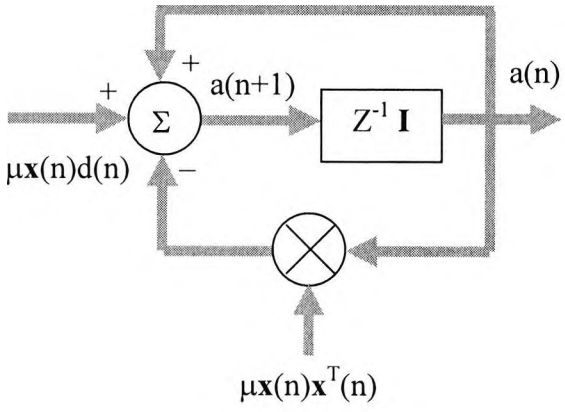

Figure 3.18: *A signal-flow graph representation of the LMS algorithm.*

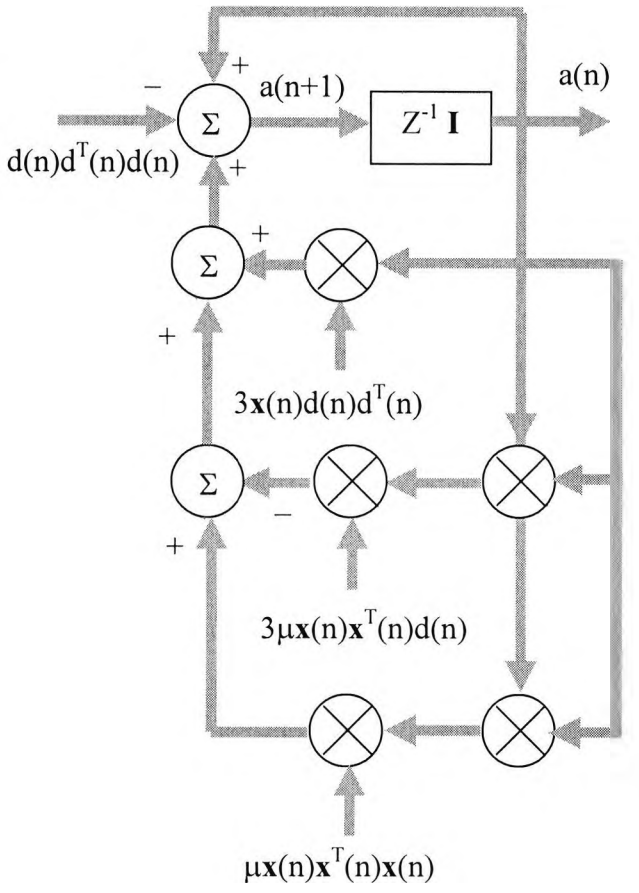

Figure 3.19: *A signal-flow graph representation of the LMF algorithm.*

2. Comparison of the performance of both the LMS and LMF algorithms

In this chapter the standard LMS and LMF predictors are applied to full cardiac cycles of the maternal transabdominal ECG signals and it is shown that the LMF predictor slightly outperforms its LMS counterpart in terms of the mean-squared error by 1 dB for the same convergence time, possibly because the LMS algorithm is limited to tracking variations in the second-order statistics domain only. The advantage of the LMF algorithm against the LMS algorithm is that when both the LMF and LMS are set to have the same step-size parameter for the weight adaptation process, the LMF will have substantially lower weight noise than the LMS. The LMF algorithm leads to a lower mis-adjustment than the LMS algorithm for the same speed of convergence. However, the main limitation of the LMS and LMF filters is their relatively slow rate of convergence, which is attributed to the exclusive use of first-order information (gradient).

3. Comparison of the performance of the LMS-based and LMF-based second- and third-order Volterra synthesisers

Second-order and third-order Volterra synthesisers are used to linearise the fetal scalp electrode, the maternal chest, and the maternal transabdominal ECG signals by removing the quadratic or the quadratic and cubic parts, respectively, and retaining only the linear part. The Volterra structures are attractive since they can deal with a general class of non-linear systems while their outputs are still linear with respect to their inputs via their linear, quadratic and cubic parts of their transfer functions.

Adaptive LMF-based second- and third-order Volterra structures are developed and applied to full cardiac cycles of the fetal scalp electrode, the maternal chest, and the maternal transabdominal ECG signals. The extension of the conventional LMS-based Volterra to the LMF-based Volterra is done to make use of the advantages of higher-order statistics, especially its robustness to Gaussian noise and its tracking capability.

Adaptive LMS- and LMF-based second- and third-order Volterra structures are used to decompose the aforementioned ECG signals into their linear, quadratic and cubic parts and retain only the linear part. The LMF-based second-order Volterra (LMFQV) takes only two cardiac cycles to converge whilst the LMS-based second-order Volterra

(LMSQV) converges in nine cardiac cycles when both structures are applied to maternal transabdominal ECG signals. Also, the LMFQV approaches convergence with an MSE which is 14 dB below that of the LMSQV. The LMF-based third-order Volterra (LMFCV) takes only two cardiac cycles to converge whilst the LMS-based third-order Volterra (LMSCV) converges in nine cardiac cycles when both structures are applied to maternal transabdominal ECG signals. After convergence of both synthesisers, the MSE of the LMFCV is 13 dB below that of the LMSCV. Hence, both the adaptive LMF-based second- and third-order Volterra structures outperform the adaptive LMS-based second- and third-order Volterra structures by 14 dB and 13 dB, respectively. The third-order Volterra structure yields a better performance in terms of the MSE than the second-order Volterra structure by approximately 20 dB. The CPU time could be reduced by eliminating redundant coefficients from the third-order Volterra synthesiser as explained in Appendix A4, Section A4.3. In practice, however, it might be prudent to compromise and use an LMF-based second-order Volterra as opposed to an LMF-based third-order Volterra structure. This would simplify the implementation of the algorithm in software or hardware and reduce the CPU time required by two orders of magnitude which will make it more attractive for on-line implementations in handheld or portable devices.

3.6 References

[1] MIT/BIH Database: ECG Database Applications Guide, 10th Edition, 1997. Harvard-MIT Division of Health Sciences and Technology, MIT Room 20A-113, Cambridge, MA 02139, USA.

[2] MIT/BIH Database: ECG Database Programmer's Guide, 9th Edition, 1997. Harvard-MIT Division of Health Sciences and Technology, MIT Room 20A-113, Cambridge, MA 02139, USA.

[3] B. Widrow et al., " Adaptive Noise Cancellation: Principles and Applications," Proceedings of IEEE, vol. 63, No. 12, pp. 1692-1716, December 1975.

[4] E. R. Ferrera and B. Widrow, " Fetal Electrocardiogram Enhancement by Time Sequenced Adaptive Filtering," IEEE Transactions on Biomedical Engineering, vol. 29, BME-29, pp. 458-460, 1982.

[5] C. A. Spiers, J. J. Soraghan, R. W. Stewart and S. Byrne, "Time-sequenced linear predictive enhancement," IEE Electronics Letters, vol. 31, No. 12, pp. 939-941,

8/6/1995.

[6] J. R. Zeidler, "Performance analysis of LMS adaptive prediction filters," IEEE Proceedings, vol. 78, No. 12, pp. 1781-1806, December 1990.

[7] E. Wallach and B. Widrow, "The Least-Mean Fourth (LMF) adaptive algorithm and its family," IEEE Transactions on Information Theory, vol. IT-30, No. 2, pp. 275-283, March 1984.

[8] S. A. Billings, "Identification of nonlinear systems- A survey," IEE Proceedings, vol. 127, Pt. D, No. 6, vol. 272-281, November 1980.

[9] S. Y. Fakhouri, "Identification of the Volterra kernels of nonlinear systems," IEE Proceedings, vol. 127, pt. D, No. 6, pp. 296-304, November 1980.

[10] T. Koh and E. J. Powers, "Second-Order Volterra Filtering and its Applications to Non-Linear System Identification," IEEE Transactions on Acoustics, Speech, and Signal Processing, vol. 33, No. 6, pp. 1445-1455, December 1985.

[11] K. I. Kim, E. J. Powers, C. P. Ritz, and R. W. Miksad, "Modelling of nonlinear systems in offshore engineering for non-Gaussian inputs," ICASSP International Conference on Acoustics, Speech, and Signal Processing, pp. 405-419, 1985.

[12] G. L. Sicuranza, G. Ramponi, "A variable-step adaptive algorithm for memory-oriented Volterra filters, IEEE Transactions on Acoustics, Speech, and Signal Processing, vol. 35, No. 10, pp. 1492-1494, October 1987.

[13] S. W. Nam, S. B. Kim, and E. J. Powers, "On the Identification of a Third-Order Volterra Non-Linear System Using a Frequency Domain Block RLS Adaptive Algorithm," ICASSP, IEEE International Conference on Acoustics, Speech, and Signal Processing, pp. 2407-2410, 1990.

[14] S. H. Tseng and E. J. Powers, "Batch and Adaptive Volterra Filtering of Cubically Non-Linear Systems with a Gaussian Input," ICASSP, IEEE International Conference on Acoustics, Speech, and Signal Processing, pp. 40-43, 1993.

[15] S. Im, S. B. Kim, and E. J. Powers, "Orthogonal Development of a Discrete Frequency Domain Third Order Volterra Model," ICASSP, IEEE International Conference on Acoustics, Speech, and Signal Processing, vol. 4, pp. 484-487, 1993.

[16] B. G. Mertzios and A. N. Venetsanopoulos, "On the implementation of the polyspectra and cumulants via Volterra kernerls," in *Time Varying Image Processing and Moving Object Recognition*, 3, V. Cappellini, (ed.), pp. 110-117, Elsevier Science B. V., 1994.

[17] S. W. Nam and E. J. Powers, "Application of Higher Order Spectral Analysis to Cubically Non-Linear System Identification," IEEE Transaction on Signal Processing, vol. 42, No. 7, pp. 1746-1765, July 1994.

[18] R. Nowak and B. Van Veen," Efficient method for identification of Volterra filter model," Signal Processing, vol. 38, pp. 417-428, 1994.

[19] S. B. Kim and E. J. Powers, "Estimation of Volterra kernels via higher-order statistical signal processing," in *Higher order statistical signal processing*, (Boashash, Powers, and Zoubier, eds.), Ch. 7, pp. 213-267, 1995.

[20] S. V. Vaseghi, *Advanced signal processing and digital noise reduction*, Wiley and Teubner, 1996.

[21] D. S. Broomhead and D. Lowe, "Multivariable Functional Interpolation and Adaptive Networks," Complex Systems, vol. 2, pp. 321-355, 1988.

[22] W. H. Press, B. P. Flannery, A. Teukolsky and W. T. Vetterling, *Numerical Recipes in C: The Art of Scientific Computing*, Cambridge University Press, 1988.

[23] W. Zgallai, M. Sabry-Rizk, P. Hardiman, and J. O'Riordan, "MUSIC-Based Bispectrum Detector: A Novel Non-Invasive Detection Method For Overlapping Fetal And Mother ECG Signals," Proceedings of the 19th IEEE International Conference on Engineering in Medicine and Biology, EMBS, pp. 72-75, USA, October 1997.

[24] S. Chen, C. F. N. Cowan and P. M. Grant, "Orthogonal Least Squares Learning Algorithm for Radial Basis Function Networks," IEEE Transactions on Neural Networks, vol. 2, pp. 302-309, 1991.

[25] M. R. Lynch, P. J. Rayner and S. B. Holden, "Removal of Degeneracy in Adaptive Volterra Networks by Dynamic Structuring," Proceedings of IEEE ICASSP, pp. 2069-2072, 1991.

[26] K. C. Nisbet, B. Mulgrew and S. McLaughlin, "A reduced complexity sub-optimal nonlinear predictor," IEE Colloquium, pp. 6/1-6/13, London, 1994.

[27] R. O. Schmidt, *A Signal Subspace Approach To Multiple Emitter Location And Spectral Estimation*, PhD Dissertation, Department of Electrical Engineering, Stanford University, USA, 1981.

[28] M. Sabry-Rizk, W. Zgallai, C. Morgan, S. El-Khafif E. R. Carson, and K. T. V. Grattan, "Novel decision strategy for P-wave detection utilising nonlinearly synthesised ECG components and their enhanced pseudospectral resonances," IEE Proceedings Science, Measurement and Technology, Special section on Medical

Signal Processing, vol. 147, No. 6, pp. 389-397, November 2000.

[29] M. Sabry-Rizk, W. Zgallai, S. El-Khafif, E. Carson, K. Grattan, "Higher- Order Ambulatory Electrocardiogram Identification and Motion Artifact Suppression With Adaptive Second- and Third-Order Volterra Filters," SPIE '98 Advanced Signal Processing Algorithms, Architectures, and Implementations VIII Vol. 3461, pp. 417-431, San Diego, USA, 19-24 July 1998.

[30] V. Volterra, *Theory of functionals and of integral and integro-differential equations*, Wiley, NY, 1959.

[31] S. Haykin, *Adaptive filter theory*, Prentice Hall, 1991.

[32] E. Ferrera, *The Time Sequenced Adaptive Filter*, PhD Thesis, Stanford University, Stanford, CA, U.S.A., 1978.

[33] B. Widrow, "Adaptive Filters. I: Fundamentals," Technical Report SU-SEL-66-125, Stanford Electronics Lab., Stanford, USA, December 1966.

[34] B. Widrow, J. McCool, M. G. Larimore and C. R. Johnson, Jr., "Stationary and non-stationary learning characteristics of the LMS adaptive filter," IEEE Proceedings, vol. 64, No. 8, pp. 1151-1162, August 1976.

[35] W. A. Gardner, "Learning characteristics of stochastic gradient descent algorithm: a general study, analysis, and critique," Signal Processing, pp. 113-133, April 1984.

[36] W. A. Gardner, "Nonstationary learning characteristics of the LMS algorithm," IEEE Transactions on Circuits and Systems, vol. 34, pp. 1199-1207, October 1987.

[37] V. J. Mathews and J. Lee, "A fast recursive least-squares second-order volterra filter," Proceedings of the IEEE International Conference on Acoustics, Speech, and Signal Processing, ICASSP, pp. 1383-1386, April 1988.

[38] C. E. Davila, A. J. Welch and H. G. Rylander, III, "A second-order adaptive Volterra filter with rapid convergence," IEEE Transactions on Acoustics, Speech, and Signal Processing, vol. 35, No. 9, pp. 1259-1263, September 1987.

[39] M. Schetzen, *The Volterra and Wiener theories of nonlinear systems*, Wiley, NY, 1980.

[40] M. J. Hinich and D. M. Patterson, "Evidence of Nonlinearity in Daily Stock Returns," Journal of Business and Economic Statistics, vol. 3, pp. 69-77, 1985.

[41] M. B. Priestley, "State-Dependent Models: A General Approach to Non-Linear Time Series Analysis," J. of Time Series Analysis, vol. 1, pt. 1, pp. 47-71, 1980.

[42] P. L. Brockett, M. J. Hinich, and D. Patterson, "Bispectral-Based Tests for the Detection of Gaussianity and Linearity in Time Series," Journal of the American Statistical Association, vol. 83, No. 403, pp. 657-664, 1988.

[43] T. Subba Rao, "The Bispectral Analysis of Nonlinear Stationary Time Series with Reference to Bilinear Time Series Models," in *Handbook of Statistics*, vol. 3, (D. Brillinger, and P. Krishnaiah, eds.), Amesterdam, Holland, pp. 293-319, 1983.

[44] R. Ashley, D. Patterson, and M. Hinich, "A Diagnostic Test for Nonlinear Serial Dependence in Time Series Fitting Errors," Journal of Time Series Analysis, vol. 7, pp. 165-178, 1986.

[45] D. M. Keenan, "A Tukey Nonadditivity-Type Test for Time Series Nonlinearity," Biometrika, vol. 72, pp. 39-44, 1985.

[46] J. D. Petruccelli and N. Davies, "A Portmanteau Test for Self Exciting Threshold Autoregressive-Type Nonlinearity in Time Series," Biometrika, vol. 73, pp. 687-694, 1986.

[47] W. S. Chang and H. Tang, "On Tests for Non-Linearity in Time Series Analysis," Journal of forecasting, vol. 5, pp. 217-228, 1986.

[48] P. M. Robinson, "Nonparametric Estimation for Time Series," Journal of Time Series Analysis, vol. 4, pp. 185-207, 1983.

[49] M. J. Hinich and D. M. Patterson, "Identification of the Coefficients in a Non-Linear Time Series of the Quadratic Types," Journal of Econometrics, vol. 30, pp. 269-288, Elsevier Science Publishers, North Holland, 1985.

[50] P. Duvaut, "Non-Linear Filtering in Signal Processing," Proceedings of the IEEE International Signal Processing Workshop on Higher-Order Statistics, pp. 9-18, France, 1991.

[51] D. H. Johnson and P. S. Rao, "On The Existence Of Gaussian Noise," IEEE Signal Processing Workshop, pp. 8.14.1-8.14.2, NY, 1990.

[52] C. L. Nikias, " Higher Order Spectral Analysis," in *Advances in Spectrum Analysis and Array Processing I* (S. Haykin, ed.), Englewood Cliffs, N. J.: Prentice Hall, 1991.

[53] H. G. Schuster, *Deterministic Chaos*, VCH, NY, 1988.

[54] S. Chen, S. A. Billings and W. Luo, "Orthogonal Least Squares Methods and Their Application to Non-linear System Identification," International Journal of Control, vol. 50 (5), pp. 1873-1896, 1989.

[55] M. Casdagli, "Nonlinear Prediction of Time Series," Physica D, vol. 35, pp. 335-356, 1989.

[56] M. J. D. Powell, "Radial Basis Functions for Multivariate Interpolation: A Review," IMA Conference on Algorithms for the Approximation of Functions and Data, RCMS Shrivenham, 1985.

[57] S. Chen and B. Mulgrew, "Overcoming Co-Channel Interference Using an Adaptive Radial Basis Function Equaliser," EURASIP Signal Processing Journal, vol. 28, pp. 91-107, 1992.

[58] T. J. Shepherd and D. S. Broomhead, "Nonlinear Signal Processing Using Radial Basis Functions," SPIE Advanced Signal Processing Algorithms, Architectures, and Implementations, vol. 1348, pp. 51-61, 1990.

[59] F. Takens, "Detecting Strange Attractors in Turbulance," *Lecture Notes in Mathematics*, pp. 366-381, Springer-Verlag, 1980.

[60] J. Doyne-Farmer, "Chaotic Attractors of an Infinite Dimensional Dynamical System," Physica D, pp. 366-393, 1982.

[61] M. C. Mackey and L. Glass, "Oscillations and Chaos in Physiological Control Systems," *Science*, vol. 197, 1977.

[62] H. P. Sava, R. Bedi, and T. E. McDonnell, "Spectral Analysis of Carpentier-Edwards Prosthetic Heart Valve Sounds in the Aortic Position Using SVD-Based Methods," IEE Colloquium, pp. 6/1-6/4, UK, 1995.

[63] J. A. Cadzow, B. Baseghi, T. Hsu, "Singular Value Decomposition Approach to Time Series Modelling," IEE Proceedings vol. 130, pt. F, No. 3, pp. 202-210, April 1983.

[64] M. Sabry-Rizk, W. Zgallai, P. Hardiman, and J. O'Riordan," Third-order cumulant signature matching technique for non-invasive fetal heart beat identification," ICASSP, IEEE International Conference on Acoustics, Speech, and Signal Processing, vol. 5, pp 3781-3784, Germany, 1997.

[65] S. Marple, *Spectral Analysis With Applications*, Prentice Hall, 1987.

[66] V. P. Stokes, H. Lanshammar, and A. Thorstensson, "Dominant pattern extraction from 3-D kinematic data," IEEE Transactions Biomedical Engineering, Vol. BME-46, pp. 100-106, 1999.

[67] G. S. Furno and W. J. Tompkins, "A learning filter for removing noise interference," IEEE Transactions on Biomedical Engineering, vol. 30, pp. 234-235, 1983.

[68] M. J. Hinich, "Test for Gaussianity and linearity of a stationary time series," Journal of time series analysis, vol. 3, No. 3, pp. 169-176, 1982.

[69] C. L. Nikias and A. P. Petropulu, *Higher Order Spectra Analysis: A Nonlinear Signal Processing Framework*, Prentice Hall, 1993.

[70] M Sabry-Rizk, W. Zgallai, A. McLean, E. R. Carson, and K. T. V. Grattan, "Virtues and Vices of Source Separation Using Linear Independent Component Analysis for Blind Source Separation of Non-linearly Coupled and Synchronised Fetal and Mother ECGs," EMBS, USA, October 2001.

[71] A. N. Kolmogorov, "Interpolation and extrapolation of stationary random sequences," 1942. Translated by the Rand Corporation, USA, April 1962.

[72] N. Wiener, *Extrapolation, interpolation, and smoothing of stationary time series with engineering applications,* Cambridge, MA: MIT Press, 1949.

[73] L. A. Zadeh, "A contribution to the theory of nonlinear systems," Journal of the Franklin Institute, Vol. 255, pp. 387-401, 1953

[74] N. Wiener, *Nonlinear problems in random theory*, NY, Wiley, 1958.

[75] D. Gabor, "Communication theory and cybernetics," IRE Transactions on Circuit Theory, Vol. CT-1, pp. 19-31, 1954.

[76] D. Gabor, W. P. L. Wilbey, and R. Woodcock, "A universal nonlinear filter, predictor and simulator which optimises itself by a learning process," Proceedings of the Institution of Electrical Engineers, London, Vol. 108, pp. 422-435, 1960.

CHAPTER FOUR

NON-INVASIVE FETAL HEARTBEAT DETECTION USING THIRD-ORDER CUMULANT SLICES MATCHING IN CONJUNCTION WITH ANN CLASSIFIERS

4.1 Introduction

4.1.1 Aim

The aim of this chapter is to describe the first hybrid system (e.g., signal processing in conjunction with classification), using the mother and fetal third-order cumulants (TOC), which carry the signature imprints of their respective QRS-complexes, in the signal processing phase. The classification phase employs an LMS-based single-hidden-layer perceptron.

4.1.2 Artificial neural network design consideration

The subject of knowledge representation inside an artificial neural network is very complicated. The subject becomes even more complicated when we have multiple sources of information activating the network, as in the case of the 2-d third-order cumulants from transabdominal ECG containing the maternal and fetal ECGs, and the uterine contraction interference signal (UCS) plus noise.

Early research studies which have not been presented in this chapter, but have been carried out under an two-and-half-year research contract*, exploited the whole multi-dimensional structures of the third- and fourth-order cumulants of the ECG signals presented in this thesis in conjunction with multi-layered feed-forward neural networks. The justification for this multi-layer perceptron network was based entirely on the assumption that by including a sufficient number of hidden layers, the network

* Permission has been granted for publications without revealing the company's name.

would be enabled to extract both third- and fourth-higher-order statistics embedded in the cumulants presented to the network input. The multi-dimensional ECG cumulants were created first, and subsequently a pre-selected number of slices were extracted and cascaded side-by-side to be presented to the input layer of the MLP. In the early days of this research, it was difficult to make a decision, just by mere observations of the available 1-d third-order cumulant slice or 2-d fourth-order cumulant slice patterns produced from the transabdominally-measured ECG signals, as to which of such slices would show a distinguishable pattern which could be matched to the corresponding mother or fetal ECG templates. Particularly, those templates of the fetal scalp electrodes which have been used as a reference, so that the fetal heartbeat detection could be verified in the midst of those complex maternal environments and counted within each maternal cardiac cycle.

In an attempt to restrict the size of the neural network to only two hidden layers, instead of three or four layers, *prior information* had to be built into the design of the MLP by using a combination of two techniques [65]: (1) restricting the network architecture through the use of network connections and (2) constraining the choice of synaptic weights by the use of *weight sharing* [70]. The issue of *prior information* was addressed in terms of the most discriminant patterns in the one-dimensional third-order cumulant slice or the two-dimensional fourth-order cumulant slices.

How to build invariances into neural network design

There exist at least three techniques for rendering classifier-type neural networks *invariant* to changes (or transformation due to an object manifestation as in speech recognition and Radar Doppler [71]). Only the first and second techniques of the following three have been applied to fetal heart monitoring:

(1) Invariance by training. A neural network has a natural ability for pattern classification. This ability may be exploited directly to obtain change invariance as follows. The network is trained by presenting it a number of different examples of the same fetal heartbeat cumulants or bispectra, with the examples being chosen to correspond to different changes (i.e., different fetal heartbeats positions in the maternal cardiac cycle) of the third-order cumulant. Provided that the number of examples is sufficiently large, and if the network is trained to learn to discriminate the different third- or fourth-order cumulants of the ECG

250 msec segments, we may then expect the network to generalise correctly changes other than those shown to it. It was found, however, from an engineering perspective, invariance by training has disadvantages. When a neural network has been trained to recognise a third-order cumulant slice in an invariant fashion with respect to known changes, it is not obvious that this training will also enable the network to recognise other representatives of different classes invariantly (e.g., cumulants of the QRS-free ECG segment). The solution was found to provide templates of the third-order cumulant slices of the QRS-free ECG segment.

(2) *Invariant feature space*. The second technique of creating an invariant classifier-type neural network rests on the premise that it may be possible to extract features that characterise the essential information content of an input data set, and which are invariant to changes of the input [70]. It has to be emphasised that this applies only to linearised ECG data sets. The important features characterising key cumulant slices, such as the diagonal and wall slices, are (i) the shape of the main lobe, and (ii) the number and positions of the side lobes. If such features are used, then the network as a classifier is relieved from the burden of having to delineate the range of changes of a fetal heartbeat, still swamped by noise and maternal contributions, with complicated decision boundaries. Indeed, the only differences that may arise between different instances of the same ordered fetal heartbeat (first heartbeat-to-first heartbeat correspondence, or second heartbeat-to-second heartbeat correspondence, etc) are due to unavoidable factors such as motion artefact and noise. The use of an invariant-feature space offers three distinct advantages; (i) The number of features applied to the network may be reduced to realistic levels; (ii) the requirements imposed on network design are relaxed; and (iii) invariance for all fetal heartbeats with respect to known changes is assured [71]; however, this approach requires *prior knowledge* of the important features. This *prior knowledge* can be acquired using a *feature detector*. A *feature detector* is employed to reduce the input data by extracting certain "*features*" that distinguish the 2-d third-order cumulants of one class (say the mother) from another class (say the fetal). This feature detector has already been used in our preliminary investigation by looking at approximately 15 slices of each of the ECG cumulants in the database, and deciding which slice in each class

provides the most discriminant features. The unique structural properties of individual diagonal, wall, and both diagonal and wall slices of the third-order cumulants (TOC) of ECG signals are the results of this *human feature detector* [54, 57]. More discussions are given in the final section of this chapter as well as a review of work done on the subject of locally structured multi-layer perceptrons which was carried out under a contract with an international company (the said company insists on confidentiality). ***This has prompted us to consider the single-hidden-layer neural network with only two cumulant slices presented at its input layer, namely, the linear non-Gaussian third-order cumulant diagonal and wall slices of the ECG signals.***

(3) *Invariance by structure*. Invariance may be imposed on a neural network by structuring its design appropriately. Specifically, synaptic connections between the neurons of the network are created such that changed versions of the same input are forced to produce the same output [70].

4.1.3 The single-hidden-layer perceptron and a one-dimensional cumulant slice

In this thesis a single-hidden-layer neural network is considered with only two cumulant slices presented at its input layer, namely, the *linear* non-Gaussian third-order cumulant diagonal and wall slices of the ECG signals. In this Chapter, third-order cumulants are used because of their ability to suppress Gaussian noise and all other noise components with symmetric probability density functions. Linearisation of the ECG data is a crucial key step. As mentioned in Chapter Three, this is accomplished by using either an LMF-based adaptive second- or third-order Volterra synthesiser. After linearisation, the third-order cumulants support linear non-Gaussianness peculiar to the signals they represent and this can be used as the discriminant features which are then fed to a single-hidden-layer perceptron with the ubiquitous back-propagation algorithm with momentum.

In general, in order to create any cumulant slice, one has to build up the whole two-dimensional cumulant structure and then choosing the appropriate co-ordinate system for the cutting plane which is used for slicing the cumulants at any arbitrary angle. This process does not apply to the special cases of the diagonal and wall slices as they are much simpler to create by freezing one time lag and letting the second lag vary as the cumulant calculation is performed as described by Eqs. (4.2) and (4.3) in

Section 4.4.1. There are mathematical formulae designed by the author which describe any arbitrarily chosen off diagonal and off wall one-dimensional slice and this helps to reduce the CPU time by 99%.

4.1.4 Layout of the Chapter

The Chapter starts by discussing the following issues; (1) ECG cumulant database, (2) classification, (3) ECG segmentation and window minimum length, (4) window overlapping, (5) calculation of an averaged fetal heart rate within one maternal cardiac cycle, (6) the effect of using more than one slice and linearisation on the classification rate, and (7) shortcomings of the cumulant matching technique. Section 4.2 presents other relevant research work on independent component analysis with its virtues and vices. Section 4.3 provides a brief description of the detection key operations of the TOC template matching technique. Section 4.4 briefly describes the equations for the TOC 1-d diagonal and wall slices, examines the effect of reducing the length of segmentation on the variance of the third-order cumulants, the effect of reducing the length of segmentation on the variance, skewness, and kurtosis for white Gaussian noise, and the effect of linearisation on third-order cumulants. Typical examples of the TOCs and their diagonal and wall slices with and without linearisation are then shown, and the TOC variance is calculated. Section 4.5 describes the back-propagation with momentum algorithm. It then describes the optimisation of the parameters of the classifier. Results are shown for maternal QRS-complex and fetal heartbeat classification rates for different TOC slices with and without linearisation employing second- and third-order Volterra synthesisers with LMF update. Summary and conclusions are given in Section 4.6.

4.1.5 Abbreviations

In this thesis, the following abbreviations are used for convenience;

Three-dimensional Third-Order Cumulants	=	TOC ,
Fetal scalp electrode cardiac cycle TOC	=	FS TOC ,
Fetal scalp electrode cardiac cycle TOC diagonal slice	=	FS TOC D,
Fetal scalp electrode cardiac cycle TOC wall slice	=	FS TOC W ,
Maternal-chest cardiac cycle TOC	=	MC TOC ,
Maternal-chest cardiac cycle TOC diagonal slice	=	MC TOC D ,
Maternal-chest cardiac cycle TOC wall slice	=	MC TOC W ,

Maternal-chest QRS-complex TOC = MC QRS TOC ,

Maternal-chest QRS-complex TOC diagonal slice = MC QRS TOC D ,

Maternal-chest QRS-complex TOC wall slice = MC QRS TOC W,

Maternal-transabdominal cardiac cycle TOC = MT TOC ,

Maternal-transabdominal cardiac cycle TOC diagonal slice = MT TOC D ,

Maternal-transabdominal cardiac cycle TOC wall slice = MT TOC W ,

Maternal-transabdominal QRS-complex TOC = MT QRS TOC ,

Maternal-transabdominal QRS-complex TOC diagonal slice= MT QRS TOC D ,

Maternal-transabdominal QRS-complex TOC wall slice = MT QRS TOC W ,

Fetal transabdominal ECG TOC diagonal slice = FT ECG TOC D,

and Fetal transabdominal ECG TOC wall slice = FT ECG TOC W .

4.1.6 ECG cumulant database

During the last decade, several ECG recordings were borrowed on loan from the North Middlesex Hospital and the Royal Free and University College Medical School. Essentially, each of the ECG recordings has one-minute duration and consists of synchronised maternal chest, maternal transabdominal and fetal scalp electrode ECG signals. Data acquisition is briefly described in Section 1.8. Such ECG recordings have been used to produce third- and fourth-order cumulants and their diagonal and wall slices. This is referred to as the cumulant database.

4.1.7 Classification

One hundred and sixty one-dimensional TOC slices (please refer to Section 2.13: 1-3) have been used as templates for the desired signals in the Artificial Neural Network (ANN) classifier. The classifier is a single-hidden-Layer Perceptrion based on a modified Back-Propagation technique [13]. The modified back-propagation algorithm has a momentum term which helps to avoid local minima [13]. A brief description is given in Section 4.5.

4.1.8 ECG segmentation and window minimum length

The duration of the fetal cardiac cycle varies from 250 msec (for a heart rate of 240 bpm) to 500 msec (for a heart rate of 120 bpm) for a range of fetal heart rate between 240 bpm and 120 bpm. The fetal QRS-complex itself occupies between 50 msec and 70 msec. In this thesis, the fetal heartbeat is detected in a flag window of

length 250 msec. This window length serves two criteria; (i) it is the minimum length yielding an acceptable upper threshold of both the deterministic and stochastic noise types inherent in the higher-order statistics of the ECG signals encountered (see Section 4.4), and (ii) this window length allows the detection of one, two, three, or four fetal heartbeats (FHBs) within one maternal transabdominal cardiac cycle. For example, for maternal heartbeat of 60 bpm, the R-wave-to-R-wave = 1000 msec, and four segments x 250 msec = one maternal cardiac cycle = possible four fetal cardiac cycles. Figure 4.1 shows the synchronised maternal chest, maternal transabdominal, and fetal scalp electrode cardiac cycles. In this particular case, there are two fetal scalp electrode cardiac cycles for each maternal cardiac cycle.

4.1.9 Window overlapping

When detecting the fetal heartbeat within the "maternal" transabdominal cardiac cycle, 90% overlapping windows, each of 250 msec duration, are scanned at a rate of 100 Hz with a sampling rate of 0.5 KHz. The overlapping percentage should be carefully chosen to compensate for the apparent loss of temporal resolution due to lengthy window which, as mentioned above, is dictated by the maximum threshold of the variance of the third-order cumulants. Assuming that the average fetal QRS-complex duration is 60 msec, this may be encountered at the beginning, middle, or end of the flag window. Hence by using a window overlapping of 90%, any fetal QRS-complex which may be missed because it starts to evolve, say, 20 msec before the end of a window, can definitely be picked up by the next one or two overlapping windows when it completes its full duration of 60 msec and has definitely reached its full peak and signature (the R-wave). If this particular QRS-complex has enough strength to be picked up by two successive overlapping windows, the algorithm will count it as one FHB. It has been found that reducing the overlapping below 90% yielded missed fetal heartbeats.

4.1.10 Calculation of an averaged fetal heart rate within one maternal cardiac cycle

The instantaneous fetal heart rate is calculated by measuring the interval between two successive R-waves and this requires pinpointing accurately the R-point of the QRS-complex. This cannot be achieved without a visual display of the R-wave. Although the ECG TOC template matching technique is very effective in detecting the

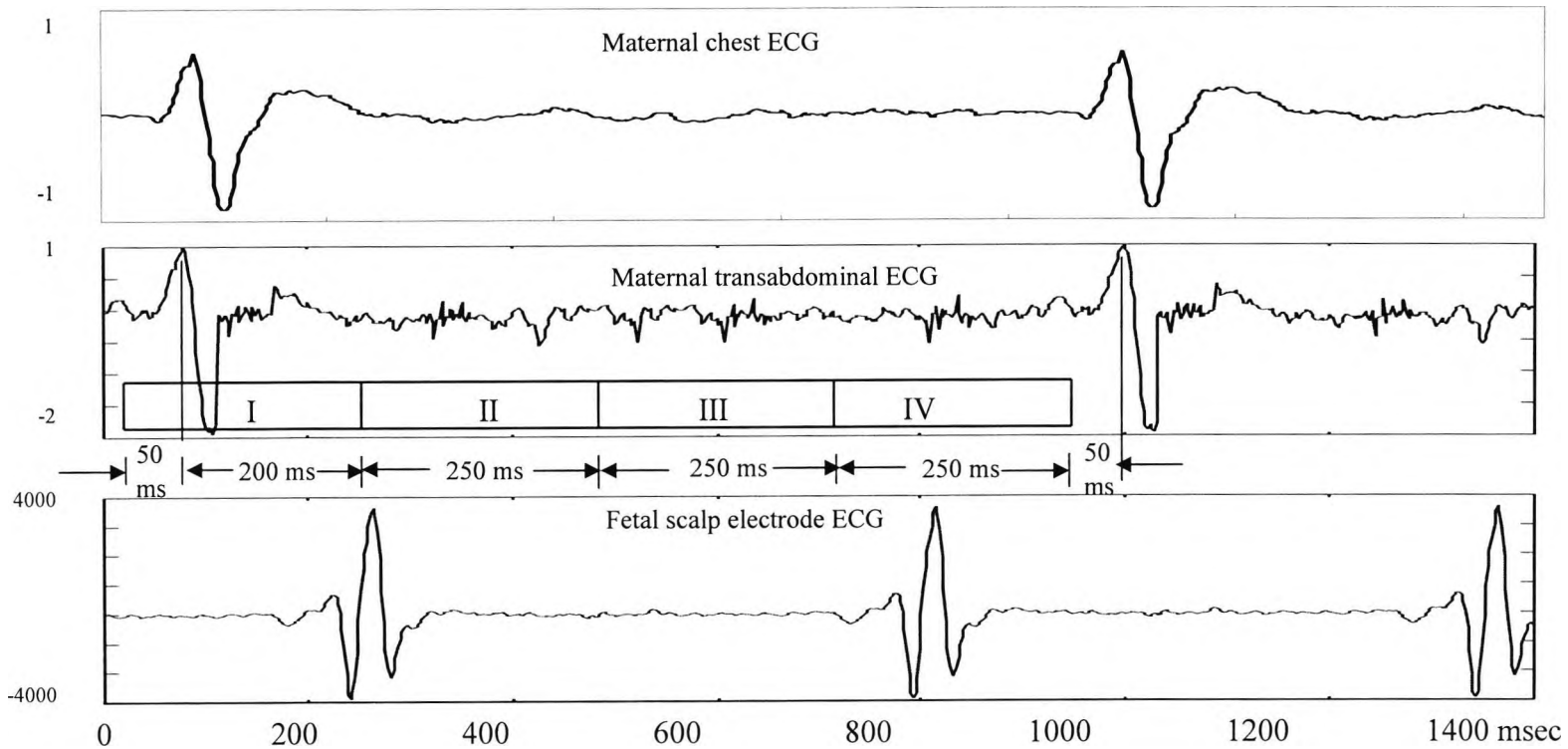

Figure 4.1: *One maternal chest cardiac cycle (upper panel), maternal transabdominal (middle panel), and the synchronised and amplified fetal ECG (lower panel). The maternal cardiac cycle begins 50 msec before the R-wave and ends 50 msec before the next R-wave. Segment I: maternal QRS-complex, segment II: the first fetal heartbeat with maternal contribution, segment III: QRS-free ECG, and segment IV: the second fetal heartbeat with maternal contribution.The subject is at the first stage of labour, 40 weeks gestation. The maternal cycle has 500 samples at a rate of 0.5 KHz. (Code: 5-14).*

occurrence of the QRS-complex as a whole even when it is completely buried in noise, it cannot locate the R-wave over a window length of 250 msec (which satisfies the criterion for the variance threshold). We have to bear in mind that, in most transabdominal ECG recordings (85%), the fetal QRS-complexes cannot be seen as they are completely masked by other signals and motion artefact. This obscurity accounts for the lower success rate of fetal heartbeat detection in all other reported and appropriately assessed fetal heartbeat detection techniques [63].

We can measure fairly accurately the adult heartbeats and calculate the instantaneous heart rate for adults [41]. Hence, by counting the number of fetal heartbeats (FHBs) that have occurred between two successive maternal R-waves, one can easily calculate the averaged FHR within the maternal cardiac cycle. Thus,

FHR = MHR x Number of FHBs / number of maternal heartbeats

On average, the maternal cardiac cycle is 1000 msec. Two maternal cardiac cycles measure 2 sec. So, detecting and displaying up to eight FHBs will take less than 2.000030 sec which is well within the manufacturers' detection-to-display interval of 3.75 sec*.

4.1.11 Combined cumulant slices and linearisation of transabdominal ECG signals

It will be shown in Section 4.5.7.2 that a linear combination of diagonal and wall slices of the TOC can improve the detection rate by up to 1% over and above the 77.8% obtainable using only either slice. Using two more arbitrary slices off-diagonal and off-wall would result in a further improvement of up to 1%. Using two slices instead of only one results in an two-fold increase in the CPU time of 1 msec using Unix WS. A Further improvement of 6% to 8% is attainable with ECG signal linearisation (removing the synthesised quadratic and cubic non-linearities from both signal and noise) using second- and third-order Volterra synthesisers, respectively. The latter results are also given in Section 4.5.7.2.

* For example, the CPU time for detecting a 250 msec segment using a Texas Instruments TMS320C40 is 20 μs.

4.1.12 Shortcoming of the TOC template matching technique

It will be shown in section 4.5.7.2 that the TOC template matching technique of linearised maternal transabdominal ECG signals can reach a high detection rate of 86%, i.e., for every 100 fetal heartbeats (FHBs) only 14 are missed. Most of the missing 14 beats in every 100 beats have been found to coincide with the maternal QRS-complexes or occur during depolarisation of the maternal P- and T-waves. Those events unavoidably lead to significant distortion of the fetal third-order cumulants. This means that the cumulant signatures will not be close to the cumulant template signature stored in the database. It will also be shown in Chapter Six that the third non-invasive MUSIC-like technique is not susceptible to the co-existence of maternal and fetal QRS-complexes or the co-existence of the maternal P-wave or T-wave and the fetal QRS-complex since the corresponding spectral peaks are usually adequately separated. Higher detection rates of up to 95.5% have been achievable using the above mentioned technique.

4.2 Other relevant research work involving cumulants based on Independent Component Analysis (ICA)

Some research workers [98, 114-115] have recently been using Independent Component Analysis (ICA), also known as Blind Source Separation (BSS), in pursuit of separating mother's and fetal ECG signals from cutaneous measurements. In the publications [62, 64-65] the ICA has been carried out under the following assumptions, the validity of each of which has been challenged in the author's joint paper [63] (a copy of our publication is given in Appendix A3); (1) Sensors (electrodes) are assumed to form an instantaneous linear mixture of mother and fetal source signals. (2) Noise is assumed to have an additive Gaussian perturbation. (3) The mother's and fetal ECG signals are assumed to be stationary and linear, mutually statistically independent and statistically independent from noise. (4) Most of the second-order and fourth-order Blind Source Separation (BSS) methods developed to date assume that all ECG third-order cumulants vanish, which shows their lack of understanding of ECG statistics, hence the need to use the fourth-order cumulants. Furthermore, a crucial factor in using Independent Component Analysis (ICA) is the accurate positioning of the individual cutaneous electrodes connected to channels numbering from six up to 32 in aid of signals' orthogonalisation.

References [62, 64-65] have succeeded in separating fetal heartbeats (FHBs) using just eight electrodes (channels). But, the collection of data used has been rather limited to clean segments taken during gestation periods, and very conveniently chosen to have very high signal-to-noise ratio (SNR), and cleverly avoiding data with intrapartum cyclic uterine contractions or serious motion artefacts. Furthermore, the aforementioned publications **have failed to include in their assessment the imminently and most frequently occurring episodes of coincident mother's and fetal heartbeats. This is the most challenging problem which is imminent in around 10% of the measured data.** As mentioned before, due to the non-linear nature of the maternal and fetal QRS-complexes and the non-linear physical channel through the uterus layers and the abdomen layers, quadratic and higher-order coupling is generated between the mother's and fetal ECGs as their separate signals propagate through the inner tissues. This also results in non-stationarity and presents a formidable detection problem even when higher-order statistics are used as DSP tools.

Independent Component Analysis (ICA) essentially requires high signal-to-noise ratios (SNRs) and has, so far, been used antepartum without appropriate assessment (i.e., no provision of fetal scalp electrode ECG reference to confirm the detection of fetal QRS-complexes) [62, 64-65].

These methods have been criticised in our paper "Virtues and Vices of Source Separation Using Linear Independent Component Analysis for Blind Source Separation of Non-linearly Coupled and Synchronised Fetal and Mother ECGs" [62] where the following issues have been raised: In our paper [99], there is evidence of non-linear quadratic and cubic coupling and non-stationarity in the transabdominally measured signals when the fetal and maternal heartbeats are coincident or even close enough. This, therefore, requires a high degree of sophistication in the non-linear modelling of both the maternal and fetal ECG signals to be able to establish the extent of quadratic coupling (cubic coupling is very weak) and incorporate it in the analysis. At this juncture, any justification of **the key assumption of linearity and mutual statistical independence** of both maternal and fetal ECG signals which is the basis for the ICA techniques, is now questionable [99]. We report in Chapter Three the use of non-linear Volterra structures which caters for quantifying the linear, quadratic, and cubic parts of both the maternal and fetal ECG signals. The subsequent analysis is much more

simplified by including only the linear non-Gaussian component of the ECG signals and noise. The analysis referred to includes; (1) the third-order cumulant template matching technique (**TOC template matching**), (2) the bispectral contour template matching technique (**BIC template matching**), and (3) the modified spectral multiple signal classification (MUSIC) with incorporated covariance matrix for uterine contraction combined with noise. It is worth reporting at the end of this short appraisal that present techniques for non-linear ICA only cater for non-linear mixtures and are definitely not adequate to separate non-linear sources such as the mother's / fetal ECGs in non-linear noise artefacts which is the case during labour.

4.3 Brief description of detection key operations

Operation 1- Creating ECG cumulant database

Please refer to Section 2.13: 1-3.

Operation 2- Detecting the maternal QRS-complexes and pinpointing their R-waves

This step includes sequential reading of the ECG recording and processing each of the 90% overlapping windows (length 250 msec) to compute the diagonal or wall slice TOC. The slice is then matched to the templates until a maternal QRS-complex is detected. Once the first MT QRS TOC D and the MT QRS TOC W have been detected, an auxiliary subroutine is used to accurately pinpoint the position of the R-wave [41]. If the second successive segment detects a maternal QRS-complex then it is discarded because it is the same complex detected twice in two adjacent windows. The whole process of window TOC template matching technique is repeated until the second maternal QRS-complex is detected and its R-wave is pinpointed. The maternal heart rate is accurately calculated from the knowledge of the current and previous R-wave positions.

Operation 3- Detecting the fetal cardiac cycles within each maternal cardiac cycle

Now the search for the fetal cardiac cycle begins at –50 msec from the position of the detected maternal R-wave even though the TOC template matching technique cannot detect fetal events under the maternal QRS-complex and as mentioned earlier fetal flag windows for this particular technique must not overlap with the first window containing the maternal QRS-complex. Window overlapping, each with fetal cumulant template

matching, continues until the first, second, and possibly third FT ECG TOC D and FT ECG TOC W signatures have been matched to at least one corresponding template for each one of them. Once the FT ECG TOC D and FT ECG TOC W have been template matched, which means fetal heartbeat detection, the window will be flagged as a detection window. If the next overlapping window detects a fetal heartbeat, it will be discarded because it is the same fetal heartbeat that has just been detected in the previous window. The number of fetal heartbeats detected within the maternal cardiac cycle is counted and the following ratio is calculated;

The average FHR = MHR x Number of FHBs / number of maternal heartbeats

In the above formula, the instantaneous maternal heart rate is previously known with some degree of accuracy, and the relative fetal to maternal heartbeat is also known within the maternal cardiac cycle. Hence, the averaged fetal heart rate can be calculated within each maternal cardiac cycle.

Operations 2 and 3 are repeated for all individual maternal cardiac cycles.

4.4 Preliminary investigations of ECG Third-order cumulants

4.4.1 Mathematical modelling of third-order cumulant 1-d slices

Definitions concerning higher-order statistics are given in Chapter 2. In this section we give definitions of third-order cumulant slices. Consider a non-Gaussian signal {X(k)} with third-order cumulants given by [1]:

$$C_3^x(\tau_1,\tau_2) = \mathrm{Cum}\{X(k), X(k+\tau_1), X(k+\tau_2)\}. \tag{4.1}$$

The calculations of the third-order cumulants (see Chapter 2) are implemented off-line due to the large CPU time required to calculate the lags in different dimensions. One way of reducing this load is to use 1-d slices of the third-order cumulants. One-dimensional slices of $C_3^x(\tau_1,\tau_2)$ can be defined as:

$$r_{2,1}^x(\tau) \underline{\underline{\nabla}} \mathrm{Cum}\{X(k), X(k), X(k+\tau)\} = C_3^x(0,\tau), \text{ and} \tag{4.2}$$

$$r^{x}_{1,2}(\tau)\underline{\underline{\nabla}}\mathrm{Cum}\{X(k), X(k+\tau), X(k+\tau)\} = \mathbf{C}^{x}_{3}(\tau,\tau). \qquad (4.3)$$

This will have the effect of reducing the CPU time by reducing the complexity of the operations by at least three orders of magnitude. The calculations of third-order cumulant slices are comparable to those of autocorrelation and take CPU time of approximately 1 msec unlike third-order cumulants, which take 1 to 3 sec to calculate depending on the segment length. The motivation behind the use of the one-dimensional TOC D or TOC W, instead of multi-dimensional sequences in the identification of mother's QRS-complexes, the first and second fetal heartbeats with maternal contribution, and QRS-free ECG, is due to excessive number crunching in the latter which can take a CPU time in excess of 1 sec. The CPU time for a diagonal slice is of the order of 1 msec. For a sampling rate of 0.5 KHz and an FHR of the order of 120 bpm, a real-time system can be easily implemented.

4.4.2 New (auxiliary) algorithm for direct calculations of 1-d TOC arbitrary slices

There are mathematical formulae designed by the author which describe any arbitrarily chosen off diagonal and off wall one-dimensional slice and this helps to reduce the CPU time by 99%. A brief description of the algorithm is given in the flowchart shown in Figure 4.6.

4.4.3 The effect of reducing the length of segmentation on the variance of the third-order cumulants for QRS-free ECG segments

To provide a reasonably accurate estimate for third-order cumulants one has to maintain the variance below a threshold value. The definition for the variance is given in Eq. (2.26). It increases with decreased data length until it seriously compromises the validity of the third-order cumulant calculations. The threshold value is established by first calculating the variance of the third-order cumulants for a very long ECG signal and then gradually reducing the signal length to that which is comparable with the deterministic signal to be detected whilst plotting the resultant variances versus signal lengths (number of samples). The results are tabulated in Table 4.1 and it is shown that reducing the data length from 250 msec to 124 msec would result in more than doubling of the variance for the third-order cumulants of the concerned ECG signal. The reason for removing the QRS-complexes prior to calculating the variance is to work in the

Time (msec)	20000	8000	4000	2000	1000	500	250	124
Variance of Cumulants	0.02	0.05	0.09	0.11	0.15	0.18	0.21	0.45

Table 4.1: *The variance of the third-order cumulants for QRS-free segments of different lengths taken from fetal scalp electrode ECG.*

realm of low signal-to-noise ratios which is encountered in weak fetal heartbeat detection.

4.4.4 The effect of reducing the length of segmentation on the variance, skewness, and kurtosis of white Gaussian noise

The fundamental reason for employing higher-order statistics to detect fetal heartbeats is based on the assumption that white Gaussian noise will not have third- or higher-order cumulants. However, the assumption is only valid for sufficiently long data length. Therefore, the effect of reducing the data length on the variance, skewness, and kurtosis of white Gaussian noise has to be investigated. White Gaussian noise is synthetically generated using the NAG library and Fortran 77, and the variance, skewness and kurtosis are calculated for different data lengths and these are tabulated in Table 4.2. The statistics start to deviate from that of Gaussian noise by more than 10% when the segment length is below 250 msec (with a variance of 1.2172).

Time (msec)	Mean	Variance	Skewness	Kurtosis
20000	-0.0016	1.0017	-0.0038	0.0648
8000	-0.0017	1.0029	-0.0046	0.1324
4000	-0.002	0.9825	-0.00656	0.1858
2000	0.0121	0.9741	0.0604	0.2631
1000	0.0411	1.0175	0.0728	0.4463
500	0.0852	1.0226	0.0902	0.7083
250	0.0917	1.0629	0.0985	0.9893
124	0.1243	1.2172	0.1371	1.6557

Table 4.2: *The effect of reducing the length of segmentation on the variance, skewness, and kurtosis of white Gaussian noise.*

4.4.5 The effect of linearisation on cumulants

In some cases the maternal transabdominal ECG signal is severely corrupted with noise and it is extremely difficult to detect the fetal heartbeat in the third-order cumulants domain. An example of this is shown in Figure 4.2 in conjunction with Figure 4.1 which shows the ordered segmentation (I, II, III, and IV) of the transabdomiannlly-measured maternal cardiac cycle. It is impossible to distinguish the QRS-free ECG segment (Figure 4.2 (a) III) and the fetal heartbeat segments (Figure 4.2 (a) II and IV) from their third-order cumulants. Linearisation (removing the quadratic and cubic parts of the signal using the optimised adaptive LMF-based third-order Volterra structure of Section 3.4- relevant parameters are found in the caption of Figure 4.2), has showed significant improvement. The parameters used are: filter order = 3, filter length = 6, delay = 5, step-size parameters = 0.002, 0.0004, 0.0001 for linear, quadratic and cubic parts, respectively.

Figure 4.2 (b) shows the third-order cumulants after synthesising the signal using a third-order Volterra structure with LMF update and retaining only the linear part of the signal. The noise is partially suppressed, and the fetal heartbeat segments (Figure 4.2 (b) II and IV) are now recognisable from the third-order cumulants. The main disadvantage of using linearisation is that it is an off-line routine. It takes CPU time of 2-3 sec to clean one full maternal transabdominal cardiac cycle. Figure 4.2 (c), (d) shows similar results using an adaptive LMS-based third-order Volterra synthesiser.

4.4.6 Typical examples of TOCs and their diagonal and wall slices

An optimised third-order Volterra structure is employed to decompose the ECG signal into its linear, quadratic, and cubic parts and retain only the linear part (the parameters are like those found in Section 4.4.5 and Figure 4.2). Figures 4.3 (a) - (e) depict five maternal transabdominal ECG signals with segmentation and their corresponding TOCs and their diagonal and wall slices for predominantly maternal QRS-complexes, the first fetal heartbeats with maternal contribution, QRS-free ECGs, and the second fetal heartbeats with maternal contribution. The diagonal and wall TOC slices of the maternal QRS-complexes, segment (I) in Figures 4.3 (a-e), are easily distinguished from the diagonal and wall TOC slices of segments (II), (III), and (IV). Furthermore, the diagonal and wall TOC slices of the fetal heartbeat segments, (II) and (IV) in Figures 4.3 (a, d-e), are distinguishable from the corresponding diagonal and wall TOC slices of the

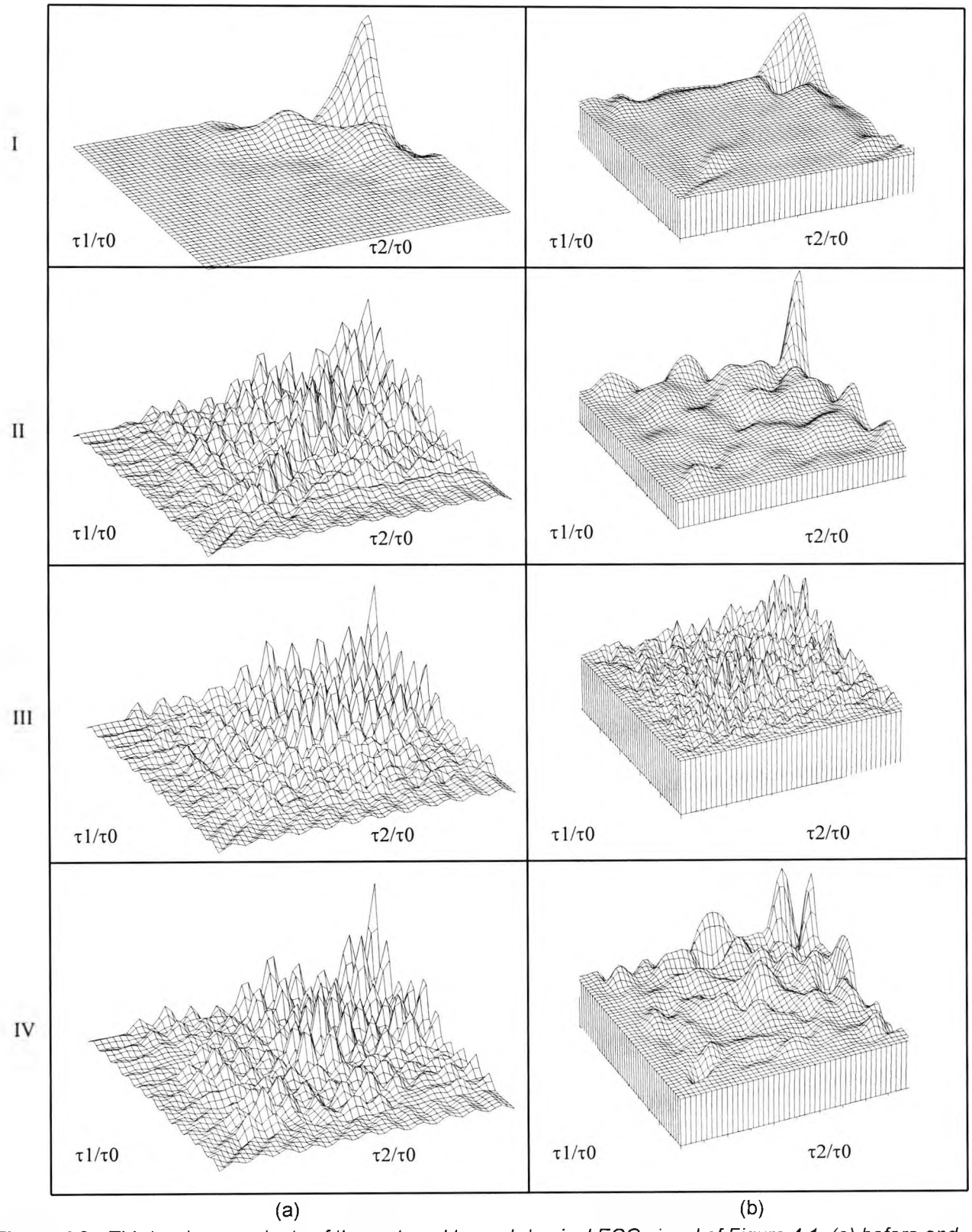

Figure 4.2: *Third-order cumulants of the maternal transabdominal ECG signal of Figure 4.1, (a) before and (b) after linearisation. The segmentation order shown on the l.h.s. of the Figure mark the following portions of the ECG: (I) predominantly maternal QRS-complex, (II) the first fetal heartbeat with maternal contribution, (III) QRS-free ECG, and (IV) the second fetal heartbeat with maternal contribution segments. Each segment is 250 msec. Linearisation has been carried out using an adaptive LMF-based Volterra synthesiser. The Volterra synthesiser parameters are: filter order = 3, filter length = 6, delay = 5, step size = 0.002, 0.0004, 0.0001 for linear, quadratic and cubic parts, respectively. (Code: 5-31).*

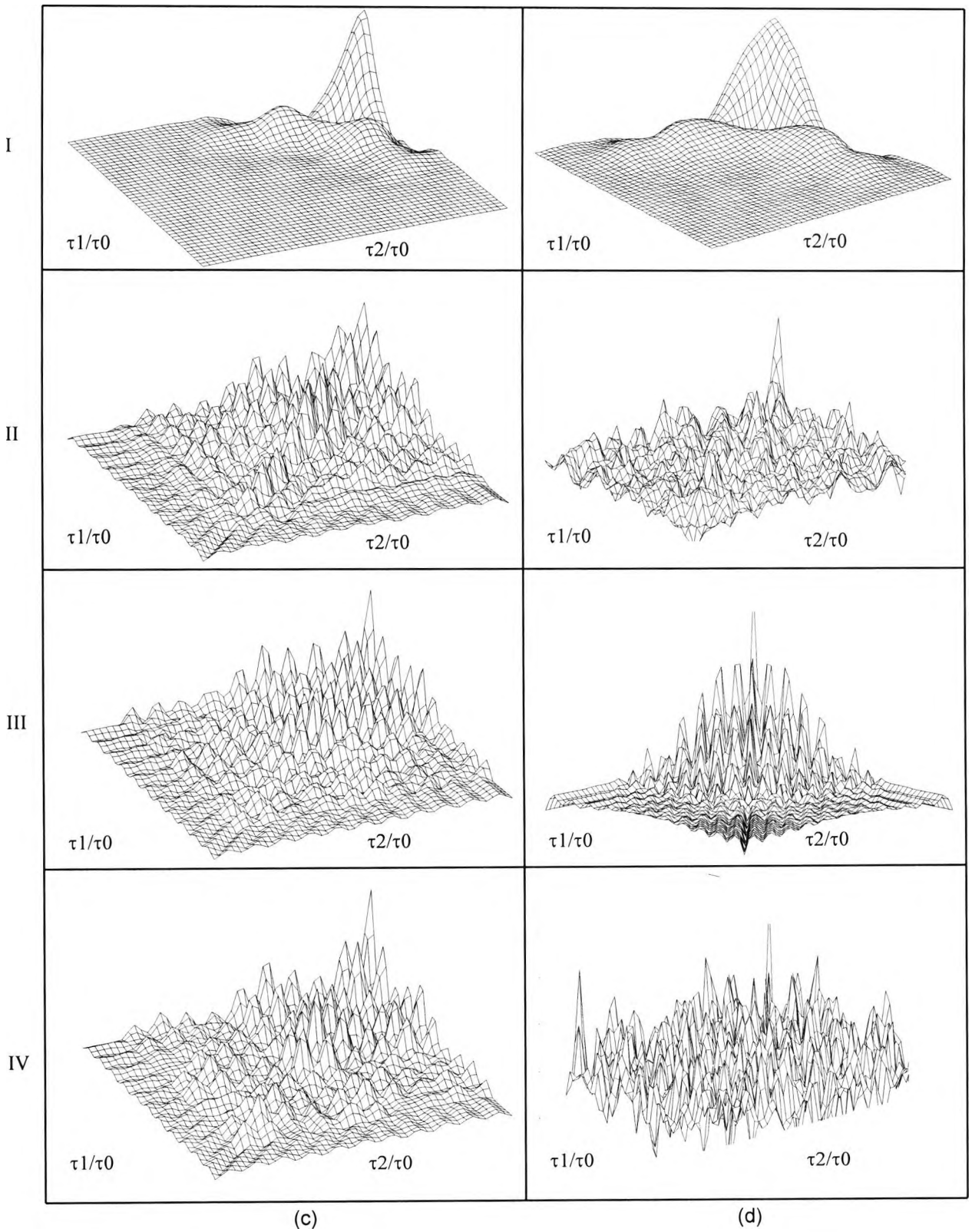

Figure 4.2 *(continued): Third-order cumulants of the maternal transabdominal ECG signal of Figure 4.1, (c) before and (d) after linearisation. The segmentation order shown on the l.h.s. of the Figure mark the following portions of the ECG: (I) predominantly maternal QRS-complex, (II) the first fetal heartbeat with maternal contribution, (III) QRS-free ECG, and (IV) the second fetal heartbeat with maternal contribution segments. Each segment is 250 msec. Linearisation has been carried out using an adaptive LMS-based Volterra synthesiser. The Volterra synthesiser parameters are: filter order = 3, filter length = 6, delay = 5, step size = 0.002, 0.0004, 0.0001 for linear, quadratic and cubic parts, respectively. (Code: 5-31).*

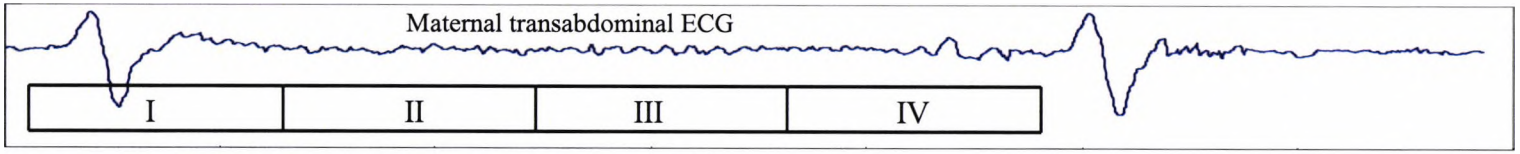

(a1)

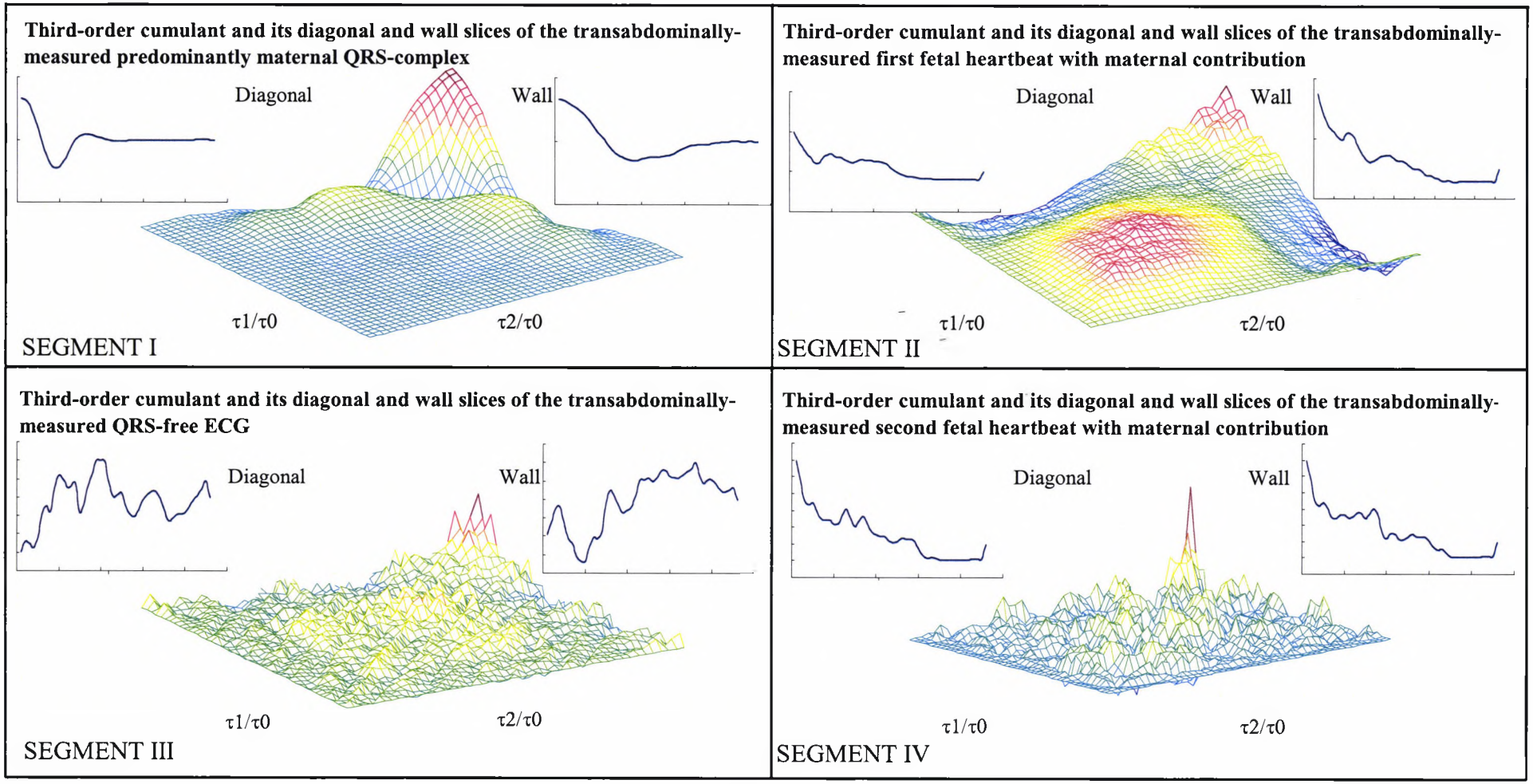

(a2)

Figure 4.3 (a1, a2): *(a1) Transabdominally-measured ECG (Code: 16-9) showing segmentation (segments I, II, III, and IV,each 250 msec). (a2) The corresponding third-order cumulants and their diagonal and walll slices (insets).(I) Predominantly maternal QRS-complex, (II) the first fetal heartbeat with maternal contribution, (III) QRS-free ECG, and (IV) the second fetal heartbeat with maternal contribution.* τ_0, τ_1,*and* τ_2 *are, respectively, the reference, first and second time lags of the third-order cumulants.A third-order Volterra structure is employed to synthesise the ECG signal into its linear, quadratic, and cubic parts and retain only the linear part.*

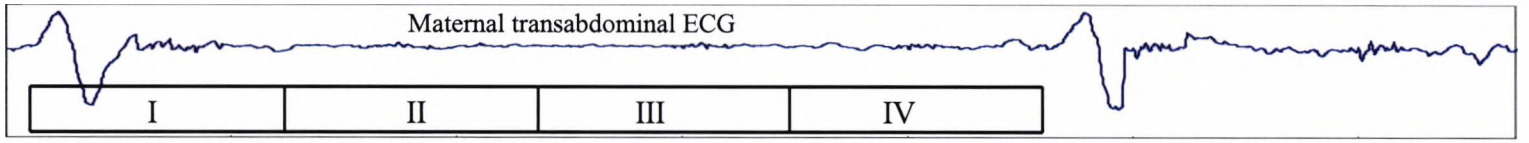

(b1)

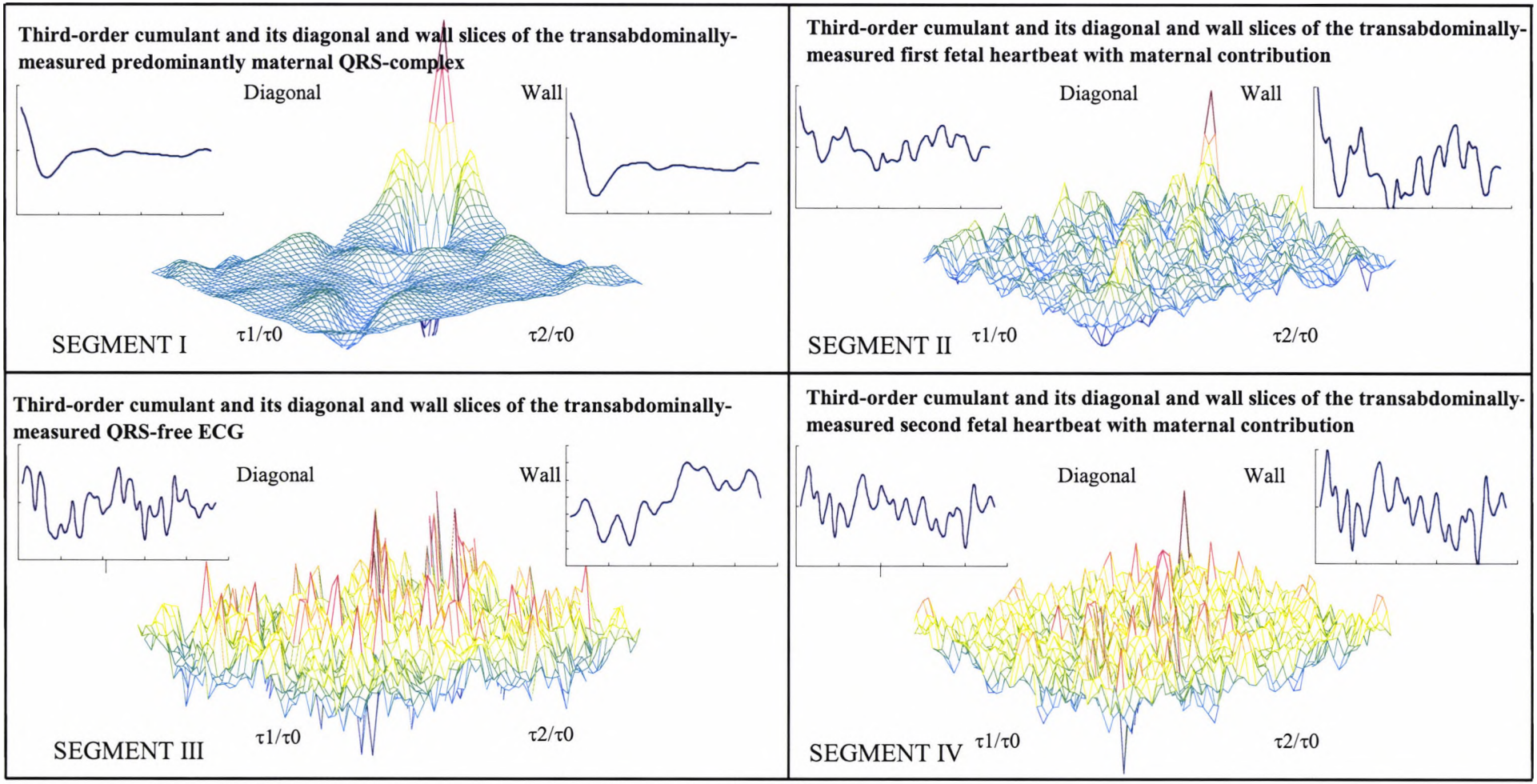

(b2)

Figure 4.3 (b1, b2): *(b1) Transabdominally-measured ECG (Code: 5-32) showing segmentation (segments I, II, III, and IV,each 250 msec). (b2) The corresponding third-order cumulants and their diagonal and walll slices (insets).(I) Predominantly maternal QRS-complex, (II) the first fetal heartbeat with maternal contribution, (III) QRS-free ECG, and (IV) the second fetal heartbeat with maternal contribution.* τ_0, τ_1, *and* τ_2 *are, respectively, the reference, first and second time lags of the third-order cumulants. A third-order Volterra structure is employed to synthesise the ECG signal into its linear, quadratic, and cubic parts and retain only the linear part.*

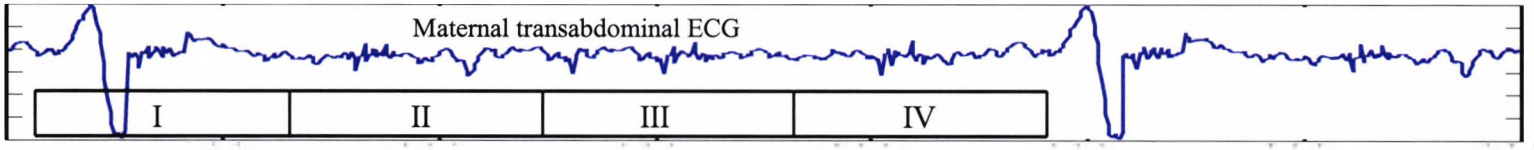

(c1)

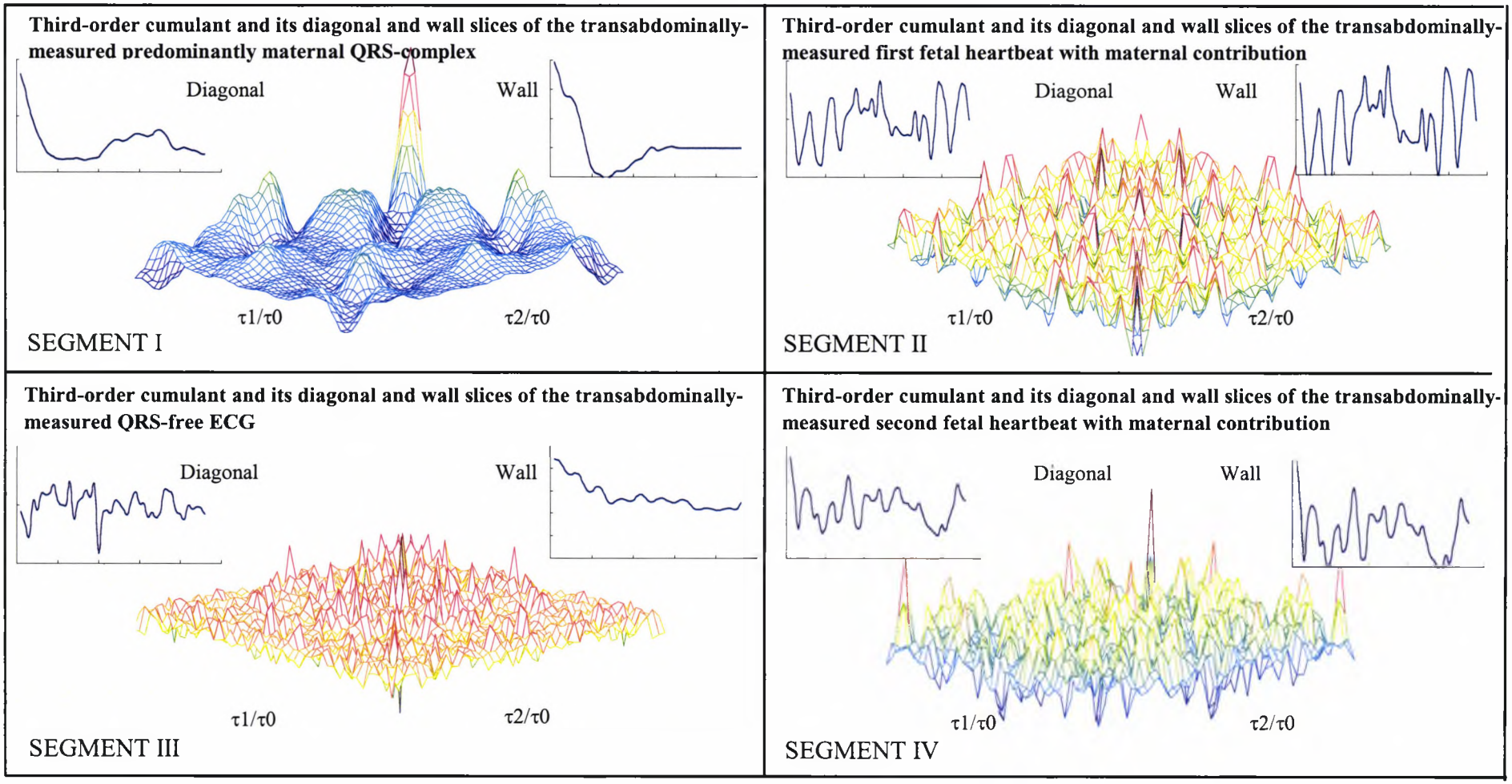

(c2)

Figure 4.3 (c1, c2): *(c1) Transabdominally-measured ECG (Code: 5-33) showing segmentation (segments I, II, III, and IV,each 250 msec). (c2) The corresponding third-order cumulants and their diagonal and walll slices (insets).(I) Predominantly maternal QRS-complex, (II) the first fetal heartbeat with maternal contribution, (III) QRS-free ECG, and (IV) the second fetal heartbeat with maternal contribution.* τ_0, τ_1, *and* τ_2 *are, respectively, the reference, first and second time lags of the third-order cumulants.A third-order Volterra structure is employed to synthesise the ECG signal into its linear, quadratic, and cubic parts and retain only the linear part.*

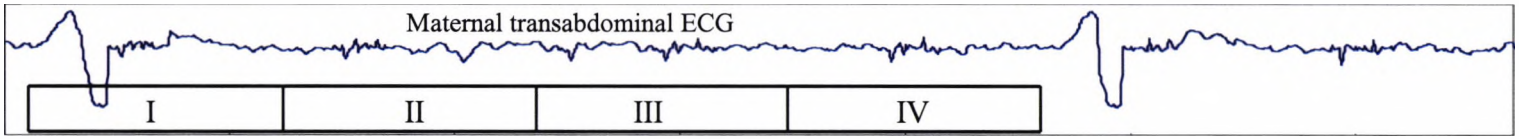

(d1)

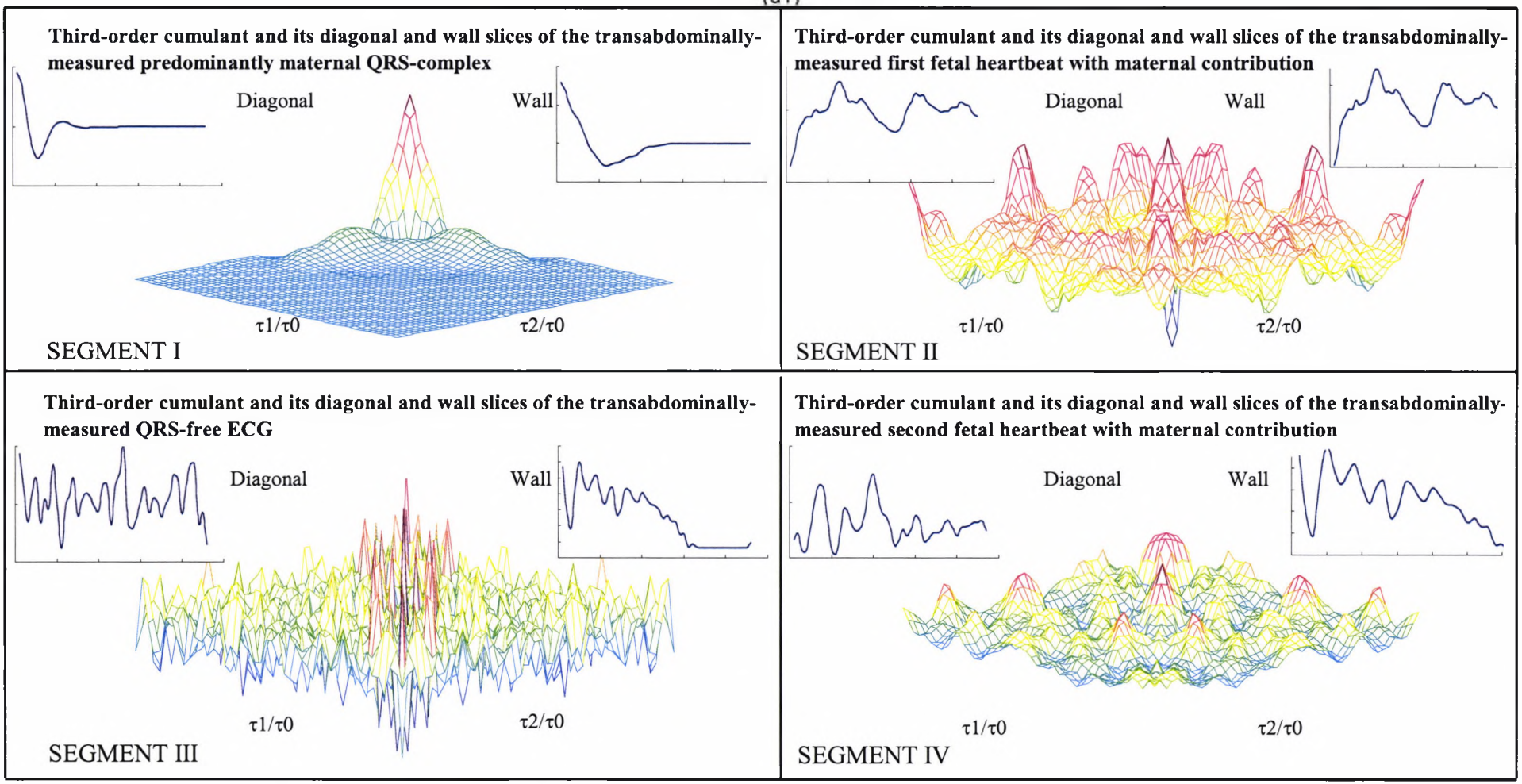

(d2)

Figure 4.3 (d1, d2): *(d1) Transabdominally-measured ECG (Code: 5-31) showing segmentation (segments I, II, III, and IV,each 250 msec). (d2) The corresponding third-order cumulants and their diagonal and walll slices (insets).(I) Predominantly maternal QRS-complex, (II) the first fetal heartbeat with maternal contribution, (III) QRS-free ECG, and (IV) the second fetal heartbeat with maternal contribution.* τ_0, τ_1, *and* τ_2 *are, respectively, the reference, first and second time lags of the third-order cumulants. A third-order Volterra structure is employed to synthesise the ECG signal into its linear, quadratic, and cubic parts and retain only the linear part.*

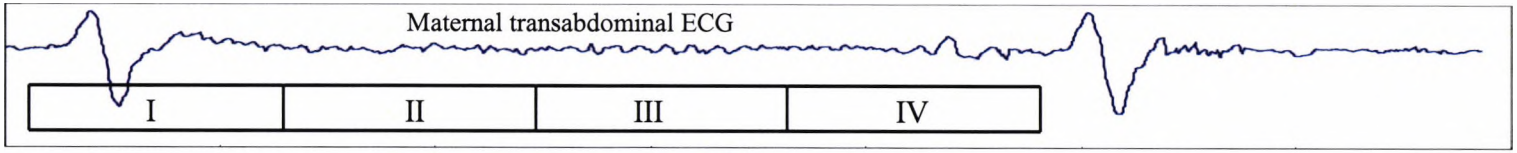

(e1)

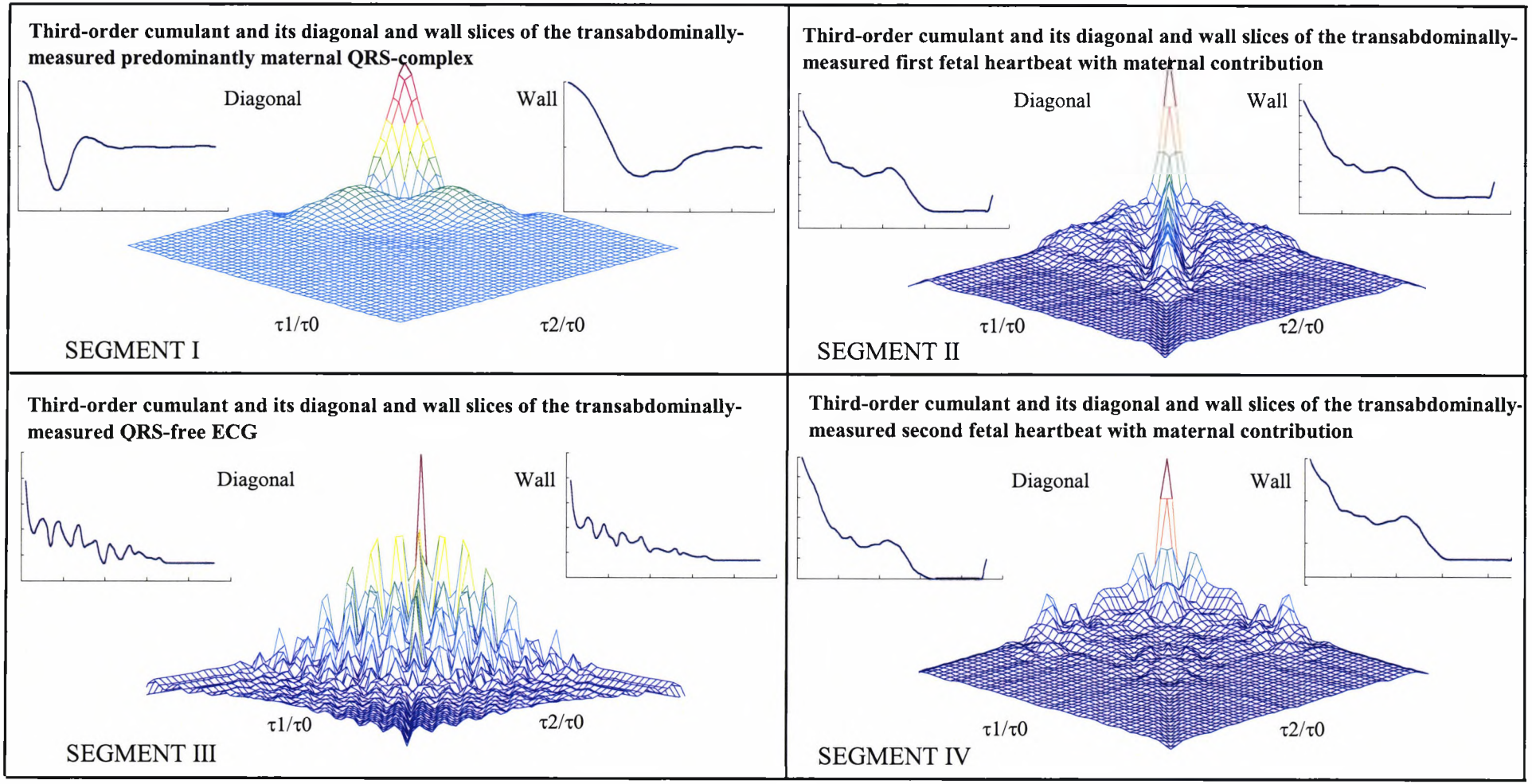

(e2)

Figure 4.3 (e1, e2): *(e1) Transabdominally-measured ECG (Code: 16-23) showing segmentation (segments I, II, III, and IV,each 250 msec). (e2) The corresponding third-order cumulants and their diagonal and walll slices (insets).(I) Predominantly maternal QRS-complex, (II) the first fetal heartbeat with maternal contribution, (III) QRS-free ECG, and (IV) the second fetal heartbeat with maternal contribution.* τ_0, τ_1,*and* τ_2 *are, respectively, the reference, first and second time lags of the third-order cumulants.*

QRS-free ECG segments (III). However, those of segments (II) and (IV) in Figures 4.3 (b) and (c) could be mistaken for QRS-free ECG segments. Note that the peaks of the QRS-free ECG segments, (III) in Figures 4.3 (b-e), are much narrower and more related to motion artefact than a signal.

4.4.7 Estimation of the cumulant matching variance

The variance of the TOC is defined as the expected value of the squared difference between the computed TOC of the 250 msec flag window of the transabdominal ECG signal and the computed TOC from the synchronised fetal scalp electrode ECG 250 msec window.

$$Var_c = E\left[(Cum(\tau_1, \tau_2)_{\text{Transabdominal}} - Cum(\tau_1, \tau_2)_{\text{fetal scalp}}\right]^2 \quad (4.4)$$

The above variance ranges from 0.64 – 4.2, average = 2.381, when calculated for 120,000 FHBs.

4.5 The single-hidden-layer perceptron back-propagation with momentum

4.5.1 Source knowledge presentation

A simplified version of the network with a single-hidden-layer is shown in Figure 4.4. As mentioned in Section 4.1, The 1-d input cumulant slices presented at the input layer of source nodes (see Figure 4.4) still has to be represented by a matrix, which may be scanned with a single neuron that has a local respective field, and the synaptic weights of the neuron are stored in corresponding locations in a layer called the feature map.

4.5.2 The back-propagation algorithm

The algorithm is based on the error-correction learning rule, and could be viewed as a generalisation of the least-mean-square (LMS) algorithm. The error back-propagation process consists of two passes through the single-hidden-layer of the network: a forward pass and a backward pass. The development of the back-propagation algorithm represents a landmark in neural networks [65] in that it provides a computationally efficient method for the training of multi-layer perceptron.

The back-propagation algorithm provides an approximation to the trajectory in weight space computed by the method of steepest descent. The smaller the learning rate,

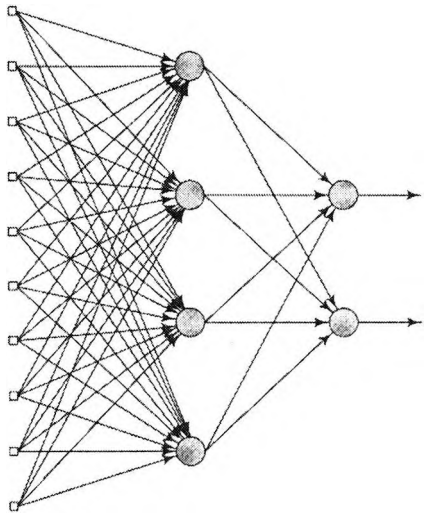

Figure 4.4: *Fully connected feed-forward network with one hidden layer and output layer.*

the smaller will be the changes of the weights in the network from one iteration to the next, and the smoother the trajectory will be in weight space. This improvement is attained at the cost of a slower rate of learning. If the learning rate parameter is too large so as to speed up the rate of learning, the resulting large changes of the weights assume such a form that the network may become unstable.

A major limitation of the back-propagation algorithms is the slow rate of convergence to a global minimum of the error-performance surface. This limitation is a distinct consequence of the fact that the algorithm operates entirely on the basis of first-order information, namely, the gradient of the error-performance surface with respect to the adjustable parameter (weights) in the single-hidden-layer perceptron.

The back-propagation learning process may be accelerated by incorporating a momentum term. The use of momentum introduces a feedback loop. This loop can have a highly beneficial effect on the learning behaviour of the back-propagation algorithm. In particular, it may have the benefit of preventing the learning process from being stuck at a local minimum on the error-performance surface of the single-hidden-layer perceptron. This simple method of increasing the rate of learning avoids the danger of instability by modifying the delta-rule by including a momentum term, which is a

positive number called the momentum constant (a review of some neural network applications of this algorithm is given in [10]).

Figure 4.4 illustrates a typical fully connected back-propagation network [66]. Each layer has a specific function. The input layer accepts an input pattern and redistributes it to all neurones in the middle layer. The output layer accepts a stimulus pattern from the middle layer and constructs the output response pattern of the network.

A back-propagation network operates in a two-step sequence during training. First, an input pattern is presented to the input layer of the network. The resulting activity flows through the network until the network's response is generated at the output layer. In the second step, the network's output is compared to the desired output for that particular input pattern. If it is not correct, an error is generated, which is propagated back through the network from the output layer back to the input layer.

4.5.3 Summary of the back-propagation network operations

To implement a full connection back-propagation network, the following formulae are used, with the notion:

$w^{(l)}$ = synaptic weight of a neuron in layer I.

$v^{(l)}$ = net internal activity levels of neurons in layer I.

$y^{(l)}$ = function signal of neuron in layer I.

$\delta^{(l)}$ = local gradient of neurons in layer I.

Each neuron consists of a linear combiner followed by a non-linearity (sigmoid function). Thus the non-linearity is distributed uniformly throughout the network. For each neuron j in layer I the net internal activity is:

$$v_j^{(l)}(n) = \sum_{i=0}^{p} w_{ji}^{(l)}(n) y_i^{(l-1)}(n). \tag{4.5}$$

For each neuron j in layer I the function signal, using the sigmoidal non-linearity, is:

$$y_j^{(l)}(n) = \frac{1}{1+\exp(-v_j^{(l)}(n))}, \tag{4.6}$$

with the derivative y`(I) = y(I) . (1-y(I)). For each neuron j in the output layer L the error signal is:

$$e_j(n) = d_j(n) - o_j(n), \tag{4.7}$$

where $d_j(n)$ is the jth element of the desired response. For each neuron j in the output layer L the local gradient is:

$$\delta_j^{(L)}(n) = e_j^{(L)}(n).o_j(n)\left[1 - o_j(n)\right], \tag{4.8}$$

while for each neuron j in layer I it is:

$$\delta_j^{(l)}(n) = y_j^{(l)}(n)\left[1 - y_j^{(l)}(n)\right]\sum_k \delta_k^{(l+1)}(n) w_{kj}^{(l+1)}(n). \tag{4.9}$$

The synaptic weights update in layer I, according to the generalised *delta-rule*, is:

$$w_{ji}^{(l)}(n+1) = w_{ji}^{(l)}(n) + \alpha\left[w_{ji}^{(l)}(n) - w_{ji}^{(l)}(n-1)\right] + \beta\delta_j^{(l)}(n) y_i^{(l-1)}(n), \tag{4.10}$$

where α is the momentum constant and β is the learning-rate parameter.

$0.0 < \beta < 1.0$ *and* $0.0 < \alpha < 1.0$.

The back-propagation algorithm provides a comparatively efficient way to compute instantaneous partial derivatives. The algorithm recursively modifies the synapses between neural fields. The algorithm first modifies the synapses between the output field and the penultimate field of hidden or interior neurons. The algorithm then uses this information to modify the synapses between the hidden fields all the way back to the synapses between the first hidden layer field and the input field. The computational complexity of the algorithm is linear. It provides a powerful device for extracting information contained in the training data and storing it in the weights of the network.

4.5.4 Optimisation of the parameters of the back-propagation algorithm

Two important parameters of the network are the learning rate (β) and the momentum constant (α). The learning rate is used to update the current weights from the previous ones. The momentum constant ensures that the weights are updated in the same previous direction even if the changes in the values of the weights are suddenly dropped to zero. This is important to avoid local minima, by giving the routine a momentum to keep moving.

Figure 4.5 shows the effect of changing the learning rate (β), the momentum constant (α) and the middle layer size on the classification of the maternal QRS-complexes and the fetal heartbeats using the TOC template matching technique. Figure 4.5 (a) shows that the classification rate increases with increasing the learning rate to a value of 0.8. Beyond this, the classification rate deteriorates because the learning is too high which makes the weights increase rapidly more than the required amounts to follow the changes in the slices. Figure 4.5 (b) shows that the momentum constant gives the best performance at a value of 0.99 for the maternal QRS-complex segments (l.h.s.) and 0.9 for the fetal heartbeat segments (r.h.s.). Values below these are not enough to push the routine towards the optimum convergence steady state values. Higher values tend to push the routine away from the desired values for convergence and miss the global minimum of the mean-squared error (MSE). Figure 4.5 (c) shows that a middle layer size of 5 x 5 achieves the highest classification rates for both the maternal QRS-complex and the fetal heartbeats segments.

4.5.5 Description of the first hybrid technique

In this chapter, a single-hidden-layer perceptron is used for the classification of the third-order cumulant slices of the maternal QRS-complexes, the first fetal heartbeat with maternal contribution, QRS-free ECG, and the second fetal heartbeat with maternal contribution from maternal transabdominal ECG segments. This is achieved using a standard back-propagation with momentum algorithm [8].

Figure 4.6 shows a flowchart of the first hybrid system. The input and output layers have a dimension of 8 x 8 and the hidden layer has a dimension of 5 x 5. The input to the first layer is the third-order cumulants diagonal and wall slices. The network is trained using TOC slice templates obtained from the maternal chest and fetal scalp electrode ECGs as

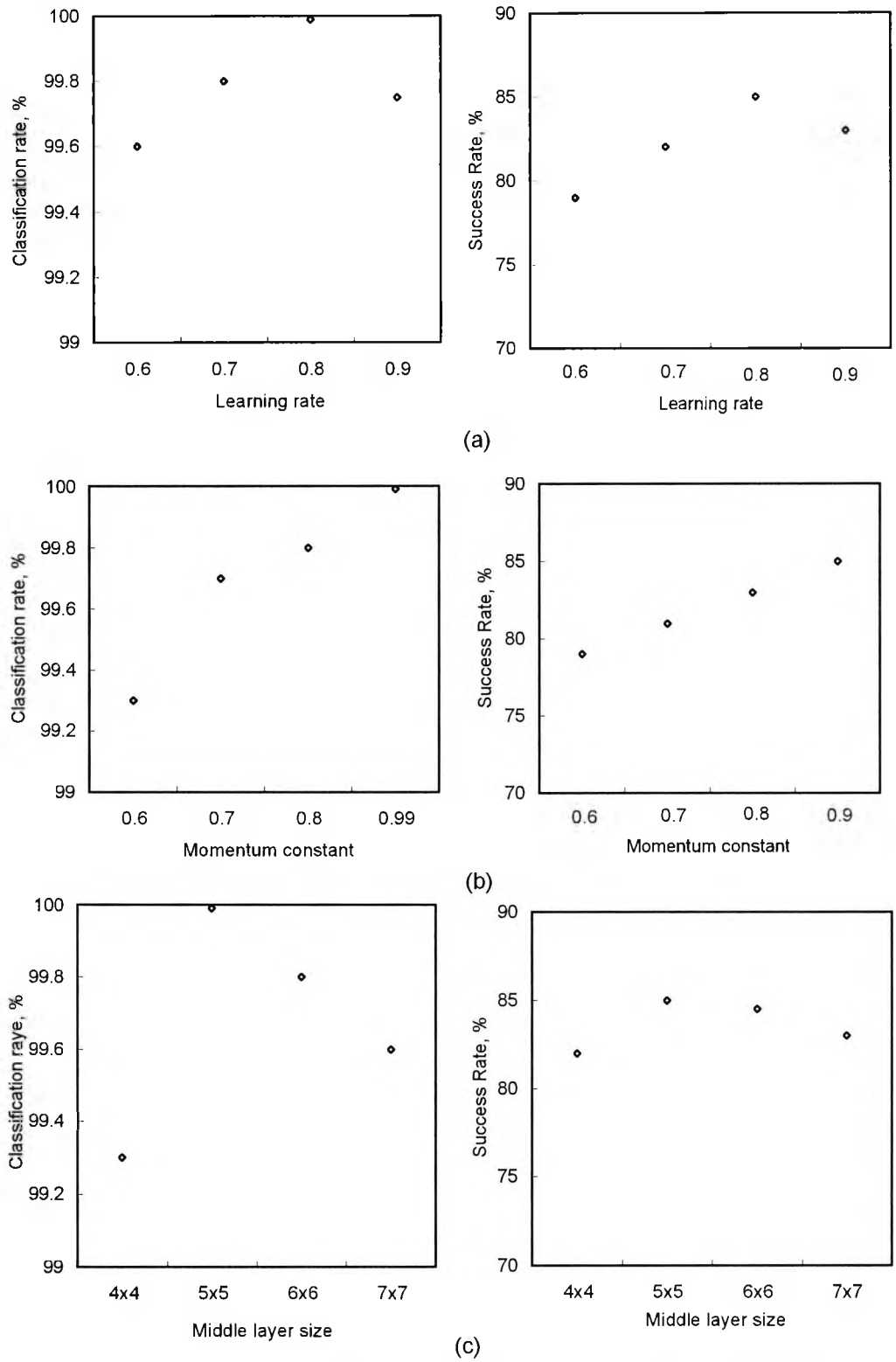

Figure 4.5: *The effect of changing (a) the learning rate, (b) the momentum constant, and (c) the middle layer size, on the classification rate of the maternal QRS-complexes (l.h.s.) and the fetal heartbeats with maternal contribution (r.h.s.) from transabdominally-measured ECG signals and employing third-order cumulant diagonal slices and their templates to be matched using a single-hidden-layer perseptron back-propagation with momentum. Performance for the maternal QRS-complex segments (l.h.s.) and the fetal heartbeat with maternal contribution segments (r.h.s.). Segment length is 250 msec each. The optimised parameters are: maternal QRS-complex classification: learning rate = 0.8, momentum constant = 0.99, and middle-layer size = 5 x 5, fetal heartbeat classification: learning rate = 0.8, momentum constant = 0.9, and middle-layer size = 5 x 5.*

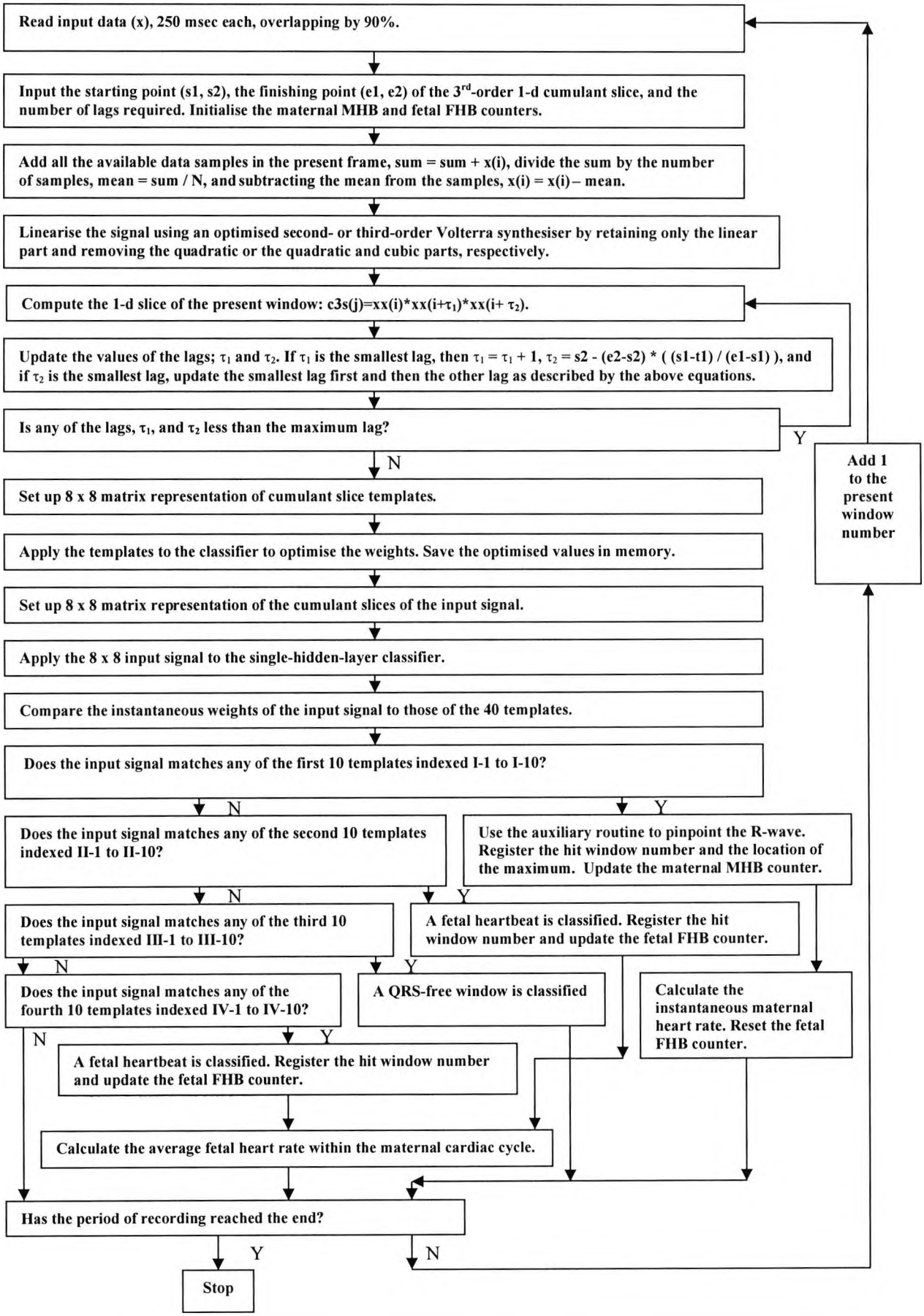

Figure 4.6: *A flowchart for the first hybrid system for non-invasive fetal heartbeat detection using TOC slices for signal processing and single-hidden-layer perceptron for classification. The system involves the implementation of a new method for calculating any arbitrary TOC slice.*

well as previously detected and earmarked transabdominal ECG segments. The latter training sequences are templates of the diagonal and wall slices of the third-order cumulants of four segments from maternal transabdominal full cardiac cycles. The input to the network is eight template patterns. These are the third-order cumulant diagonal and wall slices of four segments from one transabdominal cardiac cycle. For example the first pair are MT QRS TOC D and MT QRS TOC W, the second pair are FT ECG TOC D and FT ECG TOC W, the third pair are QRS-free TOC D and QRS-free TOC W, and the fourth pair are FT ECG TOC D and FT ECG TOC W. The network is trained over the eight patterns. The training terminates when the worst error in all patterns in one pass is less than 0.1. Typically the average error will be in the range of 0.001.

Figure 4.7 shows a block diagram of the first hybrid system. First the neural network is trained on the templates. The TOC slice templates (sets 1 to 4 in Figure 4.8) are used as input to the classifier. Each one of the 10 templates in each set is used as an input and the weights of each neuron in the classifier are optimised by changing the learning rate and the momentum constant until the error is minimised. Then the transabdominal ECG signal with 250-msec window is used as an input to the classifier. The instantaneous weights of the input signal are compared to those of the templates which are stored in the memory. The two sets of parameters are correlated. Once a signal is classified the output will be set to 1. The classification of the four segments involves a pattern-by-pattern updating rather than batch updating for the weight adjustments. This is more suitable to speed up the performance. Pattern-by-pattern updating tends to be orders of magnitude faster than batch updating. However, it should be noted that pattern-by-pattern updating is harder to parallelise.

Figure 4.8 shows the 8 x 8 matrix representation of the TOC templates shown in Figure 4.7. Those slices are diagonal, wall, diagonal and wall, and 22.5^{o} off diagonal / wall. Sets 1, 2, 3, and 4 represent, respectively, segments of predominantly maternal QRS-complex, the first fetal heartbeat with maternal contribution, QES-free ECG, and the second fetal heartbeat with maternal contribution.

Figure 4.9 shows a typical single-hidden-layer back-propagation neural network architecture with 8 inputs. It shows how the templates are used as inputs to the

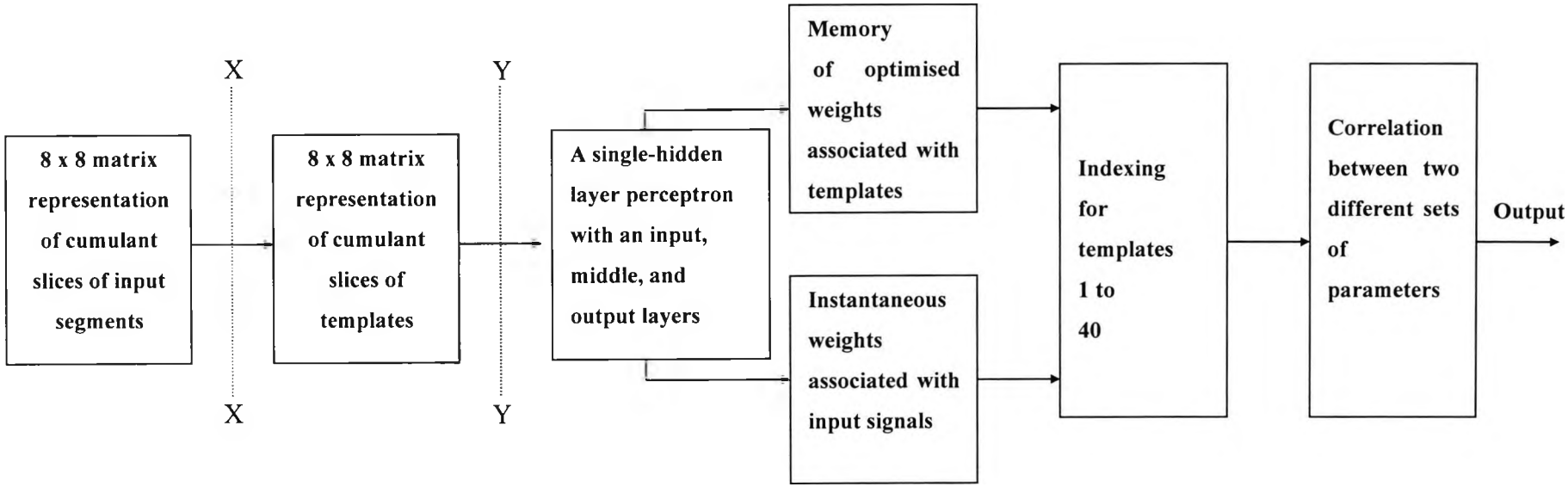

Figure 4.7: *A block diagram of the first hybrid system.*

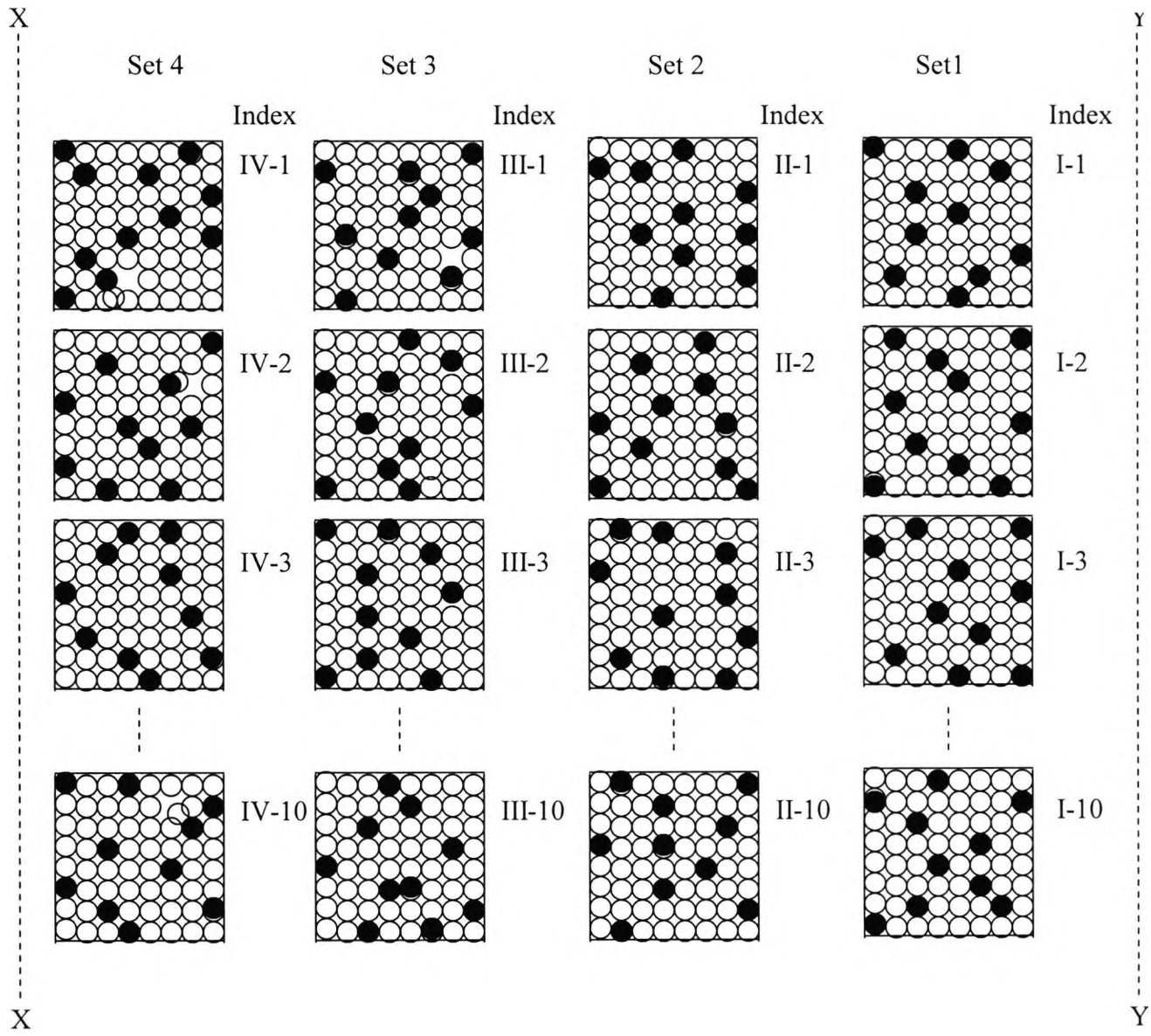

Figure 4.8: *The 8 x 8 matrix representation of cumulant slice templates shown in Figure 4.7. Those slices are diagonal, wall, diagonal and wall, and 22.5° off diagonal / wall. Sets 1, 2, 3, and 4 represent, respectively, segments of predominantly maternal QRS-complex, the first fetal heartbeat with maternal contribution, QRS-free ECG, and the second fetal heartbeat with maternal contribution.* ● *and* ○ *represent 1 and 0, respectively.*

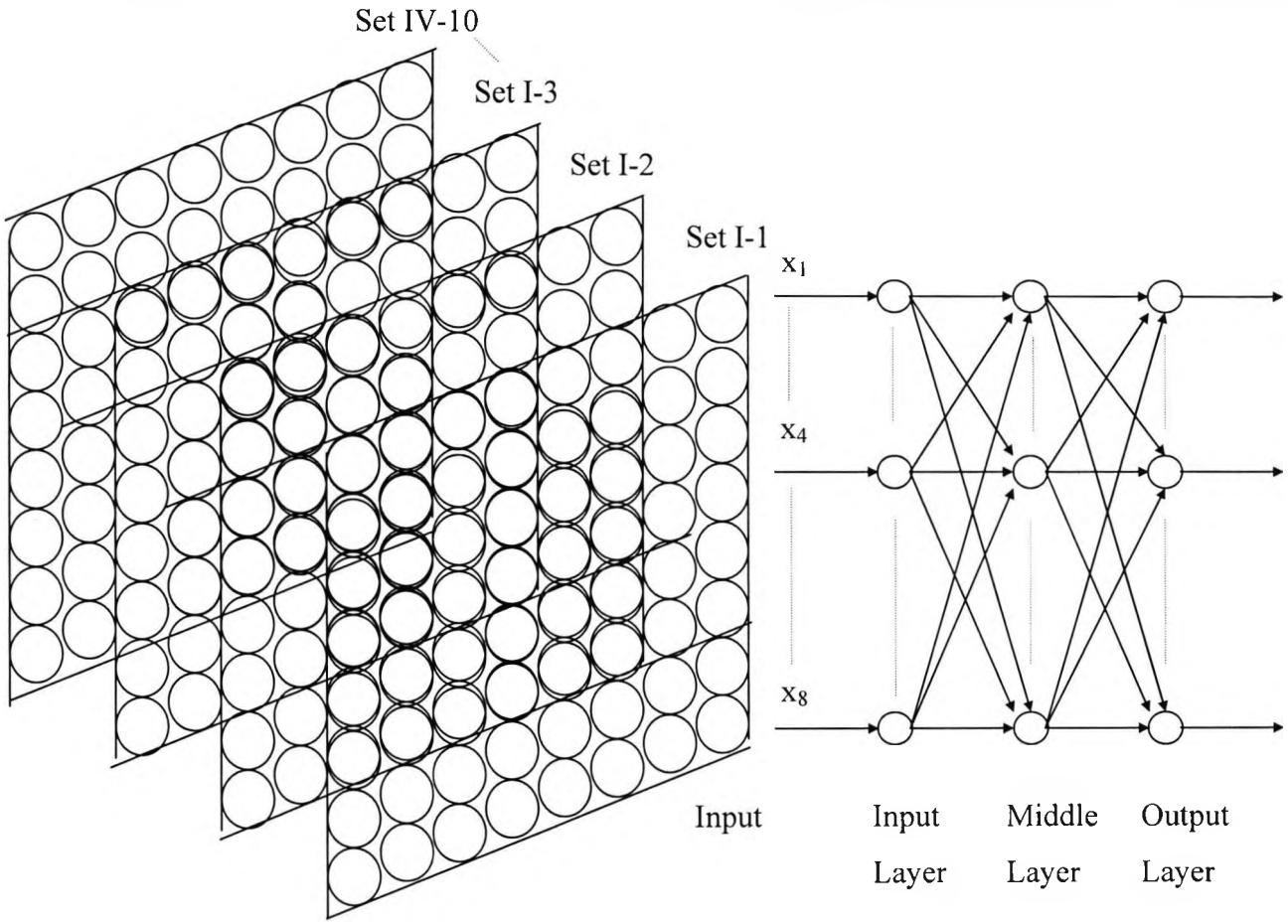

Figure 4.9: *A typical single-hidden-layer back-propagation neural network architecture.*

classifier. These will then be followed by the input signals once the classifier settles down using the templates.

Figure 4.10 shows an example of the representation of a third-order cumulant diagonal slice of a transabdominally-measured predominantly maternal QRS-complex segment by an 8 x 8 matrix to be used as an input for the classifier of Figure 4.9. The diagonal slice is represented by 0's and 1's in the 8 x 8 matrix form.

Figure 4.11 shows an example of each of the following for the classifier: (i) a True Positive (TP), (ii) a False Negative (FN), and (iii) a False Positive (FP). The first one is a predominantly maternal QRS-complex TOC diagonal slice which is correctly matched to a maternal QRS-complex TOC diagonal slice template (I-1) resulting in a true positive. The second is a first fetal heartbeat with maternal contribution TOC diagonal slice which is wrongly matched to a QRS-free TOC D template (III-3) resulting in a false negative. The third example is a QRS-free TOC D which is wrongly matched to a second fetal heartbeat with maternal contribution TOC diagonal slice (IV-2) resulting in a false positive.

4.5.6 Cumulant matching of the transabdominal maternal QRS-complexes and the fetal heartbeats to the previously identified and prepared templates

In this section we show how effectively the cumulant matching technique works with only 10 templates of maternal transabdominal QRS-complexes and 20 templates of fetal heartbeats with maternal contribution. Figures 4.12 (a) – (d) are self explanatory. Each part of the figure shows one of the four transabdominal ECG segments (data length 250 msec) and eight of the corresponding templates used for matching, and highlighting the template that is matched to the segment. An optimised third-order Volterra structure is employed to synthesise the four transabdominal ECG segments and the corresponding templates. Figure 4.12 (a) depicts the TOCs and their diagonal and wall slices (insets) for the predominantly maternal QRS-complex segment (top left panel). The rest of the figure shows eight of the ten templates of such signals. Template 2 is the one which is matched to the segment (top right panel). Figure 4.12 (b) depicts the TOCs and their diagonal and wall slices (insets) for the first fetal heartbeat with maternal contribution segment (top left panel). The rest of the figure shows eight of the ten templates of such signals. Template 2 is the one which is matched to the segment (top right panel).

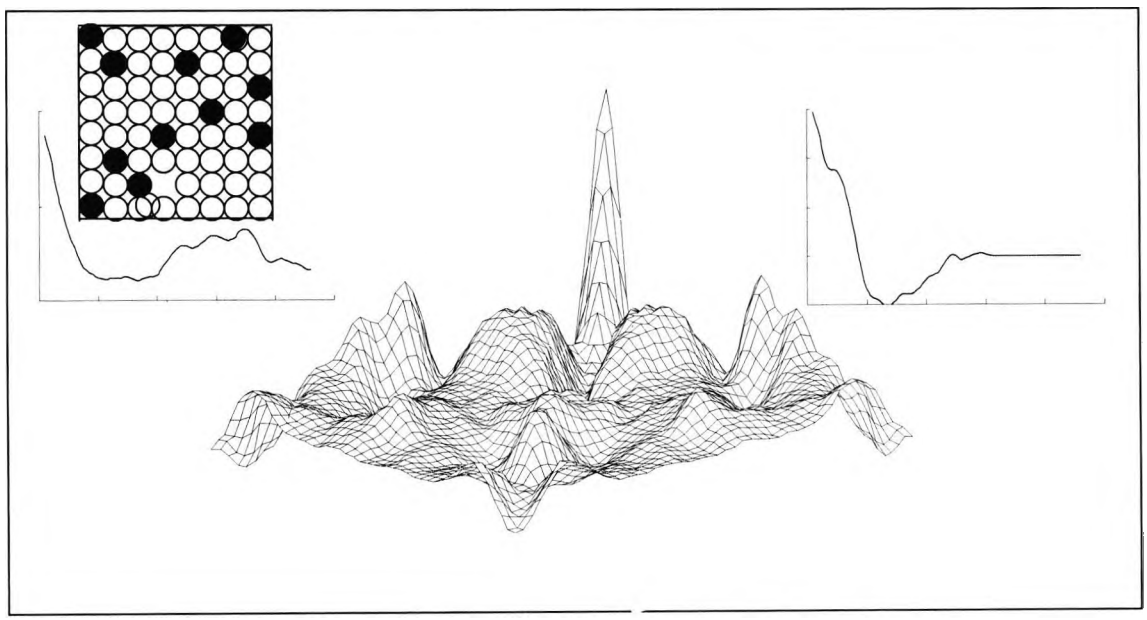

Figure 4.10: *Representation of a third-order cumulant diagonal slice of a transabdominally-measured predominantly maternal QRS-complex segment by an 8 x 8 matrix to be used as an input for the single-hidden-layer classifier of Figure 4.9.*

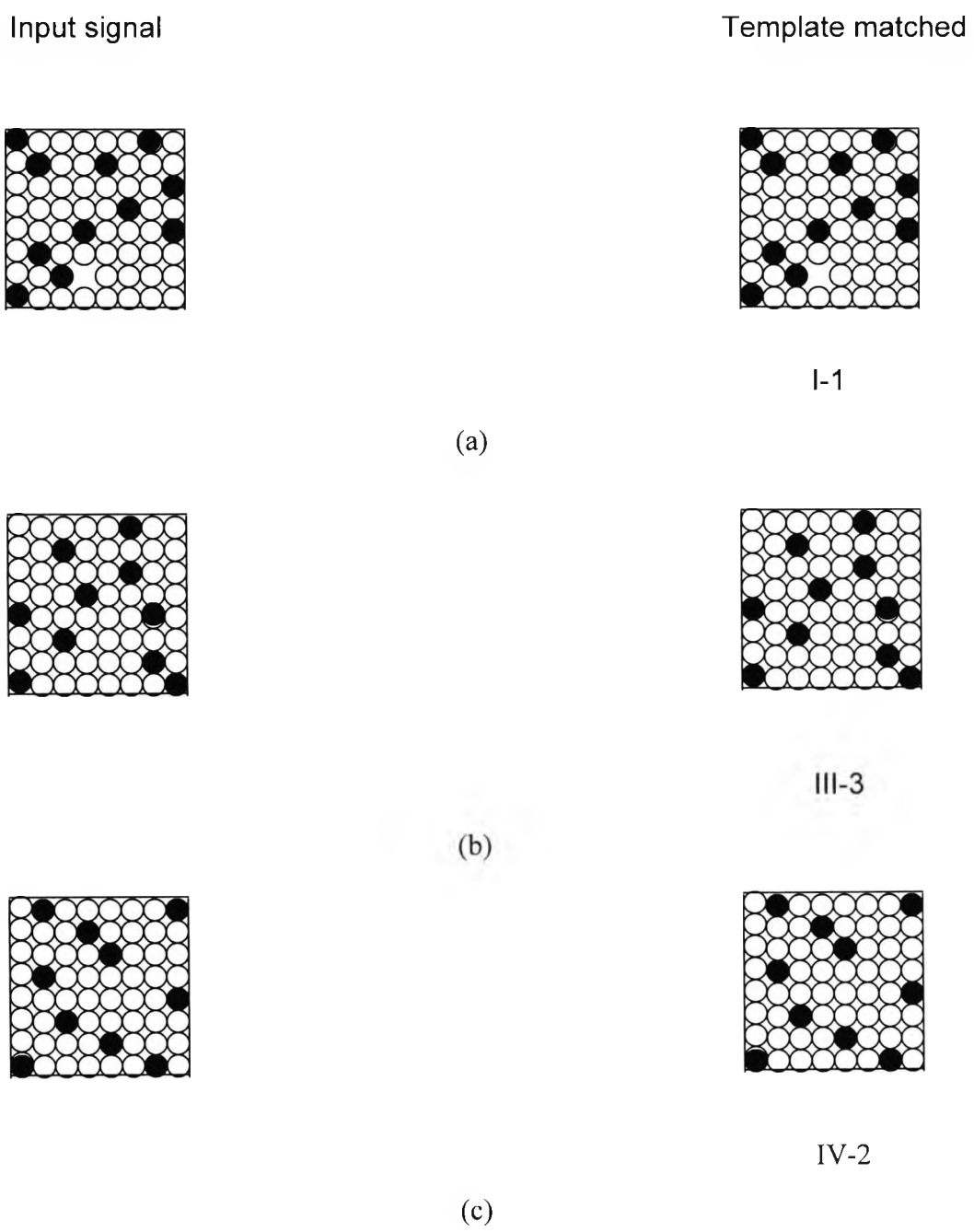

Figure 4.11: *Examples of (a) a True Positive (TP), (b) a False Negative (FN), and (c) a False Positive (FP) for the classifier. (a) A predominantly maternal QRS-complex TOC diagonal slice was correctly matched to a maternal QRS-complex TOC diagonal slice template (I-1), (b) a fetal heartbeat with maternal contribution TOC diagonal slice was wrongly matched to a QRS-free ECG TOC diagonal slice template (III-3), and (c) a QRS-free ECG TOC diagonal slice was wrongly matched to a fetal heartbeat with maternal contribution TOC diagonal slice template (IV-2).*

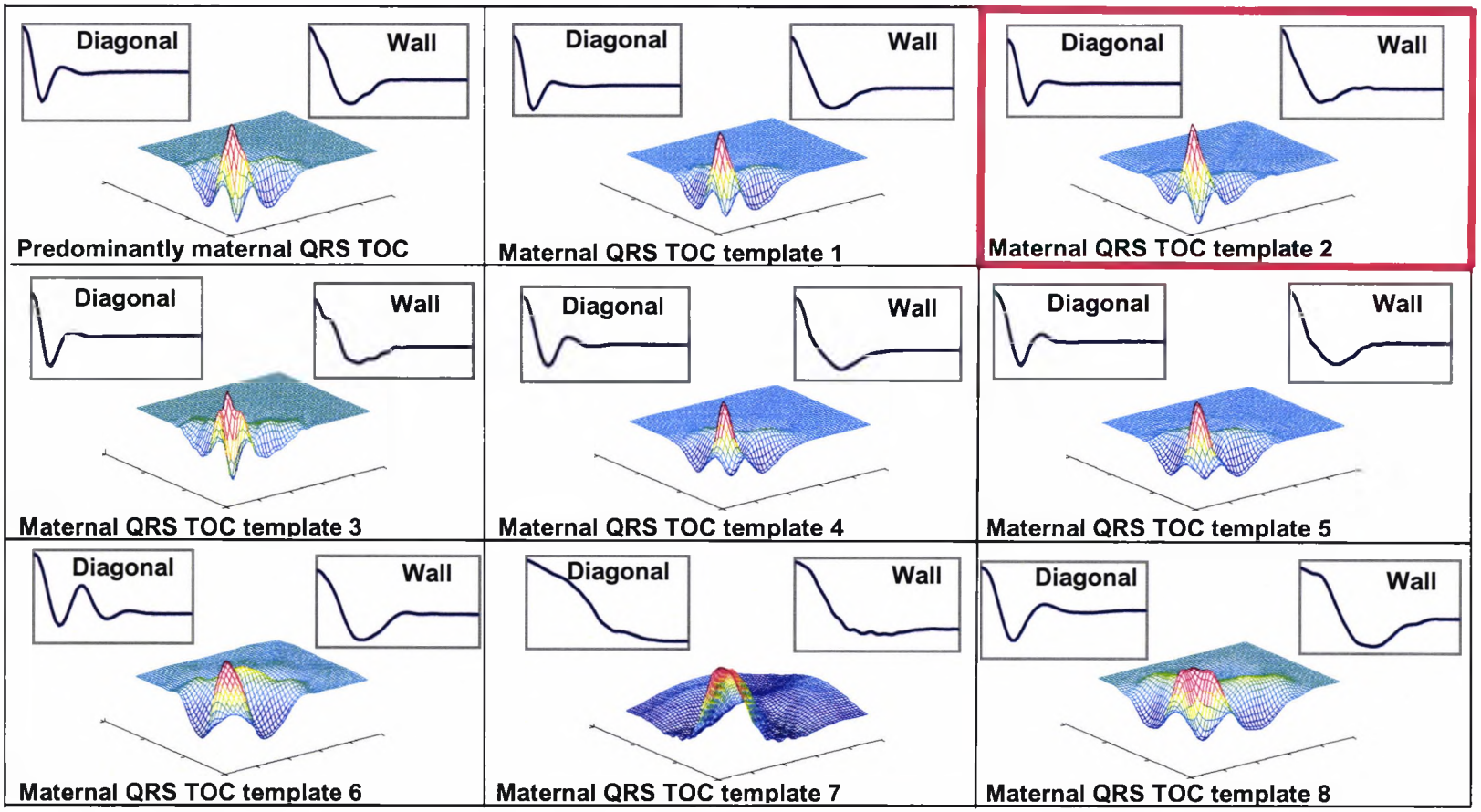

(a)

Figure 4.12 (a): *Third-order cumulants and their diagonal and wall slices (insets) for a typical example of transabdominally-measured predominantly maternal QRS-complex cumulant matching signature using the first hybrid system. The top left hand part of the figure depicts the TOC and its slices for a predominantly maternal QRS-complex. The rest of the figure shows eight of the ten templates of such signals. Template 2, at the top right hand part of the figure, is the one which is matched to the segment. The parameters of the single-hidden-layer perceptron are: learning rate = 0.80, moment constant = 0.99, and middle layer size is 5 x 5.*

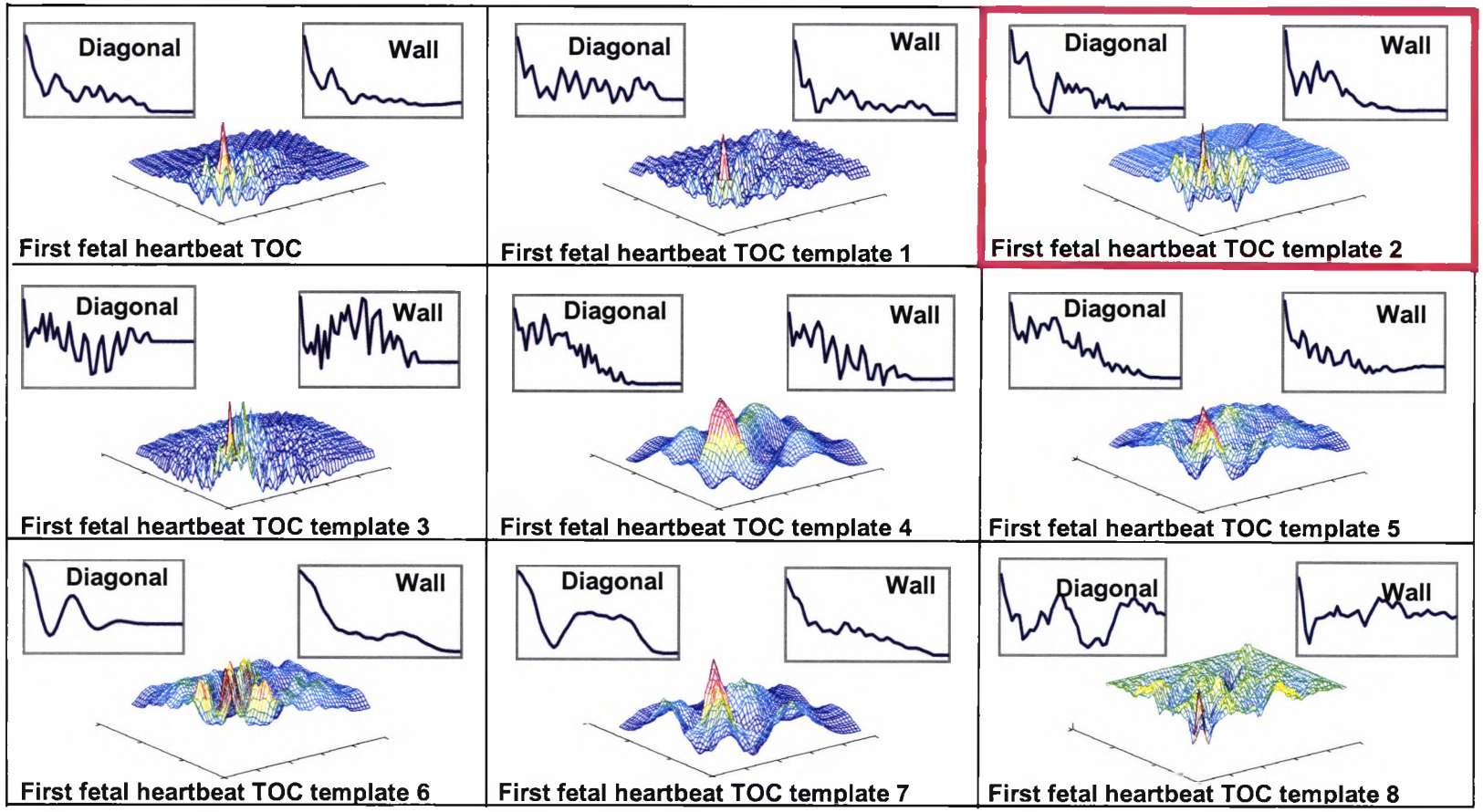

(b)

Figure 4.12 (b): *Third-order cumulants and their diagonal and wall slices (insets) for a typical example of a transabdominally-measured first fetal heartbeat with maternal contribution cumulant matching signature using the first hybrid system. The top left hand part of the figure depicts the TOC and its slices for the first fetal heartbeat with maternal contribution. The rest of the figure shows eight of the ten templates of such signals. Template 2, at the top right hand part of the figure, is the one which is matched to the segment. The parameters of the single-hidden-layer perceptron are: learning rate = 0.80, moment constant = 0.90, and middle layer size is 5 x 5.*

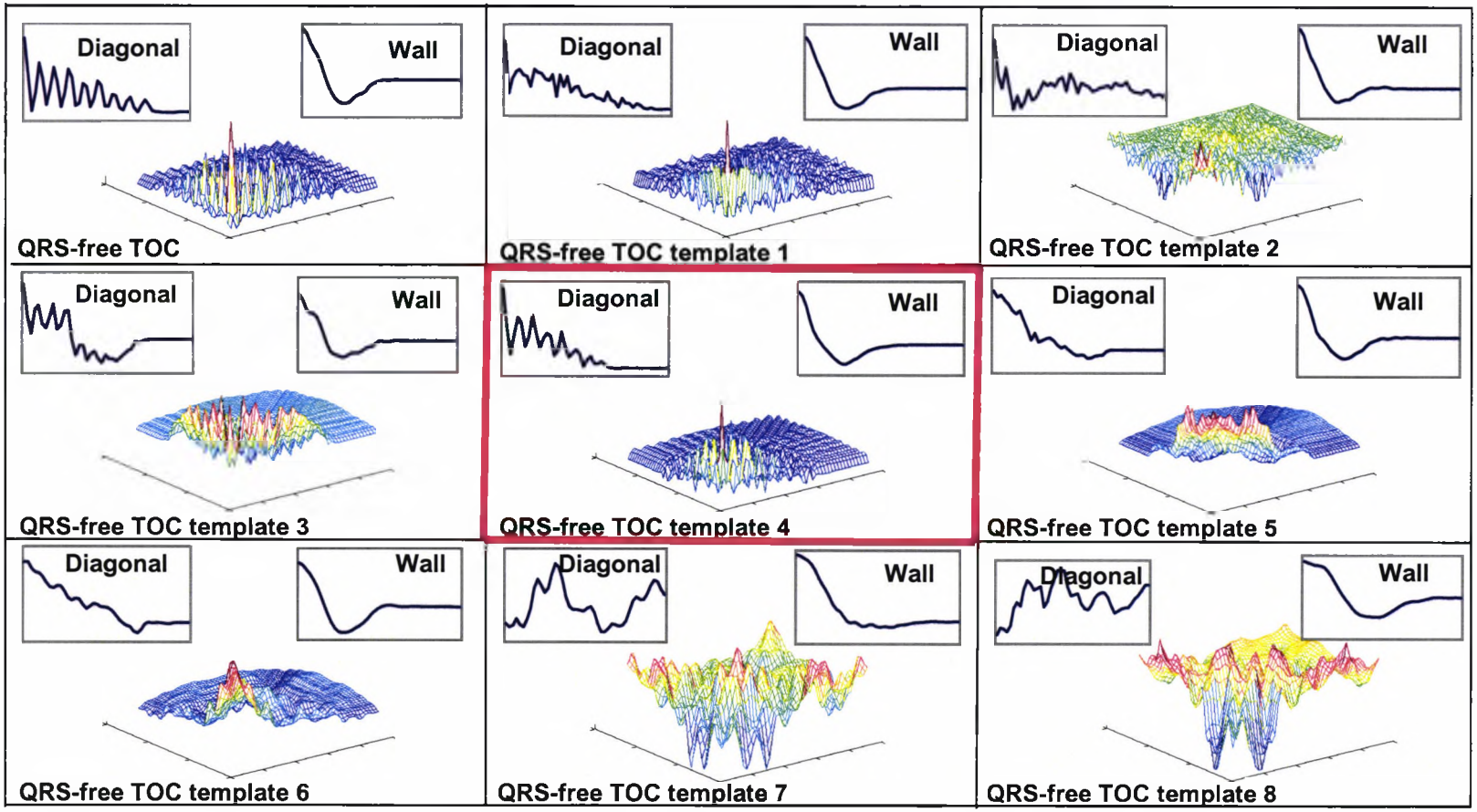

(c)

Figure 4.12 (c): *Third-order cumulants and their diagonal and wall slices (insets) for a typical example of a transabdominally-measured QRS-free ECG cumulant matching signature using the first hybrid system. The top left hand part of the figure depicts the TOC and its slices for a QRS-free ECG segment. The rest of the figure shows eight of the ten templates of such signals. Template 4, at the middle of the figure, is the one which is matched to the segment. The parameters of the single-hidden-layer perceptron are: learning rate = 0.80, moment constant = 0.90, and middle layer size is 5 x 5.*

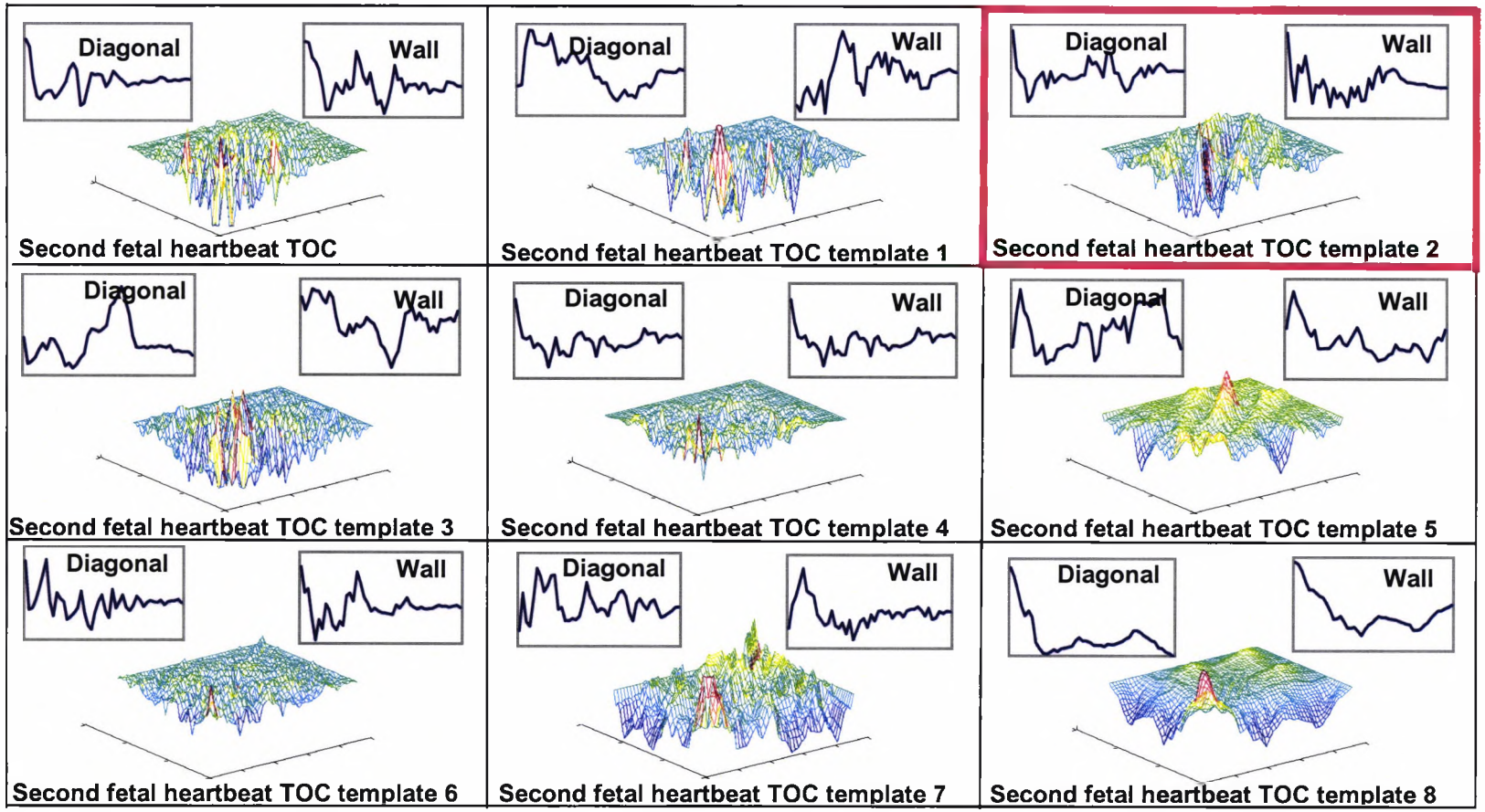

(d)

Figure 4.12 (d): *Third-order cumulants and their diagonal and wall slices (insets) for a typical example of a transabdominally-measured second fetal heartbeat with maternal contribution cumulant matching signature using the first hybrid system. The top left hand part of the figure depicts TOC and its slices for the second fetal heartbeat with maternal contribution. The rest of the figure shows eight of the ten templates of such signals. Template 2, at the top right hand part of the figure, is the one which is matched to the segment. The parameters of the single-hidden-layer perceptron are: learning rate = 0.80, moment constant = 0.90, and middle layer size is 5 x 5.*

Figure 4.12 (c) depicts the TOCs and their diagonal and wall slices (insets) for a QRS-free ECG segment (top left panel). The rest of the figure shows eight of the ten templates of such signals. Template 4 is the one which is matched to the segment (middle panel). Figure 4.12 (d) depicts the TOCs and their diagonal and wall slices (insets) for the second fetal heartbeat with maternal contribution segment (top left panel). The rest of the figure shows eight of the ten templates of such signals. Template 2 is the one which is matched to the segment (top right panel).

4.5.7 The maternal QRS-complex and the fetal heartbeat classification rates

4.5.7.1 The maternal QRS-complex classification rate

Table 4.3 shows a top classification rate of 100% for maternal QRS-complexes using the TOC template matching technique with single-hidden-layer classification. The 100% classification rate has been achievable with or without linearisation. It makes no difference to the results. However, to complete this section here is a brief description of the optimised parameters required for the maternal QRS-complex linearisation process.

Parameters

As mentioned before, this employs a second- or third-order Volterra synthesiser. Each of these synthesisers employs an LMF algorithm update. The learning rate and momentum constant are, respectively, 0.8 and 0.99. The second-order Volterra parameters are: filter length = 6, step-size parameters = 0.005, and 0.0004 for linear and quadratic parts, respectively, delay = 4. The third-order Volterra parameters are: filter length = 6, step-size parameters = 0.001, 0.0002, and 0.0004 for linear, quadratic and cubic parts, respectively, delay = 4.

Third–order Cumulant (TOC) matching template slice type and in conjunction with ANN classifiers	**TOC Diagonal slice**	**TOC Wall slice**
Classification rate (%)	**100.00**	**100.00**

Table 4.3: *The classification rate for maternal QRS-complexes using maternal transabdominally-measured ECGs and their respective TOC diagonal or wall slices.*

To calculate the maternal heart rate an auxiliary method to pinpoint the R-wave is needed. For this application we have a choice of either using the superior patent binding technique [41] or adaptive thresholding which is less accurate when one deals with deformed QRS-complexes in heart patients. The results presented here have been obtained using the latter method since all mothers' ECGs exhibit normal-to-the-patient QRS-complexes. The instantaneous maternal heart rate is calculated by dividing 60 by the R-to-R interval (in seconds). The application of this auxiliary routine leads to a maternal heart rate with an accuracy of 99.85%.

4.5.7.2 Fetal heartbeat detection quality and classification rate for the TOC template matching technique

Before attempting to assess the first hybrid technique for non-invasive fetal heartbeat detection some definitions are appropriate here:

Definitions

1- The Sensitivity (Se) is defined as the ratio of the True Positives (TP) to the sum of the True Positives and the False Negatives (FN). The sensitivity reports the percentage of true beats that are correctly classified by the algorithm.

2- The Specificity (Sp) is defined as the ratio of the True Positives (TP) to the sum of the True Positives (TP) and the False Positives (FP). It reports the percentage of classified heartbeats which are in reality true beats.

3- The classification rate: The mean value of the sensitivity and the specificity is used as the criterion for the effectiveness of the technique.

Table 4.4 shows the fetal heart detection quality and classification rate using transabdominally-measured ECGs and their respective TOC diagonal or wall slices with and without linearisation. The combined diagonal and wall slices improve the classification rate by about 1% over and above that achieved by either slice. A further improvement of about 1% is achieved by using two off-diagonal and off-wall slices. Using a second-order Volterra synthesiser results in a higher detection rate of 83.49%. The highest achievable classification rate for non-invasive fetal heartbeat detection using the first hybrid system is 86.16% when a third-order Volterra synthesiser is employed in conjunction with single-hidden-layer classifiers. Note that the classification

rate for coincident mother's and fetal QRS complexes is 0%. The classification rate of non-coincident mother's and fetal QRS-complexes is 95.55%.

Parameters

The second-order Volterra parameters are: filter length = 6, step-size parameters = 0.005, and 0.0004 for linear and quadratic parts, respectively, delay = 5. The third-order Volterra parameters are: filter length = 6, step-size parameters = 0.001, 0.0002, and 0.0004 for linear, quadratic and cubic parts, respectively, delay = 5. The learning rate and the momentum constant are 0.80 and 0.90, respectively.

Third–order Cumulant (TOC) matching template slice type with and without linearisation using Volterra and in conjunction with ANN classifiers	Detection quality				Classification rate (%)
	Se (%)	Sp (%)	FP, out of 120000	FN, out of 120000	
TOC Diagonal slice without linearization	76.24	79.38	24744	28512	77.81
TOC Wall slice without linearization	76.24	79.38	24744	28512	77.81
TOC Diagonal and Wall slices without linearization	77.13	80.24	23712	27444	78.74
TOC Diagonal, wall, diagonal and wall, and an off-diagonal and off-wall 22.5^{o} slice without linearization	78.04	81.18	22584	26352	79.69
Linearised diagonal slice using 2^{nd} order adaptive LMF Volterra synthesiser	82.37	84.61	18468	21156	83.49
Linearised wall slice using 2^{nd} order adaptive LMF Volterra synthesiser	82.37	84.61	18468	21156	83.49
Linearised diagonal slice using 3^{rd} order adaptive LMF Volterra synthesiser	84.46	87.85	14500	18648	86.16
Linearised wall slice using 3^{rd} order adaptive LMF Volterra synthesiser	84.46	87.85	14500	18648	86.16

Table 4.4: *Fetal heart detection quality and classification rate using transabdominally-measured ECG and their respective TOC diagonal or wall slices with and without linearisation. The total number of fetal heartbeats is 120,000 and the total number of maternal ECG recordings. is 30. The performance was assessed against synchronised fetal scalp heartbeats. All mothers were during the first stage of labour at 40 weeks of gestation.*

4.6 Summary and conclusions

General discussions

Early research studies which have not been presented in this chapter, but have been carried out under an two-and-half-year research contract*, exploited the whole multi-dimensional structures of the third- and fourth-order cumulants of the ECG signals presented in this thesis in conjunction with multi-layered feed-forward neural networks. The justification for this multi-layer perceptron network was based entirely on the assumption that by including a sufficient number of hidden layers, the network would be enabled to extract both third-and fourth-higher-order statistics embedded in the cumulants presented to the network input. The multi-dimensional ECG cumulants were created first and subsequently a pre-selected number of slices were extracted and cascaded side-by-side to be presented to the input layer of the MLP. In the early days of this research, it was difficult to make a decision, just by mere observations of the available 1-d third-order cumulant slice or 2-d fourth-order cumulant slice patterns produced from the transabdominally-measured ECG signals, as to which of such slices would show a distinguishable pattern which could be matched to the corresponding mother or fetal ECG templates. Particularly, those templates of the fetal scalp electrodes which have been used as a reference, so that the fetal heartbeat detection could be verified in the midst of those complex maternal environments and counted within each maternal cardiac cycle.

In an attempt to restrict the size of the neural network to only two hidden layers, instead of three or four layers, *prior information* had to be built into the design of the MLP by using a combination of two techniques [65]: (1) restricting the network architecture through the use of network connections and (2) constraining the choice of synaptic weights by the use of *weight sharing* [70]. The issue of *prior information* was addressed in terms of the most discriminant patterns in the one-dimensional third-order cumulant slice or the two-dimensional fourth-order cumulant slices. Also, those patterns, as perceived by an observer, usually change in a corresponding way as the transabdomianlly-measured data were scanned over each maternal cardiac cycle. For example, the first fetal heartbeat to occur after the mother's QRS-complex interval was

* Permission has been granted for publications without revealing the company's name.

clear from either maternal P- or maternal T-wave. Accordingly, the only change to the fetal cumulants was due to its surrounding environment, e.g., uterine contraction signals and noise artefact. The situation is not the same for the second and possibly the third fetal heartbeats within the same cardiac cycle as these may overlap with the T-wave of the present cardiac cycle or the P-wave of the next. Accordingly, a primary requirement of cumulant pattern recognition is to design a classifier that is *invariant* to such changes. In other words, a class estimate presented by an output of the classifier must not be affected by change in the cumulant structures as we scan the transabdominally-measured ECG signals from the first to the second or even third fetal heartbeat occurrences within each maternal cardiac cycle. This also applies to changing environment from one maternal cardiac cycle to the next. Particularly, as the maternal ECG including the fetal ECG override the peaks and valleys of labour contractions. We may recall, that it is crucial to monitor fetal heart rates as accurately as possible during painful contractions to assess the accelerations and decelerations of the fetal heart rates in sympathy with such electromechanical events. This has been briefly discussed in Chapter One.

There exist at least three techniques for rendering classifier-type neural networks *invariant* to changes (or transformation due to an object manifestation as in speech recognition and Radar Doppler [71]). Only the first and second techniques of the following three have been applied to fetal heart monitoring:

(1) *Invariance by training.* A neural network has a natural ability for pattern classification. This ability may be exploited directly to obtain change invariance as follows. The network is trained by presenting it a number of different examples of the same fetal heartbeat cumulants or bispectra, with the examples being chosen to correspond to different changes (i.e., different fetal heartbeats positions in the maternal cardiac cycle) of the third-order cumulant. Provided that the number of examples is sufficiently large, and if the network is trained to learn to discriminate the different third- or fourth-order cumulants of the ECG 250 msec segments, we may then expect the network to generalise correctly changes other than those shown to it. It was found, however, from an engineering perspective, invariance by training has disadvantages. When a neural network has been trained to recognise a third-order cumulant slice in an invariant fashion with respect to known changes, it is not obvious that this training will also enable the network to recognise other representatives of different classes

invariantly (e.g., cumulants of the QRS-free ECG segment). The solution was found to provide templates of the third-order cumulant slices of the QRS-free ECG segment.

(2) *Invariant feature space*. The second technique of creating an invariant classifier-type neural network rests on the premise that it may be possible to extract features that characterise the essential information content of an input data set, and which are invariant to changes of the input [70]. It has to be emphasised that this applies only to linearised ECG data sets. The important features characterising key cumulant slices, such as the diagonal and wall slices, are (i) the shape of the main lobe, and (ii) the number and positions of the side lobes. If such features are used, then the network as a classifier is relieved from the burden of having to delineate the range of changes of a fetal heartbeat, still swamped by noise and maternal contributions, with complicated decision boundaries. Indeed, the only differences that may arise between different instances of the same ordered fetal heartbeat (first heartbeat-to-first heartbeat correspondence, or second heartbeat-to-second heartbeat correspondence, ...etc) are due to unavoidable factors such as motion artefact and noise. The use of an invariant-feature space offers three distinct advantages; (i) The number of features applied to the network may be reduced to realistic levels; (ii) the requirements imposed on network design are relaxed; and (iii) invariance for all fetal heartbeats with respect to known changes is assured [71]; however, this approach requires *prior knowledge* of the important features. This has prompted us to consider the single-hidden-layer neural network with only two cumulant slices presented at its input layer, namely, the *linear* non-Gaussian third-order cumulant diagonal and wall slices of the ECG signals.

(3) *Invariance by structure*. Invariance may be imposed on a neural network by structuring its design appropriately. Specifically, synaptic connections between the neurons of the network are created such that changed versions of the same input are forced to produce the same output [70].

The single-layer perceptron operates on the premise that the patterns to be classified are linearly separable. Linear separability requires that the patterns to be classified must be sufficiently separated from each other to ensure that the decision surfaces consists of

hyper-planes*.

The perceptron convergence algorithm is non-parametric in the sense that it makes no assumptions concerning the form of the underlying probability distributions of one class or another; it operates by concentrating on errors that occur where different classes of the cumulant or spectral patterns become too close. For example, the spectral pattern of the uterine contraction shares the same spectral peak with the spectral pattern of the fetal ECG. This problem is addressed in Chapter Six. The perceptron convergence has been addressed when using the back-propagation algorithm in conjunction with either the MLP network (in earlier studies and involving the overall cumulants) or the single-hidden-layer perceptron used in this thesis in the context of the third-order cumulant slice matching hybrid classifier.

Detailed results

1. The effect of the chosen window length on the third-order cumulant variance

The transabdominal ECG signal is linearised and segmented prior to the third-order cumulant calculations. The window length is carefully chosen to serve two criteria; (i) to yield an acceptable upper threshold of both the deterministic and stochastic noise types inherent in the higher-order statistics of the ECG signals encountered, and (ii) to allow the detection of one, two, three, or four fetal heartbeats (FHBs) within one maternal transabdominal cardiac cycle.

It has also been shown that the variance of an 250 msec Gaussian noise segment is equal to 1.0629 which is close to the ideal value of 1.0. The variance would increase by more than 20% if the segment length is halved. The TOC variance of the fetal heartbeat segments has been calculated. It ranges from 0.64 to 4.2 with an average value of 2.381.

2. Calculation of averaged fetal heart rates

Templates of third-order cumulant diagonal and wall slices are used as the desired response of the single-hidden-layer perceptron in the training phase. The TOC template

* Class A and class B must not be too close to each other. Otherwise, they become non-linearly separable. Quoting from Section 13.2 of the book by Minsky and Papert, [72]: This would also hold true for the multi-layer perceptron.

matching procedure starts by matching the slices of the segments to the templates until the first and the second maternal QRS-complexes are detected and their R-wave are pinpointed. The maternal heart rate is accurately calculated from the knowledge of the current and previous R-wave positions. Then, the search for the fetal heartbeat starts at 50 msec before the first maternal R-wave and continues until we reach the second maternal R-wave. Although the ECG TOC template matching technique is very effective in detecting the occurrence of the fetal heartbeats as a whole even when it is completely buried in noise, it cannot locate the fetal R-wave over a window length of 250 msec. However, we can measure fairly accurately the maternal heartbeats and calculate the instantaneous heart rate for the mother. Hence, by counting the number of fetal heartbeats that have occurred between two successive maternal R-waves, one can easily calculate the averaged FHR within the maternal cardiac cycle;

The average FHR = MHR x Number of FHBs / number of maternal heartbeats

In the above formula, the instantaneous maternal heart rate is previously known with some degree of accuracy, and the relative fetal to maternal heartbeat is also known within the maternal cardiac cycle. Hence, the averaged fetal heart rate can be calculated within each maternal cardiac cycle.

3. Parameters of the single-hidden layer perceptron

A major limitation of the back-propagation algorithms is the slow rate of convergence to a global minimum of the error-performance surface because the algorithm operates entirely on the gradient of the error-performance surface with respect to the weights in the single-hidden-layer perceptron. The back-propagation learning process is accelerated by incorporating a momentum term. The use of momentum introduces a feedback loop which prevents the learning process from being stuck at a local minimum on the error-performance surface of the single-hidden-layer perceptron.

The network has been optimised in terms of its learning rate, momentum constant, and hidden layer size to achieve the minimum mean-squared error. The optimum learning rate is found to be 0.8. The optimum momentum constant is found to be 0.99 and 0.90 for the maternal QRS-complex and the fetal heartbeat with maternal contribution segments, respectively. The single-hidden-layer has an optimum dimension of 5 x 5.

The input to the first layer is the third-order cumulants diagonal and wall slices. The network is trained using TOC slice templates. The input to the network is eight template patterns. These are the third-order cumulant diagonal and wall slices of four segments from one transabdominal cardiac cycle. For example the first pair are maternal QRS-complex TOC diagonal and wall slices, the second pair are the first fetal heartbeat TOC diagonal and wall slices, the third pair are QRS-free ECG TOC diagonal and wall slices, and the fourth pair are the second fetal heartbeat TOC diagonal and wall slices. The network is trained over the eight patterns. The training terminates when the worst error in all patterns in one pass is less than 0.1. Typically the average error will be in the range of 0.001.

4. The classification rate for maternal QRS-complex and fetal heartbeat segments

The results of the first hybrid system indicates that a linear combination of diagonal and wall slices of the TOC can improve the detection rate by up to 1% over and above the 77.8% obtainable using only either slice. Using two more arbitrary slices off-diagonal and off-wall would result in a further improvement of up to 1%. Using two slices instead of only one results in an two-fold increase in the CPU time of 1 msec using Unix WS.

Further improvement of 6% to 8% is attainable with maternal transabdominal ECG signal linearisation employing second- and third-order Volterra synthesisers, respectively. Based on the first hybrid system using TOC slices for signal processing and subsequent single-hidden-layer classification, 100% and 86.16% classification rates have been achieved for maternal QRS-complex and fetal heartbeats, respectively. Note that the classification rates for coincident and non-coincident mother's and fetal QRS-complexes are 0% and 95.55%, respectively.

The remaining undetected 13.84% fetal heartbeats include 9.8% overlap with the maternal QRS-complexes and 4% occur during depolarisation of the maternal T-waves. Those events unavoidably lead to significant distortion of the fetal third-order cumulants. This means that the cumulant signatures will not be close to the TOC template signature stored in the database. Examples of false negatives and false positives have been found in the following cases, respectively, (i) a fetal heartbeat with

maternal contribution TOC diagonal slice was wrongly matched to a QRS-free ECG TOC diagonal slice template, and (ii) a QRS-free ECG TOC diagonal slice was wrongly matched to a fetal heartbeat with maternal contribution TOC diagonal slice template.

4.7 References

[1] C. L. Nikias and A. P. Petropulu, *Higher Order Spectral Analysis: A Nonlinear Signal Processing Framework.* A. V. Oppenheim Series editor, 1993.

[2] C. L. Nikias and M. R. Raghuveer, "Bispectrum estimation: A digital signal processing framework," Proceedings of the IEEE, vol. 75, No. 7, pp. 869-891, July 1987.

[3] H. Pozidis and A. Petropulu, "Use of selected HOS information for low variance estimate of bandlimited systems with short data records," ICASSP, IEEE International conference on Acoustics, Speech and Signal Processing, paper #DSP11.5, Seattle, Washington, USA, May 1998.

[4] M. Sabry-Rizk, W. Zgallai, P. Hardiman, and J. O'Riordan, "Blind Deconvolution - Homomorphic Analysis of Abnormalities in ECG Signals," IEE Colloquium on Blind Deconvolution, #144, pp. 5/1-9, London, UK, Sept. 1995.

[5] M. Sabry-Rizk, W. Zgallai, E. Carson, K. Grattan and R. Summers, "Higher-Order Ambulatory Electrocardiogram Identification and Motion Artifact Suppression With Adaptive Second- and Third-Order Volterra Filters," SPIE Advanced Signal Processing Algorithms, Architectures, and Implementations VIII, vol. 3461, pp. 417-431, USA, 19-24 July 1998.

[6] E. Walach and B. Widrow, "The Least-mean fourth (LMF) adaptive algorithm and its family," IEEE Trans. on Information Theory, vol. 30, No. 2, pp. 275-283, March 1984.

[7] R. Nowak and B. Van Veen, "Efficient method for identification of Volterra filter model," Signal Processing, vol. 38, pp. 417-428, 1994.

[8] M. Caudill and C. Butler, *Understanding Neural Networks: Computer Explorations*, MIT press, 1992.

[9] D. E. Rumelhart, G. E. Hinton and R. J. Williams, "Learning representations by back-propagation errors," Nature, vol. 323, pp. 533-536, 9/10/1986.

[10] N. Morgan and H. A. Bourlard, "Neural networks for statistical recognition of continuous speech," IEEE Proceedings, vol. 83, No. 5, pp. 742-758, May 1995.

[11] C. Li, C. Zheng and C. Tai, "Detection of ECG characteristic points using wavelet transforms," IEEE Transactions on Biomedical Engineering, vol. 42, No. 1, pp. 21-28, January 1995.

[12] J. M. Herbert, W. Peasgood, X. B. Huang, J. A. Crowe, M. S. Woolfson, N. Reed, and E. M. Symonds, "Antepartum fetal electrocardiogram extraction and analysis," Proceedings of Computers in Cardiology, pp. 875-877, 1993.

[13] S. Haykin, "Neural networks expand SP's horizons," IEEE Signal Processing Magazine, pp. 24-49, March 1996.

[14] D. Hatzinakos and C. L. Nikias, "Blind equalization using a tricepstrum based algorithm," IEEE Trans. on Communications, vol. 39, No. 5, pp. 669-681, May 1991.

[15] G. B. Giannakis and M. K. Tsatsanis, "Signal Detection and Classification Using Matched Filtering and Higher Order Statistics," IEEE Transactions on Acoustics, Speech, and Signal Processing, vol. 38, No. 7, July 1990.

[16] M. Sabry-Rizk, D. Romare, W. Zgallai, K. T. V. Grattan, P. Hardiman, and J. O'Riordan, "Higher order statistics (HOS) in signal processing: Are they of any use?," IEE Colloquium, Digest #111, pp. 1/1-1/6, London, May 1995.

[17] P. Ruiz and J. L. Lacoume, "Extraction of Independent Sources From Correlated Inputs: A Solution Based on Cumulants," Higher-Order Statistics Workshop, pp. 146-149, USA, 1989.

[18] C. Y. Chin and J. Y. Kung, "A Fast Phase Determination Method By A Single Cumulant Sample," Proceedings of the International Signal Processing Workshop on Higher-Order Statistics, pp. 133-136, France, 1991.

[19] C. L. Nikias and J. M. Mendel, "Signal processing with higher order spectra", IEEE Signal Processing Magazine, pp. 10-37, July 1993.

[20] L. Li and S. Haykin, "A cascaded recurrent neural networks for real time non-linear adaptive filtering, International Conference on Neural Networks, pp. 857-862, 1993.

[21] K. G. Lindecrantz and H. Lilja, "New Software QRS Detector Algorithm Suitable for Real Time Applications with Low Signal-to-Noise Ratios," Journal of Biomedical Engineering, vol. 10, pp. 280-284, May 1988.

[22] Y. C. Park et al, "On Detecting the Presence of Fetal R-Wave Using the Moving Averaged Amplitude Difference Algorithm," IEEE Transactions on Biomedical Engineering, vol. BME-39, No. 8, pp. 868-871, August 1992.

[23] D. R. Brillinger, "Some History of the Study of Higher-Order Moments and Spectra," in Proceedings of the International Signal Processing Workshop on Higher Order Statistics, Colorado, U.S.A., pp. 41-45, 1990.

[24] P. A. Delaney and D. O. Walsh, "A Bibliography of Higher-Order Spectra and Cumulants," IEEE Signal Processing Magazine, pp. 61-70, July 1994.

[25] J. A. R. Fonollosa and J. Vidal, "System Identification Using a Linear Combination of Cumulant Slices," IEEE Transactions on Signal Processing, vol. 41, No. 7, pp. 2405-2411, July 1993.

[26] C. L. Nikias, "Higher Order Spectra in Signal Processing," in EUSIPCO 89, *Signal Processing V: Theories and Applications* (L. Tarres, E. Masgrau, and M. A. Lagunas, eds.), Elsevier Publishers, Holland, pp. 35-41, 1990.

[27] R. Pan and C. L. Nikias, "The Complex Cepstrum of Higher-Order Cumulants and Nonminimum Phase System Identification," IEEE Transactions on Acoustics, Speech, and Signal Processing, vol. ASSP-36, pp. 186-205, February 1988.

[28] A. Petropulu and C. L. Nikias, "Cumulant Cepstrum of FM Signals and High Resolution Time Delay Estimation," International Conference on Acoustics, Speech, and Signal Processing, ICASSP, pp. 2642-2645, NY, April 1988.

[29] A. V. Dandawate and G. B. Giannakis, "A Triple Cross Correlation Approach for Enhancing Noisy Signals," in Proceedings of the International Signal Processing Workshop on Higher Order Statistics, Colorado, USA, pp. 212-216, 1990.

[30] A. Swami and G. B. Giannakis, "ARMA Modelling and Phase Reconstruction of Multidimensional Non-Gaussian Processes Using Cumulants," Proceedings of the IEEE International Conference on Acoustics, Speech, and Signal Processing, ICASSP, pp. 729-732, NY, 1988.

[31] J. M. Mendel, "Use of Higher Order Statistics in Signal Processing and System Theory: An Update," Proceedings of SPIE, vol. 975, Advanced Algorithms and Architectures for Signal Processing III, pp. 126-144, 1988.

[32] G. B. Giannakis, "Cumulants: A Powerful Tool in Signal Processing," Proceedings of the IEEE, vol. 75, No. 9, pp. 1333-1334, September 1987.

[33] D. Shin and C. L. Nikias, "Adaptive noise canceler for narrowband and wideband interferences using higher-order statistics," USC-SIPI Rep. #220, September 1992.

[34] F. C. Zheng, S. McLaughlin, and B. Mulgrew, "A 2nd- and 4th-Order Cumulant Based Blind Equalisation Algorithm for nonminimum phase channels," Proceedings of the International Signal Processing Workshop on Higher-Order

Statistics, Cgamrousse, France, (J. L. Lacoume, ed.), July 10-12, 1991, Elseveir Science Publishers, pp. 129-132, 1992.

[35] B. Friedlander and B. Porat, "Performance analysis of MA parameter estimation algorithms based on higher-order moments," Proceedings of IEEE ICASSP, pp. 2412-2415, NY, April 1988.

[36] M. Huzzi, "Estimation of coefficients of an autoregressive process by using higher order moments," Journal of time series analysis, vol. 2, pp. 87-93, 1981.

[37] J. K. Tugnait, "On selection of maximum cumulant lags for non-causal autoregressive model fitting," Proceedings of IEEE International Conference on Acoustics, Speech, and Signal Processing, ICASSP, pp. 2372-2375, NY, 1988.

[38] A. W. Lohmann and B. Wirnitzer, "Triple correlations," Proceedings of IEEE, vol. 72, pp. 889-901, July 1984.

[39] A. E. Cetin and A. M. Teklap, "Cumulant Based Robust System Identification," Proceedings of the International Signal Processing Workshop on Higher-Order Statistics, pp. 145-148, France, 1991.

[40] Y. H. Hu, S. Palreddy and W. J. Tompkins, "A patient-adaptable ECG beat classifier using a mixture of experts approach," IEEE Transactions on Biomedical Engineering, Vol. 44, N. 9, pp. 891-899, September 1997.

[41]] M. Sabry-Rizk, W. Zgallai, "Novel robust modified pseudo-spectral MUSIC algorithm for on-line QRS detection in electrocardiogram signals", to be published.

[42] M Sabry-Rizk, W Zgallai, E. R. Carson, K. T. V. Grattan, A. MacLean, and P. Hardiman, "Non-linear dynamic tools for characterising abdominal electro-myographic signals before and during labour," Transactions of the Institute of Measurement and Control, vol. 22, pp. 243-270, 2000.

[43] J. Jenkins, "Automated electrocardiography and arrhythmia monitoring," Prog. Card. Dis., vol. 25, No. 5, pp. 367-408, 1983.

[44] R. G. Mark, "Arrhythmia monitoring: current status and future challenges," in *Patient Monitoring and Data Management*, pp. 7-11, AAMI. Technology Analysis and Review: TAR, No. 11-85, 1985.

[45] J G McWhirter, and I. J. Clarke, "Higher order statistics, blind signal separation and multilinear algebra," IEE Colloquium, IEE, London, pp. 4/1-4/3, 1999.

[46] M. R. Lynch, P. J. Rayner and S. B. Holden, "Removal of Degeneracy in Adaptive Volterra Networks by Dynamic Structuring," Proceedings of IEEE ICASSP, pp.

2069-2072, 1991.

[47] K. C. Nisbet, B. Mulgrew and S. McLaughlin, "A reduced complexity sub-optimal nonlinear predictor," IEE Colloquium, pp. 6/1-6/13, London, 1994.

[48] A. V. Dandawate, and G. B. Giannakis, "Nonparametric polyspectral estimators for kth-order (almost) cyclostationary processes," *IEEE Transactions on Information Theory*, vol. 40, pp. 67-84, 1994.

[49] Mukhopadhyay, S. and Sircar, P., "Parametric modelling of ECG signal," *Med. Biol. Eng. Comput.*, vol. 34, pp. 171-174, 1996.

[50] Comon P, "Independent component analysis, A new concept?," Signal Processing Special Issue HOS, vol. 36, No. 3, pp. 287-314, 1994.

[51] A. Hyvarinen, "New approximation of differential entropy for independent component analysis and projection persuit," in Advances in Neural Information Processing Systems. Cambridge MA: MIT Press, vol. 10, pp. 273-279, 1999.

[52] C. Jutten and J. Herault, "Blind separation of sources- Part I: An adaptive algorithm based on neuromimetic architecture," Signal Processing, vol. 24, pp. 1-10, 1991.

[53] NAG Fortran Library Mark 19, The Numerical Algorithms Group, Oxford, UK, 1999.

[54] W. Zgallai, M. Sabry-Rizk, P. Hardiman, and J. O'Riordan, "Third-order cumulant signature matching technique for non-invasive fetal heart beat identification," ICASSP, IEEE International Conference on Acoustics, Speech, and Signal Processing, vol. 5, pp 3781-3784, Germany, 1997.

[55] J. M. Mendel, "A compendium of new theoretical results associated with using higher-order statistics in signal processing and system theory," Spectral Analysis n One or Two Dimensions, pp. 163-182, August 1990.

[56] L. De Lathauwer, B. De Moor, and J. Vandewalle, "Fetal electrocardiogram extraction by blind source separation," IEEE Transactions on Biomedical Engineering, Vol. 47, No. 5, pp. 567- 572, May 2000.

[57] M Sabry-Rizk, W. Zgallai, A. McLean, E. R. Carson, and K. T. V. Grattan, "Virtues and Vices of Source Separation Using Linear Independent Component Analysis for Blind Source Separation of Non-linearly Coupled and Synchronised Fetal and Mother ECGs," IEEE Engineering in Medicine and Biology Conference, USA, 2001.

[58] V. Zarazoso, A. K. Nandi, and E. Bacharkis, "Maternal and foetal separation using blind source separation methods," IMA Journal of Mathematics Applied in

Medicine and Biology, vol. 14, pp. 207-225, Oxford University Press, 1997.

[59] V. Zarazoso and A. K. Nandi, "Comparison between blind separation and adaptive noise cancellation techniques for fetal electrocardiogram extraction," IEE Colloquium, pp. 1/ -1/6., 1999.

[60] E. G. Lovett and K. M. Ropella, "Bispectral Analysis Of Intra-Cardiac Electrograms," IEEE Signal Processing Workshop on Higher-Order Statistics, pp. 366-368, USA, 1993.

[61] M. Sabry-Rizk, D. Romare, W. Zgallai, K. T. V. Grattan, P. Hardiman, and J. O'Riordan, "Higher order statistics (HOS) in signal processing: Are they of any use," IEE colloquium, digest #111, pp. 1/1-1/6, London, May 1995.

[62] M. Sabry-Rizk, W. Zgallai, "Higher Order Statistics Are Indispensable Tools in The Analysis of Electrocardiogram Signals," IEE Colloquium on Statistical Signal Processing, January 1999.

[63] C. Sureau, "Historical perspectives: forgotten past, unpredictable future," in *Baillier's clinical obstetrics and gynaecology, international practice and research, intrapartum surveillance*, (J Gardosi, ed.), vol. 10, No. 2, pp. 167-184, 1996.

[64] L. De Lathauwer, B. De Moor, and J. Vandewalle, "Fetal electrocardiogram extraction by blind source separation," IEEE Transactions on Biomedical Engineering, Vol. 47, No. 5, pp. 567- 572, May 2000.

[65] S. Haykin, *Neural networks*, Prentice Hall, 1998.

[66] M Caudill and C Butler, *Understanding Neural Networks: Computer Explorations*, MIT press, 1992.

[67] D. E. Rumelhart, G. E. Hinton and R. J. Williams, "Learning representations by back-propagation errors," Nature, vol. 323, pp. 533-536, 9/10/1986.

[68] P. Common, "Independent component analysis, A new concept?", Signal Processing, Vol. 21, pp. 287-314, 1994.

[69] I. J. Clarke, "Direct exploitation of non-Gaussianity as a discriminent", Proc. EUSIPCO IX, pp. 2057-60, 1998.

[70] D. E. Rumelhart, G. E. Hinton, and R. J. Williams, "Learning internal representation by error propagation," In Parallel Distributed Processing: Explorations in the Microstructure of Cognition (D. E. Rumelhart, and J. L. McClelland eds.,) vol. 1, Chapter 8. Cambridge, MA: MIT press, 1986.

[71] E. Barnard and E. Casasent, "Invariance and neural nets," IEEE Transactions on Neural Networks, vol. 2, pp. 498-508, 1991.

[72] M. L. Minsky and S. A. Papert, *Perceptrons*, Cambridge, CA, MIT Press, 1969.

CHAPTER FIVE

NON-INVASIVE FETAL HEARTBEAT DETECTION USING BISPECTRAL CONTOUR MATCHING IN CONJUNCTION WITH ANN CLASSIFIERS

5.1 Introduction

5.1.1 Aim

This chapter describes the second hybrid system (e.g., signal processing in conjunction with classification), using the mother and fetal ECG bispectral contours (BIC), which carry the signature imprints of their respective QRS-complexes, in the signal processing phase. As with the first hybrid system, the classification phase employs LMS-based single-hidden-layer classifiers. The mother's chest ECGs and the fetal scalp electrode ECGs have been used as templates or the HOS representatives in the classification. The bispectral contour matching technique is used herewith for the first time to identify the signatures of both the maternal and fetal QRS-complexes.

In the previous chapter, brief descriptions are given for the ECG database, ECG segmentation and window maximum length, window overlapping, calculation of an averaged fetal heart rate within one maternal cardiac cycle, the strategy behind creating the template database, linearisation using second- and third-order Volterra synthesisers, and single-hidden-layer perceptron design and classification criteria. In this Chapter, the same procedure is applied with the replacement of the third-order cumulant slices by the bispectral contours (usually 10 contours including the tip of the peak and are spaced by approximately 1 dB). The CPU time for the bispectrum computation is almost twice that for cumulants and 2000 times that for individual TOC slices.

It will be shown that the highest achievable Fetal Heartbeat (FHB) classification rate using the BIC template matching technique is 90.12% with reduced false positives and

negatives associated with the power spectrum-based FHB classification rate of 70%. Furthermore, the BIC has a marginally improved classification performance over and above the TOC during episodes of overlapping fetal QRS-complexes and maternal T-waves. As mentioned above, this is achieved at the expense of complexity and computation time.

5.1.2 Layout of the Chapter

It was considered prudent to report on some second-order statistics spectral estimators with and without linearisation to show the remarkable advantage gained by using the third-order statistics instead. However, this does not include appropriately chosen MUSIC-based techniques with their unique subspace structural properties and accurate estimation of the interference signal as this will be the subject of Chapter Six. The Chapter is divided as follows. Section 5.2 references previous joint work on non-invasive fetal heartbeat detection using the bispectrum. Section 5.3 refers to the detection key operations. Section 5.4 caters for displaying the effect of linearisation in conjunction with a number of second-order statistics (SOS) spectral estimators, namely, (i) the FFT, (ii) the auto-regressive (AR), (iii) the Yule-Walker, and (iv) the maximum entropy (MEM). Section 5.5 presents preliminary investigations of ECG bispectrum, including typical examples of bispectra and their contours, followed by the estimation of the variance. Section 5.6 gives a detailed description of the second hybrid system which uses several bispectral contours as the discriminants in detecting the occurrences of fetal heartbeats within each maternal cardiac cycle. Section 5.6.1 shows the results of optimising the single-hidden layer perceptron. Section 5.6.3 shows the results of maternal QRS-complex and fetal heartbeat classification with and without linearisation, and employing both second- and third-order Volterra synthesisers with LMF update. Summary and conclusions are given in Section 5.7.

5.2 Previous work

There is no reported work in the literature on the subject of non-invasive fetal heartbeat detection using the bispectrum except that jointly published by the author using the pseudo-bispectrum [35].

5.3 Detection key operations

These are exactly the same as those described in Section 4.3 except that the third-order cumulant slices are now going to be replaced by the bispectral contours.

5.4 Second-order statistics (SOS) spectral estimation

The general problem of spectral estimation is that of determining the spectral content of a signal based on a finite set of measured data [52]. Formally, the Power Spectral Density (PSD) is defined as the Fourier Transform (FT) of the Autocorrelation Function (ACF) [53]. The PSD function describes the distribution of power with frequency. Spectrum estimation is accomplished by either non-parametric or parametric methods. Non-parametric methods include FFT-based methods such as the Periodogram. Parametric methods include model identification methods such as the Auto-Regressive (AR), the Yule-Walker, and the maximum entropy (MEM). The eigenvector subspace methods are the subject of Chapter Six.

5.4.1 Non-parametric methods

The FFT-based method (The periodogram)

The PSD is calculated as

$$\hat{P}_{xx}^{A}(f) = \left| \frac{1}{N} \sum_{k=0}^{N-1} x(k).e^{-j2\pi.fk} \right|^2, \tag{5.1}$$

or the power spectral density is calculated as

$$\hat{P}_{xx}^{B}(f) = \frac{1}{1 - \hat{P}_{xx}^{A}(f)}, \qquad 0 \leq \hat{P}_{xx}^{A}(f) \leq 1. \tag{5.2}$$

The sharpness of the peaks in Eq. (5.2) is due to the non-linear warping caused by the transformation 1 / (1 - x). The apparent increase in resolution is gained at the expense of a large increase in the variance of the spectral peaks' amplitudes. Both spectral estimators contain the same information. In other words, the sharpness of the peaks of a spectral estimate is not related to its resolution. For classical methods (FFT-based), the bias of the estimator can be reduced at the expense of an increase in the variance, and vice versa. However, both types of errors cannot be reduced simultaneously. The

periodogram is an inconsistent estimator in that even though the average value converges to the true value as the data record length becomes large, the variance stays constant. The periodogram will yield statistically inconsistent (unstable) PSD estimates because the expectation operation of the PSD has been ignored. The averaged periodogram will reduce the variance, but the bias will increase. The application of temporal windows reduces the levels of the sidelobes. However, the mainlobe width will increase. The key disadvantage of the classical spectral estimation is the distortioning impact of sidelobe leakage due to the inherent windowing of finite data sets. For a finite data set, trade-offs among resolution, stability (minimising the estimate variance), and leakage suppression are necessary.

Eq. (5.2) is used to calculate the power spectrum in conjunction with a Hanning window (alpha = 0.54). The power spectrum is calculated with and without linearisation. An optimised third-order Volterra structure (see Section 3.4) is employed to decompose the ECG signal into its linear, quadratic, and cubic parts and retain only the linear part. The power spectrum of a fetal scalp electrode full cardiac cycle, data length 500 msec, is depicted in Figure 5.1 (a). There is a principal spectral peak at 30 Hz [106]. Non-linearity has not affected the frequency of the principal peak. However, removing non-linearity seems to help in sharpening it. There is apparent reduction in the spectral content at lower frequencies.

Figure 5.1 (b) shows the frequency content of a maternal chest full cardiac cycle, data length 1000 msec. There is one sharp peak at 14 Hz and three small peaks in the range of 6 Hz to 12 Hz. Note that the accurate frequency of the spectral peak of the adult QRS-complex is at 17 Hz [107] and not at 14 Hz. The FFT-based method is biased because the calculated spectral peak of the QRS-complex of the maternal chest ECG deviates from the normal frequency of the adult QRS-complexes. The removal of non-linearity sharpens the spectral peaks at 6 Hz, 10 Hz, and more so at 12 Hz, significantly.

Figure 5.1 (c) shows the frequency content of a maternal transabdominal full cardiac cycle, data length 1000 msec. There is a sharp maternal principal spectral peak at 17 Hz and four smaller peaks at 5 Hz, 13 Hz, 25 Hz, and 31 Hz. The small peak at 31 Hz may or may not correspond to the fetal principal spectral peak. The removal of non-linearity

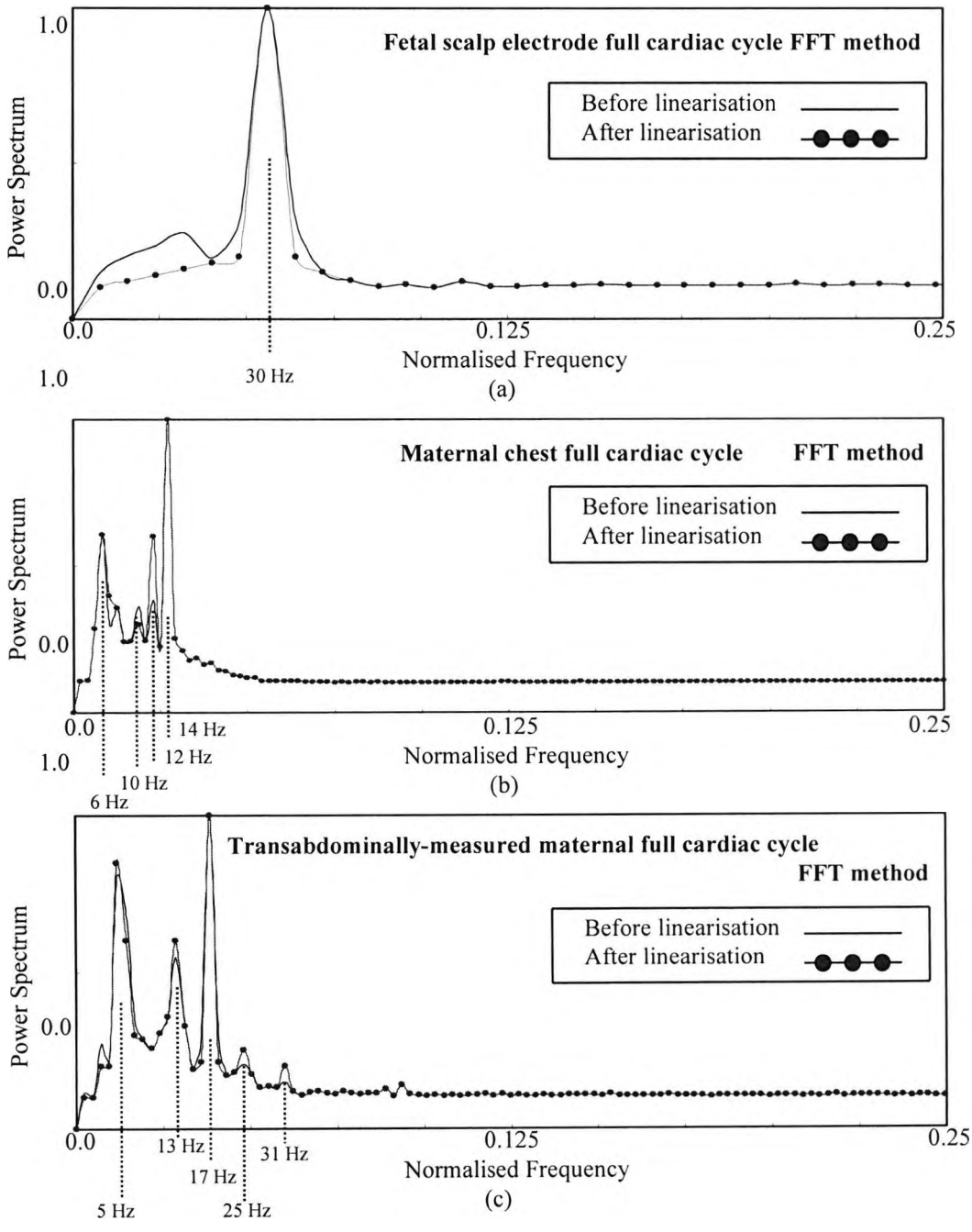

Figure 5.1: *The effect of linearisation in conjunction with the FFT-based second-order statistics (SOS) spectral estimator.* (a) *The fetal scalp electrode full cardiac cycle (Code: 5-1, data length 500 msec), (b) and (c) are the chest and transabdominaly-measured (twin electrodes) full cardiac cycles at the first stage of labour at 40 weeks, (Code: 5-1, data length 1000 msec, the maternal cardiac cycle begins 50 msec before the R-wave and ends 50 msec before the next R-wave). A Hanning window is used to calculate the power spectrum. Sampling rate = 0.5 KHz, resolution = 12 bits.*

has definitely sharpened and raised the levels of all the spectral peaks.

Figure 5.2 (a-c) shows the spectral peaks calculated using the FFT method for a fetal scalp electrode cardiac cycle, a transabdominally-measured cardiac cycle, and a segment of the maternal transabdominal ECG signal containing a fetal heartbeat with maternal contribution (inset). A Hanning window is used to calculate the power spectrum (alpha = 0.54). The power spectrum is calculated with and without linearisation. An optimised third-order Volterra structure is employed to decompose the ECG signal into its linear, quadratic, and cubic parts and retain only the linear part. The power spectrum of a fetal scalp electrode full cardiac cycle, data length 500 msec, is depicted in Figure 5.2 (a). There is a principal spectral peak at 31 Hz and other peaks at 14 Hz and 26 Hz. Non-linearity has not affected the frequency of the principal peak. However, removing non-linearity seems to help in sharpening it.

Figure 5.2 (b) shows the frequency content of a maternal transabdominal full cardiac cycle, data length 1000 msec. There are five spectral peaks at 6 Hz, 14 Hz, 20 Hz, 27 Hz, and 32 Hz. Note that there is a strong motion artefact peak at 6 Hz. There is a sharp maternal principal spectral peak at 14 Hz. Again, the FFT-based method is biased because the calculated spectral peak of the QRS-complex of the maternal chest ECG deviates from the normal frequency of the adult QRS-complexes. The small peak at 32 Hz may or may not correspond to the fetal principal spectral peak. The removal of non-linearity has definitely sharpened and raised the levels of all the spectral peaks.

Figure 5.2 (c) shows the frequency content of a segment of the maternal transabdominal ECG signal containing a fetal heartbeat with maternal contribution, data length 250 msec. There are three spectral peaks at 15 Hz, 24 Hz, and 42 Hz. There is no fetal principal spectral peak shown using the FFT method. With the removal of non-linearity, there is apparent reduction in the spectral content at lower frequencies.

5.4.2 Parametric methods

The primary motivation for many of the alternative spectral estimators has been the unsatisfactory performance of classical spectral estimators. Three parametric methods are used for spectral estimation, namely, the Auto-Regressive (AR), the Yule-Walker, and the Maximum Entropy (MEM).

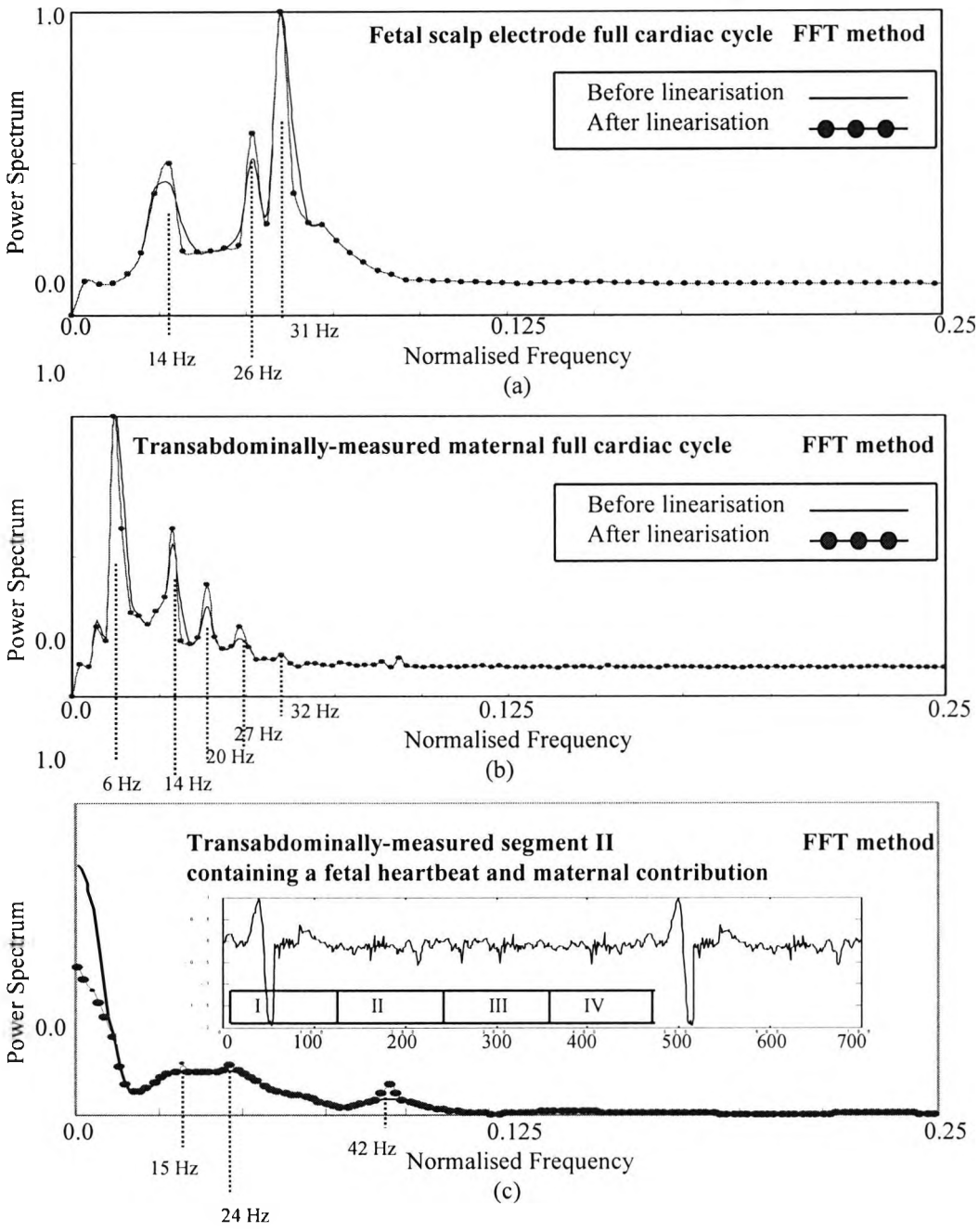

Figure 5.2: *The effect of linearisation in conjunction with the FFT-based second-order statistics (SOS) spectral estimator.* (a) The *fetal scalp electrode full cardiac cycle (data length 500 msec), (b) the transabdominally-measured maternal full cardiac cycle (twin electrodes, data length 1000 msec), and (c) segment II of the maternal transabdominal signal (inset) containing a fetal heartbeat with maternal contribution (data length 250 msec). The maternal cardiac cycle begins 50 msec before the R-wave and ends 50 msec before the next R-wave. The subject is at the first stage of labour (40 weeks gestation). A Hanning window is used to calculate the power spectrum. Sampling rate = 0.5 KHz, resolution = 12 bits.*

1. The AR method:

To estimate the PSD using an AR model we need to estimate the parameters of the model, a(1), a(2),…, a(p). The PSD is given as [53]

$$\hat{P}_{AR}(f) = \frac{\sigma^2}{\left|1 + a(1).\exp(-j2\pi f + ... + a(p).\exp(-j2\pi fp)\right|^2} \tag{5.3}$$

The incorporation of a model leads to the replacement of the general spectral estimation problem by a parameter estimation problem. If the model is accurate, but a poor spectral estimator of the parameters is used, poor (increased variance) spectral estimates will result. Different models may yield similar results, but one model may require fewer model parameters and therefore be more efficient than the other models in its representation of the data.

Figure 5.3 (a-c) shows the results of the AR method for a fetal scalp electrode cardiac cycle, a transabdominally-measured cardiac cycle, and a segment of the maternal transabdominal ECG signal containing a fetal heartbeat with maternal contribution (inset). Hanning window is used to calculate the power spectrum (alpha = 0.54). The power spectrum is calculated with and without linearisation. An optimised third-order Volterra structure is employed to decompose the ECG signal into its linear, quadratic, and cubic parts and retain only the linear part. The AR spectrum of the fetal scalp electrode full cardiac cycle, data length 500 msec, is depicted in Figure 5.3 (a). There is a sharp principal spectral peak at 30 Hz [106] and a small peak at 24 Hz. Non-linearity has not affected the frequency of the principal peak. With the removal of non-linearity, there is apparent reduction in the spectral content at lower frequencies. The sharp peaks that characterise the AR spectra are apparent in this figure.

Figure 5.3 (b) shows the AR spectrum of a maternal transabdominal full cardiac cycle, data length 1000 msec. There is a sharp maternal principal spectral peak at 15 Hz. The frequency deviation from the actual frequency of 17 Hz [107], is due to the AR bias as previously mentioned with the FFT-based method. There is a sharp motion artefact peak at 2 Hz. There is a small peak at 35 Hz which may or may not correspond to the fetal principal spectral peak. The removal of non-linearity has sharpened and raised the level of the principal spectral peak. With the removal of non-linearity, there is apparent

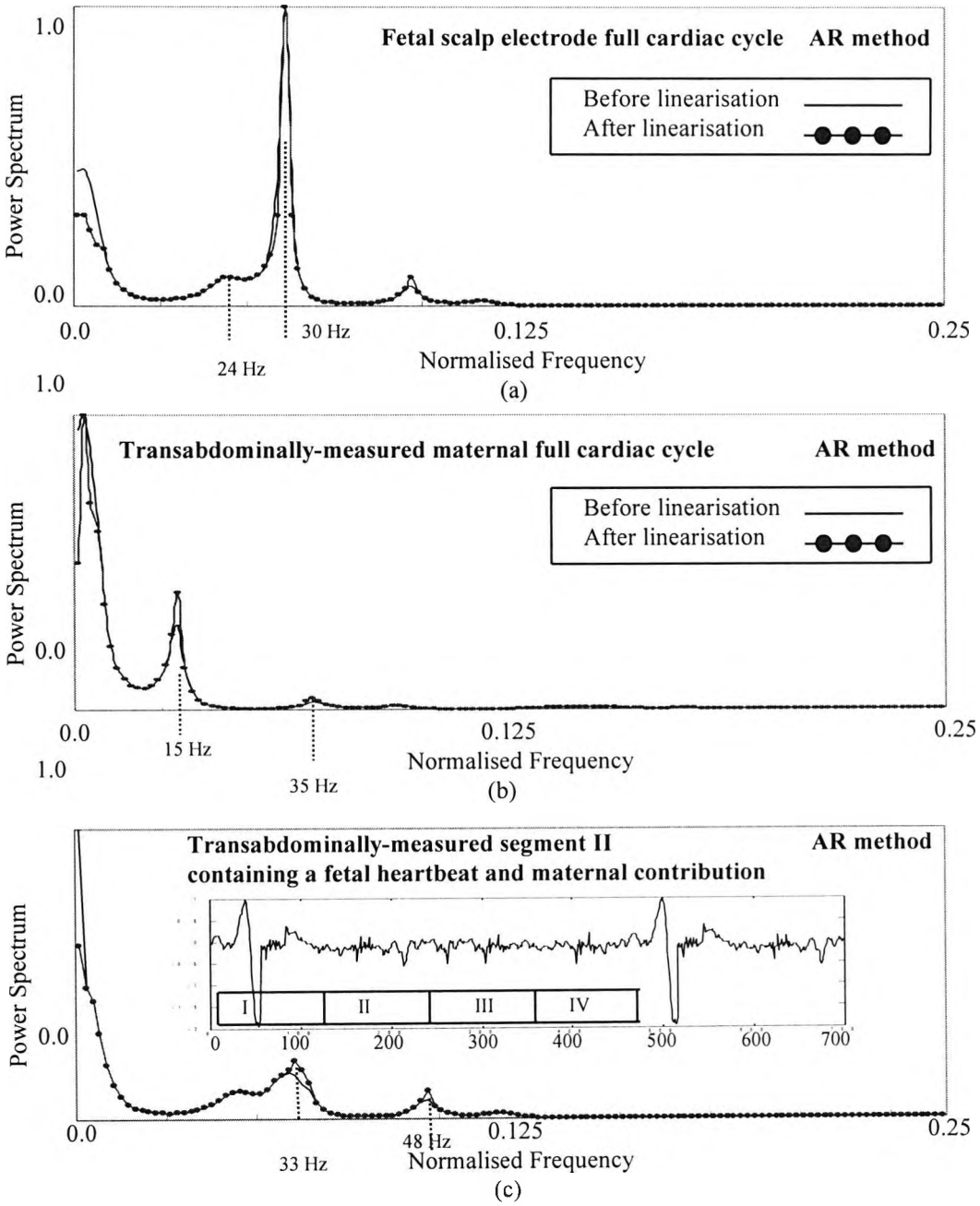

Figure 5.3: *The effect of linearisation in conjunction with the AR second-order statistics (SOS) spectral estimator. (a) The fetal scalp electrode full cardiac cycle (data length 500 msec), (b) the transabdominally-measured maternal full cardiac cycle (twin electrodes, data length 1000 msec), and (c) segment II of the maternal transabdominal signal (inset) containing a fetal heartbeat with maternal contribution (data length 250 msec). The maternal cardiac cycle begins 50 msec before the R-wave and ends 50 msec before the next R-wave. The subject is at the first stage of labour (40 weeks gestation). Model order = 11. A Hanning window is used to calculate the power spectrum. Sampling rate = 0.5 KHz, resolution = 12 bits.*

reduction in the spectral content at lower frequencies.

Figure 5.3 (c) shows the AR spectrum of a segment of the maternal transabdominal ECG signal containing a fetal heartbeat with maternal contribution, data length 250 msec. There is a small peak at 33 Hz which may or may not correspond to the fetal principal spectral peak. There is a very small peak at 48 Hz. The removal of non-linearity has sharpened and raised the level of the principal spectral peak. With the removal of non-linearity, there is apparent reduction in the spectral content at lower frequencies.

2. The Yule-Walker method

The Yule-Walker method is based on estimating the autocorrelation parameters and minimising the estimate of the prediction error power. Those parameters are obtained using the following equation [53]:

$$\frac{1}{N}\sum_{n=-\infty}^{\infty}\left(x[n]+\sum_{k=1}^{p}a[k]x[n-k]\right)*x[n-l]=0, \qquad l=1,2,....,p. \tag{5.4}$$

The autocorrelation parameters can be used to calculate the PSD in a similar way to that of Eq. (5.3). Figure 5.4 (a-c) shows the results of the Yule-Walker method for a fetal scalp electrode cardiac cycle, a transabdominally-measured cardiac cycle, and a segment of the maternal transabdominal ECG signal containing a fetal heartbeat with maternal contribution (inset). The Hanning window is used to calculate the power spectrum (alpha = 0.54). The power spectrum is calculated with and without linearisation. An optimised third-order Volterra structure is employed to decompose the ECG signal into its linear, quadratic, and cubic parts and retain only the linear part. The Yule-Walker spectrum of the fetal scalp electrode full cardiac cycle, data length 500 msec, is depicted in Figure 5.4 (a). There is a shallow principal spectral peak at 30 Hz [106]. There is a strong motion artefact at 2 Hz and a small peak at 16 Hz. Non-linearity has not affected the frequency of the principal peak. With the removal of non-linearity, there is apparent reduction in the spectral content at lower frequencies.

Figure 5.4 (b) shows the Yule-Walker spectrum of a maternal transabdominal full cardiac cycle, data length 1000 msec. There are sharp maternal principal spectral peaks

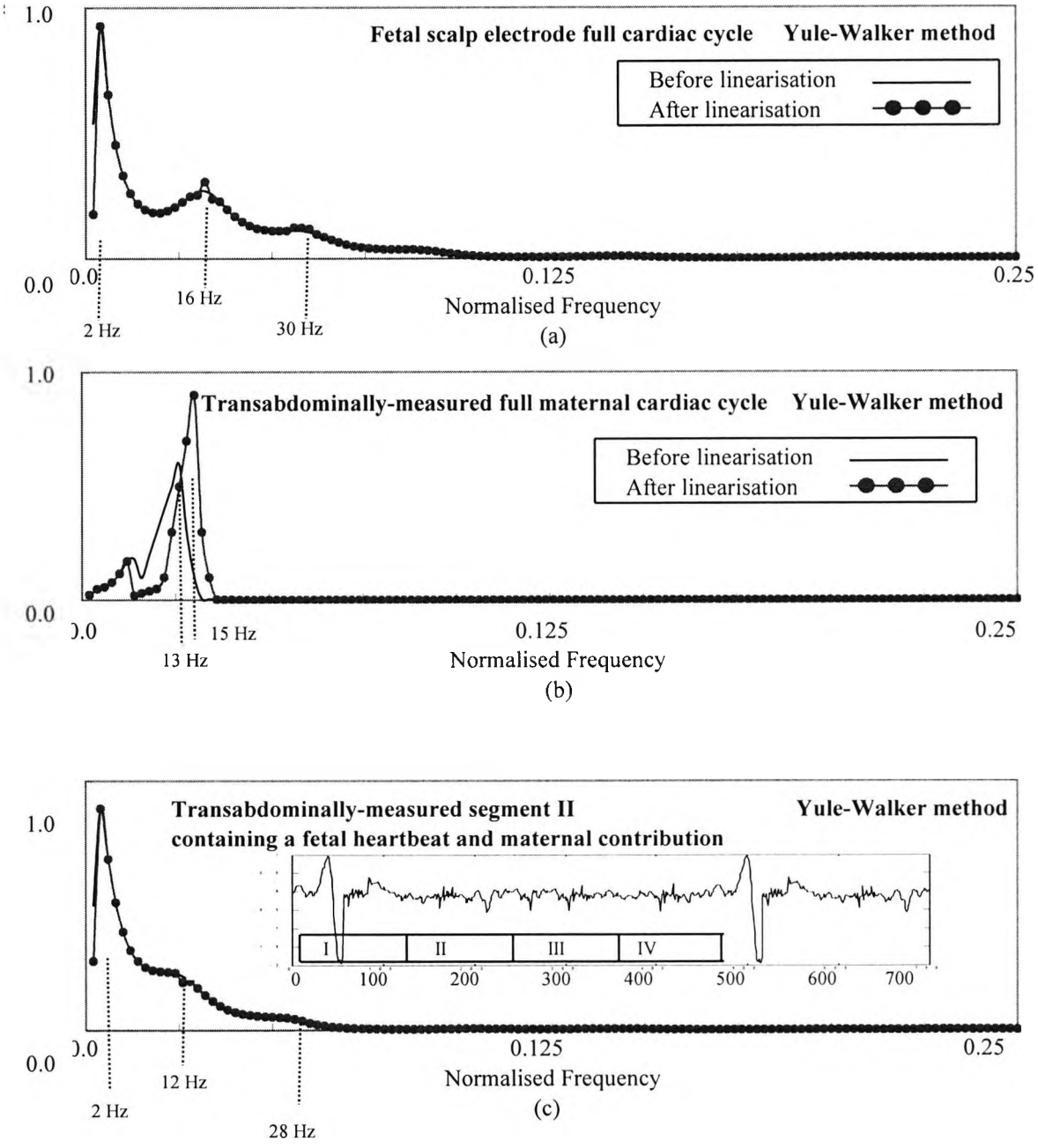

Figure 5.4: *The effect of linearisation in conjunction with the Yule-Walker second-order statistics (SOS) spectral estimator. (a) The fetal scalp electrode full cardiac cycle (data length 500 msec), (b) the transabdominally-measured maternal full cardiac cycle (twin electrodes, data length 1000 msec), and (c) segment II of the maternal transabdominal signal (inset) containing a fetal heartbeat with maternal contribution (data length 250 msec). The maternal cardiac cycle begins 50 msec before the R-wave and ends 50 msec before the next R-wave. The subject is at the first stage of labour (40 weeks gestation). Code: 35-1. SNR = 29 dB, 23 dB, and 2 dB for (a), (b), and (c), respectively. Model order = 8. A Hanning window is used to calculate the power spectrum. Sampling rate = 0.5 KHz, resolution = 12 bits.*

at 13 Hz and 15 Hz before and after linearisation, respectively. The frequency deviation from the actual frequency of 17 Hz [107], is due to the Yule-Walker bias as previously mentioned with the FFT-based method. The removal of non-linearity has sharpened and raised the level of the principal spectral peak and shifted it from 13 Hz to 15 Hz.

Figure 5.4 (c) shows the Yule-Walker spectrum of a segment of the maternal transabdominal ECG signal containing a fetal heartbeat with maternal contribution, data length 250 msec. There is a very small and shallow peak at 28 Hz which may or may not correspond to the fetal principal spectral peak. There is a very strong motion artefact at 2 Hz and a shallow peak at 12 Hz. With the removal of non-linearity, there is apparent reduction in the spectral content at lower frequencies.

The Yule-Walker method (Figure 5.4 a-c) produced shallower peaks than the AR method (Figure 5.3 a-c). This is perhaps due to the model order estimated for the former as 8 which is lower than that estimated for the latter as 11. The variation in performance among the various spectral estimation methods may often be attributed to how well the underlying assumed model matches the process under analysis. When the model is an accurate representation of the data, spectral estimates can be obtained with performance exceeding that of the classical spectral estimators (e.g., the periodogram).

3. The MEM method

The MEM method is based on maximising the entropy per sample and applying the technique of Lagragian multipliers to obtain the PSD [53]:

$$\hat{P}_{MEM}(f) = \frac{1}{\sum_{k=-p}^{p} \lambda_k \exp(-j2\pi fk)}, \tag{5.5}$$

where the λ_k's are the Lagragian multipliers. The MEM method is identical to the AR method only for Gaussian random processes and a known autocorrelation sequence of uniform spacing.

The results of the maximum entropy method (MEM) for a fetal scalp electrode cardiac cycle, a transabdominally-measured cardiac cycle, and a segment of the maternal

transabdominal ECG signal containing a fetal heartbeat with maternal contribution (inset) are shown in Figure 5.5 (a-c). The Hanning window is used to calculate the power spectrum (alpha = 0.54). The power spectrum is calculated with and without linearisation. An optimised third-order Volterra structure is employed to decompose the ECG signal into its linear, quadratic, and cubic parts and retain only the linear part (see Section 3.4). The MEM spectrum of the fetal scalp electrode full cardiac cycle, data length 500 msec, is depicted in Figure 5.5 (a). There is a principal spectral peak at 30 Hz [106]. There is a strong motion artefact at 1 Hz. Non-linearity has not affected the frequency of the fetal principal peak. With the removal of non-linearity, there is a small reduction in the spectral content at lower frequencies.

Figure 5.5 (b) shows the MEM spectrum of a maternal transabdominal full cardiac cycle, data length 1000 msec. It shows the characteristic maternal spectral peak at 15 Hz. The frequency deviation from the actual frequency of 17 Hz [107], is due to the MEM bias as previously mentioned with the FFT-based method. The removal of non-linearity has not sharpened, indeed it is broader, but only raised the level of the principal spectral peak. This might be due to a model mismatch after linearisation. With the removal of non-linearity, there is a small reduction in the spectral content at lower frequencies.

Figure 5.5 (c) shows the MEM spectrum of a segment of the maternal transabdominal ECG signal containing a fetal heartbeat with maternal contribution, data length 250 msec. There is a very shallow and small peak at 27 Hz. There is a strong motion artefact at 2 Hz. With the removal of non-linearity, there is a small reduction in the spectral content at lower frequencies. The MEM method has failed to detect the fetal peaks. One reason for this could be the low signal-to-noise ratio of the fetal ECG signal at 2 dB calculated from the singular values of segment II of the transabdominal ECG signal (see Appendix A4, Section A4.4).

There are some limitations of the second-order statistics-based spectral estimation methods. The second-order statistics methods assume that the data is stationary. The conventional methods lack sharpness of the peaks and have restricted ability to resolve spectral peaks. The FFT-based method failed to detect and resolve the peak. Also results obtained using the Maximum Entropy Method (MEM) and the Yule-Walker method did

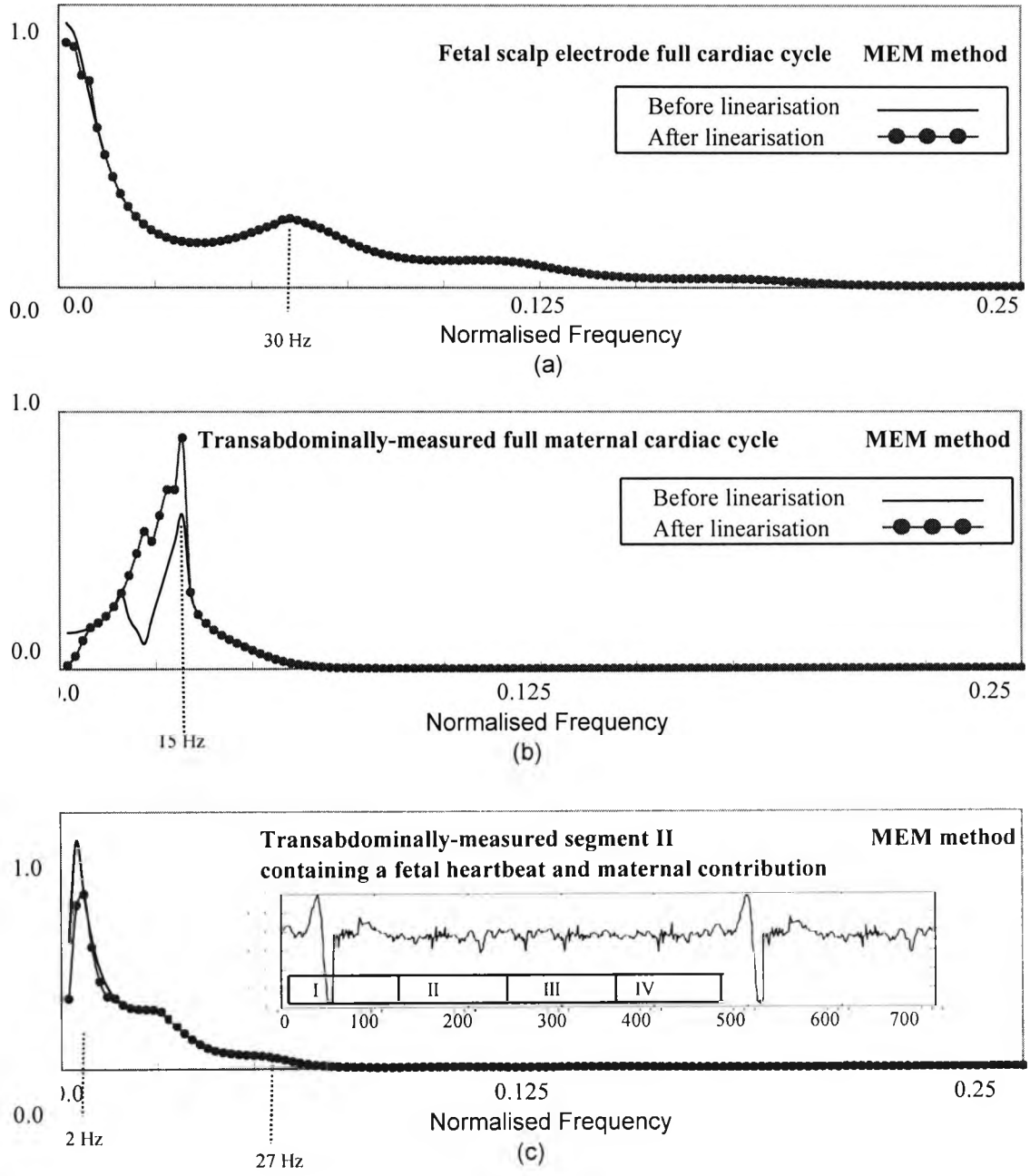

Figure 5.5: *The effect of linearisation in conjunction with the maximum entropy (MEM) second-order statistics (SOS) spectral estimator.* (a) The fetal scalp electrode full cardiac cycle (data length 500 msec), (b) the transabdominally-measured maternal full cardiac cycle (twin electrodes, data length 1000 msec), and (c) segment II of the maternal transabdominal signal (inset) containing a fetal heartbeat with maternal contribution (data length 250 msec). The maternal cardiac cycle begins 50 msec before the R-wave and ends 50 msec before the next R-wave. The subject is at the first stage of labour (40 weeks gestation). Code: 35-1. SNR = 29 dB, 23 dB, and 2 dB for (a), (b), and (c), respectively. A Hanning window is used to calculate the power spectrum. Sampling rate = 0.5 KHz, resolution = 12 bits.

not show sharp peaks for the fetal ECG. The parametric methods require an optimum choice of the model order. If the choice of the model order does not represent the information in the data then the AR will produce spurious peaks. Using the AR method, the fetal peak can be distinguished around 33 Hz albeit very small. The computational complexity of the periodogram is in the order of N $\log_2$ N, where N is the segment length. However, the computational complexities of the AR, the Yule-Walker, and the MEM methods are of the order of N^2.

5.5 Preliminary investigations of ECG bispectrum

5.5.1 Background

The nth-order cumulant spectrum of a process {x(k)} is defined as the (n-1)-dimensional Fourier transform of the nth-order cumulant sequence. The nth-order cumulant spectrum is thus defined as [3]:

$$C_n^x(\omega_1,\omega_2,\ldots,\omega_{n-1}) = \sum_{\tau_1=-\infty}^{+\infty} \cdots \sum_{\tau_{n-1}=-\infty}^{+\infty} c_n^x(\tau_1,\tau_2,\cdots,\tau_{n-1})\ e^{-j(\omega_1\tau_1+\omega_2\tau_2+\ldots+\omega_n\tau_{n-1})}, \quad (5.6)$$

where $|\omega_i| \le \pi$ for $i = 1,2,\ldots n-1$, and $|\omega_1 + \omega_2 + \ldots + \omega_{n-1}| \le \pi$

The bispectrum, n = 3, is defined as:

$$C_3^x(\omega_1,\omega_2) = \sum_{\tau 1=-\infty}^{+\infty} \sum_{\tau 2=-\infty}^{+\infty} c_3^x(\tau_1,\tau_2)\ e^{-j(\omega_1\tau 1+\omega_2\tau 2)} \quad (5.7)$$

where $c_3^x(\tau_1,\tau_2)$ is the third-order cumulant sequence. The indirect method of estimating the bispectrum is shown in Figure 5.6. Note that the computational complexity of the bispectrum is of the order of N^3.

5.5.2 Typical examples of bispectra and their contours

Data collection and pre-processing are described in Sections 1.8 and 1.9, respectively. Data segmentation is described in Section 2.13: 1-3. As mentioned in the previous chapters, linearisation is a key step in the signal processing and it is applied using an optimised third-order Volterra synthesiser to all the results included here (please see the caption of Figure 5.7 for parameters). Figures 5.7 (a-e) depict the maternal

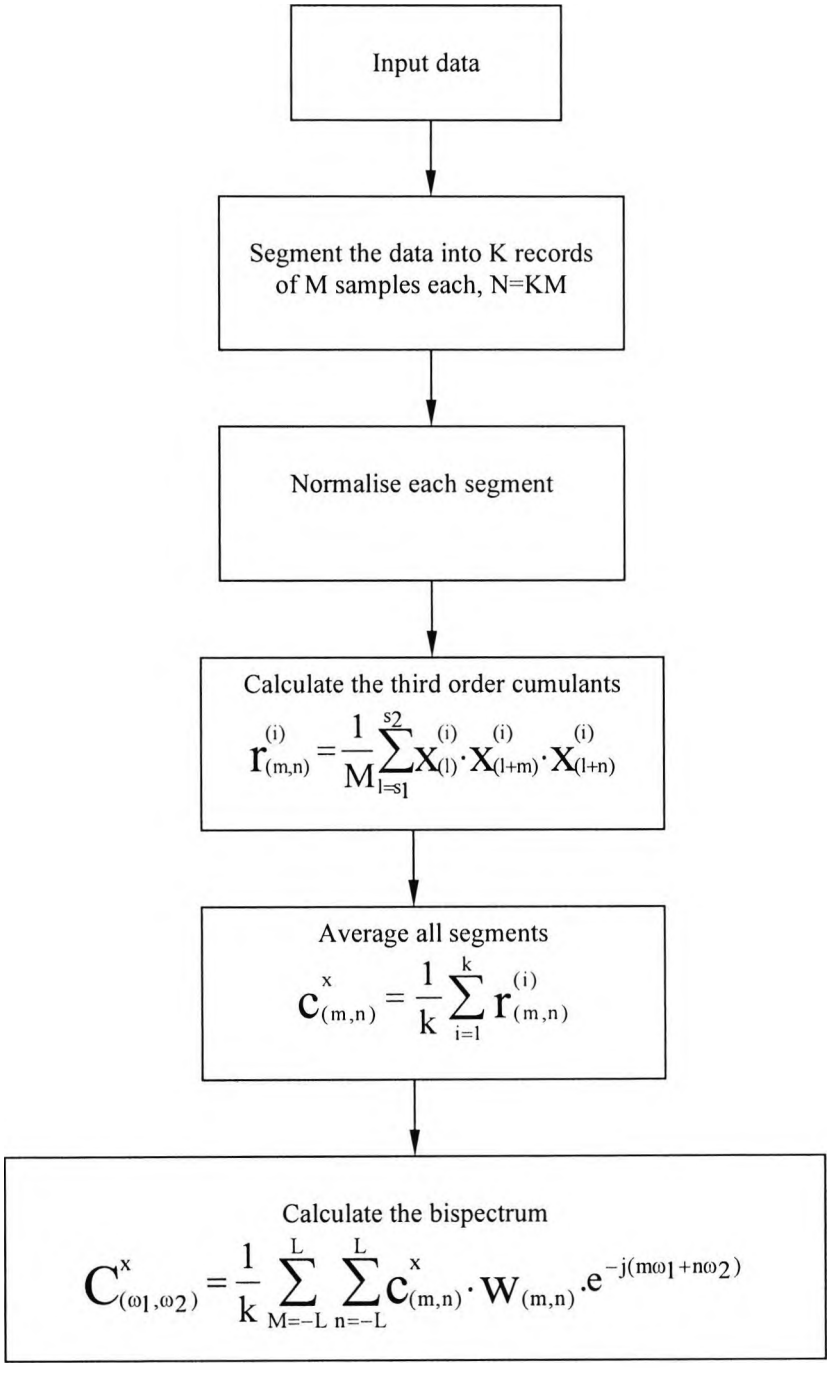

Where i=1, 2, …, k. s_1=max(0,-m,-n).
s_2=min(M-1,M-1-m,M-1-n). L<M-1,
w(m,n) is a 2-d window function.

Figure 5.6: *Flowchart of the key calculations of the bispectrum using the indirect method.*

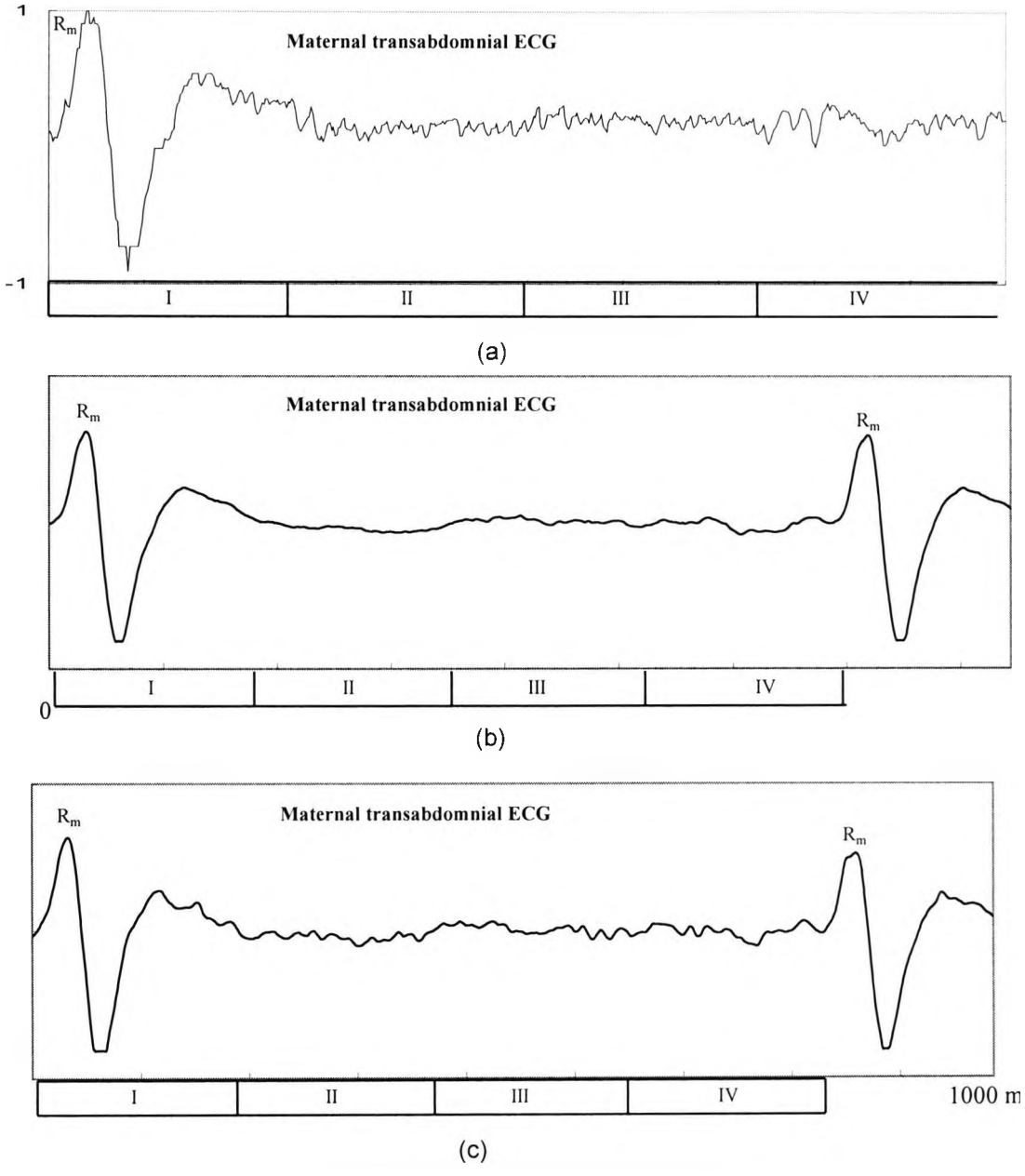

Figure 5.7: *The maternal transabdominal full cardiac cycles used to calculate the bispectrum of Figures 5.8-5.12. The ECG signals have been synthesised using an optimised third-order Volterra structure and only the linear part is retained. Segment I: predominantly maternal QRS-complex, segment II: the first fetal heartbeat with maternal contribution, segment III: QRS-free ECG, and segment IV: the second fetal heartbeat with maternal contribution. The maternal cardiac cycle begins 50 msec before the R-wave and ends 50 msec before the next R-wave. The subjects are at the first stage of labour, 40 weeks gestation. The maternal cycle has 500 samples or more at a rate of 0.5 KHz. The third-order Volterra parameters are: filter length = 6, step-size parameters = 0.001, 0.0002, and 0.0004 for linear, quadratic and cubic parts, respectively, delay = 4. The LMF parameters are: filter length = 12, step-size parameter = 0.004, delay = 6. (Code: 5, 9, 12, 16, 19).*

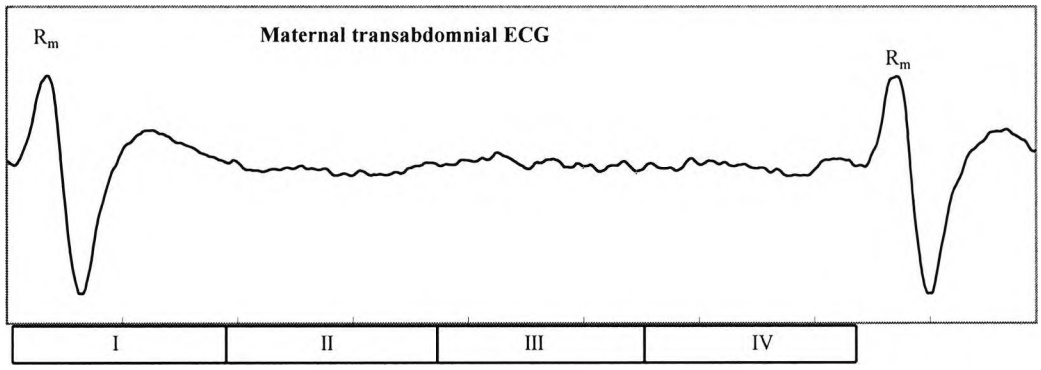

(d)

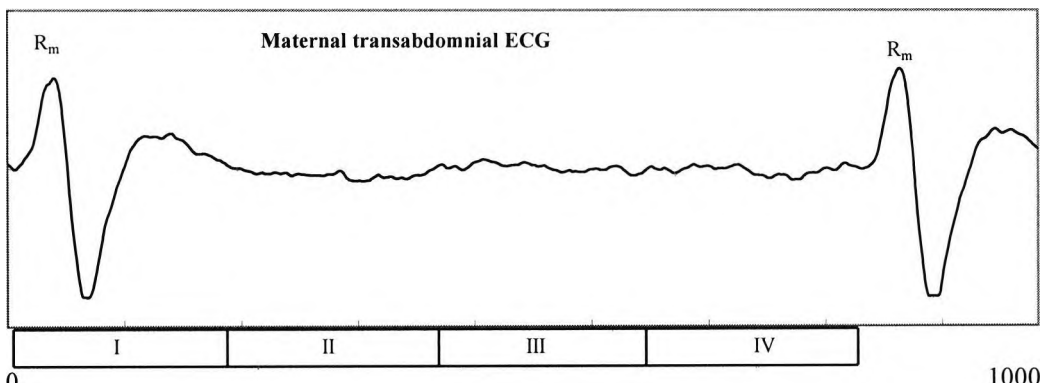

(e)

Figure 5.7 *(continued): The maternal transabdominal full cardiac cycles used to calculate the bispectrum of Figures 5.8-5.12. The ECG signals have been synthesised using an optimised third-order Volterra structure and only the linear part is retained. Segment I: predominantly maternal QRS-complex, segment II: the first fetal heartbeat with maternal contribution, segment III:QRS-free ECG, and segment IV: the second fetal heartbeat with maternal contribution. The maternal cardiac cycle begins 50 msec before the R-wave and ends 50 msec before the next R-wave. The subjects are at the first stage of labour, 40 weeks gestation. The maternal cycle has 500 samples or more at a rate of 0.5 KHz. The third-order Volterra parameters are: filter length = 6, step-size parameters = 0.001, 0.0002, and 0.0004 for linear, quadratic and cubic parts, respectively, delay = 4. The LMF parameters are: filter length = 12, step-size parameter = 0.004, delay = 6. (Code: 5, 9, 12, 16, 19).*

transabdominal ECG signals used to calculate the bispectrum of Figures 5.8 - 5.12, respectively. Figures 5.8 – 5.12 depict dual-band-pass filtered bispectra and their contours normalised to the maternal QRS-complex spectral peak for the transabdominally-measured ECG segments I, II, III, and IV. Segment I: predominantly maternal QRS-complex, segment II: the first fetal heartbeat with maternal contribution; segment III: QRS-free ECG, and segment IV: the second fetal heartbeat with maternal contribution. The dual-band-pass filter consists of two fifth-order Butterworth filters with cut-off frequencies of 10 Hz to 20 Hz, and 25 Hz to 40 Hz, respectively, a pass-band attenuation of 0.5 dB, and a stop-band attenuation larger than 70 dB. The sampling rate is 500 Hz. Optimised Kaiser weighting coefficients are used for the fetal and mother's ECGs to enhance their spectral peaks at 30 Hz and 17 Hz, respectively. The Kaiser windows are centred at frequencies of 15 Hz, 16 Hz, 17 Hz, 18 Hz, and 19 Hz for the mother's QRS-complex, and at frequencies of 28 Hz, 29 Hz, 30 Hz, 31 Hz, 32 Hz, 33 Hz, 34 Hz, 35 Hz, 36 Hz, 37 Hz, and 38 Hz for the fetal heartbeat.

Figure 5.8 (I) shows the maternal QRS-complex principal bispectral peaks and contours centred at the frequency pairs (15 Hz, 5 Hz) and (15 Hz, 20 Hz). These maternal frequency pairs with a frequency peak at 15 Hz deviate from the actual frequency of 17 Hz [35, 107], which is due to the BIC bias. The maternal optimised Kaiser window centred at 15 Hz will help to detect this deviated peak. Figure 5.8 (II) shows the first fetal heartbeat principal bispectral peak and contours at the frequency pair (28 Hz, 13 Hz). The fetal frequency peak of 28 Hz deviates from the actual frequency of 30 Hz [106], which is due to the BIC bias. The fetal optimised Kaiser window centred at 28 Hz will help to detect this deviated peak. Figure 5.8 (III) shows the QRS-free ECG bispectral peaks and contours centred at the frequency pairs (28 Hz, 3 Hz) and (28 Hz, 15 Hz). Note that although the QRS-free ECG shares the same frequencies as the fetal heartbeat, the BIC bispectral peak of the QRS-free ECG is at approximately -30 dB which is more than 15 dB lower than that of the first and second fetal heartbeats (depicted in Figure 5.8 II and IV, respectively). Figure 5.8 (IV) shows the second fetal heartbeat principal bispectral peak and contours centred at the frequency pair (28 Hz, 12 Hz). Again, the fetal frequency peak of 28 Hz deviates from the actual frequency of 30 Hz [106], which is due to the BIC bias. The fetal optimised Kaiser window centred at 28 Hz will help to detect this deviated peak.

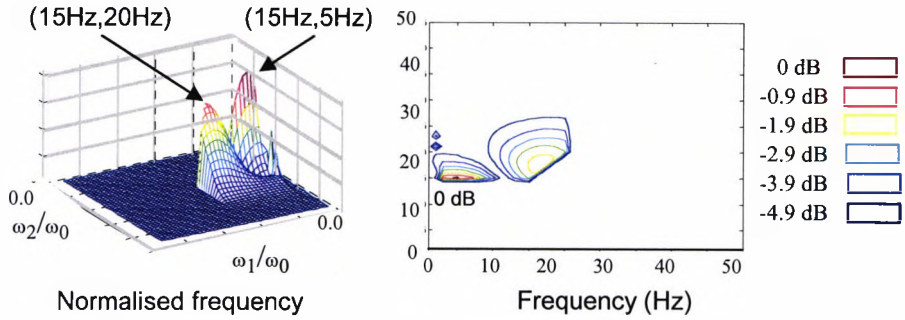

(I) The bispectrum of the transabdominally-measured predominantly maternal QRS-complex

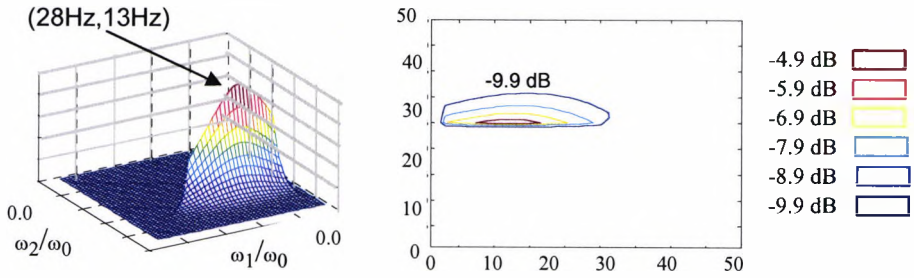

(II) The bispectrum of the first fetal heartbeat with maternal contribution

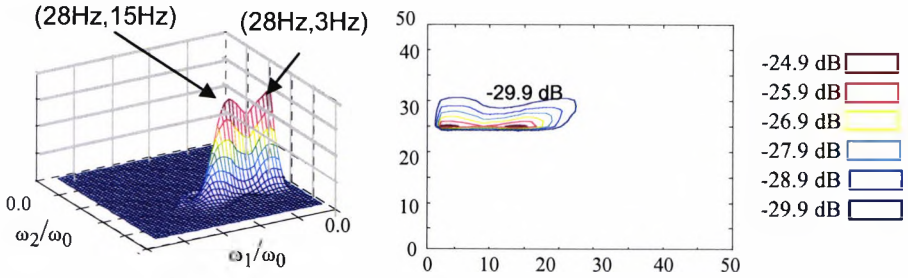

(III) The bispectrum of the QRS-free ECG

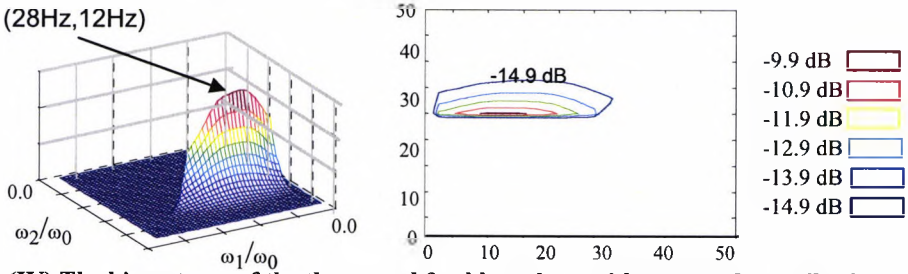

(IV) The bispectrum of the the second fetal heartbeat with maternal contribution

Figure 5.8: *Dual-band-pass filtered bispectra, Kaiser shaped window, (l.h.s.) and their contour maps normalised to the maternal QRS spectral peak (r.h.s.) for the transabdominally-measured ECG segments I, II, III, and IV shown in Fig. 5.7 (a). Segment I: predominantly maternal QRS-complex, Segment II: the first fetal heartbeat with maternal contribution; Segment III: QRS-free ECG; and Segment IV: the second fetal heartbeat with maternal contribution. The dual band-pass filter consists of two fifth-order Butterworth filters with cut-off frequencies of 10 Hz to 20 Hz, and 25 Hz to 40 Hz, respectively, and a pass-band attenuation of 0.5 dB, a stop-band attenuation larger than 50 dB. Some transabdominally-measured bispctral templates are shown in Figure 5.15 (a-d). The sampling rate is 500 Hz.(Code: 5-133).*

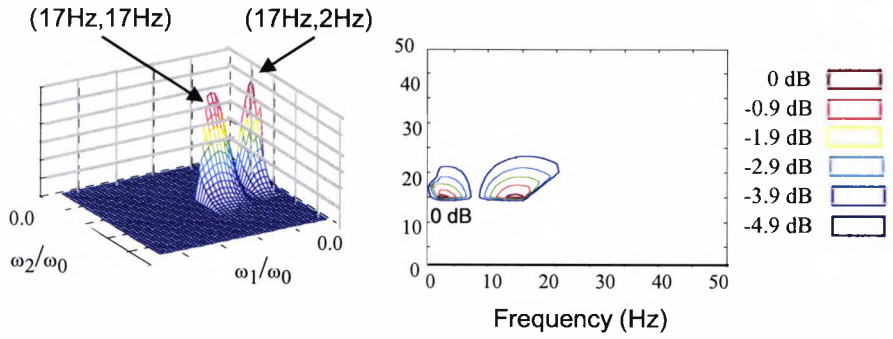

(I) The bispectrum of the transabdominally-measured predominantly maternal QRS-complex

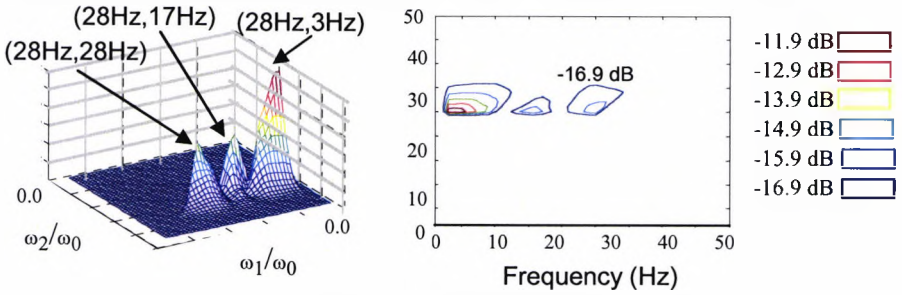

(II) The bispectrum of the the first fetal heartbeat with maternal contribution

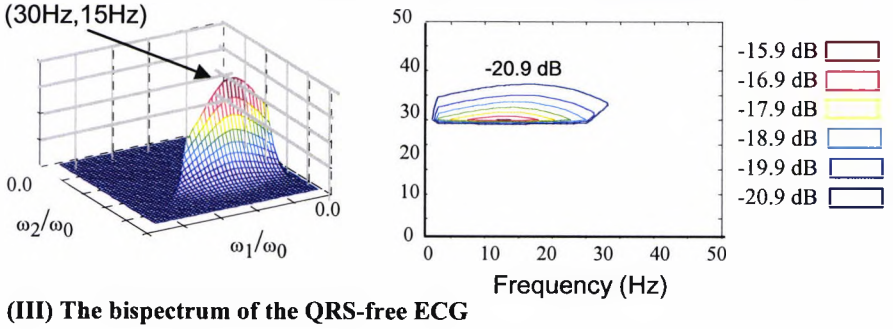

(III) The bispectrum of the QRS-free ECG

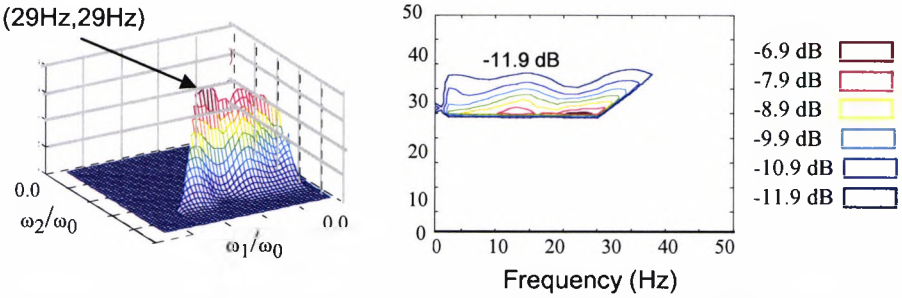

(IV) The bispectrum of the the second fetal heartbeat with maternal contribution

Figure 5.9: *Dual-band-pass filtered bispectra, Kaiser shaped window, (l.h.s.) and their contour maps normalised to the maternal QRS spectral peak (r.h.s.) for the transabdominally-measured ECG segments I, II, III, and IV shown in Fig. 5.7 (b). Segment I: predominantly maternal QRS-complex, Segment II: the first fetal heartbeat with maternal contribution; Segment III: QRS-free ECG; and Segment IV: the second fetal heartbeat with maternal contribution. The dual band-pass filter consists of two fifth-order Butterworth filters with cut-off frequencies of 10 Hz to 20 Hz, and 25 Hz to 40 Hz, respectively, and a pass-band attenuation of 0.5 dB, a stop-band attenuation larger than 50 dB. Some transabdominally-measured bispctral templates are shown in Figure 5.15 (a-d). The sampling rate is 500 Hz.(Code: 12-25).*

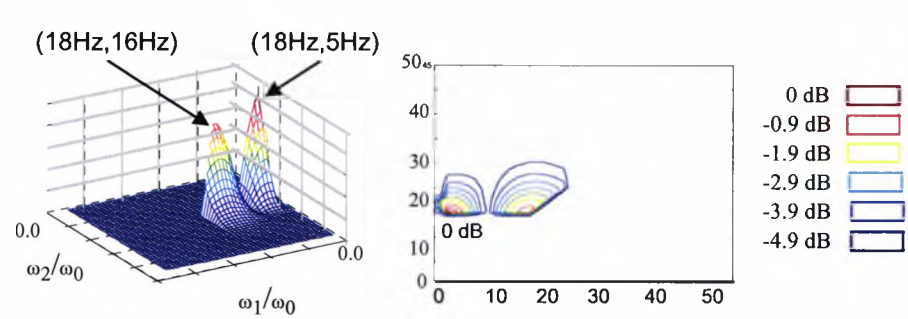

(I) The bispectrum of the transabdominally-measured predominantly maternal QRS-complex

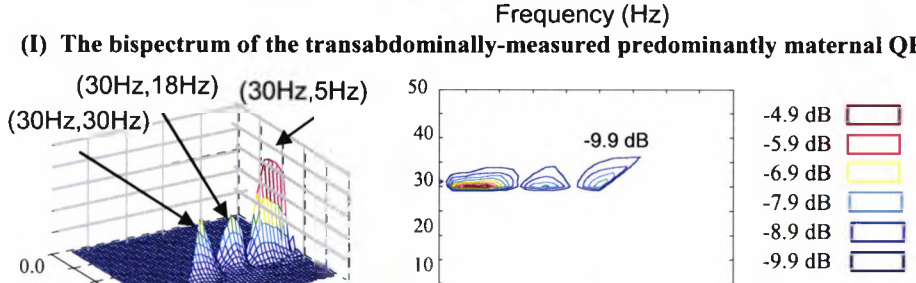

(II) The bispectrum of the first fetal heartbeat with maternal contribution

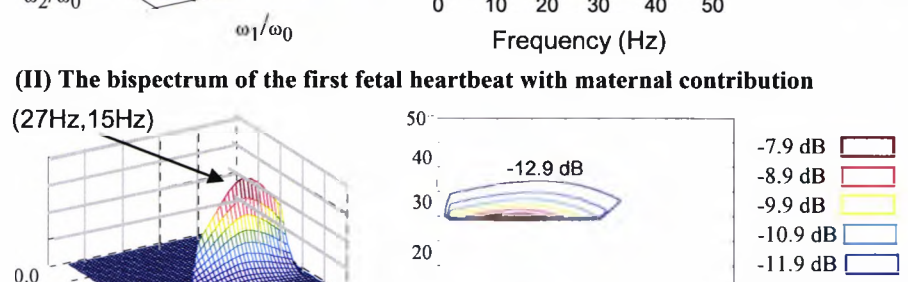

(III) The bispectrum of the QRS-free ECG

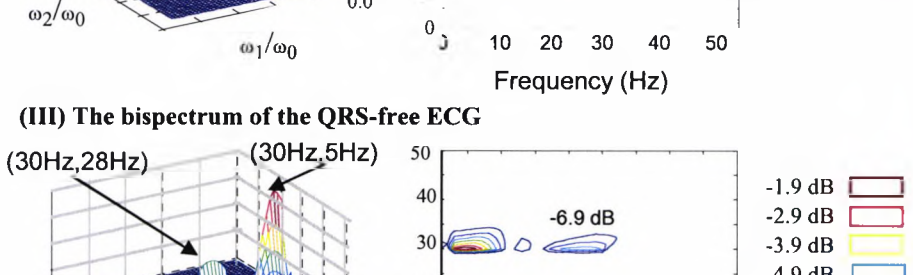

(IV) The bispectrum of the second fetal heartbeat with maternal contribution

Figure 5.10: . *Dual-band-pass filtered bispectra, Kaiser shaped window, (l.h.s.) and their contour maps normalised to the maternal QRS spectral peak (r.h.s.) for the transabdominally-measured ECG segments I, II, III, and IV shown in Fig. 5.7 (c). Segment I: predominantly maternal QRS-complex, Segment II: the first fetal heartbeat with maternal contribution; Segment III: QRS-free ECG; and Segment IV: the second fetal heartbeat with maternal contribution. The dual band-pass filter consists of two fifth-order Butterworth filters with cut-off frequencies of 10 Hz to 20 Hz, and 25 Hz to 40 Hz, respectively, and a pass-band attenuation of 0.5 dB, a stop-band attenuation larger than 50 dB. Some transabdominally-measured bispctral templates are shown in Figure 5.15 (a-d). The sampling rate is 500 Hz.(Code: 9-14).*

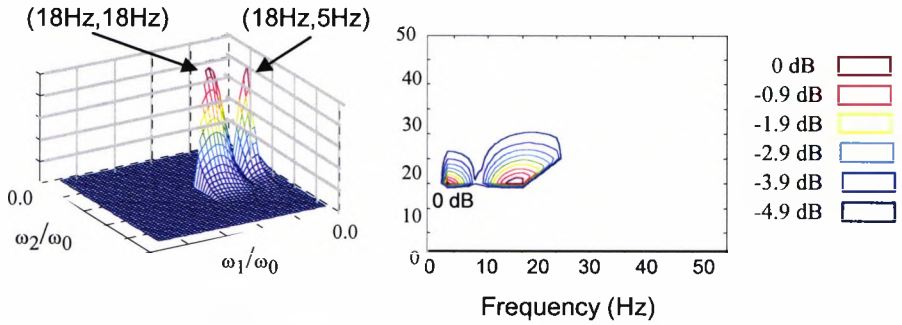

(I) The bispectrum of the transabdominally-measured predominantly maternal QRS-complex

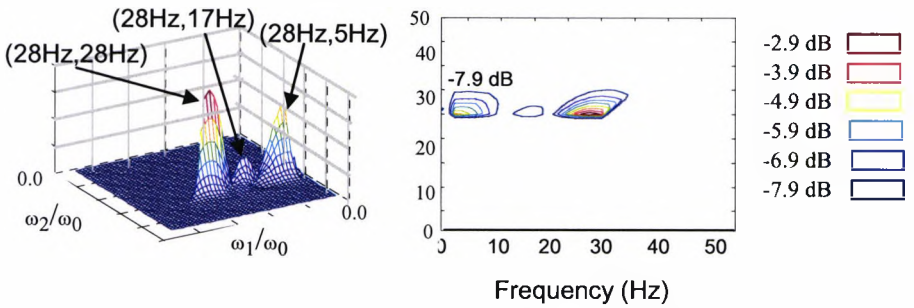

(II) The bispectrum of the combined maternal ECG and the first fetal heartbeat

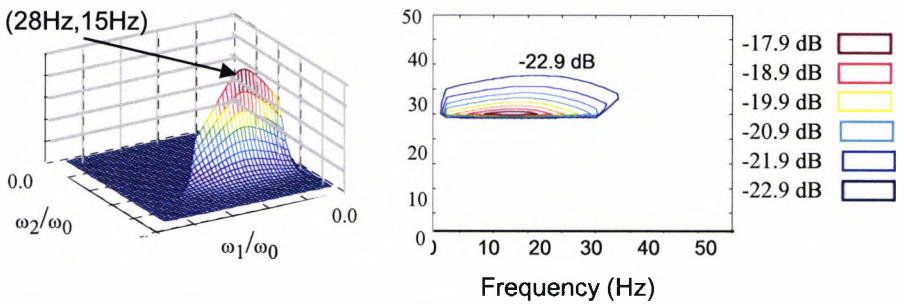

(III) The bispectrum of the QRS-free ECG

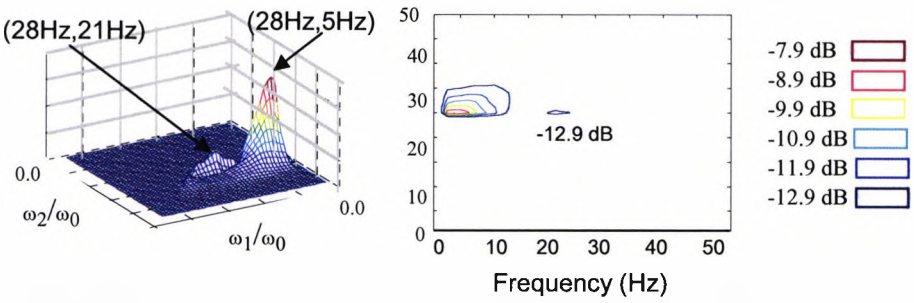

(IV) The bispectrum of the combined maternal ECG and the second fetal

Figure 5.11: *Dual-band-pass filtered bispectra, Kaiser shaped window, (l.h.s.) and their contour maps normalised to the maternal QRS spectral peak (r.h.s.) for the transabdominally-measured ECG segments I, II, III, and IV shown in Fig. 5.7 (d). Segment I: predominantly maternal QRS-complex, Segment II: the first fetal heartbeat with maternal contribution; Segment III: QRS-free ECG; and Segment IV: the second fetal heartbeat with maternal contribution. The dual band-pass filter consists of two fifth-order Butterworth filters with cut-off frequencies of 10 Hz to 20 Hz, and 25 Hz to 40 Hz, respectively, and a pass-band attenuation of 0.5 dB, a stop-band attenuation larger than 50 dB. Some transabdominally-measured bispctral templates are shown in Figure 5.15 (a-d). The sampling rate is 500 Hz.(Code: 16-2).*

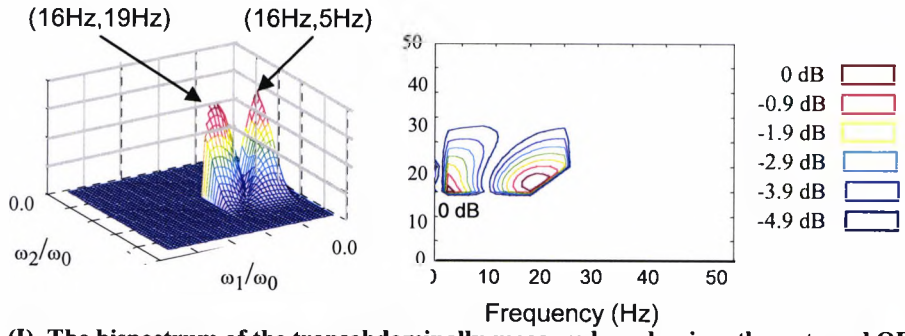

(I) The bispectrum of the transabdominally-measured predominantly maternal QRS-complex

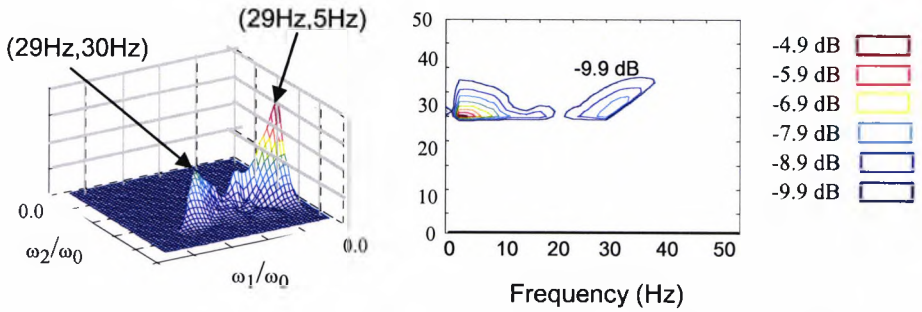

(II) The bispectrum of the combined maternal ECG and the first fetal heartbeat

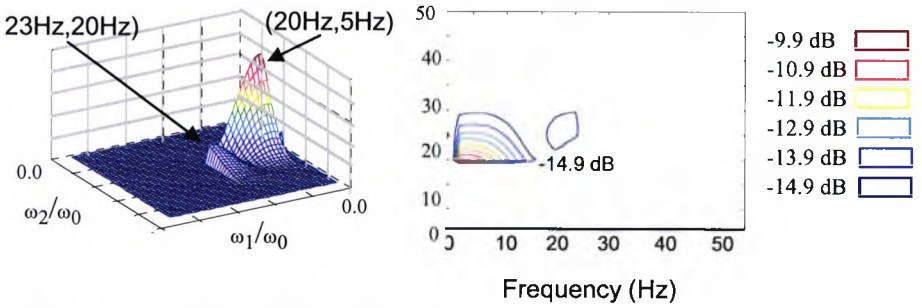

(III) The bispectrum of the QRS-free ECG

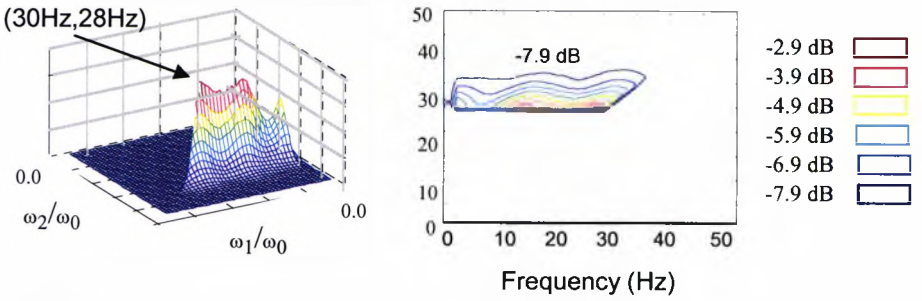

(IV) The bispectrum of the combined maternal ECG and the second fetal

Figure 5.12: *Dual-band-pass filtered bispectra, Kaiser shaped window, (l.h.s.) and their contour maps normalised to the maternal QRS spectral peak (r.h.s.) for the transabdominally-measured ECG segments I, II, III, and IV shown in Fig. 5.7 (e). Segment I: predominantly maternal QRS-complex, Segment II: the first fetal heartbeat with maternal contribution; Segment III: QRS-free ECG; and Segment IV: the second fetal heartbeat with maternal contribution. The dual band-pass filter consists of two fifth-order Butterworth filters with cut-off frequencies of 10 Hz to 20 Hz, and 25 Hz to 40 Hz, respectively, and a pass-band attenuation of 0.5 dB, a stop-band attenuation larger than 50 dB. Some transabdominally-measured bispctral templates are shown in Figure 5.15 (a-d). The sampling rate is 500 Hz.(Code: 19-2).*

Figure 5.9 (I) shows the maternal QRS-complex principal bispectral peaks and contours centred at the frequency pairs (17 Hz, 2 Hz) and (17 Hz, 17 Hz). Figure 5.9 (II) shows the first fetal heartbeat principal bispectral peaks and contours at the frequency pairs (28 Hz, 3 Hz), (28 Hz, 17 Hz), and (28 Hz, 28 Hz). The three fetal frequency peaks of 28 Hz deviate from the actual frequency of 30 Hz [106], which is due to the BIC bias. The fetal optimised Kaiser window centred at 28 Hz will help to detect this deviated peak. Figure 5.9 (III) shows the QRS-free ECG principal bispectral peak and contours centred at the frequency pair (30 Hz, 15 Hz). Note that although the BIC of the QRS-free ECG is close to the principal bispectral peak of the fetal, it is approximately at -21 dB which is 4 dB lower than that of the fetal. Figure 5.9 (IV) shows the second fetal heartbeat principal bispectral peaks and contours centred at the frequency pair (29 Hz, 29 Hz). Again, the fetal frequency peak of 29 Hz slightly deviates from the actual frequency of 30 Hz [106], which is due to the BIC bias. The fetal optimised Kaiser window centred at 29 Hz will help to detect this deviated peak.

Figure 5.10 (I) shows the maternal QRS-complex principal bispectral peaks and contours centred at the frequency pairs (18 Hz, 5 Hz) and (18 Hz, 16 Hz). These maternal frequency pairs with a frequency peak at 18 Hz slightly deviate from the actual frequency of 17 Hz [107], which is due to the BIC bias. The maternal optimised Kaiser window centred at 18 Hz will help to detect this deviated peak. Figure 5.10 (II) shows the first fetal heartbeat principal bispectral peaks and contours at the frequency pairs (30 Hz, 5 Hz), (30 Hz, 18 Hz), and (30 Hz, 30 Hz). The fetal optimised Kaiser window centred at 30 Hz will help to detect these peaks. Note that these peaks are sharper than those depicted in Figures 5.9 (II) and 5.10 (II). Figure 5.10 (III) shows the QRS-free ECG bispectral peak and contours centred at the frequency pair (27 Hz, 15 Hz). Note that the BIC of the QRS-free ECG is at approximately -12 dB which is 3 dB and 6 dB lower than that of the first and second fetal heartbeats, respectively. Figure 5.10 (IV) shows the second fetal heartbeat principal bispectral peak and contours centred at the frequency pairs (30 Hz, 5 Hz), and (30 Hz, 28 Hz). The fetal optimised Kaiser window centred at 30 Hz will help to detect these peaks.

Figure 5.11 (I) shows the maternal QRS-complex principal bispectral peak and contours centred at the frequency pairs (18 Hz, 5 Hz) and (18 Hz, 18 Hz). These maternal frequency pairs with a frequency peak at 18 Hz slightly deviate from the actual

frequency of 17 Hz [107], which is due to the BIC bias. The maternal optimised Kaiser window centred at 18 Hz will help to detect this deviated peak. Figure 5.11 (II) shows the first fetal heartbeat principal bispectral peaks and contours at the frequency pairs (28 Hz, 5 Hz), (28 Hz, 17 Hz) and (28 Hz, 28 Hz). These three fetal frequency pairs with frequency peaks at 28 Hz slightly deviate from the actual frequency of 30 Hz [106], which is due to the BIC bias. The fetal optimised Kaiser window centred at 28 Hz will help to detect this deviated peak. Figure 5.11 (III) shows the QRS-free ECG bispectral peak and contours centred at the frequency pair (28 Hz, 15 Hz). Note that although the BIC of the QRS-free ECG is at the same frequency of the first fetal heartbeat but it is at approximately -23 dB which is 15 dB lower than that of the first fetal heartbeat and 10 dB lower than that of the second fetal heartbeat, depicted in Figure 5.11 (IV). Note that both fetal heartbeats have bispectral peaks that are sharper than that of the QRS-free ECG segment. Figure 5.11 (IV) shows the second fetal heartbeat biaspectral peaks and contours centred at the frequency pairs (28 Hz, 5 Hz), and (28 Hz, 21 Hz). The two fetal frequency pairs with frequency peaks at 28 Hz slightly deviate from the actual frequency of 30 Hz [106], which is due to the BIC bias. The fetal optimised Kaiser window centred at 28 Hz will help to detect this deviated peak.

Figure 5.12 (I) shows the maternal QRS-complex principal bispectral peaks centred at the frequency pairs (16 Hz, 5 Hz) and (16 Hz, 19 Hz). These maternal frequency pairs with a frequency peak at 16 Hz slightly deviate from the actual frequency of 17 Hz [107], which is due to the BIC bias. The maternal optimised Kaiser window centred at 16 Hz will help to detect this deviated peak. Figure 5.12 (II) shows the first fetal heartbeat principal bispectral peaks at the frequency pairs (29 Hz, 5 Hz) and (29 Hz, 30 Hz). These fetal frequency pairs with a frequency peak at 29 Hz slightly deviate from the actual frequency of 30 Hz [106], which is due to the BIC bias. The fetal optimised Kaiser window centred at 29 Hz will help to detect this deviated peak. Figure 5.12 (III) shows the QRS-free ECG bispectral principal peaks centred at the frequency pairs (20 Hz, 5 Hz) and (23 Hz, 20 Hz). Note that the BIC of the QRS-free ECG is at approximately -15 dB which is 5 dB lower than that of the first fetal heartbeat and 7dB lower than that of the second fetal heartbeat. Figure 5.12 (IV) shows the second fetal heartbeat principal bispectral peak centred at the frequency pair (30 Hz, 28 Hz). The fetal optimised Kaiser window centred at 30 Hz will help to detect this deviated peak.

5.5.3 Estimation of the bispectral contour matching variance

The variance of the BIC is defined as the expected value of the squared difference in frequency (in Hz) between the computed BIC of the 250 msec flag window of the transabdominal ECG signal and the computed BIC from the synchronised fetal scalp electrode ECG 250 msec window.

$$Var_b = E\left[(Bis(\omega_1, \omega_2)_{\text{Transabdominal}} - Bis(\omega_1, \omega_2)_{\text{fetal scalp}}\right]^2 \quad (5.8)$$

The above variance ranges from 0.47 – 3.3, average = 1.716, when calculated for 120,000 FHBs. The variance indicates the deviation of the frequency of the BIC (in Hz) of the transabdominal ECG signal from that of the fetal scalp electrode around 30 Hz.

5.6 The single-hidden-layer perceptron employing the back-propagation with momentum algorithm

As mentioned in Chapter Four, single-hidden-layer perceptron classifiers are trained in a supervised manner with the back-propagation algorithm which is based on the error-correction learning rule. The back-propagation algorithm provides a computationally efficient method for the training of the classifiers. The back-propagation algorithm is a first-order approximation of the steepest descent technique. It depends on the gradient of the instantaneous error surface in weight space. The algorithm is therefore stochastic in nature. It has a tendency to zigzag its way about the true direction to a minimum on the error surface. Consequently, it suffers from a slow convergence property. A momentum term is employed to speed up the performance of the algorithm. The classifier used here is exactly the same as that used in Section 4.5.

5.6.1 Optimisation of the parameters of the back-propagation algorithm

Figure 5.13 shows the effect of changing the learning rate (β), the momentum constant (α) and the middle layer size on the classification of the maternal QRS-complexes and the fetal heartbeats using the BIC template matching technique. The effect of changing the learning rate on the classification rate is shown in Figure 5.13 (a). Small values of β are not able to track the variations in the bispectral contours. For classification of the bispectral contours, β reaches its optimum value at 0.2. For values larger than 0.2, the

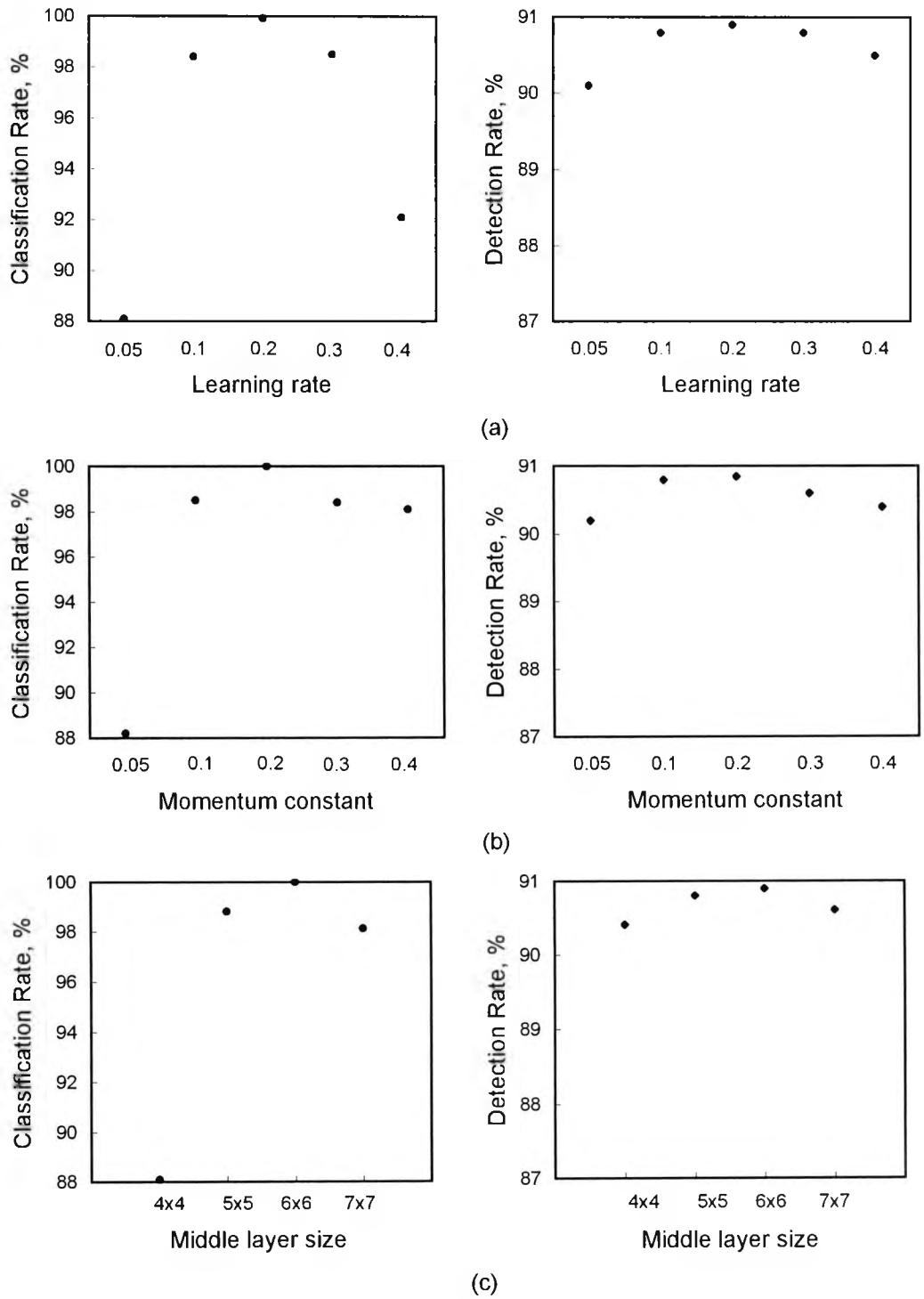

Figure 5.13: *The effect of changing (a) the learning rate, (b) the momentum constant, and (c) the middle layer size on the classification rate of the maternal QRS-complexes (l.h.s.) and fetal heartbeats (r.h.s.) from transabdominally-measured ECG signals and employing bispectral contours and their templates to be matched using a single-hidden-layer perceptron back-propagation algorithm with momentum. Performance for predominantly maternal QRS-complex segments (l.h.s.) and fetal heartbeats with maternal contribution segments (r.h.s.). Data length 250 msec. The optimised parameters for the BIC classification are: learning rate = 0.2, momentum constant = 0.2, and middle-layer size = 6 x 6. (Code: 5-1-100).*

output values are too large so that the difference with respect to the reference signal (template) will increase. This leads to larger error that will be fed back to the network, which will lead to slower convergence. The network will take long time to converge, or it might not converge at all. The optimum value of the momentum constant is found to be 0.2, as depicted in Figure 5.13 (b). Smaller values are not enough to push the adaptations to avoid local minima. While larger values tend to affect the routine detrimentally by bypassing the global minimum. The performance deteriorates significantly as the learning rate and the momentum constant diverge from their optimum values. The number and size of the middle layers were investigated by trial and error. There is a trade off between networks that should be small enough to allow faster implementation, and larger networks in size and number of hidden layers which are very slow and can not be implemented on-line using the current technology. Large networks could have complex relationships that represent non-linearities that might not exist in the real signals at all. The optimum parameters indicated in Figure 5.13 are calculated without considering the CPU time factor which might render those parameters undesirable for real-time applications. The CPU time for training is in the range of 17 to 60 sec. The average mean-squared error (MSE) is 0.04. The worst error is 0.1, which is the criterion for convergence. The implemented neural network has a single middle layer size of 6 x 6 as shown in Figure 5.13 (c). The number of passes (epochs) required for training varied from 6 to 14.

5.6.2 Bispectral contour template matching of the trabsabdominal maternal QRS-complex and fetal heartbeat to the previously identified and prepared templates

In this section we show how effective the bispectral contour template matching technique works with only 10 templates of maternal transabdominal QRS-complexes and 20 templates of fetal heartbeats with maternal contribution. A flowchart of the bispectral contour template matching technique is given in Figure 5.14. Figures 5.15 (a) – (d) are self explanatory. Each part of the figure shows one of the four transabdominal ECG segments (data length 250 msec) and three of the corresponding templates used for matching, and highlighting the template that was matched to the segment. An optimised third-order Volterra structure is employed to synthesise the four segments and the corresponding templates. Figure 5.15 (a) depicts the bispectral contour for the

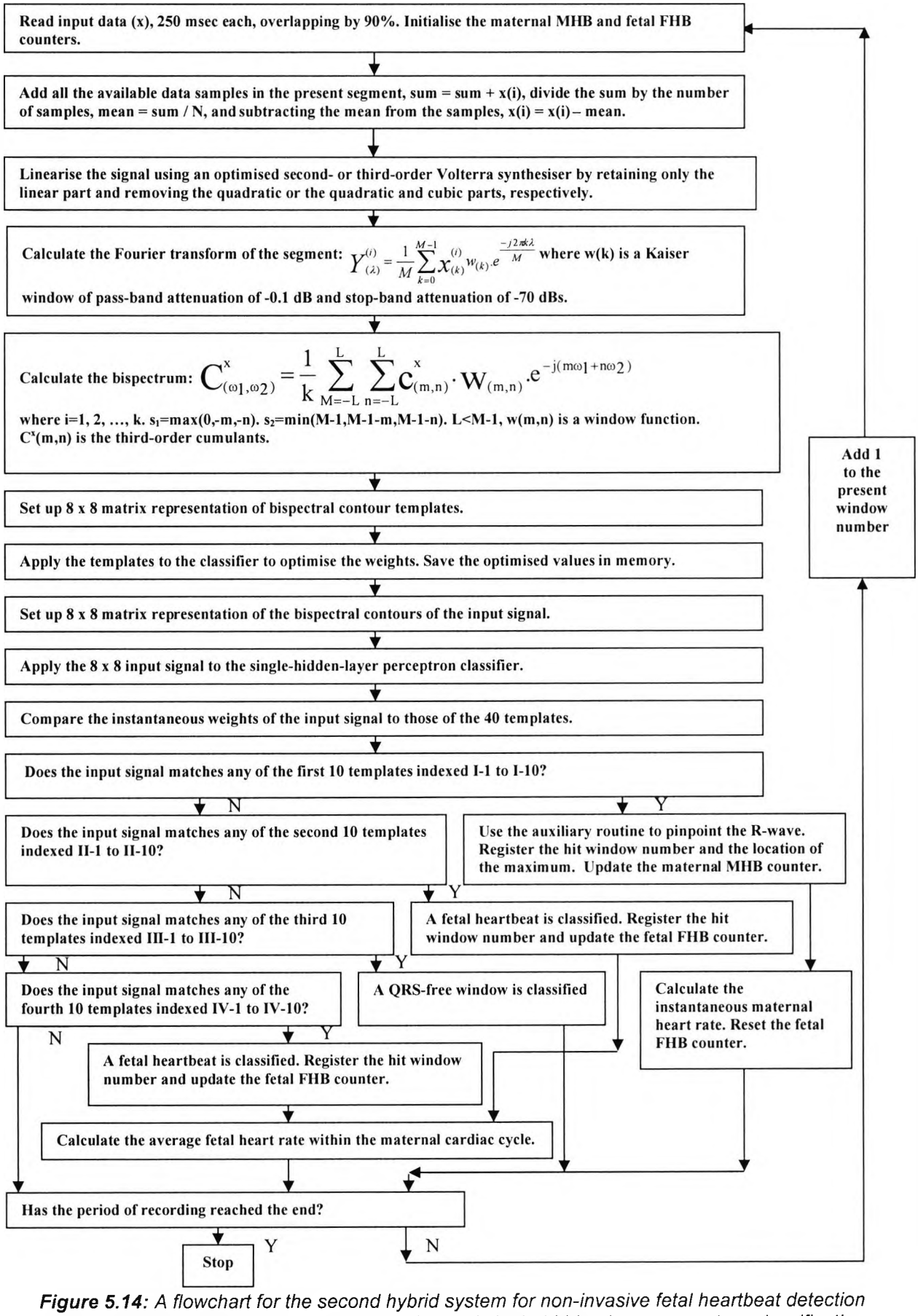

Figure 5.14: *A flowchart for the second hybrid system for non-invasive fetal heartbeat detection using bispectral contours for signal processing and single-hidden-layer perceptron classification.*

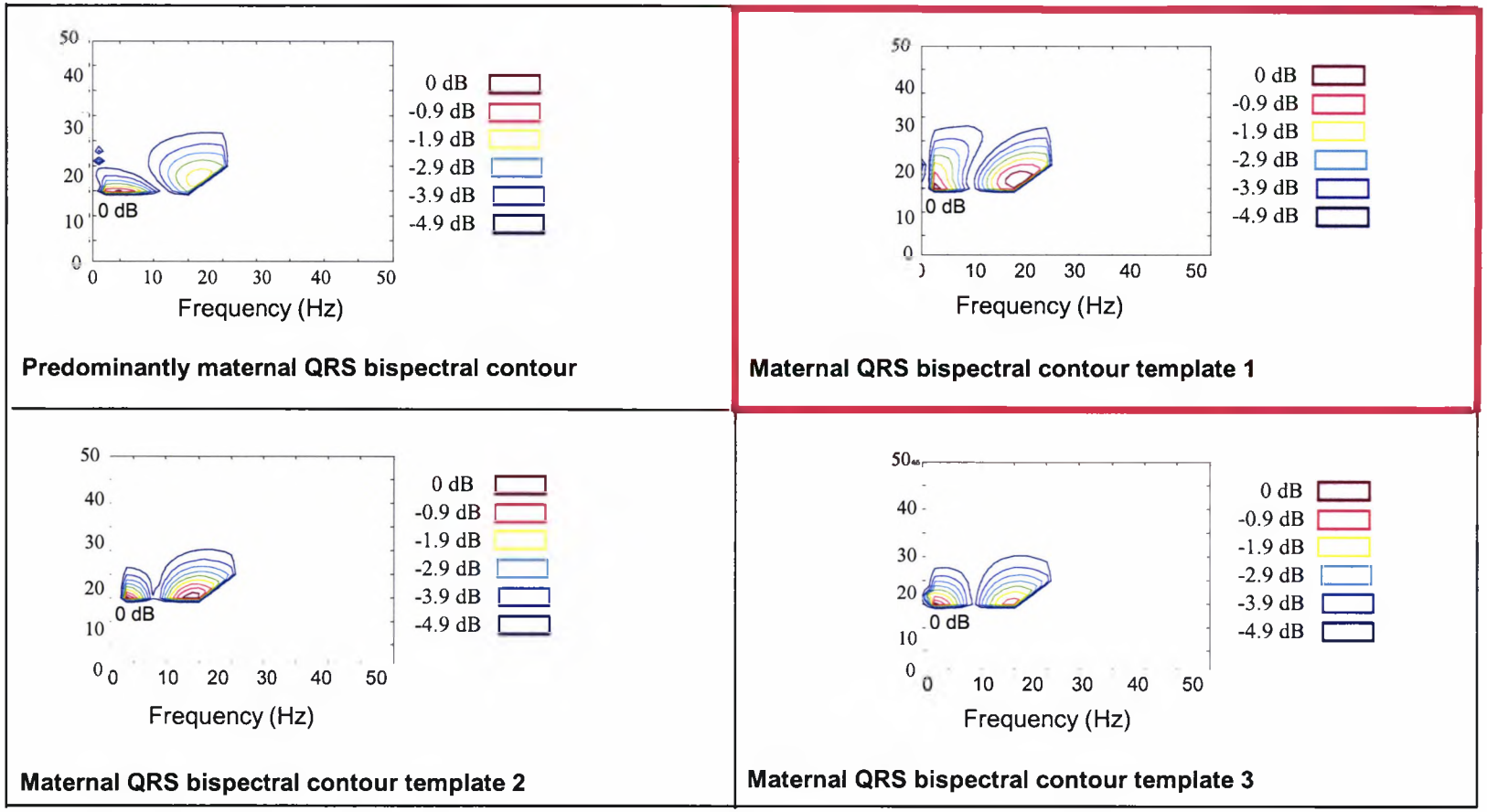

(a)

Figure 5.15 (a) *: Dual-band-pass filtered bispectral contours, Kaiser shaped window, for a typical example of a transabdominally-measured predominantly maternal QRS-complex segment using the second hybrid system. The top left hand part of the figure depicts the bispectral contour for the predominantly maternal QRS-complex segment. The rest of the figure shows three of the ten templates of such signals. Template 1, at the top right hand part of the figure, is the one which is matched to the segment. The parameters of the single-hidden layer perceptron classifier are: learning rate = 0.20, moment constant = 0.2, and middle layer size is 6 x 6. The bispectrum is computed using the indirect method. Optimised Kaiser windows centred at frequencies of 15 Hz, 16 Hz, 17 Hz, 18 Hz, and 19 Hz for the mother's QRS-complex are used. The dual-band-pass filter consists of two fifth-order Butterworth filters with cut-off frequencies of 10 Hz to 20 Hz, and 25 Hz to 40 Hz, respectively, and a pass-band attenuation of 0.5 dB, a stop-band attenuation larger than 70 dB.*

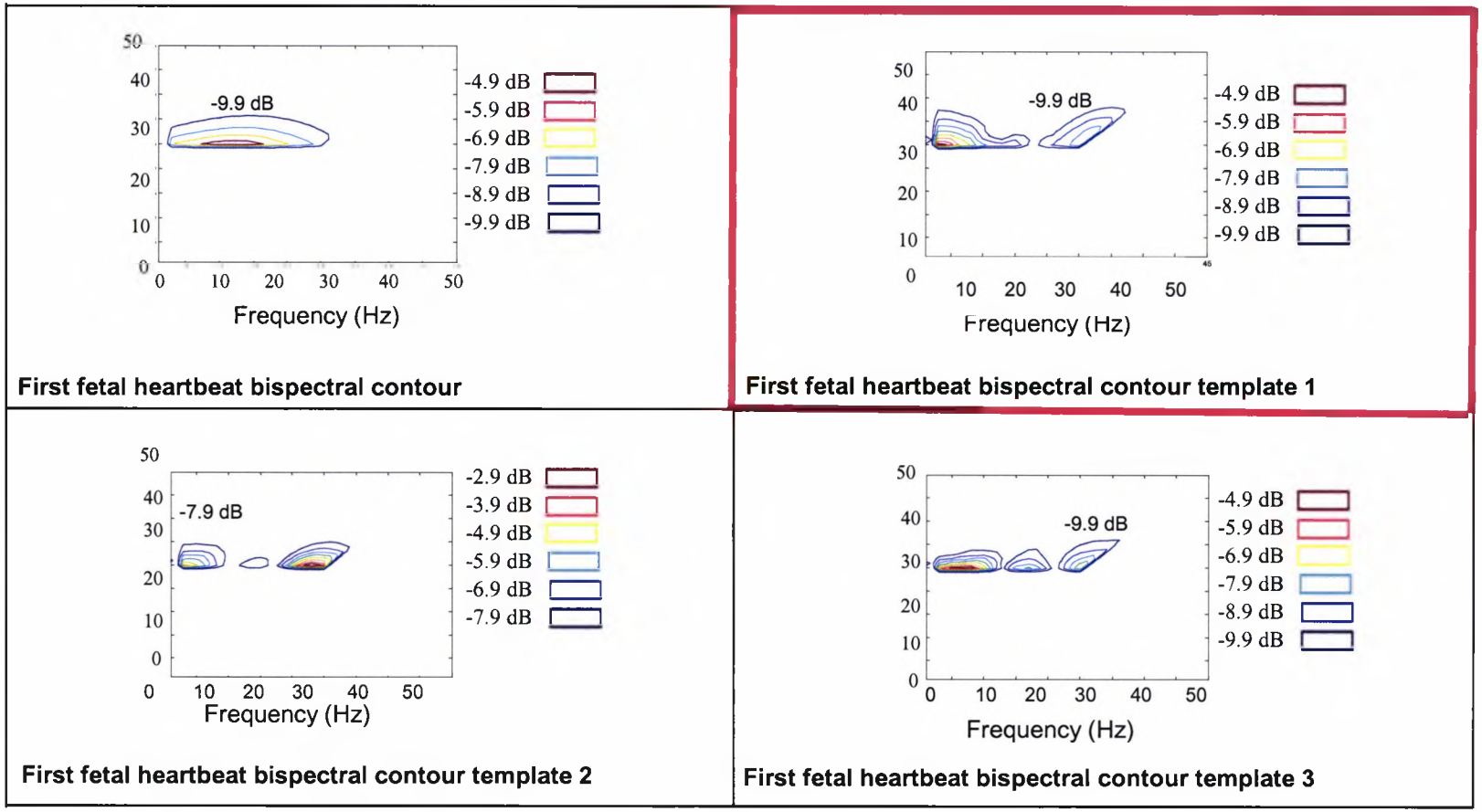

(b)

Figure 5.15 (b): *Dual-band-pass filtered bispectral contours, Kaiser shaped window, for a typical example of a transabdominally-measured first fetal heartbeat with maternal contribution segment using the second hybrid system. The top left hand part of the figure depicts the bispectral contour for the first fetal heartbeat with maternal contribution segment. The rest of the figure shows three of the ten templates of such signals. Template 1, at the top right hand part of the figure, is the one which is matched to the segment. The parameters of the classifier are: learning rate = 0.20, moment constant = 0.20, and middle layer size is 6 x 6. The bispectrum is computed using the indirect method. Optimised Kaiser windows centred at frequencies of 28 Hz, 29 Hz, 30 Hz, 31 Hz, 32 Hz, 33 Hz, 34 Hz, 35 Hz, 36 Hz, 37 Hz, and 38 Hz for the fetal heartbeat are used. The dual-band-pass filter consists of two fifth-order Butterworth filters with cut-off frequencies of 10 Hz to 20 Hz, and 25 Hz to 40 Hz, respectively, and a pass-band attenuation of 0.5 dB, a stop-band attenuation larger than 70 dB.*

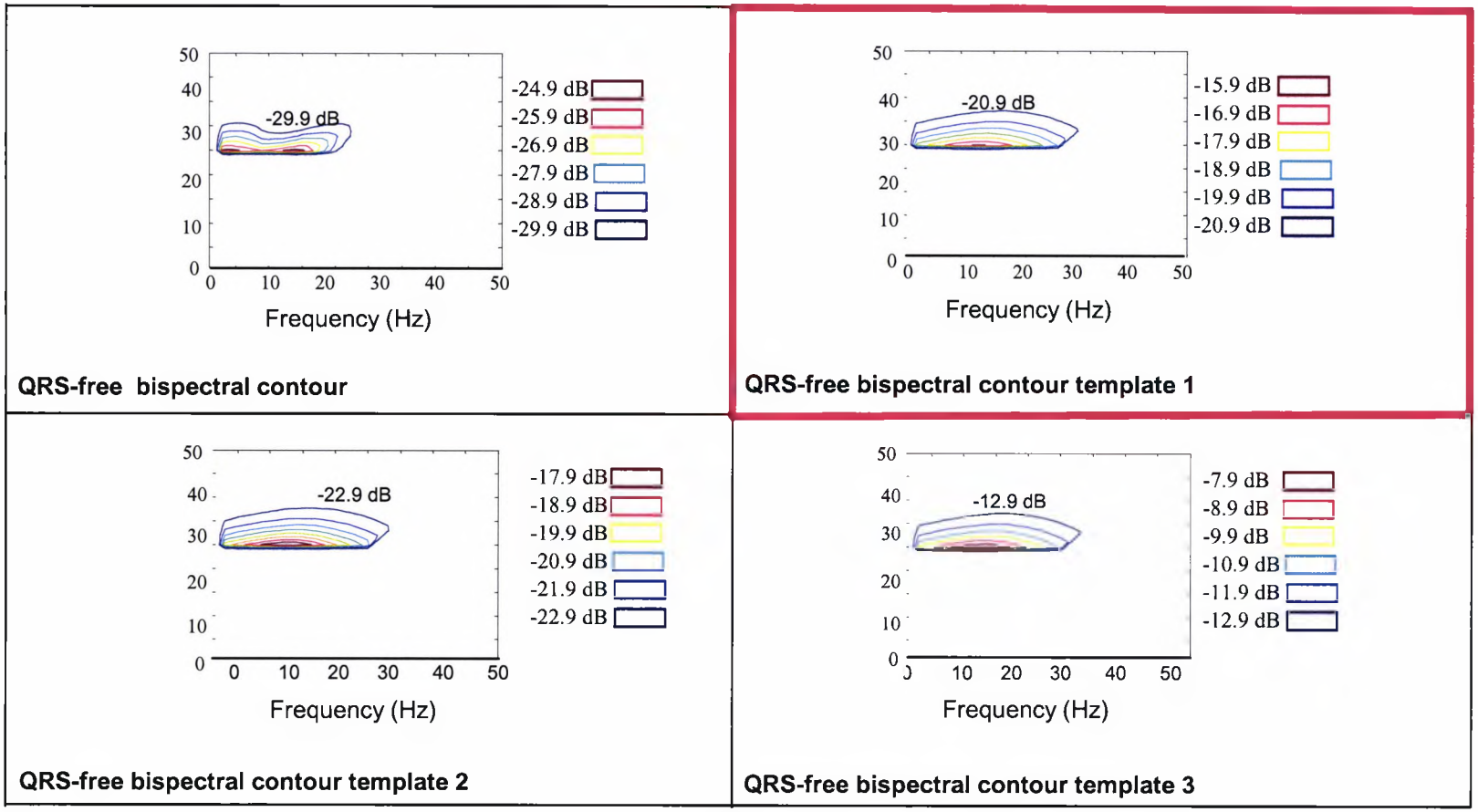

(c)

Figure 5.15 (c) *: Dual-band-pass filtered bispectral contours, Kaiser shaped window, for a typical example of a transabdominally-measure QRS-free ECG segment using the second hybrid system. The top left hand part of the figure depicts the bispectral contour for a QRS-free ECG segment. The rest of the figure shows three of the ten templates of such signals. Template 1, at the top right hand part of the figure, is the one which is matched to the segment. The parameters of the classifier are: learning rate = 0.20, moment constant = 0.20, and middle layer size is 6 x 6. The bispectrum is computed using the indirect method. Optimised Kaiser windows centred at frequencies of 28 Hz, 29 Hz, 30 Hz, 31 Hz, 32 Hz, 33 Hz, 34 Hz, 35 Hz, 36 Hz, 37 Hz, and 38 Hz are used. The dual-band-pass filter consists of two fifth-order Butterworth filters with cut-off frequencies of 10 Hz to 20 Hz, and 25 Hz to 40 Hz, respectively, and a pass-band attenuation of 0.5 dB, a stop-band attenuation larger than 70 dB.*

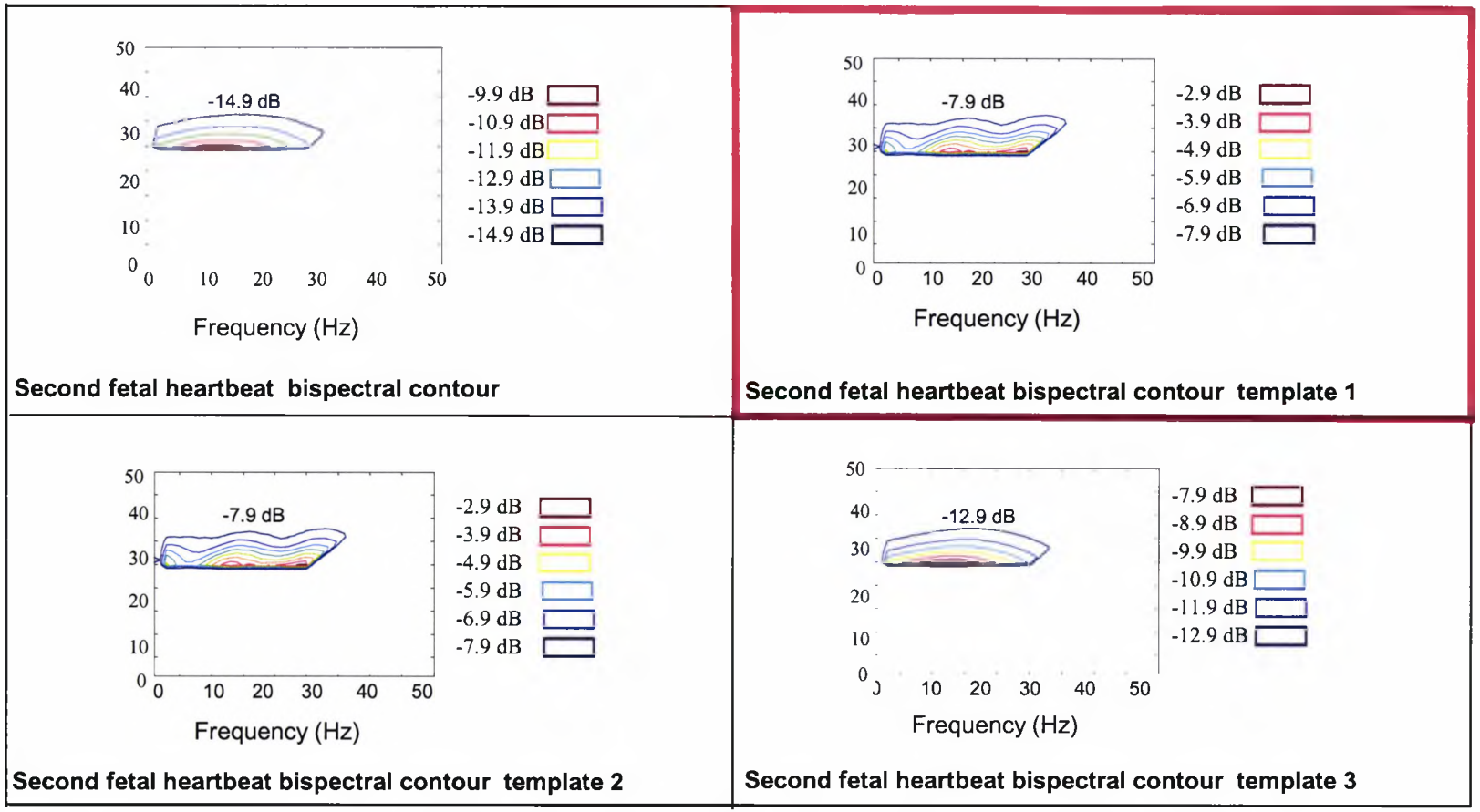

(d)

Figure 5.15 (d) *: Dual-band-pass filtered bispectral contour, Kaiser shaped window, for a typical example of a transabdominally-measured second fetal heartbeat with maternal contribution segment using the second hybrid system. The top left hand part of the figure depicts the bispectral contour for the second fetal heartbeat with maternal contribution. The rest of the figure shows three of the ten templates of such signals. Template 1, at the top right hand part of the figure, is the one which is matched to the segment. The parameters of the classifier are: learning rate = 0.20, moment constant = 0.20, and middle layer size is 6 x 6. The bispectrum is computed using the indirect method. Optimised Kaiser windows centred at frequencies of 28 Hz, 29 Hz, 30 Hz, 31 Hz, 32 Hz, 33 Hz, 34 Hz, 35 Hz, 36 Hz, 37 Hz, and 38 Hz for the fetal heartbeat are used. The dual-band-pass filter consists of two fifth-order Butterworth filters with cut-off frequencies of 10 Hz to 20 Hz, and 25 Hz to 40 Hz, respectively, and a pass-band attenuation of 0.5 dB, a stop-band attenuation larger than 70 dB.*

predominantly maternal QRS-complex segment (top left panel). The rest of the figure shows three of the ten templates of such signals. Template 1 is the one which is matched to the segment (top right panel). Figure 5.15 (b) depicts the bispectral contour for the first fetal heartbeat with maternal contribution segment (top left panel). The rest of the figure shows three of the ten templates of such signals. Template 1 is the one which is matched to the segment (top right panel). Figure 5.15 (c) depicts the bispectral contour for a QRS-free ECG segment (top left panel). The rest of the figure shows three of the ten templates of such signals. Template 1 is the one which is matched to the segment (top right panel). Figure 5.15 (d) depicts the bispectral contour for the second fetal heartbeat with maternal contribution segment (top left panel). The rest of the figure shows three of the ten templates of such signals. Template 1 is the one which is matched to the segment (top right panel).

The classification of the four segments involves a pattern-by-pattern updating rather than batch updating for the weight adjustments. This is more suitable to speed up the performance. Pattern-by-pattern updating tends to be orders of magnitude faster than batch updating. However, it should be noted that pattern-by-pattern updating is harder to parallelise.

5.6.3 The maternal QRS-complex and the fetal heartbeat Classification rates

5.6.3.1 The maternal QRS-complex classification rate

Table 5.1 shows a top classification rate of 100% for maternal QRS-complexes using bispectral contours for signal processing and single-hidden-layer perceptron classification. The 100% maternal QRS-complex classification rate has been achievable with or without linearisation. It makes no difference to the results. However, to complete this section a brief description of the optimised parameters required for the linearisation process will be given.

To calculate the maternal heart rate an auxiliary method to pinpoint the R-wave is needed. For this application we have a choice of either using the superior patent binding technique [105] or adaptive thresholding which is less accurate when one deals with deformed QRS-complexes in heart patients. The results presented here have been

obtained using the latter method since all mothers' ECGs exhibit normal-to-the-patient QRS-complexes. The instantaneous maternal heart rate is calculated by dividing 60 by

Spectral matching template in conjunction with ANN classifiers	**The power spectrum**	**The bispectrum contours**
Classification rate	**99.84**	**100.00**

Table 5.1: *The classification rate for the maternal QRS-complex using maternal transabdominally-measured ECGs and their respective power spectrum and bispectral contours.*

the R-to-R interval (in seconds). The application of this auxiliary routine leads to a maternal heart rate with an accuracy of 99.85%.

Parameters

The second-order Volterra parameters are: filter length = 6, step-size parameters = 0.005, and 0.0004 for linear and quadratic parts, respectively, delay = 3. The third-order Volterra parameters are: filter length = 6, step-size parameters = 0.001, 0.0002, and 0.0004 for linear, quadratic and cubic parts, respectively, delay = 4. A dual-band-pass filter is applied to the bispectrum, the first has a band-pass of 10 Hz to 20 Hz and the second has a band-pass of 25 Hz to 40 Hz. Optimised Kaiser windows centred at frequencies of 15 Hz, 16 Hz, 17 Hz, 18 Hz, and 19 Hz for the mother's spectrum, and at frequencies of 28 Hz, 29 Hz, 30 Hz, 31 Hz, 32 Hz, 33 Hz, 34 Hz, 35 Hz, 36 Hz, 37 Hz, and 38 Hz for the fetal spectrum are used in both the power spectrum and the BIC.

5.6.3.2 Fetal heartbeat detection quality and classification rate for the bispectral contour template matching technique

Before attempting to assess the second hybrid technique for non-invasive fetal heartbeat detection some definitions are appropriate here:

Definitions

1- The Sensitivity (Se) is defined as the ratio of the True Positives (TP) to the sum of the True Positives and the False Negatives (FN). The sensitivity reports the percentage of true beats that are correctly classified by the algorithm.

2- The Specificity (Sp) is defined as the ratio of the True Positives (TP) to the sum of

the True Positives (TP) and the False Positives (FP). It reports the percentage of classified heartbeats which are in reality true beats.

3- The classification rate: The mean value of the sensitivity and the specificity is used as the criterion for the effectiveness of the technique.

Table 5.2 summarises the results of the fetal heartbeat detection using the power spectrum method (second-order statistics), and the bispectrum contour template matching technique. In this section, optimised adaptive LMF-based second- and third-order Volterra synthesisers are employed.

The power spectrum method has a classification rate of 71.47%. By using the second hybrid system the classification rate increased to 87.72% without linearisation, and to 88.28% and 90.12% using second- and third-order Volterra synthesisers with LMF

Spectral matching template type with and without linearisation using Volterra and in conjunction with ANN classifiers	Detection quality				Classification rate (%)
	Se (%)	Sp (%)	FP, out of 120000	FN, out of 120000	
Power spectrum with linearisation	**71.29**	**71.44**	**34272**	**34537**	**71.37**
Bispectral contour without linearisation	**87.97**	**87.46**	**15048**	**14436**	**87.72**
Linearised bispectral contour using 2nd order adaptive LMF Volterra synthesiser	**88.53**	**88.04**	**14352**	**13764**	**88.28**
Linearised bispectral contour using 3rd order adaptive LMF Volterra synthesiser	**90.53**	**89.73**	**12324**	**11364**	**90.12**

Table 5.2: *Fetal heart detection quality and classification rate using transabdominally-measured ECG and their respective power spectrum and bispectral contours with and without linearisation. The total number of fetal heartbeats is 120,000 and the total number of maternal ECG recordings is 30. The performance was assessed against synchronised fetal scalp heartbeats. All mothers were during the first stage of labour at 40 weeks of gestation.*

update, respectively. The second hybrid method has an improvement of 19% and 4% in the classification rate over and above that achieved with the second-order statistics and the TOC template matching technique, respectively. Note that the classification rate of the coincident mother's and fetal QRS-complexes is 0%. The classification rate of non-coincident mother's and fetal QRS-complexes is 99.21%.

Parameters

The second-order Volterra parameters are: filter length = 6, step-size parameters = 0.005, and 0.0004 for linear and quadratic parts, respectively, delay = 5. The third-order Volterra parameters are: filter length = 6, step-size parameters = 0.001, 0.0002, and 0.0004 for linear, quadratic and cubic parts, respectively, delay = 5. A dual-band-pass filter is applied to the bispectrum, the first has a band-pass of 10 Hz to 20 Hz and the second has a band-pass of 25 Hz to 40 Hz. Optimised Kaiser windows centred at frequencies of 15 Hz, 16 Hz, 17 Hz, 18 Hz, and 19 Hz for the mother's spectrum, and at frequencies of 28 Hz, 29 Hz, 30 Hz, 31 Hz, 32 Hz, 33 Hz, 34 Hz, 35 Hz, 36 Hz, 37 Hz, and 38 Hz for the fetal spectrum are used in both the power spectrum and the BIC.

5.7 Summary and conclusions

General discussions

The hybrid bispectral contour matching technique is an extension to the hybrid cumulant matching technique presented in the previous chapter. Therefore, the choice of the NN classifier is based on the general discussion presented previously. *Prior information* remain as valuable assets and are very much exploited herein. It is the matching of the horizontal 2-d bispectral contours that has been used in the BIC template matching technique instead of the 1-d polar bispectral slices. Because in order to use the 1-d polar bispectrum slices effectively, one needs to use a minimum of 24 polar slices to facilitate capturing the most rapid changes in the bispectrum including null features that could be used as discriminant patterns. Whereas for BIC contours, provided that they are horizontally cut at a maximum number of 10 levels, a good quality discriminant picture can be made available for the neural network classifier. For example, it is very unlikely that maxima and troughs are missed because of any changes in their respective positions.

Approximately 50,000 maternal cardiac cycles have been included in the analysis. The numbers of bispectral contours compound templates are 10 for the maternal chest, 10 for the fetal scalp, and 140 for the transabdominally-measured 250 msec segments, respectively. Each bispectral compound template is made of 10 horizontal templates at different levels. Starting from a normalised 0 dB and going down in steps of 1 dB each to a – 10 dB.

The maternal transabdominal ECG signal is linearised using an optimised LMF-based second- or third-order Volterra synthesiser. The second-order Volterra synthesiser parameters are: filter length = 6, step-size parameters = 0.005, and 0.0004 for linear and quadratic parts, respectively, delay = 5. The third-order Volterra synthesiser parameters are: filter length = 6, step-size parameters = 0.001, 0.0002, and 0.0004 for linear, quadratic and cubic parts, respectively, delay = 5. The transabdominal ECG signal is segmented into four segments containing; (I) The maternal QRS-complex, (II) the first fetal heartbeat with maternal contribution, (III) QRS-free ECG, and (IV) the second fetal heartbeat with maternal contribution. To segment the transabdominal ECG signals, the window length is carefully chosen to; (i) Yield an acceptable upper threshold of both the deterministic and stochastic noise types inherent in the higher-order statistics of the ECG signals encountered, and (ii) allow the detection of one, two, three, or four fetal heartbeats (FHBs) within one maternal transabdominal cardiac cycle.

The classification procedure starts by matching the bispectral contours of the segments to those of the templates until the first and the second mother's QRS-complexes are detected and their R-waves are pinpointed. The maternal heart rate is accurately calculated from the knowledge of the current and previous R-wave positions. Then, the search for the fetal heartbeat starts at 50 msec before the first maternal R-wave and continues until we reach the second maternal R-wave. Although the ECG bispectral contour template matching technique is very effective in detecting the occurrence of the fetal heartbeats as a whole in the frequency domain even when it is completely buried in noise, it cannot locate the R-wave in the time domain over a window length of 250 msec. However, we can measure fairly accurately the maternal heartbeats and calculate the instantaneous heart rate for the mother. Hence, by counting the number of fetal heartbeats that have occurred between two successive maternal R-waves, one can easily calculate the averaged FHR within the maternal cardiac cycle;

The average FHR = MHR x Number of FHBs / number of maternal heartbeats

In the above formula, the instantaneous maternal heart rate is previously known with some degree of accuracy, and the relative fetal to maternal heartbeat is also known within the maternal cardiac cycle. Hence, the averaged fetal heart rate can be calculated within each maternal cardiac cycle.

Detailed results

1. The effect of window length on the bispectral contour variance

The variance of the bispectrum for the optimum window length of 250 msec with FHB occurrence ranges from 0.47 to 3.3 with an average value of 1.716. Note that the variance of the bispectrum is smaller than that of the third-order cumulants. A further 15% increase in the variance of the bispectrum is due to an increase in the maternal heartbeat from 60 bpm to 100 bpm. The latter has resulted in an 30% decrease in segment size.

2. Parameters of the single-hidden layer perceptron

The network has been optimised in terms of its learning rate, momentum constant, and hidden layer size to achieve the minimum mean-squared error. The optimum learning rate is found to be 0.2. The optimum momentum constant is found to be 0.2. The single-hidden-layer has an optimum dimension of 6 x 6. The input to the first layer is the bispectral contours of the four transabdominally-measured ECG segments. The network is trained using the BIC templates. During the training phase, the input to the network is four template patterns. These are the BIC of four segments from one transabdominal cardiac cycle. For example the first is the maternal QRS-complex BIC, the second is the first fetal heartbeat BIC, the third is the QRS-free ECG BIC, and the fourth is the second fetal heartbeat BIC. The network is trained over ten templates of each of the four segments. The training terminates when the worst error in all patterns in one pass is less than 0.1. Typically the average error will be in the range of 0.001.

3. The classification rate for maternal QRS-complex and fetal heartbeat segments

Results obtained from 30 cases using the non-invasive transabdominally-measured ECG signal, with the simultaneous fetal scalp electrode ECG signal as a reference, show that

the second hybrid method has a classification rate of 100% for normal, healthy maternal QRS-complexes and 90.12% for fetal heartbeats. It has been shown that an improvement of 1% to 3% is attainable with ECG signal linearisation employing second- and third-order Volterra synthesisers, respectively. Conventional methods (based on the power spectrum) of fetal heartbeat detection have a success rate in the range of 70%. The second hybrid system has a significantly higher classification rate.

The classification rate of fetal heartbeats for non-coincident mother's and fetal QRS-complexes is 99.21%. The classification rate of fetal heartbeats for coincident mother's and fetal QRS-complexes is 0%. This means that the hybrid bispectral contours technique fails to resolve the fetal beat when both the mother and fetal QRS-complexes are synchronised.

The bispectral contour template matching technique improved the classification rate by approximately 4% over and above that of the third-order cumulant template matching technique. The difference in performance is not due to better resolvability of the latter over the former in the case of coincident mother's and fetal QRS-complexes, as both techniques fail in this respect. But, it is due to the fact that the BIC template matching technique can resolve a few of the fetal QRS-complexes occurring within the T-wave region of the mother.

5.7 References

[1] J. M. Mendel, "A compendium of new theoretical results associated with using higher-order statistics in signal processing and system theory," Spectral Analysis in One or Two Dimensions, pp. 163-182, August 1990.

[2] E. Walach and B Widrow, "The Least-Mean Fourth (LMF) adaptive algorithm and its family," IEEE Transactions on Information Theory, vol. IT-30, No. 2, pp. 275-283, March 1984.

[3] M. C. Dogan and J. M. Mendel, "Antenna Array Noise Re-conditioning by Cumulants", Proceedings of the IEEE Signal Processing Workshop on Higher Order Statistics, CA, 1993.

[4] C. L. Nikias and A. P. Petropulu," Higher Order Spectral Analysis: A Nonlinear Signal Processing Framework". A. V. Oppenheim Series editor, 1993.

[5] V. Zarazoso and A. K. Nandi, "Comparison between blind separation and

adaptive noise cancellation techniques for fetal electrocardiogram extraction," IEE Colloquium, pp. 1/ -1/6., 1999.

[6] C. Li, C. Zheng and C. Tai, "Detection of ECG characteristic points using wavelet transforms," IEEE Transactions on Biomedical Engineering, vol. 42, No. 1, pp. 21-28, January 1995.

[7] J. M. Herbert, W. Peasgood, X. B. Huang, J. A. Crowe, M. S. Woolfson, N. Reed, and E. M. Symonds, "Antepartum fetal electrocardiogram extraction and analysis," Proceedings of Computers in Cardiology, pp. 875-877, 1993.

[8] S. Haykin, "Neural networks expand SP's horizons," IEEE Signal Processing Magazine, pp. 24-49, March 1996.

[9] E. G. Lovett and K. M. Ropella, "Bispectral Analysis Of Intra-Cardiac Electrograms," IEEE Signal Processing Workshop on Higher-Order Statistics, pp. 366-368, USA, 1993.

[10] S. Szilagyi, L. Szilagyi and L. David, "Comparison Between Neural Network-Based Adaptive Filtering And Wavelet Transform for ECG Characteristics Points Detection," Proceedings of the 19th IEEE International Conference on Engineering in Medicine and Biology, EMB, pp. 272-274, USA, November, 1997.

[11] C. L. Nikias and J. M. Mendel, "Signal processing with higher order spectra", IEEE Signal Processing Magazine, pp. 10-37, July 1993.

[12] Q. Xue, Y. H. Hu, and W. J. Tompkins, "Neural network-based adaptive matched filtering for QRS detection," IEEE transactions on Biomedical Engineering, Vol. BME-39, No. 4, pp. 317-328, April 1992.

[13] N. J. Outram, E. C. Ifeachor, and P. Van Eet Velt, "Optimal Enhancement of the Fetal Electrocardiogram During Labour," in IEE colloquium on Signal Processing in Cardiology, Digest No. 1995/043, pp. 5/1-5/5, March 1995.

[14] N. J. Outram and E. C. Ifeachor, "Techniques for Detection and Classification of the Fetal QRS Complex," in IEE Colloquium on Applications of Neural Networks to Signal Processing, Digest No. 1994/248, pp. 10/1-10/3, December 1994.

[15] N. J. Outram et al., "Techniques for Optimal Enhancement and Feature Extraction of the Fetal Electrocardiogram," IEE Proceedings A, 1994.

[16] E. C. Ifeachor and O. J. Outram, "Fuzzy Logic Concepts for Pattern Analysis of Changes in Fetal Electrocardiogram," Proceedings of the International Conference on Neural Networks and Expert Systems in Medicine and Health Care, (E. C. Ifeachor and K. G. Rosen, eds.), Plymouth, UK, pp. 353-362, August 1994.

[17] J. J. Soraghan et al., "Linear and Nonlinear Adaptive ECG Signal Enhancement- A Comparative Study," IEE Colloquium on Signal Processing in Cardiology, Digest No. 1995/043, pp. 7/1-7/8, March 1995.

[18] S. Haykin, *Neural Networks:- A comprehensive Foundation*, Macmillan, NY, 1994.

[19] D. R. Brillinger, "Some History of the Study of Higher-Order Moments and Spectra," in Proceedings of the International Signal Processing Workshop on Higher Order Statistics, Colorado, U.S.A., pp. 41-45, 1990.

[20] P. A. Delaney and D. O. Walsh, "A Bibliography of Higher-Order Spectra and Cumulants," IEEE Signal Processing Magazine, pp. 61-70, July 1994.

[21] D. R. Brillinger and M. Rosenblatt, "Asymptotic Theory of Kth Order Spectra," in *Spectral Analysis of Time Series* (B. Harris, ed.), pp. 189-232, Wiley, NY, 1967.

[22] D. R. Brillinger, "An Introduction to Polyspectra," Annals of Mathematical Statistics, vol. 36, pp. 1351-1374, 1965.

[23] T. Barnett et al., "Bispectrum Analysis of Electroencephalogram Signals During Waking and Sleeping," Science, vol. 172, pp. 401-402, 1971.

[24] K. S. Lii, M. Rosenblatt, and C. W. Van Atta, "Bispectral Measurements in Turbulence," Journal of Fluid Mechanics, Vol. 77, pp. 45-62, 1976.

[25] K. Hasselmann, W. Munk, and G. MacDonald, "Bispectra of Ocean Waves," in Time Series Analysis (M. Rosenballt, ed.), Wiley, NY, pp. 125-139, 1963.

[26] Y. C. Kim and E. J. Powers, "Digital Bispectral Analysis and its Applications to Nonlinear Wave Interactions," IEEE Transactions on Plasma Science, vol. PS-7, pp. 120-131, 1979.

[27] M. J. Hinich and C. S. Clay, "The Application of the Discrete Fourier Transform in the Estimation of Power Spectra, Coherence, and Bispectra of Geophysical Data," Review of Geophysics, vol. 6, pp. 347-363, 1968.

[28] C. L. Nikias, "Higher Order Spectra in Signal Processing," in EUSIPCO 89, *Signal Processing V: Theories and Applications* (L. Tarres, E. Masgrau, and M. A. Lagunas, eds.), Elsevier Publishers, Holland, pp. 35-41, 1990.

[29] J. M. Mendel, "Tutorial on Higher Order Statistics (Spectra) in Signal Processing and System Theory: Theoretical Results and Some Applications," Proceedings of the IEEE, vol. 79, No. 3, pp. 278-305, March 1991.

[30] I. Jouny and E. K. Walton, " Applications of the Bispectrum in Radar Signature Analysis and Target Identification," Proceedings of the International Signal Processing Workshop on Higher-Order Statistics, Cgamrousse, France, (J. L.

Lacoume, ed.), July 10-12, 1991, Elseveir Science Publishers, pp. 197-200, 1992.

[31] C. L. Nikias, "ARMA bispectrum approach to nonminimum phase system identification," IEEE Transaction on Acoustics, Speech, and Signal Processing, vol. ASSP-36, pp. 513-524, April 1988.

[32] M. R. Raghuveer and C. L. Nikias, "Bispectrum estimation via parametric modeling," Signal Processing, Special issue on modern trends of spectral analysis, vol. 10, pp. 35-48, Jan. 1986.

[33] A. W. Lohmann and B. Wirnitzer, "Triple correlations," Proceedings of IEEE, vol. 72, pp. 889-901, July 1984.

[34] M Richter, T Schreiber, and D Kaplan, "Fetal ECG Extraction with Non-Linear State-Space Projections," IEEE Transactions on Biomedical Engineering, vol. 45, No. 1, pp. 133-137, January 1998.

[35] W. Zgallai, M. Sabry-Rizk, , P. Hardiman, and J. O'Riordan, "MUSIC-Based Bispectrum Detector: A Novel Non-Invasive Detection Method For Overlapping Fetal and Maternal ECG Signals," Proceedings of the 19th IEEE International Conference on Engineering in Medicine and Biology, EMBS, pp. 72-75, USA, October 1997.

[36] G. Bienvenue and I. Kopp, principe de la goniometrie passive adaptative, GRETSI, 106/1-106/10, 1979.

[37] M. Viebeg and P. Stoica, Editorial Note, in Special Issue on Subspace Methods, Part I: Array Signal Processing and Subspace Computations, Signal Processing, vol. 50 No. 1,2, pp. 1-3, April 1996.

[38] P. Stoica and A. Nehorai "MUSIC, maximum likelihood and Cramér-Rao bound," IEEE Transaction on Acoustics, Speech, and Signal Processing, vol. 37, pp. 720-741, 1989.

[39] P. Kumaresan and D. W. Tuffs, "Estimating the angles of multiple plane waves," IEEE Transactions AES, vol. 19 , No. 1, Jan 1983.

[40] S. S. Reddi, "Multiple source location- A digital approach," IEEE Transactions AES, vol. 15, pp. 95-105, 1979.

[41] B. Friedlander and A. Weiss, "Direction finding using spatial smoothing with interpolated arrays," IEEE Transactions AES, vol. 28, pp. 574-587, April 1992.

[42] T. J. Shan, M. Wax, T. Kailath, "On spatial smoothing for directions of arrival estimation of coherent signals," IEEE Transactions Acoustics, Speech and Signal Processing, vol. 33, No. 4, pp. 806-811, 1985.

[43] A J Barabell, "Improving the resolution of performance of eigenstructure-based direction-finding algorithms," Proc ICASSP, vol. 83, pp. 336-339, 1983.

[44] H. Krim and M. Viebeg, "Two decades of array signal processing research: The parametric approach," IEEE Signal Processing Magazine, vol. 13, No. 4, pp. 67-94, July 1996.

[45] M. Viebeg, B Ottersten, "Sensor array processing based on subspace fitting," IEEE Transactions on Signal Processing, vol. 39, No. 5, pp. 1110-1121, may 1991.

[46] M. Viebeg, B Ottersten, and T Kailath, "Detection and estimation in sensor array using weighted subspace fitting," IEEE Transactions on Signal Processing, vol. 39, No. 11, pp. 2436-2449, November 1991.

[47] A. Paulraj, R Roy and T Kailath, "A subspace rotation approach to signal parametric estimation," IEEE Proceedings, vol. 74, No. 7, pp. 1044-1045, July 1986.

[48] R. Roy and T Kailath, "ESPRIT, estimation of signal parameters via rotational invariance techniques," IEEE Transactions on Acoustics Speech, and Signal Processing, vol. 37, No. 7, pp. 984-995, July 1989.

[49] R. Roy, B. Ottersten, A. L. Swindlehurst and T. Kailath, "Multiple invariance ESPRIT," Proceedings 22nd Asilomar Conference on Signals, Systems and Computers, pp. 583-587, 1988.

[50] S. Haykin, *Adaptive filter theory*, Prentice Hall, 1991.

[51] R. Schmidt, "Multiple emitter location and signal parameter estimation," Proceedings of RADC Spectrum Estimation Workshop, pp. 243-258, 1979.

[52] S. Marple, *Spectral Analysis With Applications*, Prentice Hall, 1987.

[53] S. Kay, *Modern Spectral Estimation: Theory and Applications*, Prentice Hall, 1987.

[54] MIT/BIH Database: ECG Database Applications Guide, 10th Edition, 1997. Harvard-MIT Division of Health Sciences and Technology, MIT Room 20A-113, Cambridge, MA 02139, USA.

[55] MIT/BIH Database: ECG Database Programmer's Guide, 9th Edition, 1997. Harvard-MIT Division of Health Sciences and Technology, MIT Room 20A-113, Cambridge, MA 02139, USA.

[56] V. Zarazoso, A. K. Nandi, and E. Bacharkis, "Maternal and foetal separation using blind source separation methods," IMA Journal of Mathematics Applied in Medicine and Biology, vol. 14, pp. 207-225, Oxford University Press, 1997.

[57] R. O. Schmidt, *A Signal Subspace Approach To Multiple Emitter Location And Spectral Estimation*, PhD Dissertation, Department of Electrical Engineering, Stanford University, USA, 1981.

[58] D. Spielman, A. Paulraj and T. Kailath, "Performance Analysis Of The Music Algorithm," Proceedings of the IEEE International Conference on Acoustics, Speech, and Signal Processing, ICASSP, pp. 1909-1912, Japan, April 1986.

[59] R. Schmidt and R. Franks, "Multiple RF Signal Processing: An Experimental System," IEEE Transactions on Antennas and Propagation, vol. AP-34, pp. 281-190, March 1986.

[60] R. Kumaresan and D. W. Tufts, "Estimating The Angles Of Arrival Of Multiple Plane Waves," IEEE Transactions on Aerospace Electronic Systems, vol. AES-19, pp. 134- 139, 1983.

[61] U. Nickel, "Algebraic Formulation Of Kumaresan-Tufts Super resolution Method, Showing Relation to ME and MUSIC Methods," IEE Proceedings, vol. 135, pt. F, pp. 7-10, 1988.

[62] J. F. Yang and M. Kaveh, "Adaptive Algorithms For Tracking Roots Of Spectral Polynomials," IEEE International Conference on Acoustics, Speech, and Signal Processing, ICASSP, pp. 1162-1169, Scotland, 1989.

[63] J. F. Yang and M. Kaveh, "Adaptive Eigenspace Algorithms For Direction Or Frequency Estimation And Tracking," IEEE Transactions on Acoustics, Speech, and Signal Processing, vol. ASSP-36, pp. 241-251, 1988.

[64] M. Kaveh and A. J. Barabell, "The Statistical Performance of the MUSIC and the Minimum-Norm Algorithms in Resolving Plane Waves in Noise," IEEE Trans. on Acoustics, Speech, and Signal Processing, vol. ASSP-34, pp. 331341, 1986.

[65] P. Stoica and A. Nehorai, "MUSIC, Maximum Likelihood, and Cramer-Rao Bound," IEEE Transactions on Acoustics, Speech, and Signal Processing, vol. ASSP-37, pp. 720-741, 1989.

[66] C. Van Loan, "Matrix Computation In Signal Processing," Chapter 4 in *Selected Topics In Signal Processing,* S. Haykin, ed., Prentice Hall, 1989.

[67] R. R. Mohler and F. J. Bugnon, "A Second-Order Eigenstructure Array Processor," Higher-Order Statistics Workshop, pp. 152-155, USA, 1989.

[68] E. Moulines and J. F. Cardoso, "Second-Order Versus Fourth-Order MUSIC Algorithms," Proceedings of the International Signal Processing Workshop on Higher-Order Statistics, pp. 247-250, France, 1991.

[69] J. Parthasarathy and S. Prasad, "Eigenspace Algorithms For Estimating The Polyspectral Parameter Of Harmonic Signals," IEEE Signal Processing Workshop on Higher-Order Statistics, pp. 290-294, USA, 1993.

[70] P. P. Kanjilal, S. Palit, and G. Saha, "Fetal ECG Extraction from Single Channel Maternal ECG Using Singular Value Decomposition," IEEE Transactions on Biomedical Engineering, vol. 44, No. 1, pp. 51-59, January 1997.

[71] M Richter, T Schreiber, and D Kaplan, "Fetal ECG Extraction with Non-Linear State-Space Projections," IEEE Transactions on Biomedical Engineering, vol. 45, No. 1, pp. 133-137, January 1998.

[72] E Ciccinelli, A Bortone, I Carbonara et al, "Improved equipment for abdominal fetal electrocardiogram recording: description and clinical evaluation," International Journal of Biomedical Computing, vol. 35, No. 3, pp. 193-205, 1994.

[73] Q. Xue, Y. H. Hu, and W. J. Tompkins, " Neural network-based adaptive matched filtering for QRS detection," IEEE transactions on Biomedical Engineering, Vol. BME-39, No. 4, pp. 317-328, April 1992.

[74] M. Kristensson, M. Jansson, and B. Ottersten, "Further results and insights on subspace based sinusoidal frequency estimation," IEEE Transactions on Signal Processing, Vol. 49, No. 12, pp. 2962-2974, December 2001.

[75] A Eriksson, P. Stoica, and T Soderstorm, "Markov-based eigenanalysis method for frequency estimation," IEEE Transactions on Signal Processing, Vol. 42, pp. 586-594, March 1994.

[76] A. Graham, *Kronecker products and matrix calculus with applications*. London UK: Ellis Horwwod, 1981.

[77] W. Zgallai, M. Sabry-Rizk, P. Hardiman, and J. O'Riordan, "Third-order cumulant signature matching technique for non-invasive fetal heart beat identification," ICASSP, IEEE International Conference on Acoustics, Speech, and Signal Processing, vol. 5, pp 3781-3784, Germany, 1997.

[78] A. O. Steindhart, "Householder transformations in signal processing," IEEE Acoustics, Speech, and Signal Processing magazine, vol. 5, pp. 4-12, 1988.

[79] A. S. Householder, "Unitary traniangulization of a nonsymmetric matrix," Journal of the Association of Comput. Mach., Vol. 5, pp. 339-342, 1958.

[80] G. H. Golub, and A. H. Kahan, "Calculating the singular values and the pseudo-inverse of a matrix," Journal of SIAM Numer. Anal. B., vol. 2, pp. 205-224, 1965.

[81] P. O. Borjesson et al, "Adaptive QRS Detection Based on Maximum a Posteriori

Estimation," IEEE Trans. on Biomedical Engineering, vol. 29, pp. 341-351, 1982.

[82] J. Pan and W. J. Tompkins, "A Real-Time QRS Detection Algorithm," IEEE Transactions on Biomedical Engineering, vol. BME-32, pp. 230-236, 1985.

[83] P. S. Hamilton and W. J. Tompkins, "Quantitative Investigation on QRS Detection Rules Using MIT/BIH Arrhythmia Databases," IEEE Transactions on Biomedical Engineering, vol. BME-33, pp. 1157-1165, 1986.

[84] M.L. Ahlstrom and W.J. Tompkins, "Automated high-speed analysis of holter tapes with microcomputers," IEEE Trans. Biomed. Eng., vol. 30, pp. 651-657, Oct. 1983.

[85] R.A. Balda, Trends in Computer-Processed Electrocardiograms. Amsterdam: North Holland, 1977, pp. 197-205.

[86] J. Fraden and M.R. Neumann, "QRS wave detection," Med. Bioi. Eng. Comput., vol. 18, pp. 125-132,1980.

[87] D. Gustafson, "Automated VCG interpretation studies using signal analysis techniques," R-I044 Charles Stark Draper Lab., Cambridge, MA,1977.

[88] A. Ligtenberg and M. Kunt, " A robust-digital QRS-detection algorithm for arrhythmia monitoring," Comput, Biomed.Res., vol. 16, pp. 273-286, 1983.

[89] B., Cellar, Y.C.C. Grace, and C. Phillips, "ECG analysis and processing using wavelets and other methods," Biomed. Eng. Appl. Basis Commun., vol. 9, no. 2, pp. 81-90,1997.

[90] Y.H. Hu, W.J. Tompkins, J.L. Urrusti, and V.X. Afonso, "Applications of artificial neural networks for ECG signal detection and classification," J. Electrocardiology, vol. 26 (Suppl.), pp. 66-73,1993.

[91] M.G. Strintzis, G. Stalidis, X. Magnisalis, and N. Maglaveras, "Use of neural networks for electrocardiogram (ECG) feature extraction, recognition and classification," Neural Netw. World, vol. 3, no. 4, pp. 313-327,1992.

[92] A. Kyrkos, E. Giakoumakis, and G. Carayannis, "Time recursive prediction techniques on QRS detection problem," in Proc. 9th, Annu. Conf. IEEE Engineering in Medicine and Biology Society, 13-16 Nov., Boston, MA, pp. 1885-1886, 1987.

[93] D.A. Coast, R.M. Stem, G.G. Cano, and S.A. Briller, "An approach to cardiac arrhythmia analysis using hidden Markov models," IEEE Trans. Biomed. Eng., vol. 37, pp. 826-836, 1990.

[94] P.E. Trahanias," An approach to QRS complex detection using mathematical

morphology," IEEE Trans. Biomed. Eng., vol. 40, no. 2, pp. 201-205,1993.

[95] A. Ruha, S. Sallinen, and S. Nissila, "A real-time microprocessor QRS detector system with a 1-ms timing accuracy for the measurement. Of ambulatory HRV," IEEE Trans. Biomed. Eng., vol. 44, pp. 159-167, 1997.

[96] R. Poli, S. Cagnoni, and G. Valli, "Genetic design of optimum linear and nonlinear QRS detectors," IEEE Trans. Biomed. Eng., vol. 42, pp. 1137-1141, 1995.

[97] S.-K. Zhou, J.-T. Wang, and J.-R. Xu, "The real-time detection of QRS-comp1ex using the envelop of ECG," in Proc. 10th Annu. Int. Conf., IEEE Engineering in Medicine and Biology Society, New Orleans, LA, 1988, p. 38.

[98] F. Gritzali, "Towards a generalized scheme for QRS detection in ECG waveforms," Signal Processing, vol. 15, pp. 183-192, 1988.

[99] G. Belforte, R. De Mori, and F. Ferraris, "A contribution to the automatic processing of electrocardiograms using syntactic methods," IEEE Trans. Biomed. Eng., vol. 26, pp. 125-136, Mar. 1979.

[100] B.-V. Kower, C. Hennig, and R. Orglmeister, "QRS detection using zero crossing counts," submitted for publication, 2001.

[101] M. Sabry-Rizk, D. Romare, W. Zgallai, K. T. V. Grattan, P. Hardiman, and J. O'Riordan, "Higher order statistics (HOS) in signal processing: Are they of any use," IEE colloquium, digest #111, pp. 1/1-1/6, London, May 1995.

[102] M. Sabry-Rizk, W. Zgallai, "Higher Order Statistics Are Indispensable Tools in The Analysis of Electrocardiogram Signals," IEE Colloquium on Statistical Signal Processing, January 1999.

[103] L. De Lathauwer, B. De Moor, and J. Vandewalle, "Fetal electrocardiogram extraction by blind source separation," IEEE Transactions on Biomedical Engineering, Vol. 47, No. 5, pp. 567- 572, May 2000.

[104] M Sabry-Rizk, W. Zgallai, A. McLean, E. R. Carson, and K. T. V. Grattan, "Virtues and Vices of Source Separation Using Linear Independent Component Analysis for Blind Source Separation of Non-linearly Coupled and Synchronised Fetal and Mother ECGs," IEEE Engineering in Medicine and Biology Conference, USA, 2001.

[105] M. Sabry-Rizk, W. Zgallai, "Novel robust modified pseudo-spectral MUSIC algorithm for on-line QRS detection in electrocardiogram signals", to be published.

[106] M. Sabry-Rizk, W. Zgallai E. R. Carson, K. T. V. Grattan, P. Hardiman, P. Thompson and A. Maclean, "Modified MUSIC Pseudospectral Analysis Reveals Common Uterus and Fetal Heart Resonances During Labour Contractions", the 22nd Annual International Conference of the IEEE Engineering in Medicine and Biology Society, EMB2000, USA, 23-28/7/2000.

[107] M. Sabry-Rizk, W. Zgallai, C. Morgan, S. El-Khafif' E. R. Carson, and K. T. V. Grattan, "Novel decision strategy for P-wave detection utilising nonlinearly synthesised ECG components and their enhanced pseudospectral resonances," IEE Proceedings Science, Measurement and Technology, Special section on Medical Signal Processing, vol. 147, No. 6, pp. 389-397, November 2000.

CHAPTER SIX

MODIFIED SPECTRAL MUSIC WITH WEIGHTED SUBSPACES AND INCORPORATED COVARIANCE MATRIX FOR COMBINED UTERINE CONTRACTION AND NOISE ARTEFACT

6.1 Introduction

6.1.1 Aim

Presented in this Chapter is the third and most successful FHR detection technique. It is aimed at enhancing the spectral resolution of characteristic peaks uniquely identifying individual ECG signals contained in the transabdominally-measured data, namely, the QRS-complexes of the mother and the fetal. It is based, in the first instance, on partitioning two subspaces; the first subspace contains the ECG signal bearing the mother and fetal, and the second orthogonal subspace contains the uterine contraction interference signal (UCS) plus noise. This is reminiscent of, but more superior to, the conventional multiple signal classification (MUSIC) spectral estimator which exploits the orthogonality between the signal and noise subspaces provided that the noise is additive white Gaussian. In this new version of modified spectral MUSIC, subsequent separation of the mother and fetal QRS-complexes is performed in their shared signal subspace.

6.1.2 How is the separation of the coexisting or non-coexisting mother's and fetal QRS-complexes performed?

The spectral content of the mother's QRS-complex and that of the fetus are different and indeed unique. The mother's QRS-complex principal spectral peak is found around 17 Hz, and the fetal QRS-complex principal spectral peak is found around 30 Hz.

Accordingly, such individual spectral content can be exploited herewith in the identification and detection of either signal within the maternal cardiac cycle. The Kaiser filtered weighted MUSIC previously published algorithm has been devoted to identifying in the frequency domain anomalous QRS-complexes and P-waves such as P-on-T-waves and P-on-QRS-complex episodes for adult patients [37]. However, for FHR detection in labour one has to overcome two major problems in the transabdominally-measured ECG data, namely, poor signal spectral resolution and the influence of the coexisting labour contraction signals* [62] which not only exhibit a fairly broad spectrum, but also are uniquely characterised by having localised energy resonances, one of which is seriously overlapping with the fetal distinctive strong peaks which will be used as the fetal spike event. The fetal heartbeat detection is accomplished by thresholding the enhanced fetal spikes in the frequency domain. The most challenging problem is, therefore, not only to enhance the quality and resolution of the mother and fetal QRS-complexes' principal pseudo-spectral peaks, abbreviated as MPPP and FPPP, respectively, but also to nudge the uterine contraction interference signals (UCS) plus noise into a separate subspace which will be named the interference subspace (I-subspace), whereby orthogonalisation is forced between the I-subspace and the signal subspace (S-subspace) containing both the mother and / or the fetal QRS signature imprints.

At this juncture of time, it is worth writing a statement or two about the meaning of *windowed* data in the literature [79]. Starting with a scalar-valued process, it is well-known that subspace-based identification of sinusoidal frequencies is possible if the scalar-valued data is *windowed* to form a low-rank vector-valued process. MUSIC- and ESPRIT-like estimators have, for some time, been applied to this vector model. The rank properties of certain weighting functions and residual covariance matrices were left as an open question in [37]. The statistical properties of subspace methods when applied to *windowed* (or weighted) data models are inevitably different from models where the low-rank structure is physically present in the system (such as an antenna array in directional finding applications). In this chapter, the so called temporal

*** Labour contractions behave like deterministic, non-linear, and chaotic signals when considered over a sufficiently long data sample of almost 10 sec or longer [62]. However, for an 250 msec segment they exhibit noise-like characteristics.**

window is restricted to 250 msec and is not aimed at a specific rank reduction (as sometimes referred to in the literature as an optimum window). Following this brief discussion, it has been decided not to attempt to answer the effect of the rank properties of the Kaiser weighted MUSIC.

In this thesis, the Kaiser filter weights are applied to each of the 250 msec window (segment) and the weights are optimised to enhance the principal peaks of either QRS-complex in their respective temporal domains.

In pursuing separation of signals and interference signals, or signals and noise, two auxiliary methods have been used based on the concepts of *oriented energy* and *signal-to-signal ratio*, and *the Gram-Schmidt orthogonalisation.* This is done in addition to the MUSIC well established Generalised Singular Value Decomposition (GSVD) which deals with partitioning signal and coloured noise (as opposed to Gaussian noise) subspaces.

6.1.3 What distinguishes this subspace-based technique from the previously published subspace-based technique for adults [37]?

The novelty of this technique rests on its dealing with the UCS during the strong and most painful peaks of labour contractions which are, apart from their noise-like characteristics, heavily contaminated with other noise artefact. To pave the way for the studies based on this technique, it is prudent to discuss the relevant issues. This is done in the following sections. Before we proceed with such issues it is convenient to provide a layout of this chapter.

6.1.4 Layout of the Chapter

Section 6.2 provides discussions of some relevant issues. These issues include the role of ECG linearisation and the issue of coincident mother and fetal QRS-complexes. Section 6.3 addresses some problems associated with mother and fetal spectral resolution in a labour environment, and the proposed solutions. Section 6.4 reviews some relevant previous studies that paved the way for the development of the new technique. Section 6.5 presents a detailed statement of research. It describes a particular class of modified MUSIC, namely, *the sequentially optimised and weighted spectral MUSIC* algorithm, also involving a *reconfigured interference plus noise subspace* to

incorporate *the modified covariance matrix of the uterine activity* in such a spectral estimator. For convenience, the mathematical formulation of the conventional MUSIC is presented in Section 6.6. Section 6.7 is devoted to the mathematical formulation of the new class of MUSIC, and deals with the incorporation of the modified covariance matrix of the linearised non-Gaussian uterine contraction interference signal (UCS) in the sequentially optimised and weighted MUSIC. Also, the concepts of oriented energy and signal-to-signal ratio, and the alternative projection method of Gram-Schmidt orthogonalisation are then briefly described. Results are detailed in Section 6.8. Summary and conclusions are given in Section 6.9.

6.2 Discussions of relevant issues

6.2.1 The role of linearisation in FHR applications confined to this thesis

The two novel hybrid techniques presented in Chapters Four and Five exploit the Gaussian-free TOC and BIC unique signatures of individual mother's and fetal QRS-complex templates. The QRS higher-order statistics signature templates are then incorporated in the memory of an LMS-based classifier in order to obtain high fetal heartbeat classification rates of the incoming TOCs or BICs of the transabdominally-measured ECG signals that contain the mother's QRS, or the fetal QRS, or both QRSs. Therefore, placing both the TOC-based and the BIC-based techniques in the same conceptual hybrid framework which combines both signal processing and neural network classification. The classification rates for the hybrid TOC-based and the hybrid BIC-based FHR techniques are 86.16% and 90.12%, respectively. The difference in performance is not due to better resolvability of the latter in the frequency domain over the former in the time domain when dealing with episodes of coincident mother and fetal QRS-complexes, as both techniques fail in this respect. Rather, it is due to the fact that the BIC technique can resolve a few of fetal QRS-complexes occurring within the T-wave region of the mother. Unfortunately, the non-linear transabdominally-measured ECG signals are always contaminated by the non-linear labour uterine contraction interference signals (UCS) and some non-linear noise, and this renders their HOS representatives as distorted candidates which makes difficult the matching between the HOS templates and the transabdominal ECG components, namely, the mother and fetal QRS-complexes. The HOS templates created from measuring the mother's chest ECG and the fetal scalp electrode ECG databases are

themselves non-linear and must be linearised alongside with their transabdominal counterparts before incorporating them in the classifiers. They are, however, not as much influenced by uterine contraction and other artefacts associated with the transabdominally-measured counterparts. **Linearisation** is, therefore, of crucial importance in the signal processing phase of all the above mentioned ECG signals. Linearisation is performed by means of synthesising the non-linearity of all ECG signals; the mother's chest (template), the fetal scalp electrode (template), and the transabdominally-measured with noise, into their quadratic and cubic components using adaptive LMS-based Volterra filters (see Figure 2.1). Only the linear components are retained for further processing. By removing the non-linearity from the ECG signals, we are left with the **linear* non-Gaussian TOC and BIC**. This minimises non-linear sourced distortions and in general improves the quality of the HOS representative templates and drastically improves the fetal heart detection rates during labour. There is a set of allowable deformation of the HOS templates due to morphological variations** and non-Gaussian noise artefact.

6.2.2 Coincident mother and fetal QRS-complexes

The mother and fetal QRS-complexes often coincide making it impossible to separate them using any time-domain-based technique. Even with the higher-order statistics TOC, as reported earlier, there is a 13.8% failure rate due to 9.8% mother QRS and fetal QRS coincidences, and 4% fetal QRS and maternal T-wave coincidences. The BIC failure rate of 9.8% is purely due to mother QRS and fetal QRS coincidences as there is a shortcoming in acquiring sufficiently high resolution to separate the bispectral peaks of the mother and fetal QRS-complexes. The overlapping of the fetal QRSs and the maternal T-waves can be resolved by the BIC template matching technique. The above percentages of QRS-complex coincident episodes have been found in the 50,000 maternal heartbeat database. The alternative is to try to resolve them in the

* The ECG quadratic and cubic components and their HOS have been used in other studies beyond the scope of this thesis [39-40].

** When sets of HOS templates are created from the mother's chest ECG signals and the fetal scalp electrode ECG signals, certain deformations are allowed to cater for morphological variations in each ECG recordings, which may not be obvious to the discerning eye, and certainly does not affect the performance of the QRS neural network classifiers. This is done by randomly selecting QRS-complexes over the first few cardiac cycles.

frequency-domain. More detailed analyses are given in Section 6.3.5. The modified spectral MUSIC, which is the subject of this Chapter, is motivated, at least in part, by the shortcoming of all other techniques to detect FHBs when masked by the mother's QRS-complex. The other motivation is to combat interference and noise using only second-order statistics. The following sections are designed to promote awareness of the problems and solutions encountered in the implementation of the third and most successful FHB detection technique.

6.3 Specific problems associated with mother and fetal spectral resolution in a labour environment, and solutions

6.3.1 The New tailored subspace-based spectral estimation of mother's and fetal QRS-complexes during labour

Now, we seek to exploit a multiple signal classification (MUSIC) methodology which incorporates a tailor-made subspace fitting for individual QRS spectral signatures based on *a priori* information. In a simplified term, if we ignore the influence of the uterine contraction interference signals for a moment, the technique is based on weighting the covariance matrix of the transabdominally-measured signals, which in turn uniquely modifies the signal and noise subspaces with the view that this will enhance and retain only those terms (eigenvectors) that result in the mother QRS principal pseudo-spectral peak at 17 Hz, or if we wish, the fetal QRS principal pseudo-spectral peak at 30 Hz as depicted in Figure 6.1 (not at the same time). This figure has been brought forward prematurely from Section 6.8 in order to visualise the important spectral characteristics of the mother and fetal and appreciate the difference between their spectral contents. In essence, one could say that, in the absence of uterine contraction interference signals and assuming white Gaussian noise* presence, this is a specially** weighted MUSIC-like technique. It will be recognised in the following sections that, both the signal and noise subspaces will have been modified or reconfigured by two tailor-made weighting Kaiser functions, one is aimed at enhancing the mother QRS spectral peak and the other is aimed at enhancing the fetal QRS spectral peak. Obviously, the two

* Most MUSIC-based estimation techniques require the additive noise to be white and Gaussian.

** The tailor-made weighting function is the Kaiser filter [7] which has been used in all our ECG analysis over the last decade [37-38, 40-42]. For further information, see Appendix A6 and Figures 5.15 (a-d).

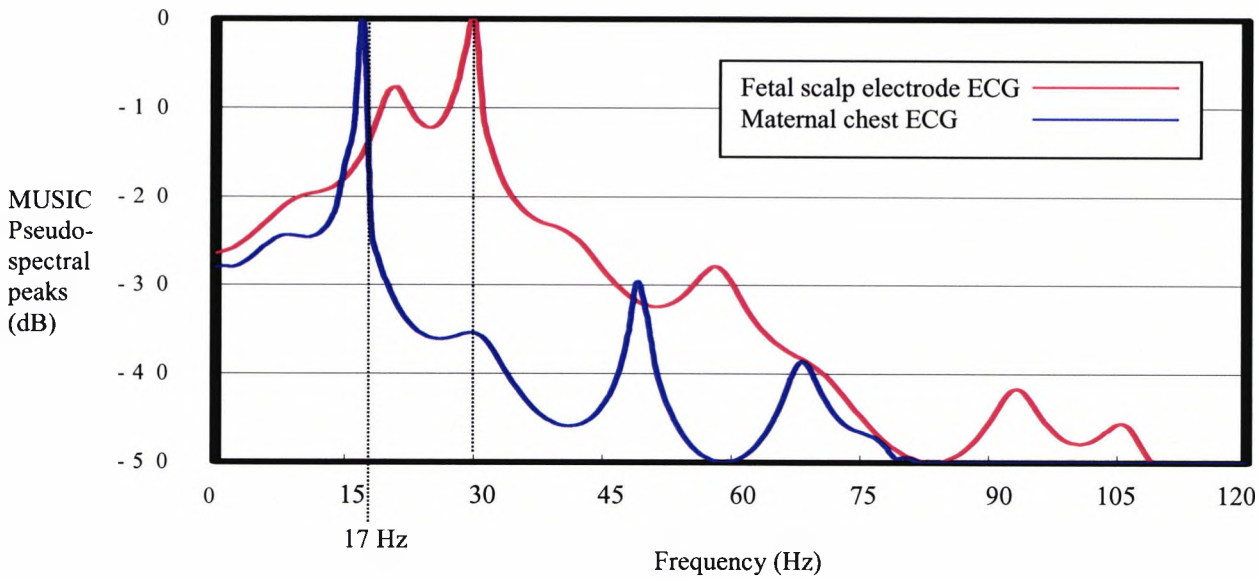

***Figure 6.1**: Normalised specially weighted MUSIC-like pseudo-spectrum for fetal scalp electrode, and maternal chest full cardiac cycles. Optimised Kaiser weighting coefficients are used for the fetal and mother ECGs to enhance their spectral peaks at 30 Hz and 17 Hz, respectively. The maternal cardiac cycle begins 50 msec before the R-wave and ends 50 msec before the next R-wave. The subject is at end of term, 40 weeks. Model order is 11 and 4, respectively, for the signal and noise subspaces. (Code: 5-1).*

Kaiser weighting functions will be applied sequentially as the same data segment is scanned twice. Again, this technique detects the fetal heartbeat in an 250-msec flag window by thresholding the resultant principal pseudo-spectral peak (FPPP) in the frequency domain, counts the number of beats in every maternal cardiac cycle, and computes the averaged FHR per maternal cycle. The computer algorithm has to first pinpoint two successive R-waves of the mother's QRS-complexes, and then divides the cardiac cycle into four segments 250 msec each, starting with a reference point approximately 50 msec before the first R-wave and ends at 50 msec before the second R-wave. Dr. Sabry-Rizk and Mr Zgallai have devised a very accurate adult QRS-complex detection scheme. Since the mother's QRS segment is scanned twice "sequentially" to establish the fetal presence, it may be prudent to use parallel signal processing and divide the input data into two streams in order to achieve simultaneous scanning and weighted MUSIC processing, each with different Kaiser weighting functions. The problem of synchronisation can be solved by allowing for a certain lag of around 20 μsec (using Unix WS) which counts for the difference between computing times of the Kaiser weighted mother's and fetal pseudo-spectral patterns and additional signal processing. The time allocated to the former is devoted to the identification of the maternal QRS-complex in the frequency domain and subsequent pinpointing of the R-wave in the time domain within the 250-msec segment, using a sophisticated technique [72] which permits very accurate instantaneous MHR. The time allocated to the latter is devoted to the identification of the fetal QRS-complex in the frequency domain and thresholding of the fetal principal peak (FPPP). The fetal R-wave cannot be pinpointed in the time domain because the fetal QRS-complex is usually buried under noise and motion artefact and it is rather difficult to detect. Therefore, the presence of the fetal is blindly registered over the entire 250-msec flag window. For a fixed window length of 250 msec, the fetal CPU time required for the above mentioned operations is less than the mother CPU time by 20 μsec using Unix WS. The algorithm is limited to identifying and registering each fetal heartbeat occurrence within the flag window and counting the number of FHBs within each maternal cardiac cycle. Therefore, the fetal heart rate will not be instantaneous, instead it will be related to the mother heart rate, which can be as accurate as 99.85% [72], for each individual maternal cardiac cycle.

Essentially, this subspace-based technique depends on *a priori* information of the mother and fetal spectral content particularly the characteristics and allocations of their

respective principal peaks and, therefore, requires initial familiarisation with the dominant spectral features of the following ECG signals' template databases; (a) the mother's chest, (b) the fetal scalp electrode, (c) the uterine contraction interference signals, and (d) noise artefact. Unlike the two HOS-based techniques described in the previous chapters, the spectral templates will not be required in the fetal identification process, rather they are merely used to observe possible spectral variations in adults and fetals and to implement a multiple overlapping window structure in the frequency domain for each of the fetal and mother principal pseudo-spectral peaks. In general, the Kaiser weighted spectral MUSIC estimator routine seeks to orthogonalise the signal and noise subspaces using a commercial singular value decomposition (SVD) subroutine based on the assumption of additive white Gaussian noise, after incorporating the appropriate Kaiser weighting coefficients into the frequency localiser function within the routine. Obviously, any commercial SVD presumes an identity matrix for the noise which is not the case of the linearised non-Gaussian interference signals (UCS) and the accompanying linearised non-Gaussian motion artefact. An immediate solution is to use the generalised singular value decomposition (GSVD) which is not based on white Gaussian noise and can deal with coloured and non-Gaussian noise provided that the coloured noise covariance matrix is known *a priori* or can be estimated. This obviously leads us to the next important operation to be performed, namely, the development and incorporation of a modified covariance matrix of the UCS in the interference subspace (I-subspace)* associated with the transabdominal ECG signals. The I-subspace may now contain the UCS plus noise as opposed to the noise-only subspace associated with the conventional MUSIC. This is now the second modification introduced to the I-subspace which will be orthogonalised and separated from the signal subspace (S-subspace) containing both the mother and fetal QRS-complexes by performing the generalised singular value decomposition (GSVD)** [29, 32-33].

* which replaces the noise subspace in the MUSIC estimator.

** The principle which is used to decompose any information matrix into orthogonal component dyads or modes. Generalised SVD implies that no assumption is being made of white Gaussian during the implementation of the SVD. Instead, coloured or non-Gaussian noise is used in the mathematical formulation which makes the orthogonalisation of signal subspace and noise subspace much more sophisticated [29, 32-33].

The concept of oriented energy and signal-to-signal ratio will also be used when performing the GSVD to separate the above mentioned subspaces. This will be briefly discussed in Section 6.7.3.

Having explained the concept of the modified weighted UCS covariance matrix incorporated MUSIC-like technique some detailed analyses are now in order. We may recall that the individual ECG spectral content for the mother and the fetal have been depicted in Figure 6.1. The Principal Pseudo-spectral Peaks (PPPs) of the mother's QRS-complex at 17 Hz is coloured blue, and the fetal principal pseudo-spectral peak at 30 Hz is coloured red. However, there may be small frequency variations in the 17 Hz and 30 Hz centres in each adult ECG and each fetal ECG due to normal morphological changes, or indeed from one ECG to another [41-43]. This may necessitates the provision of several overlapping windows centred at 15 Hz, 16 Hz, 17 Hz, 18 Hz, and 19 Hz for the mother, and 28 Hz, 29 Hz, 30 Hz, 31 Hz, 32 Hz, 33 Hz, 34 Hz, 35 Hz, 36 Hz, 37 Hz, and 38 Hz for the fetal.

The word "pseudo" is usually encountered in frequency estimation methods that do not result in the actual power spectrum of the underlying process [1-2]. The power spectrum for an adult's standard ECG may or may not show the principal peak at 17 Hz [50, 64], due to lack of resolution. **Even if one uses other eigenvector-based spectral techniques without the means to mitigate the effect of an unknown noise field, the desired resolution is not guaranteed. In other words, the noise field must be accurately incorporated in the subspace either by measuring it without a signal or by estimating it using AR modelling.**

6.3.2 The UCS short-term and long-term statistical behaviour

The nature of the UCS changes with the length of the observation data. For instance, if the UCS is observed over 10,000 samples it can be modelled as deterministic, non-linear, and chaotic signals [34-36, 62]. However, when observed over an 250-msec window, the UCS may look just like noise. This prompts us to use at least two methods to orthogonalise the signal and interference subspaces. The first method is the GSVD assuming that the UCS is just like coloured non-Gaussian noise. The second method is using the concept of oriented energy and signal-to-signal ratio. A third method may involve the Gram-Schmidt orthogonalisation routine. The choice of the method rather

depends on which one would yield minimum residual UCS in the QRS-complex subspace. Now follows a summary of the UCS short- and long-term statistics which have been analysed and accurately modelled using a new special non-linear structure by Dr. Sabry-Rizk and Mr. Zgallai over a number of years [34-36, 62] and the relevant tests, namely, the Hinich linearity test [66] and the chaoticity test [67-70].

Short-term statistics (data length 250 msec)

1- The modified covariance matrix of the UCS, $\mathbf{I}_{noise}$ matrix, is correlated because its off diagonal elements are non-zero. The Hinich Test for Gaussianity was applied to the $\mathbf{I}_{noise}$ matrix. The matrix does not satisfy the hypothesis of Gaussianity at a confidence level of 95%. The Gaussianity parameter, S-Gauss, was calculated to be 163.5 which is different from 0 for the Gaussianity assumption to be valid. So it is assumed that the $\mathbf{I}_{noise}$ matrix is non-Gaussian.

2- The statistics of the $\mathbf{I}_{noise}$ matrix are calculated from the following equations for the variance, skewness, and kurtosis;

$$\text{The variance is defined as } \gamma_2^x \underline{\underline{\nabla}} c_2^x(0) = \frac{1}{2\pi} \int_{-\pi}^{\pi} C_2^x(\omega).d\omega \tag{6.1}$$

$$\text{The skewness as } \gamma_3^x \underline{\underline{\nabla}} c_3^x(0,0) = \frac{1}{(2\pi)^2} \int_{-\pi}^{\pi}\int_{-\pi}^{\pi} C_3^x(\omega_1,\omega_2).d\omega_1.d\omega_2 \tag{6.2}$$

and the kurtosis as

$$\gamma_4^x \underline{\underline{\nabla}} c_4^x(0,0,0) = \frac{1}{(2\pi)^3} \int_{-\pi}^{\pi}\int_{-\pi}^{\pi}\int_{-\pi}^{\pi} C_4^x(\omega_1,\omega_2,\omega_3).d\omega_1.d\omega_2.d\omega_3 \tag{6.3}$$

The variance of $\mathbf{I}_{noise}$ equals 0.957, the skewness equals 1.321, and the Kurtosis equals 2.637. The skewness and kurtosis are calculated from the third- and fourth-order statistics of the $\mathbf{I}_{noise}$ which confirms that $\mathbf{I}_{noise}$ is non-Gaussian because its higher-order statistics are not equal to zero.

3- The statistics of $\mathbf{I}_{noise}$ are different from the Uniform and Laplace noise which do not support third-order statistics because they are symmetrically

distributed. They are also different from the Exponential and Rayleigh because its second, third- and fourth-order statistics are not related by one constant, e.g., λ, α.

Long-term statistics (data length 10,000 msec)

The UCS signal, when considered over a sufficiently long data sample of length 10,000 or more [62], is deterministic, chaotic, and multi-fractal. Essentially, the multi-fractility is indicative of normality in this case. Based on the Hinich linearity test and the Hurst component analysis test [63] which will now be described.

Tests

The Hinich linearity test [66]:

The test is based on the observation that for a linear process the skewness will be constant [66]. In the Hinich linearity test, the inter-quartile range of the estimated bicoherence squared is computed; a quantity, Λ, proportional to the mean value of the bicoherence squared is also computed; the theoretical inter-quartile range of a chi-square random variable with two degrees of freedom and non-centrality parameter, Λ, is then computed. The linearity hypothesis should be rejected if the estimated and theoretical inter-quartile ranges are very different from one another. The non-centrality parameter is

$$\Lambda = \frac{2N}{\left(1+\rho^{-1}\right)^3}\Gamma_s \tag{6.4}$$

where Λ is the non-centrality parameter, N is the number of samples, ρ is the signal-to-noise ratio, and Γ_s is the skewness of the signal. The estimated and theoretical inter-quartile ranges are 268.91 and 42.59, respectively. Hence, the non-linearity hypothesis was accepted.

The Chaoticity Hurst component test [67-70]:

The test is based on the observation that multi-fractal signals can be decomposed into many subsets characterised by different local Hurst exponents, h, which quantify the local singular behaviour and relate to the local scaling of the signal. The local value of h is extracted using the Wavelet theory. The local exponent, h, is evaluated through the modulus of the maxima values of the wavelet transform at each point of the signal. A

function Zq(a) is defined as the sum of the qth powers of the local maxima of the modulus of the wavelet transform coefficients at scale a. The scaling of that partitioning function, Zq(a), is estimated. For small scales we expect the partitioning function Zq(a) scales as a power law,

$$Zq(a) \cong a^{t(q)} \tag{6.5}$$

For certain values of q, the exponents t(q) have familiar meanings. In particular, t(2) is related to the scaling exponent of the Fourier power spectra,

$$S(f) \cong 1/f^{b}, \text{ as } b = 2 + t(2). \tag{6.6}$$

For positive q, Zq(a) reflects the scaling of the large fluctuations and strong singularities, whereas for negative q, Zq(a) reflects the scaling of the small fluctuations and weak singularities. For multi-fractal signals, t(q) is a non-linear function:

$$t(q) = q\,h - D(h), \tag{6.7}$$

where h = dt/ dq is not constant. The fractal dimension D(h) is related to t(q) through a Legendre transform:

$$D(h) = q\,h - t(q) \tag{6.8}$$

The local Hurst exponents, h, quantify the local singular behaviour and thus relate to the local scaling of the time series. Using the 10,000 samples of the UCS, the partitioning function was calculated for scales a > 8 and for values of q ranges from -5 to 5. It was found that t(q) is a non-linear function of q; also D(h) has non-zero values for a broad range of the local Hurst exponents, h, which indicates that the corresponding UCS is a multi-fractal signal [62]. The range of scaling exponents ($0 < h < 0.4$) with non-zero fractal dimension D(h) indicates that the fluctuations in the UCS exhibit anti-correlated behaviour ($h = 1/2$ corresponds to uncorrelated behaviour; $h > 1/2$ corresponds to correlated behaviour). Hence, the UCS is a deterministic, non-linear, and chaotic signal.

6.3.3 *The UCS spectral characteristics*

The UCS broad spectrum will now be briefly addressed. It has been found from previous research studies [52-53] that, the spectrum of UCS may include comparatively strong narrowband spectral components centred around 5 Hz, 30 Hz, 45 Hz, 60 Hz, and 90 Hz in addition to some broadband components. Figure 6.2 depicts UCS spectral characteristics before and after linearisation using a third-order Volterra synthesiser. Figure 6.3 depicts the effect of linearisation on the UCS's bicoherence squared. Linearisation has resulted in an average reduction of about 9 dB in spectral peaks at frequency pairs of (32 Hz,18 Hz), (32 Hz,48 Hz), and (48 Hz,32 Hz), which are strongly overlapping with the fetal frequency pairs depicted in Figure 6.4 (a,b) at (30 Hz, 7 Hz), (30 Hz, 18 Hz), and (30 Hz, 26 Hz).

In particular, the uterine contraction component at 30 Hz usually masks the principal spectral components of the fetal [52]. The most challenging problem is, therefore, the isolation of the fetal Principal Pseudo-spectral Peak (FPPP) at 30 Hz in the presence of the UCS peak at the same frequency [39-41]. This Chapter proposes using a new pseudo-spectral localiser which incorporates the modified covariance matrix representing the uterine contraction interference signals plus coexisting noise artefact, and seeks to reduce the influence of background uterine activities in the pseudo-spectral MUSIC localisation procedure by partitioning the two subspaces; one contains the desired signal parameters and the other contain the UCS parameters. An accurate estimate of the UCS modified covariance matrix, however, is needed to be incorporated in the pseudo-spectral localiser. For this purpose, a portion of the data that contains only noise fields and does not contain any signal information such as the P-waves or the QRS-complexes is utilised. When such a segment of the data that is P-wave- and QRS-complex-free is sufficiently long for the MUSIC pseudo-spectral localiser (in this case 250 msec or 250 samples at 1 KHz sampling rate), an accurate estimate of the UCS modified covariance matrix can be obtained.

6.3.4 The criteria used in the evaluation of spectral estimation methods

In evaluating spectral and spatio-temporal estimation methods employed in Radar, Sonar, and biomedical signals such as electroencephalogram and magnetocardiogram, three criteria are usually used. The first is ***resolution***: the ability of an estimate to reveal the presence of two equal-energy sources which have nearly equal bearings. When the

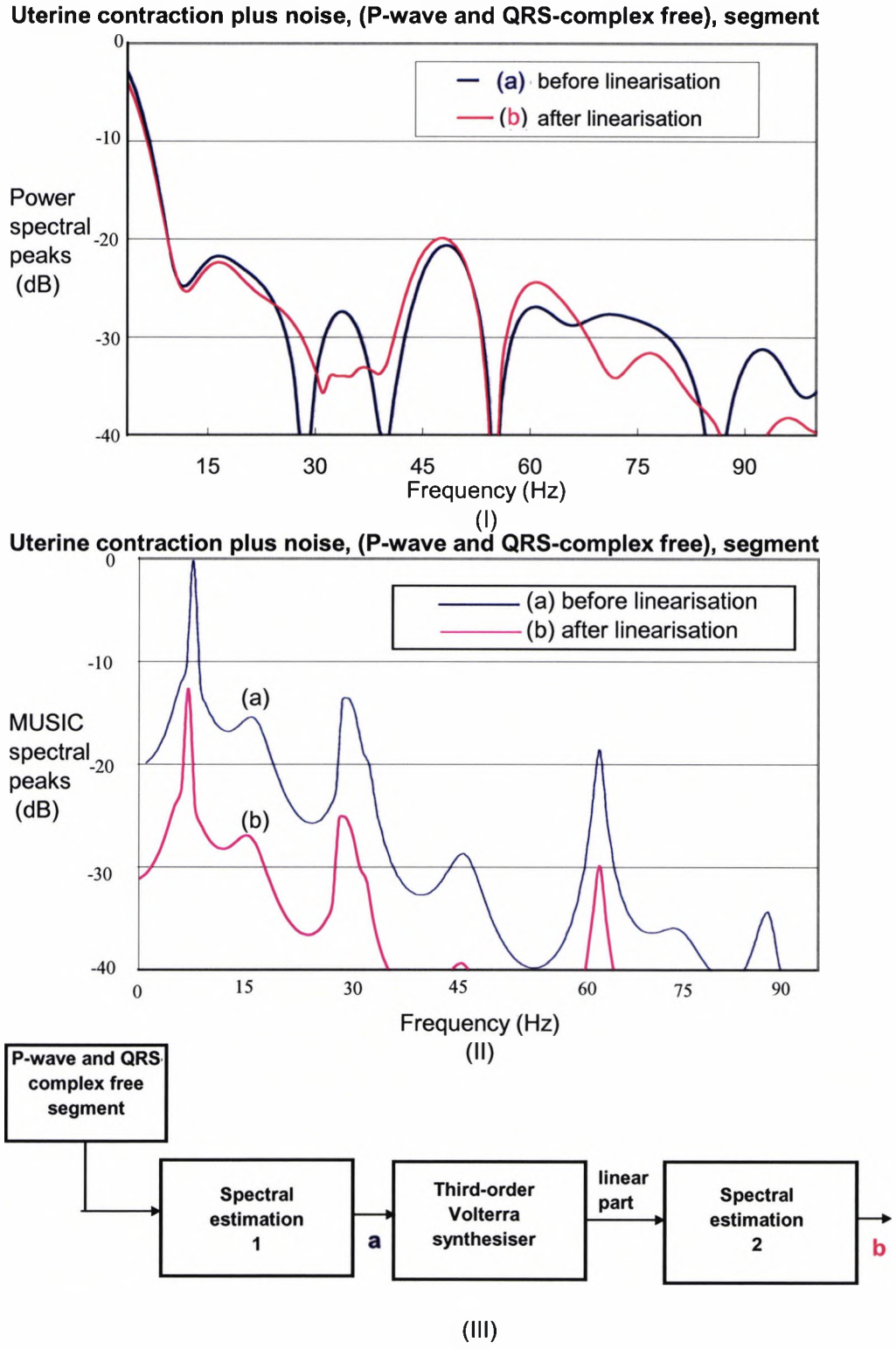

Figure 6.2: *Spectral properties of a uterine contraction plus noise segment. (I) Power spectrum (in dB) and (II) Kaiser shaped weighted MUSIC pseudo-spectral peaks (in dB) before (a) and after (b) linearisation using only the linear part of the output of a third-order Volterra synthesiser. The output consists of the linear, quadratic, and cubic parts of the transabdominally-measured ECG 250 msec segment, and free of both P-waves and QRS-complexes. (III) Linearisation signal processing used in Figures (I) and (II). The Welch averaged periodogram method is used to calculate the power spectrum. The MUSIC model order is 11 and 4 for the signal and noise subspaces, respectively. Optimised Kaiser weighting coefficients were used. Volterra synthesiser parameters are: filter length = 6, delay = 2, step-size parameters =0.001, 0.0001, 0.00001, for linear, quadratic and cubic parts, respectively. Code: 9-67.*

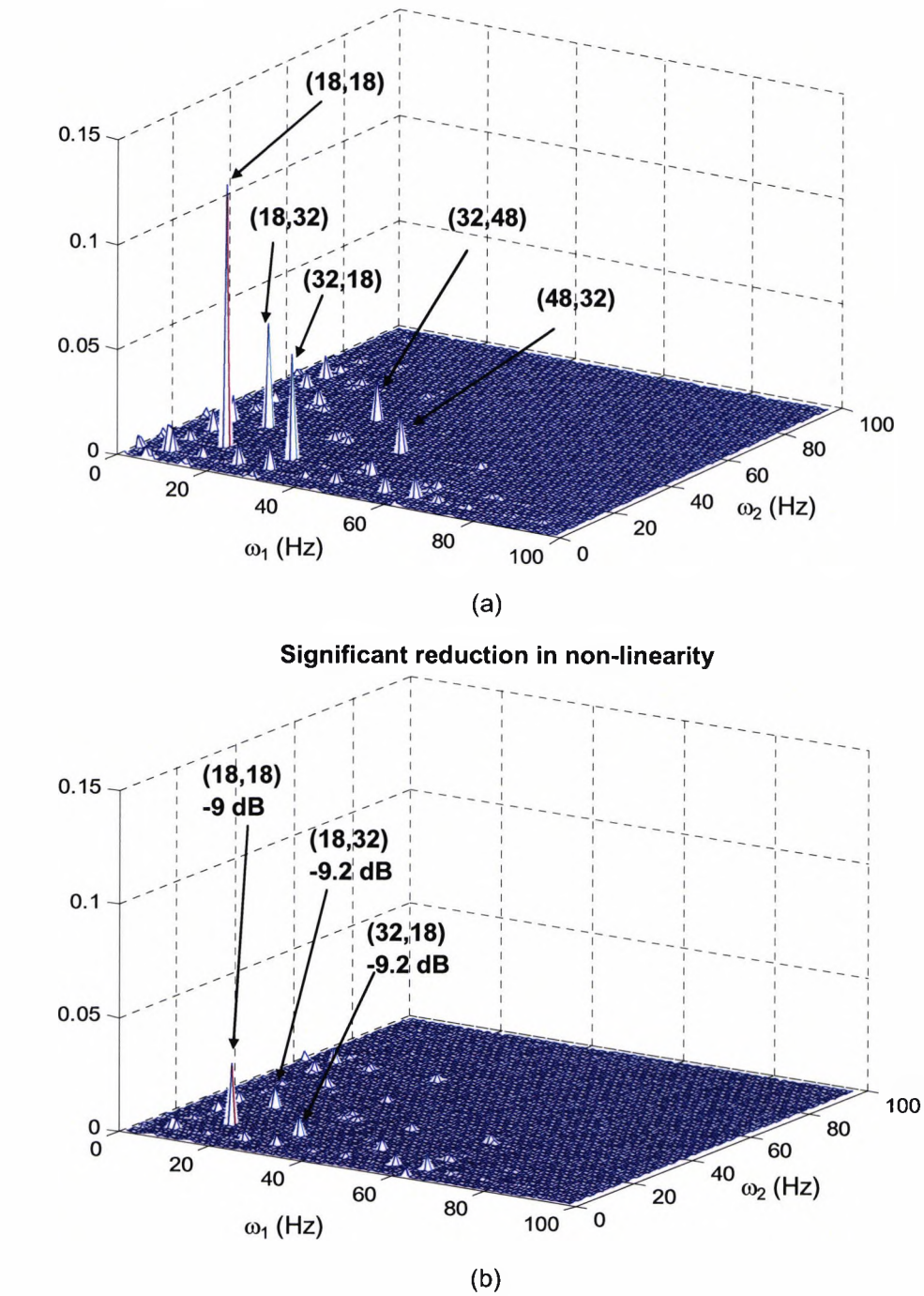

Figure 6.3: *The bicoherence squared (Kaiser shaped window) of the transabdominally-measured ECG 250 msec segment which is free from both the P-waves and the QRS-complexes (a) before and (b) after linearisation using a third-order Volterra synthesiser.* Retaining only the linear part results in a significant reduction in artefact. The direct method was used to calculate the bispectrum and then normalised with the Welch averaged periodogram to obtain the bicoherence squared. * The Volterra synthesiser parameters are: filter length = 6, delay = 2, step-size parameters =0.001, 0.0001, 0.00001, for linear, quadratic and cubic parts, respectively. Code: 9-67.*

First fetal heartbeat bispectral contour

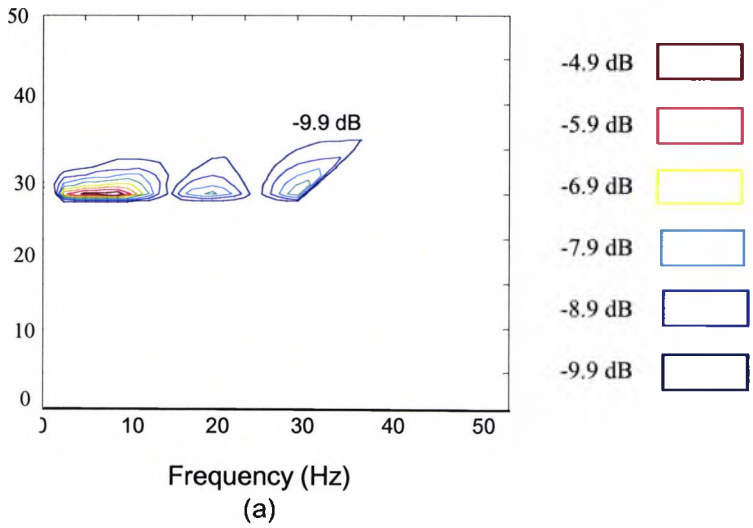

Fetal scalp electrode bispectral contour

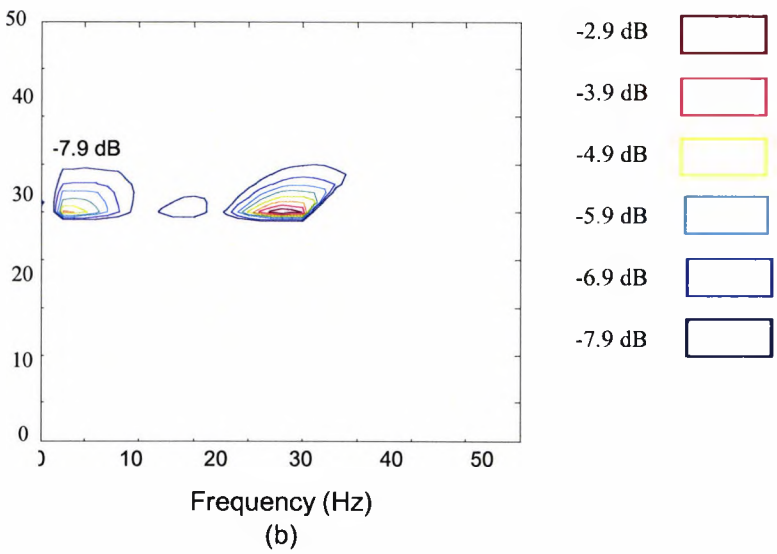

Figure 6.4: *(a) Bispectral contours for the transabdominally-measured ECG 250 msec segment containing the first fetal heartbeat with maternal contribution. (b) Bispectral contours for the synchronised fetal scalp electrode ECG. The bispectrum is calculated using the direct method with a Kaiser window applied to the 250 msec segment.*

two signal sources are resolved, two distinctive peaks are present in the spectrum; if not resolved, only one peak is found. A spectral estimate yielding the sharpest peak usually implies that the bearing has been resolved. However, the sharpness of a peak can always be increased by raising the spectrum to a power greater than one. Such a computation does not increase the accuracy to which source bearings can be distinguished. In the case presented in this thesis a fetal heartbeat is detected only when the fetal principal peak at 30 Hz raises above a predetermined threshold. Therefore, it is of crucial importance to eliminate any other contribution to the spectrum at this particular frequency. The FPPP artificial sharpness will have a marginal effect on the outcome in a fully automated system.

The second criterion is the ***bias of the estimate***. When one source is present, the bias (the error in the location of the spectral peak) is usually zero (the estimate is unbiased). However, when the two sources are present, the bias is usually non-zero. These two criteria of the "goodness" of a spectrum may conflict: Good resolution is often obtained at the expense of a biased estimate. In the fetal case, the higher the bias, the more the deviation of the detected FPPP away from the actual FPPP at around 30 Hz will be.

The third criterion is ***variability***: the range of frequencies "bearings" over which the location of a spectral peak can be expected to vary. Analytical evaluation of the variability for a given spectral estimate is usually difficult. From a practical point of view, the first, second, and possibly third fetal heartbeat within one maternal cardiac cycle may exhibit frequencies at 28 Hz, 29 Hz, 30 Hz, ..., 37Hz, and 38 Hz while the actual fetal scalp measured frequencies are much more confined to a range of 30 Hz to 32 Hz. This is primarily due to the second and third fetal QRS-complexes overlapping with the maternal T-wave or the next P-wave within the fourth segment of the maternal cardiac cycle.

6.3.5 The Problem of coincident mother's and fetal QRSs

Difficult situations arise in which the maternal and fetal heart rates are almost commensurate. Episodes of coincident or near coincident mother's and fetal QRS-complexes have been found in about 10% of the transabdominal ECG data. In such episodes about every ten seconds a fetal heartbeat coincides with the maternal QRS-complex. This is similar to one problem which has often arisen in Radar

applications [54] and it revolves around having two coincident targets with different temporal and spectral characteristics. Such a problem and others different in nature (Sonar, and underground buried objects) have been dealt with using one or two of the following spectral estimation methods that are based on partitioning the signal and noise subspaces; (i) the conventional multiple signal classification (MUSIC) method [4], (ii) the Pisarenko harmonic decomposition method [71], (iii) the eigenvector method [1-2], and (iv) the minimum norm method [1-2]. Such subspace parameter or frequency estimation methods differ only in what "sub-subspace" of the noise subspace they each use [1, 21, 51].

The best candidate in the literature of modern super-resolution spectral methods, which can accommodate both peak resolvability and modification to either the signal subspace or the so called noise subspace is the spectral multiple signal classification (MUSIC). The MUSIC is a highly popular eigenvector-based suboptimal parameter (or frequency) estimation method which has partly supplanted the optimal and more traditional Maximum Likelihood (ML) approach because the MUSIC is computationally more efficient and offers estimation performance comparable with that of the ML method in lower SNR or shorter data sample.

6.4 Previous studies have paved the way for the new development

6.4.1 Joint publications

In previous publications, second- and third-order weighted spectral MUSIC techniques to detect adult's QRS-complexes and anomalous P-waves, e.g., P-on-T waves and P-on-QRS waves which are extremely difficult to spot by observing ECG recordings have been presented [37-38]. The fetal heartbeat detection scheme which recognises prominent FPPP and appropriately reconfigures the signal and noise subspaces to enhance the FPPP against all background contamination is reminiscent of the previously published scheme which was aimed at adult's QRS-complex and P-wave detection schemes. Now, a few reconfigured and optimised subspace templates for the fetal QRS principal pseudo-spectral peaks (FPPPs) have to be purposely developed from clinical databases (see Sections 1.8 and 4.1.6). For brevity, the spectral estimate will be referred to as the weighted spectral MUSIC because by virtue of definition the conventional MUSIC is not weighted. However, the high success rate which has been achieved using the weighted spectral MUSIC to detect adult's QRS-complexes and P-waves cannot be

guaranteed in detecting FPPPs which is sometimes at –20 dB (normalised to the MPPPs), and overlapping with strong spectral components attributed to non-QRS signals and uterine activities in noise even after the quintessential linearisation process. The incorporation, therefore, of a modified covariance matrix representing the instantaneous uterine activity within the realm of the maternal cardiac cycle, into the weighted spectral MUSIC algorithm is the second most crucial step (the first being linearisation of the ECG) in separating coincident mother's and fetal QRS-complexes during labour in the linearised weighted spectral MUSIC fetal heartbeat detection.

6.4.2 Virtues and vices of the conventional MUSIC

The MUSIC algorithm is a product of an eigenvector-based projection approach to the mathematical formulation of the temporal problem of estimating the frequencies of complex sinusoids in additive noise. Basically, the rationale of such an approach is to partition the observation space (observed or measured data), spanned by the eigenvectors of a correlation matrix (or data covariance matrix), into two subspaces that are referred to as the signal subspace and the noise subspace. It has to be emphasised that the noise is assumed to be white Gaussian [57-60]. The algorithm forms a null spectrum with the noise-subspace eigenvectors of the data correlation matrix and then searches iteratively for nulls in this spectrum. The MUSIC, in this spectral form, needs to perform a computationally expensive, say, $\mathcal{M}$-dimensional iterative search for $\mathcal{L}$ extrema of a highly non-linear scalar function to estimate the $\mathcal{M}$ parameters of all $\mathcal{L}$ signal frequency sources. Clearly, the signal is a continuous function, but as it is recorded, say, every 1 msec, it can be thought of as a vector of dimensionality as large as the number of milliseconds in the subject's mean heart cycle, or in our case the 250 msec temporal window. Whether this iteration converges to the global (rather than the local) optimum and the speed of convergence depend on the availability of *a priori* estimates of the number of spectral peaks in the maternal and fetal ECG signal subspaces and noise subspaces close to the actual global optimum (the model order for the signal and noise subspaces). If the $\mathcal{L}$-dimensional signal subspace is estimated perfectly, then the signal frequencies are simply found at the $\mathcal{L}$ global maximisers. Any errors in our estimate would yield a single global maximum and at least ($\mathcal{L}$-1) local maxima. Finding the first frequency source is simple over a sufficiently densely sampled signal grid. Identifying the remaining local maxima becomes more difficult since non-linear search techniques may miss shallow or adjacent peaks and return to a

previous peak. Any "peak-picking" algorithm would rapidly become complex and subjective as the model order increases. In order to avoid such a problem when dealing with transabdominally-measured combined maternal and fetal signals, we now introduce the sequentially optimised, weighted MUSIC.

6.5 Detailed statement of research

6.5.1 The sequentially optimised, weighted MUSIC algorithm

The novelty of the sequentially optimised, weighted MUSIC applied to first enhance the mother's principal pseudo-spectral peak and then the fetal principal pseudo-spectral peak is to avoid the above mentioned peak-picking problem entirely. We, instead, remove the component of the signal subspace that is spanned by the first maternal source with its principal lobes and sidelobes and then perform a search to find the fetal frequency source as the new global maximiser over the modified subspace. In this way, we replace the problem of finding $\mathcal{L}$ local maxima with one in which we find the frequency sources as $\mathcal{L}$ global maxima over their respective modified signal subspaces. To expand on this, the algorithm first reads the data sample (250 msec window) and uses an optimum weighting function developed from the mother's chest ECG which yields the MPPP at around 17 Hz [38]. And then the algorithm goes back and re-reads the same data sample having modified the subspace with a newly weighted function which is developed entirely from the fetal scalp electrode database and yields the FPPP at around 30 Hz (this can be adjusted to cater for FPPPs at 28 Hz, 29 Hz, 30 Hz, 31 Hz, 32 Hz, …., 37 Hz, and 38 Hz).

6.5.2 The reconfigured interference plus noise subspace to incorporate the modified covariance matrix of the linearised non-Gaussian uterine activity in the weighted MUSIC estimator

In an exhaustive study recently completed on abdominal electromyographic signals (AEMG) during labour contractions [35], it has been demonstrated in the most convincing way possible that the underlying dynamics of such contractions are indeed multi-fractal chaotic. Work is now in progress to identify a system of non-linear differential equations responsible for the generation of different classes of labour contractions, particularly pre-term cases. The best we can do at present is to build a non-linear model that captures the underlying non-linear dynamics responsible for the generation of such chaotic contractions. The modelling of chaotic physiological systems

from stimulus-response data has advanced in recent years. Most notably, the introduction of a new family of embedded multi-step Volterra-like structures [36] which exploits the non-linear signal dynamics embedded in the attractor and integrates them in the design of such structures to gauge the long-term behaviour of the dynamics. Short data samples that can be classified as predominantly uterine noise artefact must be isolated within the maternal cardiac cycle and the computation of $\mathbf{I}_{noise}$ which represents the modified covariance matrix is performed right at the start of the algebraic matrix formulation as will be shown in Section 6.8.

The data portions earmarked for the UCS modified covariance matrix ($\mathbf{I}_{noise}$) are 250 msec long (see Figure 6.9), falling mostly within segments III in the case of those maternal cardiac cycles that are free from coincident mother and fetal QRS-complexes in segments I, **OR** in segments II and IV for maternal cardiac cycles that do exhibit occurrences of coincident mother and fetal QRS-complexes in Segments I.

6.6 Mathematical formulation of the conventional MUSIC (The analysis given in this section is based on *Adaptive filter theory*, S. Haykin, Ch. 12, pp. 445-455, Prentice Hall, 2nd edition, 1991, [1]).

6.6.1 Conventional MUSIC assumptions

Consider a received signal {u(i)} that consists of L complex sinusoids whose complex amplitudes are α_1, α_2, ..., α_L and whose angular frequencies are ω_1, ω_2, ..., ω_L, respectively. Specifically, u(i) of the received signal is written as [1]:

$$u(i) = \sum_{l=1}^{L} \alpha_l \exp(j\omega_l i) + v(i), \qquad i = 0, 1, \ldots, N-1 \tag{6.9}$$

where $v(i)$ is a complex sample of additive receiver noise, and N is the total data length. The following assumptions are made:

1- The complex sinusoidal components of the received signal are uncorrelated with each other, which means that

$$E[\alpha_k \alpha_l^*] = \begin{cases} P_l, & k = l \\ 0, & k \neq l \end{cases} \tag{6.10}$$

2- The receiver noise is white, which means that

$$E[v_i v_j^*] = \begin{cases} \sigma^2, & j = i \\ 0, & j \neq i \end{cases} \tag{6.11}$$

6.6.2 Data processing

For the processing (filtering) of data, it is proposed to use a transversal filter of length M + 1 as indicated in Figure 6.5. Given the time series of Eq. (6.9), the problem then is to estimate the unknown amplitudes and unknown frequencies contained in the time series.

6.6.3 Data Matrix

Given the time series of length N as in Eq. (6.9) and the transversal filtering structure of length M + 1 as in Figure 6.5, we may define the data matrix **A** by writing

$$\mathbf{A}^H = \underbrace{\begin{bmatrix} u(M) & \cdots & u(N-1) \\ u(M-1) & \cdots & u(N-2) \\ \vdots & & \vdots \\ u(0) & \cdots & u(N-M+1) \end{bmatrix}}_{\text{forward half}} \quad \underbrace{\begin{bmatrix} u^*(0) & \cdots & u^*(N-M+1) \\ u^*(1) & \cdots & u^*(N-M+2) \\ \vdots & & \vdots \\ u^*(M) & \cdots & u^*(N-1) \end{bmatrix}}_{\text{backward half}} \tag{6.12}$$

The elements constitute the left half of the matrix $\mathbf{A}^H$ in Eq. (6.12) represent the various sets of tap inputs used for forward filtering. The complex conjugated elements constituting the right half of the matrix $\mathbf{A}^H$ represent the corresponding sets of tap inputs used for backward filtering. Note that in the forward or backward half in Eq. (6.12), as we move from one column of $\mathbf{A}^H$ to the next, we drop one input sample and add a new

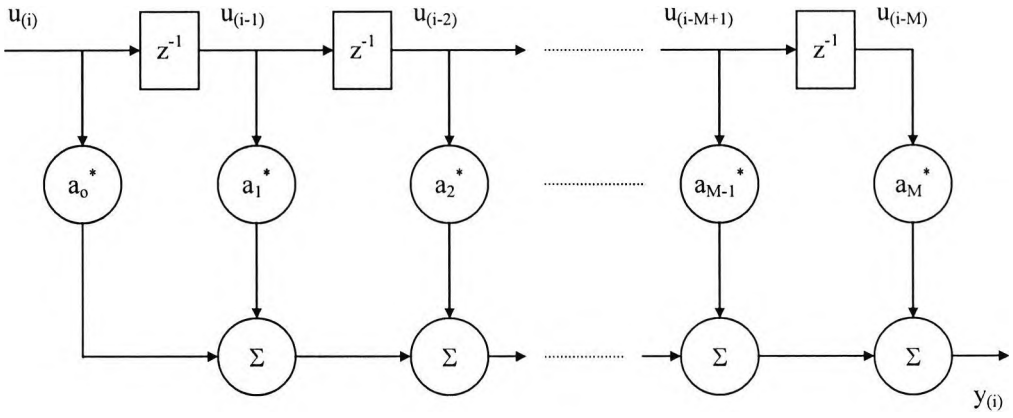

Figure 6.5: *Transversal filter for temporal processing.*

one, and of course reorder the data. This has the effect of temporal smoothing.

6.6.4 The conventional MUSIC algorithm

To motivate the development of the multiple signal classification (MUSIC) algorithm [4-6], consider first the (M + 1)-by-(M + 1) ensemble averaged covariance matrix **R** for an input signal that consists of L uncorrelated zero-mean complex sinusoids and an additive white-noise process of zero mean and variance σ^2, as in Eq. (6.9). The angular frequencies of the sinusoids are denoted by $\omega_1, \omega_2, \ldots, \omega_L$, and their average power by $P_1, P_2, \ldots, P_L$. We may thus express the ensemble-averaged covariance matrix **R** in the following form:

$$\mathbf{R} = \mathbf{S}\,\mathbf{D}\,\mathbf{S}^H + \sigma^2\,\mathbf{I}, \tag{6.13}$$

where **I** is the (M + 1)-by-(M + 1) identity matrix. The rectangular matrix **S** is the (M + 1)-by-L frequency matrix defined by:

$$\mathbf{S} = [\mathbf{s}_1, \mathbf{s}_2, \ldots, \mathbf{s}_L] = \begin{bmatrix} 1 & 1 & \cdots & 1 \\ \exp(-j\omega_1) & \exp(-j\omega_2) & \cdots & \exp(-j\omega_L) \\ \exp(-j2\omega_1) & \exp(-j2\omega_2) & \cdots & \exp(-j2\omega_L) \\ \vdots & \vdots & \vdots & \vdots \\ \exp(-jM\omega_1) & \exp(-jM\omega_2) & \cdots & \exp(-jM\omega_L) \end{bmatrix} \quad (6.14)$$

Note that the lth column of the matrix **S**, namely, the vector $\mathbf{s}_l$ is determined by the lth complex sinusoid of angular frequency ω_l. The diagonal matrix **D** in Eq. (6.13) is the K-by-K covariance matrix of the sinusoids, defined by

$$\mathbf{D} = \text{diag}(P_1, P_2, ..., P_L), \quad (6.15)$$

Let $\lambda_1 \geq \lambda_2 \geq .. \geq \lambda_{M+1}$ denote the eigenvalues of **R**, and $\nu_1 \geq \nu_2 \geq .. \geq \nu_{M+1}$ denote the eigenvalues of $\mathbf{S}\,\mathbf{D}\,\mathbf{S}^H$, respectively. Then, from the representation shown in Eq. (6.13) we deduce that

$$\lambda_i = \nu_i + \sigma^2, \qquad i = 1, 2, ...M + 1 \quad (6.16)$$

We assume that the signal matrix **S** is of full column rank L, which is justified if the L complex sinusoids in the time series of Eq. (6.9) have distinct frequencies, and the L columns of the matrix **S** are, therefore, linearly independent. This assumption then implies that the (M + 1 - L) smallest eigenvalues of the matrix $\mathbf{S}\,\mathbf{D}\,\mathbf{S}^H$ are equal to zero. Correspondingly, the smallest eigenvalue of the covariance matrix **R** is equal to σ^2 with multiplicity (M + 1 – L), as shown by

$$\lambda_i = \begin{cases} \nu_i + \sigma^2, & i = 1,....,L \\ \sigma^2, & i = L+1,....,M+1 \end{cases} \quad (6.17)$$

Note that, in general, $v_i \neq P_i$, i = 1, 2, …, L. Figure 6.6 illustrates a plot of λ_i versus i for L = 8 and M = 10, assuming an additive white noise background. Such a plot is referred to as an eigen-spectrum.

Let $\mathbf{q}_1$, $\mathbf{q}_2$, …, $\mathbf{q}_{M+1}$ denote the eigenvectors of the covariance matrix **R**. All the (M + 1 – L) eigenvectors associated with the smallest eigenvalues of **R** satisfy the relation

$$\mathbf{R}\,\mathbf{q}_i = \sigma^2\,\mathbf{q}_i, \qquad i = L + 1, \ldots, M + 1 \tag{6.18}$$

or equivalently,

$$(\mathbf{R} - \sigma^2\mathbf{I})\,\mathbf{q}_i = \mathbf{0}, \qquad i = L + 1, \ldots, M + 1 \tag{6.19}$$

Using Eq. (6.13), we may rewrite Eq. (6.19) as

$$\mathbf{S}\,\mathbf{D}\,\mathbf{S}^H\,\mathbf{q}_i = \mathbf{0}, \qquad i = L + 1, \ldots, M + 1 \tag{6.20}$$

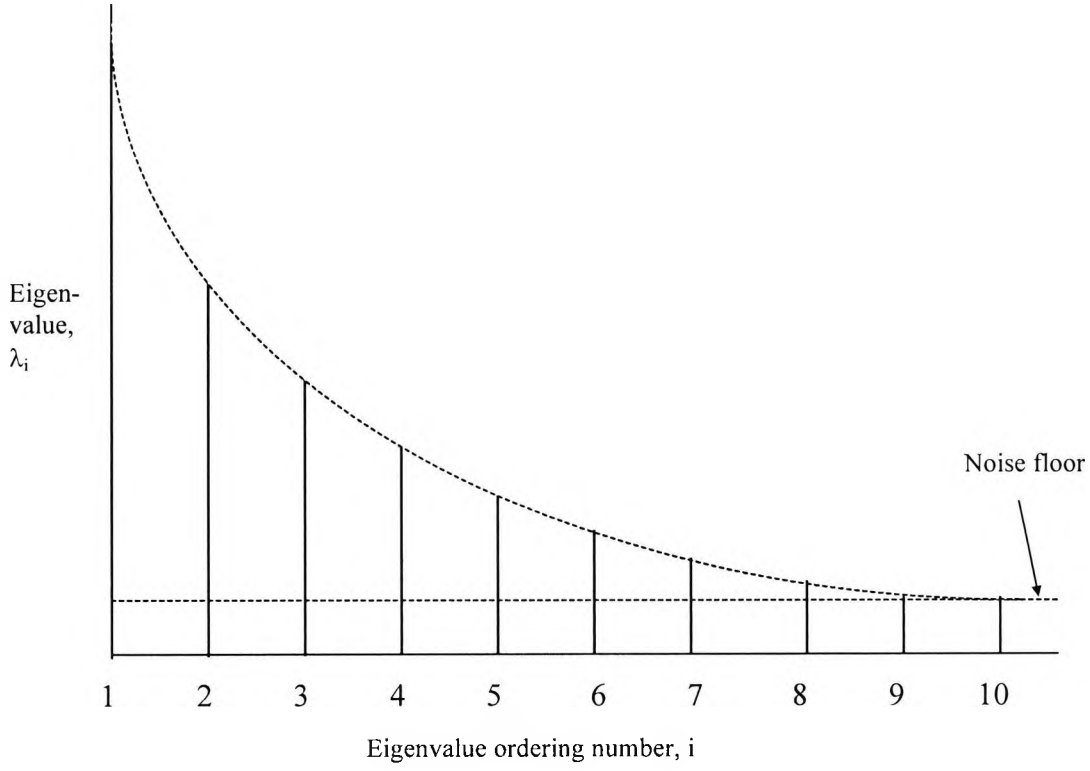

Figure 6.6: *An eigen-spectrum.*

Since the matrix **S** is assumed to be of full column rank L and since the matrix **D** is diagonal with all entries being non-zero, which is a consequence of Eq. (6.10), it follows from Eq. (6.20) that

$$\mathbf{S}^H \mathbf{q}_i = \mathbf{0}, \qquad i = L + 1, \ldots, M + 1 \tag{6.21}$$

or more explicitly, from the line of Eq. (6.14)

$$\mathbf{s}_l^H \mathbf{q}_i = \mathbf{0}, \qquad \begin{matrix} i = L + 1, \ldots, M + 1 \\ l = 1, 2, \ldots, L \end{matrix} \tag{6.22}$$

where the vector $\mathbf{s}_l$ constitutes the lth column of matrix **S**.

A fundamental property of the eigenvectors of a covariance matrix is that they are orthogonal to each other. Hence, the eigenvectors $\mathbf{q}_1, \ldots, \mathbf{q}_L$ span a subspace that is the orthogonal complement of the space spanned by the eigenvectors $\mathbf{q}_{L+1}, \ldots, \mathbf{q}_{M+1}$. Accordingly, we deduce from Eq. (6.21) that

$$\text{span } \{\mathbf{s}_1, \ldots, \mathbf{s}_L\} = \text{span } \{\mathbf{q}_1, \ldots, \mathbf{q}_L\} \tag{6.23}$$

The span $\{\mathbf{s}_1, \ldots, \mathbf{s}_L\}$refers to a subspace that is defined by the set of all linear combinations of the vectors $\mathbf{s}_1, \ldots, \mathbf{s}_L$. The span $\{ \mathbf{q}_1, \ldots, \mathbf{q}_L\}$is similarly defined.

Thus, the eigenvalue decomposition of the (M + 1)-by-(M + 1) covariance matrix **R** of superimposed complex sinusoids in noise suggests the following two important observations:

1- The space spanned by the eigenvectors of **R** consists of two disjoint subspaces: One subspace called the signal plus noise subspace, is spanned by the eigenvectors associated with the L largest eigenvalues of **R**. The second subspace, called the noise subspace, is spanned by the eigenvectors associated with the (M + 1 – L) smallest eigenvalues of **R**. These two subspaces are orthogonal complement of each other. This first observation follows from Eq. (6.22).

2- Given the eigenvectors of **R**, we may define the frequencies of the complex sinusoids in the input signal by searching for those sinusoidal signal vectors $\mathbf{s}_k$ that are orthogonal to the noise subspace. This second observation follows from Eq. (6.21).

6.6.5 Practical Considerations

We may use a sample average that equals the scaled version of the covariance matrix $\mathbf{\Phi}$, as shown by

$$\hat{\mathbf{R}} = \frac{1}{2(N-M)}\mathbf{\Phi}, \tag{6.24}$$

where $\mathbf{\Phi}$ is itself related to the data matrix **A** as follows

$$\mathbf{\Phi} = \mathbf{A}^H\mathbf{A}, \tag{6.25}$$

and the scaling factor, 1 / [2 . (N - M)], accounts for the fact that the time averaging is performed over 2 (N - M) data points. In any event, let $\mathbf{v}_1, \mathbf{v}_2, \ldots, \mathbf{v}_{M+1}$ denote the eigenvectors of the estimate $\hat{\mathbf{R}}$. In accordance with observation 1, we may define a set of eigenvectors $\mathbf{v}_1, \mathbf{v}_2, \ldots, \mathbf{v}_L$ associated with the L largest eigenvalues of the estimate $\hat{\mathbf{R}}$, and a set of eigenvectors $\mathbf{v}_{L+1}, \ldots, \mathbf{v}_{M+1}$ associated with the (M + 1 – L) smallest eigenvalues of $\hat{\mathbf{R}}$. Let

$$\mathbf{V}_N = [\mathbf{v}_{L+1}, \ldots, \mathbf{v}_{M+1}] \tag{6.26}$$

and

$$\mathbf{V}_s = [\mathbf{v}_1, \mathbf{v}_2, \ldots, \mathbf{v}_L]. \tag{6.27}$$

We naturally have

$$\mathbf{V}_N^H\mathbf{V}_s = \mathbf{0} \tag{6.28}$$

which is in line with observation 1. However, owing to the presence of uncertainty in

the eigenvector estimates, $\mathbf{v}_1$, $\mathbf{v}_2$, ..., $\mathbf{v}_{M+1}$, arising because of the finite number of samples used to generate $\hat{\mathbf{R}}$, the orthogonality relations of Eq. (6.21) that are responsible for observation 2 no longer hold. In the context of the latter point, we can search for the signal vectors that are most closely orthogonal to the noise subspace. Accordingly, in the MUSIC algorithm it is proposed to estimate the angular frequencies of the complex sinusoids in the input signal as the peaks of the MUSIC spectrum estimate:

$$\hat{S}_{MUSIC}(\omega) = \frac{1}{\sum_{i=L+1}^{M+1} \left| \mathbf{s}^H \mathbf{v}_i \right|^2} = \frac{1}{\mathbf{s}^H(\omega)\mathbf{V}_N \mathbf{V}_N^H \mathbf{s}(\omega)} \tag{6.29}$$

where the variable frequency vector or frequency scanning vector $\mathbf{s}(\omega)$ is defined by

$$\mathbf{s}^T(\omega) = [1, e^{-jw}, \ldots, e^{-jw(M-L)}] \tag{6.30}$$

The product $\mathbf{V}_N \mathbf{V}_N^H$ represents a projection on the noise subspace.

Eq. (6.29) for the MUSIC spectrum* is based on the use of a projection matrix related to the noise subspace. It can be shown that the MUSIC spectrum may also be computed using the formula

$$\hat{S}_{MUSIC}(\omega) = \frac{1}{M + 1 - \mathbf{s}^H(\omega)\mathbf{V}_s \mathbf{V}_s^H \mathbf{s}(\omega)} \tag{6.31}$$

where M + 1 is the dimension of the data matrix, $\mathbf{V}_s \mathbf{V}_s^H$ is the projection matrix on the signal subspace, and $\mathbf{s}(\omega)$ is a frequency scanning vector. Note that although this formula and that of Eq. (6.29) are mathematically equivalent, they make different computational demands. Appendix A9 describes a summary of the conventional MUSIC

* Note that the $\hat{S}_{MUSIC}(\omega)$ is based on a single realisation of the underlying stochastic process represented by the given data matrix **A**. As such, it represents an estimate of the exact MUSIC spectrum based on the eigen-decomposition of the ensemble-averaged covariance matrix of the process, hence the use of a hat in the symbol $\hat{S}_{MUSIC}(\omega)$.

algorithm and some computational considerations.

6.7 Mathematical formulation of the incorporation of I_{noise} in the sequentially weighted MUSIC

6.7.1 Weighted MUSIC for mother's and fetal QRS principal pseudo-spectral peaks

Eq. (6.29) is the formula used in the MUSIC algorithm for estimating the frequencies of complex sinusoids that are corrupted by additive white noise. Note that in this formula all the singular vectors that constitute the matrix $\mathbf{V}_N$, in accordance with Eq. (6.22) are weighted equally.

Since the mother's and fetal QRS-complex principal pseudo-spectral peaks (MPPPs) and (FPPPs) occur around 17 Hz and 30 Hz, respectively, it is prudent to introduce some sort of optimised weighting functions, $\mathbf{W}_{mi}$ and $\mathbf{W}_{fi}$, to enhance the mother's and fetal QRS-complex principal pseudo-spectral peaks (MPPPs) and (FPPPs) around 17 Hz and 30 Hz, respectively. This weighting is considered crucial factor in isolating the principal pseudo-spectral peaks in both the mother's and the fetal QRS-complexes. Appendix A6 describes such a weighting filter based on Kaiser window [7].

The weighted MUSIC for the mother's and fetal QRS-complexes is described by Eqs. (6.32) – (6.33), respectively:

$$\hat{S}_{MUSIC}(\omega) = \frac{1}{\sum_{i=L+1}^{M+1} \mathbf{W}_{mi} \left| \mathbf{s}^H \mathbf{v}_i \right|^2}, \tag{6.32}$$

$$\hat{S}_{MUSIC}(\omega) = \frac{1}{\sum_{i=L+1}^{M+1} \mathbf{W}_{fi} \left| \mathbf{s}^H \mathbf{v}_i \right|^2}. \tag{6.33}$$

6.7.2 The sequentially optimised weighted MUSIC with the incorporation of the modified covariance matrix of the UCS, I_{noise}

The theory of the MUSIC described in this chapter has been based on the assumption

that the additive noise process {v(i,k)} is white and satisfies the following condition

$$E[v(i,k)v^*(j,k)] = \begin{cases} \sigma^2, & j = i \\ 0, & j \neq i \end{cases} \tag{6.34}$$

where the variance σ^2 is common. In other words, the covariance matrix of the noise process {v(i,k)} consists of a diagonal matrix equal to σ^2 **I**, where **I** is an identity matrix. Correspondingly, the ensemble-averaged covariance matrix of the received signal process {u(i,k)}has the form given in Eq. (6.5), reproduced here for convenience

$$\mathbf{R} = \mathbf{S}\,\mathbf{D}\,\mathbf{S}^H + \sigma^2\,\mathbf{I}, \tag{6.35}$$

where the matrices **S** and **D** are the (M + 1)-by-L frequency matrix and the diagonal matrix defined by the average power in the input signal, respectively.

In a more general case of a coloured noise background, the covariance matrix of the noise process {v(i,k)} takes on a non-diagonal structure. Correspondingly, the covariance matrix of the received signal process {u(i,k)}is modified as follows

$$\mathbf{R} = \mathbf{S}\,\mathbf{D}\,\mathbf{S}^H + \mathbf{I}_{noise} \tag{6.36}$$

where $\mathbf{I}_{noise}$ is the covariance matrix of the UCS plus noise {v(i,k)}. The MUSIC algorithm may indeed be generalised to deal with this new situation.

Here is a brief description of the generalisation process. In the above equation we assumed that the noise and signal are uncorrelated. Let us denote $\tilde{\mathbf{g}}_i$ as an eigenvector obtained by solving the generalised eigenvalue problem

$$\mathbf{R}\,\tilde{\mathbf{g}}_i = \lambda_i\,\mathbf{I}_{noise}\,\tilde{\mathbf{g}}_i. \tag{6.37}$$

Using $\tilde{\mathbf{g}}_i$, it is easy to show that

$$(\mathbf{R} - \mathbf{I}_{noise})\,\tilde{\mathbf{g}}_i = \mathbf{S}\,\mathbf{D}\,\mathbf{S}^H\,\tilde{\mathbf{g}}_i = \mathbf{0} \qquad \text{for } i = L+1, \ldots, M+1. \tag{6.38}$$

Since both **S** and **D** are full rank matrices, the above equation results in

$$\mathbf{S}^H \tilde{\mathbf{g}}_i = \mathbf{0} \qquad \text{for } i = L+1, \ldots, M+1. \tag{6.39}$$

Eq. (6.39) indicates that the spectral peaks of the frequency scanning vector $\mathbf{S}^H(\omega)$ can be found by checking the orthogonality between the modified and weighted noise subspace projector $\tilde{\mathbf{G}}_N \tilde{\mathbf{G}}_N^H$ and the sinusoidal vectors. Here $\tilde{\mathbf{G}}_N$ is defined as

$$\tilde{\mathbf{G}}_N = [\tilde{\mathbf{g}}_{L+1}, \ldots, \tilde{\mathbf{g}}_{M+1}]. \tag{6.40}$$

The eigenvectors are normalised in such a way that

$$\tilde{\mathbf{g}}_i^H \mathbf{I}_{noise} \tilde{\mathbf{g}}_i = \delta_{ij}, \tag{6.41}$$

where δ_{ij} is Kronecker's delta = 1 when i = j, and δ_{ij} = 0 when i ≠ j. Therefore, the spectral MUSIC localiser for correlated noise is given by

$$\mathbf{J}(x) = \frac{1}{\lambda_{min}\left[\mathbf{S}^H \tilde{\mathbf{G}}_N \tilde{\mathbf{G}}_N^H \mathbf{S}\ \mathbf{S}^H \mathbf{I}_{noise}^{-1} \mathbf{S}\right]} \tag{6.42}$$

where $\lambda_{min}(.,.)$ indicates the generalised minimum eigenvalue of the matrix pair given in parenthesis. This thesis proposes using the above localiser to reduce the influence of background noise due to uterine activity and other non-Gaussian ECG noise in the spectral MUSIC localisation procedure. An accurate estimate of the noise covariance matrix, however, is needed to use the localiser. For this purpose, one should find a portion of the data that is at least predominantly occupied by noise, if not completely free from any signals. For transabdominally-measured ECG signals, such a portion can be found in a data portion taken in segments free from mother's and fetal QRSs and maternal P-waves.

6.7.3 The concepts of oriented energy and signal-to-signal ratio

This section describes the concepts of oriented energy and oriented signal-to-signal ratio of a vector sequence and shows their relationships with the SVD and GSVD. The

justification behind using the signal-to-signal ratio is to cater for partitioning two subspaces, each contains at least one signal, namely, the signal subspace (S-subspace) containing the mother and fetal QRS-complexes and the interference subspace (I-subspace) containing the UCS.

Consider a sequence of p-vectors $\{\mathbf{a}_k\}$, k = 1, ..., q, and arrange them as the columns of a p x q matrix, **A**. Then $E_e[\mathbf{A}]$, the energy of the vector set in the direction of unit vector $\mathbf{e} \subset \mathcal{R}^p$, is defined as

$$E_e[\mathbf{A}] = \sum_{K=1}^{q} (\mathbf{e}^T \mathbf{a}_k)^2 = \| \mathbf{e}^T \mathbf{A} \|^2 \qquad (6.43)$$

There exists a relationship between the singular values and vectors of the matrix **A** and its directions of extremal oriented energy as follows:

$$E_{u_i}[\mathbf{A}] = \| \mathbf{u}_i^T \mathbf{A} \|^2 = \sigma_i^2 \qquad (6.44)$$

where $\mathbf{u}_i$ is a column vector of **U** in the SVD of **A** (see Appendix A10) and σ_i is the corresponding singular value of **A**. Moreover, we know from linear algebra that each $\mathbf{u}_i$ contains the coefficients of a linear combination of the rows of **A**, such that $\| \mathbf{u}_i^T \mathbf{A} \mathbf{A}^T \mathbf{u}_i \| = \| \mathbf{u}_i^T \mathbf{A} \|^2$ reaches extremal value, which equals σ_i^2. In other words, the columns $\mathbf{u}_i$, of the **U**-matrix in the SVD of **A** provide directions in the column space of **A** for which the oriented energy is extremal. Therefore, the SVD of a matrix **A** finds r_A = rank (**A**) orthonormal directions of extremal oriented energy.

The oriented signal-to-signal ratio, R_e [**A**, **B**], of two sets of p-vectors $\{\mathbf{a}_k\}$ and $\{\mathbf{b}_k\}$, (k = 1, ..., q), in the direction of unit vector $\mathbf{e} \subset \mathcal{R}^p$, is defined as

$$R_e [\mathbf{A}, \mathbf{B}] = E_e[\mathbf{A}] / E_e[\mathbf{B}] = \| \mathbf{e}^T \mathbf{A} \|^2 / \| \mathbf{e}^T \mathbf{B} \|^2 \qquad (6.45)$$

In analogy with the oriented energy-SVD relationship, a relationship between the oriented signal-to-signal ratio concept and the GSVD exists. If the GSVD of matrices **A** and **B** is given as in the GSVD theorem of Appendix A11; then

$$R_e [\mathbf{A}, \mathbf{B}] = (\alpha_i / \beta_i)^2 \quad \text{for } \mathbf{e} = x_i / \| x_i \| \qquad (6.46)$$

For proof see [73-75]. Applied to the signal separation problem, this can be interpreted as follows: assume that **A** contains p signals that are all mixed with an unwanted signal, while **B** contains only contributions from the unwanted signal. The GSVD of the matrix pair (**A**, **B**) then looks for directions in the column space of **A** and **B** for which the oriented ratio of wanted signal to unwanted signal is extremal.

6.7.4 Gram-Schmidt orthogonalisation: An alternative projection method

Now the third orthogonalisation method will be briefly described. In order to facilitate partial or total elimination of the uterine contraction interference signal (UCS) from the composite transabdominal ECG signal (**TECG**) the two signals with noise must first be linearised. This helps to get rid of higher-order trends and may render the signals linear and non-Gaussian. Then the latter composite signal is Gram-Schmidt (GS) orthogonalised [76-78] with the former (the unwanted signal) and projected onto it (see Appendix A13). Both signals can be measured. However, the UCS still contains low levels of the **TECG** signal, e.g., T- and u-waves. Essentially, the **TECG** signal occupies the whole cardiac cycle.

Figure 6.7 illustrates how the composite transabdominal ECG signal (**TECG** = MECG + FECG + the uterine contraction interference signal (UCS) + noise) is represented by the vector OA and Gram-Schmidt (GS) orthogonalised with the UCS represented by the vector OB. The signal OE is perpendicular to the UCS signal, which is free from any component that might correspond to the UCS.

6.7.5 Summary of the sequentially optimised, weighted MUSIC with the incorporation of the modified covariance matrix of the uterine contraction interference signal ($\mathbf{I}_{noise}$)

A flowchart for the sequentially optimised, weighted MUSIC with the incorporation of the modified covariance matrix of the uterine contraction interference signal, $\mathbf{I}_{noise}$, is given in Figure 6.8.

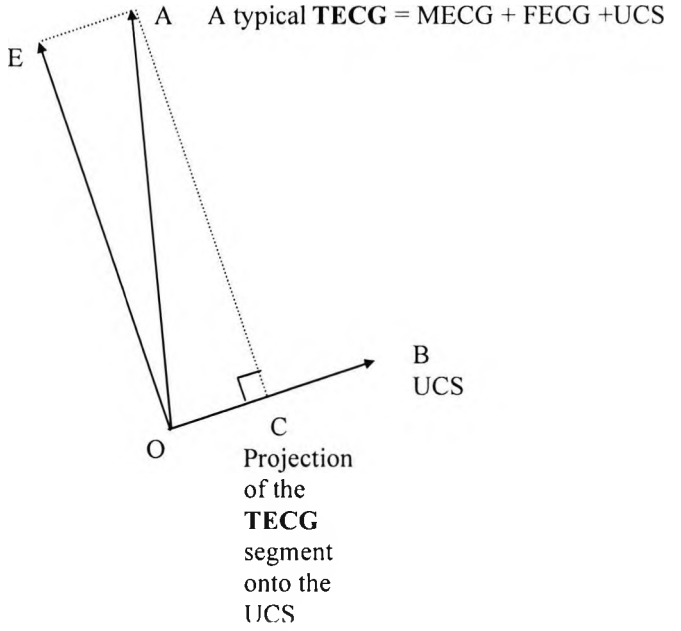

***Figure 6.7**: The composite transabdominal ECG signal (**TECG** = MECG + FECG + the uterine contraction interference signal (UCS) + noise) is represented by the vector OA and Gram-Schmidt (GS) orthogonalised with the UCS represented by the vector OB. The signal OE is perpendicular to the UCS signal, which is free from any component that might correspond to the UCS.*

To be continued

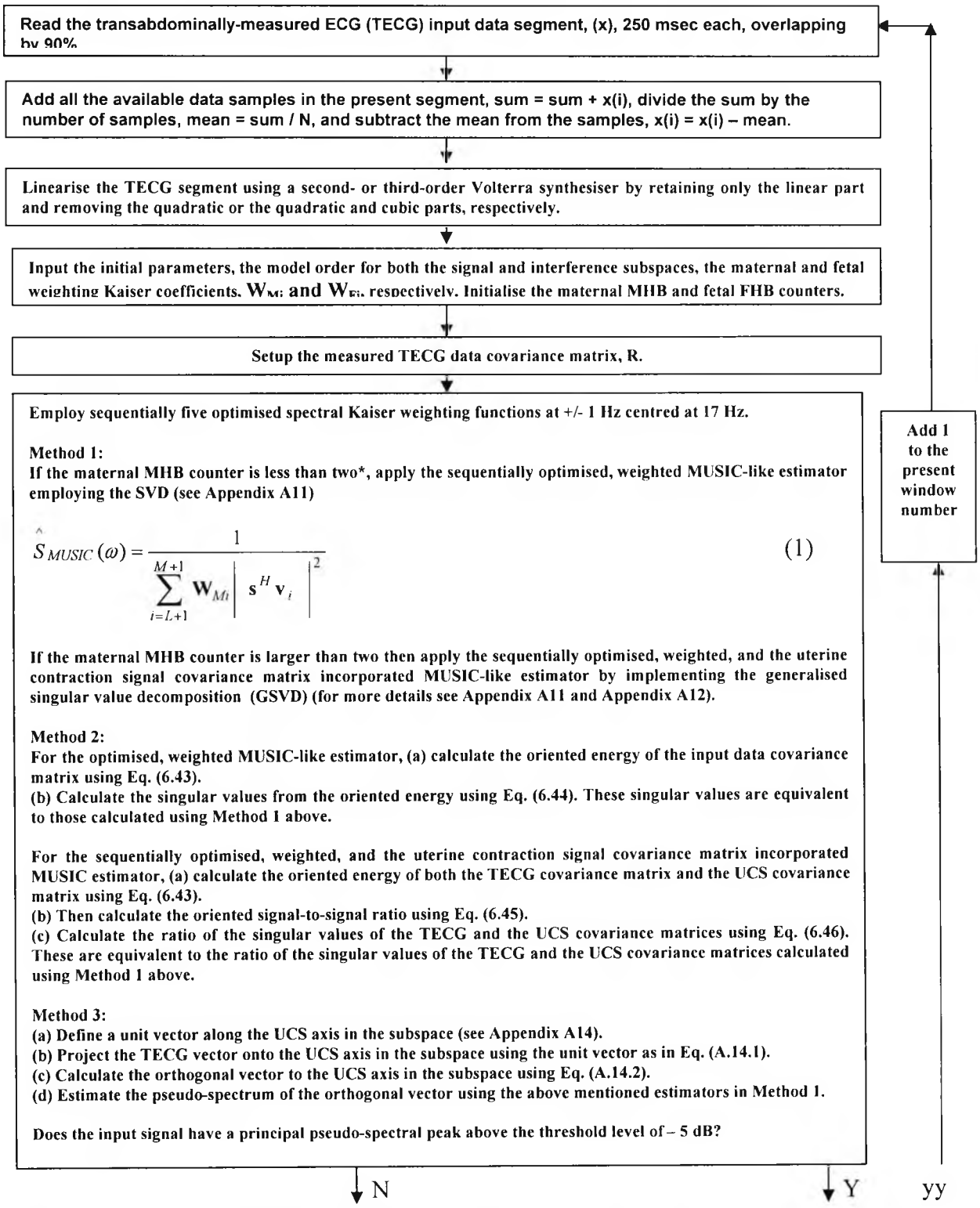

Figure 6.8: *A flowchart for the third system for non-invasive fetal heartbeat detection using both the sequentially optimised, weighted MUSIC-like technique and the sequentially optimised, weighted and the uterine contraction interference signal covariance matrix incorporated MUSIC technique.*

* *For the first cardiac cycle, the sequentially optimised, weighted MUSIC estimator is used. During the first cardiac cycle, the QRS-free ECG segment is used to estimate the uterine contraction interference signal covariance matrix, I_{noise}. Then the sequentially optimised, weighted and the uterine contraction interference signal covariance matrix incorporated MUSIC estimator could be used starting from the second maternal cardiac cycle.*

continued

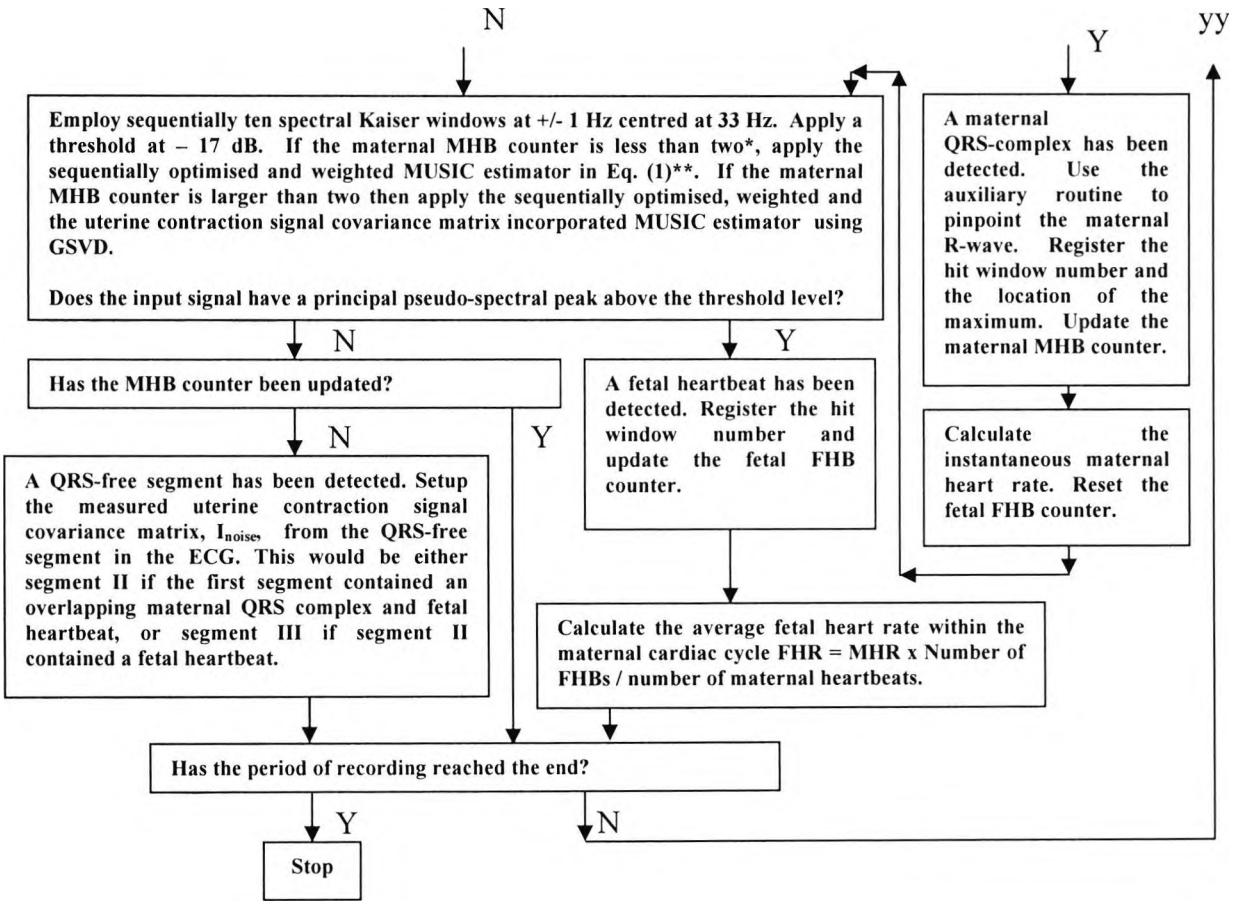

Figure 6.8 *(continued): A flowchart for the third system for non-invasive fetal heartbeat detection using both the sequentially optimised, weighted MUSIC technique and the sequentially optimised, weighted and the uterine contraction interference signal covariance matrix incorporated MUSIC technique.*

* *For the first cardiac cycle, the sequentially optimised and weighted MUSIC estimator is used. During the first cardiac cycle, the QRS-free ECG segment is used to estimate the uterine contraction signal covariance matrix, I_{noise}. Then the sequentially optimised, weighted and the uterine contraction signal covariance matrix incorporated MUSIC estimator could be used starting from the second maternal cardiac cycle.*

** Replace $\mathbf{W}_{Mi}$ by $\mathbf{W}_{Fi}$.

6.8 Results

6.8.1 Data collection and pre-processing

Data collection and pre-processing are described in Sections 1.8 and 1.9, respectively. The data portions earmarked for the UCS modified covariance matrix ($\mathbf{I}_{noise}$) are 250 msec long (see Figure 6.9), falling mostly within segments III in the case of those maternal cardiac cycles that are free from coincident mother and fetal QRS-complexes in segments I, **OR** in segments II and IV for maternal cardiac cycles that do exhibit occurrences of coincident mother and fetal QRS-complexes in Segments I.

6.8.2 Results for the sequentially optimised, weighted MUSIC with and without the incorporation of the UCS modified covariance matrix ($\mathbf{I}_{noise}$)

First, the sequentially optimised, weighted spectral MUSIC localiser of Eqs. (6.32-6.33) is applied to the transabdominally-measured ECG four segments depicted in Figure 6.9 (a-g).

Figure 6.10 (A) depicts the resultant pseudo-spectrum of segments I, II, III, and IV shown in Figure 6.9 (a). The maternal MPPP is clearly detected at 17 Hz as shown at the top left hand part of the Figure. The FPPP of the first fetal heart beat, which is coincident with the maternal QRS-complex in segment I (with maternal and fetal R-wave separation of 40 msec), was detected at 30 Hz and can be seen at the inset of the top left hand part of the Figure. The FPPP of the second fetal heartbeat is detected at 32 Hz as can be seen in the bottom left hand part of the Figure. The top and bottom parts of the Figure at the right hand side are QRS-free segments. **Comment**: Clear Fetal Principal Peaks (FPPs) at 30 Hz and 32 Hz in segments I and III, respectively.

Next the proposed localiser of Eq. (6.42) employing the sequentially optimised, weighted MUSIC with the incorporation of the UCS modified covariance matrix ($\mathbf{I}_{noise}$) is applied to the same segments. The UCS modified covariance matrix is calculated using the data portion in segment II. The results are shown in Figure 6.10 (B). The maternal MPPP is detected at 17 Hz as shown at the top left hand part of the Figure. The FPPP of the first fetal heart beat, which is coincident with the maternal QRS-complex in segment I (with maternal and fetal R-wave separation of 40 msec), is detected at 30 Hz and can be seen at the inset of the top left hand part of the Figure. The FPPP of the second fetal heartbeat is detected at 32 Hz as can be seen in the bottom left hand part of

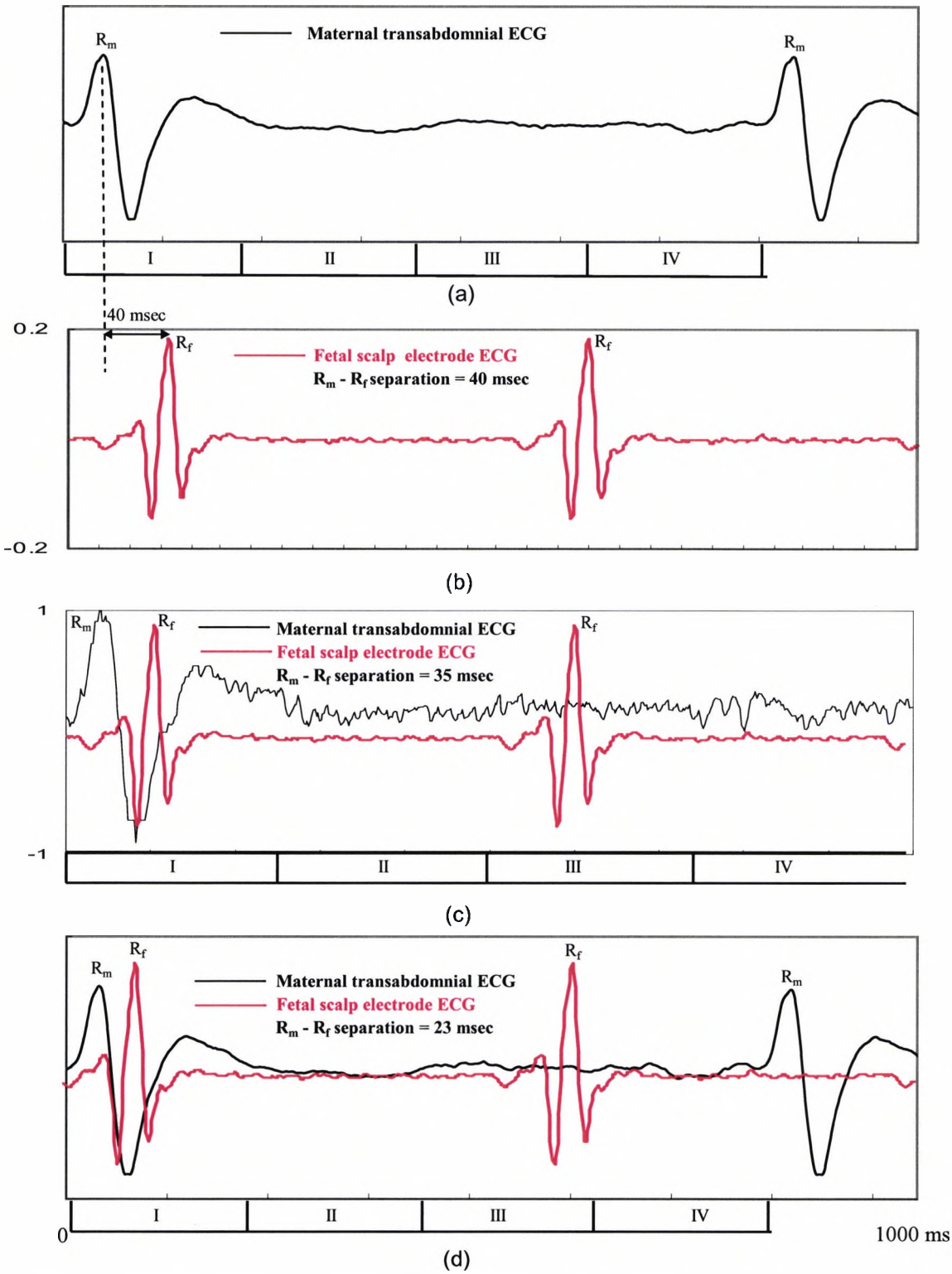

Figure 6.9: Coincident mother's and fetal QRS-complexes. (*a) A typical maternal transabdominal cardiac cycle, (b) the synchronised and amplified fetal ECG signal measured using two electrodes; one electrode is clipped to the fetal scalp, and the other is attached to the maternal thigh. The R-wave separation is 40 msec. (c), (d), (e), (f), and (g) are superimposed and synchronised maternal transabdominal and fetal scalp ECGs with maternal R-wave to fetal R-wave separation of 35 msec, 23 msec, 18 msec, 14 msec, and 9 msec, respectively. The maternal cardiac cycle begins 50 msec before the R-wave and ends 50 msec before the next R-wave. The subject is at the first stage of labour, 40 weeks gestation. The maternal cycle has 500 samples or more at a rate of 0.5 KHz. (Code: 5, 9, 12, 16, 19). Segment I: maternal QRS, segment II: the first fetal heartbeat with maternal contribution, segment III: QRS-free ECG, and segment IV: the second fetal heartbeat with maternal contribution.*

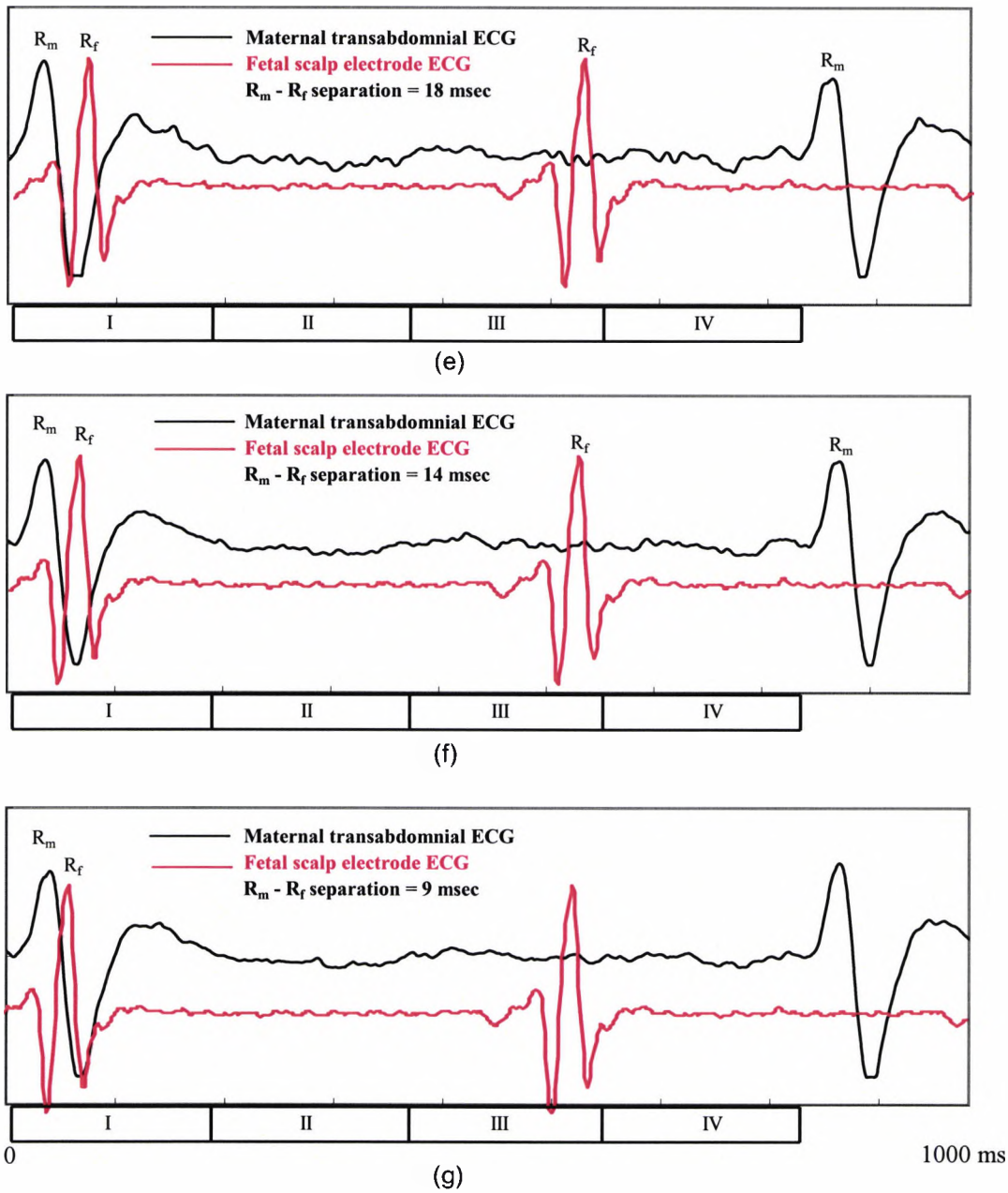

Figure 6.9 *(continued): Coincident mother's and fetal QRS-complexes.(a) A typical maternal transabdominal cardiac cycle, (b) the synchronised and amplified fetal ECG signal measured using two electrodes; one electrode is clipped to the fetal scalp, and the other is attached to the maternal thigh. The R-wave separation is 40 msec. (c), (d), (e), (f), and (g) are superimposed and synchronised maternal transabdominal and fetal scalp ECGs with maternal R-wave to fetal R-wave separation of 35 msec, 23 msec, 18 msec, 14 msec, and 9 msec, respectively. The maternal cardiac cycle begins 50 msec before the R-wave and ends 50 msec before the next R-wave. The subject is at the first stage of labour, 40 weeks gestation. The maternal cycle has 500 samples or more at a rate of 0.5 KHz. (Code: 5, 9, 12, 16, 19). Segment I: maternal QRS, segment II: the first fetal heartbeat with maternal contribution, segment III: QRS-free ECG, and segment IV: the second fetal heartbeat with maternal contribution.*

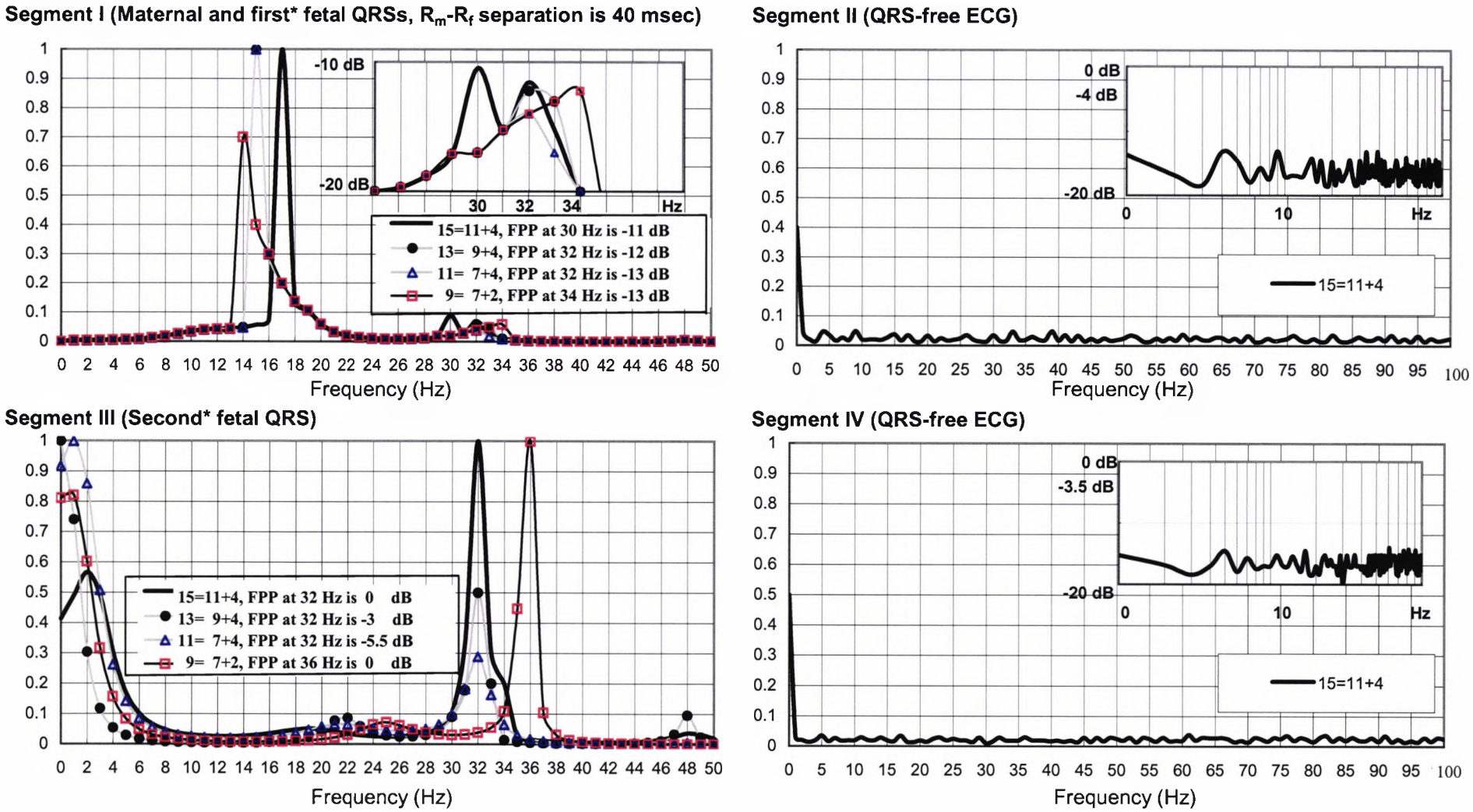

Figure 6.10 A: *Weighted spectral MUSIC for the transabdominally-measured ECG signal of Figure 6.9 (a). Both mother's and fetal QRS-complexes coexist in segment I with their respective R-wave separation at 40 msec. Fetal Principal Peak (FPP) at 32 Hz indicates the presence of a second fetal QRS in segment III, while the content of segments II and IV are chiefly noise artefacts.* ***Comment****: Clear Fetal Principal Peaks (FPPs) at 30 Hz and 32 Hz in segments I and III, respectively. * within the maternal cardiac cycle.*

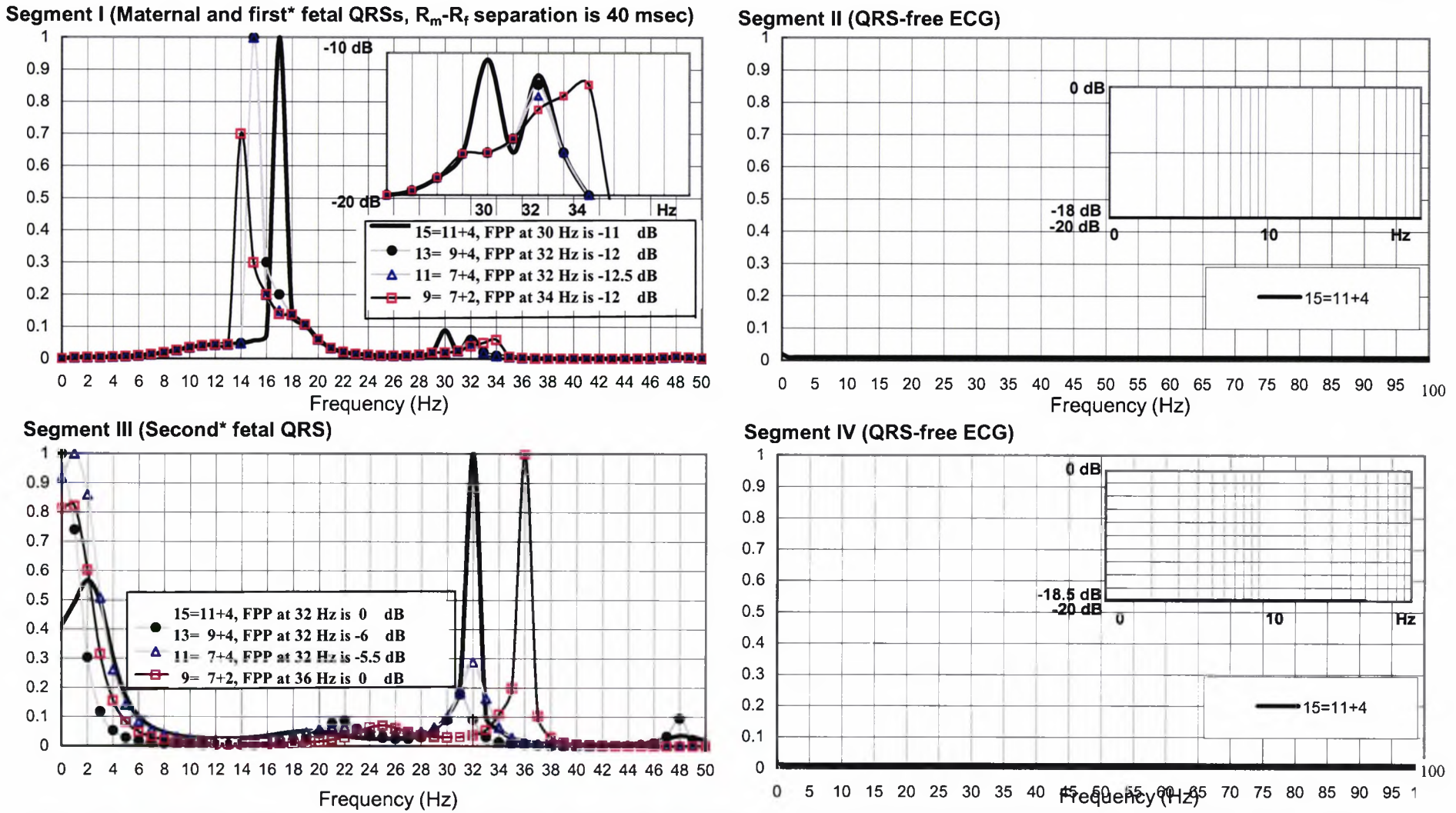

Figure 6.10 B: *Weighted and I_{noise} incorporated spectral MUSIC for the transabdominally-measured ECG signal of Figure 6.9 (a). Both mother's and fetal QRS-complexes coexist in segment I with their respective R-wave separation at 40 msec. Fetal Principal Peak (FPP) at 32 Hz indicates the presence of a second fetal QRS in segment III, while segments II and IV contain noise artefacts. * within the maternal cardiac cycle.* ***Comments*** *: Clear Fetal Principal Peaks (FPPs) at 30 Hz and 32 Hz in segments I and III, respectively. When I_{noise} is incorporated the MUSIC peaks are less sensitive to small deviations in the model order. By incorporating the I_{noise} the FPPs tend to be sharper at 32 Hz when there are small deviations in the model order such as 13=9+4 and 11=7+4. There is an appreciable noise artefact reduction in the QRS-free segments.*

the Figure. The top and bottom parts of the Figure at the right hand side are QRS-free segments. **Comments**: Clear Fetal Principal Peaks (FPPs) at 30 Hz and 32 Hz in segments I and III, respectively. When $\mathbf{I}_{noise}$ is incorporated the MUSIC peaks are less sensitive to small deviations in the model order. By incorporating the $\mathbf{I}_{noise}$ the FPPs tend to be sharper at 32 Hz when there are small deviations in the model order such as 13=9+4 and 11=7+4. There is an appreciable noise artefact reduction in the QRS-free segments.

Figure 6.11 (A) and (B) show the results using the sequentially optimised, weighted MUSIC with and without the incorporation of the UCS modified covariance matrix for the case of maternal and fetal R-wave separation of 35 msec as depicted in Figure 6.9 (c). Figure 6.11 (A) shows similar results to those of Figure 6.10 (A) using the sequentially optimised, weighted MUSIC, with the maternal FPPP at 17 Hz shown at the top left hand part of the Figure, the FPPP of the first fetal heartbeat at 30 Hz shown in the inset of the top left hand part of the Figure, and the FPPP of the second fetal heartbeat at 32 Hz shown at the bottom left hand part of the Figure. **Comments**: The same as in Figure 6.10 (A).

With the incorporation of the UCS modified covariance matrix, Figure 6.11 (B) shows that the FPPP of the second fetal heartbeat at the bottom left hand part of the Figure is sharper than that of Figure 6.11 (A) using the sequentially optimised, weighted MUSIC. Also, the peak is now shifted to 30 Hz using the model order 15 = 11 + 4. **Comments**: The same as in Figure 6.10 B. Furthermore, the second fetal FPP is much sharper with $\mathbf{I}_{noise}$ incorporated. Sharper peaks. There is an appreciable noise artefact reduction in the QRS-free segments.

Figure 6.12 (A) and (B) show the results using the sequentially optimised, weighted MUSIC with and without the incorporation of the UCS modified covariance matrix for the case of maternal and fetal R-wave separation of 23 msec as depicted in Figure 6.9 (d). In Figure 6.12 (A), note that the MPPP at the top left hand part of the Figure is now shifted from 17 Hz to 16 Hz using the model order of 15 = 11 + 4. The FPPPs of both the first and second fetal heartbeats are detected at 30 Hz at the top and bottom left hand parts of the Figure, respectively. **Comments**: There is a shift in the Mother's QRS Principal Pseudo-spectral Peak (MPPP) from 17 Hz to 16 Hz.

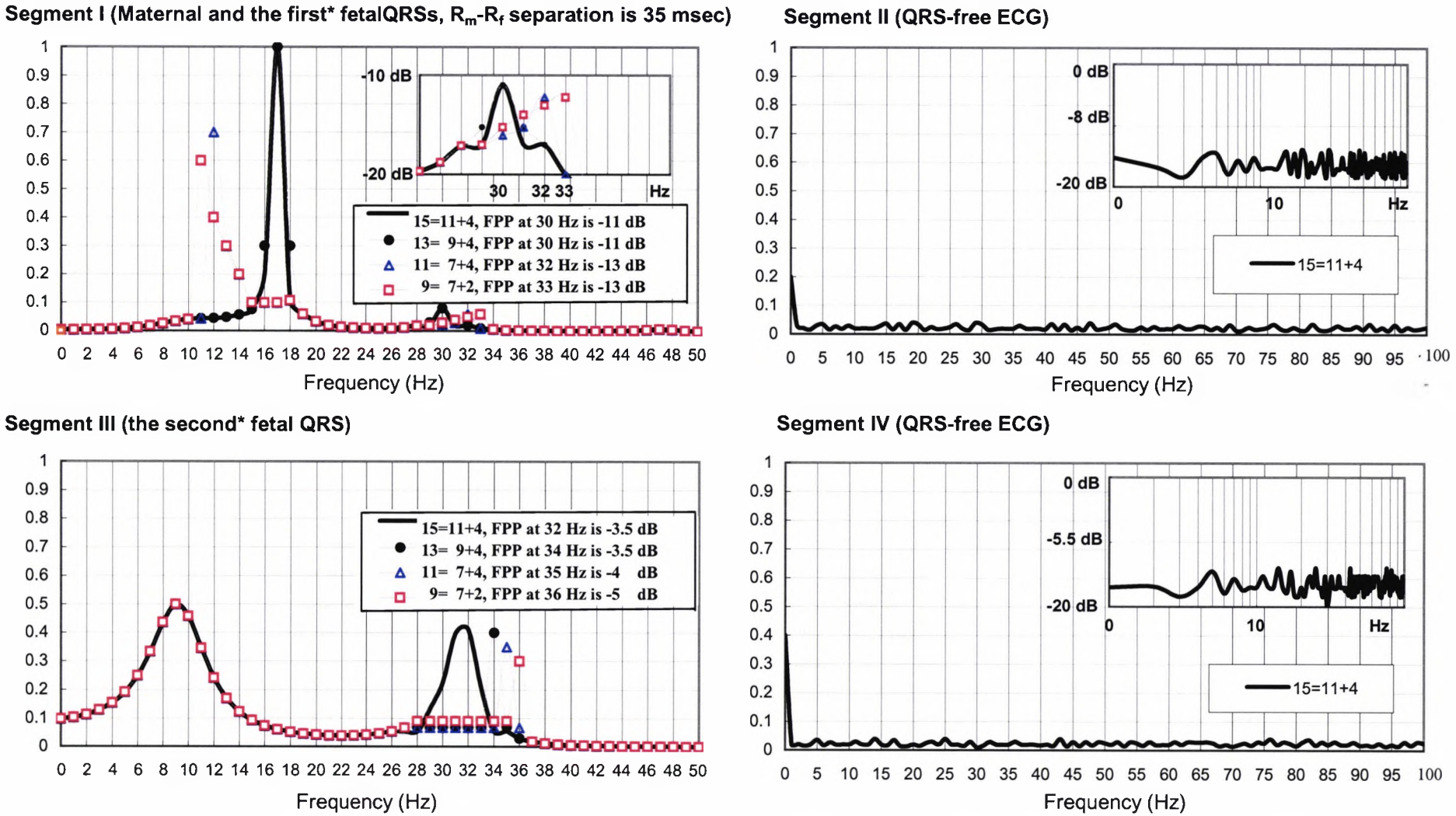

Figure 6.11 A: *Weighted spectral MUSIC for the transabdominally-measured ECG signal of Figure 6.9 (c). Both mother's and fetal QRS-complexes coexist in Segment I with their respective R-wave separation at 35 msec. Fetal principal peak (FPP) indicates the presence of a second fetal QRS in segment III, while Segments II and IV contain noise artefact. * within the maternal cardiac cycle.* ***Comments*** *: The same as in Figure 6.10 A.*

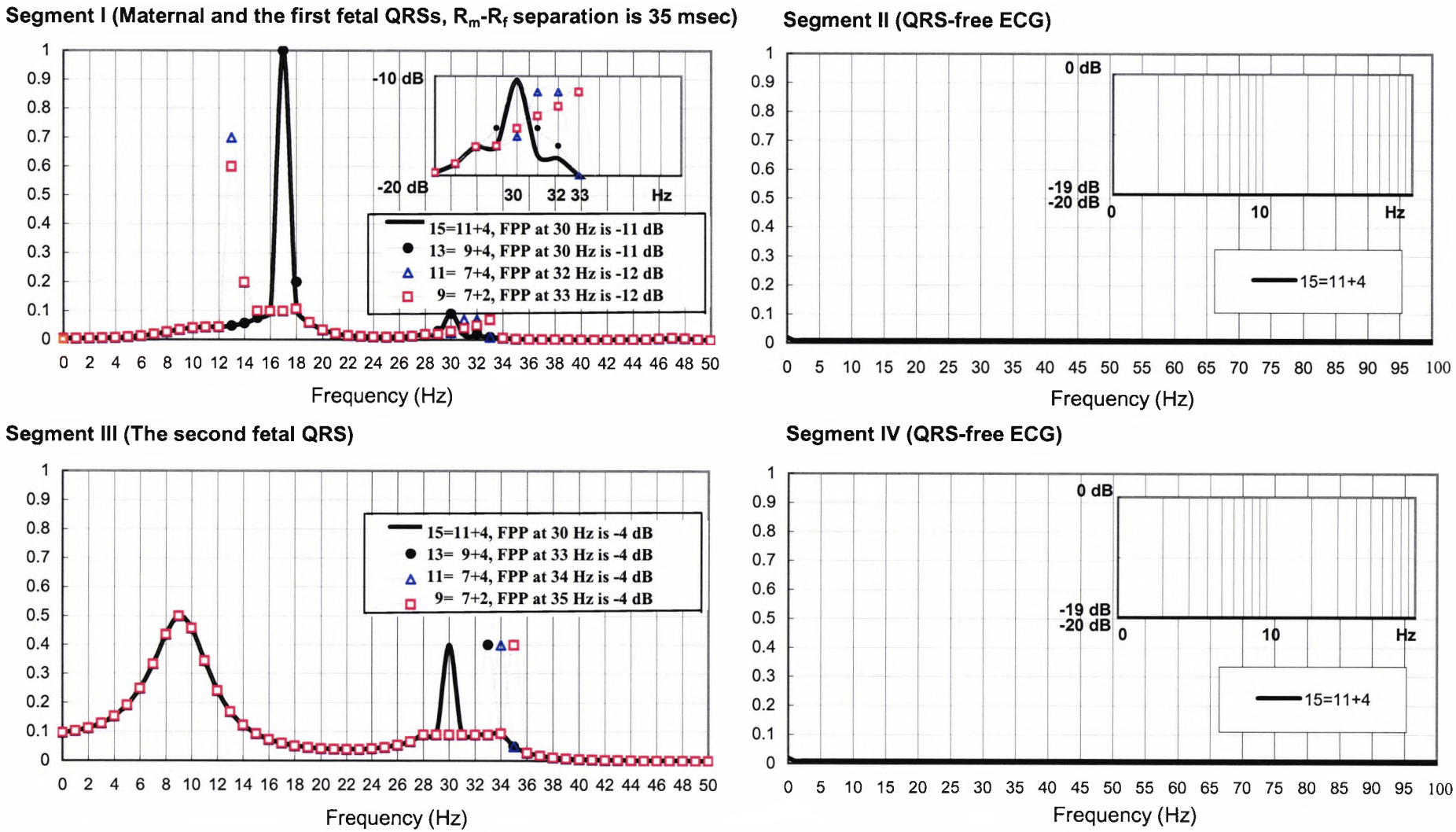

Figure 6.11 B: *Weighted and I_{noise}-incorporated spectral MUSIC for the transabdominally-measured ECG signal of Figure 6.9 (c). Both mother's and fetal QRS-complexes coexist in Segment I with their respective R-wave separation at 35 msec. Fetal principal peak (FPP) indicates the presence of a second fetal QRS in segment III, while Segments II and IV contain noise artefact. * within the maternal cardiac cycle.* ***Comments****: The same as in Figure 6.10 B. Furthermore, the second fetal FPP is much more sharper with I_{noise} incorporated. sharper peaks. There is an appreciable noise artefact reduction in the QRS-free segments.*

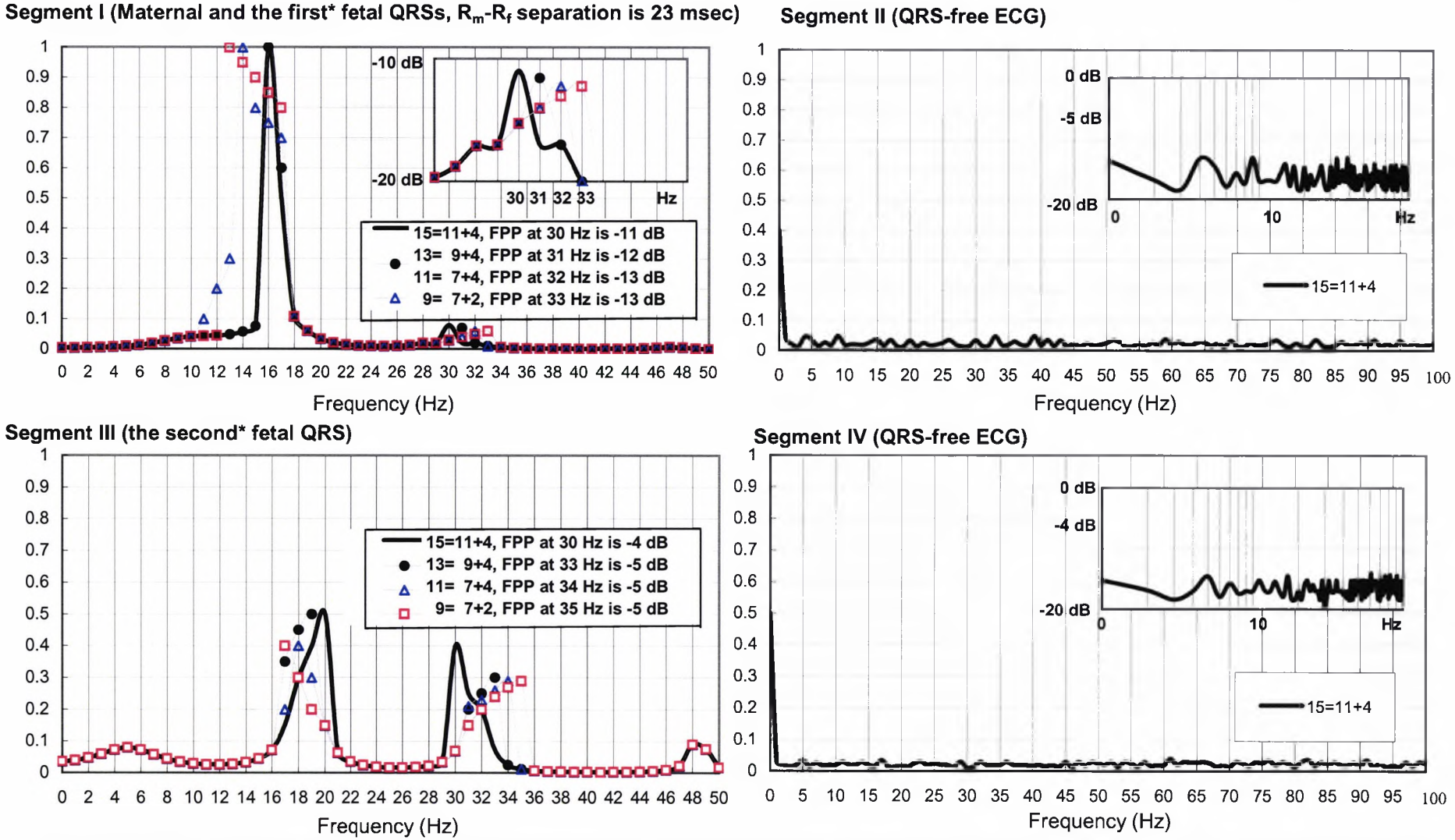

Figure 6.12 A: *Weighted spectral MUSIC for the transabdominally-measured ECG signal of Figure 6.9 (d). Both mother's and fetal QRS-complexes coexist in Segment I with their respective R-wave separation at 23 msec. Fetal principal peak (FPP) indicates the presence of a second fetal QRS in segment III, while Segments II and IV contain noise artefact. * within the maternal cardiac cycle.* ***Comments****: There is a shift in the Mother's QRS Principal Peak (MPP) from 17 Hz to 16 Hz.*

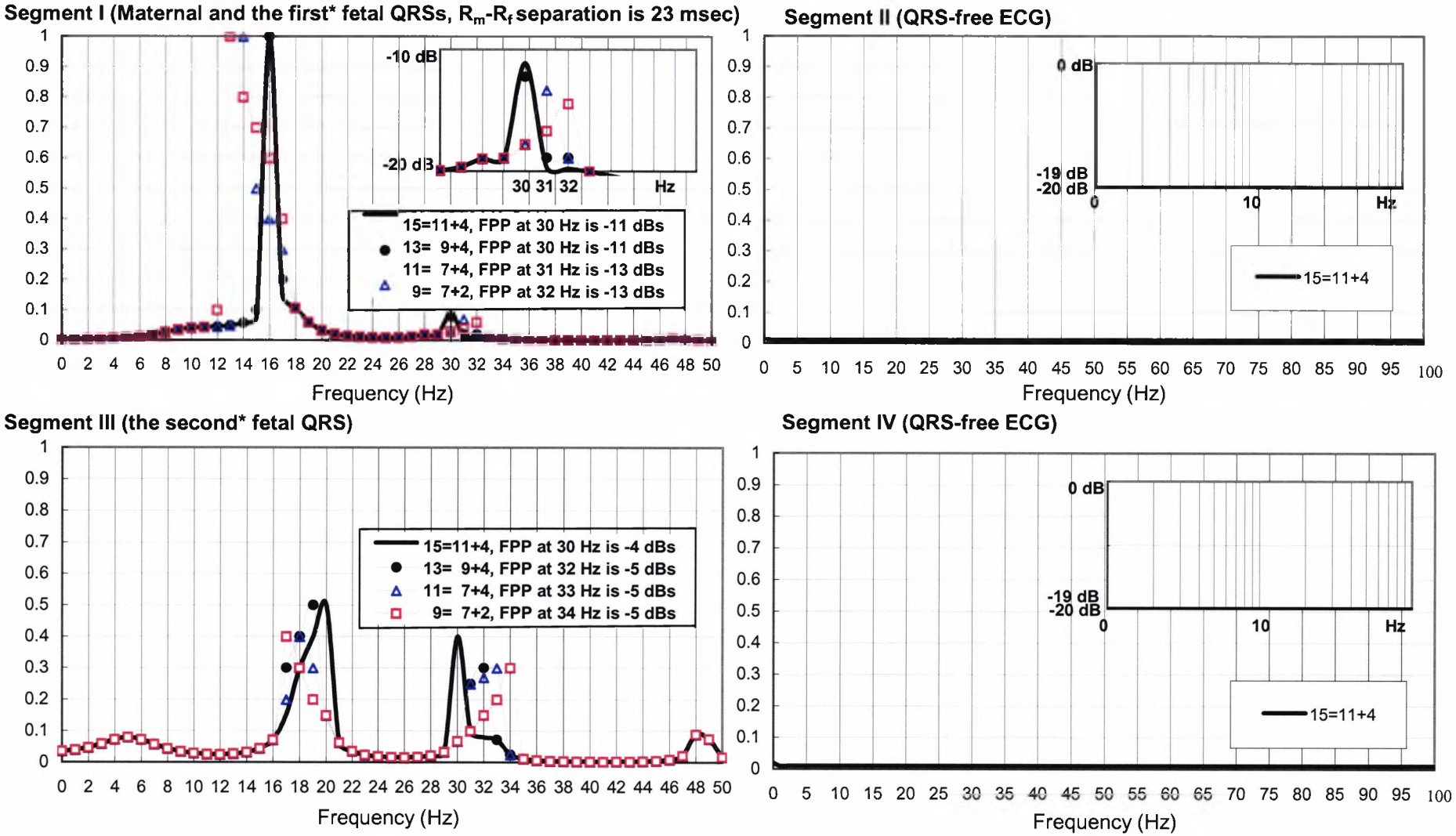

Figure 6.12 B: *Weighted and I_{noise}-incorporated spectral MUSIC for the transabdominally-measured ECG signal of Figure 6.9 (d). Both mother's and fetal QRS-complexes coexist in Segment I with their respective R-wave separation at 23 msec. Fetal principal peak (FPP) indicates the presence of a second fetal QRS in segment III, while Segments II and IV contain noise artefact. * within the maternal cardiac cycle.* ***Comments****: In addition to comments of Figure 6.10 B, sharper Mother Principal Peak (MPP) at 16 Hz. The FPP is less sensitive to a small deviation from the optimum model order, 11+4, as in the case of the model order 9+4. Both yield the same FPP. There is an appreciable noise artefact reduction in the QRS-free segments.*

With the incorporation of the UCS modified covariance matrix, Figure 6.12 (B) shows that the MPPP at the top left hand part of the Figure is shifted from 17 Hz to 16 Hz and is also sharper. The FPPP of the first fetal heartbeat is detected at 30 Hz using model orders of 15 = 11 + 4 and 13 = 9 + 4. **Comments**: In addition to the comments of Figure 6.10 B, sharper Mother Principal Peak (MPP) at 16 Hz. The FPP is less sensitive to a small deviation from the optimum model order, 11+4, as in the case of the model order 9+4. Both yield the same FPP. There is an appreciable noise artefact reduction in the QRS-free segments.

Figure 6.13 (A) and (B) show the results using the sequentially optimised, weighted MUSIC with and without the incorporation of the UCS modified covariance matrix for the case of maternal and fetal R-wave separation of 18 msec as depicted in Figure 6.9 (e). Figure 6.13 (A) depicts the maternal MPPP at 17 Hz shown at the top left hand part of the Figure, the FPPP of the first fetal heartbeat at 30 Hz shown in the inset of the top left hand part of the Figure, and the FPPP of the second fetal heartbeat at 31 Hz shown at the bottom left hand part of the Figure. **Comments**: No additional comments.

With the incorporation of the UCS modified covariance matrix, Figure 6.13 (B) shows that the MPPP at the top left hand part of the Figure is detected at 17 Hz. The FPPPs of the first and second fetal heartbeats are both detected at 30 Hz as shown at the top and bottom left hand parts of the Figure, respectively. **Comments**: There is an appreciable noise artefact reduction in the QRS-free segments. No additional comments.

Figure 6.14 (A) and (B) show the results using the sequentially optimised, weighted MUSIC with and without the incorporation of the UCS modified covariance matrix for the case of maternal and fetal R-wave separation of 14 msec as depicted in Figure 6.9 (f). Figure 6.14 (A) shows the maternal MPPP at 17 Hz shown at the top left hand part of the Figure, the FPPP of the first fetal heartbeat is shifted at 31 Hz shown in the inset of the top left hand part of the Figure. The FPPP of the second fetal heartbeat is at 30 Hz shown at the bottom left hand part of the Figure. **Comments**: 1) As a result of the close proximity of R_m and R_f, the FPPP exhibits increased sensitivity to small deviations from the optimal model order in segment I. 2) Also, there is a loss of resolution for FPPP in segment III.

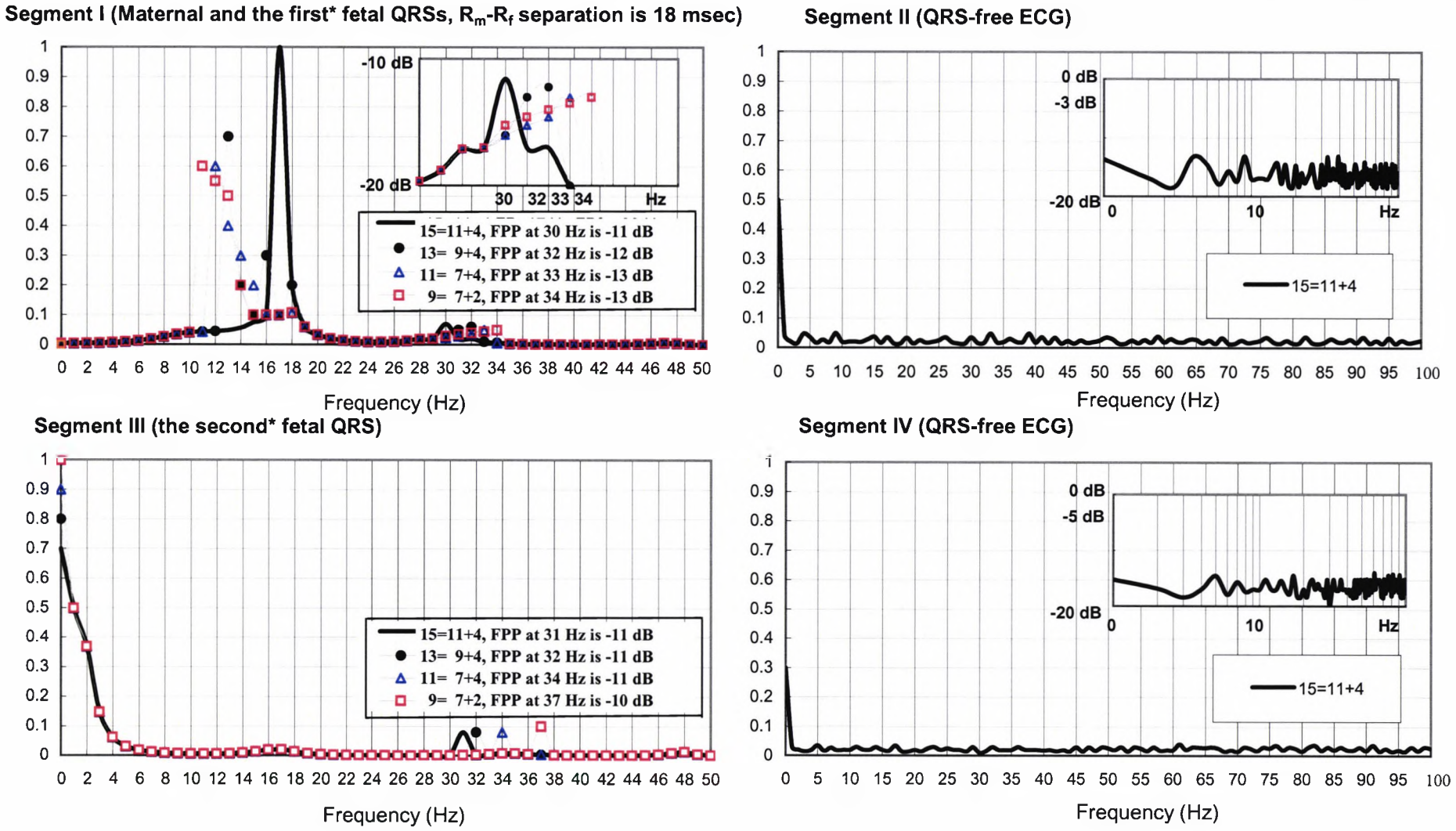

Figure 6.13 A: *Weighted spectral MUSIC for the transabdominally-measured ECG signal of Figure 6.9 (e). Both mother's and fetal QRS-complexes coexist in Segment I with their respective R-wave separation at 18 msec. Fetal principal peak (FPP) indicates the presence of a second fetal QRS in segment III, while Segments II and IV contain noise artefact. * within the maternal cardiac cycle.* ***Comments*** *: No additional comments.*

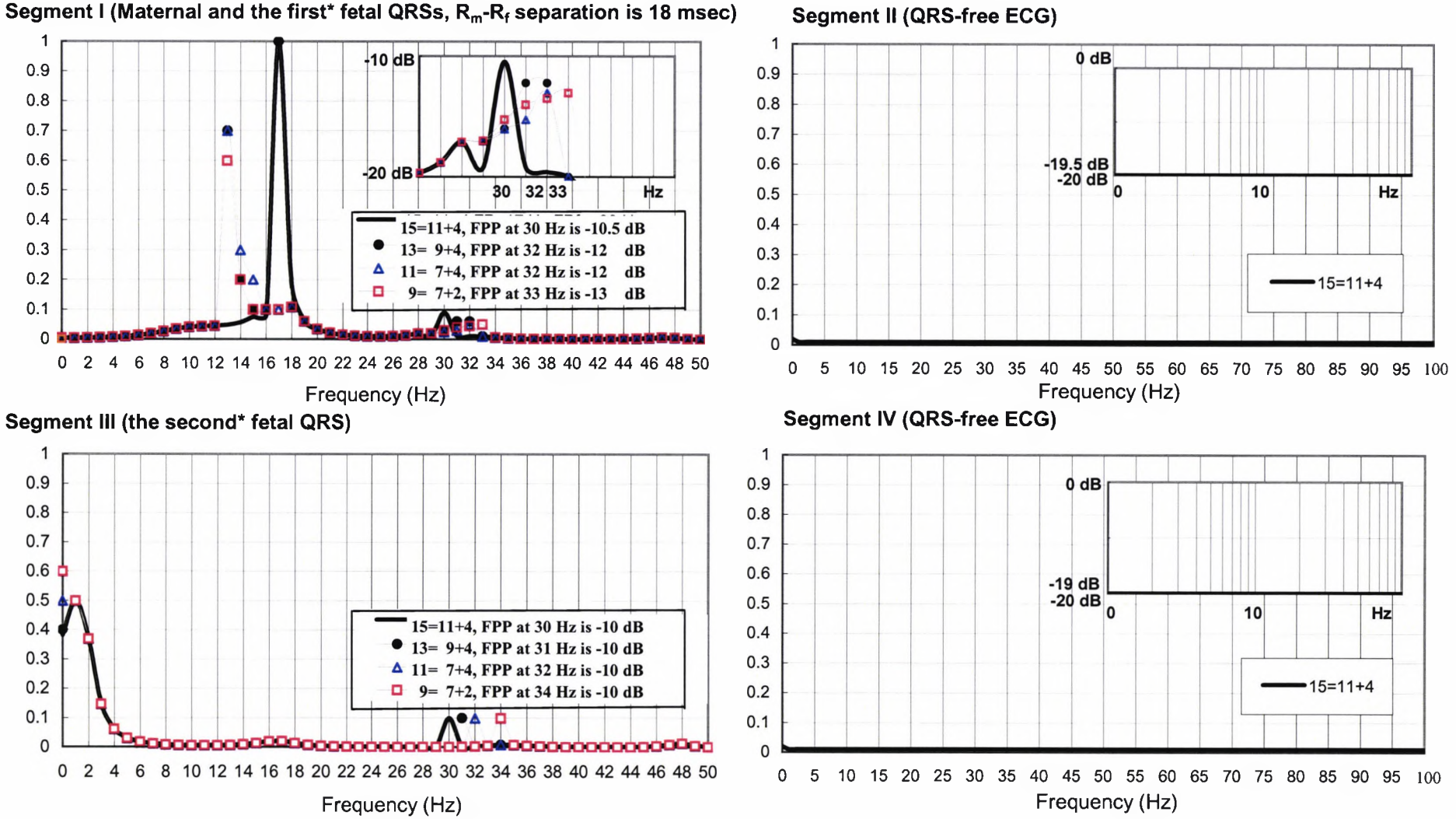

Figure 6.13 B: *Weighted and* I_{noise} *incorporated spectral MUSIC for the transabdominally-measured ECG signal of Figure 6.9 (e). Both mother's and fetal QRS-complexes coexist in Segment I with their respective R-wave separation at 18 msec. Fetal principal peak (FPP) indicates the presence of a second fetal QRS in segment III, while Segments II and IV contain noise artefact. * within the maternal cardiac cycle.* ***Comments****: There is an appreciable noise artefact reduction in the QRS-free segments. No additional comments.*

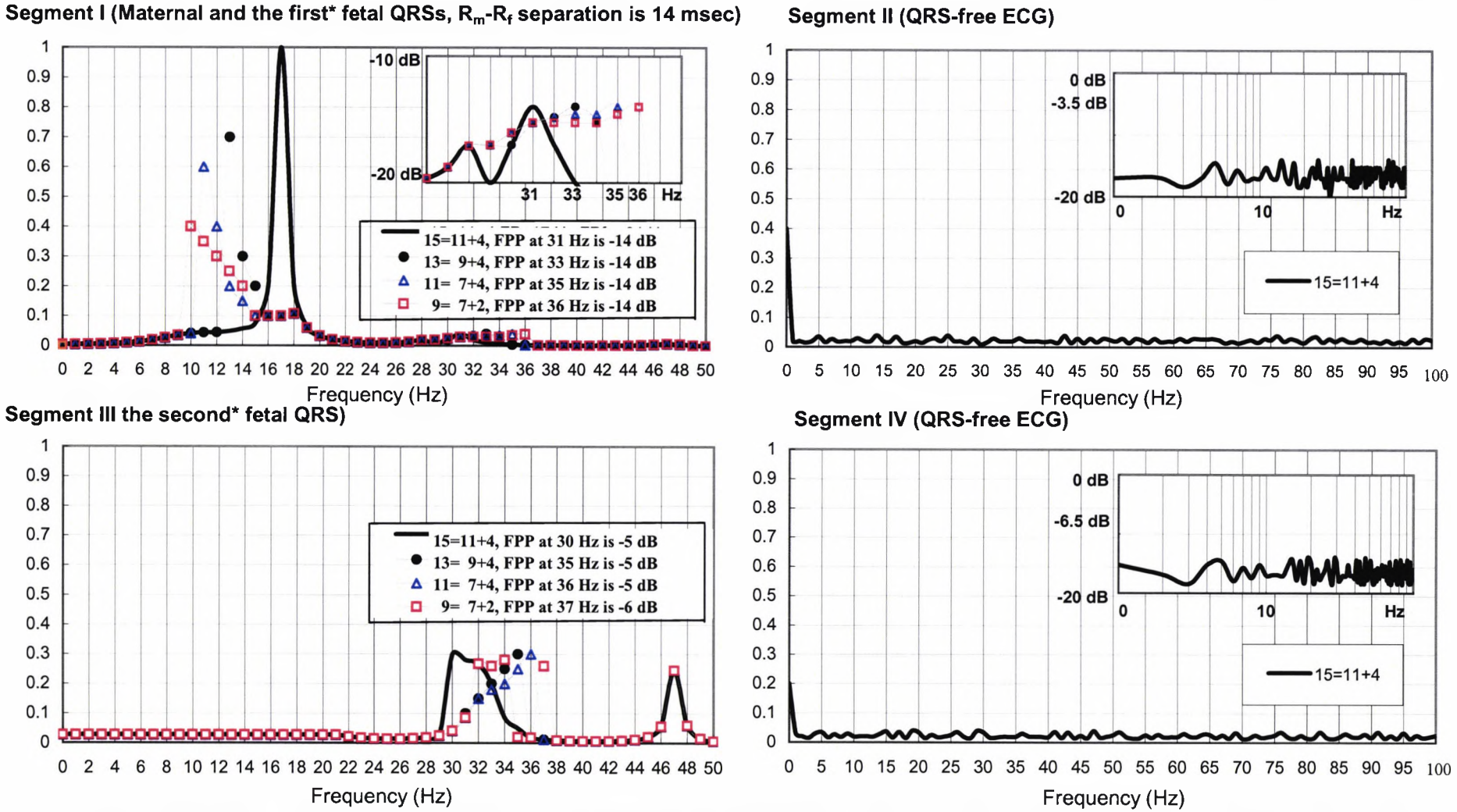

Figure 6.14 A: *Weighted spectral MUSIC for the transabdominally-measured ECG signal of Figure 6.9 (f). Both mother's and fetal QRS-complexes coexist in Segment I with their respective R-wave separation at 14 msec. Fetal principal peak (FPP) indicates the presence of a second fetal QRS in segment III, while Segments II and IV contain noise artefact. * within the maternal cardiac cycle.* ***Comments****: 1) As a result of the close proximity of R_m and R_f, the FPP exhibits increased sensitivity to small deviations from the optimal model order in segment I. 2) Also, there is a loss of resolution for FPP in segment III.*

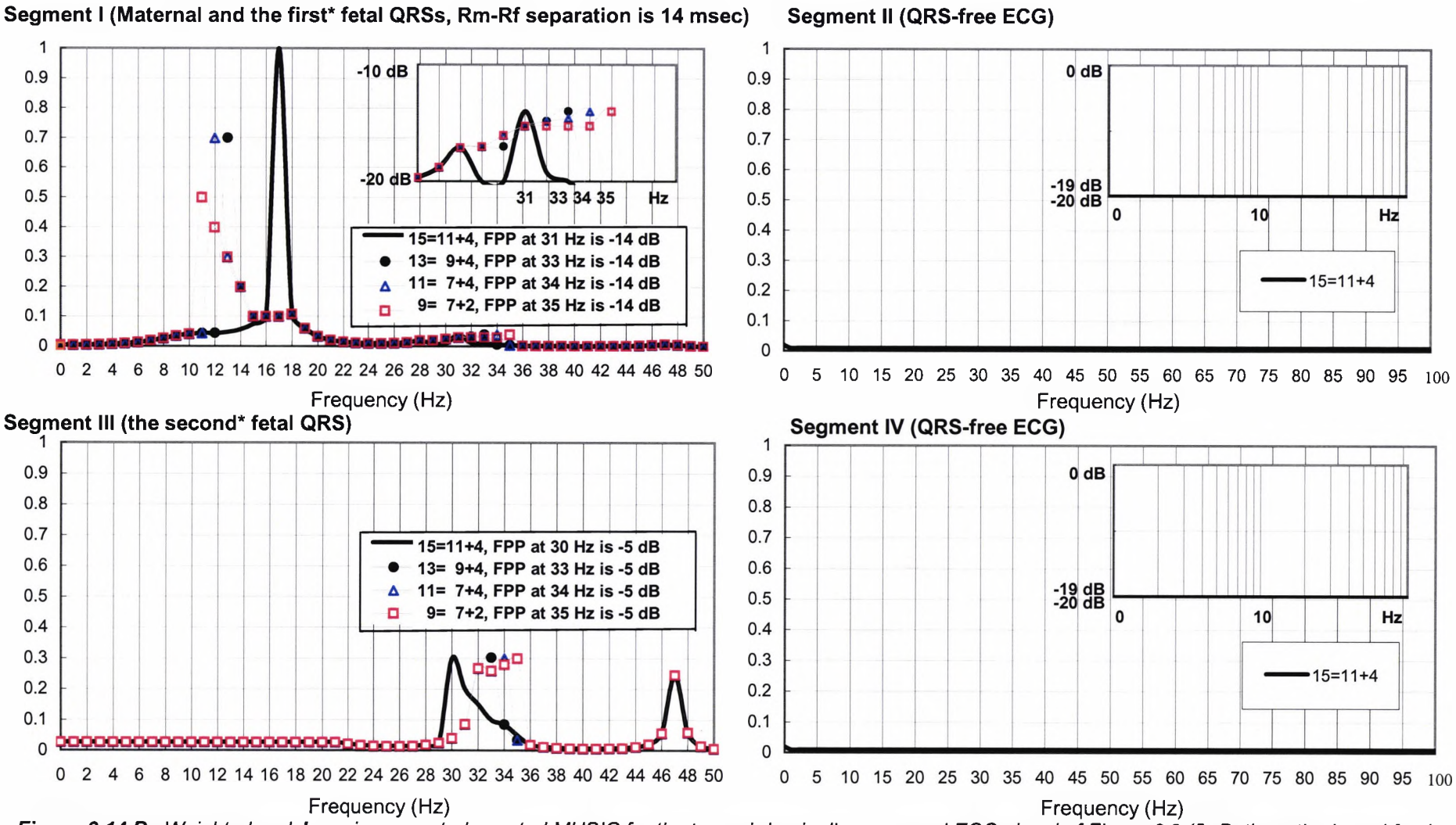

Figure 6.14 B: *Weighted and* I_{noise} *incorporated spectral MUSIC for the transabdominally-measured ECG signal of Figure 6.9 (f). Both mother's and fetal QRS-complexes coexist in Segment I with their respective R-wave separation at 14 msec. Fetal principal peak (FPP) indicates the presence of a second fetal QRS in segment III, while Segments II and IV contain noise artefact. * within the maternal cardiac cycle.* ***Comments*** *: The same comments as in weighted spectral MUSIC of Figure 6.14 A. There is an appreciable noise artefact reduction in the QRS-free segments.*

With the incorporation of the UCS modified covariance matrix, Figure 6.14 (B) shows similar results to those of Figure 6.14 (A). **Comments**: The same as in Figure 14 (A). There is an appreciable noise artefact reduction in the QRS-free segments.

Figure 6.15 (A) and (B) show the results using the sequentially optimised, weighted MUSIC with and without the incorporation of the UCS modified covariance matrix for the case of maternal and fetal R-wave separation of 9 msec as depicted in Figure 6.9 (g). Figure 6.15 (A) depicts the maternal MPPP at 17 Hz shown at the top left hand part of the Figure, the FPPP of the first fetal heartbeat is shifted at 31 Hz shown in the inset of the top left hand part of the Figure. The FPPP of the second fetal heartbeat is at 31 Hz shown at the bottom left hand part of the Figure. **Comments**: 1) As a result of close proximity, the FPPP tends to broaden. 2) Also, as a result of the close proximity of R_m and R_f, the FPPP exhibits increased sensitivity to small deviations from the optimal model order in segment I.

Figure 6.15 (B) depicts the results of the $\mathbf{I}_{noise}$ incorporation for the transabdominally-measured ECG signal of Figure 6.9 (g). Both mother's and fetal QRS-complexes coexist in Segment I with their respective R-wave separation at 9 msec. The fetal principal peak (FPPP) indicates the presence of a second fetal QRS in segment III, while Segments II and IV contain noise artefact. **Comments**: The same comments applied to close proximity as in Figure 6.15 A. However, the fetal FPP is stronger and sharper around 31 Hz, and there is significant noise reduction in the QRS-free segments.

Comments

1. ***The effect of proximity of Rm and Rf on the frequency deviation of the FPPPs.*** The new MUSIC algorithm is capable of detecting fetal heartbeats, at a rate of almost 92%, when the mother and fetal R-waves are almost synchronised, provided that appropriate sequential weightings for the mother and the fetal are maintained throughout. As the separation between the mother and fetal R-waves is increased, there is a slight increase in the corresponding detection rate and a decrease in the **FPPP** frequency deviations.

2. ***The effect of the I_{noise} incorporation on the FPPP***: The incorporation of the covariance matrix of the **UCS** not only helps to strengthen and sharpen the **FPPPs** in some cases and hence improves the resolution, but also reduces the sensitivity of the **FPPPs** to any small deviations from the optimal model order.

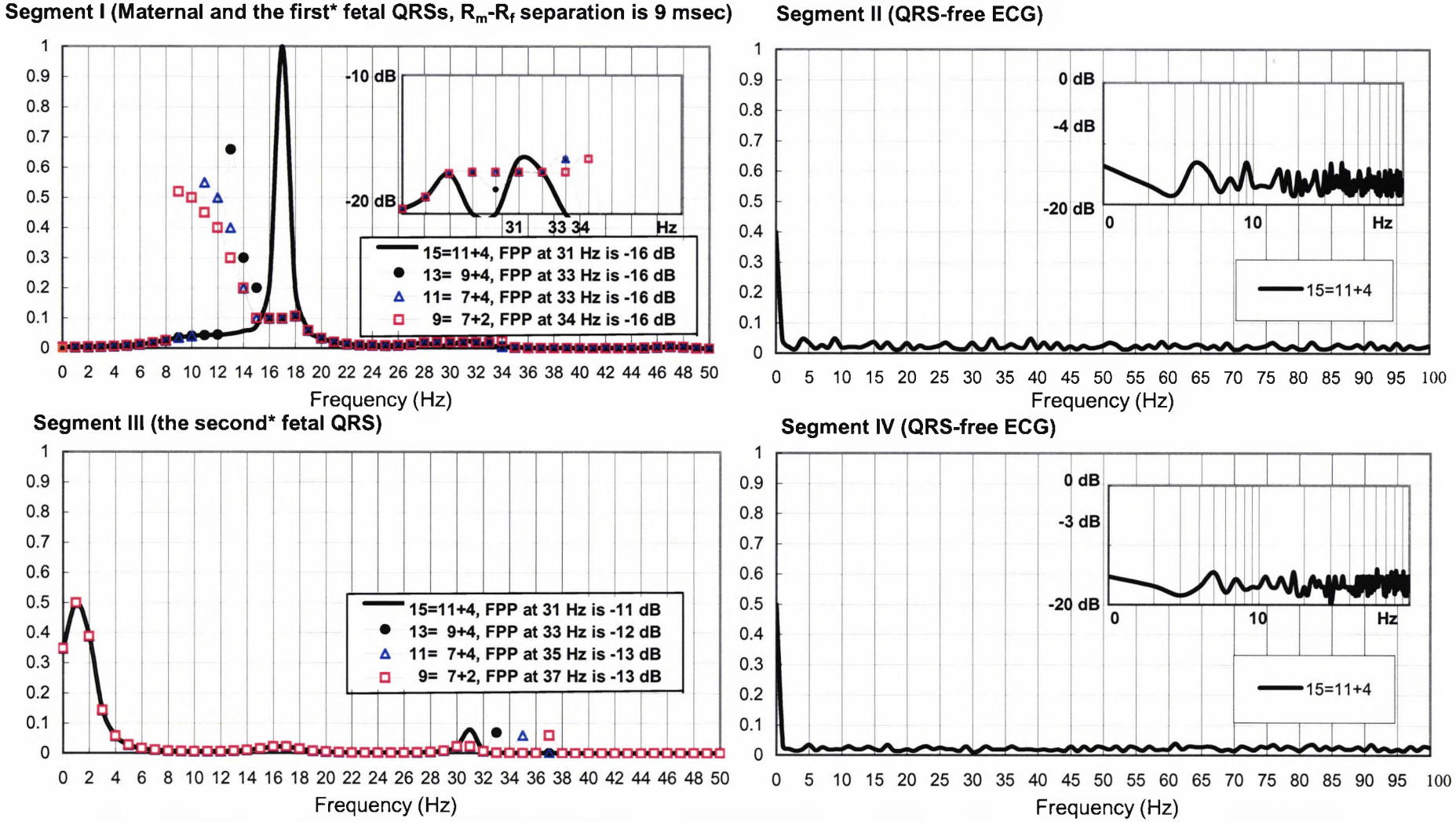

Figure 6.15 A: *Weighted spectral MUSIC for the transabdominally-measured ECG signal of Figure 6.9 (g). Both mother's and fetal QRS-complexes coexist in Segment I with their respective R-wave separation at 9 msec. Fetal principal peak (FPP) indicates the presence of a second fetal QRS in segment III, while Segments II and IV contain noise artefact. * within the maternal cardiac cycle.* ***Comments*** *: 1) As a result of close proximity, FPP tends to broaden. 2) Also, as a result of the close proximity of R_m and R_f, the FPP exhibits increased sensitivity to small deviations from the optimal model order in segment I.*

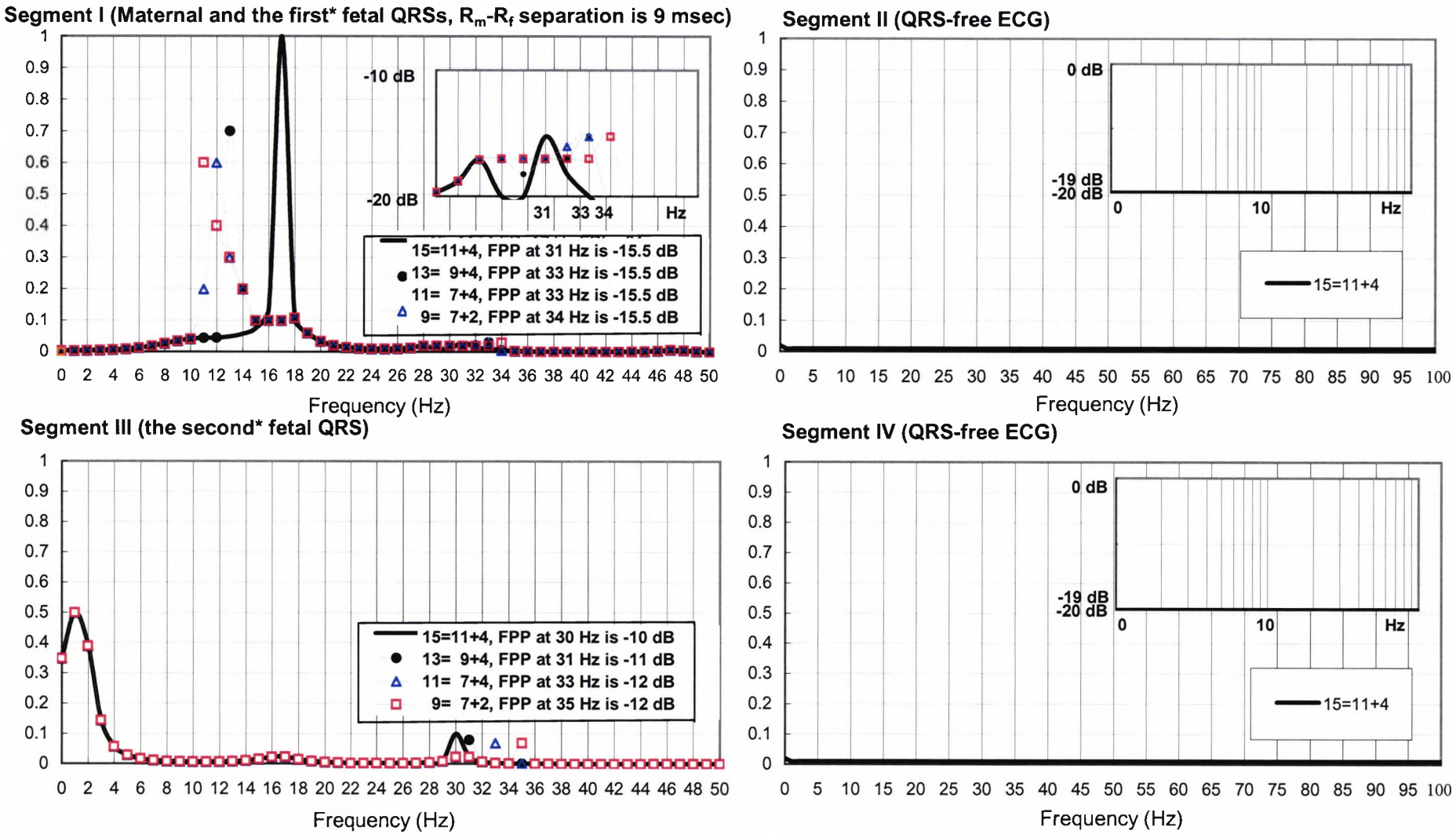

Figure 6.15 B: *Weighted and I_{noise} incorporated spectral MUSIC for the transabdominally-measured ECG signal of Figure 6.9 (g). Both mother's and fetal QRS-complexes coexist in Segment I with their respective R-wave separation at 9 msec. Fetal principal peak (FPP) indicates the presence of a second fetal QRS in segment III, while Segments II and IV contain noise artefact. * within the maternal cardiac cycle.* ***Comments****: The same comments applied to close proximity as in Figure 6.15 A. However, the fetal FPP is stronger and sharper around 31 Hz, and there is an appreciable noise artefact reduction in the QRS-free segments.*

3. ***The effect of the I_{noise} incorporation on the fetal heart detection rate.*** The sequentially optimised, weighted MUSIC has resulted in the following fetal heart detection rates: (i) 89.23%, 97.51%, and 91.20% for coincident, non-coincident mother and fetal QRS-complexes, and overall average, respectively. The sequentially optimised, weighted, and $\mathbf{I}_{noise}$ incorporated MUSIC has resulted in the following fetal heart detection rates: (i) 93.52%, 99.35%, and 95.50% for coincident, non-coincident mother and fetal QRS-complexes, and overall average, respectively. The results have been verified by the recording of the instantaneous scalp fetal heart rate.

6.8.3 The bias of the conventional MUSIC, and the sequentially optimised, weighted MUSIC with and without the I_{noise} UCS modified covariance matrix incorporation when applied to mother's and fetal QRS-complex segments

A statistical measure could be described as an unbiased estimate when the expected value of the estimated statistic is equal to the true value, asymptotically. For example a frequency estimate is said to be unbiased if

$$E\left|\hat{f}(\omega)\right| = f(\omega). \tag{6.47}$$

The bias is defined as the difference between the true value and the expected value. Hence,

$$\text{Bias} = E\left|\hat{f}(\omega)\right| - f(\omega). \tag{6.48}$$

In the case of mother's and fetal QRS-complexes the true values of the spectral peaks are taken to be those obtained from the mother's chest ECG and fetal scalp electrode ECG, respectively. The expected values of the estimates are those obtained using the 250 msec segments from the maternal transabdominal ECG signal for a predominantly maternal QRS segment and a fetal heartbeat with maternal contribution. Those true values and estimates were calculated for 1000 segments using the following three

methods: (i) the conventional MUSIC, (ii) the sequentially optimised, weighted MUSIC, and (iii) the sequentially optimised, weighted and $\mathbf{I}_{noise}$ incorporated MUSIC. The results are shown in Table 6.1 and 6.2, respectively, for mother's and fetal QRS segments.

For the mother's and fetal QRS-complex, the more deviation of the detected frequency of the MPPP at around 17 Hz and the FPPP around 30 Hz, respectively, from the respective actual frequency, the higher the bias will be.

	The conventional MUSIC	**The sequentially optimised and weighted MUSIC**	**The sequentially optimised, weighted, and $\mathbf{I}_{noise}$ incorporated MUSIC**
Bias	1.97	1.54	1.23

Table 6.1: *The bias of three spectral methods used to estimate the principal spectral peaks of 1000 transabdominally-measured mother's QRS-complex segments. These methods are the conventional MUSIC, and the sequentially optimised, weighted MUSIC with and without the incorporation of the UCS modified covariance matrix.*

	The conventional MUSIC	**The sequentially optimised and weighted MUSIC**	**The sequentially optimised, weighted, and $\mathbf{I}_{noise}$ incorporated MUSIC**
Bias	3.84	3.32	2.15

Table 6.2: *The bias of three spectral methods used to estimate the principal spectral peaks of 1000 transabdominally-measured fetal heartbeat with maternal contribution segments. These methods are the conventional MUSIC, and the sequentially optimised, weighted MUSIC with and without the incorporation of the UCS modified covariance matrix.*

6.8.4 Estimation of the FPPP variance

The variance of the third detection method is defined as the expected value of the squared difference between the computed FPPP of the 250 msec flag window of the transabdominal ECG signal and the computed FPPP from the synchronised fetal scalp electrode ECG 250 msec window.

$$Var_M = E\left[(\hat{S}_{MUSIC}(\omega)_{Transabdominal} - \hat{S}_{MUSIC}(\omega)_{fetal\ scalp}\right]^2 \quad (6.49)$$

The variance ranges from 0 – 8, average = 4.127, when calculated for 120,000 FHBs.

6.9 Summary and conclusions

General comments

1. Modifications to the conventional MUSIC

The modified spectral MUSIC is motivated, at least in part, by the shortcoming of all other techniques to detect FHBs when masked by the mother's QRS-complex. The other motivation is to combat interference and noise using only second-order statistics. However, by limiting ourselves to only the second-order statistics whilst dealing with non-linear signals and non-linear noise, we have succumbed to face all sorts of problems. The one which stands out is the problem of the uterine contraction interference signal (UCS) and noise artefact, which do not easily conform to any specific probability distribution as the statistics change with time and eventually take on a chaotic nature for sufficiently long data. And to make matter even worse, the spectrum of the UCS contains resonances with a strong peak around 30 Hz overlapping the fetal principal pseudo-spectral peak. We have found from previous published work that, by removing non-linearity from the ECG signals, we can, in fact, enhance the resonances of the fetal spectrum and weaken or suppress the resonances of the background UCS. Therefore, a systematic approach was adopted and by breaking down the unsolvable problem, a tractable solution was obtained. This approach is summarised as follows; (i) linearise the whole ECG data, (ii) do not include any unqualified assumptions regarding noise statistics, (iii) deal with the actual second-order statistics of the interfering signals and noise, and (iv) perform all the eigen-structured MUSIC mathematical formulation based on the actual ECG signals and the actual *residual* UCS interference plus artefact, and not on a hypothetical Gaussian or non-Gaussian noise for that matter. The latter necessitates isolating and measuring the UCS plus noise and examining its short-term properties within the 250 msec frame, and then incorporate its covariance matrix into the mathematical formulation of the MUSIC.

2. How has previous research paved the way to the above systematic approach?

It is well-known that the conventional eigen-structured MUSIC has been developed on the basis of the second-order statistics (correlation matrix) of the data, and the additive spatially or temporally white Gaussian noise model [4]. In the presence of non-Gaussian noise which does not fit any workable model, the MUSIC fails as an estimator. In the

mid 1990s, the author and supervisor considered a cumulant-based MUSIC as a natural progression to providing a solution to the problem of fetal ECG detection in a noisy environment. The subject of cumulant-based MUSIC was formulated by R. Pan and C. L. Nikias [80] in an attempt to circumvent the noise-modelling problem and exploit the property of noise-free cumulants in the identification of harmonics. In theory, cumulants could be made free from Gaussian-noise for sufficiently long data. However, even if the cumulant-based MUSIC is susceptible to the changes in the probability distributions of the labour noise cocktail, if nothing is done about it. This had resulted in a limited success in fetal heart monitoring. Fortunately, this has played a definitive role in tackling the unavoidable problem of noise-modelling of the non-linear uterine contraction artefacts. However, this has proven to be a cumbersome problem due to the non-conformative behaviour of the *raw* multi-resonances UCS. Such an UCS, in the presence of the strong mother's QRS-complex, takes on a different form from that in a QRS-free environment. (This difference prevails in the higher-order statistical domains). As we discovered by conducting a separate investigation to study the chaotic behaviour of uterine contraction signals [62]. The obvious solution then was to tame all the transabdominally-measured ECG data by getting rid of the intrinsic non-linearities prior to any signal- or noise-modelling and subspace restructuring. It has been found more tractable to deal with linear non-Gaussian data rather than non-linear data. Essentially, efforts were diverted to isolating and measuring the uterine contraction interference signal (UCS) in a QRS-free interval as the maternal cardiac cycle is scanned segment by segment. And then linearise and compute its *residual* covariance matrix to be embedded in its respective reconfigured subspace. This subspace can be made orthogonal to the other subspace containing both the mother's and fetal QRS-complexes. In conclusion, in pursuing the eigen-structured MUSIC, no assumptions have been made whatsoever on the type of accompanying noise.

3. The UCS short-term and long-term statistical behaviour

The nature of the UCS changes with the length of the observation data. The UCS when observed over 10,000 samples was found to be deterministic, non-linear, and chaotic signal*. However, when observed over an 250-msec window, the UCS behaves more or

* *The definition of determinism is that future events are set causally by past events. So the next points to the closest point should describe the past events to the measurements at each point and we can therefore predict future events by taking an average of these points.*

less like noise. In pursuing separation of signals and interference signals, or signals and noise, two auxiliary methods have been used based on the concepts of *oriented energy* and *signal-to-signal ratio*, and *the Gram-Schmidt orthogonalisation*. This is done in addition to the MUSIC well established Generalised Singular Value Decomposition (GSVD) which deals with partitioning signal and coloured noise (as opposed to Gaussian noise) subspaces. The results presented in this chapter are based on the latter.

The rest was relatively easy and focused on separating two subspaces: **(1) The first S-subspace** contains either the covariance matrix of the coincident mother and fetal QRS-complexes, or predominantly one QRS-complex, and **(2) the second I-subspace** contains the modified covariance matrix of the *residual* uterine contraction interference signal (UCS).

4. How is the separation of the coexisting or non-coexisting mother's and fetal QRS-complexes performed?

The spectral content of the mother's QRS-complex and that of the fetus are different and indeed unique. The mother's QRS-complex principal spectral peak is found around 17 Hz., and the fetal QRS-complex principal spectral peak is found around 30 Hz. Accordingly, such individual spectral content can be exploited herewith in the identification and detection of either signal within the maternal cardiac cycle. The Kaiser filtered weighted MUSIC previously published algorithm has been devoted to identifying, in the frequency domain, anomalous QRS-complexes and P-waves such as P-on-T-waves and P-on-QRS-complex episodes for adult patients [37]. However, for FHR detection in labour, one has to overcome two major problems in the transabdominally-measured ECG data, namely, poor signal spectral resolution and the influence of the coexisting labour contraction signals which not only exhibit a fairly broad spectrum, but also is uniquely characterised by having localised energy resonances, one of which is seriously overlapping with the fetal distinctive strong peak around 30 Hz which represents the fetal spike. The fetal heartbeat detection is accomplished by thresholding the enhanced fetal spikes in the frequency domain. The most challenging problem is, therefore, not only to enhance the quality and resolution of the mother and fetal QRS-complexes' principal pseudo-spectral peaks, abbreviated as **MPPP** and **FPPP**, respectively, but also to suppress the UCS resonances and nudge its modified covariance matrix into a separate subspace which is named the interference

subspace (**I-subspace**). Orthogonalisation is forced between the **I-subspace** and the signal subspace (**S-subspace**) containing either the covariance matrix of both the mother's and fetal QRS-complexes or predominantly one QRS-complex. Again, depending on the coefficients of the Kaiser filter, the desired QRS-complex will prevail and the other will be attenuated. The data segment containing both mother's and fetal QRS-complexes can be read and re-read sequentially, or is divided into two separate streams and weighted differently in parallel so that individual QRS-complex principal peaks can be thresholded and detected simultaneously.

5. The choice of the window length

When choosing the window length, two factors were considered to be of importance; (1) To maximise the temporal resolution for the fetal heartbeat detection (the window segment should be short enough to capture the fetal heartbeat with the highest possible temporal resolution); and (2) the window length should be sufficiently long to limit the MUSIC variance. The Kaiser filter weights are applied to each of the 250 msec window (segment) and the weights are optimised to enhance the principal peaks of either QRS-complex in their respective temporal domains.

The rank properties of certain weighting functions and residual covariance matrices were left as an open question in this thesis.

6. What does distinguish this subspace-based technique from the previously published subspace-based technique for adults [37]?

The novelty of this technique rests on its dealing with the UCS during the strong and most painful peaks of labour contractions which are, apart from their noise-like characteristics, heavily contaminated with other noise artefact. Short data samples that can be classified as predominantly uterine noise artefact have been isolated within the maternal cardiac cycle and the computation of $\mathbf{I}_{noise}$ which represents the modified covariance matrix is performed and incorporated in the modified spectral MUSIC steering vector prior to the GSVD orthogonalisation. The 250 msec data portions earmarked for the UCS modified covariance matrix ($\mathbf{I}_{noise}$) fall mostly within segments III in the case of those maternal cardiac cycles that are free from coincident mother and fetal QRS-complexes in segments I, **OR** in segments II and IV for maternal cardiac cycles that do exhibit occurrences of coincident mother and fetal

QRS-complexes in Segments I.

7. Successful detection of coincident mother and fetal QRS-complexes has resulted in an increase of 9.3% and 5.4% over and above the TOC and the BIC template matching techniques, respectively.

The mother and fetal QRS-complexes often coincide making it impossible to separate them using any time-domain-based technique. Even with the higher-order statistics TOC, as reported earlier, there is a 13.8% failure rate, partially due to 9.8% rate of QRS-complex coincidences, and the rest, 4% rate, is due to overlapping fetal QRS-complex and maternal T-wave. The BIC failure rate of 9.8% is purely due to QRS-complex coincidences as there is a shortcoming in acquiring sufficiently high resolution to separate the bispectral peaks of the mother and fetal QRS-complexes. The overlapping of the fetal QRSs and the maternal T-waves can be resolved by the BIC template matching technique. The above percentages of QRS-complex coincident episodes have been found in the 50,000 maternal heartbeat database. The alternative is to try to resolve them in the frequency-domain.

Detailed results

1. Summary of short-term statistics of the modified covariance matrix of the UCS, I_{noise} matrix

- The modified covariance matrix of the UCS, $\mathbf{I}_{noise}$ matrix, is correlated because its off diagonal elements are non-zero.
- The Hinich Test for Gaussianity was applied to the $\mathbf{I}_{noise}$ matrix. The matrix does not satisfy the hypothesis of Gaussianity at a confidence level of 95%. The Gaussianity parameter, S-Gauss, was calculated to be 163.5 which is different from 0 for the Gaussianity assumption to be valid. So it is assumed that the $\mathbf{I}_{noise}$ matrix is non-Gaussian.
- The statistics of the $\mathbf{I}_{noise}$ matrix are calculated from the following equations for the variance, skewness, and kurtosis;

The variance is defined as $\gamma_2^x \underline{\underline{\nabla}} c_2^x(0) = \frac{1}{2\pi}\int_{-\pi}^{\pi} C_2^x(\omega).d\omega$

The skewness as $\gamma_3^x \underline{\underline{\nabla c}}_3^x(0,0) = \frac{1}{(2\pi)^2} \int_{-\pi}^{\pi} \int_{-\pi}^{\pi} C_3^x(\omega_1, \omega_2).d\omega_1.d\omega_2$

and the kurtosis as

$$\gamma_4^x \underline{\underline{\nabla c}}_4^x(0,0,0) = \frac{1}{(2\pi)^3} \int_{-\pi}^{\pi} \int_{-\pi}^{\pi} \int_{-\pi}^{\pi} C_4^x(\omega_1, \omega_2, \omega_3).d\omega_1.d\omega_2.d\omega_3$$

- The variance of $\mathbf{I}_{noise}$ equals 0.957, the skewness equals 1.321, and the Kurtosis equals 2.637. The skewness and kurtosis are calculated from the third- and fourth-order statistics of the $\mathbf{I}_{noise}$ which confirms that $\mathbf{I}_{noise}$ is non-Gaussian because its higher-order statistics are not equal to zero.
- The statistics of $\mathbf{I}_{noise}$ are different from the Uniform and Laplace noise which do not support third-order statistics because they are symmetrically distributed. They are also different from the Exponential and Rayleigh because its second, third- and fourth-order statistics are not related by one constant, e.g., λ, α.

2. Multiple overlapping windows to track deviations in the MPPP and FPPP frequencies

Up to five overlapping and optimised Kaiser weighted windows have been used in the detection of the following mother's QRS-complex principal spectral peaks; 15 Hz, 16 Hz, **17 Hz**, 18 Hz, and 19 Hz. Up to ten overlapping and optimised Kaiser weighted windows have been used in the detection of the following fetal QRS-complex principal spectral peaks; 28 Hz, 29 Hz, **30 Hz**, 31 Hz, 32 Hz, 33 Hz, 34 Hz, 35 Hz, 36 Hz, 37 Hz, and 38 Hz. The optimised Kaiser weights for the mother and fetal have been given in Appendix A6. Because there are inevitable deviations in the **17 Hz** and the **30 Hz** of the mother and fetal QRS-complex pseudo-spectra, respectively.

3. The choice of the model order

As with any eigen-structured MUSIC estimator, the model order has to be chosen very carefully. The optimum model order is **eleven for the signal** and **four for the noise**. **The method presented in this chapter is not sensitive to small deviations in the model order.**

4. Calculations of the bias and variance of the sequentially optimised, weighted, and I_{noise} incorporated MUSIC

Assume a mother's heart rate of 60 bpm yielding a cardiac cycle length of 1000 msec. Each maternal cardiac cycle has been divided into four segments (temporal windows) of 250 msec each. If the mother's heart rate reaches say, 100 bpm the individual segmentation length is reduced by 100 msec reducing the segment length to 150 msec. And this would result in an increase in the variance of 15%. The effect on the QRS- interval is marginally small as a normal interval is from 90 msec to 110 msec. The segmentation usually starts at 50 msec before the mother's R-wave and continues until the end of the first segment, albeit 250 msec or 163 msec. The other three equal segments are increased or decreased according to the mother's heart rate. It was reported earlier that a decrease in the temporal window, or the segment length, can increase the variance by up to 15% of the value assigned to the critical 250 msec.

Common definitions of the bias and variance are found in *Modern Spectral Estimation: Theory and Applications*, by S. Kay, Prentice Hall, 1987, [21].

- *The bias of the modified spectral MUSIC.* The bias is defined as the averaged differences in frequencies, over 10,000 cases, of the transabdominally-measured fetal MUSIC peaks and those of the fetal scalp electrode. It was shown that the sequentially optimised, weighted, and I_{noise} incorporated MUSIC has a bias of 1.23 and 2.15 for mother's and fetal principal spectral peaks, respectively. This is lower than that of the conventional MUSIC by approximately 45%. The improvement in the bias is because the principal spectral peaks of the fetal heartbeat segment are closer to that calculated from the fetal scalp electrode segment. For the mother's QRS-complex, the more deviation of the detected frequency of the MPPP around 17 Hz from that of the mother's chest ECG, the higher the bias will be. Similarly, for the fetal QRS-complex, the more deviation of the detected frequency of the FPPP around 30 Hz from that of the fetal scalp electrode, the higher the bias will be.

- *The variance of the modified spectral MUSIC.* The variance is defined as the averaged, squared differences in frequencies, over 10,000 cases, of the transabdominally-measured fetal MUSIC peaks and those of the fetal scalp

electrode. The variance of the fetal principal spectral peaks ranges from 0 to 8, with an average value of 4.127.

5. Performance analysis of fetal heart monitoring in cases of coincident and non-coincident mother's and fetal QRS-complexes

Assuming a mother's heart rate of 60 bpm yielding a cardiac cycle length of 1000 msec. Each maternal cardiac cycle has been divided into four equal segments (temporal windows) of 250 msec. The average rate by which the first fetal event coincides with the QRS-complex of the mother is 9.8%, based on 50,000 maternal cardiac cycles. When the two QRSs of the mother and fetal coincide in segment I, segment II is usually free from such events and may be taken as the UCS plus noise artefact segment. On average, the second fetal heartbeat occurs in segment III. And if there is a third fetal heartbeat (i.e., the fetal heart rate is three times the mother's), then it is likely to occur over both the fourth segment of the present cycle and the first segment of the next cycle. In most cases, we have encountered two fetal heartbeat occurrences within each maternal cardiac cycle. When the mother's heart rate goes up during painful labour contractions, we still found more or less two fetal heartbeat occurrences within each maternal cardiac cycle. The deceleration of the fetal heart rate after the peak of labour contractions is normal and not proven to be related to the mother's heartbeat as her heart will still be racing for a while after the peak of contractions.

The effect of proximity of the mother's and fetal R-wave on the frequency deviation of the fetal principal spectral peak around 30 Hz, and on the fetal heart detection rate

Performance analysis has included the effect of proximity of the mother's and fetal R-wave on the frequency deviation of the fetal principal spectral peak around 30 Hz, and on the fetal heart detection rate, in all observed cases of coincident mother and fetal QRS-complexes. The sequentially optimised, weighted, and $\mathbf{I}_{noise}$ incorporated MUSIC algorithm has been applied to approximately 50,000 maternal cardiac cycles, including 4,873 coincident QRS-complexes cases. The results are tabulated in Table 6.3.

It can be clearly seen that even for a fixed model order of 11 and 4 for the signal and noise subspace, respectively, the new MUSIC algorithm is capable of detecting fetal heartbeats, at a rate of almost 92%, when the mother and fetal R-waves are almost

Averaged R_m-R_f separation (msec)	**40**	**35**	**25**	**20**	**15**	**7**	**0**
Frequency deviation in the fetal FPPP ± (Hz)	**1.73**	**1.92**	**2.09**	**2.17**	**2.31**	**2.52**	**2.74**
Number of overlapping windows	**5**	**5**	**5**	**5**	**8**	**9**	**10**
Average detection rate (%)	**93.81**	**93.63**	**93.56**	**93.49**	**93.24**	**92.35**	**91.83**

Table 6.3: *The effect of proximity of the mother's and fetal R-wave on the frequency deviation of the fetal principal spectral peak around 30 Hz, and on the fetal detection rate. The total number of fetal heartbeats is 120,000. The number of coincident mother and the first fetal QRS-complexes is 4,873. The average fetal heart detection rate is 93.52% for coincident mother and the first fetal QRS-complexes within the maternal cardiac cycle. Otherwise, the average fetal heart detection rate is 99.5% for the second or third occurrences of fetal heartbeats within the maternal cardiac cycle.* ***The overall fetal heart detection rate for the 120,000 FHBs is 95.5%.*** *The model order is fixed at 11 and 4 for the signal and noise subspace, respectively.*

synchronised, provided that appropriate sequential weightings for the mother and the fetal are maintained throughout.

As the separation between the mother and fetal R-waves is increased, we can see a slight increase in the corresponding detection rate and a decrease in the **FPPP** frequency deviations.

The effect of the incorporation of the UCS modified covariance matrix on the fetal principal pseudo-spectral peak

The incorporation of the covariance matrix of the **UCS** helps to strengthen and sharpen the **FPPPs** for the optimum model order and in some cases it appears to be tolerant to a change in the model order from 11 and 4 to 9 and 4 for the signal and noise subspace, respectively. It has also resulted in a significant noise artefact reduction in the QRS-free segments.

The effect of the incorporation of the UCS modified covariance matrix on the fetal heart detection rate

The sequentially optimised, weighted and $\mathbf{I}_{noise}$ incorporated MUSIC has resulted in the following fetal heart detection rates: (i) 93.52% for coincident mother and fetal QRS-complexes, (ii) 99.35% for non-coincident mother and fetal QRS-complexes, and (iii) 95.50% overall average.

Without the incorporation of the UCS modified covariance matrix into the mathematical formulation of the sequentially optimised, weighted MUSIC, the following fetal heart detection rates have been obtained: (i) 89.23% as opposed to the 93.52% for coincident mother and fetal QRS-complexes, (ii) 97.51% as opposed to the 99.35% for non-coincident mother and fetal QRS-complexes. Because in the former no "appropriate noise model" was assumed in the analysis, and (iii) 91.20% overall average.

6.10 References

[1] S. Haykin, *Adaptive filter theory*, Prentice Hall, 1991.

[2] S. Marple, *Spectral Analysis With Applications*, Prentice Hall, 1987.

[3] P. Stoica and A. Nehorain, "MUSIC, maximum likelihood, and Cramer-Rao bound," IEEE Transactions on Acoustics, Speech, and Signal Processing, Vol. 37, pp. 720-741, 1988.

[4] R. Schmidt, "Multiple emitter location and signal parameter estimation," Proceedings of RADC Spectrum Estimation Workshop, pp. 243-258, 1979.

[5] R. O. Schmidt, *A Signal Subspace Approach To Multiple Emitter Location And Spectral Estimation*, PhD Dissertation, Department of Electrical Engineering, Stanford University, USA, 1981.

[6] R. Schmidt and R. Franks, "Multiple DF Signal Processing: An Experimental System," IEEE Transactions on Antennas and Propagation, vol. AP-34, pp. 281-190, March 1986.

[7] J. F. Kaiser, "Nonrecursive digital filter design using the Io-sinh window function," in Selected Papers in Digital Signal Processing, II, NY, IEEE, 1976.

[8] G. G. Golub, F. T. Luk, and M. L. Overton, "A block Lanczos method for computing the singular values and corresponding singular vectors of a matrix," ACM Transactions on Mathematical Software," Vol. 7, pp. 149-169, 1981.

[9] S. Van Huffel, J. Vandewelle, and A. Haegmans, "An efficient and reliable algorithm for computing the singular subspace of a matrix, associated with its smallest singular values," Jounral of Computational and Applied Mathematics, Vol. 19, pp. 313-330, 1987.

[10] S. Van Huffel, and J. Vandewelle, "The partial total least squares algorithm," Journal of Computational and Applied Mathematics, Vol. 21, pp. 333-341, , 1988.

[11] P. Stoica, and A. Nehroai, "MUSIC, Maximum Likelihood, and Cramer-Rao bound: Further results and comparisons," IEEE Transactions on Acoustics, Speech, and Signal Processing, Vol. 38, No. 12, pp. 2140-2150, December 1990.

[12] B. Friedlander and A. Weiss, "Direction finding using spatial smoothing with interpolated arrays," IEEE Transactions AES, vol. 28, pp. 574-587, April 1992.

[13] T. J. Shan, M. Wax, T. Kailath, "On spatial smoothing for directions of arrival estimation of coherent signals," IEEE Transactions Acoustics, Speech and Signal Processing, vol. 33, No. 4, pp. 806-811, 1985.

[14] A J Barabell, "Improving the resolution of performance of eigenstructure-based direction-finding algorithms," Proc ICASSP, vol. 83, pp. 336-339, 1983.

[15] D. Spielman, A. Paulraj and T. Kailath, "Performance Analysis Of The Music Algorithm," Proceedings of the IEEE International Conference on Acoustics, Speech, and Signal Processing, ICASSP, pp. 1909-1912, Japan, April 1986.

[16] U. Nickel, "Algebraic Formulation Of Kumaresan-Tufts Super resolution Method, Showing Relation to ME and MUSIC Methods," IEE Proceedings, vol. 135, pt. F, pp. 7-10, 1988.

[17] E. Moulines and J. F. Cardoso, "Second-Order Versus Fourth-Order MUSIC Algorithms," Proceedings of the International Signal Processing Workshop on Higher-Order Statistics, pp. 247-250, France, 1991.

[18] A. O. Steindhart, "Householder transformations in signal processing," IEEE Acoustics, Speech, and Signal Processing magazine, vol. 5, pp. 4-12, 1988.

[19] A. S. Householder, "Unitary traniangulization of a nonsymmetric matrix," Journal of the Association of Comput. Mach., Vol. 5, pp. 339-342, 1958.

[20] G. H. Golub, and A. H. Kahan, "Calculating the singular values and the pseudo-inverse of a matrix," Journal of SIAM Numer. Anal. B., vol. 2, pp. 205-224, 1965.

[21] S. Kay, *Modern Spectral Estimation: Theory and Applications*, Prentice Hall, 1987.

[22] M. Kaveh and A. J. Barabell, "The statistical performance of the MUSIC and the

minimum-norm algorithms for resolving plane waves in noise," IEEE Transactions on Acoustics, Speech, and Signal Processing, vol. ASSP-34, pp. 331-341, April 1986.

[23] H. Wang and M. Kaveh, "Performance of narrowband signal-subspace processing," Proceedings of the 1986 IEEE International Conference on Acoustics, Speech, and Signal Processing, Tokyo, Japan, pp. 589-592, April 1986.

[24] D. Spielman, A. Paluraj, and T. Kailath, "Performance analysis of the MUSIC algorithm," Proceedings of the 1986 IEEE International Conference on Acoustics, Speech, and Signal Processing, Tokyo, Japan, pp. 1909-1912, April 1986.

[25] X. Dongxin, J. C. Principe, and W. Hsiao-Chun, "Generalized eigendecomposition with an on-line local algorithm," IEEE Signal Processing Letters, Vol. 5, No. 11, pp. 298-301 , November 1998.

[26] E. Oja, "A simplified neuron model as a principal component analyzer," Journal of Math. Biol., Vol. 15, pp. 267-273, 1982.

[27] S. Y. Kung, K. I. Diamantaras, and J. S. Taur, "Adaptive principal component extraction (APEX) and applications," IEEE Transactions on Signal Processing, Vol. 42, May 1994.

[28] J. Mao and K. Jain, "Artificial neural networks for feature extraction and multivariate data projection," IEEE Transactions on Neural Networks, Vol. 6, March 1995.

[29] J. C. Principe, D. Xu, and C. Wang, "Generalised Oja's rule for linear discriminant analysis with Fisher criterion," Proceedings of the International Conference on Acoustics, Speech, and Signal Processing, pp. 3401, 3404, 1997.

[30] J. C. Principe, and D. Xu, "Classification with linear networks using an on-line constrained LDA algorithm," Proceedings of the IEEE Workshop on Neural Networks for Signal Processing VII, pp. 286-295, 1997.

[31] K. I. Diamanataras, and S. J. Kung, Principal component neural networks: Theory and applications, New York, Wiley, 1996.

[32] C. Chatterjee, V. P. Roychowdury, J. Ramos, and M. D. Zolowski, "Self-organizing algorithms for generalised eigen-decomposition," IEEE Transactions on Neural Networks, vol. 8, 1997.

[33] R. D. DeGroat, "Noniterative Subspace Tracking," IEEE Transactions on Signal Processing, Vol. 40, No. 3, pp. 571-577, March 1992.

[34] M. Sabry-Rizk, W. Zgallai, A. MacLean, K. T. V. Grattan, E. R. Carson, "The

Application of a Novel Class of Embedded Dynamic Cubic Volterra to Long-Term Prediction of Chaotic and Multi-Fractal Electromyographic Signals During Labour," the 4th International Conference on Neural Networks and Expert Systems in Medicine and Healthcare, Greece, June 2001.

[35] M. Sabry-Rizk, W. Zgallai, E. R. Carson, K. T. V.Grattan, A. MacLean, and P. Hardiman, "Non-linear dynamic tools for characterising abdominal electromyographic signals before and during labour," Transactions of the Institute of Measurement and Control, Vol. 22, pp. 243-270, 2000.

[36] M. Sabry-Rizk, W. Zgallai "Novel Volterra Predictor Based on State-Space Equilibrium of Nonlinear Single- or Multi-Fractal Signals" Proceedings of the SPIE's 45th Annual Meeting, the International symposium on Optical Science and Technology, SPIE2000, Advanced Signal Processing Algorithms, Architectures, and Implementations X, USA, Vol. 4116, pp. 322-333, 30/7-4/8/2000.

[37] M. Sabry-Rizk, W. Zgallai, C. Morgan, S. El-Khafif E. R. Carson, and K. T. V. Grattan, "Novel decision strategy for P-wave detection utilising nonlinearly synthesised ECG components and their enhanced pseudospectral resonances," IEE Proceedings Science, Measurement and Technology, Special section on Medical Signal Processing, vol. 147, No. 6, pp. 389-397, November 2000.

[38] M. Sabry-Rizk, W. Zgallai, E. R. Carson, S. El-Khafif, C. Morgan, and K. T. V. Grattan "Novel decision strategy for P wave detection utilising non-linearly synthesised ECG components and their enhanced pseudospectral resonances", IASTED-SIP 2001, Honolulu, Hawaii, USA, August 2001.

[39] M Sabry-Rizk, W. Zgallai, A. McLean, E. R. Carson, and K. T. V. Grattan, "Virtues and Vices of Source Separation Using Linear Independent Component Analysis for Blind Source Separation of Non-linearly Coupled and Synchronised Fetal and Mother ECGs," IEEE Engineering in Medicine and Biology Conference, USA, 2001.

[40] M. Sabry-Rizk, W. Zgallai, "Higher Order Statistics Are Indispensable Tools in The Analysis of Electrocardiogram Signals," IEE Colloquium on Statistical Signal Processing, January 1999.

[41] M. Sabry-Rizk, W. Zgallai, E. R. Carson, S. El-Khafif, C. Morgan, and K. T. V. Grattan "Novel decision strategy for P wave detection utilising non-linearly synthesised ECG components and their enhanced pseudospectral resonances", IEE

International conference, MEDSIP2000, Bristol, UK, September 2000.

[42] M. Sabry-Rizk, W. Zgallai E. R. Carson, K. T. V. Grattan, P. Hardiman, P. Thompson and A. Maclean, "Modified MUSIC Pseudospectral Analysis Reveals Common Uterus and Fetal Heart Resonances During Labour Contractions", the 22nd Annual International Conference of the IEEE Engineering in Medicine and Biology Society, EMB2000, USA, 23-28/7/2000.

[43] M. Sabry-Rizk, W. Zgallai, E. R. Carson A. MacLean, K. T. V. Grattan, "Multi-fractility in Fetal Heart Beat Dynamics," 2nd European Medical & Biological Engineering Conference Vienna (Austria), December 04-08, 2002.

[44] E. Cicinelli, A. Bartone, I. Carbonara, G. Incampo, M. Bachicchio, G. Ventura, S. Montanaro, and G. Aloisio, "Improved equipment for abdominal fetal electrocardiogram recording: description and clinical evaluation," Int. J. Biol. Med. Comput., Vol. 5, pp. 193-205, 1994; D. Callaerts et al., "Description of a real time system to extract the fetal electrocardiogram," Clin. Pgys. Physiol. Meas., Vol. 10, Suppl. B., pp. 7-10, 1989; D. Callaerts, B. DeMoor, J. Vanderville, W. Sansen, "Comparison of SVD methods to extract the fetal electrocardiogram," Med. Biol. Eng. Comput., Vol. 28, pp. 217-224, 1990.

[45] J. Vanderschoot, D. Callaerts, W. Sansen, J. Vaderwalle, G. Vantrappen, and J. Janssens, "Two methods for optimal MECG elimination and FECG detection from skin electrode signals," IEEE Transactions on Biomedical Engineering, Vol. BME-34, No. 3, pp. 233-242, 1987.

[46] L. De Lathauwer, B. De Moor, and J. Vanderwelle, "Fetal electrocardiogram extraction by blind source subspace separation", IEEE Transactions on Biomedical Engineering, Vol. BME-47, No. 5, pp. 567572-, 2000.

[47] D. Callaerts, J. Vanderschoot, J. Vanderwelle, W. Sansen, G. Vantrappen, and J. Sansen, "Fetal electrocardiogram measuring method and equipment (FMME)," J. Perinatal Medicine, World Symp. On Computers in the Care of Mother, Fetus, and Newborn, Vol. 15, suppl. 1, no. 4, pp. 33, 1987.

[48] D. Callaerts, J. Vanderwelle, W. Sansen, J. Janssens, and G. Vantrappen, "Acquisition and processing of the antepartum FECG," in A Critical Appraisal of Fetal surveillance, H. P. Van Dejin, and F. J. A. Copray, Eds., Amesterdam, The Netherlands: Elsevier Science B. V., pp. 371-380, 1994.

[49] J. Vanderschoot, G. Vantrappen, J. Jansens, J. Vanderwelle, and W. Sansen, "A reliable method for fetal ECG extraction from abdominal recordings," in Medical

Informatics Europe 84 Lecture Notes in Medical Informatics, F. H. Roger, et al., Eds., Berlin, Germany: Springer Verlag, vol. 24, pp. 249-254, 1984.

[50] W. J. Tompkins, *Biomedical digital signal processing*, Prentice Hall, 1993.

[51] S. Marple, *Spectral Analysis With Applications*, Prentice Hall, 1987.

[52] M. Sabry-Rizk, W. Zgallai E. R. Carson, K. T. V. Grattan, P. Hardiman, P. Thompson and A. Maclean, "Modified MUSIC Pseudospectral Analysis Reveals Common Uterus and Fetal Heart Resonances During Labour Contractions", the 22nd Annual International Conference of the IEEE Engineering in Medicine and Biology Society, EMB2000, USA, 23-28/7/2000.

[53] M. Sabry-Rizk, W. Zgallai, A. MacLean, and E. R. Carson, "Multi-fractility in labour contraction dynamics," The 2nd Joint Conference of the IEEE Engineering in Medicine and Biology Society and the Biomedical Engineering Society,23-26 October 2002, Houston, Texas, USA.

[54] S. Haykin, A. Steinhardt, "Adaptive Radar detection and estimation," A volume in the Wiley Series in Remote Sensing, J. A. Kong, Series Editor, J. Wiley and sons, inc., 1992.

[55] D. Callaerts, B. DeMoor, J. Vanderville, and W. Sansen, "Comparison of SVD methods to extract the fetal electrocardiogram," Med. Biol. Eng. Comput., Vol. 28, pp. 217-224, 1990.

[56] A. Van Oosterom and J Alsters, "Removing the maternal component in the fetal ECG using singular value decomposition," In Electrocardiography '83. I. Ruttkay-Nedecky and P. MacFarlane, Eds., Exceptra Medicine, Amesterdam, The Netherlands, pp. 171-176, 1984.

[57] A. Van Oosterom, "Spatial filtering of the fetal electrocardiogram," J. Perinat. Med., Vol. 14, No. 6, pp. 411-419, 1986.

[58] D. Callaerts, J. Vanderschoot, J. Vandewalle, W. Vantrappen, and J. Janssens, "An adaptive on-line method for the extraction of the complete fetal electrocardiogram from cutaneous multilead recordings," J. Perinat. Med., Vol. 14, No. 6, pp. 421-433, 1986.

[59] D. Callaerts, J. Vanderschoot, J. Vandewalle, and W. Sansen, "An on-line adaptive algorithm for signal processing using SVD," In Signal Processing III, Elsevier Science/ North Holland/, Amesterdam, The Netherlands, EURASIP 86, The Hague, pp. 953-956, 1986.

[60] B. N. Parlett, *The Symmetric eigenvalue problem*, Prentice Hall, Englewood, Cliffs,

New Jersey, USA, 1980.

[61] J. C. Mosher et al., "Multiple dipole modelling and localisation from spatio-temporal MEG data," IEEE Transactions on Biomedical Engineering, Vol. 39, pp. 541-557, June 1992.

[62] [81] M Sabry-Rizk, W Zgallai, E. R. Carson, K. T. V. Grattan, A. MacLean, and P. Hardiman Non-linear dynamic tools for characterising abdominal electromyographic signals before and during labour. Trans Inst Measurement and Control, vol. 22, pp. 243-270, 2000.

[63] P. Ch. Ivanov, L. A. Nunes Amaral, A. L. Goldberger, S. Havlin, M. G. Rosenblums, Z. R. Struzik, and H. E. Stanley, "Multifractality in human heartbeat dynamics", Nature, vol. 399, pp. 461-465, 3 June 1999.

[64] N. V. Thakor, J. G. Webster, and W. J. Tompkins, "Estimation of QRS complex power spectra for design of QRS filters," IEEE Transactions on Biomedical Engineering, vol. 31, pp. 702-706, 1984.

[65] M. Sabry-Rizk, W. Zgallai, P. Hardiman, and J. O'Riordan, "MUSIC-Based Bispectrum Detector: A Novel Non- Invasive Detection Method For Overlapping Fetal And Mother ECG Signals," Proceedings of the 19th IEEE International Conference on Engineering in Medicine and Biology, EMBS, pp. 72- 75, USA, October 1997.

[66] M. J. Hinich, "Test for Gaussianity and linearity of a stationary time series," Journal of time series analysis, vol. 3, No. 3, pp. 169-176, 1982.

[67] H. E. Hurst, "Long-term storage capacity of reservoirs," Transactions of the American Society of Civil Engineers,Vol. 116, pp. 770-808, 1951.

[68] T. Vicsek, Fractal Growth Phenomena, 2nd edition, World Scientific, Singapore, 1993.

[69] H. Takayasu, Fractals in the physical sciences, Manchester University Press, UK, 1997.

[70] H. E. Stanley, in Fractals and disordered systems, 2nd edition, A. Bunde and S. Halvin, eds., pp. 1 – 68, Springer, Brerlin, 1996.

[71] V. F. Pisarenko, "The retrieval of harmonics from a covariance function," Geophys. J. Roy. Astron. Soc., Vol. 33, pp. 347-366, 1973.

[72] M. Sabry-Rizk, W. Zgallai, "Novel robust modified pseudo-spectral MUSIC algorithm for on-line QRS detection in electrocardiogram signals", to be published.

[73] B. De Moor, J. Vanderwalle, and J. Staar, Oriented energy and oriented signal-to signal ratio concepts in the analysis of vector sequences and time series, In SVD and signal processing: algorithms, applications, and architectures. E. Deprettere, (Ed.) North Holland, pp. 209-232, 1987.

[74] B. De Moor, Mathematical concepts and techniques for modelling of static and dynamic systems, PhD. Thesis, Dept. of Electrical Engineering, Katholieke Universiteit, Leuven, Belgium, June 1988.

[75] J. Vanderwalle, D. Callaerts, "Singular value decomposition: a powerful concept and tool in signal processing," Proc. Conf. On Mathematics in Signal Processing, Warwick, 1988.

[76] S. Haykin, *Adaptive filter theory*, Prentice Hall, 1991.

[77] R. Schmidt, "Multiple emitter location and signal parameter estimation," Proceedings of RADC Spectrum Estimation Workshop, pp. 243-258, 1979.

[78] J. C. Mosher et al., "Multiple dipole modelling and localisation from spatio-temporal MEG data," IEEE Trans. Biomedical Engineering, Vol. 39, pp. 541-557, June 1992.

[79] M. Kristensson, M. Jansson, and B. Ottersten, "Further results and insights on subspace sinusoidal frequency estimation," IEEE Transactions on Signal Processing, vol. 49, No. 12, pp. 2962-2974 , December 2001.

[80] R. Pan and C. L. Nikias, "Harmonic decomposition methods in cumulant domains," Proc. ICASSP'88, pp. 2356-2359, NY, 1988.

CHAPTER SEVEN

FINAL CONCLUSIONS

The three proposed non-invasive state-of-the-art signal processing techniques

The thesis proposes and evaluates **three** state-of-the-art signal processing techniques to detect fetal heartbeats within each maternal cardiac cycle, during labour contractions, using only a pair of transabdominal electrodes. A second pair of electrodes may be used for the mother's chest ECG. The first and second techniques are, namely, the structured third-order cumulant-slice-template matching and the bispectral-contours-template matching for fetal QRS identification, respectively. The third technique is based on the modified and appropriately weighted spectral multiple signal classification (MUSIC) with incorporated covariance matrix for uterine contraction noise-like interfering signals also contaminated with noise. Essentially, two modifications to the standard MUSIC have been developed in order to enhance the performance of the spectral estimator in our applied work. The first modification involves the introduction of an optimised weighting function to the segmented ECG covariance matrix, and is chiefly aimed at enhancing the fetal QRS major spectral peak which occurs at around 30 Hz against the mother QRS major spectral peak usually occurring around 17 Hz and all other noise contributions. Additional optional pseudo-bispectral enhancement to sharpen the maternal and fetal spectral peaks in particular when the mother and fetal R-waves are temporally coincident has been achieved. The second modification to the spectral MUSIC is the removal of the unjustified assumption that only white Gaussian noise is present and the incorporation of the actual measured labour uterine contraction covariance matrix in reconfigured subspace analysis. This inevitably leads to the generalised eigenvectors – eigenvalues decomposition modern signal processing. This is now coined the modified, interference incorporated pseudo-spectral MUSIC. The above mentioned first and second techniques are higher-order statistics-based (HOS) and

hybrid involving both signal processing and NN classifiers. The third technique is second-order statistics-based (SOS).

In all techniques, the removal of signal non-linearity with the aid of non-linear Volterra synthesisers plays a crucial part in the fetal detection integrity. Essentially, Chapter Two has provided a complete coverage of the application of higher-order statistics to ECG data, and Chapter Three has exploited the non-linear Volterra synthesiser in relation to the concept of ECG signal and noise linearisation. The adaptively optimised parameters of the LMS-based and the LMF-based second- and third-order Volterra synthesisers were given in all the relevant figure captions in this thesis. During a clinical trial in a London hospital, a PC was provided by our software with fixed optimised Volterra parameters, and this has not changed the outcome as given in this conclusion. Also, the parameters of the single-hidden-layer perceptron classifier were fixed.

The thesis has covered **current** non-invasive FHR monitoring techniques and has given adequate appraisal to all other non-invasive **modern signal processing techniques**, including those based on higher-order statistics, wavelet transform, and non-linear dynamic modelling. None of such techniques had been properly assessed against a reference fetal scalp electrode, and in the majority of cases the fetal heartbeat is visible in their moderate-to-high SNR ECG data.

Adequate individual chapter's discussions and conclusions have been presented and will not be repeated here for brevity and because it is now prudent to concentrate on conclusions that are only relevant to the three non-invasive signal processing techniques presented in this thesis, and given in Chapters Four, Five, and Six.

Data acquisition

The extraction and subsequent analysis of the fetal electrocardiogram (FECG) from the maternal abdomen (transabdominally) can potentially provide the clinician with an indication of fetal status. Currently, such FECG assessment can be performed during labour, using signals obtained from a scalp electrode. This is invasive and undesirable during labour, and may even be the cause of fetal infection in an otherwise normal healthy labour. This is not an overstatement, particularly before the onset of labour, as it necessitates rupturing the maternal sack which contains the amniotic fluid, prematurely,

to allow access to and clipping of the fetal scalp. Assuming of course that the fetal is not in a breached position, e.g., head first. It is, therefore, very desirable to be able to monitor the fetal ECG transabdominally without any loss of signals, as in the case of the ultrasound mode, during antepartum and intrapartum. It is particularly valuable to have continuous transabdominal FECG monitoring before, during, and after each painful uterine contraction **peak** as this determines whether the fetal responds normally to this enormous pressure which is attributed to perfect precession electromechanical activities, as previously investigated in the higher-order statistical domains by Dr. M. Sabry-Rizk and Mr. Zgallai under a research contract. This has been mentioned briefly in the thesis. The Doppler ultrasound requires skill to operate and position the transducer so as to acquire the fetal ultrasound, making it unsuitable for long-term ambulatory monitoring. The opposite is true for our PC-based techniques, because there is no sensitivity as to whereabouts the electrode pair is positioned on the abdomen. In fact, the techniques presented here can pick up the occurrences of the fetal heartbeat from a pair of bipolar electrodes placed on the mother's chest, albeit at –13 dB or so measured from the mother's R-wave. This is because HOS-based techniques, when appropriately exploited with a view of minimising the Gaussian noise and identifying the range and extent of distortion, and provided that the latter does not affect the discriminant properties of the cumulants or their bispectra which applies to fetal/mother ECG, can be used in adaptive discriminant patterns "robustification".

Signals obtained from the maternal thorax and abdomen via a specially designed four-channel isolation amplifier which has a flat frequency response between 0.5 and 100 Hz and 3 dB points at 0.05 and 250 Hz. This extended low frequency response, together with the accompanying flat phase response, minimises distortion of the low frequency components in the FECG such as the P- and T-waves which could hinder precise clinical diagnosis.

Transabdominal signals are taken in either vertical or horizontal directions, with electrodes spaced about 25 cm apart and equidistant with the umbilicus. These transabdominal signals consist of maternal and fetal ECG complexes (typical amplitudes of 100 μv and 20 μv, respectively) as well as a variety of noise sources. In order to make these signals' magnitudes suitable for digitisation, amplification by a factor of 10,000 is required. Digitisation is performed at a sampling rate of 500 Hz with 16-bit resolution.

The electrodes used are the wet gel disposable (silver/silver/chloride) type. The fetal scalp electrode is clipped to its head. The common reference electrode is attached to the mother's thigh. The skin is first cleaned with alcohol-saturated cotton wool to remove grease, dirt and dead skin, thus decreasing the skin electrode impedance.

Problems associated with obtaining suitable traces include large baseline drift (which can cause amplifier saturation), abdominal muscle noise which can swamp the ECG signals, and 50 Hz interference. All has been dealt with in the thesis, particularly the challenging problem of labour uterine contraction.

Critical data segmentation for the second- and third-order statistics-based techniques

Because the fetal heart detection techniques presented in the thesis rely on adequate mother QRS-complex detection in the first instance, the emphases here are on delineating the boundary of each maternal cardiac cycle by first detecting the mother's QRS-complexes. This is followed by dividing the cardiac cycle into four segments, coded as I, II, III, and IV (segment I contains the mother's QRS-complex and any fetal heartbeat), with a view to improve both the temporal and spectral resolutions, as well as limiting the HOS variances and the MUSIC variance. On average, the cardiac cycle is 1,000 msec for a mother's heart rate of 60 bpm. Therefore, individual segments have equal length of 250 msec. This also applies to the synchronised fetal scalp electrode ECG signal, but with a typical fetal QRS-complex length of 60 msec, as opposed to a normal QRS-complex range between 90 msec and 110 msec in adults. It is very common to have two fetal heartbeats in each maternal cardiac cycle. It is less common to have three fetal heartbeats in each maternal cardiac cycle. Four fetal occurrences within a maternal cardiac cycle is a rare event. As the mother's heart rate increases or decreases, this inevitably affects the QRS-complex resolution in both the time and the frequency domains, as well as the corresponding variance. Naturally, the ECG segment length ranges from 150 msec to 300 msec, for a corresponding range of mother's heart rate from 100 bpm to 50 bpm. The behaviour of the uterine contraction interference signals takes on the form of short-term noise-like. As opposed to its long-term non-linear chaotic behaviour.

Data scenarios

The above mentioned four segments were coded as I, II, III, and IV, each of length 250 msec. These four coded segments have often ascribed to one of the following scenarios;

Scenario 1:

(I) Segment I, 0 – 250 msec; Predominantly maternal QRS-interval (no fetal heartbeat present),

(II) Segment II, 251 msec – 500 msec; The first fetal heartbeat with maternal contribution,

(III) Segment III, 501 msec – 750 msec; QRS-free ECG, and

(IV) Segment IV, 751 msec – 1000 msec; The second fetal heartbeat with maternal contribution.

Scenario 2:

(I) Segment I, 0 – 250 msec; Both maternal and fetal QRS-complexes,

(II) Segment II, 251 msec – 500 msec; QRS-free ECG,

(III) Segment III, 501 msec – 750 msec; The second fetal heartbeat with maternal contribution, and

IV) Segment IV, 751 msec – 1000 msec; Either QRS-free ECG or possibly the third fetal heartbeat with maternal contribution.

The short-term statistical behaviour of the uterine contraction interference signals (UCS)

The nature of the UCS changes with the length of the observation data. For instance, if the UCS is observed over 10,000 samples it can be modelled as deterministic, non-linear, chaotic, and multi-fractal signals [1-4]. First, we need to quantify the long-term statistics before we refer to short-term statistics.

UCS Long-term statistics (data length 10,000 msec). Essentially, the multi-fractility is indicative of normality in this case. Based on the Hinhch linearity test and the Hurst component analysis test which will now be described.

The Hinich linearity test: The test is based on the observation that for a linear process the skewness will be constant. In the Hinich linearity test, the inter-quartile range of the estimated bicoherence squared is computed; a quantity, Λ, proportional to the mean value of the bicoherence squared is also computed; the theoretical inter-quartile range of

a chi-square random variable with two degrees of freedom and non-centrality parameter, Λ, is then computed. The linearity hypothesis should be rejected if the estimated and theoretical inter-quartile ranges are very different from one another. The non-centrality parameter is $\Lambda = \frac{2N}{\left(1+\rho^{-1}\right)^3}\Gamma_s$, where Λ is the non-centrality parameter, N is the number of samples, ρ is the signal-to-noise ratio, and Γ is the skewness of the signal. The estimated and theoretical inter-quartile ranges are 268.91 and 42.59, respectively. Hence, the non-linearity hypothesis was accepted.

The Chaoticity Hurst component test: The test is based on the observation that multi-fractal signals can be decomposed into many subsets characterised by different local Hurst exponents, h, which quantify the local singular behaviour and relate to the local scaling of the signal. The local value of h is extracted using the Wavelet theory. The local exponent, h, is evaluated through the modulus of the maxima values of the wavelet transform at each point of the signal. A function Zq(a) is defined as the sum of the qth powers of the local maxima of the modulus of the wavelet transform coefficients at scale a. The scaling of that partitioning function, Zq(a), is estimated. For small scales we expect the partitioning function Zq(a) scales as a power law, $Zq(a) \cong a^{t(q)}$. For certain values of q, the exponents t(q) have familiar meanings. In particular, t(2) is related to the scaling exponent of the Fourier power spectra, $S(f) \cong 1/f^{b}$, as b = 2 + t(2). For positive q, Zq(a) reflects the scaling of the large fluctuations and strong singularities, whereas for negative q, Zq(a) reflects the scaling of the small fluctuations and weak singularities. For multi-fractal signals, t(q) is a non-linear function: t(q) = q h - D(h), where h = dt/ dq is not constant. The fractal dimension D(h) is related to t(q) through a Legendre transform: D(h) = q h - t(q). The local Hurst exponents, h, quantify the local singular behaviour and thus relate to the local scaling of the time series. Using the 10,000 samples of the UCS, the partitioning function was calculated for scales a > 8 and for values of q ranges from -5 to 5. It was found that t(q) is a non-linear function of q; also D(h) has non-zero values for a broad range of the local Hurst exponents, h, which indicates that the corresponding UCS is a multi-fractal signal. The range of scaling exponents ($0 < h < 0.4$) with non-zero fractal dimension D(h) indicates that the fluctuations in the UCS exhibit anti-correlated behaviour (h = 1/2 corresponds to uncorrelated behaviour; h > 1/2 corresponds to correlated behaviour). Hence, the UCS is a deterministic, non-linear, and chaotic signal.

UCS Short-term statistics (data length 250 msec)

1- The Hinich Test for Gaussianity was applied to the 250 msec UCS segments The UCS does not satisfy the hypothesis of Gaussianity at a confidence level of 95%. The Gaussianity parameter, S-Gauss, was calculated to be 163.5 which is different from 0 for the Gaussianity assumption to be valid. So it is assumed that the UCS is non-Gaussian.

2- The statistics of the UCS are calculated from the following equations for the variance, skewness, and kurtosis;

The variance is defined as $\gamma_2^x \underline{\underline{\nabla}} c_2^x(0) = \frac{1}{2\pi}\int_{-\pi}^{\pi} C_2^x(\omega).d\omega$,

the skewness as $\gamma_3^x \underline{\underline{\nabla}} c_3^x(0,0) = \frac{1}{(2\pi)^2}\int_{-\pi}^{\pi}\int_{-\pi}^{\pi} C_3^x(\omega_1,\omega_2).d\omega_1.d\omega_2$,

and the kurtosis as

$\gamma_4^x \underline{\underline{\nabla}} c_4^x(0,0,0) = \frac{1}{(2\pi)^3}\int_{-\pi}^{\pi}\int_{-\pi}^{\pi}\int_{-\pi}^{\pi} C_4^x(\omega_1,\omega_2,\omega_3).d\omega_1.d\omega_2.d\omega_3$. The variance of the UCS equals 0.957, the skewness equals 1.321, and the Kurtosis equals 2.637. The skewness and kurtosis are calculated from the third- and fourth-order statistics of the UCS which confirms that the UCS is non-Gaussian because its higher-order statistics are not equal to zero.

3- The statistics of the UCS are also different from the Uniform and Laplace noise which do not support third-order statistics because they are symmetrically distributed. It is also different from the Exponential and Rayleigh because its second, third- and fourth-order statistics are not related by one constant, e.g., λ, α.

Characteristics of the motion artefact noise. The second- and third-order statistics of a motion artefact noise segment of 10,000 samples were extracted from the MIT/BIH NSR and AR databases. On the one hand, the power spectrum has proven not to be accurate enough to be relied upon in a thesis like this which deals with the higher-order statistics of motion artefact. On the other hand, the bispectrum depicts many frequencies in the triangle region of (0 Hz,0 Hz), (0 Hz,35 Hz) and (35 Hz,0 Hz). These bispectral frequencies of motion artefact would be overlapping with those of the mother's and fetal QRS-complexes, albeit at around –20 dB level. However, the level of

noise at the QRS-complex spectra is comparatively small, and the effect of motion artefact on the detection of QRS-complexes is not noticeable. The bicoherence squared is rather confined to very low frequencies.

The first hybrid system: The third-order cumulant slice template matching in conjunction with a single-layer perceptron

Early research studies which have not been presented in this thesis, but have been carried out under an two-and-half-year research contract, exploited the whole multi-dimensional structures of the third- and fourth-order cumulants of the ECG signals presented in this thesis in conjunction with multi-layered feed-forward neural networks. The justification for this multi-layer perceptron network was based entirely on the assumption that by including a sufficient number of hidden layers, the network would be enabled to extract both third-and fourth-higher-order statistics embedded in the cumulants presented to the network input. The multi-dimensional ECG cumulants were created first and subsequently a pre-selected number of slices were extracted and cascaded side-by-side to be presented to the input layer of the MLP. In the early days of this research, it was difficult to make a decision, just by mere observations of the available 1-d third-order cumulant slice or 2-d fourth-order cumulant slice patterns produced from the transabdominally-measured ECG signals, as to which of such slices would show a distinguishable pattern which could be matched to the corresponding mother or fetal ECG templates. Particularly, those templates of the fetal scalp electrodes which have been used as a reference, so that the fetal heartbeat detection could be verified in the midst of those complex maternal environments and counted within each maternal cardiac cycle.

Current research studies have focused on the use of a single-hidden-layer perceptron and a one-dimensional cumulant slice. There are mathematical formulae and software developed by the author which deal with any arbitrarily chosen off diagonal and off wall one-dimensional slice and this helps to reduce the CPU time by 99%.

Detailed results

1. The effect of the chosen window length on the third-order cumulant variance

The transabdominal ECG signal is linearised and segmented prior to the third-order cumulant calculations. The window length is carefully chosen to serve two criteria; (i) to yield an acceptable upper threshold of both the deterministic and stochastic noise types inherent in the higher-order statistics of the ECG signals encountered, and (ii) to allow the detection of one, two, three, or four fetal heartbeats (FHBs) within one maternal transabdominal cardiac cycle.

It has also been shown that the variance of a Gaussian noise segment of the same length is equal to 1.0629 which is close to the ideal value of 1.0. The variance would increase by more than 20% if the segment length is halved. The TOC variance of the fetal heartbeat segments has been calculated. It ranges from 0.64 to 4.2 with an average value of 2.381.

2. Calculation of averaged fetal heart rates

Templates of third-order cumulant diagonal and wall slices are used as the desired response of the single-hidden-layer perceptron in the training phase. The TOC template matching procedure starts by matching the slices of the segments to the templates until the first and the second maternal QRS-complexes are detected and their R-wave are pinpointed. The maternal heart rate is accurately calculated from the knowledge of the current and previous R-wave positions. Then, the search for the fetal heartbeat starts at 50 msec before the first maternal R-wave and continues until we reach the second maternal R-wave. Although the ECG TOC template matching technique is very effective in detecting the occurrence of the fetal heartbeats as a whole even when it is completely buried in noise, it cannot locate the fetal R-wave over a window length of 250 msec. However, we can measure fairly accurately the maternal heartbeats and calculate the instantaneous heart rate for the mother. Hence, by counting the number of fetal heartbeats that have occurred between two successive maternal R-waves, one can easily calculate the averaged FHR within the maternal cardiac cycle;

The average FHR = MHR x Number of FHBs / number of maternal heartbeats

In the above formula, the instantaneous maternal heart rate is previously known with some degree of accuracy, and the relative fetal to maternal heartbeat is also known within the maternal cardiac cycle. Hence, the averaged fetal heart rate can be calculated within each maternal cardiac cycle.

3. Parameters of the single-hidden layer perceptron

A major limitation of the back-propagation algorithms is the slow rate of convergence to a global minimum of the error-performance surface because the algorithm operates entirely on the gradient of the error-performance surface with respect to the weights in the single-hidden-layer perceptron. The back-propagation learning process is accelerated by incorporating a momentum term. The use of momentum introduces a feedback loop which prevents the learning process from being stuck at a local minimum on the error-performance surface of the single-hidden-layer perceptron.

The network has been optimised in terms of its learning rate, momentum constant, and hidden layer size to achieve the minimum mean-squared error. The optimum learning rate is found to be 0.8. The optimum momentum constant is found to be 0.99 and 0.90 for the maternal QRS-complex and the fetal heartbeat with maternal contribution segments, respectively. The input layer size of the neural network is 8 x 8. The single-hidden-layer has an optimum dimension of 5 x 5. The input to the first layer is the third-order cumulants diagonal and wall slices. The network is trained using TOC slice templates. The input to the network is eight template patterns. These are the third-order cumulant diagonal and wall slices of four segments from one transabdominal cardiac cycle. For example the first pair are the maternal QRS-complex TOC diagonal and wall slices, the second pair are the first fetal heartbeat TOC diagonal and wall slices, the third pair are QRS-free ECG TOC diagonal and wall slices, and the fourth pair are the second fetal heartbeat TOC diagonal and wall slices. The network is trained over the eight patterns. The training terminates when the worst error in all patterns in one pass is less than 0.1. Typically the average error will be in the range of 0.001.

4. The classification rate for maternal QRS-complex and fetal heartbeat segments

The results of the first hybrid system indicates that a linear combination of diagonal and wall slices of the TOC can improve the detection rate by up to 1% over and above the

77.8% obtainable using only either slice. Using two more arbitrary slices off-diagonal and off-wall would result in a further improvement of up to 1%. Using two slices, instead of only one, result in an two-fold increase in the CPU time of 1 msec using Unix WS.

Further improvement of 6% to 8% is attainable with maternal transabdominal ECG signal linearisation employing second- and third-order Volterra synthesisers, respectively. Based on the first hybrid system using TOC slices for signal processing and subsequent single-hidden-layer classification, 100% and 86.16% classification rates have been achieved for maternal QRS-complex and fetal heartbeats, respectively. Note that the classification rates for coincident and non-coincident mother's and fetal QRS-complexes are 0% and 95.55%, respectively.

The remaining undetected 13.84% fetal heartbeats include 9.8% overlap with the maternal QRS-complexes and 4% occur during depolarisation of the maternal T-waves. Those events unavoidably lead to significant distortion of the fetal third-order cumulants. This means that the cumulant signatures will not be close to the TOC template signature stored in the database. Examples of false negatives and false positives have been found in the following cases, respectively, (i) a fetal heartbeat with maternal contribution TOC diagonal slice was wrongly matched to a QRS-free ECG TOC diagonal slice template, and (ii) a QRS-free ECG TOC diagonal slice was wrongly matched to a fetal heartbeat with maternal contribution TOC diagonal slice template.

The averaged classification rate is 86.16% for 120,000 fetal heartbeats.
Fetal heartbeats falling within the maternal QRS-complex have not been detected.

The second hybrid system: The bispectral contours template matching in conjunction with a single-hidden-layer perceptron

The hybrid bispectral contour matching technique is an extension to the above cumulant-based hybrid technique. Therefore, the choice of the NN classifier is based on the general discussion presented previously. *Prior information* remains as a valuable asset and is very much exploited herein. It is the matching of the horizontal 2-d bispectral contours that has been used in the BIC template matching technique instead of the 1-d polar bispectral slices. Because in order to use the 1-d polar bispectrum slices

effectively, one needs to use a minimum of 24 polar slices to facilitate capturing the most rapid changes in the bispectrum including null features that could be used as discriminant patterns. Whereas for BIC contours, provided that they are horizontally cut at a maximum number of 10 levels, a good quality discriminant picture can be made available for the neural network classifier. For example, it is very unlikely that maxima and troughs are missed because of any changes in their respective positions.

Approximately 50,000 maternal cardiac cycles have been included in the analysis. The numbers of bispectral contours compound templates are 10 for the maternal chest, 10 for the fetal scalp, and 140 for the transabdominally-measured 250 msec segments, respectively. Each bispectral compound template is made of 10 horizontal templates at different levels. Starting from a normalised 0 dB and going down in steps of 1 dB each to a – 10 dB.

The maternal transabdominal ECG signal is linearised using an optimised LMF-based second- or third-order Volterra synthesiser. The second-order Volterra synthesiser parameters are: filter length = 6, step-size parameters = 0.005, and 0.0004 for linear and quadratic parts, respectively, delay = 5. The third-order Volterra synthesiser parameters are: filter length = 6, step-size parameters = 0.001, 0.0002, and 0.0004 for linear, quadratic and cubic parts, respectively, delay = 5. The transabdominal ECG signal is segmented into four segments containing; (I) The maternal QRS-complex, (II) the first fetal heartbeat with maternal contribution, (III) QRS-free ECG, and (IV) the second fetal heartbeat with maternal contribution. To segment the transabdominal ECG signals, the window length is carefully chosen to; (i) Yield an acceptable upper threshold of both the deterministic and stochastic noise types inherent in the higher-order statistics of the ECG signals encountered, and (ii) allow the detection of one, two, three, or four fetal heartbeats (FHBs) within one maternal transabdominal cardiac cycle.

The classification procedure starts by matching the bispectral contours of the segments to those of the templates until the first and the second mother's QRS-complexes are detected and their R-waves are pinpointed. The maternal heart rate is accurately calculated from the knowledge of the current and previous R-wave positions. Then, the search for the fetal heartbeat starts at 50 msec before the first maternal R-wave and continues until we reach the second maternal R-wave. Although the ECG bispectral

contour template matching technique is very effective in detecting the occurrence of the fetal heartbeats as a whole in the frequency domain even when it is completely buried in noise, it cannot locate the R-wave in the time domain over a window length of 250 msec. However, we can measure fairly accurately the maternal heartbeats and calculate the instantaneous heart rate for the mother. Hence, by counting the number of fetal heartbeats that have occurred between two successive maternal R-waves, one can easily calculate the averaged FHR within the maternal cardiac cycle;

The average FHR = MHR x Number of FHBs / number of maternal heartbeats

In the above formula, the instantaneous maternal heart rate is previously known with some degree of accuracy, and the relative fetal to maternal heartbeat is also known within the maternal cardiac cycle. Hence, the averaged fetal heart rate can be calculated within each maternal cardiac cycle.

Detailed results

1. The effect of window length on the bispectral contour variance

The variance of the bispectrum for the optimum window length of 250 msec with FHB occurrence ranges from 0.47 to 3.3 with an average value of 1.716. Note that the variance of the bispectrum is smaller than that of the third-order cumulants. A further 15% increase in the variance of the bispectrum is due to an increase in the maternal heart beat from 60 bpm to 100 bpm. The latter has resulted in a 40% decrease in segment size.

2. Parameters of the single-hidden layer perceptron

The network has been optimised in terms of its learning rate, momentum constant, and hidden layer size to achieve the minimum mean-squared error. The optimum learning rate is found to be 0.2. The optimum momentum constant is found to be 0.2. The input layer dimensions are 8 x 8. The single-hidden-layer has an optimum dimension of 6 x 6. The input to the first layer is the bispectral contours of the four transabdominally-measured ECG segments. The network is trained using the BIC templates. During the training phase, the input to the network is four template patterns. These are the BIC of four segments from one transabdominal cardiac cycle. For example the first is the maternal QRS-complex BIC, the second is the first fetal heartbeat BIC, the third is the

QRS-free ECG BIC, and the fourth is the second fetal heartbeat BIC. The network is trained over ten templates of each of the four segments. The training terminates when the worst error in all patterns in one pass is less than 0.1. Typically the average error will be in the range of 0.001.

3. The classification rate for maternal QRS-complex and fetal heartbeat segments

The indirect method of calculating the bispectrum has been employed. The CPU time is 2 sec. Results obtained from 30 cases using the non-invasive transabdominally-measured ECG signal, with the simultaneous fetal scalp electrode ECG signal as a reference, show that the second hybrid method has a classification rate of 100% for normal, healthy maternal QRS-complexes and 90.12% for fetal heartbeats. It has been shown that an improvement of 1% to 3% is attainable with ECG signal linearisation employing second- and third-order Volterra synthesisers, respectively. Conventional methods (based on the power spectrum) of fetal heartbeat detection have a success rate in the range of 70%. The second hybrid system has a significantly higher classification rate.

The classification rate of fetal heartbeats for non-coincident mother's and fetal QRS-complexes is 99.21%. The classification rate of fetal heartbeats for coincident mother's and fetal QRS-complexes is 0%. This means that the hybrid bispectral contours technique fails to resolve the fetal beat when both the mother and fetal QRS-complexes are synchronised.

The bispectral contour template matching technique improved the classification rate by approximately 4% over and above that of the third-order cumulant template matching technique. The difference in performance is not due to better resolvability of the latter over the former in the case of coincident mother's and fetal QRS-complexes, as both techniques fail in this respect. But, it is due to the fact that the BIC template matching technique can resolve a few of the fetal QRS-complexes occurring within the T-wave region of the mother.

The averaged classification rate is 90.12% for 120,000 fetal heartbeats.

Fetal heartbeats falling within the maternal QRS-complex have not been detected.

Fetal heartbeats falling within the maternal P- and T-waves have been detected.

The third system: The Sequentially optimised weighted and uterine contraction interference signal modified covariance matrix incorporated MUSIC

The third technique is based on the modified and appropriately weighted spectral multiple signal classification (MUSIC) with incorporated covariance matrix for uterine contraction noise-like interfering signals also contaminated with noise. Essentially, two modifications to the standard MUSIC have been developed in order to enhance the performance of the spectral estimator in our applied work. The first modification involves the introduction of an optimised weighting function to the segmented ECG covariance matrix, and is chiefly aimed at enhancing the fetal QRS major spectral peak which occurs at around 30 Hz against the mother QRS major spectral peak usually occurring around 17 Hz and all other noise contributions. Additional optional pseudo-bispectral enhancement to sharpen the maternal and fetal spectral peaks, in particular when the mother and fetal R-waves are temporally coincident, has been achieved. The second modification to the spectral MUSIC is the removal of the unjustified assumption that only white Gaussian noise is present and the incorporation of the actual measured labour uterine contraction covariance matrix in reconfigured subspace analysis. This inevitably leads to the generalised eigenvectors – eigenvalues decomposition modern signal processing. This is now coined the modified, interference incorporated pseudo-spectral MUSIC.

The novelty of this technique rests on its dealing with the UCS during the strong and most painful peaks of labour contractions which are, apart from their noise-like characteristics, heavily contaminated with other noise artefact. Short data samples that can be classified as predominantly uterine noise artefact have been isolated within the maternal cardiac cycle and the computation of the USC covariance matrix which represents the modified covariance matrix is performed and incorporated in the modified spectral MUSIC steering vector prior to the GSVD orthogonalisation. The 250 msec data portions earmarked for the UCS modified covariance matrix fall mostly within segments III in the case of those maternal cardiac cycles that are free from coincident mother and fetal QRS-complexes in segments I, **OR** in segments II and IV

for maternal cardiac cycles that do exhibit occurrences of coincident mother and fetal QRS-complexes in Segments I.

The spectral characteristics of the uterine contraction interference signal

It has been found from previous research studies [4-5] that, the spectrum of the uterine contraction interference signals may include comparatively strong narrowband spectral components centred around 5 Hz, 30 Hz, 45 Hz, 60 Hz, and 90 Hz in addition to some broadband components. Several figures in Chapter Six have depicted the UCS spectral characteristics before and after linearisation using an optimised third-order Volterra synthesiser. Linearisation has resulted in an average reduction of about 9 dB in spectral peaks at frequency pairs of (32 Hz,18 Hz), (32 Hz,48 Hz), and (48 Hz,32 Hz), which are strongly overlapping with the fetal frequency pairs at (30 Hz, 7 Hz), (30 Hz, 18 Hz), and (30 Hz, 26 Hz).

Modifications to the conventional MUSIC

The modified spectral MUSIC is motivated, at least in part, by the shortcoming of all other techniques to detect FHBs when masked by the mother's QRS-complex. The other motivation is to combat interference and noise using only second-order statistics. However, by limiting ourselves to only the second-order statistics whilst dealing with non-linear signals and non-linear noise, we have succumbed to face all sorts of problems. The one which stands out is the problem of the uterine contraction interference signal (UCS) and noise artefact, which do not easily conform to any specific probability distribution as the statistics change with time and eventually take on a chaotic nature for sufficiently long data. And to make matter even worse, the spectrum of the UCS contains resonances with a strong peak around 30 Hz overlapping the fetal principal pseudo-spectral peak. We have found from previous published work that, by removing non-linearity from the ECG signals, we can, in fact, enhance the resonances of the fetal spectrum and weaken or suppress the resonances of the background UCS. Therefore, a systematic approach was adopted and by breaking down the unsolvable problem, a tractable solution was obtained. This approach is summarised as follows; (i) linearise the whole ECG data, (ii) do not include any unqualified assumptions regarding noise statistics, (iii) deal with the actual second-order statistics of the interfering signals and noise, (iv) perform all the eigen-structured MUSIC mathematical formulation based on the actual ECG signals and the actual *residual* UCS interference

plus artefact, and not on a hypothetical Gaussian or non-Gaussian noise for that matter, and (v) optimise the weighting functions for the covariance matrix of the segmented data based on the natural spectral peaks of the mother's at around 17 Hz against that of the fetal at around 30 Hz, or of the fetal against that of the mother's. This is done sequentially by re-scanning the mother's QRS segment, or by splitting the data in halves in two parallel streams, and applying the appropriate optimised weighting function to the corresponding stream. In (iv), it is necessary to isolate and measure the UCS plus noise and examining its short-term properties within the 250 msec frame, and then incorporate its covariance matrix into the mathematical formulation of the MUSIC.

In pursuing separation of signals and interference signals, or signals and noise, two auxiliary methods have been used based on the concepts of *oriented energy* and *signal-to-signal ratio*, and *the Gram-Schmidt orthogonalisation*. This is done in addition to the MUSIC well established Generalised Singular Value Decomposition (GSVD) which deals with partitioning signal and coloured noise (as opposed to Gaussian noise) subspaces.

The rest was relatively easy and focused on separating two subspaces: **(1) The first S-subspace** contains either the covariance matrix of the coincident mother and fetal QRS-complexes, or predominantly one QRS-complex, and **(2) the second I-subspace** contains the modified covariance matrix of the *residual* uterine contraction interference signal (UCS).

How is the separation of the coexisting or non-coexisting mother's and fetal QRS-complexes performed?

The spectral content of the mother's QRS-complex and that of the fetus are different and indeed unique. The mother's QRS-complex principal spectral peak is found around 17 Hz., and the fetal QRS-complex principal spectral peak is found around 30 Hz. Accordingly, such individual spectral content can be exploited herewith in the identification and detection of either signal within the maternal cardiac cycle. The Kaiser filtered weighted MUSIC previously published algorithm has been devoted to identifying in the frequency domain anomalous QRS-complexes and P-waves such as P-on-T-waves and P-on-QRS-complex episodes for adult patients [6]. Similarly, the optimised Kaiser filtered weighted MUSIC can be applied to detect the fetal

QRS-complex principal spectral peak. This will be appropriately addressed shortly. However, for FHR detection in labour one has to overcome two major problems in the transabdominally-measured ECG data, namely, poor signal spectral resolution and the influence of the coexisting labour contraction signals which not only exhibit a fairly broad spectrum, but also is uniquely characterised by having localised energy resonances, one of which is seriously overlapping with the fetal distinctive strong peak around 30 Hz which represents the fetal spike. The fetal heartbeat detection is accomplished by thresholding the enhanced fetal spikes in the frequency domain. The most challenging problem is, therefore, not only to enhance the quality and resolution of the mother and fetal QRS-complexes' principal pseudo-spectral peaks, abbreviated as MPPP and FPPP, respectively, but also to suppress the UCS resonances and nudge its modified covariance matrix into a separate subspace which is named the interference subspace (I-subspace).

Orthogonalisation is forced between the I-subspace and the signal subspace (S-subspace) containing either the covariance matrix of both the mother's and fetal QRS-complexes or predominantly one QRS-complex. Again, depending on the coefficients of the Kaiser filter, the desired QRS-complex will prevail and the other will be attenuated. The data segment containing both mother's and fetal QRS-complexes can be read and re-read sequentially, or is divided into two separate streams and weighted differently in parallel so that individual QRS-complex principal peaks can be thresholded and detected simultaneously.

Detailed results

1. Multiple overlapping windows to track deviations in the MPPP and FPPP frequencies

Up to five overlapping and optimised Kaiser weighted windows have been used in the detection of the following mother's QRS-complex principal spectral peaks; 15 Hz, 16 Hz, **17 Hz**, 18 Hz, and 19 Hz. Up to ten overlapping and optimised Kaiser weighted windows have been used in the detection of the following fetal QRS-complex principal spectral peaks; 28 Hz, 29 Hz, **30 Hz**, 31 Hz, 32 Hz, 33 Hz, 34 Hz, 35 Hz, 36 Hz, 37 Hz, and 38 Hz. Because there are inevitable deviations in the **17 Hz** and the **30 Hz** of the mother and fetal QRS-complex pseudo-spectra, respectively.

2. The choice of the model order

As with any eigen-structured MUSIC estimator, the model order has to be chosen very carefully. The optimum model order is **eleven for the signal** and **four for the noise**. **The method presented in this chapter is not sensitive to small deviations in the model order** as revealed in Section 6.8.

3. Calculations of the bias and variance of the sequentially optimised weighted, and UCS covariance matrix incorporated MUSIC

The bias of the modified spectral MUSIC. It was shown that the sequentially optimised weighted, and UCS covariance matrix incorporated MUSIC has a bias of 1.23 and 2.15 for mother's and fetal principal spectral peaks, respectively. This is lower than that of the conventional MUSIC by approximately 45%. The improvement in the bias is because the principal spectral peaks of the fetal heartbeat segment are closer to that calculated from the fetal scalp electrode segment. For the mother's QRS-complex, the more deviation of the detected frequency of the MPPP around 17 Hz from that of the mother's chest ECG, the higher the bias will be. Similarly, for the fetal QRS-complex, the more deviation of the detected frequency of the FPPP around 30 Hz from that of the fetal scalp electrode, the higher the bias will be.

The variance of the modified spectral MUSIC. The variance of the fetal principal spectral peaks ranges from 0 to 8, with an average value of 4.127.

4. Performance analysis of fetal heart monitoring in cases of coincident and non-coincident mother's and fetal QRS-complexes

Assuming a mother's heart rate of 60 bpm yields a cardiac cycle length of 1000 msec. Each maternal cardiac cycle has been divided into four equal segments (temporal windows) of 250 msec. The average rate by which the first fetal event coincides with the QRS-complex of the mother is 9.8%, based on 50,000 maternal cardiac cycles. When the two QRSs of the mother and fetal coincide in segment I, segment II is usually free from such events and may be taken as the UCS plus noise artefact segment. On average, the second fetal heartbeat occurs in segment III. And if there is a third fetal heartbeat (i.e., the fetal heart rate is three times the mother's), then it is likely to occur over both the fourth segment of the present cycle and the first segment of the next cycle. In most cases, we have encountered two fetal heartbeat occurrences within each maternal cardiac cycle. When the mother's heart rate goes up during painful labour contractions, we still

found more or less two fetal heartbeat occurrences within each maternal cardiac cycle. The deceleration of the fetal heart rate after the peak of labour contractions is normal and not proven to be related to the mother's heartbeat as her heart will still be racing for a while after the peak of contractions.

The effect of proximity of the mother's and fetal R-wave on the frequency deviation of the fetal principal spectral peak around 30 Hz, and on the fetal heart detection rate

Performance analysis has included the effect of proximity of the mother's and fetal R-wave on the frequency deviation of the fetal principal spectral peak around 30 Hz, and on the fetal heart detection rate, in all observed cases of coincident mother and fetal QRS-complexes. The sequentially optimised weighted, and UCS covariance matrix incorporated MUSIC algorithm has been applied to approximately 50,000 maternal cardiac cycles, including 4,873 coincident QRS-complexes cases. The results are tabulated in Table 7.1.

It can be clearly seen that even for a fixed model order of 11 and 4 for the signal and noise subspace, respectively, the new MUSIC algorithm is capable of detecting fetal heartbeats, at a rate of almost 92%, when the mother and fetal R-waves are almost synchronised, provided that appropriate sequential weightings for the mother and the fetal are maintained throughout.

As the separation between the mother and fetal R-waves is increased, we can see a slight increase in the corresponding detection rate and a decrease in the **FPPP** frequency deviations.

The effect of the incorporation of the UCS modified covariance matrix on the fetal principal pseudo-spectral peak

The incorporation of the covariance matrix of the **UCS** helps to strengthen and sharpen the **FPPPs** for the optimum model order and in some cases it appears to be tolerant to a change in the model order from 11 for the signal and 4 for the noise to 9 for the signal and 4 for the noise. It has also resulted in a significant noise artefact reduction in the QRS-free segments.

Averaged R_m-R_f separation (msec)	**40**	**35**	**25**	**20**	**15**	**7**	**0**
Frequency deviation in the fetal FPPP ± (Hz)	**1.73**	**1.92**	**2.09**	**2.17**	**2.31**	**2.52**	**2.74**
Number of overlapping windows	**5**	**5**	**5**	**5**	**8**	**9**	**10**
Average detection rate (%)	**93.81**	**93.63**	**93.56**	**93.49**	**93.24**	**92.35**	**91.83**

Table 7.1: *The effect of proximity of the mother's and fetal R-wave on the frequency deviation of the fetal principal spectral peak around 30 Hz, and on the fetal detection rate. The total number of fetal heartbeats is 120,000. The number of coincident mother and the first fetal QRS-complexes is 4,873.* ***The average fetal heart detection rate is 93.52% for coincident mother and the first fetal QRS-complexes within the maternal cardiac cycle. Otherwise, the average fetal heart detection rate is 99.35% for the second or third occurrences of fetal heartbeats within the maternal cardiac cycle. The overall fetal heart detection rate for the 120,000 FHBs is 95.5%.*** *Model order is fixed at 11 for the signal and 4 for the noise.*

The effect of the incorporation of the UCS modified covariance matrix on the fetal heart detection rate

The sequentially optimised weighted, and UCS covariance matrix incorporated MUSIC has resulted in the following fetal heart detection rates: (i) 93.52% for coincident mother and fetal QRS-complexes, (ii) 99.35% for non-coincident mother and fetal QRS-complexes, and (iii) 95.50% overall average.

Without the incorporation of the UCS modified covariance matrix into the mathematical formulation of the sequentially optimised, weighted MUSIC, the following fetal heart detection rates have been obtained: (i) 89.23% as opposed to the 93.52% for coincident mother's and fetal QRS-complexes, (ii) 97.51% as opposed to the 99.35% for non-coincident mother's and fetal QRS-complexes. Because in the former no "appropriate noise model" was assumed in the analysis, and (iii) 91.20% overall average.

The average fetal heart detection rate is 93.52% for coincident mother and the first fetal QRS-complexes within the maternal cardiac cycle.
Otherwise, the average fetal heart detection rate is 99.5% for the second or third occurrences of fetal heartbeats within the maternal cardiac cycle.
The overall fetal heart detection rate for the 120,000 FHBs is 95.5%.

Final remarks

The author would like to recommend the third system for non-invasive fetal heartbeat detection. It has the highest fetal heartbeat detection rate of 95.5%. It can detect fetal heartbeats falling within the maternal QRS-complex even when the mother's R-wave and the fetal-'s R-wave are synchronised. There is no need for the pseudo-bispectral enhancement to sharpen the maternal and fetal spectral peaks, as this is done at the expense of bispectrum computations, which results in an increase in the CPU time and does not improve the detection rate. Furthermore, one cannot implement the simple thresholding technique for detecting the fetal spectral spikes as in the one-dimensional MUSIC-based pseudo-spectrum presented in this thesis. There is no requirement to licence the use of NN classifiers in clinics, as in the case of the first and the second hybrid techniques. The **VLSI** implementation of the tracking and updating of the GSVD has already been developed for code division multiple access (CDMA), and some algorithms are based on subspace tracking by Moonen et al. [7].

References

[1] M. Sabry-Rizk, W. Zgallai, A. MacLean, K. T. V. Grattan, E. R. Carson, "The Application of a Novel Class of Embedded Dynamic Cubic Volterra to Long-Term Prediction of Chaotic and Multi-Fractal Electromyographic Signals During Labour," the 4th International Conference on Neural Networks and Expert Systems in Medicine and Healthcare, Greece, June 2001.

[2] M. Sabry-Rizk, W. Zgallai, E. R. Carson, K. T. V.Grattan, A. MacLean, and P. Hardiman, "Non-linear dynamic tools for characterising abdominal electromyographic signals before and during labour," Transactions of the Institute of Measurement and Control, Vol. 22, pp. 243-270, 2000.

[3] M. Sabry-Rizk, W. Zgallai, A. MacLean, and E. R. Carson, "Multi-fractility in labour contraction dynamics," The 2nd Joint Conference of the IEEE Engineering in Medicine and Biology Society and the Biomedical Engineering Society, 23-26

October 2002, Houston, Texas, USA.

[4] M. Sabry-Rizk, W. Zgallai "Novel Volterra Predictor Based on State-Space Equilibrium of Nonlinear Single- or Multi-Fractal Signals" Proceedings of the SPIE's 45th Annual Meeting, the International symposium on Optical Science and Technology, SPIE2000, Advanced Signal Processing Algorithms, Architectures, and Implementations X, USA, Vol. 4116, pp. 322-333, 30/7-4/8/2000.

[5] M. Sabry-Rizk, W. Zgallai E. R. Carson, K. T. V. Grattan, P. Hardiman, P. Thompson and A. Maclean, "Modified MUSIC Pseudospectral Analysis Reveals Common Uterus and Fetal Heart Resonances During Labour Contractions", the 22nd Annual International Conference of the IEEE Engineering in Medicine and Biology Society, EMB2000, USA, 23-28/7/2000.

[6] M. Sabry-Rizk, W. Zgallai, C. Morgan, S. El-Khafif E. R. Carson, and K. T. V. Grattan, "Novel decision strategy for P-wave detection utilising nonlinearly synthesised ECG components and their enhanced pseudospectral resonances," IEE Proceedings Science, Measurement and Technology, Special section on Medical Signal Processing, vol. 147, No. 6, pp. 389-397, November 2000.

[7] M. Moonen, P. Van Dooren, J. Vandewalle, "A singular value decomposition updating algorithm for subspace tracking", SIAM J. Matirx Anal Appl., Vol. 13, No. 4, pp. 1015-1038, October 1992.

APPENDIX A1

List of Publications

[1] M Sabry-Rizk, W Zgallai, E. R. Carson, K. T. V. Grattan, A. MacLean, and P. Hardiman Non-linear dynamic tools for characterising abdominal electromyographic signals before and during labour. Trans Inst Measurement and Control, vol. 22, pp. 243-270, 2000.

[2] M. Sabry-Rizk, W. Zgallai, C. Morgan, S. El-Khafif E. R. Carson, and K. T. V. Grattan, "Novel decision strategy for P-wave detection utilising nonlinearly synthesised ECG components and their enhanced pseudospectral resonances," IEE Proceedings Science, Measurement and Technology, Special section on Medical Signal Processing, vol. 147, No. 6, pp. 389-397, November 2000.

[3] M. Sabry-Rizk, W. Zgallai, E. R. Carson A. MacLean, K. T. V. Grattan, "Multi-fractility in Fetal Heart Beat Dynamics," 2nd European Medical & Biological Engineering Conference Vienna (Austria), December 04-08, 2002.

[4] M. Sabry-Rizk, W. Zgallai, A. MacLean, and E. R. Carson, "Multi-fractility in labour contraction dynamics," The 2nd Joint Conference of the IEEE Engineering in Medicine and Biology Society and the Biomedical Engineering Society,23-26 October 2002, Houston, Texas, USA.

[5] M Sabry-Rizk, W. Zgallai, A. McLean, E. R. Carson, and K. T. V. Grattan, "Virtues and Vices of Source Separation Using Linear Independent Component Analysis for Blind Source Separation of Non-linearly Coupled and Synchronised Fetal and Mother ECGs," EMBS 2001.

[6] M. Sabry-Rizk, W. Zgallai, A. MacLean, K. T. V. Grattan, E. R. Carson, "The Application of a Novel Class of Embedded Dynamic Cubic Volterra to Long-Term Prediction of Chaotic and Multi-Fractal Electromyographic Signals During Labour," the 4th International Conference on Neural Networks and Expert Systems in Medicine and Healthcare, Greece, June 2001.

[7] M. Sabry-Rizk, W. Zgallai, E. R. Carson, S. El-Khafif, C. Morgan, and K. T. V.

Grattan "Novel decision strategy for P wave detection utilising non-linearly synthesised ECG components and their enhanced pseudospectral resonances", IASTED-SIP 2001, Honolulu, Hawaii, USA, August 2001.

[8] M. Sabry-Rizk, W. Zgallai E. R. Carson, K. T. V. Grattan, P. Hardiman, P. Thompson and A. Maclean, "Modified MUSIC Pseudospectral Analysis Reveals Common Uterus and Fetal Heart Resonances During Labour Contractions", the 22nd Annual International Conference of the IEEE Engineering in Medicine and Biology Society, EMB2000, USA, 23-28/7/2000.

[9] M. Sabry-Rizk, W. Zgallai "Novel Volterra Predictor Based on State-Space Equilibrium of Nonlinear Single- or Multi-Fractal Signals" SPIE's 45th Annual Meeting, the International symposium on Optical Science and Technology, SPIE2000, Advanced Signal Processing Algorithms, Architectures, and Implementations X, USA, vol. 4116, pp. 322- 333, 30/7-4/8/2000.

[10] M. Sabry-Rizk, W. Zgallai, E. R. Carson, S. El-Khafif, C. Morgan, and K. T. V. Grattan "Novel decision strategy for P wave detection utilising non-linearly synthesised ECG components and their enhanced pseudospectral resonances", IEE International conference, MEDSIP2000, Bristol, UK, September 2000.

[11] M. Sabry-Rizk, W. Zgallai, S. El-Khafif, E. Carson and K. Grattan, "Highly Accurate Higher Order Statistics Based Neural Network Classifier of Specific Abnormality in Electrocardiogram Signals," ICASSP99, Vol. II, Speech processing II Audio and Electrtoacoustics Neural Networks for Signal Processing, pp. 1033-1036, USA, 15- 19/3/1999.

[12] M. Sabry-Rizk, S. El-Khafif, E. Carson, W. Zgallai, K. Grattan, C. Morgan and P. Hardiman, "Suspicious Polyphase Patterns of Normal Looking ECGs Provide Fast Early Diagnoses of a Coronary Artery Disease," IEEE Proceedings of the joint EMBS/BMES conference, pp. 979, 13-16 October 1999.

[13] M. Sabry-Rizk, W. Zgallai, "Higher Order Statistics Are Indispensable Tools in The Analysis of Electrocardiogram Signals," IEE Colloquium on Statistical Signal Processing, January 1999.

[14] M. Sabry-Rizk, W. Zgallai, S. El-Khafif, E. Carson, K. Grattan, "Higher- Order Ambulatory Electrocardiogram Identification and Motion Artifact Suppression With Adaptive Second- and Third-Order Volterra Filters," SPIE '98 Advanced Signal Processing Algorithms, Architectures, and Implementations VIII Vol. 3461, pp. 417-431, San Diego, USA, 19-24 July 1998.

[15] M. Sabry-Rizk, W. Zgallai, P. Hardiman, and J. O'Riordan, "MUSIC-Based Bispectrum Detector: A Novel Non- Invasive Detection Method For Overlapping Fetal And Mother ECG Signals," Proceedings of the 19th IEEE International Conference on Engineering in Medicine and Biology, EMBS, pp. 72- 75, USA, October 1997.

[16] W. Zgallai, M. Sabry-Rizk, P. Hardiman, and J. O'Riordan, "Third-order cumulant signature matching technique for non-invasive fetal heart beat identification," ICASSP, IEEE International Conference on Acoustics, Speech, and Signal Processing, vol. 5, pp 3781-3784, Germany, 1997.

[17] M. Sabry-Rizk, W. Zgallai, P. Hardiman, and J. O'Riordan, "Applications of higher order cepstral techniques in problems of fetal heart signal extraction," SPIE, International Symposium on Optical Science and Measurements, Vol. 2846, pp. 395-411, Colorado, USA, August 1996.

[18] M. Sabry-Rizk, W. Zgallai, P. Hardiman, and J. O'Riordan, "Blind deconvolution-homomorphic analysis of abnormalities in ECG signals," IEE colloquium, #144, pp. 5/1-9, London, 1995.

[19] M. Sabry-Rizk, W. Zgallai, P. Hardiman, and J. O'Riordan, " Applications of adaptive polycepstral based filtering to ECG analysis," in proceedings of the international workshop on medical and biological signal processing, (E. C. Ifeachor, ed.), pp. 14-19 Plymouth, UK, September, 1995.

[20] M. Sabry-Rizk, D. Romare, W. Zgallai, K. T. V. Grattan, P. Hardiman and J. O'Riordan "Higher order statistics (HOS) in signal processing: Are they of any use?," IEE Colloquium, Digest #111, pp. 1/1-1/6, London, May 1995.

APPENDIX A2

A2.1 Independent Component Analysis (ICA)

Assume the following basic linear statistical model:

$$Y = \mathbf{M}\, X + N \tag{A2.1}$$

in which $Y \in \mathcal{R}^I$ is referred to as the observation vector, $X \in \mathcal{R}^J$ is called the source vector and $N \in \mathcal{R}^I$ represents additive noise. $\mathbf{M} \in \mathcal{R}^{IxJ}$ is the mixing matrix.

The goal of ICA consists of the estimation of the transfer matrix **M** and / or the corresponding realisations of the source vector X, given only realisations of the output vector Y, under the following assumptions:

- the columns of **M** are linearly independent;
- the components of X are mutually statistically independent, as well as statistically independent from the noise components.

Most of the current ICA algorithms rely on the first assumption for identifiability. The second assumption is the actual key ingredient for ICA. It is a very strong hypothesis, but also quite natural in lots of applications.

It is impossible to determine the norm of columns of **M** in Eq. (A2.1), since a rescaling of these vectors can be compensated by the inverse scaling of the source signal values. Similarly the ordering of the source signals, having no physical meaning, cannot be identified. For non-Gaussian sources, these indeterminacies are the only way in which an ICA solution is not unique [8], [20].

The ICA assumptions do not allow to distinguish between the signal and the noise term in Eq. (A2.1). Hence, the source signals will be estimated as X, by a simple matrix multiplication

$$\hat{X} = \mathbf{W}^T\, Y. \tag{A2.2}$$

As an example, $\mathbf{W}^T$ can take the form of the pseudo-inverse $\mathbf{M}\uparrow$, with $\mathbf{M}$ an estimate of the mixing matrix. More generally, various beamforming strategies [22] can be applied.

Exploitation of the fact that the source signals are uncorrelated leads to a classical principal component analysis (PCA), which only allows to estimate the sources as well as the mixing matrix up to an orthogonal transformation. To illustrate this, let us assume that the sources have unit variance. Then we have (we omit the noise term at this point, for clarity)

$$\mathbf{C}_Y = \mathbf{M}\,\mathbf{M}^T \qquad \text{(A2.3}\}$$

in which $\mathbf{C}_Y$ is the covariance matrix of Y. Substitution of the singular value decomposition (SVD) of the mixing matrix $\mathbf{M} = \mathbf{U}\,\mathbf{S}\,\mathbf{V}^T$ shows that the eigenvalue decomposition (EVD) of the observed covariance allows to estimate the column space of $\mathbf{M}$ while the factor $\mathbf{V}$ remains unknown

$$\mathbf{C}_Y = \mathbf{U}\,\mathbf{S}^2\,\mathbf{U}^T = (\mathbf{U}\,\mathbf{S})\,(\mathbf{U}\,\mathbf{S})^T. \qquad \text{(A2.4)}$$

As is well known, $\mathbf{U}$ and $\mathbf{S}$ might be found directly, in a numerically more reliable way, from the SVD of the observed dataset [13].

The solution to the ICA problem lies in the fact that the assumption of statistical independence is stronger than the notion of uncorrelated signals. Statistical independence is not only a claim on the second-order statistics of the signals, but also on their higher order statistics (HOS) [16]. More precisely, it is not sufficient that the source covariance $\mathbf{C}_x$ is a diagonal matrix, in addition, the higher-order cumulants of the source vector should be diagonal higher-order tensors. (A higher-order tensor can intuitively be imagined as a multi-way matrix, of which the entries are characterised by more than two indexes; its diagonal is defined as the entries for which all the indexes are equal.)

If we focus at the fourth-order level (third-order cumulants vanish for even probability density functions), then we have the following. The fourth-order cumulant $C_x(^4)$ of a real zero-mean stochastic vector X is defined by

$$C_x(^4)i_1i_2i_3i_4 = E\{Xi_1\ Xi_2\ Xi_3\ Xi_4\} - E\{Xi_1\ Xi_2\}E\{Xi_3\ Xi_4\}$$
$$-E\{Xi_1\ Xi_3\}E\{Xi_2\ Xi_4\} - E\{Xi_1\ Xi_4\}E\{Xi_2\ Xi_3\} \qquad \text{(A2.5)}$$

for all index values; E denotes the expectation. For every component Xi of X that has a non-zero mean, Xi has to be replaced by Xi -E{Xi}. It can be proven that the link between the cumulant of the observations and the cumulant of the sources is a straight generalisation of its second-order counterpart, Eq. (A2.3)

$$\left(C_Y^{(4)}\right)_{i_1i_3i_3i_4} = \sum_{j_1j_2j_3j_4} (M)_{i_1j_1}(M)_{i_2j_2}(M)_{i_3j_3}(M)_{i_4j_4}(C_X^{(4)})_{j_1j_2j_3j_4} \qquad \text{(A2.6)}$$

for all index values, in which $C_x(^4)$ is diagonal. A nice property is that higher-order cumulants are insensitive to additive Gaussian noise. Eq. (A2.6) means that the unknown mixing matrix M is not only a diagonaliser of the covariance matrix C_Y, but also of the cumulant tensor $C_Y(^4)$, which leads to a sufficient amount of constraints to solve the problem. From an algebraic point of view, this means that the ICA solution can be obtained by means of multi-linear generalisations of the EVD (see e.g., [6, 8, 10]). Actually, since the first paper on the subject [14], ICA has become a hot topic in the signal processing world. Apart from multi-linear algebra, solutions have been based on principles of neural networks and information theory, ([7], [15] and the references therein).

Although generally PCA does not allow to identify the mixing matrix nor the source signals, there are some cases in which it does lead to a reasonably good source separation. A straightforward example consists of the situation in which the mixing matrix has mutually orthogonal columns (having mutually distinct norms, if we assume that the sources have unit variance), as is clear from Eq. (A2.4). A second example is the situation in which the source variances are very different (assuming that the norms of the corresponding columns of **M** have a comparable magnitude). Next, consider a setup with, e.g., two sources, of which the variances are given by σ_1^2 and σ_2^2, with $\sigma_1^2 >> \sigma_2^2$. Reference [21] proved that in this case PCA yields, for both source estimates, an interference-to-signal ratio of the order of σ_2^2 / σ_1^2. This corresponds to the fact that the dominant eigenvector of C_y turns out to be an accurate estimate of the first column of **M** in this scenario; the second eigenvector however, is not necessarily a

good estimate of the second column of **M** but it is approximately orthogonal to the first one. In the context of research on ICA, similar results have independently been obtained in [11] and [19].

A2.2 Extraction of the FECG by means of BSSS

The propagation of q bioelectric sources to an array of p body surface electrodes ($p \geq q$), can be formulated as

$$Y(t) = \mathbf{M}\, X(t) + N(t) \qquad \text{(A2.7)}$$

where $Y(t) = (y_1(t) \ldots y_p(t))^T$ contains the potential recordings, $X(t) = (x_1(t) \ldots x_q(t))^T$ contains the signal values of the bioelectric sources, and the noise on each channel is represented by $N(t) = (n_1(t) \ldots n_p(t))^T$. The matrix **M** describes the propagation from source to electrode, i.e., its entry with row number i and column number j gives the gain of the jth bioelectric source signal with respect to the ith channel data ($1 \leq i \leq p$; $1 \leq j \leq q$). It is natural to assume that the different bioelectric sources, since they originate at different locations, correspond to different mechanisms, etc, can be approximately modelled as statistically independent. The noise components $n_i(t)$ ($1 \leq i \leq p$) are assumed to be Gaussian, with variance σ_N^2 .mutually independent as well as independent from the source signals.

As a conclusion the derivation of the antepartum FECG from multi-lead cutaneous recordings can be considered as an example of blind source subspace separation (BSSS), as discussed in Section A2.1, in which however the sources are of a multi-dimensional nature; we will use the term blind source subspace separation (BSSS). The fact that only the different source subspaces have to be separated, instead of all the source components, allows to reduce the computational cost, in comparison to conventional ICA, without loss of medical information. For, example, in the Jacobi type algebraic algorithms of [6, 8, 10] the multi-dimensional character of the sources limits the number of Jacobi rotation angles that have to be identified, since rotations of the basis vectors within one and the same source subspace are irrelevant.

Since there is a large gap between the amplitudes of the MECG and the FECG, a good separation can already be expected from merely PCA, as explained in section A2.1. This is the philosophy behind the important class of SVD techniques for the extraction of the FECG [3-5]. To enhance the performance, one often tries to choose the electrode positions in a way that is more or less likely to correspond to an orthogonal transfer (see Section A2.1), but this is still a matter of heuristic rules and trial-and-error.

Conceptually, the higher-order processing step in ICA may add the following advantages to the second-order approach.

- It is possible to enhance the quality of separation: whereas the PCA error only decreases proportionally to the ratio of the power of the weak source versus the power of the strong source, ICA directly aims at a correct reconstruction of the mixing matrix. In case the higher order ICA step would fail, one can still resort to the results of the PCA, which forms the first step in many ICA algorithms.
- The propagation of the electrical signals can be characterised in an essentially unique way. We mention three important implications:

  1. The transfer vectors indicate how strongly the different electrodes capture each source signal; from this information, better measurement positions might be deduced. The positioning of the electrodes is still the most crucial factor of the success of the PCA method [5].

  2. An important aspect in the evaluation of the fetal wellbeing is the quantification of fetal movements [4]. At this moment the required information can only be obtained by echocardiography or, simply, by asking the mother. The number of significant changes in the FECG subspace, which could be obtained from an on-line adaptive ICA implementation could be very useful information here.

  3. The properties of the human body as a conducting medium are, in their own, subject of medical research [18]. The study of the propagation of the fetal heart signal to the mother's skin is an important sub-aspect [17]. The transfer matrix can provide more understanding with respect to the propagation of electrical signals through the body.

- The physician can resort to a more intuitive interpretation of the results: the separation of the measured signals into statistically independent source signals

with a physical meaning, is easier to interpret than a decomposition in time-orthogonal principal components.

The FECG extraction is formulated as a blind identification problem, since it is less meaningful in practice to resort to a more parametric approach:

- The transfer coefficients are subject to a large uncertainty: the development of propagation models is still in its infancy. Moreover, it is clear that length, weight, contour, etc. are significantly different from patient to patient.
- The geometrical and resistivity parameters of the body of a single patient are not constant in time. Fetal growth, a different position of the fetus in the uterus, the variation in the characteristics of the amniotic fluid and the placenta during pregnancy, the changing geometry, ... etc., imply important changes of the transfer matrix.
- For the application in medical diagnosis and treatment it is crucial that unexpected ECG patterns can be detected and examined. For example, the parametric formulation of the quasi-periodicity of a regular heart rate pattern would hamper the detection of extra systoles (extra heartbeats between the regular beat-to-beat pattern).
- Potentially interesting is also the application of BSSS to cardiac electrical imaging, a recent generalisation of the ECG, in which more information is acquired by using a larger array of (e.g., 200) electrodes to record a sequence of "electrical images" of the body [2]. This technique can be seen as an emerging modality for medical imaging, complementary to, e.g., computed tomography and magnetic resonance imaging; it is worth mentioning that in Japan the technique is already common practice.

A2.3 REFERENCES

[1] B. Baslijns and L. De Lathauwer, "Real-time Extl:aclie van Medische Informatie uit Foetale Hartzignalen," master's thesis, ElecL Eng. Dept. (ESAT), K. U. Leuven (in Dutch), Leuyen, Belgium; July 1992.

[2] D. H. Brooks and R. S. McLeod, "Electrical imaging of the heart," IEEE Signal Processing Magazine., pp. 24-42, Jan. 1997.

[3] D. Callaerts, J. Vanderschoot, J. Vandewalle, W. Sansen, G. Vantrappen, and J.

Janssens, "Fetal electrocardiogram measuring method and equipment (FMME)," J Perinatal Medicine, World Symp. on Computers in the Care of Mother, Fetus, and Newborn, vol. i5, supp. 1, no.4, p. 33, Mar.1987.

[4] D. Callaerts, "Signal Separation Based on Singular Value Decomposition and their Application to the Real-time Extraction of the Fetal Electrocardiogram from Cutaneous Recordings," Ph.D. dissertation, K. U. Leuven, E. E. Dept., Dec. 1989.

{5] D. Callaerts, J. Vandewalle, W. Sansen, J. Janssens, and G. Vantrappen, "Acquisition and processing of the antepartum FECG," in A Critical Appraisal of Fetal Surveillance, H. P. van Deijn and F. J. A. Copray, Eds, Amsterdam, The Netherlands: Elsevier Science B.V., 1994, pp. 371-380.

[6] I-F. Cardoso and A. Souloumiac, "Blind beamforming for non-Gaussian signals," Inst. Elect. Eng. Proc.-F., vol. 140, no.6, pp. 362-370, 1994.

[7] I.-F. Cardoso, C.lutten, and P. Loubaton, Eds., in Proc. lst Int. Workshop Independent Component Analysis and Blind Signal Separation (ICA'99), Aussois, France, Ian. 1999.

[8] P. Comon, "Independent component analysis, a new concept?," Signal Processing (Special Issue Higher Order Statistics), vol. 36, no.3, pp. 287-314, Apr. 1994.

[9] L. De Lathauwer, D. Callaerts, B. De Moor, and I. Vandewalle, "Fetal electrocardiogram extraction by source subspace separation," in Proc. IEEE SP/ATHOS Workshop on HOS, Girona, Spain, June 1995, pp. 134-138.

[10] L. De Lathauwer, B. De Moor, and I. Vandewalle, "Blind source separation by simultaneous third-order tensor diagonalization," in Proc. EU SIPCO-96, vol. 3, Trieste, Italy, Sept. 13, 1996, pp. 2089-2092.

[11] L. De Lathauwer, "Signal Processing Based on Multilinear Algebra," Ph.D. dissertation, Elect. Eng. Dept, K. U. Leuven, (ESAT), Leuven, Belgium, Sept. 1997.

[12] L. De Lathauwer, B. De Moor, and I. Vandewalle, "Fetal electrocardiogram extraction by blind source subspace separation," Leuven, Belgium, Tech. Rep. 98-127,1998.

[13] G. H. Golub 'and C. F. Van Loan, Matrix Computations, 3rd ed. Baltimore, MD: Johns Hopkins Univ. Press, 1996.

[14] I. Herault, C. Iutten, and B. Aus, "Detection de grandeurs primitives dans un mebcsage composite par une architecture neuromimetique en apprentissage non supervise," in Proc. 10th GRETSI Colloquium, Nice, France, May 24, 1985, pp.

1017-1022.

[15] T.-W. Lee, Independent Component Analysis: Theory and Applications. Norwell, MA: Kluwer Academic, Sept. 1998.

[16] C, L. Nikias and I. M. Mendel, "Signal processing with higher order spectra," IEEE Signal Processing Mag., pp. 10-37, Iuly 1993.

[17] T. Oostendorp, "Modeling the Fetal ECG," Ph.D. dissertation, K. U. Nijmegen, The Netherlands, 1989.

[18] R. Plonsey, Bioelectric Phenomena, New York: McGraw-Hill, 1969.

[19] N. Thirion, "Separation d'Ondes en Prospection Sismique," Ph.D. dissertation, CEPHAG, Grenoble, France, Sept. 1995.

[20] L. Tong, R. Liu, V. Soon, and Y.-F. Huang, "Indeterminacy and identifiability of blind identification," IEEE.Trans. Circuits Syst., vol. 38, pp. 499-509, May 1991.

[21] I. Vanderschoot, G. Vantrappen, I. Ianssens, I. Vandewa1le, and W. Sansen, " A reliable method for fetal ECG extraction from abdominal recordings," in Medical Informatics Europe 84, Lecture Notes in Medical informatics, F. H. Roger et al., Eds. Berlin, Germany: Springer Verlag, 1984, vol. ,24, pp. 249-254.

[22] B. D. Van Veen and K. M. Buckley, "Beamforming: A versatile approach to spatial filtering," IEEE Acoust. Speech, Signal Processing Mag., pp. 4-24, Apr. 1988.

APPENDIX A3

Virtues and Vices of Source Separation Using Linear Independent Component Analysis for Blind Source Separation of Non-linearly Coupled and Synchronised Fetal and Mother ECGs

M Sabry-Rizk, W. Zgallai, A. McLean[1], E. R. Carson*, and K. T. V. Grattan

Electrical, Electronic and Information Engineering Department, and *Centre for Measurement and Information in Medicine, City University London, Northampton Square, London EC1V OHB, UK. Tel: +44 20 7477 8937, Fax: +44 20 7477 8568, Email: m.sabry-rizk@city.ac.uk. [1] Department of Obstetrics and Gynaecology, Royal Free and University College Medical School, London, UK.

Abstract: In this paper, we address the imminent problem which arises when researchers unjudiciously use a linear and instantaneous (memoryless) model for the source mixing structures of independent component analysis (ICA), also known as blind source separation (BSS), in persuit of separating noisy and frequently non-stationary combined mother and fetal electrocardiogram (ECG) signals from cutaneous measurements under the following false assumptions. (1) Sensors (electrodes) are instantaneous linear mixtures of mother and fetal source signals. (2) Noise is an additive Gaussian perturbation. (3) Mother and fetal ECG signals are assumed to be stationary and linear, mutually statistically independent and statistically independent from noise. (4) Most of the second-order (SO) and fourth-order (FO) blind source separation (BSS) methods developed this last decade assume that third-order cumulants vanish hence the need to use FO. All these assumptions are not valid and will be challenged. We will expose these vices without providing any significant contributions for overcoming them. Rather, we provide a framework for investigations which are based on conformal mapping of non-linear mixtures and novel dynamic non-linear structures with time-variant memory to cater for quadratic coupling between mother and fetal which is quasi-periodical and the concomitant (quasi) cyclo-stationarity. Results given here show linear ICA shortfalls in non-stationary environment which is precipitated by quadratic coupling between mother and fetal ECGs during events of synchronised QRS complexes and P-waves and account for more than 20% of the 100,000 maternal cardiac cycles obtained from several clinical trials.

Keywords: Non-invasive fetal electrocardiogram, Blind source separation, linear / non-linear independent component analysis, quadratically coupled sources, non-linear and non-stationary mixtures.

I. DISCUSSIONS

I.1 Issues for discussions

- The unsuitability of using linear independent component analysis (ICA) or blind source separation (BSS) to the problem of separating fetal heartbeat from transabdominally measured signals.
- Wrong assumptions and conditions for solutions to the above problem.
- Evidence of non-linear coupling and (quasi) cyclo-stationarity in the transabdominally measured signals.
- Present techniques for non-linear ICA only cater for non-linear mixtures and may not be adequate for non-linear mixtures of individually non-linear mother / fetal ECGs.

I.2 Linear Independent Component Analysis (ICA)

Blind source separation is to recover unobservable independent sources (or signals) from multiple observed data masked by linear mixing. Most existing algorithms for linear mixing models stem from the theory of the independent component analysis (ICA) [1]-[3]. Most of the second-order (SO) and fourth-order (FO) blind source separation methods developed this decade are aimed at blindly separating statistically independent sources that are assumed zero-mean, stationary and ergodic. Nevertheless, in many situations of practical interest, such as in non-invasive fetal heartbeat identification, the combined sources measured transabdominally are (quasi) cyclo-stationary due to non-linear coupling. In these conditions it becomes important to wonder whether the performance of these current SO and FO blind source separation methods which have been developed for stationary source may be affected by the potential non-stationarity of the latter limiting the analysis to the SO and FO cumulant-based blind source separation methods, the purpose of this paper is to bring some answers to this important question by looking at the non-linearity, quadratic coupling and non-stationarity during events of synchronised QRS complexes and P-waves.

I.3 Wrong Assumptions in Mother and Fetal Source Separation

Recently, Lathauwer et al. [4-9], Zarzoso et al. [10] have attempted to separate mother and fetal electrocardiograms from cutaneous 8-32 channel recordings, by exploiting the second- and fourth-order statistics because notably the solution to the ICA problem lies in the fact that the assumption of statistical independence is a key factor. Statistical independence is relatively strong assumption but it is plausible in many contexts because it arises from a lack of physical relationship between the various sources. However, they focus at the second-order and fourth-order level based on the wrong assumption that the third-order cumulants for

mother and fetal vanish (which is not true). Third-order cumulants do exist for mother and fetal ECGs and have been successfully exploited in many analyses [24].

Researchers in this field justify using linear mixtures based on inaccuracies in the assumption that the transfer from bioelectric current sources to body surface electrodes can be considered linear and resistive [21]. Even if this is justified as first approximation, the non-linearities which characterise individual mother and fetal cardio-electrical activities [22], [23] will interact during their propagation through various body layers and mix with motion artefact, before they are finally picked up as the ECG signals by electrodes on the skin surface. It is important to realise that the cardiac signals have to penetrate through a complex system experiencing various effects and there is evidence of spectral tuning between the fetal heartbeat and uterus contractions [26], [27]. However, only evidence of quadratic coupling between the mother and fetal ECGs will be given in this paper due to lack of space. It is worth mentioning that in previous publications [22], [23] we provided evidence of non-Gaussian and multiplicative noise in individual ECGs.

The main drawback of these techniques, therefore, is their underlying simplistic assumptions, namely, linear sources, linear mixtures, and additive model for noise. Also, we strongly oppose the claim that third-order cumulants vanish for either mother or fetal ECG [24]. In fact, the utilisation of the third-order cumulants to extract fetal heart signals from the maternal ECG has proven to be a very robust technique provided that the observed signals are non-linearly filtered and if necessary the linearised signals are deconvovled from any multiplicative noise before the third-order cumulant matching process is carried out [24], [25]. Furthermore, only 1-d diagonal slice is needed for the identification and reconstruction process [25], [30]. These publications prove beyond doubt that the pdfs for both mother and fetal ECGs are not even and third-order cumulants do exist.

I.4 Non-linear Mixing Update

For non-linear mixing models, many difficulties occur and both the linear ICA theory and existing linear de-mixing algorithms are no longer applicable because of the complexity of non-linear characteristics. In addition, there is no guarantee for the uniqueness of the solution of non-linear blind source separation unless additional constraints are imposed on the mixing transformation [11].

So far several authors studied the difficult problem of the non-linear blind source separation and proposed a few efficient de-mixing algorithms [11]-[14], [15-19]. In addition, the extension of related linear ICA theories to the context of non-linear mixtures has resulted in the development of non-linear ICA. The so-called non-linear ICA is to employ a non-linear function to transform the non-linear mixtures such that the outputs become statistically independent after the transformation. However, this transformation is not unique without some specific constraints on the function of non-linear mixing. If s_1 and s_2 are two independent random variables, then $f(s_1)$ and $g(s_2)$ are also statistically independent regardless of the non-linear functions f and g (see Fig. 1). At this junction we stress that if s_1 and s_2 are themselves non-linear then we suggest a total review to the present non-linear ICA theory.

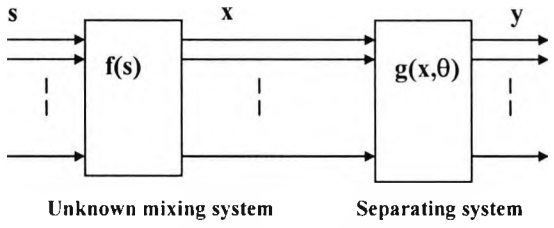

Figure 1: *Non-linear mixing and separating systems for blind signal separation.*

I.5 Framework for Our Non-linear Model

We have succeeded in non-linearly modelling fetal and mother ECGs, and in conformal mapping their mixing structures using embedded Volterra-like structures with extended memory [28]. Modifications to the memory of these structures have been introduced to cater for non-stationarity [29]. In the next section we provide evidence of non-linear quadratic coupling between mother and fetal respective ECGs and non-stationarity. This is followed by attempting to exploit linear ICA in mother / fetal source separation using eight electrodes and resulting in several misses during events of synchronised mother / fetal QRS complexes and P-waves. In general, in the context of linear ICA, it is assumed that each sensor receives a mixture of all the source signals: if there are fewer sources than sensors the received mixture of signals is linearly invertible: ideally the separating matrix should approximate the inverse of the mixing matrix.

II. RESULTS

Data Acquisition (I) for the purpose of identification of quadratic coupling and the concomitant non-stationarity

The data collection process included obtaining data from pregnant women at various stages of gestation. Abdominal electromyographic signals were obtained with consent of women using a pair of electrodes, Sonicaid 8000, a Pentium II PC and an interface card. Figs. 2 and 3 are self explanatory and show clear manifestations of quadratic coupling and non-stationarity through the exploitation of the bicoherence squared of transabdominally measured ECGs when the QRS-complexes and P-waves of mother / fetal overlap. The scalp electrode was deemed necessary and was used as a marker for fetal heartbeats. Fig. 5 shows blind source separation results after carrying out a novel non-linear identification procedure on the data of Fig. 4(a), using an embedded Volterra-like structure with an extended memory and modified to cater for time-variant non-linearity. Three key channels are shown after the identification of the previously missing first, fourth, and seventh fetal heartbeats [28], [29].

Data Acquisition (II) for the purpose of repeating linear Independent Component Analysis

As in Data acquisition (I) but the number of surface electrodes is eight (minimum).

Linear ICA Results were obtained following the same procedures and algorithms in [4] and are shown in Fig. 4. Note that the first, fourth and seventh fetal signals have not been identified and marked X in Fig. 4(b). The missing fetal complexes are almost invariably coincident with maternal QRS complexes or P-waves. These missing fetal complexes were recovered using an embedded Volterra-like structure with an extended memory and modified to cater for time-variant non-linearity [28], [29].

III. CONCLUSIONS

We have extolled one virtue and several vices of exploiting linear independent component analysis in separating mother and fetal electrocardiogram sources from cutaneous measurements. Linear ICA works well in separating mother and fetal sources under two conditions, namely, high signal-to-noise ratios and non-overlapping mother / fetal QRS complexes and P-waves. We provided evidence of quadratic coupling between the mother and fetal electrocardiograms which increases with the proximity of the occurrences of their respective QRS-complexes and P-waves. This results in non-stationarity which is manifested in the OT triangle of the bicoherence squared. We have shown that, by giving one typical result due to lack of space, in as many cases as more than 20% in the 100,000 maternal cardiac cycles obtained from clinical trials, synchronised mother / fetal QRS-complexes cannot be detected using linear ICA. The need for higher-order statistics in linear / non-linear independent component analysis does not preclude using the third-order cumulants in the concerned problem. For moderate noise (antepartum) and when the uterus is not contracting fiercefully as in labour, the separation is feasible resorting only to second-order statistics provided that non-linearity is removed from the transabdominally-measured ECGs.

REFERENCES

[1] C. Jutten and J. Herault, "Blind separation of sources: part I: An adaptive algorithm based on neuromimetic architecture," Signal Processing, vol. 24, pp. 1-20, 1991.

[2] P. Comon, "Independent component analysis- A new concept?," Signal Processing, vol. 36, pp. 287-314, 1994.

[3] A. Hyvarinen, "New approximation of differential entropy for independent component analysis and projection persuit," in Advances in Neural Information Processing Systems. Cambridge MA: MIT Press, vol. 10, pp. 273-279, 1999.

[4] L. De Lathauwer, B. De Moor, and J. Vandewalle, "Fetal electrocardiogram extraction by blind source separation," IEEE Transactions on Biomedical Engineering, vol. 47, No. 5, pp. 567-572, May 2000.

[5] L. De Lathauwer, B. De Moor, and J. Vandewalle, "Blind source separation by simultaneous third-order tensor diagonalisation," in Proc. EUSIPCO, Italy, vol. 3, pp. 2089-2092, 1996.

[6] L. De Lathauwer, B. De Moor, and J. Vandewalle, "Fetal electrocardiogram extraction by blind source separation," ESAT/SISTA, Leuven, Belgium, Tech. Rep. 98-127, 1998.

[7] G. H. Golub and C. F. Van Loan, *Matrix Computations*, 3rd ed. Baltimore, MD: Johns Hopkins Univ. Press, 1996.

[8] C. L. Nikias and J. M. Mendel, "Signal processing with higher order spectra," IEEE Signal Processing Magazine, pp. 10-37, July 1993.

[9] L. Tong, R. Liu, V. Soon, and Y.-F. Huang, "Indeterminacy and indetifiablity of blind identification," IEEE Transactions on Circuits and Systems, vol. 38, pp. 499-509, May 1991.

[10] V. Zarzoso and A. K. Nandi, "Blind separation of independent sources for virtually any source probability density function," IEEE Transactions on Signal Processing, vol. 47, No. 9, pp. 2419-2431, September 1999.

[11] G. Burel, "Blind separation of sources: A nonlinear neural algorithm," Neural Networks, vol. 5, pp. 937-947, 1992.

[12] G. Deco and W. Brauer, "Nonlinear higher-order statistical decorrelation by volume-conserving neural architectures," Neural Networks, vol. 8, pp. 525-535, 1995.

[13] P. Pajunen, A. hyvarinen, and J. Karhunen, "Nonlinear blind source separation by self-organizing maps," in Progress in Neural Information Processing: Proc. ICONIP, New York, vol. 2, pp. 1207-1210, 1996.

[14] P. Pajunen, "Blind source separation using algorithmic information theory," in Neurocomput: Elsevir, vol. 22, pp. 35-48, 1998.

[15] Hermann and H.-H. Yang, "Perspectives and limitations of self-organizing maps in blind separation of source signals," in Progress in Neural Information Processing: Proc. ICONIP, New York, vol. 2, pp. 1211-1216, 1996.

[16] J. K. Lin, D. G. Grier, and J. D. Cowan, "Source separation and density estimation by faithful equivariant SOM," in *Advances in Neural Information Processing Systems*. Cambridge MA: MIT Press, vol. 9, 1997.

[17] H.-H. Yang, S. Amari, and A. Cichocki, "Information backpropagation for blind separation of sources from nonlinear mixture," in Proc. IEEE ICN, TX, pp. 2141-22146, 1997.

[18] A. Taleb, C. Jutten, and S. Olympieff, "Source separation in post nonlinear mixtures: An entropy-based algorithm," in Proc. ESANN, pp. 208902092, 1998.

[19] A. Hyvarinen and P. Pajunen, "Nonlinear independent component analysis: Existence and uniqueness results," Neural Networks, vol. 12, pp. 429-439, 1999.

[20] T.-W. Lee, B. Koehler, and B. U. Orglmeister, "Blind source separation of nonlinear mixing model," in Proc. IEEE Workshop, Neural Networks for Signal Processing, VII, pp. 405-415, Oct. 1997.

[21] R. Plonsey, *Bioelectric phenomena*, New York: McGrew Hill, 1969.

[22] M. Sabry-Rizk, W. Zgallai, C. Morgan, S. ElKhafif

E. R. Carson, and K. T. V. Grattan, "Novel decision strategy for P-wave detection utilising nonlinearly synthesised ECG components and their enhanced pseudospectral resonances," *IEE Proceedings Science, Measurement and Technology*, Special section on Medical Signal Processing, vol. 147, No. 6, pp. 389-397, November 2000.

[23] M. Sabry-Rizk, W. Zgallai, S. El-Khafif, E. Carson, K. Grattan, "Higher- Order Ambulatory Electro-cardiogram Identification and Motion Artifact Suppression With Adaptive Second- and Third-Order Volterra Filters," SPIE '98 Advanced Signal Processing Algorithms, Architectures, and Implementations VIII Vol. 3461, pp. 417-431, San Diego, USA, 19-24 July 1998.

[24] W. Zgallai, M. Sabry-Rizk, P. Hardiman, and J. O'Riordan, "Third-order cumulant signature matching technique for non-invasive fetal heart beat identification," ICASSP, IEEE International Conference on Acoustics, Speech, and Signal Processing, vol. 5, pp 3781-3784, Germany, 1997.

[25] W. Zgallai, *The application of higher-order statistics and non-linear filtering to non-invasive fetal Electrocardiogram (ECG) detection*, PhD Thesis, City University, London, UK, June 2001.

[26] M Sabry-Rizk, W Zgallai, E. R. Carson, K. T. V. Grattan, A. MacLean, and P. Hardiman Non-linear dynamic tools for characterising abdominal electro-myographic signals before and during labour. *Trans Inst Measurement and Control*, vol. 22, pp. 243- 270, 2000.

[27] M. Sabry-Rizk, W. Zgallai E. R. Carson, K. T. V. Grattan, P. Hardiman, P. Thompson and A. Maclean, "Modified MUSIC Pseudospectral Analysis Reveals Common Uterus and Fetal Heart Resonances During Labour Contractions", the 22nd Annual International Conference of the IEEE Engineering in Medicine and Biology Society, EMB2000, USA, 23-28/7/2000.

[28] M. Sabry-Rizk, W. Zgallai "Novel Volterra Predictor Based on State-Space Equilibrium of Nonlinear Single- or Multi-Fractal Signals" SPIE's 45th Annual Meeting, the International symposium on Optical Science and Technology, Advanced Signal Processing Algorithms, Architectures, and Implementations X, USA, vol. 4116, pp. 322-333, 30/7-4/8/2000.

[29] M. Sabry-Rizk and W. Zgallai, "Modelling of synchronised fetal and mother electrocardiogram signals using Volterra-like structures," to be submitted to IEEE Transactions on Signal Processing, 2001.

[30] M. Sabry-Rizk, W. Zgallai, "On-Line Non-Invasive Fetal Heart Cumulant Detection Using A Neural Network," To be submitted to IEEE Transaction on Biomedical Engineering, 2001.

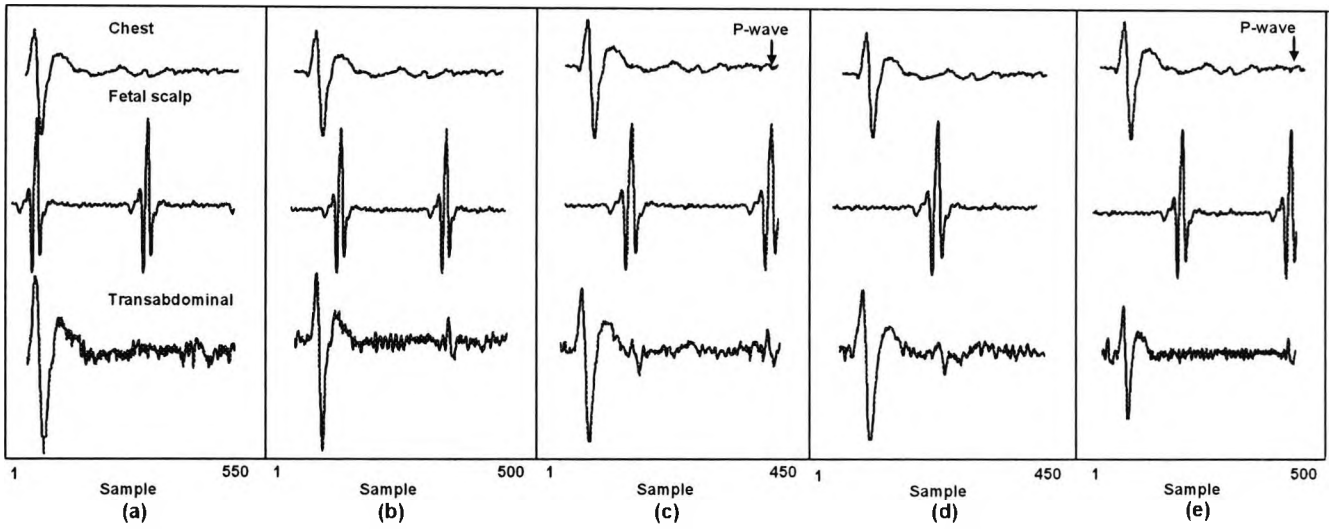

Figure 2: *Simultaneous recordings of maternal chest ECG (top), fetal scalp ECG (middle) and transabdominal ECG (bottom). (a) The fetal and maternal QRS complexes severely overlapping (synchronised). (c) Fetal QRS-on-ST segment. The second fetal QRS complex within the maternal cycle coincides with her P-wave. (e) Fetal QRS-on-ST segment. The second fetal QRS complex within the maternal cycle coincides with her P-wave.*

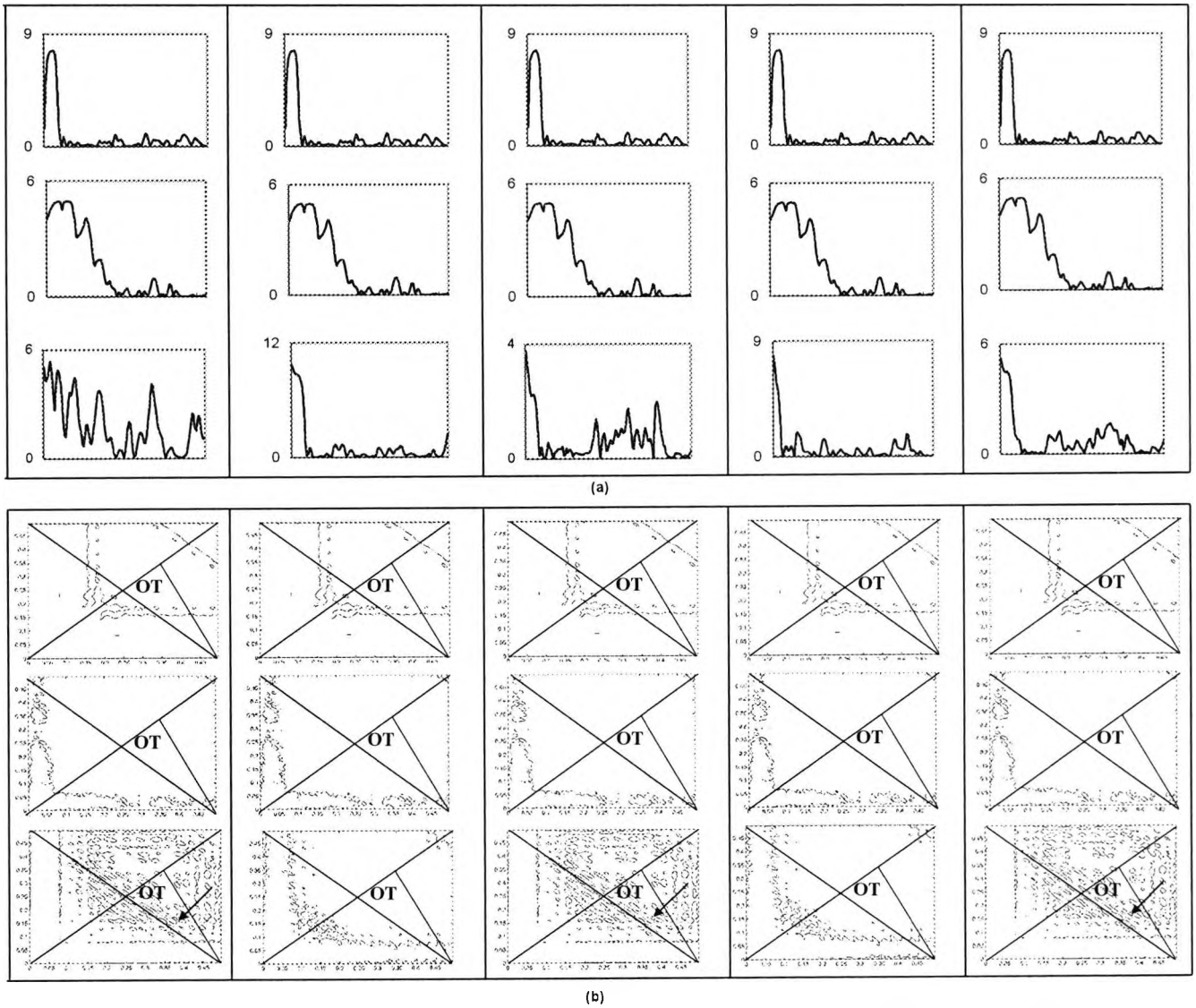

Figure 3: *Exploitation of the bicoherence squared of simultaneous recordings (see Figure 2) of maternal chest ECG (top rows in (a)-(b)), transabdominal ECG (bottom rows in (a)-(b)), and fetal scalp ECG (middle rows in (a)-(b)), to detect quadratic coupling and non-stationarity, particularly during events of synchronised maternal and fetal QRS complexes and P-waves. (a) Diagonal slices and (b) the corresponding contours with arrowheads pointing at activities in the OT region indicative of non-stationarity [16].*

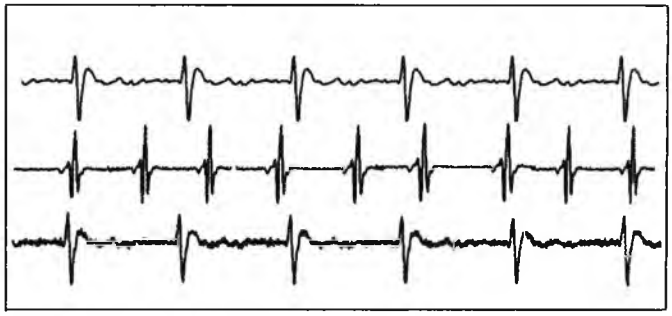

(a)

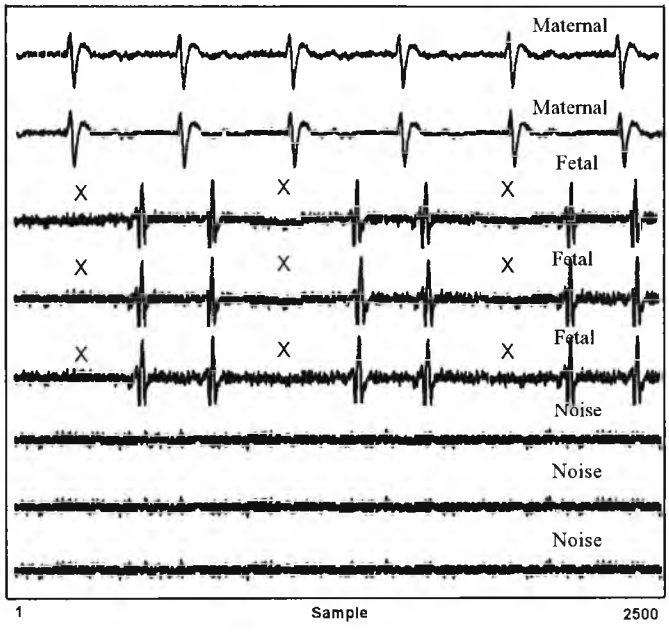

(b)

Figure 4: *Simultaneous recordings of maternal and fetal ECGs.*
(a) Maternal chest (top), fetal scalp (middle) and transabdominal ECG signals of length 2500 samples including five maternal cycles and 9 fetal cycles. The fetal scalp recording was deemed necessary and was used as a marker for fetal heartbeats.
(b) Outputs of 8 channel after applying blind source separation using second-order (SO) and fourth-order (FO) cumulants of the data. Channels 1 and 2 show the maternal signal. Channels 3, 4 and 5 are amplified to show the fetal signals. Note the first, fourth and seventh fetal signals have not been identified and are marked X. The missing fetal complexes are almost invariably coincident with either maternal QRS complexes or P-waves. The remaining channels, namely, 6, 7 and 8 are noise channels.

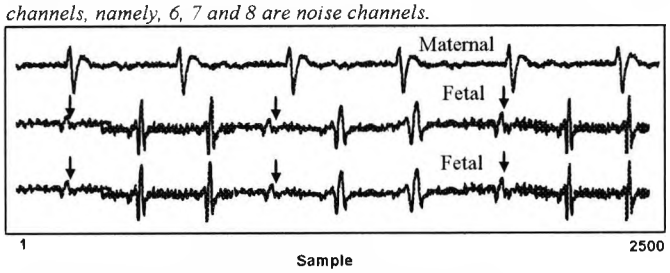

Figure 5: *Blind source separation results after carying out a novel non-linear identification procedure on the data of Fig. 4 (a), using an embedded Volterra-like structure with an extended memory and modified to cater for time-variant non-linearity. Three key channels are shown after the identification of the previously missing first, fourth and seventh fetal heartbeats (arrowheads).*

APPENDIX A4

LINEARITY AND GAUSSIANITY TESTS, VOLTERRA STRUCTURES, AND SIGNAL TO NOISE RATIO

A4.1 Non-Gaussianity and non-linearity tests

If a signal is Gaussian, its third- (and fourth-) order cumulants must be zero [1]. In practice, sample estimates of cumulants will not be exactly zero. So, we need a test to determine whether or not estimated quantities are significantly different from zero in a statistical sense. For a linear non-Gaussian signal, the absolute value of the bicoherence squared is a constant [1]. Again, sample estimates of the bicoherence squared will not be constant, and we need a test to determine whether the non-constancy is statistically significant [2]. The bispectrum of the signal is estimated and smoothed; tests are then conducted to see whether the bispectral values are significantly different from zero. The basic idea is that estimates of the bispectrum are asymptotically complex normal; hence, the energy in the bispectrum is chi-square distributed; the number of degrees of freedom depends upon the FFT length and the smoothing window.

In the Gaussianity test, the null hypothesis is that the data have zero bispectrum (Gaussian). The computed probability of false alarm (PFA) value is the probability that the value of the chi-squared random variable with the indicated degrees of freedom will exceed the computed test statistic. The PFA value indicates the false alarm probability in accepting the alternate hypothesis, that the data have non-zero bispectrum. Usually, the null hypothesis is accepted if the PFA is greater than 0.05 (i.e., it is risky to accept the alternate hypothesis).

The power of the test is dependent on the skewness of the signal, but independent of the skewness of the noise, assuming that it is known or can be estimated. The probability of the detection is the probability that the detection statistic will exceed a threshold where the detection statistic under the alternative hypothesis in non-central chi-square with 2K degrees of freedom, where K is the number of bifrequency pairs in the principal domain.

The non-centrality parameter is

$$\Lambda = \frac{2N}{\left(1+\rho^{-1}\right)^3}\Gamma_s \qquad \text{(A4.1)}$$

where Λ is the non-centrality parameter, N is the number of samples, ρ is the signal-to-noise ratio, and Γ_s is the skewness of the signal.

Since the non-centrality parameter has a linear dependence on the skewness of the signal and approximately a cubic dependence on the SNR, at low average SNR it is necessary for the skewness of the signal to increase by a factor of 8 to achieve a 3 dB improvement in detection performance. Also, because of the cubic dependence on the SNR, the detection ratio exhibits a rapid increase in probability of detection from near 0 probability to near a probability of 1 over a small SNR range of only 4 – 5 dB.

The non-centrality parameter also has a linear dependence on N, the sample size. Thus, it is necessary to increase the sample size by a factor of 8 for a fixed value of the skewness of the signal to achieve a 3 dB improvement in detection performance at low average SNR. The bispectrum detector can detect non-Gaussian signals at low average SNR for reasonable sample sizes, and reasonable values of the weighted average skewness. Thus, it appears that the bispectrum can be used to detect a non-Gaussian signal even in the presence of quite low SNR.

In the Linearity test, the inter-quartile range of the estimated bicoherence squared is computed; a quantity, Λ, proportional to the mean value of the bicoherence squared is also computed; the theoretical inter-quartile range of a chi-square random variable with two degrees of freedom and non-centrality parameter, Λ, is then computed. The linearity

hypothesis should be rejected if the estimated and theoretical inter-quartile ranges are very different from one another [2]. In the following analysis a smoothing parameter (cparm) value of 0.51 and an FFT length of 256 are used. The sequences to be tested have different number of samples.

A4.2 Non-Gaussianity and non-linearity tests when applied to the linear, quadratic and cubic parts of the Volterra synthesiser

We now test the linear, quadratic and cubic parts of fetal scalp electrode, maternal chest and maternal transabdominal ECG signals which were used to represent these signals. It is shown in Table A4.1 below that the parameter S-Gauss is larger than zero in all cases. This indicates that the linear parts of the fetal scalp electrode, maternal chest and maternal transabdominal ECG signals as well as the linear parts of quadratic and cubic Volterra predictors are all non-Gaussian. Also, the quadratic part of quadratic and cubic Volterra as well as the cubic part of cubic Volterra predictors are also all non-Gaussian. The last six rows of the table are for signal-free segments with noise artefacts that were isolated from transabdominal cardiac cycles. Table A4.1 shows that the linear part of the noise is also non-Gaussian.

A linear non-Gaussian process can be generated if an output signal is generated by a non-linear filtering operation satisfying a truncated Volterra functional expansion. A linear time series will have third-order cumulant values if the input is not normal (its probability density function is not Gaussian) and the impulse response is linear. If the relationship between the input and the output is non-linear, like in the case of a Volterra predictor, then the output is non-Gaussian even if the input is Gaussian. That could be the explanation for the linear part of the Volterra synthesiser which is linear and non-Gaussian.

A good test statistic to test for linear non-Gaussian or non-linear signals is to use the bicoherence [2-3]. If a linear signal is Gaussian then the values of its bispectrum and bicoherence are zero at all frequencies. If a non-Gaussian signal is linear then all its bicoherence values are constants. However, if the value of the bicoherence is frequency dependent then the signal is non-linear [1].

Signal	S-Gauss	R (estimate)	R (theory)
FECG linear	147	25.8149	37.7603
FECG linear of quadratic	139	23.0438	39.1932
FECG quadratic of quadratic	3912	861.8194	78.7328
FECG linear of cubic	126	20.9268	34.3863
FECG quadratic of cubic	3459	826.4141	70.1212
FECG cubic of cubic	4178	458.7681	76.3572
MECG linear	408	27.6948	21.4091
MECG linear of quadratic	379	26.8153	20.9630
MECG quadratic of quadratic	6302	617.6984	87.9746
MECG linear of cubic	316	30.0503	17.9819
MECG quadratic of cubic	7044	671.3088	99.4456
MECG cubic of cubic	11290	875.6768	118.5841
AbdECG linear	151	31.6286	43.5039
AbdECG linear of quadratic	173	32.2683	35.2109
AbdECG quadratic of quadratic	9524	639.6858	116.5349
AbdECG linear of cubic	191	38.8798	28.5174
AbdECG quadratic of cubic	2145	820.3422	103.5432
AbdECG cubic of cubic	7193	710.2506	94.9496
Noise artefact, linear	8940	63.9564	42.3918
Noise artefact, linear of quadratic	7694	57.7569	46.8452
Noise artefact, quadratic of quadratic	9536	325.4379	52.1645
Noise artefact, linear of cubic	7216	55.6703	42.3918
Noise artefact, quadratic of cubic	10832	402.9357	51.8291
Noise artefact, cubic of cubic	13500	163.5049	32.8104

***Table A4.1**: Statistics for Gaussianity and linearity tests for Volterra linear, quadratic and cubic parts of fetal scalp, maternal chest, transabdominal ECG signals, and also for a signal-free segment of transabdominal cardiac cycles containing only noise artefacts. (code: 5-1).*

For the quadratic and cubic parts of the quadratic and cubic Volterra synthesisers, the estimated and theoretical inter-quartile ranges are not close to each other as shown when comparing the last two columns of Table A4.1. Hence, the non-linearity hypothesis was accepted. This is the case for both the quadratic and cubic parts of fetal scalp electrode, maternal chest, and maternal transabdominal ECG signals, as well as the signal-free

noise artefacts. However, for the linear parts of all the aforementioned signals, the differences between the theoretical and estimated values in Table A4.1 are not very large, hence the linearity assumption is accepted. It is concluded that the linear parts of the Volterra predictors are non-Gaussian and linear. However, the quadratic and cubic parts are both non-Gaussian and non-linear.

The linear and quadratic parts of the quadratic Volterra synthesiser, and the linear, quadratic and cubic parts of the cubic Volterra synthesisers can be quantified in percentages as shown in Table A4.2. The percentage of quadratic and cubic non-linearity in fetal scalp electrode, maternal chest, maternal transabdominal ECG signals and that of signal-free noise artefacts are less than 4%. Therefore, the largest part of the ECG signal is linear and non-Gaussian.

With respect to the overall transabdominal signal, it is noticed that the fetal signal is usually 10 – 20% of the maternal signal and the noise is about 5 – 15%. It is noticed that in about 50% of the transabdominal ECG cycles the level of the fetal and noise signals are the same and that the fetal is buried in noise with an SNR in the range of ±2 dB. Calculations of the SNR will be explained in section A4.4. The SNR is calculated for

Signal type	L	Q	C
Chest	96.35	3.65	_
	95.90	3.55	0.55
Fetal scalp	96.00	4.00	_
	95.55	3.85	0.60
Transabdomianl	96.25	3.75	_
	95.75	3.60	0.65
Noise artefacts	97.55	2.45	_
	97.09	2.55	0.36

Table A4.2: *The percentage of the overall maternal chest, fetal scalp, maternal transabdominal ECG signal, and noise artefacts in the synthesised linear, quadratic and cubic parts of the Volterra structure. L, Q, and C denote the linear, quadratic, and cubic parts, respectively. A blank entry under C in the first column on the right hand side indicates a quadratic synthesiser with no cubic part. Code: 5-1.*

the maternal transabdominal ECG signal investigated for linearity and Gaussianity. Using the method of section A4.4 it was found that the maternal SNR is in the range of 20 dB to 25 dB and the fetal SNR is in the range of –2 dB to +5 dB. The tests also confirmed that the signals are stationary within the maternal cardiac cycle.

A4.3 Coefficients Elimination for Volterra Structures

State subspace reduction techniques are used to determine how many of the coefficients can arbitrarily be set to zero without degrading the performance of the predictor. Starting with a full-rank Volterra predictor of quadratic, cubic only and quadratic and cubic structures, the mean -squared error of each predictor is calculated after elimination of some of the coefficients. The direct method of coefficient elimination could be summarised as follows [7]:

(i) Calculate the eigenvalues and eigenvectors of the correlation matrix ϕ_{zz} and hence estimate the rank L. The eigenvectors are collected into a rank matrix $\mathbf{V}$ which is partitioned $\mathbf{V} = [\mathbf{V}_s \quad \mathbf{V}_n]$ and indexed such that the eigenvectors which span the signal subspace are given by, $\mathbf{V}_s = [\mathbf{v}_1 \quad \mathbf{v}_2 \Lambda \, \mathbf{v}_L]$ and those which span the noise subspace are $\mathbf{V}_n = [\mathbf{v}_{L+1} \quad \Lambda \, \mathbf{v}_M]$.

(ii) Project each axis vector onto the signal subspace. The lengths of the projections are d_j. The vector $\mathbf{d}$ that contains these lengths is defined as, $\mathbf{d} = \text{diag}(\mathbf{V}_s\mathbf{V}_s^T)$. The L indices with the largest projections give the indices of the non-linearities that will be retained. The remainder indicates those weights that will be set to zero.

(iii) The matrix φ_{zz} is reduced in size by removing the rows and columns corresponding to the discarded direction- the axis associated with the shortest projection lengths. This gives an L x L matrix φ'_{zz}. Similarly the M vector φ_{zx} is reduced in size by removing the rows corresponding to the discarded directions. This gives an L vector φ'_{zx}. A set of normal equations $\varphi'_{zz}\mathbf{a}' = \varphi'_{zx}$ is solved for the L vector $\mathbf{a}'$ which contains the desired non-zero elements of $\mathbf{a}$.

A4.4 Signal to Noise Ratio

In real signal applications, one cannot separate the signal and the noise. The SNR is defined from the singular values of rectangular data matrix, $\boldsymbol{R}_x$, constructed for a cyclic or quasi-periodic data as follows.

$$\boldsymbol{R}_x = \begin{bmatrix} x(1) & x(2) & ..... & x(l_f) \\ x(l_f+1) & x(l_f+2) & ..... & x(2l_f) \\ ..... & ..... & ..... & ..... \\ ..... & ..... & ..... & ..... \\ x((L-1)l_f+1) & x((L-1)l_f+2) & ..... & x(Ll_f) \end{bmatrix}, \tag{A4.2}$$

where each row in this matrix contains one period of the signal, l_f is the fundamental period length, which is defined as the smallest of the most frequently occurring stride-cycles, and L is the number of periods used for calculating the matrix. Applying the SVD to this matrix the SNR can be calculated as follows [8]:

$$\text{SNR} = \frac{\sum_{i=1}^{p} s_i^2}{\sum_{i=p+1}^{l_f} s_i^2}, \tag{A4.3}$$

where s_i, i=1,2,.....l_f are the singular values of $\boldsymbol{R}_x$ and p is the number of dominant singular values, which theoretically constitute the signal subspace and the sum of squares of these p singular values represent the energy content of the signal. For strictly periodic process with no noise the total energy is s_1^2.

A4.5 References

[1] C. L. Nikias and A. P. Petropulu, *Higher Order Spectra Analysis: A Nonlinear Signal Processing Framework*, Prentice Hall, 1993.

[2] M. J. Hinich, "Test for Gaussianity and linearity of a stationary time series," Journal of time series analysis, vol. 3, No. 3, pp. 169-176, 1982.

[3] T. Subba Rao, "The Bispectral Analysis of Nonlinear Stationary Time Series with Reference to Bilinear Time Series Models," in *Handbook of Statistics*, vol. 3, (D. Brillinger, and P. Krishnaiah, eds.), Amesterdam, Holland, pp. 293-319, 1983.

[4] S. Chen, C. F. N. Cowan and P. M. Grant, "Orthogonal Least Squares Learning Algorithm for Radial Basis Function Networks," IEEE Transactions on Neural Networks, vol. 2, pp. 302-309, 1991.

[5] M. R. Lynch, P. J. Rayner and S. B. Holden, "Removal of Degeneracy in Adaptive Volterra Networks by Dynamic Structuring," Proceedings of IEEE ICASSP, pp. 2069-2072, 1991.

[6] S. Haykin, *Adaptive filter theory*, Prentice Hall, 1991.

[7] K. C. Nisbet, B. Mulgrew and S. McLaughlin, "A reduced complexity sub-optimal nonlinear predictor," IEE Colloquium, pp. 6/1-6/13, London, 1994.

[8] V. P. Stokes, H. Lanshammar, and A. Thorstensson, "Dominant pattern extraction from 3-D kinematic data," IEEE Transactions Biomedical Engineering, Vol. BME-46, pp. 100-106, 1999.

APPENDIX A5

THE MIT-BIH DATABASE

A.5.1 The MIT-BIH Normal Sinus Rhythm Database

This database includes 18 long-term ECG recordings of subjects referred to the Arrhythmia Laboratory at Boston's Beth Israel Hospital (now the Beth Israel Deaconess Medical Center). Subjects included in this database were found to have had no significant arrhythmias; they include 5 men, aged 26 to 45, and 13 women, aged 20 to 50.

A5.2 The MIT-BIH Arrhythmia Database

Since 1975, the laboratories at Boston's Beth Israel Hospital (now the Beth Israel Deaconess Medical Center) and at MIT have supported the research into arrhythmia analysis and related subjects. One of the first major products of that effort was the MIT-BIH Arrhythmia Database, which was completed in 1980. The database was the first generally available set of standard test material for evaluation of arrhythmia detectors, and has been used for that purpose as well as for basic research into cardiac dynamics at about 500 sites worldwide. Originally, the database was distributed on 9-track half-inch digital tape at 800 and 1600 bpi, and on quarter-inch IRIG-format FM analogue tape. In August, 1989, a CD-ROM version of the database was produced; since that time, it has been on CD-ROM only.

The MIT-BIH Arrhythmia Database contains 48 half-hour excerpts of two-channel ambulatory ECG recordings, obtained from 47 subjects studied by the BIH Arrhythmia Laboratory between 1975 and 1979. Twenty-three recordings were chosen at random from a set of 4000 24-hour ambulatory ECG recordings collected from a mixed population of inpatients (about 60%) and outpatients (about 40%) at Boston's Beth Israel

Hospital; the remaining 25 recordings were selected from the same set to include less common but clinically significant arrhythmias that would not be well-represented in a small random sample.

The recordings were digitized at 360 samples per second per channel with 11-bit resolution over a 10 mV range. Two or more cardiologists independently annotated each record; disagreements were resolved to obtain the computer-readable reference annotations for each beat (approximately 110,000 annotations in all) included with the database.

A5.3 Description of data sets 105, 108 and 203 of the MIT-BIH Arrhythmia Database

Record 105 (MLII, V1; female, age 73)

Medications: Digoxin, Nitropaste, Pronestyl

Beats	**Before 5:00**	**After 5:00**	**Total**
Normal	405	2121	2526
PVC	12	29	41
Unclassifiable	-	5	5
Total	417	2155	2572

Ventricular ectopy

- 41 isolated beats

Rhythm	**Rate**	**Episodes**	**Duration**
Normal sinus rhythm	78-102	1	30:06

Signal quality	**Episodes**	**Duration**
Both clean	31	22:18
Upper noisy	3	0:10
Lower noisy	28	3:27
Both noisy	23	4:06
Unreadable	4	0:04

Notes:

The PVCs are uniform. The predominant feature of this tape is high-grade noise and artifact.

Points of interest:

5:27 Artifact

7:57 PVC

15:16 Normal sinus rhythm

17:52 Artifacts

22:02 Noise

26:45 PVC

27:27 Noise

28:08 Noise

29:07 Noise

Record 108 (MLII, V1; female, age 87)

Medications: Digoxin, Quinaglute

Beats	**Before 5:00**	**After 5:00**	**Total**
Normal	279	1461	1740
APC	1	3	4
PVC	3	13	16
Fusion PVC	-	2	2
Junctional escape	-	1	1
Blocked APC	2	9	11
Total	285	1489	1774

Supraventricular ectopy

- 4 isolated beats

Ventricular ectopy

- 14 isolated beats
- 2 couplets

Rhythm	Rate	Episodes	Duration
Normal sinus rhythm	44-78	1	30:06

Signal quality	Episodes	Duration
Both clean	19	24:05
Upper noisy	3	0:16
Lower noisy	12	2:45
Both noisy	8	3:01

Notes:

There is borderline first degree AV block and sinus arrhythmia. The PVCs are multiform. The lower channel exhibits considerable noise and baseline shifts.

Points of interest:

0:22	PVC,	blocked	APC,	noise	
4:51		Interpolated		PVC	
7:41		Axis		shift	
8:13	PVC,	blocked	APC,	fusion	PVC
10:55		Sinus		arrhythmia	
18:08		Fusion	PVC-PVC	couplet	
20:05		Junctional	escape	beat	
24:20		Blocked	APC,	APCs	
28:10				Noise	
29:00	Noise				

Record 203 (MLII, V1; male, age 43)

Medications: Coumadin, Digoxin, Heparin, Hygroton, Lasix

Beats	Before 5:00	After 5:00	Total
Normal	426	2103	2529
Aberrated APC	2	-	2
PVC	71	373	444

Fusion PVC	-	1	1
Unclassifiable	-	4	4
Total	499	2481	2980

Supraventricular ectopy

- 2 isolated beats

Ventricular ectopy

- 238 isolated beats
- 64 couplets
- 13 runs of 3 beats
- 6 runs of 4 beats
- 1 run of 7 beats
- 1 run of 9 beats

Rhythm	**Rate**	**Episodes**	**Duration**
Normal sinus rhythm	63-173	1	2:43
Atrial flutter	61-180	2	5:14
Atrial fibrillation	54-180	20	21:32
Ventricular trigeminy	100-116	1	0:04
Ventricular tachycardia	124-189	21	0:33

Signal quality	**Episodes**	**Duration**
Both clean	21	24:28
Upper noisy	20	3:17
Lower noisy	7	1:49
Both noisy	8	0:30
Unreadable	1	0:02

Notes:

The PVCs are multiform. There are QRS morphology changes in the upper channel due to axis shifts. There is considerable noise in both channels, including muscle artifact and baseline shifts. This is a very difficult record, even for humans!

Points of interest:

5:00 Ventricular tachycardia, 4 beats and 9 beats
13:14 Atrial fibrillation, ventricular couplets
15:02 Noise
22:02 Ventricular couplet, PVCs
23:25 Noise
24:04 PVCs
24:46 Noise
26:39 Ventricular tachycardia, 7 beats
26:51 Ventricular couplet, PVCs
27:15 Ventricular tachycardia, 3 beats

APPENDIX A6

Kaiser window and weighted MUSIC

A.6.1 Kaiser window

The first modification to the MUSIC algorithm is done by modifying Eq. (6.29) by introducing the parameter W_{MFk} which represents a Kaiser window function [1] to the denominator. Kaiser Window was introduced by Kaiser based on discrete-time approximations of the prolate spheroidal wave functions. For the Rectangular, Bartlett, Hanning, Hamming, and Blackman windows, the width of the mainlobe is inversely proportional to the number of samples, N. However, the minimum stop-band attenuation is independent of the window length and is a function of the selected window. Hence, to meet a desired stop-band attenuation, the designer is forced to select a window that meets the design specifications. It is worth noting that windows with low sidelobe levels have broader mainlobe widths, hence requiring an increase in the order of the filter N to achieve the desired transition width. The Kaiser window has a variable parameter β_k which can be varied to control the sidelobe level with respect to the mainlobe peak. As in other windows, the mainlobe width can be adjusted by changing the length of the window, which in turn adjusts the transition width of the filter. Therefore, the FIR filter can be efficiently designed using the Kaiser window. The Kaiser window is defined by [2]:

$$W_{mfk}(i) = \begin{cases} \dfrac{I_o\left(2\beta\sqrt{\dfrac{i}{N-1}-\left(\dfrac{i}{N-1}\right)^2}\right)}{I_o(\beta_k)} & 0 \le i \le N-1 \\ 0 & \textit{elsewhere} \end{cases} \qquad \text{(A6.1)}$$

where $I_o(x)$ is the modified zeroth-order Bessel function of the first kind. β controls the way the window function tapers at the edges in the time domain. $I_o(x)$ is normally

evaluated using the following power series expansion

$$I_0(x) = 1 + \sum_{k=1}^{L} \left[\frac{(x/2)^k}{k!} \right]^2 \qquad \text{(A6.2)}$$

where typically L < 25. An algorithm due to Kaiser gives an efficient implementation of this equation. When $\beta = 0$, the Kaiser window corresponds to the rectangular window, and when it is equal to 5.44, the resulting window is very similar, though not identical, to the Hamming window. The value of β is determined by the stoop-band attenuation requirements and may be estimated from one of the following empirical relationships:

$$\beta = 0 \qquad \text{if } A \leq 21 \text{ dB}, \qquad \text{(A6.3)}$$

$$\beta = 0.5842\,(A - 21)^{0.4} + 0.07886\,(A - 21) \qquad \text{if } 21 \text{ dB} < A < 50 \text{ dB}, \qquad \text{(A6.4)}$$

$$\beta = 0.1102\,(A - 8.7) \qquad \text{if } A \geq 50 \text{ dB}, \qquad \text{(A6.5)}$$

where $A = -20 \log_{10}(\delta)$ is the stop-band attenuation, $\delta = \min(\delta_p, \delta_s)$, since the pass-band and stop-band ripples are nearly equally, δ_p is the desired pass-band ripple and δ_s is the desired stop-band ripple. The number of filter coefficients, N, is given by

$$N \geq \frac{A - 7.95}{14.36 \Delta f}, \qquad \text{(A6.6)}$$

where Δf is the normalised transition bandwidth. The values of β and N are used to compute the coefficients for the Kaiser window, w(n). Eq. (A6.5) was used to calculate β for the Kaiser weighting coefficients of the maternal QRS-complex and the fetal heartbeat. β is equal to 6.127 for the former and 6.291 for the latter.

A.6.2 Summary of the window method

1- Specify the ideal or desired frequency response, $H_D(\omega)$.

2- Obtain the impulse response, $h_D(n)$, by evaluating the inverse Fourier

Transform.

3- Select a window function that satisfies the pass-band or attenuation specifications and then determine the number of coefficients using the appropriate relationship between the length and the transition bandwidth, Δf (expressed as a fraction of the sampling frequency).

4- Obtain values of w(n) for the chosen window function and the values of the actual coefficients, h(n), by multiplying $h_D(n)$ by w(n):

$$H(n) = h_D(n) \,.\, w(n). \tag{A6.7}$$

It is clear that the window method is straightforward and requires a minimal amount of computational effort. Indeed the coefficients could be obtained with a pocket calculator.

A.6.3 The sequentially optimised and weighted MUSIC

Kaiser has shown that these Kaiser windows are nearly optimum in the sense of having the largest energy in the mainlobe for a given peak sidelobe amplitude. The Kaiser window is used to design a band-pass filter with a pass-band attenuation of -1 dB, minimum stop-band attenuation of -70 dBs, centre frequencies of 17 Hz and 30 Hz, respectively, for the maternal QRS-complex and the fetal heartbeat pseudo-spectral peaks. The coefficients are arranged in an (M - p + 1) x (M - p + 1) matrix to be multiplied by the eignvectors $\mathbf{v}_N$. The matrix of the coefficients can be written as

$$W_{MFk} = \begin{bmatrix} w_{m+1,m+1} & w_{m+1,m+2} \cdots w_{m+1,p+1} \\ w_{m+2,m+1} & w_{m+2,m+2} \cdots w_{m+2,p+1} \\ \cdots & \\ w_{p+1,m+1} & w_{p+1,m+2} \cdots w_{p+1,p+1} \end{bmatrix} \tag{A6.8}$$

Hence, using Eq. (6.29) and Eq. (A6.8), the sequentially optimised and weighted MUSIC-like estimator can be expressed as

$$P(\omega) = \frac{1}{\begin{bmatrix} w_{1,m+1} & w_{1,m+2} \cdots w_{1,p+1} \\ w_{2,m+1} & w_{2,m+2} \cdots w_{2,p+1} \\ \cdots & \\ w_{p+1,m+1} & w_{p+1,m+2} \cdots w_{p+1,p+1} \end{bmatrix} x \begin{bmatrix} 1 & e^{-j\omega} & \cdots e^{-jp\omega} \end{bmatrix} x \begin{bmatrix} v_{1,m+1} & v_{1,m+2} \cdots v_{1,p+1} \\ v_{2,m+1} & v_{2,m+2} \cdots v_{2,p+1} \\ \cdots & \\ v_{p+1,m+1} & v_{p+1,m+2} \cdots v_{p+1,p+1} \end{bmatrix}}$$

$$x \frac{1}{\begin{bmatrix} v^*_{1,m+1} & v^*_{2,m+1} \cdots v^*_{p+1,m+1} \\ v^*_{1,m+2} & v^*_{2,m+2} \cdots v^*_{p+1,m+2} \\ \cdots & \\ v^*_{1,p+1} & v^*_{2,p+1} \cdots v^*_{p+1,p+1} \end{bmatrix} x \begin{bmatrix} 1 \\ e^{j\omega} \\ \cdots \\ e^{jp\omega} \end{bmatrix}} \qquad \text{(A6.9)}$$

where W_{MFk} can be substituted by W_{Mk} and W_{Fk} for the optimised Kaiser weighted coefficients for the maternal QRS-complex and the fetal heartbeat principal pseudo-spectral peaks, respectively.

A.6.4 The Kaiser coefficients of the mother's QRS-complex

1.149253201 0.982169251 0.801737734 0.5925466 1.04843858
1.663712032 1.319756997 1.559402251 4.151685019 0.435111232
0.824357818 10.03305689 0.075439403 1.446923527 1.005492549
1.13881777 1.010125525 1.112982675 1.054177077 14.64811754
0.40118421 0.939932725 0.948944957 2.150512959 0.945435035
21.48580419 1.908443233 0.094936534 4.192797563 1.223595741
1.119754804 1.006219947 1.357271858 0.6978442 0.654189942
1.094963727 1.121518925 1.318576272 0.249476968 2.081067575
1.961844113 0.552354621 0.102612073 0.295653014 3.50365836
1.0856573 0.956078205 1.120611657 1.102615456 0.794066179
1.337215004 0.596200716 1.583603059 29.95636544 1.303502603
5.169873516 0.179132663 1.207634773 1.163927888 0.785620906
1.040099881 0.851976195 1.907881902 1.213525766 0.715962719

0.114764147	0.947099501	0.910392996	1.686797484	1.245412981
0.008450692	1.196556966	1.910813112	0.507330829	0.016670668
0.99233444	0.66477291	1.760347078	1.091776693	1.440875468
0.567751505	0.772229192	0.579324678	2.83806498	42.73184927
0.584904481	2.454985943	13.40233916	0.726946252	0.051635255
0.952095924	0.079214662	1.532946061	0.30245571	0.944576488
0.549883899	0.915100567	4.059789248	0.012779603	0.500212911
1.18714481	3.190683557	3.742827594	572.8851749	0.491998759
0.927451369	1.971692587	1.209602742	9.289796672	0.708884569
2.005875641	0.928383856	0.282982863	2.005875641	0.928383856
1.149253201	0.982169251	0.801737734	0.5925466	1.04843858
1.663712032	1.319756997	1.559402251	4.151685019	0.435111232
0.824357818	10.03305689	0.075439403	1.446923527	1.005492549
1.13881777	1.010125525	1.112982675	1.054177077	14.64811754
0.40118421	0.939932725	0.948944957	2.150512959	0.945435035
21.48580419	1.908443233	0.094936534	4.192797563	1.223595741
1.119754804	1.006219947	1.357271858	0.6978442	0.654189942
1.094963727	1.121518925	1.318576272	0.249476968	2.081067575
1.961844113	0.552354621	0.102612073	0.295653014	3.50365836
1.0856573	0.956078205	1.120611657	1.102615456	0.794066179
1.337215004	0.596200716	1.583603059	29.95636544	1.303502603
5.169873516	0.179132663	1.207634773	1.163927888	0.785620906
1.040099881	0.851976195	1.907881902	1.213525766	0.715962719
0.114764147	0.947099501	0.910392996	1.686797484	1.245412981
0.008450692	1.196556966	1.910813112	0.507330829	0.016670668
0.99233444	0.66477291	1.760347078	1.091776693	1.440875468
0.567751505	0.772229192	0.579324678	2.83806498	42.73184927
0.584904481	2.454985943	13.40233916	0.726946252	0.051635255
0.952095924	0.079214662	1.532946061	0.30245571	0.944576488
0.549883899	0.915100567	4.059789248	0.012779603	0.500212911
1.18714481	3.190683557	3.742827594	572.8851749	0.491998759
0.927451369	1.971692587	1.209602742	9.289796672	0.708884569

A.6.5 The Kaiser coefficients of the fetal QRS-complex

0.803229457	0.626593323	2.49683354	0.15361307	5.33129127
0.162722894	3.076774741	0.920867196	1.166246566	0.797130643
2.346422448	0.217684209	0.65551547	0.565556635	3.368241266
0.195887916	0.489199233	12.23374436	1.133958792	0.033388051
1.418882219	0.937142227	0.92990052	1.047629904	0.271307778
1.423502329	15.77151233	0.496852819	0.814036855	0.437447316
0.795920399	17.15792848	2.103969067	1.748417424	1.056282753
1.144236728	0.298480952	0.945546959	1.026432666	1.022538206
0.712360331	1.514267466	1.097885191	0.86826119	0.891178146
0.02376525	7.238226829	0.244058715	0.98435139	53.70934865
0.442183146	0.314025664	0.95566187	1.031065453	3.134019749
0.031398548	0.944362516	1.369261662	2.38156286	0.58063022
2.826424829	0.64493068	6.958807533	0.668229781	0.966307464
3.804444914	0.370741375	0.959978893	1.031835537	1.163190792
2.347118826	0.213052688	1.078287642	1.09813755	0.671659551
0.275104293	1.093838379	0.609301348	2.21998696	2.079125547
0.796784829	60.65080259	0.964544114	1.016735978	0.74765748
1.494590521	13.30912445	0.04418504	0.853962113	0.543696095
2.170038053	1.216310945	0.304590322	7.144329049	0.14033888
4.513104819	1.659777066	0.966235902	0.986550086	0.564061404
0.443196011	1.23378891	1.627844817	1.345310968	1.275908042
5.662452698	0.487965395	0.143509155	6.197482327	0.047165648
2.064756017	1.274750618	1.493817321	2.064756017	1.274750618
0.803229457	0.626593323	2.49683354	0.15361307	5.33129127
0.162722894	3.076774741	0.920867196	1.166246566	0.797130643
2.346422448	0.217684209	0.65551547	0.565556635	3.368241266
0.195887916	0.489199233	12.23374436	1.133958792	0.033388051
1.418882219	0.937142227	0.92990052	1.047629904	0.271307778
1.423502329	15.77151233	0.496852819	0.814036855	0.437447316
0.795920399	17.15792848	2.103969067	1.748417424	1.056282753
1.144236728	0.298480952	0.945546959	1.026432666	1.022538206
0.712360331	1.514267466	1.097885191	0.86826119	0.891178146
0.02376525	7.238226829	0.244058715	0.98435139	53.70934865

0.442183146 0.314025664 0.95566187 1.031065453 3.134019749
0.031398548 0.944362516 1.369261662 2.38156286 0.58063022
2.826424829 0.64493068 6.958807533 0.668229781 0.966307464
3.804444914 0.370741375 0.959978893 1.031835537 1.163190792
2.347118826 0.213052688 1.078287642 1.09813755 0.671659551
0.275104293 1.093838379 0.609301348 2.21998696 2.079125547
0.796784829 60.65080259 0.964544114 1.016735978 0.74765748
1.494590521 13.30912445 0.04418504 0.853962113 0.543696095
2.170038053 1.216310945 0.304590322 7.144329049 0.14033888
4.513104819 1.659777066 0.966235902 0.986550086 0.564061404
0.443196011 1.23378891 1.627844817 1.345310968 1.275908042
5.662452698 0.487965395 0.143509155 6.197482327 0.047165648

A.6.6 References

[1] J. F. Kaiser, "Nonrecursive digital filter design using the Io-sinh window function," in Selected Papers in Digital Signal Processing, II, NY, IEEE, 1976.

[2] M. H. Er, et al., "FIR filters,", in "The circuits and filters Handbook", W.K. Chen, Ed., CRC, Press, IEEE Press, 1995.

APPENDIX A7

An example of the covariance matrix of the uterine contraction signal, I_{noise} matrix

The list below is an example of the (M + 1) x (M + 1) covariance matrix of the uterine contraction signal, $\mathbf{I}_{noise}$ matrix, with M + 1 = 15 for QRS-free ECG segment. Note that the symbol E denotes the power of 10, for example 5.08E-02 = 0.0508.

```
I(1,1) = 0.235247       I(1,2) = -0.158353      I(1,3) = 0.209564
I(1,4) = -0.419537      I(1,5) = 0.321579       I(1,6) = -0.318482
I(1,7) = 0.0353         I(1,8) = -0.181454      I(1,9) = 0.341014
I(1,10) = -0.214313     I(1,11) = 0.10929       I(1,12) = -2.13E-02
I(1,13) = 0.25098       I(1,14) = 5.08E-02      I(1,15) = 0.021315
I(2,1) = 0.229518       I(2,2) = -0.221884      I(2,3) = 0.23763
I(2,4) = -0.306377      I(2,5) = -0.150243      I(2,6) = -0.271848
I(2,7) = 5.62E-02       I(2,8) = 7.54E-02       I(2,9) = -0.462363
I(2,10) = 3.95E-04      I(2,11) = -0.082602     I(2,12) = -0.11737
I(2,13) = -0.379269     I(2,14) = 2.37E-02      I(2,15) = -0.246573
I(3,1) = 0.23081        I(3,2) = -0.25103       I(3,3) = 0.2281
I(3,4) = -0.10165       I(3,5) = 1.02E-01       I(3,6) = 0.235588
I(3,7) = -0.122746      I(3,8) = 0.32383        I(3,9) = 7.36E-02
I(3,10) = 0.52176       I(3,11) = 0.237379      I(3,12) = 0.134566
I(3,13) = -3.47E-02     I(3,14) = -0.28245      I(3,15) = 0.16305
I(4,1) = 0.245352       I(4,2) = -0.38121       I(4,3) = 0.05392
I(4,4) = 0.0673         I(4,5) = -0.341524      I(4,6) = 0.111
I(4,7) = -0.3501        I(4,8) = 2.26E-02       I(4,9) = -9.12E-02
I(4,10) = -0.3531       I(4,11) = 3.45E-02      I(4,12) = 0.22684
I(4,13) = 0.30625       I(4,14) = 0.3716        I(4,15) = 0.12334
I(5,1) = 0.2267         I(5,2) = -0.30301       I(5,3) = -2.33E-02
I(5,4) = 0.2144         I(5,5) = 0.0203         I(5,6) = 0.31505
I(5,7) = -6.73E-02      I(5,8) = -0.313         I(5,9) = 0.2396
I(5,10) = 4.57E-03      I(5,11) = -0.31817      I(5,12) = -0.24915
I(5,13) = 3.40E-02      I(5,14) = -0.11496      I(5,15) = -0.32968
I(6,1) = 0.22616        I(6,2) = -0.245         I(6,3) = -0.2223
I(6,4) = 0.25672        I(6,5) = -0.23427       I(6,6) = -1.01E-01
I(6,7) = 0.03596        I(6,8) = -0.31684       I(6,9) = -0.14591
I(6,10) = -2.18E-02     I(6,11) = 0.33621       I(6,12) = -0.2489
I(6,13) = -0.16776      I(6,14) = -0.16711      I(6,15) = 0.3707
I(7,1) = 0.24647        I(7,2) = -0.12459       I(7,3) = -0.33743
I(7,4) = 0.1416         I(7,5) = 0.26863        I(7,6) = 4.57E-02
I(7,7) = 0.4021         I(7,8) = 0.08021        I(7,9) = 1.78E-02
I(7,10) = 1.10E-02      I(7,11) = 2.47E-02      I(7,12) = 0.45762
I(7,13) = -0.209        I(7,14) = 0.34504       I(7,15) = -0.2026
I(8,1) = 0.23062        I(8,2) = 5.99E-07       I(8,3) = -0.4217
I(8,4) = 2.75E-08       I(8,5) = -0.1366        I(8,6) = -0.329
I(8,7) = 3.53E-07       I(8,8) = 0.3886         I(8,9) = -4.22E-08
I(8,10) = 3.49E-07      I(8,11) = -0.0722528    I(8,12) = 7.93E-07
I(8,13) = 0.433995      I(8,14) = -0.4          I(8,15) = 2.73E-06
I(9,1) = 0.252472       I(9,2) = 0.1326         I(9,3) = -0.344034
I(9,4) = -0.12166       I(9,5) = 0.2746         I(9,6) = 4.87E-02
I(9,7) = -0.4127        I(9,8) = 0.0807         I(9,9) = -1.78E-02
I(9,10) = -1.61E-02     I(9,11) = 2.85E-02      I(9,12) = -0.4695
I(9,13) = -0.206        I(9,14) = 0.3406        I(9,15) = 0.2028
I(10,1) = 0.2448        I(10,2) = 0.245         I(10,3) = -0.063235
I(10,4) = -0.2572       I(10,5) = -0.2427       I(10,6) = -1.03E-01
```

I(10,7) = -0.31456	I(10,8) = -0.31663	I(10,9) = 0.121
I(10,10) = 2.10E-02	I(10,11) = 0.33621	I(10,12) = 0.22697
I(10,13) = -0.15876	I(10,14) = -0.1512	I(10,15) = -0.38004
I(11,1) = 0.25705	I(11,2) = 0.3135	I(11,3) = -3.30E-02
I(11,4) = -0.21454	I(11,5) = 0.0212	I(11,6) = 0.33505
I(11,7) = 7.11E-02	I(11,8) = -0.328	I(11,9) = -0.265
I(11,10) = -5.75E-03	I(11,11) = -0.3317	I(11,12) = 0.2815
I(11,13) = 3.73E-02	I(11,14) = -0.13469	I(11,15) = 0.3684
I(12,1) = 0.253521	I(12,2) = 0.321464	I(12,3) = 0.123942
I(12,4) = 0.10163	I(12,5) = -0.3524745	I(12,6) = 0.11108
I(12,7) = 0.093	I(12,8) = 2.36E-02	I(12,9) = 9.32E-02
I(12,10) = 0.3431	I(12,11) = 4.33E-02	I(12,12) = -0.25584
I(12,13) = 0.289625	I(12,14) = 0.351962	I(12,15) = -0.114351
I(13,1) = 0.2501	I(13,2) = 0.3043	I(13,3) = 0.2282
I(13,4) = 0.1015	I(13,5) = 1.01E-01	I(13,6) = 0.269855
I(13,7) = 0.15274	I(13,8) = 0.3278	I(13,9) = -7.35E-02
I(13,10) = -0.5421	I(13,11) = 0.06273	I(13,12) = -0.137456
I(13,13) = -4.13E-02	I(13,14) = -0.28924	I(13,15) = -0.163
I(14,1) = 0.23495	I(14,2) = 0.24518	I(14,3) = 0.26776
I(14,4) = 0.31263	I(14,5) = -0.1502	I(14,6) = -0.2718
I(14,7) = -5.82E-02	I(14,8) = 7.85E-02	I(14,9) = 0.4523
I(14,10) = -3.64E-04	I(14,11) = -0.096	I(14,12) = 0.1253
I(14,13) = -0.3892	I(14,14) = 2.48E-02	I(14,15) = 0.2365
I(15,1) = 0.2252	I(15,2) = 0.17883	I(15,3) = 0.2095
I(15,4) = 0.4395	I(15,5) = 0.3515	I(15,6) = -0.3184
I(15,7) = -0.061	I(15,8) = -0.17144	I(15,9) = -0.351
I(15,10) = 0.227341	I(15,11) = 0.10179	I(15,12) = 2.37E-02
I(15,13) = 0.247	I(15,14) = 5.08E-02	I(15,15) = -0.1157

APPENDIX A8

Matrix Terminology and Definitions

A8.1 Definitions

Consider an m x n matrix **A** with elements a_{ij}, i = 1, 2, …, m; j = 1, 2, …, n. The transpose of **A**, which is denoted by $\mathbf{A}^T$, is defined as the n x m matrix with elements a_{ij}, or

$$[\mathbf{A}^T]_{ij} = a_{ji}. \tag{A8.1}$$

Similarly, the hermitian transpose (or conjugate transpose) is denoted by $\mathbf{A}^H$ and is defined as the n x m matrix with elements

$$[\mathbf{A}^H]_{ij} = a^*_{ji}. \tag{A8.2}$$

For a real matrix, $\mathbf{A}^H = \mathbf{A}^T$.

A square matrix is one for which m = n. A real square matrix is a symmetric matrix if $\mathbf{A}^T = \mathbf{A}$, and a complex square matrix is symmetric if $\mathbf{A}^H = \mathbf{A}$.

The rank of a matrix is the number of linearly independent rows or columns, whichever is less. The inverse of a square n x n matrix is the square n x n matrix $\mathbf{A}^{-1}$, for which

$$\mathbf{A}^{-1}\mathbf{A} = \mathbf{A}\mathbf{A}^{-1} = \mathbf{I} \tag{A8.3}$$

where **I** is the n x n identity matrix. The inverse will exist if and only if the rank of **A** is n. If the inverse does not exist, **A** is singular.

The determinant of a square n x n matrix is denoted by det (**A**). It is computed as

$$\det(\mathbf{A}) = \sum_{j=1}^{n} a_{ij} C_{ij} , \tag{A8.4}$$

where

$$C_{ij} = (-1)^{i+j} M_{ij} . \tag{A8.5}$$

M_{ij} is the determinant of the sub-matrix of **A** obtained by deleting the ith row and jth column and is termed the minor of a_{ij}.

A complex square n x n matrix **A** is positive semi-definite if it is hermitian and its hermitian form is non-negative or

$$\mathbf{x}^{H} \mathbf{A} \mathbf{x} \geq 0 \tag{A8.6}$$

for all $\mathbf{x} \neq 0$. If the hermitian form is strictly positive, the matrix is positive definite. Similarly, a real square n x n matrix **A** is positive semi-definite if **A** is symmetric and

$$\mathbf{x}^{T} \mathbf{A} \mathbf{x} \geq 0 \tag{A8.7}$$

for all $\mathbf{x} \neq 0$. A quadratic form Q is defined as

$$Q = \sum_{i=1}^{n} \sum_{j=1}^{n} a_{ij} x_i x_j \tag{A8.8}$$

for real a_{ij} and x_i. If the quadratic form is strictly positive, **A** is positive definite.

A partitioned m x n matrix **A** is one which is expressed in terms of its sub-matrices. An example is the 2 x 2 partitioning

$$\mathbf{A} = \begin{bmatrix} \mathbf{A}_{11} & \mathbf{A}_{12} \\ \mathbf{A}_{21} & \mathbf{A}_{22} \end{bmatrix} \tag{A8.9}$$

A.8.2 Special Matrices

A diagonal matrix is a square n x n matrix with $a_{ij} = 0$ for $i \neq j$ or all elements off the principal diagonal are zero. A diagonal matrix appears as

$$\mathbf{A} = \begin{bmatrix} a_{11} & 0 & \cdots & 0 \\ 0 & a_{22} & \cdots & 0 \\ \cdot & \cdot & \cdot & \cdot \\ \cdot & \cdot & \cdot & \cdot \\ \cdot & \cdot & \cdot & \cdot \\ 0 & 0 & \cdots & a_{nn} \end{bmatrix}. \tag{A8.10}$$

The inverse of a diagonal matrix is found by simply inverting each element on the principal diagonal.

A generalisation of the diagonal matrix is the square n x n block diagonal matrix

$$\mathbf{A} = \begin{bmatrix} \mathbf{A}_{11} & \mathbf{0} & \cdots & \mathbf{0} \\ \mathbf{0} & \mathbf{A}_{22} & \cdots & \mathbf{0} \\ \cdot & \cdot & \cdot & \cdot \\ \cdot & \cdot & \cdot & \cdot \\ \cdot & \cdot & \cdot & \cdot \\ \mathbf{0} & \mathbf{0} & \cdots & \mathbf{A}_{nn} \end{bmatrix} \tag{A8.11}$$

in which sub-matrices $\mathbf{A}_{ii}$ are square and the other sub-matrices are identically zero. The dimensions of the sub-matrices need not be identical.

The exchange matrix **J** is defined as the square n x n matrix

$$\mathbf{J} = \begin{bmatrix} 0 & \cdots & 0 & 1 \\ 0 & \cdots & 1 & 0 \\ \cdot & \cdot & \cdot & \cdot \\ \cdot & \cdot & \cdot & \cdot \\ \cdot & \cdot & \cdot & \cdot \\ 1 & \cdots & 0 & 0 \end{bmatrix}. \qquad \text{(A8.12)}$$

A lower triangular n x n square matrix is defined as

$$\mathbf{L} = \begin{bmatrix} a_{11} & 0 & \cdots & 0 \\ a_{21} & a_{22} & \cdots & 0 \\ \cdot & \cdot & \cdot & \cdot \\ \cdot & \cdot & \cdot & \cdot \\ \cdot & \cdot & \cdot & \cdot \\ a_{n1} & a_{n2} & \cdots & a_{nn} \end{bmatrix}. \qquad \text{(A8.13)}$$

The inverse of a lower triangular matrix is also a lower triangular matrix.

Similarly, an upper triangular square n x n matrix is defined as

$$\mathbf{U} = \begin{bmatrix} a_{11} & a_{12} & \cdots & a_{1n} \\ 0 & a_{22} & \cdots & a_{2n} \\ \cdot & \cdot & \cdot & \cdot \\ \cdot & \cdot & \cdot & \cdot \\ \cdot & \cdot & \cdot & \cdot \\ 0 & 0 & \cdots & a_{nn} \end{bmatrix}. \qquad \text{(A8.14)}$$

The inverse of an upper triangular matrix is also an upper triangular matrix.

A real square n x n matrix is orthogonal if

$$\mathbf{A}^{-1} = \mathbf{A}^{T}. \tag{A8.15}$$

For a matrix to be orthogonal the columns (and rows) must be orthonormal or if $\mathbf{a}_i$ denotes the ith column (or row), the conditions

$$\mathbf{a}_i^{T}\mathbf{a}_j = \begin{cases} 0 & \text{for } i \neq j \\ 1 & \text{for } i = j \end{cases} \tag{A8.16}$$

must be satisfied. A complex square n x n matrix is unitary if

$$\mathbf{A}^{-1} = \mathbf{A}^{H}. \tag{A8.17}$$

To be unitary the matrix **A** must satisfy

$$\mathbf{a}_i^{H}\mathbf{a}_j = \begin{cases} 0 & \text{for } i \neq j \\ 1 & \text{for } i = j \end{cases} \tag{A8.18}$$

A.8.3 Matrix manipulation and formulation

$$(\mathbf{A}\,\mathbf{B})^{T} = \mathbf{B}^{T}\,\mathbf{A}^{T} \tag{A8.19}$$

$$(\mathbf{A}\,\mathbf{B})^{H} = \mathbf{B}^{H}\,\mathbf{A}^{H} \tag{A8.20}$$

$$(\mathbf{A}^{T})^{-1} = (\mathbf{A}^{-1})^{T} \tag{A8.21}$$

$$(\mathbf{A}^{H})^{-1} = (\mathbf{A}^{-1})^{H} \tag{A8.22}$$

$$(\mathbf{A}\,\mathbf{B})^{-1} = \mathbf{B}^{-1}\,\mathbf{A}^{-1} \tag{A8.23}$$

$$\det(\mathbf{A}^T) = \det(\mathbf{A}) \tag{A8.24}$$

$$\det(\mathbf{A}^H) = \det^*(\mathbf{A}) \tag{A8.25}$$

$$\det(c\,\mathbf{A}) = c^n \det(\mathbf{A}), \text{ where c is a scalar} \tag{A8.26}$$

$$\det(\mathbf{A}\,\mathbf{B}) = \det(\mathbf{A}) \det(\mathbf{B}) \tag{A8.27}$$

$$\det(\mathbf{A}^{-1}) = 1 / \det(\mathbf{A}) \tag{A8.28}$$

APPENDIX A9

Computational considerations and summary of the conventional MUSIC algorithm

The theory leading to the development of the MUSIC algorithm has been based on the ensemble-averaged correlation matrix, $\hat{\mathbf{R}}$, or its time-averaged counterpart, $\hat{\mathbf{\Phi}}$. We may thus compute the MUSIC spectrum of Eq. (6.29) by performing an eigen-analysis on the correlation matrix $\hat{\mathbf{\Phi}}$ to compute the noise subspace represented by $\mathbf{V}_N$. From a computational viewpoint, however, a more efficient approach is to perform a singular value decomposition on the data matrix **A** directly. The products of this decomposition are represented by the singular values $\sigma_1, \sigma_2, \ldots, \sigma_{M+1}$, the associated right singular vectors $\mathbf{v}_1, \mathbf{v}_2, \ldots, \mathbf{v}_{M+1}$, and a set of left singular vectors. Insofar as the application of the MUSIC algorithm is concerned, the left singular vectors of **A** are of no interest. On the other hand, the squares of the singular values of the data matrix **A** and the associated right singular vectors are of particular interest because they are respectively, the same as the eigenvalues of the correlation matrix, $\mathbf{\Phi} = \mathbf{A}^H\mathbf{A}$, and the associated eigenvectors. In computing the MUSIC spectrum, the following points are noteworthy:

1- The MUSIC algorithm assumes knowledge of the model order, that is, the number of complex sinusoids contained in the transversal filter input.

2- The singular values of the data matrix **A** do not actually enter the computation of the MUSIC spectrum. Rather, they are used merely as a tool for identifying those right singular vectors of **A** that constitute the noise subspace. Although this role may appear to be of a secondary nature, nevertheless, it is crucial to the successful application of the MUSIC algorithm.

3- The MUSIC algorithm requires knowledge of only $M + 1 - L$ smallest singular values of the data matrix **A**. For such a requirement we may use a standard routine to compute the $M + 1$ singular values and associates singular vectors of the data matrix **A**; we may then identify the $M + 1 - L$ smallest singular values

and therefore retain the associated right singular vectors for use in the MUSIC algorithm. A more efficient procedure, however, is to use an SVD algorithm tailor-made for solving the problem at hand.

Table A.9.1 presents a summary of the MUSIC algorithm. Figure A.9.1 presents a block diagram of the essential steps involved in the computation of the MUSIC algorithm.

---

1) Use the time series {u(i)} to set up a data matrix **A**.

2) Compute the M+1-L smallest singular values $\sigma_{L+1}, \ldots, \sigma_{M+1}$ and therefore identify the right singular vectors $\mathbf{v}_{L+1}, \ldots, \mathbf{v}_{M+1}$. Hence, define the matrix

$$\mathbf{V}_N = [\mathbf{v}_{L+1}, \mathbf{v}_{L+2}, \cdots, \mathbf{v}_{M+1}].$$

3) Compute the projection matrix on the noise subspace, defined by the product $\mathbf{V}_N\mathbf{V}_N^H$. Hence, compute the MUSIC spectrum estimate

$$\hat{S}_{MUSIC}(\omega) = \frac{1}{\mathbf{s}^H(\omega)\mathbf{V}_N\mathbf{V}_N^H\mathbf{s}(\omega)}$$

for a varying values of angular frequency ω in the scanning vector

$$\mathbf{s}(\omega)=[1, e^{-j\omega}, \ldots, e^{-j\omega M}]^T, \quad -\pi<\omega<\pi.$$

4) Estimate the angular frequencies of the complex sinusoids in the time series {u(i)} by locating the spectral peaks of $\hat{S}_{MUSIC}(\omega)$.

Table A.9.1: *Summary of the MUSIC algorithm*

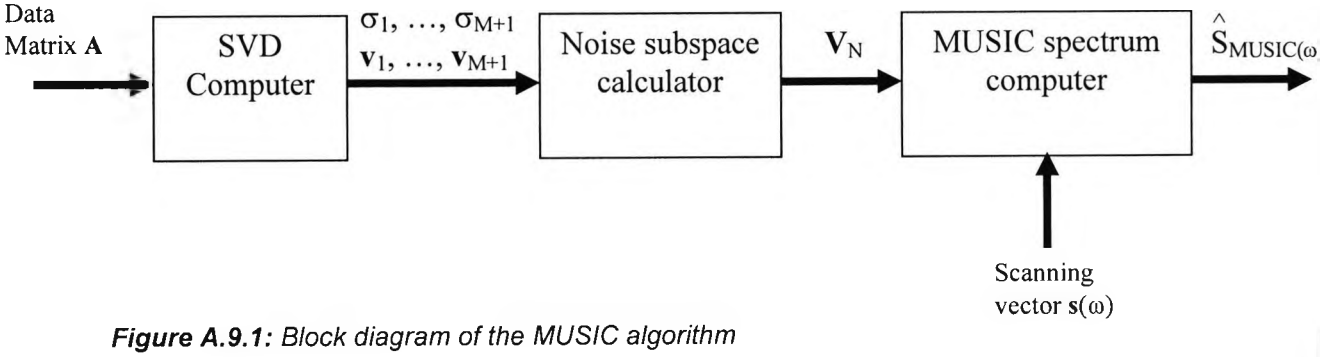

Figure A.9.1: *Block diagram of the MUSIC algorithm*

Appendix A10

Singular value decomposition (SVD) and the generalised singular value decomposition (GSVD): basic theorems

The singular value decomposition (Autonne-Eckart-Young) theorem

For any real p x q matrix **A**, there exists a real factorisation

$$\mathbf{A}_{p,q} = \mathbf{U}_{p,p}\, \Sigma_{p,p}\, \mathbf{V}^{T}_{p,q} \quad (\text{for } p < q), \tag{A10.1}$$

in which the matrix **U** is orthogonal ($\mathbf{U}\,\mathbf{U}^T = \mathbf{U}^T\,\mathbf{U} = \mathbf{I}_p$), the matrix **V** contains p orthonormal columns ($\mathbf{V}^T\,\mathbf{V} = \mathbf{I}_p$) and $\Sigma_{p,p}$ is a real diagonal matrix with non-negative diagonal elements, called the singular values, σ_i, of the matrix **A** [1].

The generalised singular value decomposition (GSVD)

Let **A** be a p x q and **B** a p x k matrix ($p < q$ and $p < k$) then there exist matrices $\mathbf{U}_A$ (q x p) and $\mathbf{U}_B$ (k x p), both with p orthonormal columns, and a non-singular p x p matrix **X** such that

$$\mathbf{A} = \mathbf{X}^{-T}\, \mathbf{D}_A\, \mathbf{U}_A{}^T \text{ and} \tag{A10.2}$$

$$\mathbf{B} = \mathbf{X}^{-T}\, \mathbf{D}_B\, \mathbf{U}_B{}^T, \tag{A10.3}$$

where $\mathbf{D}_A = \text{daig}\,(\alpha_1, \ldots, \alpha_p)$ and $\mathbf{D}_B = \text{diag}(\beta_1, \ldots, \beta_p)$, $(\alpha_i, \beta_i \geq 0)$, are square diagonal p x p matrices and $\alpha_1/\beta_1 \geq \alpha_2/\beta_2 \geq \ldots \geq \alpha_r/\beta_r$, r = rank (**B**) [1]. The elements of the set $\sigma(\mathbf{A}, \mathbf{B}) = (\alpha_1/\beta_1, \ldots, \alpha_r/\beta_r)$ are referred to as the generalised singular values of **A** and **B**.

References

[1] G. H. Golub, and A. H. Kahan, "Calculating the singular values and the pseudo-inverse of a matrix," J. of SIAM Numer. Anal. B., vol. 2, pp. 205-224, 1965.

Appendix A11

Previously published papers based on SVD methods to extract the fetal ECG from cutaneous electrode signals [1]

Three methods making use of the singular value decomposition (SVD) of a measurement matrix to extract the fetal ECG from cutaneously recorded electrode signals were presented and compared [1].

In the first method, a set of six or more potential signals, p, is recorded from electrodes placed on the maternal skin [2]. After sampling, a p x q data matrix $\boldsymbol{M}$ is constructed, where each row of $\boldsymbol{M}$ consists of the q samples of one signal. The SVD of the data matrix, given by $\boldsymbol{M} = \mathbf{U}\,\Sigma\,\mathbf{V}^{\mathrm{T}}$, provides under certain conditions of electrode placement, an efficient way to construct an MECG-free fetal electrocardiogram.

If the maternal ECG is sufficiently strongly present in the recordings, compared with the presence of the fetal ECG, then the singular spectrum Σ of $\boldsymbol{M}$ can be partitioned into three groups

$$\Sigma = \begin{pmatrix} \Sigma_M & 0 & 0 \\ 0 & \Sigma_F & 0 \\ 0 & 0 & \Sigma_O \end{pmatrix} \qquad \text{(A11.1)}$$

where Σ_M contains r_M singular values, associated with the maternal heart, Σ_F contains r_F singular values, associated with the fetal heart, and Σ_O contains $r_O = p - r_M - r_F$ singular values, associated with other possible sources of bioelectric activity and noise. A number of orthonormal singular directions correspond to each group of singular values, to form a subspace of the p-dimensional column space of the data matrix $\boldsymbol{M}$,

spanned by the columns of **U**. This results in a maternal subspace (dimension r_M), a fetal subspace (dimension r_F) and a subspace for other sources of electrical activity (dimension r_o).

The advantages of this method are: (i) the resultant signals are optimal with respect to extremal oriented energy, and (ii) the resultant fetal signals are orthogonal and form a set of principal fetal signals, independent of the physical orientation of the fetal heart.

The disadvantages of this method are: (i) no general electrode placement strategy can be used, because for each subject the most ideal electrode positions have to be looked for, and (ii) this method is not suitable during labour.

The second method is an on-line approach to the technique in [3]. It composes a matrix $\boldsymbol{M}_M$ as a sequence of several (5 - 10) maternal QRS intervals, selected from the data matrix $\boldsymbol{M}$. Some of these intervals may contain a P-wave, while others also contain a T-wave, such that the subspace associated with the maternal heart is described much better than before, when only one maternal QRS-complex was selected [1]. Then the SVD of $\boldsymbol{M}_M$ is computed and the left singular matrix $\mathbf{U}_M$ is partitioned into

$$\begin{matrix} & r_M & p - r_M \\ \mathbf{U}_M = (\mathbf{U}_1 & & \mathbf{U}_2) \; p, \end{matrix} \qquad \text{(A11.2)}$$

with r_M the estimated dimension of the maternal subspace.

Instead of selecting a fetal QRS interval, the whole data matrix $\boldsymbol{M}$ is projected onto $\mathbf{U}_2$, the complement of the maternal subspace.

$$\mathbf{A}_{(p\text{-}rM),q} = \mathbf{U}_2^T \boldsymbol{M} \qquad \text{(A11.3)}$$

This matrix **A** then contains no MECG contribution any more.

The disadvantages of this method include: (i) it relies on the fetal signals being sufficiently strong (relative to all other unwanted signals present in the recordings) so that the direction of maximum orientation energy of **A**, found in $\mathbf{u}_{A1}$, provides the MECG-free linear combination of the $p - r_M$ signals of **A**, (ii) there is a more

complicated initialisation of the on-line procedure than that of the first method, and (iii) concerning the signal-to-noise ratio, it is expected that this method is suboptimal in the same way as [3]. This method is useful when only a fetal trigger is required, as the signal obtained is not a complete FECG [4].

A third method is proposed based on the generalised singular value decomposition (GSVD) and interpreted with the new concept of oriented signal-to-signal ratio [1]. From Appendix A10, we know that the GSVD of the pair (**A**, **B**) looks for non-orthogonal directions, denoted x_i, of extremal oriented signal-to-signal ratio. Let α_i / β_i be the generalised singular values of **A** and **B**, arranged in non-increasing order. Then, the column x_i of **X,** which is a non-singular p x p matrix, in the GSVD of (**A**, **B**) (see Eqs. A.10.2 and A.10.3) is a vector for which the oriented energy of matrix **A** is α_i / β_i times larger than the oriented energy of matrix **B** (cf. concepts of signal-to-signal ratio, [6]).

Therefore, arrange the p recorded potential signals in a p x q data matrix ***M*** and compose a matrix **B** as a sequence of several maternal QRS intervals, not coinciding with fetal complexes. This means that the matrix **B** only contains contributions from the unwanted signal, the MECG. The GSVD of the matrix pair (***M***, **B**) can then be written as

$$\boldsymbol{M} = \mathbf{X}^{-T}\,\mathbf{D}_M\,\mathbf{U}_M{}^T \qquad \text{(A11.4)}$$

$$\mathbf{B} = \mathbf{X}^{-T}\,\mathbf{D}_B\,\mathbf{U}_B{}^T \qquad \text{(A11.5)}$$

All columns of **X** provide, after normalisation, a linear combination of the p recorded potential signals, in which the oriented signal (in ***M***)- to-signal (in **B**)-ratio is extremal. Only some of them contain an MECG-free fetal heart signal. Concerning the computation of the **X** matrix in the GSVD of a matrix pair (**A**, **B**), a very important observation is stated in the following theorem [7].

Theorem and proof: Four–step method for GSVD computation: The computation of the **X** matrix in the GSVD of a matrix pair (**A**, **B**) can be performed by the following four-step method [7]:

Step 1: Compute the SVD of **B**

$$\mathbf{B} = \mathbf{U}_B \, \Sigma_B \, \mathbf{V}_B^T \tag{A11.6}$$

Step 2: Define a transformation $\mathbf{Q} = \Sigma_B^{-1} \, \mathbf{U}_B^T$ on the matrix $\mathbf{A}$ such that

$$\mathbf{Q} \, \mathbf{A} = \mathbf{A}^* = \Sigma_B^{-1} \, \mathbf{U}_B^T \, \mathbf{A}. \tag{A11.7}$$

Step 3: Compute the SVD of $\mathbf{A}^*$

$$\mathbf{A}^* = (\mathbf{U}_A^*) \, (\Sigma_A^*) \, (\mathbf{V}_A^*)^T. \tag{A11.8}$$

Step 4: Compute the $\mathbf{X}$ matrix in the GSVD of ($\mathbf{A}$, $\mathbf{B}$) as

$$\mathbf{X} = \mathbf{Q}^T \, \mathbf{U}_A^* = \mathbf{U}_B \, \Sigma_B^{-1} \, \mathbf{U}_A^*. \tag{A11.9}$$

Proof: Suppose that the GSVD of a matrix pair ($\mathbf{A}$, $\mathbf{B}$) is given by Eqs. (A10.2-A10.3), then

$$\mathbf{A} \, \mathbf{A}^T = \mathbf{X}^{-T} \, \mathbf{D}_A^2 \, \mathbf{X}^{-1} \tag{A11.10}$$

$$\mathbf{B} \, \mathbf{B}^T = \mathbf{X}^{-T} \, \mathbf{D}_B^2 \, \mathbf{X}^{-1} \tag{A11.11}$$

In other words, the p x p matrix $\mathbf{X}$ diagonalises both $\mathbf{A} \, \mathbf{A}^T$ and $\mathbf{B} \, \mathbf{B}^T$. The corresponding generalised symmetric eigenvalue problem then has the following formulation:

$$\mathbf{A} \, \mathbf{A}^T \, \mathbf{x}_i = \lambda_i \, \mathbf{B} \, \mathbf{B}^T \, \mathbf{x}_i \tag{A11.12}$$

with λ_i the ith generalised eigenvalue. In the first step of the procedure the SVD of $\mathbf{B}$ is computed, such that

$$\mathbf{B} \, \mathbf{B}^T = \mathbf{U}_B \, \Sigma_B^2 \, \mathbf{U}_B^T = \mathbf{Q}^{-1} \, \mathbf{Q}^{-T} \tag{A11.13}$$

Substitution into Eq. (A11.12) then gives

$$\mathbf{A} \, \mathbf{A}^T \, \mathbf{x}_i = \lambda_i \, \mathbf{Q}^{-1} \, \mathbf{Q}^{-T} \, \mathbf{x}_i \tag{A11.14}$$

This can also be written as

$$(\mathbf{Q}\,\mathbf{A}\,\mathbf{A}^T\,\mathbf{Q}^T)\,(\mathbf{Q}^{-T}\,\mathbf{x}_i) = \lambda_i\,(\mathbf{Q}^{-T}\,\mathbf{x}_i) \qquad \text{(A11.15)}$$

and this is nothing more than a normal symmetric eigenvalue problem. Diagonalisation with an orthonormal matrix $\mathbf{U}\,\mathbf{A}^*$ of the symmetric matrix $\mathbf{Q}\,\mathbf{A}\,\mathbf{A}^T\,\mathbf{Q}^T$ and comparison with Eq. (A11.10) results in

$$\mathbf{X} = \mathbf{Q}^T\,\mathbf{U}\,\mathbf{A}^* = \mathbf{U}_B\,\Sigma_B^{-1}\,\mathbf{U}\,\mathbf{A}^* \qquad \text{(A11.16)}$$

As already mentioned, experiments showed that the transfer for the signals coming from the maternal heart is nearly time-invariant, such that the **B** matrix has to be constructed and decomposed only once as a kind of initialisation. The rest of the method can again be performed, using the on-line adaptive strategy, but now with an initial projection matrix equal to $\mathbf{U}_B\,\Sigma_B^{-1}$, which is now a non-orthogonal matrix.

The disadvantages of this method include: (i) a rather complicated initialisation of the on-line procedure (visual selection of data intervals) is required, and (ii) no principal signals are obtained, because the signals are not orthogonal.

References

[1] D. Callaerts, B. DeMoor, J. Vanderville, and W. Sansen, "Comparison of SVD methods to extract the fetal electrocardiogram," Med. Biol. Eng. Comput., Vol. 28, pp. 217-224, 1990.

[2] A. Van Oosterom and J Alsters, "Removing the maternal component in the fetal ECG using singular value decomposition," In Electrocardiography '83. I. Ruttkay-Nedecky and P. MacFarlane, Eds., Exceptra Medicine, Amesterdam, The Netherlands, pp. 171-176, 1984.

[3] A. Van Oosterom, "Spatial filtering of the fetal electrocardiogram," J. Perinat. Med., Vol. 14, No. 6, pp. 411-419, 1986.

[4] D. Callaerts, J. Vanderschoot, J. Vandewalle, W. Vantrappen, and J. Janssens, "An adaptive on-line method for the extraction of the complete fetal electrocardiogram from cutaneous multilead recordings," J. Perinat. Med., Vol. 14, No. 6, pp. 421-433, 1986.

[5] D. Callaerts, J. Vanderschoot, J. Vandewalle, and W. Sansen, "An on-line adaptive

algorithm for signal processing using SVD," In Signal Processing III, Elsevier Science/ North Holland/, Amesterdam, The Netherlands, EURASIP 86, The Hague, pp. 953-956, 1986.

[6] G. H. Golub, and A. H. Kahan, "Calculating the singular values and the pseudo-inverse of a matrix," Journal of SIAM Numer. Anal. B., vol. 2, pp. 205-224, 1965.

[7] B. N. Parlett, *The Symmetric eigenvalue problem*, Prentice Hall, Englewood, Cliffs, New Jersey, USA, 1980.

APPENDIX A12

The concepts of oriented energy and signal-to-signal ratio*

This Appendix describes the concepts of oriented energy and oriented signal-to-signal ratio of a vector sequence and shows their relations with SVD and GSVD.

A12.1 Definition 1: Oriented energy:

Consider a sequence of p-vectors $\{\mathbf{a}_k\}$, k = 1, …, q, and arrange them as the columns of a p x q matrix, **A**. Then $E_e[\mathbf{A}]$, the energy of the vector set in the direction of unit vector $\mathbf{e} \subset \mathcal{R}^p$, is defined as

$$E_e[\mathbf{A}] = \sum_{K=1}^{q} (\mathbf{e}^T \mathbf{a}_k)^2 = \| \mathbf{e}^T \mathbf{A} \|^2 \qquad \text{(A12.1)}$$

There exists a relationship between the singular values and vectors of the matrix **A** and its directions of extremal oriented energy as follows:

$$E_{ui}[\mathbf{A}] = \| \mathbf{u}_i^T \mathbf{A} \|^2 = \sigma_i^2 \qquad \text{(A12.2)}$$

where $\mathbf{u}_i$ is a column vector of **U** in the SVD of **A** and σ_i is the corresponding singular value of **A**. For proof see [2-3]. Moreover, we know from linear algebra that each $\mathbf{u}_i$ contains the coefficients of a linear combination of the rows of **A**, such that

* The material presented here is based on the works by:

1- B. De Moor, J. Vanderwalle, and J. Staar, *Oriented energy and oriented signal-to signal ratio concepts in the analysis of vector sequences and time series*, In *SVD and signal processing: algorithms, applications, and architectures*. E. Deprettere, (Ed.) North Holland, pp. 209-232, 1987.

2- B. De Moor, *Mathematical concepts and techniques for modelling of static and dynamic systems*, PhD. Thesis, Dept. of Electrical Engineering, Katholieke Universiteit, Leuven, Belgium, June 1988.

3- J. Vanderwalle, D. Callaerts, "Singular value decomposition: a powerful concept and tool in signal processing," Proc. Conf. On Mathematics in Signal Processing, Warwick, 1988.

$\| \mathbf{u}_i^T \mathbf{A} \mathbf{A}^T \mathbf{u}_i \| = \| \mathbf{u}_i^T \mathbf{A} \|^2$ reaches extremal value, which equals σ_i^2. In other words, the columns $\mathbf{u}_i$, of the **U**-matrix in the SVD of **A** provide directions in the column space of **A** for which the oriented energy is extremal. Therefore, the SVD of a matrix **A** finds r_A = rank (**A**) orthonormal directions of extremal oriented energy.

A12.2 Definition 2: Oriented signal-to-signal ratio

The oriented signal-to-signal ratio, R_e [**A**, **B**], of two sets of p-vectors $\{\mathbf{a}_k\}$ and $\{\mathbf{b}_k\}$, (k = 1, …, q), in the direction of unit vector $\mathbf{e} \subset \mathcal{R}^p$, is defined as

$$R_e [\mathbf{A}, \mathbf{B}] = E_e[\mathbf{A}] / E_e[\mathbf{B}] = \| \mathbf{e}^T \mathbf{A} \|^2 / \| \mathbf{e}^T \mathbf{B} \|^2 \qquad \text{(A12.3)}$$

In analogy with the oriented energy-SVD relationship, a relationship between the oriented signal-to-signal ratio concept and the GSVD exists. If the GSVD of matrices **A** and **B** is given as in the GSVD theorem of Appendix A11; then

$$R_e [\mathbf{A}, \mathbf{B}] = (\alpha_i / \beta_i)^2 \quad \text{for } \mathbf{e} = x_i / \| x_i \| \qquad \text{(A12.4)}$$

For proof see [1-3]. Applied to the signal separation problem, this can be interpreted as follows: assume that **A** contains p signals that are all mixed with an unwanted signal, while **B** contains only contributions from the unwanted signal. The GSVD of the matrix pair (**A**, **B**) then looks for directions in the column space of **A** and **B** for which the oriented ratio of wanted signal to unwanted signal is extremal. This was illustrated for the FECG-MECG separation problem.

References

[1] B. De Moor, J. Vanderwalle, and J. Staar, *Oriented energy and oriented signal-to-signal ratio concepts in the analysis of vector sequences and time series*, In SVD and signal processing: algorithms, applications, and architecxtures. E. Deprettere, (Ed.) North Holland, pp. 209-232, 1987.

[2] B. De Moor, Mathematical concepts and techniques for modelling of static and dynamic systems, PhD. Thesis, Department of Electrical Engineering, Katholieke Universiteit, Leuven, Belgium, June 1988.

[3] J. Vanderwalle, D. Callaerts, "Singular value decomposition: a powerful concept and tool in signal processing," Proc. Conf. On Mathematics in Signal Processing, Warwick, 1988.

APPENDIX A13

An alternative projection method: The composite transabdominal ECG signal (TECG = MECG + FECG + the uterine contraction signal (UCS) + noise) is Gram-Schmidt orthogonalised with the UCS

In order to facilitate partial or total elimination of the uterine contraction signal (UCS) from the composite transabdominal ECG signal (**TECG**), the two signals with noise must first be linearised. This helps to get rid of higher-order trends and may render the signals linear and non-Gaussian. Then the latter composite signal is Gram-Schmidt (GS) orthogonalised with the former (the unwanted signal) and projected onto it. Both signals can be measured. However, the UCS still contains low levels of the **TECG** signal, e.g., T- and u-waves. Essentially, the **TECG** signal occupies the whole cardiac cycle.

Figure A13.1 illustrates the segmentation of the composite transabdominal ECG (**TECG**) signals into four segments. Figure A13.2 illustrates how the composite transabdominal ECG signal (**TECG** = MECG + FECG + the uterine contraction signal (UCS) + noise) is represented by the vector OA, and Gram-Schmidt (GS) orthogonalised with the UCS represented by the vector OB. The signal OE is perpendicular to the UCS signal, which is free from any component that might correspond to the UCS.

In order to find the projection of a 250 msec **TECG** segment represented by the vector OA onto the UCS vector OB and then subtract it from the segment itself, we perform Gram-Schmidt (GS) orthogonalisation [1-3] between these two signals.

1) Let u = OB / ||OB|| be the unit vector along the UCS axis.
2) The projection OC of a typical 250 msec transabdominal ECG segment on the UCS axis is the following inner product:

$$OC = OB \cdot u \qquad \text{(A13.1)}$$

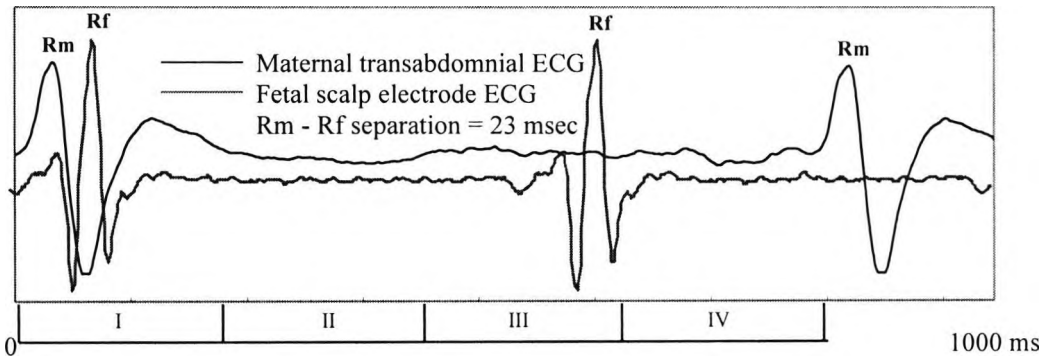

***Figure A13.1**: Superimposed and synchronised maternal transabdominal and fetal scalp electrode ECG signals with maternal R-wave to fetal R-wave separation of 23 msec. The maternal cardiac cycle begins 50 msec before the R-wave and ends 50 msec before the next R-wave. The subject is at the first stage of labour, 40 weeks gestation. The maternal cycle has 500 samples or more at a rate of 0.5 KHz. (Code: 12). Segment I: maternal QRS-complex, segment II: the first fetal heartbeat with maternal contribution, segment III: QRS-free ECG, and segment IV: the second fetal heartbeat with maternal contribution.*

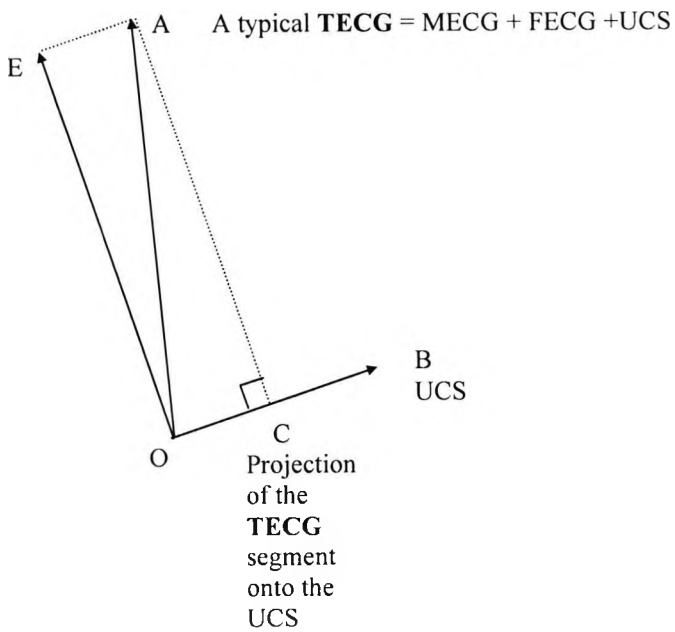

***Figure A13.2**: The composite transabdominal ECG signal (**TECG** = MECG + FECG + the uterine contraction signal (UCS) + noise) is represented by the vector OA, and Gram-Schmidt (GS) orthogonalised with the UCS represented by the vector OB. The signal OE is perpendicular to the UCS signal, which is free from any component that might correspond to the UCS.*

3) The orthogonal vector to the UCS vector is then given by the following formula:

$$OE = OA - u\,(\,OA\,.\,u\,)$$

$$= OA - \frac{OB}{\|\,OB\,\|}\left(OA.\frac{OB}{\|\,OB\,\|}\right) \qquad \text{(A13.2)}$$

or more explicitly,

$$OE(n) = OA(n) - u(n)\left[\sum_{i=1}^{N} OA(i)u(i)\right], \qquad n = 1, 2, \ldots, N, \qquad \text{(A13.3)}$$

where

$$u(n) = \frac{OB(n)}{\sum_{j=1}^{N} OB(j)^2}, \qquad n = 1, 2, \ldots, N. \qquad \text{(A13.4)}$$

Each segment of the transabdominal ECG signal (**TECG** = MECG + FECG + the uterine contraction signal (UCS) + noise) contains either the P-wave, the QRS-complex, or both, (segments I, III, IV as shown in Figure A13.1) will be orthogonalised with the remaining uterine contraction signal (UCS) known to be free from the P-waves and the QRS- complexes (segment II in Figure A13.1).

The algorithm thus measures from a given 250 msec **TECG** segment the amount of the uterine contraction signal (UCS) and subtracts it from the transabdominal ECG (**TECG**) data during acquisition and storage.

References

[1] S. Haykin, *Adaptive filter theory*, Prentice Hall, 1991.

[2] R. Schmidt, "Multiple emitter location and signal parameter estimation," Proceedings of RADC Spectrum Estimation Workshop, pp. 243-258, 1979.

[3] J. C. Mosher et al., "Multiple dipole modelling and localisation from spatio-temporal MEG data," IEEE Trans. Biomedical Engineering, Vol. 39, pp. 541-557, June 1992.